

Neurovascular
Malformation
Solutions

Ischemic Stroke
and Carotid Artery
Disease Solutions

For more information or a product demonstration,
contact your local MicroVention representative:



MicroVention, Inc.
Worldwide Headquarters
1311 Valencia Avenue
Tustin, CA 92780 USA
MicroVention UK Limited
MicroVention Europe, S.A.R.L.
MicroVention Deutschland GmbH

PH +1.714.247.8000

PH +44 (0) 191 258 6777

PH +33 (1) 39 21 77 46

PH +49 211 210 798-0

Smooth and stable.

Target Detachable Coils deliver consistently smooth deployment and exceptional microcatheter stability. Designed to work seamlessly together for framing, filling and finishing. Target Coils deliver the high performance you demand.

For more information, please visit www.strykerneurovascular.com/Target or contact your local Stryker Neurovascular sales representative.



Target®
DETACHABLE COILS

BARRICADE™ COIL SYSTEM

COILS THAT PERFORM

Cost Analysis of Cerebral Aneurysms Treated with the Barricade Coil System, A Retrospective Review

22 Patients Treated ♦ 114 Total Barricade Coils Used ♦ 8.2mm Mean Aneurysm Size

RIGHT PERICALLOSAL ANEURYSM

LEFT ICA TERMINUS ANEURYSM



PRE-TREATMENT

POST-TREATMENT



PRE-TREATMENT

POST-TREATMENT

“ I have successfully treated a wide range of aneurysms with the Barricade Coil System. I am impressed with the overall performance of the coils and the realized cost savings.”

-Yince Loh, M.D.

COILS THAT SAVE \$

\$110,000*
SAVED

Images and data courtesy of Yince Loh, M.D., Seattle, WA

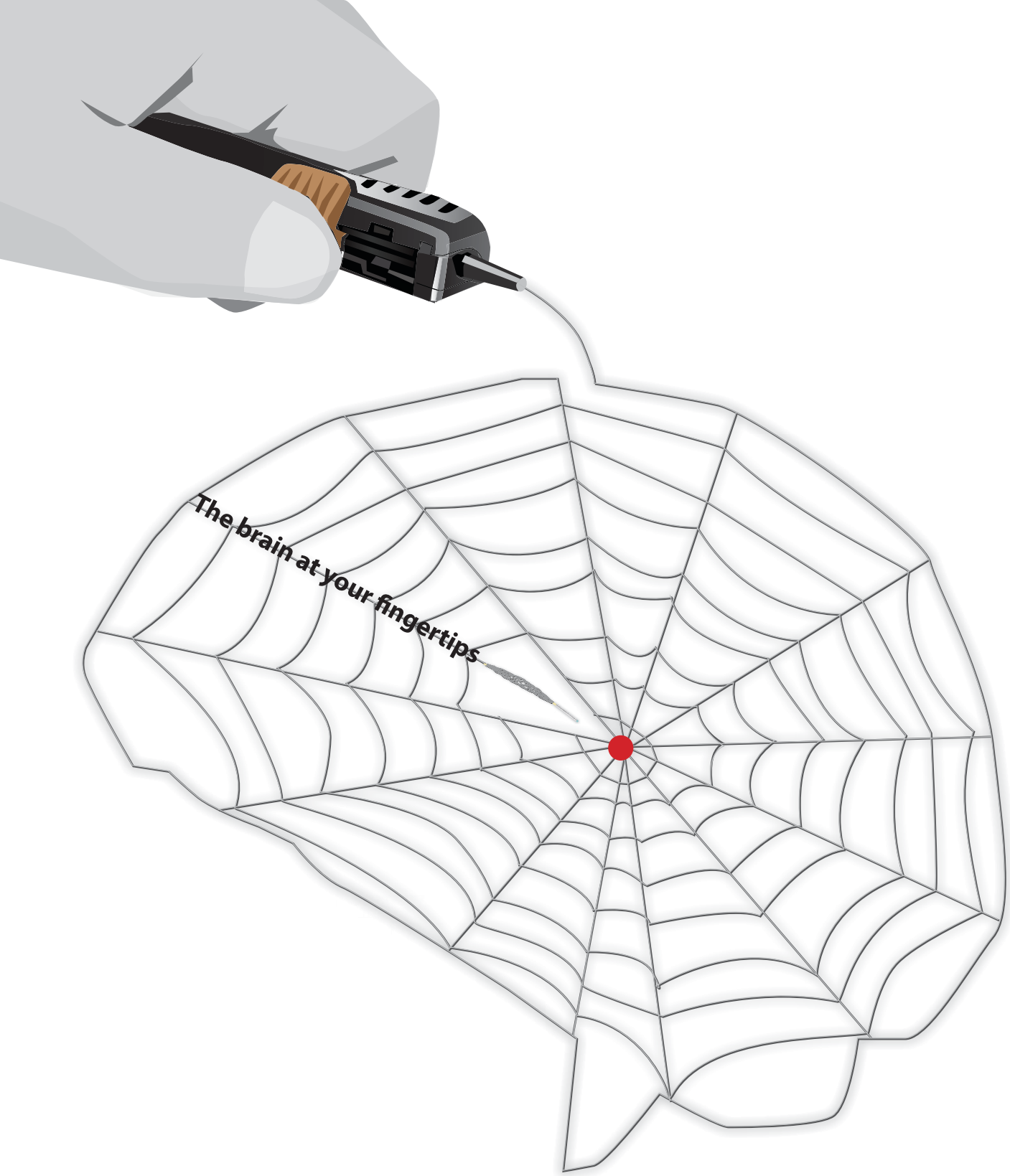
* Estimated savings in this case, data on file.

The Barricade Coil System is intended for the endovascular embolization of intracranial aneurysms and other neurovascular abnormalities such as arteriovenous malformations and arteriovenous fistulae. The System is also intended for vascular occlusion of blood vessels within the neurovascular system to permanently obstruct blood flow to an aneurysm or other vascular malformation and for arterial and venous embolizations in the peripheral vasculature. Refer to the instructions for use for complete product information.

18 TECHNOLOGY DRIVE #169, IRVINE CA 92618 | p: 949.788.1443 | f: 949.788.1444
WWW.BLOCKADEMEDICAL.COM

MKTG-050 Rev. A





The brain at your fingertips

 **Rapid Medical**

www.rapid-medical.com > tigertriever

The Foundation of the ASNR Symposium 2017: *Discovery and Didactics* April 22-23, 2017

ASNR 55th Annual Meeting: *Diagnosis and Delivery* April 24-27, 2017



Long Beach Convention & Entertainment Center
© Long Beach Convention & Visitors Bureau

Jacqueline A. Bello, MD, FACR
ASNR 2017 Program Chair/President-Elect

Programming developed in cooperation with and appreciation of the...

American Society of Functional Neuroradiology (ASFNR)

Kirk M. Welker, MD

American Society of Head and Neck Radiology (ASHNR)

Rebecca S. Cornelius, MD, FACR

American Society of Pediatric Neuroradiology (ASPNR)

Susan Palasis, MD

American Society of Spine Radiology (ASSR)

Joshua A. Hirsch, MD, FACR, FSIR

Society of NeuroInterventional Surgery (SNIS)

Blaise W. Baxter, MD

American Society of Neuroradiology (ASNR)

Health Policy Committee

Robert M. Barr, MD, FACR

Computer Sciences & Informatics (CSI) Committee

John L. Go, MD, FACR

Research Scientist Committee

Dikoma C. Shungu, PhD and Timothy, P.L. Roberts, PhD

The International Hydrocephalus Imaging Working Group (IHIWG)/CSF Flow Group

William G. Bradley, Jr., MD, PhD, Harold L. Rekate, MD and Bryn A. Martin, PhD

Register Now!

Visit 2017.asnr.org for more information.



ASNR 55th Annual Meeting

c/o American Society of Neuroradiology
800 Enterprise Drive, Suite 205 • Oak Brook, Illinois 60523-4216
Phone: 630-574-0220 • Fax: 630 574-0661 • 2017.asnr.org



ASFNR ASHNR ASPNR ASSR SNIS

THE FOUNDATION OF THE ASNR



Come to the beach! Please join us in Long Beach, California, April 22-27, 2017, for the 55th Annual Meeting of the ASNR. Known for its 5.5 miles of Pacific Ocean waterfront, this southern California beach resort boasts a blend of city sophistication and seaside serenity. ASNR is delighted to provide a “4D” focus for this meeting, as depicted by our meeting logo: **Discovery and Didactics** for The Foundation of the ASNR Symposium 2017: **Diagnosis and Delivery** for the ensuing Annual Meeting Program.

Centered on Discovery and Didactics, the symposium will feature sessions on “What’s New?” in the role neuroimaging plays defining CNS disease mechanisms and how to best prepare for “What’s Next?” for our subspecialty in terms of training, teaching, and leading the process of lifelong learning. The annual meeting programming will address best practices in Diagnosis and Delivery, as we strive to provide value, promote quality in better health and care and consider cost. Our discussions will consider how to navigate the changing landscape of healthcare reform and reimbursement as subspecialists in a field that is changing at an equally “fast forward” pace!



Hyatt Regency Long Beach
© Hyatt Regency Long Beach



Westin Long Beach
© The Westin Long Beach

CALL FOR AJNR EDITORIAL FELLOWSHIP CANDIDATES

ASNR and AJNR are pleased once again to join efforts with other imaging-related journals that have training programs on editorial aspects of publishing for trainees or junior staff (3–5 years after training), including Radiology (Olmsted fellowship), AJR (Figley and Rogers fellowships), JACR (Bruce J. Hillman fellowship), and Radiologia.

2017 Candidate Information and Requirements

GOALS

- Increase interest in “editorial” and publication-related activities in younger individuals.
- Increase understanding and participation in the AJNR review process.
- Incorporate into AJNR’s Editorial Board younger individuals who have previous experience in the review and publication process.
- Fill a specific need in neuroradiology not offered by other similar fellowships.
- Increase the relationship between “new” generation of neuroradiologists and more established individuals.
- Increase visibility of AJNR among younger neuroradiologists.

ACTIVITIES OF THE FELLOWSHIP

- Serve as Editorial Fellow for one year. This individual will be listed on the masthead as such.
- Review at least one manuscript per month for 12 months. Evaluate all review articles submitted to AJNR.
- Learn how electronic manuscript review systems work.
- Be involved in the final decision of selected manuscripts together with the Editor-in-Chief.
- Participate in all monthly Senior Editor telephone conference calls.
- Participate in all meetings of the Editors and Publications Committee during the annual meetings of ASNR and RSNA as per candidate’s availability. The Foundation of the ASNR will provide \$2000 funding for this activity.
- Evaluate progress and adjust program to specific needs in annual meeting or telephone conference with the Editor-in-Chief.
- Embark on an editorial scientific or bibliometric project that will lead to the submission of an article to AJNR or another appropriate journal as determined by the Editor-in-Chief. This project will be presented by the Editorial Fellow at the ASNR annual meeting.
- Serve as liaison between AJNR and ASNR’s Young Professionals Network and the 3 YPs appointed to AJNR as special consultants. Participate in meetings and telephone calls with this group. Design one electronic survey/year, polling the group regarding readership attitudes and wishes.
- Recruit trainees as reviewers as determined by the Editor-in-Chief.
- Participate in Web improvement projects.
- Serve as Guest Editor for an issue of AJNR’s News Digest with a timely topic.

QUALIFICATIONS

- Be a fellow in neuroradiology from North America, including Canada (this may be extended to include other countries).
- Be a junior faculty neuroradiology member (< 3 years) in either an academic or private environment.
- Be an “in-training” or member of ASNR in any other category.

APPLICATION

- Include a short letter of intent with statement of goals and desired research project. CV must be included.
- Include a letter of recommendation from the Division Chief or fellowship program director. A statement of protected time to perform the functions outlined is desirable.
- Applications will be evaluated by AJNR’s Senior Editors and the Chair of the Publications Committee prior to the ASNR meeting. The name of the selected individual will be announced at the meeting.
- Applications should be received by March 1, 2017 and sent to Ms. Karen Halm, AJNR Managing Editor, electronically at khalm@asnr.org.

Official Journal:

American Society of Neuroradiology
American Society of Functional Neuroradiology
American Society of Head and Neck Radiology
American Society of Pediatric Neuroradiology
American Society of Spine Radiology

EDITOR-IN-CHIEF

Jeffrey S. Ross, MD

Professor of Radiology, Department of Radiology,
Mayo Clinic College of Medicine, Phoenix, AZ

SENIOR EDITORS

Harry J. Cloft, MD, PhD

Professor of Radiology and Neurosurgery,
Department of Radiology, Mayo Clinic College of
Medicine, Rochester, MN

Thierry A.G.M. Huisman, MD

Professor of Radiology, Pediatrics, Neurology, and
Neurosurgery, Chairman, Department of Imaging
and Imaging Science, Johns Hopkins Bayview,
Director, Pediatric Radiology and Pediatric
Neuroradiology, Johns Hopkins Hospital,
Baltimore, MD

C.D. Phillips, MD, FACR

Professor of Radiology, Weill Cornell Medical
College, Director of Head and Neck Imaging,
New York-Presbyterian Hospital, New York, NY

Pamela W. Schaefer, MD

Clinical Director of MRI and Associate Director of
Neuroradiology, Massachusetts General Hospital,
Boston, Massachusetts, Associate Professor,
Radiology, Harvard Medical School, Cambridge, MA

Charles M. Strother, MD

Professor of Radiology, Emeritus, University of
Wisconsin, Madison, WI

Jody Tanabe, MD

Professor of Radiology and Psychiatry,
Chief of Neuroradiology,
University of Colorado, Denver, CO

STATISTICAL SENIOR EDITOR

Bryan A. Comstock, MS

Senior Biostatistician,
Department of Biostatistics,
University of Washington, Seattle, WA

EDITORIAL BOARD

Ashley H. Aiken, *Atlanta, GA*
Lea M. Alhilali, *Phoenix, AZ*
John D. Barr, *Dallas, TX*
Ari Blitz, *Baltimore, MD*
Barton F. Branstetter IV, *Pittsburgh, PA*
Jonathan L. Brisman, *Lake Success, NY*
Julie Bykowski, *San Diego, CA*
Keith Cauley, *Danville, PA*
Asim F. Choudhri, *Memphis, TN*
Alessandro Cianfoni, *Lugano, Switzerland*
J. Matthew Debnam, *Houston, TX*
Seena Dehkharghani, *New York, NY*
Colin Derdeyn, *Iowa City, IA*
Rahul S. Desikan, *San Francisco, CA*
Yonghong Ding, *Rochester, MN*
Clifford J. Eskey, *Hanover, NH*
Saeed Fakhran, *Phoenix, AZ*
Massimo Filippi, *Milan, Italy*
Allan J. Fox, *Toronto, Ontario, Canada*
Wende N. Gibbs, *Los Angeles, CA*
Christine M. Glastonbury, *San Francisco, CA*
John L. Go, *Los Angeles, CA*
Allison Grayev, *Madison, WI*
Brent Griffith, *Detroit, MI*
Wan-Yuo Guo, *Taipei, Taiwan*
Ajay Gupta, *New York, NY*
Rakesh K. Gupta, *Lucknow, India*
Lotfi Hacein-Bey, *Sacramento, CA*
Christopher P. Hess, *San Francisco, CA*
Andrei Holodny, *New York, NY*
Benjamin Huang, *Chapel Hill, NC*
George J. Hunter, *Boston, MA*
Mahesh V. Jayaraman, *Providence, RI*
Valerie Jewells, *Chapel Hill, NC*
Christof Karmonik, *Houston, TX*
Timothy J. Kaufmann, *Rochester, MN*
Hillary R. Kelly, *Boston, MA*
Toshibumi Kinoshita, *Akita, Japan*
Kenneth F. Layton, *Dallas, TX*
Michael M. Lell, *Nürnberg, Germany*
Michael Lev, *Boston, MA*
Karl-Olof Lovblad, *Geneva, Switzerland*
Franklin A. Marden, *Chicago, IL*
M. Gisele Matheus, *Charleston, SC*
Joseph C. McGowan, *Merion Station, PA*
Stephan Meckel, *Freiburg, Germany*
Christopher J. Moran, *St. Louis, MO*
Takahisa Mori, *Kamakura City, Japan*
Suresh Mukherji, *Ann Arbor, MI*
Amanda Murphy, *Toronto, Ontario, Canada*
Alexander J. Nemeth, *Chicago, IL*
Sasan Partovi, *Cleveland, OH*
Laurent Pierot, *Reims, France*
Jay J. Pillai, *Baltimore, MD*
Whitney B. Pope, *Los Angeles, CA*

Andrea Poretti, *Baltimore, MD*
M. Judith Donovan Post, *Miami, FL*
Tina Young Poussaint, *Boston, MA*
Joana Ramalho, *Lisbon, Portugal*
Otto Rapalino, *Boston, MA*
Álex Rovira-Cañellas, *Barcelona, Spain*
Paul M. Ruggieri, *Cleveland, OH*
Zoran Rumboldt, *Rovinj-Rovigno, Croatia*
Amit M. Saindane, *Atlanta, GA*
Erin Simon Schwartz, *Philadelphia, PA*
Lubdha M. Shah, *Salt Lake City, UT*
Aseem Sharma, *St. Louis, MO*
J. Keith Smith, *Chapel Hill, NC*
Maria Vittoria Spampinato, *Charleston, SC*
Gordon K. Sze, *New Haven, CT*
Krishnamoorthy Thamburaj, *Hershey, PA*
Cheng Hong Toh, *Taipei, Taiwan*
Thomas A. Tomsick, *Cincinnati, OH*
Aquila S. Turk, *Charleston, SC*
Willem Jan van Rooij, *Tilburg, Netherlands*
Arastoo Vossough, *Philadelphia, PA*
Elysa Widjaja, *Toronto, Ontario, Canada*
Max Wintermark, *Stanford, CA*
Ronald L. Wolf, *Philadelphia, PA*
Kei Yamada, *Kyoto, Japan*
Carlos Zamora, *Chapel Hill, NC*

EDITORIAL FELLOW

Daniel S. Chow, *San Francisco, CA*

SPECIAL CONSULTANTS TO THE EDITOR

AJNR Blog Editor

Neil Lall, *Denver, CO*

Case of the Month Editor

Nicholas Stence, *Aurora, CO*

Case of the Week Editors

Juan Pablo Cruz, *Santiago, Chile*
Sapna Rawal, *Toronto, Ontario, Canada*

Classic Case Editor

Sandy Cheng-Yu Chen, *Taipei, Taiwan*

Facebook Editor

Peter Yi Shen, *Sacramento, CA*

Health Care and Socioeconomics Editor

Pina C. Sanelli, *New York, NY*

Physics Editor

Greg Zaharchuk, *Stanford, CA*

Podcast Editor

Yvonne Lui, *New York, NY*

Twitter Editor

Jennifer McCarty, *Atlanta, Georgia*

YOUNG PROFESSIONALS ADVISORY COMMITTEE

Asim K. Bag, *Birmingham, AL*
Anna E. Nidecker, *Sacramento, CA*
Peter Yi Shen, *Sacramento, CA*

Founding Editor
Juan M. Taveras

Editors Emeriti
Mauricio Castillo, Robert I. Grossman,
Michael S. Huckman, Robert M. Quencer

Managing Editor
Karen Halm

Assistant Managing Editor
Laura Wilhelm

Executive Director, ASNR
Mary Beth Hepp

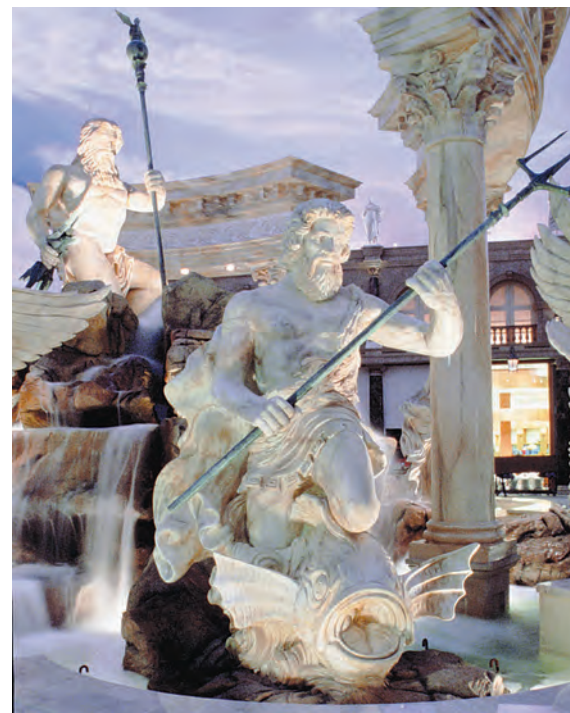
Director of Communications, ASNR
Angelo Artemakis



51st Annual Meeting

American Society of
**Head & Neck
Radiology**

Head and Neck Imaging in the City of Lights



Caesars Palace • Las Vegas, NV

September 16 – 20, 2017
(Saturday - Wednesday)

Please contact Educational Symposia at 813-806-1000 or ASHNR@edusymp.com or visit www.ASHNR.org for additional information.

INTRODUCING FULLY AUTOMATED STROKE APPLICATIONS



ZERO CLICK

Calculation of infarct
penumbra & mismatch

AUTOMATED STROKE REPORT

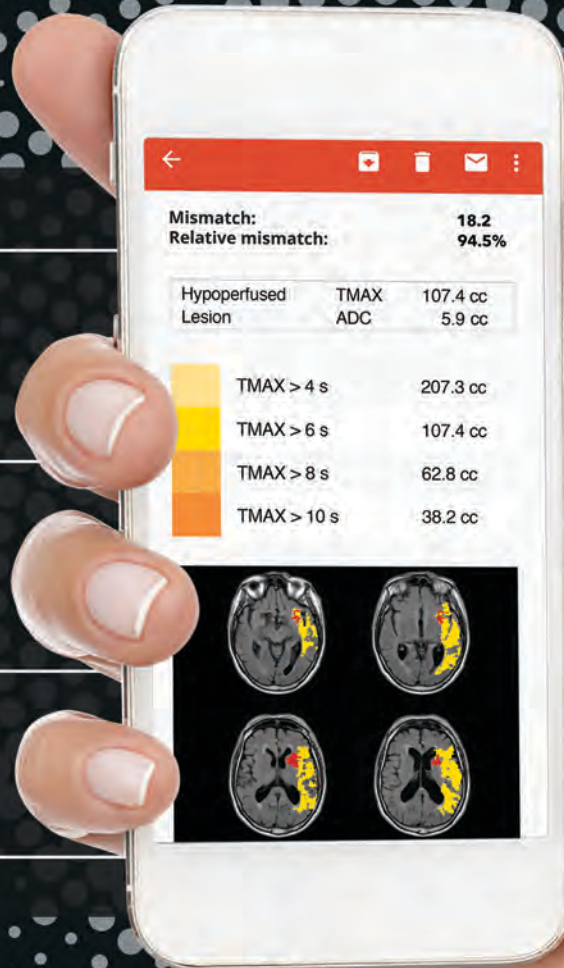
(MRI & CT) by email

VENDOR-NEUTRAL

& easy integration
into IT systems

Ask for a free trial

www.olea-medical.com



“ Innovation is in our DNA. ”

* FDA cleared



Improved diagnosis for life™

Trevo® XP ProVue Retrievers

See package insert for complete indications, complications, warnings, and instructions for use.

INDICATIONS FOR USE

- The Trevo Retriever is indicated for use to restore blood flow in the neurovasculature by removing thrombus for the treatment of acute ischemic stroke to reduce disability in patients with a persistent, proximal anterior circulation, large vessel occlusion, and smaller core infarcts who have first received intravenous tissue plasminogen activator (IV t-PA). Endovascular therapy with the device should start within 6 hours of symptom onset.
- The Trevo Retriever is indicated to restore blood flow in the neurovasculature by removing thrombus in patients experiencing ischemic stroke within 8 hours of symptom onset. Patients who are ineligible for intravenous tissue plasminogen activator (IV t-PA) or who fail IV t-PA therapy are candidates for treatment.

COMPLICATIONS

Procedures requiring percutaneous catheter introduction should not be attempted by physicians unfamiliar with possible complications which may occur during or after the procedure. Possible complications include, but are not limited to, the following: air embolism; hematoma or hemorrhage at puncture site; infection; distal embolization; pain/headache; vessel spasm, thrombosis, dissection, or perforation; emboli; acute occlusion; ischemia; intracranial hemorrhage; false aneurysm formation; neurological deficits including stroke; and death.

COMPATIBILITY

3x20mm retrievers are compatible with Trevo® Pro 14 Microcatheters (REF 90231) and Trevo® Pro 18 Microcatheters (REF 90238). 4x20mm retrievers are compatible with Trevo® Pro 18 Microcatheters (REF 90238). 4x30mm retrievers are compatible with Excelsior® XT-27® Microcatheters (150cm x 6cm straight REF 275081) and Trevo® Pro 18 Microcatheters (REF 90238). 6x25mm Retrievers are compatible with Excelsior® XT-27® Microcatheters (150cm x 6cm straight REF 275081). Compatibility of the Retriever with other microcatheters has not been established. Performance of the Retriever device may be impacted if a different microcatheter is used.

Balloon Guide Catheters (such as Merci® Balloon Guide Catheter and FlowGate® Balloon Guide Catheter) are recommended for use during thrombus removal procedures.

Retrievers are compatible with the Abbott Vascular DOC® Guide Wire Extension (REF 22260).

Retrievers are compatible with Boston Scientific RHV (Ref 421242).

SPECIFIC WARNINGS FOR INDICATION 1

- The safety and effectiveness of the Trevo Retrievers in reducing disability has not been established in patients with large core infarcts (i.e., ASPECTS ≤ 7). There may be increased risks, such as intracerebral hemorrhage, in these patients.
- The safety and effectiveness of the Trevo Retrievers in reducing disability has not been established or evaluated in patients with occlusions in the posterior circulation (e.g., basilar or vertebral arteries) or for more distal occlusions in the anterior circulation.

WARNINGS APPLIED TO BOTH INDICATIONS

- Administration of IV t-PA should be within the FDA-approved window (within 3 hours of stroke symptom onset).
- Contents supplied STERILE, using an ethylene oxide (EO) process. Nonpyrogenic.
- To reduce risk of vessel damage, adhere to the following recommendations:
 - Take care to appropriately size Retriever to vessel diameter at intended site of deployment.
 - Do not perform more than six (6) retrieval attempts in same vessel using Retriever devices.
 - Maintain Retriever position in vessel when removing or exchanging Microcatheter.
- To reduce risk of kinking/fracture, adhere to the following recommendations:
 - Immediately after unsheathing Retriever, position Microcatheter tip marker just proximal to shaped section. Maintain Microcatheter tip marker just proximal to shaped section of Retriever during manipulation and withdrawal.
 - Do not rotate or torque Retriever.
 - Use caution when passing Retriever through stented arteries.
- Do not resterilize and reuse. Structural integrity and/or function may be impaired by reuse or cleaning.
- The Retriever is a delicate instrument and should be handled carefully. Before use and when possible during procedure, inspect device carefully for damage. Do not use a device that shows signs of damage. Damage may prevent device from functioning and may cause complications.

- Do not advance or withdraw Retriever against resistance or significant vasospasm. Moving or torquing device against resistance or significant vasospasm may result in damage to vessel or device. Assess cause of resistance using fluoroscopy and if needed resheat the device to withdraw.
- If Retriever is difficult to withdraw from the vessel, do not torque Retriever. Advance Microcatheter distally, gently pull Retriever back into Microcatheter, and remove Retriever and Microcatheter as a unit. If undue resistance is met when withdrawing the Retriever into the Microcatheter, consider extending the Retriever using the Abbott Vascular DOC guidewire extension (REF 22260) so that the Microcatheter can be exchanged for a larger diameter catheter such as a DAC® catheter. Gently withdraw the Retriever into the larger diameter catheter.
- Administer anti-coagulation and anti-platelet medications per standard institutional guidelines.

PRECAUTIONS

- Prescription only – device restricted to use by or on order of a physician.
- Store in cool, dry, dark place.
- Do not use open or damaged packages.
- Use by “Use By” date.
- Exposure to temperatures above 54°C (130°F) may damage device and accessories. Do not autoclave.
- Do not expose Retriever to solvents.
- Use Retriever in conjunction with fluoroscopic visualization and proper anti-coagulation agents.
- To prevent thrombus formation and contrast media crystal formation, maintain a constant infusion of appropriate flush solution between guide catheter and Microcatheter and between Microcatheter and Retriever or guidewire.
- Do not attach a torque device to the shaped proximal end of DOC® Compatible Retriever. Damage may occur, preventing ability to attach DOC® Guide Wire Extension.



Concentric Medical
301 East Evelyn Avenue
Mountain View, CA 94041

Stryker Neurovascular
47900 Bayside Parkway
Fremont, CA 94538

strykerneurovascular.com

Date of Release: SEP/2016

EX_EN_US

Copyright © 2016 Stryker
NV00018973.AB

Target® Detachable Coil

See package insert for complete indications, contraindications, warnings and instructions for use.

INTENDED USE / INDICATIONS FOR USE

Target Detachable Coils are intended to endovascularly obstruct or occlude blood flow in vascular abnormalities of the neurovascular and peripheral vessels.

Target Detachable Coils are indicated for endovascular embolization of:

- Intracranial aneurysms
- Other neurovascular abnormalities such as arteriovenous malformations and arteriovenous fistulae
- Arterial and venous embolizations in the peripheral vasculature

CONTRAINDICATIONS

None known.

POTENTIAL ADVERSE EVENTS

Potential complications include, but are not limited to: allergic reaction, aneurysm perforation and rupture, arrhythmia, death, edema, embolus, headache, hemorrhage, infection, ischemia, neurological/intracranial sequelae, post-embolization syndrome (fever, increased white blood cell count, discomfort), TIA/stroke, vasospasm, vessel occlusion or closure, vessel perforation, dissection, trauma or damage, vessel rupture, vessel thrombosis. Other procedural complications including but not limited to: anesthetic and contrast media risks, hypotension, hypertension, access site complications.

WARNINGS

- Contents supplied STERILE using an ethylene oxide (EO) process. Do not use if sterile barrier is damaged. If damage is found, call your Stryker Neurovascular representative.
- For single use only. Do not reuse, reprocess or resterilize. Reuse, reprocessing or resterilization may compromise the structural integrity of the device and/or lead to device failure which, in turn, may result in patient injury, illness or death. Reuse, reprocessing or resterilization may also create a risk of contamination of the device and/or cause patient infection or cross-infection, including, but not limited to, the transmission of infectious disease(s) from one patient to another. Contamination of the device may lead to injury, illness or death of the patient.

- After use, dispose of product and packaging in accordance with hospital, administrative and/or local government policy.

- This device should only be used by physicians who have received appropriate training in interventional neuroradiology or interventional radiology and preclinical training on the use of this device as established by Stryker Neurovascular.**

- Patients with hypersensitivity to 316LVM stainless steel may suffer an allergic reaction to this implant.
- MR temperature testing was not conducted in peripheral vasculature, arteriovenous malformations or fistulae models.
- The safety and performance characteristics of the Target Detachable Coil System (Target Detachable Coils, InZone Detachment Systems, delivery systems and accessories) have not been demonstrated with other manufacturer's devices (whether coils, coil delivery devices, coil detachment systems, catheters, guidewires, and/or other accessories). Due to the potential incompatibility of non Stryker Neurovascular devices with the Target Detachable Coil System, the use of other manufacturer's device(s) with the Target Detachable Coil System is not recommended.
- To reduce risk of coil migration, the diameter of the first and second coil should never be less than the width of the ostium.
- In order to achieve optimal performance of the Target Detachable Coil System and to reduce the risk of thromboembolic complications, it is critical that a continuous infusion of appropriate flush solution be maintained between a) the femoral sheath and guiding catheter, b) the 2-tip microcatheter and guiding catheters, and c) the 2-tip microcatheter and Stryker Neurovascular guidewire and delivery wire. Continuous flush also reduces the potential for thrombus formation on, and crystallization of infusate around, the detachment zone of the Target Detachable Coil.
- Do not use the product after the “Use By” date specified on the package.
- Reuse of the flush port/dispenser coil or use with any coil other than the original coil may result in contamination of, or damage to, the coil.
- Utilization of damaged coils may affect coil delivery to, and stability inside, the vessel or aneurysm, possibly resulting in coil migration and/or stretching.
- The fluoro-saver marker is designed for use with a Rotating Hemostatic Valve (RHV). If used without an RHV, the distal end of the coil may be beyond the alignment marker when the fluoro-saver marker reaches the microcatheter hub.

- If the fluoro-saver marker is not visible, do not advance the coil without fluoroscopy.
- Do not rotate delivery wire during or after delivery of the coil. Rotating the Target Detachable Coil delivery wire may result in a stretched coil or premature detachment of the coil from the delivery wire, which could result in coil migration.
- Verify there is no coil loop protrusion into the parent vessel after coil placement and prior to coil detachment. Coil loop protrusion after coil placement may result in thromboembolic events if the coil is detached.
- Verify there is no movement of the coil after coil placement and prior to coil detachment. Movement of the coil after coil placement may indicate that the coil could migrate once it is detached.
- Failure to properly close the RHV compression fitting over the delivery wire before attaching the InZone® Detachment System could result in coil movement, aneurysm rupture or vessel perforation.
- Verify repeatedly that the distal shaft of the catheter is not under stress before detaching the Target Detachable Coil. Axial compression or tension forces could be stored in the 2-tip microcatheter causing the tip to move during coil delivery. Microcatheter tip movement could cause the aneurysm or vessel to rupture.
- Advancing the delivery wire beyond the microcatheter tip once the coil has been detached involves risk of aneurysm or vessel perforation.
- The long term effect of this product on extravascular tissues has not been established so care should be taken to retain this device in the intravascular space.

Damaged delivery wires may cause detachment failures, vessel injury or unpredictable distal tip response during coil deployment. If a delivery wire is damaged at any point during the procedure, do not attempt to straighten or otherwise repair it. Do not proceed with deployment or detachment. Remove the entire coil and replace with undamaged product.

- After use, dispose of product and packaging in accordance with hospital, administrative and/or local government policy.

CAUTIONS / PRECAUTIONS

- Federal Law (USA) restricts this device to sale by or on the order of a physician.
- Besides the number of InZone Detachment System units needed to complete the case, there must be an extra InZone Detachment System unit as back up.

- Removing the delivery wire without grasping the introducer sheath and delivery wire together may result in the detachable coil sliding out of the introducer sheath.
- Failure to remove the introducer sheath after inserting the delivery wire into the RHV of the microcatheter will interrupt normal infusion of flush solution and allow back flow of blood into the microcatheter.
- Some low level overhead light near or adjacent to the patient is required to visualize the fluoro-saver marker; monitor light alone will not allow sufficient visualization of the fluoro-saver marker.
- Advance and retract the Target Detachable Coil carefully and smoothly without excessive force. If unusual friction is noticed, slowly withdraw the Target Detachable Coil and examine for damage. If damage is present, remove and use a new Target Detachable Coil. If friction or resistance is still noted, carefully remove the Target Detachable Coil and microcatheter and examine the microcatheter for damage.
- If it is necessary to reposition the Target Detachable Coil, verify under fluoroscopy that the coil moves with a one-to-one motion. If the coil does not move with a one-to-one motion or movement is difficult, the coil may have stretched and could possibly migrate or break. Gently remove both the coil and microcatheter and replace with new devices.
- Increased detachment times may occur when:
 - Other embolic agents are present.
 - Delivery wire and microcatheter markers are not properly aligned.
 - Thrombus is present on the coil detachment zone.
- Do not use detachment systems other than the InZone Detachment System.
- Increased detachment times may occur when delivery wire and microcatheter markers are not properly aligned.
- Do not use detachment systems other than the InZone Detachment System.



Stryker Neurovascular
47900 Bayside Parkway
Fremont, CA 94538

strykerneurovascular.com

Date of Release: MAR/2016

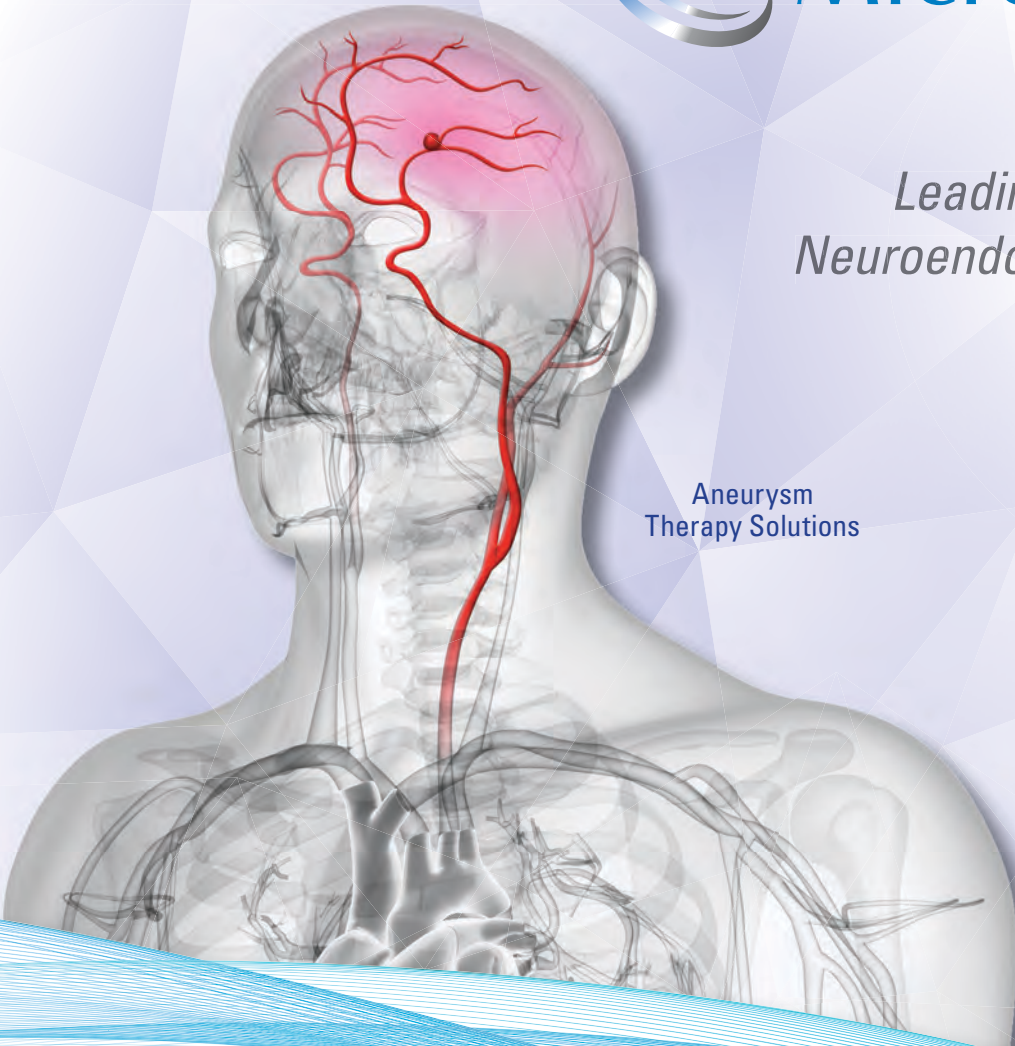
EX_EN_US

Copyright © 2016 Stryker
NV00018669.AB



*Leading the Way in
Neuroendovascular Therapy*

Aneurysm
Therapy Solutions



**A 360-Degree Approach to
Performance Based Solutions**

microvention.com

MICROVENTION is a registered trademark of MicroVention, Inc. Refer to Instructions for Use for additional information. © 2016 MicroVention, Inc. 11/16

NEW

Indication for Trevo[®] Retrievers

A New Standard of Care in Stroke



FIRST

mechanical thrombectomy device
indicated to reduce disability in stroke.*

FIRST

new treatment indication for
stroke in 20 years.

Trevo XP

PROVUE RETRIEVER

Success accelerated.

*The Trevo Retriever is indicated for use to restore blood flow in the neurovasculature by removing thrombus for the treatment of acute ischemic stroke to reduce disability in patients with a persistent, proximal anterior circulation, large vessel occlusion, and smaller core infarcts who have first received intravenous tissue plasminogen activator (IV t-PA). Endovascular therapy with the device should start within 6 hours of symptom onset.

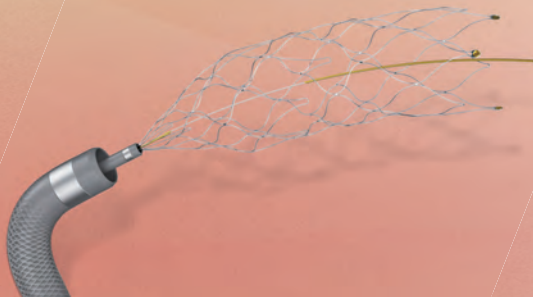
INNOVATIVE SOLUTIONS for the treatment of neurovascular diseases



DERIVO[®] Embolisation Device and ACCLINO[®] flex Stent
for the treatment of intracranial aneurysms



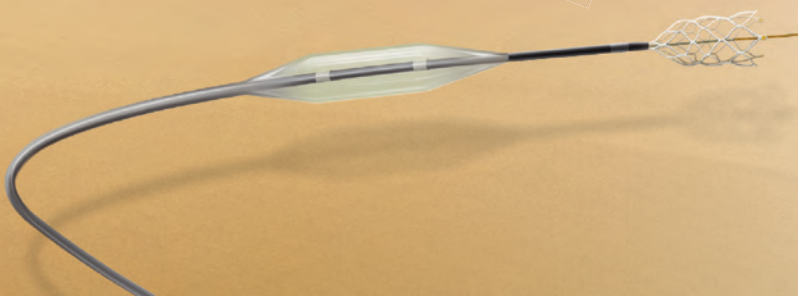
NeuroSlider[®] Microcatheter



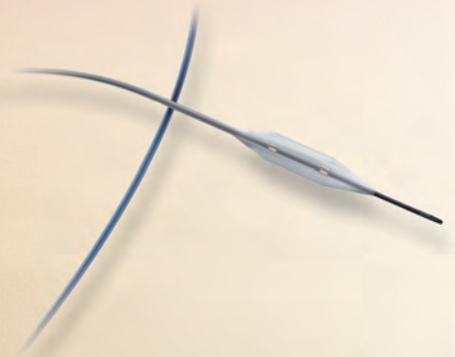
APERIO[®] Thrombectomy Device, NeuroSlider[®] and NeuroBridge[®] for acute stroke care



NeuroBridge[®] Intermediate Catheter



CREDO[®] Stent with NeuroSpeed[®] PTA Balloon Catheter
for the treatment of intracranial stenosis



NeuroSpeed[®] PTA Balloon Catheter

CREDO[®] Stent only available within ASSISTENT – Acandis Stenting of Intracranial STENosis-regisTry

AJNR

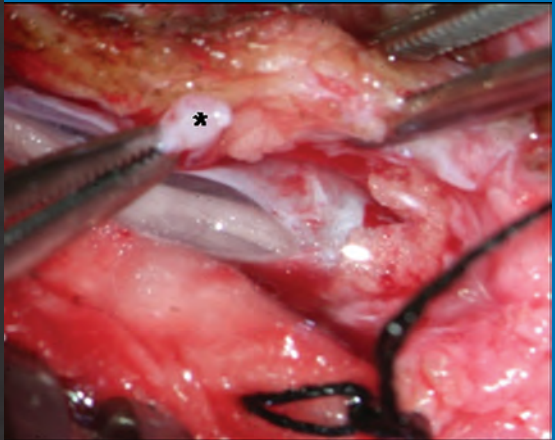
AMERICAN JOURNAL OF NEURORADIOLOGY

JANUARY 2017
VOLUME 38
NUMBER 1
WWW.AJNR.ORG

THE JOURNAL OF DIAGNOSTIC AND
INTERVENTIONAL NEURORADIOLOGY

Third window abnormalities
Limited dorsal myeloschisis and dermal sinus
Arteriovenous shunt detection with ASL

Official Journal ASNR • ASFNR • ASHNR • ASPNR • ASSR



AJNR

AMERICAN JOURNAL OF NEURORADIOLOGY

JANUARY 2017
VOLUME 38
NUMBER 1
WWW.AJNR.ORG

Publication Preview at www.ajnr.org features articles released in advance of print. Visit www.ajnrblog.org to comment on AJNR content and chat with colleagues and AJNR's News Digest at <http://ajnrdigest.org> to read the stories behind the latest research in neuroimaging.

- 1 **PERSPECTIVES** *M.E. Adin*
- REVIEW ARTICLE**
- 2 **Spectrum of Third Window Abnormalities: Semicircular Canal Dehiscence and Beyond** *M.-L. Ho, et al.* **HEAD & NECK**
- GENETICS VIGNETTE**
- 10 **Genetics of Frontotemporal Dementia** *F.W. Rohlfing, et al.*
- GENERAL CONTENTS**
- 12 **Emergency Department MRI Scanning of Patients with Multiple Sclerosis: Worthwhile or Wasteful?** *J. Pakpoor, et al.* **ADULT BRAIN**
- 18 **Hippocampal and Deep Gray Matter Nuclei Atrophy Is Relevant for Explaining Cognitive Impairment in MS: A Multicenter Study** *D. Damjanovic, et al.* **ADULT BRAIN**
- 25 **Influence of Small Vessel Disease and Microstructural Integrity on Neurocognitive Functioning in Older Individuals: The DANTE Study Leiden** *J.E.F. Moonen, et al.* **ADULT BRAIN**
- 31 **Measuring Brain Tissue Integrity during 4 Years Using Diffusion Tensor Imaging** *D. Ontaneda, et al.* **ADULT BRAIN**
- 39 **Clinicoradiologic Correlations of Cerebral Microbleeds in Advanced Age** *I. Barnaure, et al.* **ADULT BRAIN**
- 46 **Body Temperature Modulates Infarction Growth following Endovascular Reperfusion** *S. Dehkharghani, et al.* **ADULT BRAIN**
- 52 **Collateral Assessment by CT Angiography as a Predictor of Outcome in Symptomatic Cervical Internal Carotid Artery Occlusion** *S. Sundaram, et al.* **ADULT BRAIN**
- 58 **Acute Ischemic Stroke Infarct Topology: Association with Lesion Volume and Severity of Symptoms at Admission and Discharge** *S. Payabvash, et al.* **ADULT BRAIN**
- 64 **Structural Brain Network Reorganization in Patients with Neuropsychiatric Systemic Lupus Erythematosus** *X. Xu, et al.* **ADULT BRAIN**
- 71 **Intracranial Arteriovenous Shunting: Detection with Arterial Spin-Labeling and Susceptibility-Weighted Imaging Combined** *J. Hodel, et al.* **ADULT BRAIN**

 	77	Diagnostic Value of Brain Calcifications in Adult-Onset Leukoencephalopathy with Axonal Spheroids and Pigmented Glia <i>T. Konno, et al.</i>	ADULT BRAIN
  	84	Endovascular Therapy of M2 Occlusion in IMS III: Role of M2 Segment Definition and Location on Clinical and Revascularization Outcomes <i>T.A. Tomsick, et al., for the IMS III Investigators</i>	INTERVENTIONAL
	90	Impact of Modified TICI 3 versus Modified TICI 2b Reperfusion Score to Predict Good Outcome following Endovascular Therapy <i>C. Dargazanli, et al.</i>	INTERVENTIONAL
  	97	Emergent Endovascular Management of Long-Segment and Flow-Limiting Carotid Artery Dissections in Acute Ischemic Stroke Intervention with Multiple Tandem Stents <i>S.A. Ansari, et al.</i>	INTERVENTIONAL EXTRACRANIAL VASCULAR
	105	Treatment of Intra- and Extracranial Aneurysms Using the Flow-Redirection Endoluminal Device: Multicenter Experience and Follow-Up Results <i>F. Drescher, et al.</i>	INTERVENTIONAL EXTRACRANIAL VASCULAR
 	113	Flow Diverters in the Treatment of Pediatric Cerebrovascular Diseases <i>M. Barburuglu, et al.</i>	INTERVENTIONAL PEDIATRICS
 	119	Flow Conditions in the Intracranial Aneurysm Lumen Are Associated with Inflammation and Degenerative Changes of the Aneurysm Wall <i>J. Cebal, et al.</i>	INTERVENTIONAL
	127	Embolization of Intracranial Dural Arteriovenous Fistulas Using PHIL Liquid Embolic Agent in 26 Patients: A Multicenter Study <i>S. Lamin, et al.</i>	INTERVENTIONAL
	132	Quantifying the Cerebral Hemodynamics of Dural Arteriovenous Fistula in Transverse Sigmoid Sinus Complicated by Sinus Stenosis: A Retrospective Cohort Study <i>W.-Y. Guo, et al.</i>	INTERVENTIONAL
 	139	The Effects of Acetazolamide on the Evaluation of Cerebral Hemodynamics and Functional Connectivity Using Blood Oxygen Level-Dependent MR Imaging in Patients with Chronic Steno-Occlusive Disease of the Anterior Circulation <i>J. Wu, et al.</i>	FUNCTIONAL
	146	Impact of Neuroradiology-Based Peer Review on Head and Neck Radiotherapy Target Delineation <i>S. Braunstein, et al.</i>	HEAD & NECK
	154	Performance of CT in the Preoperative Diagnosis of Cervical Lymph Node Metastasis in Patients with Papillary Thyroid Cancer: A Systematic Review and Meta-Analysis <i>C.H. Suh, et al.</i>	HEAD & NECK
    	162	White Matter Injury and General Movements in High-Risk Preterm Infants <i>C. Peyton, et al.</i>	PEDIATRICS
	170	Automated Processing of Dynamic Contrast-Enhanced MRI: Correlation of Advanced Pharmacokinetic Metrics with Tumor Grade in Pediatric Brain Tumors <i>S. Vajapeyam, et al.</i>	PEDIATRICS
	176	Limited Dorsal Myeloschisis and Congenital Dermal Sinus: Comparison of Clinical and MR Imaging Features <i>S.M. Lee, et al.</i>	PEDIATRICS SPINE
 	183	Associations between Measures of Structural Morphometry and Sensorimotor Performance in Individuals with Nonspecific Low Back Pain <i>K. Caeyenberghs, et al.</i>	SPINE
 	192	Dynamic Contrast-Enhanced MR Perfusion of Intradural Spinal Lesions <i>V. Cuvinciuc, et al.</i>	SPINE
	195	First-Pass Contrast-Enhanced MR Angiography for Pretherapeutic Diagnosis of Spinal Epidural Arteriovenous Fistulas with Intradural Venous Reflux <i>S. Mathur, et al.</i>	SPINE INTERVENTIONAL
	200	First-Pass Contrast-Enhanced MR Angiography in Evaluation of Treated Spinal Arteriovenous Fistulas: Is Catheter Angiography Necessary? <i>S. Mathur, et al.</i>	SPINE INTERVENTIONAL

206 **Comparison of Time-Resolved and First-Pass Contrast-Enhanced MR Angiography in Pretherapeutic Evaluation of Spinal Dural Arteriovenous Fistulas** *S. Mathur, et al.*

SPINE
INTERVENTIONAL

MEMORIAL

213 **Henry J.M. Barnett** *A.J. Fox*

215 **35 YEARS AGO IN AJNR**

ONLINE FEATURES

LETTERS

E1 **Comment on “Aneurysms Associated with Brain Arteriovenous Malformations”** *F. Clarençon, et al.*

E5 **Reply** *S.K. Rammos, et al.*

E6 **More Transparency Is Needed in the Reporting of Clinical Research Studies** *X. Armoiry, et al.*

E8 **Reply** *W. Brinjikji, et al.*

E9 **Survey of Head and Neck Practice** *D.M. Yousem, et al.*

E10 **Reply** *Y. Anzai*

BOOK REVIEWS *R.M. Quencer, Section Editor*

Please visit www.ajnrblog.org to read and comment on Book Reviews.



Sagittal T2-weighted MRI shows an intraspinal tract separate from the filum terminale or nerve roots. The attachment site of the tract is the spinal cord just above the conus medullaris. A low-lying conus and dorsal tenting of the spinal cord at the tract-cord union are present. Photograph obtained during the operation shows a thick tract adhering to the dorsal aspect of the spinal cord.



Indicates Editor's Choices selection



Indicates Fellows' Journal Club selection



Indicates open access to non-subscribers at www.ajnr.org



Indicates article with supplemental on-line table



Indicates article with supplemental on-line photo



Indicates article with supplemental on-line video



Evidence-Based Medicine Level 1



Evidence-Based Medicine Level 2



Title: Hul Gil. According to Wikipedia, the first known cultivation of opium poppies was in Mesopotamia, approximately 3400 BCE, by Sumerians, who called the plant hul gil, or the "joy plant." Nowadays in Mesopotamia, where I took this picture, poppies are not popular or cultivated but they are widely seen around the fields during a short period in the mid-spring season. It is truly fascinating to see the transition of all those naked fields to a canvas covered with flowers of all kinds of colors as far as the eye can see. But, even in a garden where all the flowers are individually beautiful, some stand out and look "more beautiful." That said, there seems to be a little confounder for the case of the poppy standing erect in the picture above (remember papaverine is also an opium alkaloid). More of the Dr. Adin's works can be seen on Instagram with the handle @unsuz.adam.

Mehmet Emin Adin, Radiologist, Silvan Dr. Yusuf Azizoglu State Hospital, Silvan, Diyarbakir, Turkey

Spectrum of Third Window Abnormalities: Semicircular Canal Dehiscence and Beyond

 M.-L. Ho,  G. Moonis,  C.F. Halpin, and  H.D. Curtin



ABSTRACT

SUMMARY: Third window abnormalities are defects in the integrity of the bony structure of the inner ear, classically producing sound-/pressure-induced vertigo (Tullio and Hennebert signs) and/or a low-frequency air-bone gap by audiometry. Specific anatomic defects include semicircular canal dehiscence, perilymphatic fistula, enlarged vestibular aqueduct, dehiscence of the scala vestibuli side of the cochlea, X-linked stapes gusher, and bone dyscrasias. We discuss these various entities and provide key examples from our institutional teaching file with a discussion of symptomatology, temporal bone CT, audiometry, and vestibular-evoked myogenic potentials.

ABBREVIATIONS: EVAS = enlarged vestibular aqueduct syndrome; SSCCD = superior semicircular canal dehiscence

Third window abnormalities are defects in the integrity of the bony structure of the inner ear, first described by Minor et al in 1998.¹ In 2008, Merchant and Rosowski² proposed a universal theory for the underlying mechanism of hearing loss accompanying these defects. Normal sound conduction is transmitted through the oval and round windows, which serve as fluid interfaces between air in the middle ear and perilymphatic fluid spaces of the inner ear. Various conditions can enlarge existing bony channels or create additional defects in the bony labyrinth, producing hydrodynamic third windows. Potential third windows include bony dehiscence of the semicircular canals, enlargement of the opening of the vestibular aqueduct, dehiscence of the scala vestibuli side of the cochlea, and abnormal bony thinning between the cochlea and vascular channels. At audiometry, there is a characteristic low-frequency air-bone gap due to decreased air conduction and increased bone conduction.²

Figure 1A illustrates the mechanism of air-conducted sound in normal ears, and Fig 1B demonstrates how third window shunt-

ing effects decrease air conduction. The 2 physiologic windows between the middle and inner ear are the oval window, which transmits vibrations from the auditory ossicles, and the round window of the cochlea. With air conduction, there is physiologic entrainment of the oval and round windows due to coupling by incompressible perilymph. Pressure differences between the cochlear perilymphatic spaces activate hair cells and create the perception of sound. In the presence of a third window, incoming acoustic energy from the oval window is shunted away, decreasing transmission to the round window. This result reduces sound perception because less acoustic energy is available to the hair cells.

In contrast, Fig 1C illustrates the mechanism of bone-conducted sound in normal ears, and Fig 1D demonstrates how third window shunting effects paradoxically increase bone conduction. With bone conduction, vibrations throughout the otic capsule produce differential outward motion of the oval and round windows, due to unequal impedance of these 2 structures. The pressure difference across the basilar membrane creates the perception of sound. The presence of a third window involving the semicircular canals, vestibular aqueduct, or scala vestibuli side of the cochlea lowers the apparent impedance. This feature has the opposite effect of increasing sound perception in proportion to the differential acoustic energy across the basilar membrane.²

In this article, we discuss the spectrum of third window abnormalities, including superior semicircular canal dehiscence (SSCCD), posterior semicircular canal dehiscence, perilymphatic fistula, enlarged vestibular aqueduct, X-linked stapes gusher, and bone dyscrasias. We review the literature for each disease entity and provide key examples from our institutional teaching file with

From the Department of Radiology (M.-L.H.), Mayo Clinic, Rochester, Minnesota; Department of Radiology (G.M.), Columbia University, New York, New York; and Departments of Otolaryngology (C.F.H.) and Radiology (H.D.C.), Massachusetts Eye and Ear Infirmary, Boston, Massachusetts.

Paper previously presented at: Morrison Research Day, May 23, 2011, Beth Israel Deaconess Radiology, Boston, Massachusetts; Resident Research Day, June 10, 2011, Beth Israel Deaconess Medical Center, Boston, Massachusetts; Annual Meeting of the American Society of Neuroradiology and the Foundation of the ASNR Symposium, June 4–9, 2011; Seattle, Washington; and Annual Meeting of the Eastern Neuroradiological Society, September 15–18, 2011, Chatham, Massachusetts.

Please address correspondence to Mai-Lan Ho, MD, Department of Radiology, Mayo Clinic, 200 First St SW, Rochester, MN 55905; e-mail: ho.mai-lan@mayo.edu

 Indicates open access to non-subscribers at www.ajnr.org

<http://dx.doi.org/10.3174/ajnr.A4922>

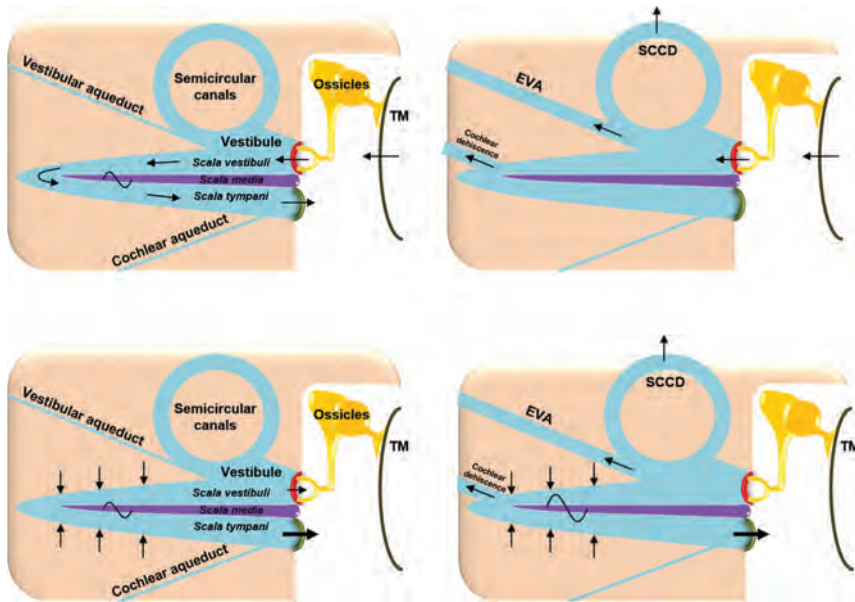


FIG 1. Mechanisms of air- and bone-conducted sound in healthy and third window anatomy. *A*, Normal air conduction. Vibrations of the tympanic membrane are transmitted inward through the auditory ossicles and oval window. Energy is then conducted through the incompressible perilymph, producing equal and outward motion of the round window. The difference in vibration between the oval and round windows generates a pressure gradient across the basilar membrane, activating hair cells and creating the perception of sound. *B*, Decreased air conduction in third window anatomy. Due to shunting across third windows (semicircular canal dehiscence [SCCD], EVAS, cochlear dehiscence), there is decreased energy transmission from the oval window to the round window. The decrease in pressure gradient across the basilar membrane yields reduced sound perception. *C*, Normal bone conduction. Vibrations are transmitted throughout the otic capsule. This transmission results in differential outward motion of the oval and round windows due to unequal impedance of these 2 structures. The resulting pressure difference across the basilar membrane enables sound perception. *D*, Increased bone conduction in third window anatomy. Due to shunting across third windows, there is decreased motion of the oval window on the scala vestibuli side of the cochlea. However, the motion of the round window on the scala tympani side is unchanged. This phenomenon artifactually elevates the pressure difference across the basilar membrane, resulting in increased sound perception. TM indicates tympanic membrane; yellow, auditory ossicles; beige, otic capsule; red, oval window; green, round window; blue, perilymph; purple, basilar membrane. Adapted with permission from Merchant SN, Rosowski JJ. Conductive hearing loss caused by third window lesions of the inner ear. *Otol Neurotol* 2008;29:282–89.

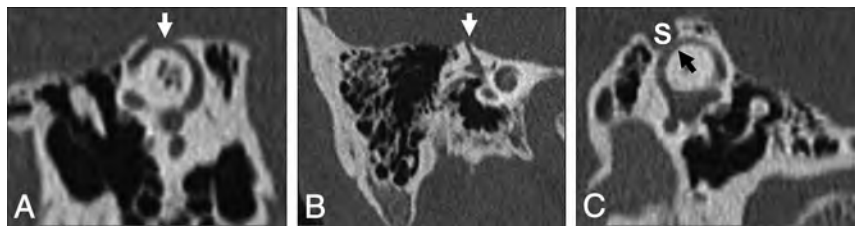


FIG 2. Temporal bone CT in the Pöschl (*A*) and Stenvers (*B*) planes demonstrating a large defect (*arrows*) in the roof of the right superior semicircular canal. *C*, Temporal bone CT Pöschl reconstruction demonstrates dehiscence of the left superior semicircular canal (*arrow*) into the superior petrosal sinus (*S*).

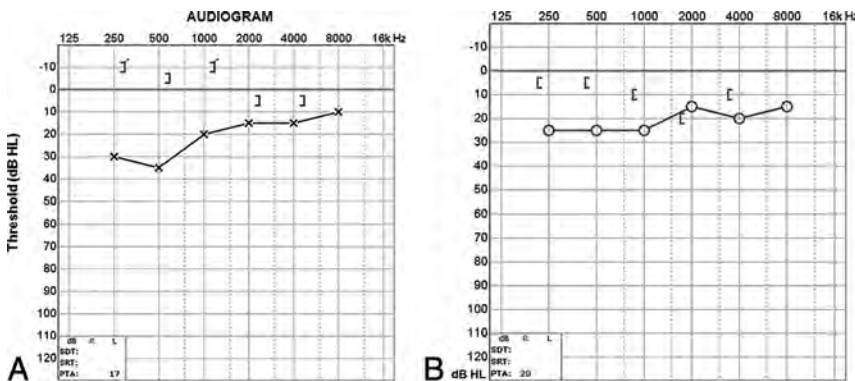


FIG 3. *A*, Audiogram of the right superior semicircular canal dehiscence with increased bone conduction (*brackets*) and decreased air conduction (*crosses*). The air-bone gap exceeds 10 dB at low sound frequencies (<1 kHz), the range at which acoustic energy is readily dissipated (described in the text). *B*, Audiogram of left superior semicircular canal dehiscence into the superior petrosal sinus. There is increased bone conduction (*brackets*) and decreased air conduction (*circles*), similar to typical SSCCD.

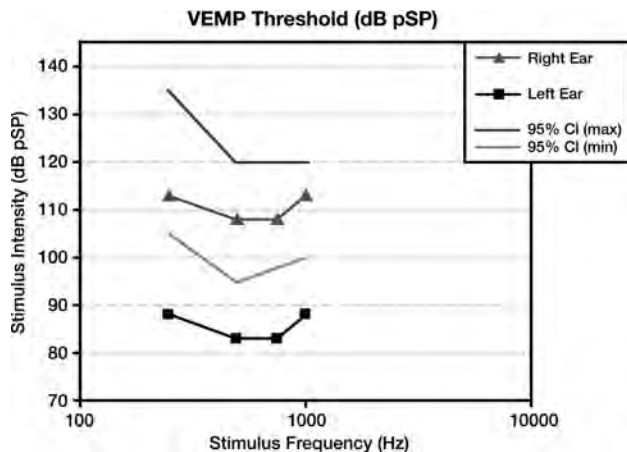


FIG 4. Vestibular-evoked myogenic potentials in superior semicircular canal dehiscence. Compared with the normal right ear (triangle) range (lines), the left ear demonstrates an abnormally sensitive response threshold (squares) across all tested stimulus frequencies. The lower thresholds indicate increased excitation of otolithic organs due to third window acoustic transmission.

discussion of symptomatology, temporal bone CT, audiometry, and vestibular-evoked myogenic potentials.

Superior Semicircular Canal Dehiscence

Superior semicircular canal dehiscence refers to focal loss of the bony wall of the superior semicircular canal. The prevalence is reported as 2.1%–10.7% on temporal bone CT and 0.5%–0.6% at postmortem studies. SSCCD is idiopathic, though the proposed risk factors include congenital underdevelopment of bone overlying the semicircular canal, shear stress from trauma, increased pressure due to Valsalva maneuvers, and gradual erosion by vascular pulsations.^{3–10} A special subset of SSCCD involves dehiscence of the superior semicircular canal into the superior petrosal sinus, which normally grooves the superior margin of the petrous sinus, which normally grooves the superior margin of the petrous portion of the temporal bone. Neurovascular foramina can serve as potential windows between the middle and inner ear but are normally not associated with abnormalities of sound transmission due to their small cross-sectional area. Vascular abnormalities that enlarge the foramina and/or communicate with the bony labyrinth can produce clinically significant acoustic dissipation. It is theorized that acoustic decompression through the dura mater acts as a third window equivalent, permitting shunting of acoustic energy into the subarachnoid space or into the vessel itself.^{2,11,12}

Patients with SSCCD typically present with vertigo and nystagmus induced by loud noises (Tullio phenomenon) or increases in external auditory canal pressure (Hennebert sign).⁵ High-resolution temporal bone CT images (maximum thickness, 0.5–0.625 mm) should be evaluated to avoid volume averaging, which can obscure a focal osseous defect. Multiplanar reconstructions and reformats parallel to (Pöschl plane) and perpendicular to (Stenvers plane) the superior semicircular canal are used to demonstrate the dehiscence to best advantage (Fig 2).^{3,8,9}

At audiometry, a characteristic air-bone gap results from increased bone and decreased air conduction. This phenomenon occurs most significantly at lower sound frequencies (below 1 kHz), a range at which acoustic energy is readily dissipated (Fig 3). At higher frequencies, there is a small or no gap because propor-

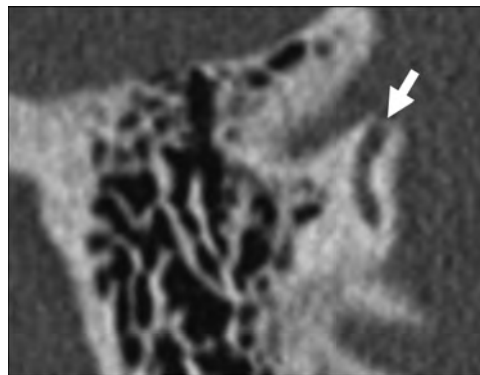


FIG 5. Posterior semicircular canal dehiscence. Temporal bone CT in the coronal plane demonstrates a defect (arrow) in the roof of the posterior semicircular canal.

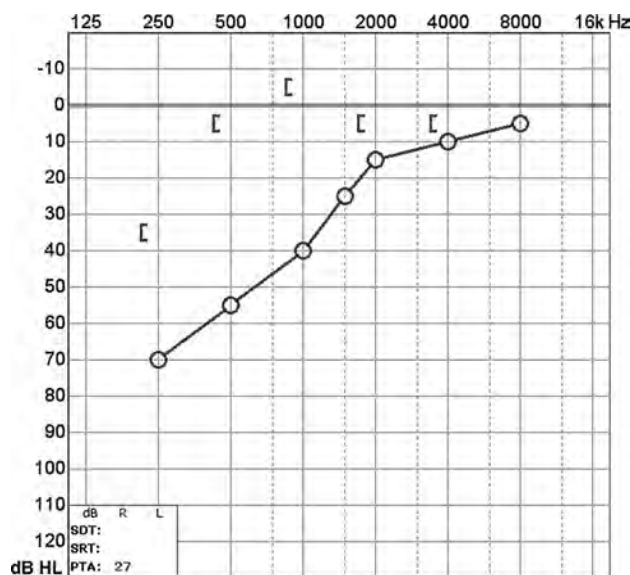


FIG 6. Audiogram of posterior semicircular canal dehiscence with increased bone conduction (brackets) and decreased air conduction (circles). Findings are compatible with posterior semicircular canal dehiscence (described in the text).

tionally less acoustic energy is shunted by the third window. Vestibular-evoked myogenic potential testing may show abnormally low response thresholds on the side of pathology. The effective impedance is reduced; this reduction results in increased transmission of acoustic energy at the saccule (Fig 4). Because middle ear pathology can also produce an air-bone gap, tympanometry and acoustic reflexes may be tested to verify that the air-bone gap does not result from an inefficient middle ear.^{3,10}

At Massachusetts Eye and Ear Infirmary, 116 patients (161 ears) with SSCCD were included in the teaching file from 2000 to 2011. Of these, 5/161 ears demonstrated dehiscence into the superior petrosal sinus. Reported symptoms included hearing loss in 60/116 patients (52%), vertigo in 54/116 (46%), pulsatile tinnitus in 35/116 (30%), autophony in 31/116 (27%), and oscillopsia in 16/116 (14%). Audiometry was evaluable in 92 ears, with 71/92 ears (77%) supporting the diagnosis of semicircular canal dehiscence and 21/92 (23%) being normal. Vestibular-evoked myogenic potential testing was evaluable in 39 ears, with 22/39

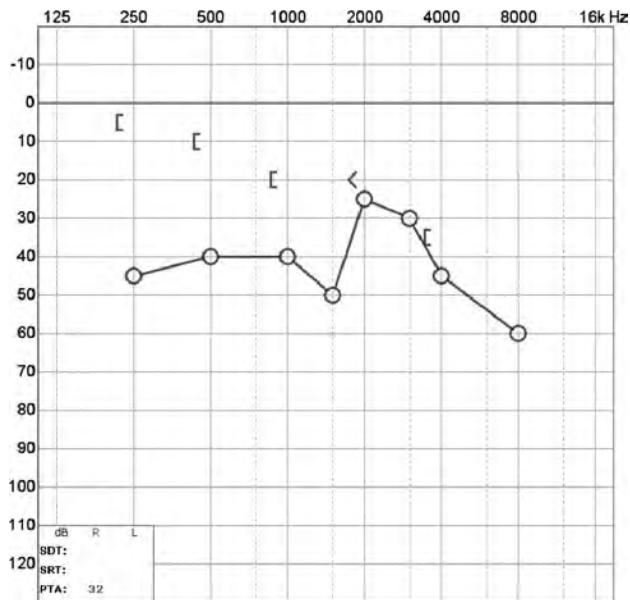


FIG 10. Audiogram of carotid-cochlear dehiscence. There is increased bone conduction (brackets) and decreased air conduction (circles), with a progressively larger air-bone gap at lower frequencies. In this case, the ipsilateral acoustic reflex was present, indicating that the ossicular chain was free to move with the action of the stapedius muscle. Therefore no middle ear pathology such as serous otitis, otosclerosis, or cholesteatoma was responsible for the air-bone gap.

etiology is chronic infection/inflammation, such as cholesteatoma or otitis media. The lateral semicircular canal is most frequently involved due to its location directly adjacent to the middle ear (Fig 7). On audiometry, cholesteatoma demonstrates a characteristic air-bone gap of middle ear origin, which is present at both low and high sound frequencies due to superimposed ossicular chain pathology (Fig 8).^{3,16,17} Rarely, cochlear-carotid dehiscence with the absence of the intervening bony partition can also occur (Fig 9). On audiometry, this condition demonstrates an air-bone gap that is greater at lower frequencies, similar to other third windows (Fig 10).¹⁸⁻²⁰

Other potential causes of perilyabyrinthine fistula include trauma (Fig 11), an operation, and benign and neoplastic masses (Fig 12). Transverse temporal bone fractures are more likely to involve the petrous pyramid and violate the otic capsule. With this background abnormality, it is difficult or impossible to identify superimposed third window effects. In such cases, hearing is generally unrecoverable and audiometry is not performed, so a typical third window effect cannot be demonstrated.^{21,22}

At Massachusetts Eye and Ear Infirmary, 43 patients (60 ears) with perilyabyrinthine fistula of the semicircular canals, vestibule, and/or scala vestibuli side of the cochlea were included in the teaching file from 2000 to 2011. Etiologies were inflammatory in 45/60 (75%), traumatic/iatrogenic in 9/60 (15%), and neoplastic in 6/60 (10%). Anatomic sites of involvement included the lateral semicircular canal in 31/60 (52%), the superior semicircular canal in 12/60 (20%), the posterior semicircular canal in 4/60 (7%), the cochlea in 13/60 (22%), and the vestibule in 11/60 (18%). Reported symptoms included hearing loss in 21/43 (49%), vertigo in 13/43 (31%), otorrhea in 13/43 (30%), and otalgia in 10/43 (23%).

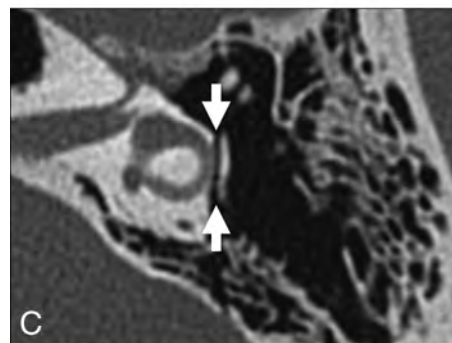
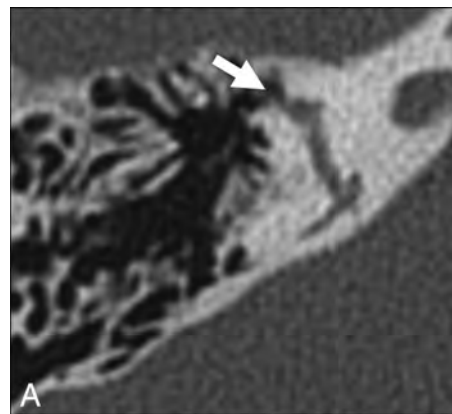


FIG 11. Traumatic causes of perilyabyrinthine fistula. A, Transverse temporal bone fracture through the superior semicircular canal (arrow). B, Transverse temporal bone fracture across the bony vestibule (arrow). C, Transverse temporal bone fracture through the otic capsule (arrows) with unroofing of the lateral semicircular canal.

Enlarged Vestibular Aqueduct

Enlarged vestibular aqueduct syndrome (EVAS) is a pathologic enlargement of the vestibular aqueduct at the level of the endolymphatic duct. In EVAS, the connection of the vestibular aqueduct to the vestibule is larger than normal, and this connection acts as a third window transmitting acoustic energy through the aqueduct to the dura. CT criteria are classically based on the transverse dimension of the vestibular aqueduct (Valvassori criterion: midpoint of ≥ 1.5 mm; Cincinnati criteria: midpoint of ≥ 1 mm or operculum of ≥ 2 mm), though the adjacent posterior semicircular canal often serves as a standard reference.²³⁻²⁷ Normative values by using the 45° oblique (Pöschl) projection have recently been established as 0.3–0.9 mm (mean, 0.5 mm) at the midpoint.²⁸ The finding is frequently bilateral and can be seen either in

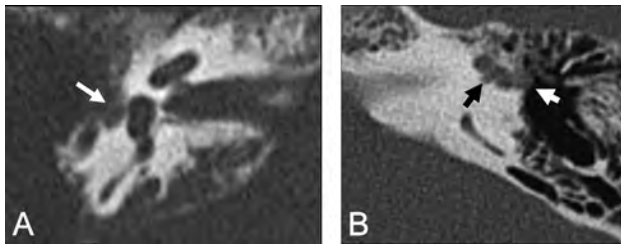


FIG 12. Neoplastic causes of perilymphatic fistula. *A*, Squamous cell carcinoma. Axial CT scan shows destructive soft tissue filling the middle ear and eroding through the otic capsule (*arrow*). *B*, Facial nerve venous malformation. Axial CT scan shows a lobulated soft-tissue density extending from the geniculate ganglion (*white arrow*) through the otic capsule and into the superior semicircular canal (*black arrow*).

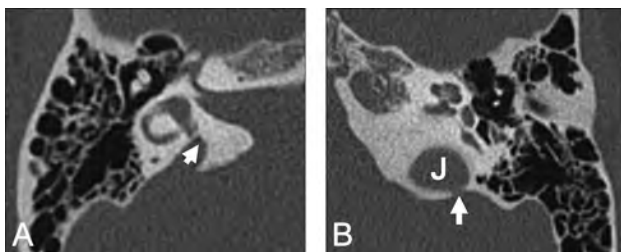


FIG 13. *A*, Enlarged vestibular aqueduct syndrome. Axial CT scan shows a dilated vestibular aqueduct (*arrow*) at its junction with the vestibule. *B*, Axial CT scan shows dehiscence of the vestibular aqueduct (*arrow*) into the jugular foramen (*J*).

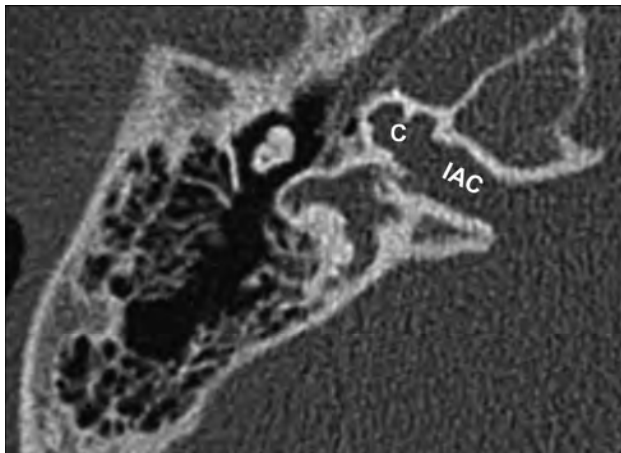


FIG 14. X-linked stapes gusher. Axial CT scan shows a dysplastic cochlea (*C*) with a modiolar deficiency and absence of the lamina cribrosa, resulting in a direct communication with an enlarged internal auditory canal (*IAC*).

isolation or with various congenital conditions, including Pendred syndrome; coloboma, heart defect, atresia choanae (also known as choanal atresia), retarded growth and development, genital abnormality, and ear abnormality (*CHARGE* syndrome); and branchio-oto-renal syndrome. It has been reported that dehiscence of the vestibular aqueduct into the jugular bulb also exhibits third window mechanics (*Fig 13*).²⁹⁻³³

At audiometry, patients present with a complex and variable pattern of hearing loss. The sensorineural component of hearing loss is thought to result from potential associated cochleovestibular malformations and manifests at higher sound frequencies.

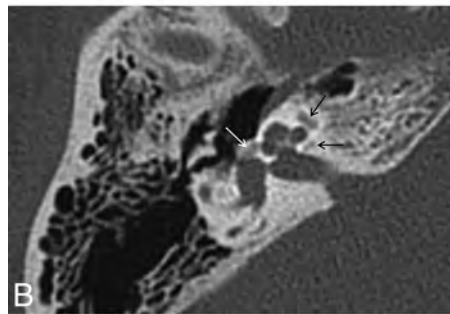
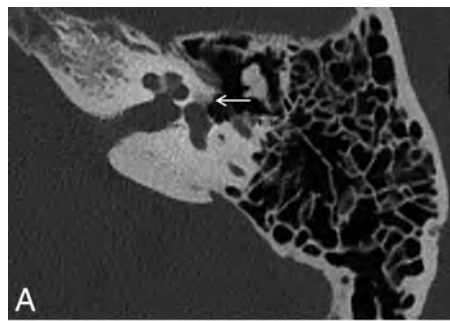


FIG 15. Otospongiosis. *A*, Fenestral otospongiosis. Axial CT scan shows lucency at the fissula ante fenestram (*arrow*). *B*, Fenestral and retrofenestral otospongiosis. Axial CT scan shows lucency at the fissula ante fenestram (*white arrow*) and surrounding the cochlea (*black arrows*). *C*, Advanced otospongiosis. Axial CT scan late in the course of disease demonstrates a complete ring of pericochlear lucency.

The conductive component of hearing loss results from acoustic energy dissipation through an enlarged third window where the vestibular aqueduct joins the vestibule. This is evidenced by an audiometric air-bone gap at low frequencies but may be missed if bone conduction is not measured, particularly in young children who cannot tolerate a full audiologic examination.^{2,34-37} Vestibular-evoked myogenic potential studies may demonstrate increased vestibular organ responses on the side of pathology.^{38,39}

At Massachusetts Eye and Ear Infirmary, 98 patients (165 ears) with EVAS were included in the teaching file from 2000 to 2011. Sixty of 165 ears (36%) demonstrated associated cochleovestibular malformations. Reported symptoms at the time of imaging included hearing loss in 67/98 patients (68%) and vertigo in 6/98 (6%). Audiogram findings for EVAS varied widely, demonstrating mixed sensorineural and conductive components. Six patients

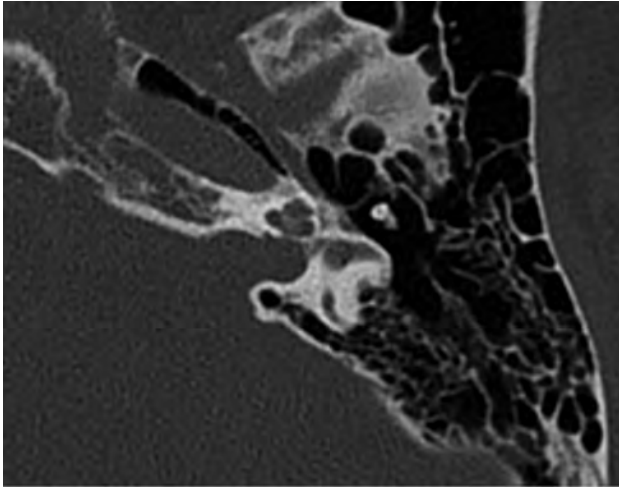


FIG 16. Osteogenesis imperfecta. Axial CT scan shows otic capsule demineralization with multiple vague lucencies, including the fissa ante fenestram, pericochlear region, and area adjacent to the internal auditory canal. Radiologically, this is indistinguishable from otospongiosis.

(7 ears) demonstrated vestibular aqueduct dehiscence into the jugular bulb. Audiometry was evaluative in 7 ears, with 1/7 (14%) showing the classic air-bone gap of the third window disorder.

X-Linked Stapes Gusher

X-linked stapes gusher is a congenital disorder resulting from a loss-of-function mutation in the *POU3F4* gene at the DFN3 locus of the X chromosome. Patients are almost exclusively male and present with mixed hearing loss at birth, rapidly progressing to severe deafness in the first decade.^{40,41} Female carriers of the gene may be healthy or may have less severe hearing loss.^{42,43} The spectrum of abnormalities on CT includes cochlear hypoplasia with modiolary deficiency, absence of the lamina cribrosa, an enlarged internal auditory canal, and an enlarged labyrinthine facial nerve canal (Fig 14).⁴⁴⁻⁴⁷

On audiometry, patients with X-linked stapes gusher typically demonstrate a mixed hearing loss. The sensorineural component of hearing loss results from the cochleovestibular malformation. The conductive component results from absence of the lamina cribrosa, which normally separates the basal turn of the cochlea from the internal auditory canal. Therefore, there is direct communication of CSF between the subarachnoid and perilymphatic spaces, acting as a third window.^{2,48}

At Massachusetts Eye and Ear Infirmary, 9 patients (18 ears) with X-linked stapes gusher were included in the teaching file from 2000 to 2011. On CT, all patients demonstrated bilateral temporal bone abnormalities. One hundred percent of patients had hearing loss, with mixed sensorineural and conductive components on audiometry.

Bone Dyscrasias

Bone dyscrasias such as Paget disease, osteogenesis imperfecta, and otospongiosis are rarely reported in conjunction with third window mechanics. In the adult, the bony labyrinth is composed of mature avascular enchondral bone, which undergoes virtually no remodeling after development. Metabolic bone diseases decrease the acoustic impedance both into and out of the bone, presumably acting as an anatomically diffuse or “distributed” third

window (Figs 15 and 16). Postmortem micro-CT and temporal bone histology have demonstrated communications between the middle and inner ear that are too small to visualize on conventional CT. Air-bone gaps on audiometry have been reported in the literature but may be obscured by large conductive losses.^{2,49-54}

CONCLUSIONS

Third window lesions classically present with auditory (hearing loss) and vestibular (Tullio and Hennebert syndromes) symptoms. On temporal bone CT, specific anatomic defects include superior semicircular canal dehiscence, posterior semicircular canal dehiscence, perilyabyrinthine fistula, enlarged vestibular aqueduct, X-linked stapes gusher, and bone dyscrasias. Awareness of the various etiologies and correlation with an audiological examination will help in diagnosing this multifaceted disorder.

ACKNOWLEDGMENT

We thank Garyfallia Pagonis for her expert assistance with graphics.

Disclosures: Gul Moonis—*UNRELATED*: Other: a blind reader for RadMD. Chris F. Halpin—*UNRELATED*: Payment for Lectures (including service on Speakers Bureaus): Auris Medical. Comments: travel to a conference in Dallas in 2015 on sudden sensory loss. Hugh D. Curtin—*UNRELATED*: Payment for Lectures (including service on Speakers Bureaus): International Institute for Continuing Medical Education, Comments: lectures in Continuing Medical Education courses; Royalties: Elsevier (book royalties).

REFERENCES

- Minor LB, Solomon D, Zinreich JS, et al. **Sound- and/or pressure-induced vertigo due to bone dehiscence of the superior semicircular canal.** *Arch Otolaryngol Head Neck Surg* 1998;124:249–58 CrossRef Medline
- Merchant SN, Rosowski JJ. **Conductive hearing loss caused by third-window lesions of the inner ear.** *Otol Neurotol* 2008;29:282–89 CrossRef Medline
- Chien WW, Carey JP, Minor LB. **Canal dehiscence.** *Curr Opin Neurology* 2011;24:25–31 CrossRef Medline
- Stimmer H, Hamann KF, Zeiter S, et al. **Semicircular canal dehiscence in HR multislice computed tomography: distribution, frequency, and clinical relevance.** *Eur Arch Otorhinolaryngol* 2012;269:475–80 CrossRef Medline
- Crovetto M, Whyte J, Rodriguez OM, et al. **Anatomo-radiological study of the superior semicircular canal dehiscence: radiological considerations of superior and posterior semicircular canals.** *Eur J Radiol* 2010;76:167–72 CrossRef Medline
- Chen EY, Paladin A, Phillips G, et al. **Semicircular canal dehiscence in the pediatric population.** *Int J Pediatr Otorhinolaryngol* 2009;73:321–27 CrossRef Medline
- Loke SC, Goh JP. **Incidence of semicircular canal dehiscence in Singapore.** *Br J Radiol* 2009;82:371–73 CrossRef Medline
- Cloutier JF, Bélair M, Saliba I. **Superior semicircular canal dehiscence: positive predictive value of high-resolution CT scanning.** *Eur Arch Otorhinolaryngol* 2008;265:1455–60 CrossRef Medline
- Sequeira SM, Whiting BR, Shimony JS, et al. **Accuracy of computed tomography detection of superior canal dehiscence.** *Otol Neurotol* 2011;32:1500–05 CrossRef Medline
- Yuen HW, Boeddinghaus R, Eikelboom RH, et al. **The relationship between the air-bone gap and the size of superior semicircular canal dehiscence.** *Otolaryngol Head Neck Surg* 2009;141:689–94 CrossRef Medline
- McCall AA, McKenna MJ, Merchant SN, et al. **Superior canal dehiscence syndrome associated with the superior petrosal sinus in pediatric and adult patients.** *Otol Neurotol* 2011;32:1312–19 CrossRef Medline
- Koo JW, Hong SK, Kim DK, et al. **Superior semicircular canal dehiscence.**

- cence syndrome by the superior petrosal sinus. *J Neurol Neurosurg Psychiatry* 2010;81:465–67 CrossRef Medline
13. Krombach GA, DiMartino E, Schmitz-Rode T, et al. **Posterior semicircular canal dehiscence: a morphologic cause of vertigo similar to superior semicircular canal dehiscence.** *Eur Radiol* 2003;13:1444–50 Medline
 14. Nomiya S, Cureoglu S, Kariya S, et al. **Posterior semicircular canal dehiscence: a histopathologic human temporal bone study.** *Otol Neurotol* 2010;31:1122–27 CrossRef Medline
 15. Gopen Q, Zhou G, Poe D, et al. **Posterior semicircular canal dehiscence: first reported case series.** *Otol Neurotol* 2010;31:339–44 CrossRef Medline
 16. Shinnabe A, Hara M, Hasegawa M, et al. **Clinical characteristics and surgical benefits and problems of chronic otitis media and middle ear cholesteatoma in elderly patients older than 70 years.** *Otol Neurotol* 2012;33:1213–17 CrossRef Medline
 17. Ikeda R, Kobayashi T, Kawase T, et al. **Risk factors for deterioration of bone conduction hearing in cases of labyrinthine fistula caused by middle ear cholesteatoma.** *Ann Otol Rhinol Laryngol* 2012;121:162–67 CrossRef Medline
 18. Lund AD, Palacios SD. **Carotid artery-cochlear dehiscence: a review.** *Laryngoscope* 2011;121:2658–60 CrossRef Medline
 19. Young RJ, Shatzkes DR, Babb JS, et al. **The cochlear-carotid interval: anatomic variation and potential clinical implications.** *AJNR Am J Neuroradiol* 2006;27:1486–90 Medline
 20. Penido Nde O, Borin A, Fukuda Y, et al. **Microscopic anatomy of the carotid canal and its relations with cochlea and middle ear.** *Braz J Otorhinolaryngol* 2005;71:410–14 CrossRef Medline
 21. Kang HM, Kim MG, Boo SH, et al. **Comparison of the clinical relevance of traditional and new classification systems of temporal bone fractures.** *Eur Arch Otorhinolaryngol* 2012;269:1893–99 CrossRef Medline
 22. Dahiya R, Keller JD, Litofsky NS, et al. **Temporal bone fractures: otic capsule sparing versus otic capsule violating clinical and radiographic considerations.** *J Trauma* 1999;47:1079–83 CrossRef Medline
 23. Berrettini S, Forli F, Bogazzi F, et al. **Large vestibular aqueduct syndrome: audiological, radiological, clinical, and genetic features.** *Am J Otolaryngol* 2005;26:363–71 CrossRef Medline
 24. Valvassori G, Clemis J. **The large vestibular aqueduct syndrome.** *Laryngoscope* 1978;88:273–78 Medline
 25. Boston M, Halsted M, Meinzen-Derr J, et al. **The large vestibular aqueduct: a new definition based on audiologic and computed tomography correlation.** *Otolaryngol Head Neck Surg* 2007;136:972–77 CrossRef Medline
 26. Sennaroglu L, Saatci I. **A new classification for cochleovestibular malformations.** *Laryngoscope* 2002;112:2230–41 CrossRef Medline
 27. Saliba I, Gingras-Charland ME, St-Cyr K, et al. **Coronal CT scan measurements and hearing evolution in enlarged vestibular aqueduct syndrome.** *Int J Pediatr Otorhinolaryngol* 2012;76:492–99 CrossRef Medline
 28. Lookabaugh S, Kelly HR, Carter MS, et al. **Radiologic classification of superior canal dehiscence: implications for surgical repair.** *Otol Neurotol* 2015;36:118–25 CrossRef Medline
 29. Hourani R, Carey J, Yousem DM. **Dehiscence of the jugular bulb and vestibular aqueduct: findings on 200 consecutive temporal bone computed tomography scans.** *J Comput Assist Tomogr* 2005;29:657–62 CrossRef Medline
 30. Friedmann DR, Eubig J, Winata LS, et al. **Prevalence of jugular bulb abnormalities and resultant inner ear dehiscence: a histopathologic and radiologic study.** *Otolaryngol Head Neck Surg* 2012;147:750–56 CrossRef Medline
 31. Friedmann DR, Eubig J, Winata LS, et al. **A clinical and histopathologic study of jugular bulb abnormalities.** *Arch Otolaryngol Head Neck Surg* 2012;138:66–71 CrossRef Medline
 32. Kupfer RA, Hoesli RC, Green GE, et al. **The relationship between jugular bulb-vestibular aqueduct dehiscence and hearing loss in pediatric patients.** *Otolaryngol Head Neck Surg* 2012;146:473–77 CrossRef Medline
 33. Friedmann DR, Le BT, Pramanik BK, et al. **Clinical spectrum of patients with erosion of the inner ear by jugular bulb abnormalities.** *Laryngoscope* 2010;120:365–72 CrossRef Medline
 34. Mimura T, Sato E, Sugiura M, et al. **Hearing loss in patients with enlarged vestibular aqueduct: air-bone gap and audiological Bing test.** *Int J Audiol* 2005;44:466–69 CrossRef Medline
 35. Arjmand EM, Webber A. **Audiometric findings in children with a large vestibular aqueduct.** *Arch Otolaryngol Head Neck Surg* 2004;130:1169–74 CrossRef Medline
 36. Merchant SN, Nakajima HH, Halpin C, et al. **Clinical investigation and mechanism of air-bone gaps in large vestibular aqueduct syndrome.** *Ann Otol Rhinol Laryngol* 2007;116:532–41 CrossRef Medline
 37. Zhou G, Gopen Q, Kenna MA. **Delineating the hearing loss in children with enlarged vestibular aqueduct.** *Laryngoscope* 2008;118:2062–66 CrossRef Medline
 38. Zhou G, Gopen Q. **Characteristics of vestibular evoked myogenic potentials in children with enlarged vestibular aqueduct.** *Laryngoscope* 2011;121:220–25 CrossRef Medline
 39. Sheykholslami K, Schmerber S, Habiby Kermany M, et al. **Vestibular-evoked myogenic potentials in three patients with large vestibular aqueduct.** *Hear Res* 2004;190:161–68 CrossRef Medline
 40. Schild C, Prera E, Lüblinghoff N, et al. **Novel mutation in the homeobox domain of transcription factor POU3F4 associated with profound sensorineural hearing loss.** *Otol Neurotol* 2011;32:690–94 CrossRef Medline
 41. Friedman RA, Bykhovskaya Y, Tu G, et al. **Molecular analysis of the POU3F4 gene in patients with clinical and radiographic evidence of X-linked mixed deafness with perilymphatic gusher.** *Ann Otol Rhinol Laryngol* 1997;106:320–25 CrossRef Medline
 42. Huang BY, Zdanski C, Castillo M. **Pediatric sensorineural hearing loss, part 2: syndromic and acquired causes.** *AJNR Am J Neuroradiol* 2012;33:399–406 CrossRef Medline
 43. Marlin S, Moizard MP, David A, et al. **Phenotype and genotype in females with POU3F4 mutations.** *Clin Genet* 2009;76:558–63 CrossRef Medline
 44. Papadaki E, Prassopoulos P, Bizakis J, et al. **X-linked deafness with stapes gusher in females.** *Eur J Radiol* 1998;29:71–75 CrossRef Medline
 45. Talbot JM, Wilson DF. **Computed tomographic diagnosis of X-linked congenital mixed deafness, fixation of the stapedial footplate, and perilymphatic gusher.** *Am J Otol* 1994;15:177–82 Medline
 46. Kumar G, Castillo M, Buchman CA. **X-linked stapes gusher: CT findings in one patient.** *AJNR Am J Neuroradiol* 2003;24:1130–32 Medline
 47. Cremers CW, Snik AF, Huygen PL, et al. **X-linked mixed deafness syndrome with congenital fixation of the stapedial footplate and perilymphatic gusher (DFN3).** *Adv Otorhinolaryngol* 2002;61:161–67 Medline
 48. Snik AF, Hombergen GC, Mylanus EA, et al. **Air-bone gap in patients with X-linked stapes gusher syndrome.** *Am J Otol* 1995;16:241–46 Medline
 49. Makarem AO, Linthicum FH. **Cavitating otosclerosis.** *Otol Neurotol* 2008;29:730–31 CrossRef Medline
 50. Makarem AO, Hoang TA, Lo WW, et al. **Cavitating otosclerosis: clinical, radiologic, and histopathologic correlations.** *Otol Neurotol* 2010;31:381–84 CrossRef Medline
 51. Richard C, Linthicum FH Jr. **An unexpected third window in a case of advanced cavitating otosclerosis.** *Otol Neurotol* 2012;33:e47–48 CrossRef Medline
 52. Merchant SN, Rosowski JJ, McKenna MJ. **Superior semicircular canal dehiscence mimicking otosclerotic hearing loss.** *Adv Otorhinolaryngol* 2007;65:137–45 Medline
 53. Van Rompaey V, Potvin J, van den Hauwe L, et al. **Third mobile window associated with suspected otosclerotic foci in two patients with an air-bone gap.** *J Laryngol Otol* 2011;125:89–92 CrossRef Medline
 54. Santos F, McCall AA, Chien W, et al. **Otopathology in osteogenesis imperfecta.** *Otol Neurotol* 2012;33:1562–66 CrossRef Medline

Genetics of Frontotemporal Dementia

F.W. Rohlfig and R.K. Tu

ABBREVIATION: FTD = frontotemporal dementia

HISTORY OF FRONTOTEMPORAL DEMENTIA

In 1892, Arnold Pick, a neuropsychiatrist at the University of Prague, made the first description of frontotemporal dementia (FTD). In his case report, “On the relationship between senile atrophy of the brain and aphasia,” he described a 71-year-old man who developed progressive aphasia and apraxia. Upon autopsy, the patient’s brain showed asymmetric atrophy.¹

Pathologically, FTD is associated with atrophy of the frontal and/or temporal lobes, gliosis, neuronal swelling, and eventual microvacuolation.^{2,3} Pick bodies are hyperphosphorylated tau accumulations in the neuronal cytoplasm, which may be found with silver staining but are not pathognomonic for the disease.⁴ TAR DNA-binding proteins are hyperphosphorylated, ubiquitinated, cleaved proteins and are the most commonly found neuropathology in FTD.⁵

FTD is an uncommon disease compared with other neurodegenerative disorders such as Alzheimer disease. However, in presenile dementia, FTD incidence is similar to that of Alzheimer disease. In a study of 50–59-year-old patients in Rochester, Minnesota, incidence of FTD cases and Alzheimer cases were both found to be 3.3/100,000 person years.⁶ In Cambridge, United Kingdom, FTD incidence was found to be 3.5/100,000 person years, whereas Alzheimer disease incidence was 4.2/100,000 person years.⁷ Although FTD is considered a presenile dementia, 20%–25% of patients with FTD are older than 65 years. The median survival is 6 ± 1.1 years.^{8,9}

WHAT ARE THE CLINICAL MANIFESTATIONS OF FRONTOTEMPORAL DEMENTIA?

FTD has 3 main clinical manifestation groups based on dominant symptoms at diagnosis. The first is the frontal variant or behav-

ioral variant, which may represent 70% of FTD.⁵ Frontal variant FTD results in alterations in interpersonal skills and behavior. Persons may show uninhibited behavior, disinhibition, apathy, or new obsessions or rituals, usually first noticed by a close contact of the patient.^{2,10}

Progressive nonfluent aphasia variant is another manifestation group where patients present with word-finding difficulty. Speech can become nonfluent, but comprehension remains intact.^{2,10}

Semantic dementia group is characterized by the loss of semantic memory. Patients may present with loss of word understanding and the inability to use or recall certain words. Instead, patients use less precise substitute terms and phrases. Speech remains fluent.^{2,8,10}

In time, most manifestations of FTD converge and overlap, expressing multiple symptoms causing increased impairment.⁵

ARE THERE GENETIC TYPES OF FTD?

Approximately 20%–40% of FTD cases have a family history of disease, and 10% of FTD cases are inherited in an autosomal dominant fashion.¹¹ The most notable variants are found in *MAPT* (microtubule-associated protein tau), *C9ORF72*, and *PGRN* (progranulin).^{8,10}

Mutations in the gene *MAPT* on chromosome 17 have been found to be associated with Pick bodies and FTD. *MAPT* mutations have been shown to be responsible for 11% of overall FTD cases.¹²

C9ORF72 mutations result in hexanucleotide repeat expansions; however, the mechanism behind this expansion is unclear, and the length of repeats has not been shown to correlate with severity. *C9ORF72* mutations have shown to result in 6% of overall FTD cases.¹²

PGRN gene mutations on chromosome 17 likely result in lysosomal impairment and cause ubiquitin-positive cytoplasmic and intranuclear inclusions. *PGRN* mutations have been found to result in 10% of total FTD cases and 22% of familial FTD cases.¹³

From the Departments of Radiology (F.W.R.) and Neuroradiology (R.K.T.), George Washington University School of Medicine and Health Sciences, Washington, DC; and Progressive Radiology–Foxhall MRI (R.K.T.), Washington, DC.

Please address correspondence to Raymond K. Tu, 2121 K St NW, Ste 100, Washington, DC 20037; e-mail: frohlfingiv@gmail.com

<http://dx.doi.org/10.3174/ajnr.A4972>

IS THERE DIAGNOSTIC TESTING FOR FTD?

Currently, diagnosis of FTD is based on clinical characteristic signs of continual change in behavior and language with the exclusion of delirium and psychotic disorders. Imaging is used to confirm the diagnosis by visualizing atrophy at the frontal and/or temporal lobes and exclude other diagnoses, including tumor, stroke, or infection.

WHAT IS THE ROLE OF IMAGING IN FTD?

MR imaging is useful in excluding other diagnoses and can show atrophy of the frontal and/or temporal lobes with sparing of the posterior cortical areas to support the diagnosis of FTD.¹⁴

Other methods besides the standard T1 MR imaging have recently been used to evaluate FTD. Imaging of patients with frontal variant FTD has shown gray matter atrophy of the frontal and temporal lobes, with the right usually more affected than the left. Other affected structures include anterior cingulate, anterior insula, and subcortical structures. Patients with semantic FTD commonly present with atrophy of the temporal lobes, with the left more commonly affected than the right. Patients with progressive nonfluent aphasia FTD present initially with atrophy in the left inferior frontal lobe, insula, and premotor cortex.¹⁴

T2 and proton density-weighted MR imaging of FTD have shown increased white matter signal intensity in either the frontal or temporal lobes.³

DTI of frontal variant FTD has shown bilateral frontal and temporal lobe changes of the white matter. Semantic FTD has shown asymmetrical (left more than right) changes. Progressive nonfluent aphasia FTD has shown white matter changes in the dorsal language pathways.¹⁴

Resting-state fMRI has been used to analyze changes in FTD. However, results have been contradictory and inconclusive.¹⁴

Arterial spin-labeling perfusion MR imaging in frontal variant FTD has shown hypoperfusion in the frontal regions, anterior cingulate, and thalamus.¹⁴

SPECT and PET in FTD show hypometabolism in the frontal and temporal lobes, with progressive nonfluent aphasia variant showing more hypometabolism in the temporal lobes and frontal variant FTD showing more hypoperfusion in the frontal lobes. This technique may be useful and assist in diagnosis when MR does not show atrophy of frontal or temporal lobes.^{2,14}

CONCLUSIONS

Diagnosis of FTD still rests on a characteristic clinical examination. Of the imaging modalities, SPECT and PET studies appear to be a sensitive diagnostic tool. Structural imaging is contributory when atrophy is present; however, characteristic signs of FTD may not be present early in the disease process. Genetic and idiopathic forms of FTD have similar imaging and genetic mutations, suggesting a common pathophysiology.

REFERENCES

1. Pearce J. **Pick's disease.** *J Neurol Neurosurg Psychiatry* 2003;74:169 CrossRef Medline
2. Kirshner H. **Frontotemporal dementia and primary progressive aphasia: an update.** *Curr Neurol Neurosci Rep* 2010;10:504–11 CrossRef Medline
3. Kitagaki H, Mori E, Hirono N, et al. **Alteration of white matter MR signal intensity in frontotemporal dementia.** *AJNR Am J Neuroradiol* 1997;18:367–78 Medline
4. Spillantini MG, Goedert M. **Tau pathology and neurodegeneration.** *Lancet Neurol* 2013;12:609–22 CrossRef Medline
5. Seltman RE, Matthews BR. **Frontotemporal lobar degeneration: epidemiology, pathology, diagnosis and management.** *CNS Drugs* 2012;26:841–70 CrossRef Medline
6. Knopman DS, Petersen RC, Edland SD, et al. **The incidence of frontotemporal lobar degeneration in Rochester, Minnesota, 1990 through 1994.** *Neurology* 2004;62:506–08 CrossRef Medline
7. Mercy L, Hodges JR, Dawson K, et al. **Incidence of early-onset dementias in Cambridgeshire, United Kingdom.** *Neurology* 2008;71:1496–99 CrossRef Medline
8. Weder ND, Aziz R, Wilkins K, et al. **Frontotemporal dementias: a review.** *Ann Gen Psychiatry* 2007;6:15 CrossRef Medline
9. Hodges JR, Davies R, Xuereb J, et al. **Survival in frontotemporal dementia.** *Neurology* 2003;61:349–54 CrossRef Medline
10. Warren JD, Rohrer JD, Rossor MN. **Frontotemporal dementia.** *BMJ* 2013;347:f4827 CrossRef Medline
11. Rohrer JF, Guerreiro R, Vandrovцова J, et al. **The heritability and genetics of frontotemporal lobar degeneration.** *Neurology* 2009;73:1451–56 CrossRef Medline
12. Seelaar H, Kamphorst W, Rosso SM, et al. **Distinct genetic forms of frontotemporal dementia.** *Neurology* 2008;71:1220–26 CrossRef Medline
13. Gass J, Cannon A, Mackenzie IR, et al. **Mutations in progranulin are a major cause of ubiquitin-positive frontotemporal lobar degeneration.** *Hum Mol Genet* 2006;15:2988–3001 CrossRef Medline
14. Rohrer JD, Rosen HJ. **Neuroimaging in frontotemporal dementia.** *Int Rev Psychiatry* 2013;25:221–29 CrossRef Medline

Emergency Department MRI Scanning of Patients with Multiple Sclerosis: Worthwhile or Wasteful?

J. Pakpoor, D. Saylor, I. Izbudak, L. Liu, E.M. Mowry, and D.M. Yousem

ABSTRACT

BACKGROUND AND PURPOSE: The increasing use of the emergency department MR imaging scanner at our institution raises questions about its added value to certain patient groups. We hypothesized that the use of emergency department MR imaging for identifying active demyelination in MS patients presenting with new neurologic symptoms would be of low yield.

MATERIALS AND METHODS: Electronic medical records were reviewed for patients with MS who had emergency department MR imaging scans for a suspected MS exacerbation between March 1, 2014, and March 1, 2016. Details surrounding patient disposition, imaging, diagnosis, and management were determined.

RESULTS: Of 115 patients in our study, 48 (41.7%) were ultimately diagnosed with an MS exacerbation. Nearly all patients with MS exacerbations (87.5%, 42/48) had active demyelination on their emergency department MR imaging, identified on 30.6% (33/108) of brain MRIs and 20.4% (19/93) of spinal MRIs. The presence of active demyelination at MRI was significantly associated with the ultimate diagnosis of an MS exacerbation ($P < .001$). MR imaging activity isolated to the spinal cord (ie, not found on concurrent brain MR imaging) was present in only 9 of 93 (9.7%) cases. Pseudoexacerbations accounted for 18 of the alternative diagnoses.

CONCLUSIONS: Emergency department MR imaging is a worthwhile endeavor from a diagnostic standpoint for MS exacerbations despite not being part of the diagnostic criteria. This finding has corresponding downstream impact on management decisions to admit and/or administer intravenous steroids. However, we raise the question of whether clinicians over-rely on emergency department imaging for making exacerbation diagnoses. Additionally, spinal MR imaging is of questionable value as an addition to brain MR imaging due to a low yield of isolated spinal disease.

ABBREVIATIONS: AD = active demyelination; ED = emergency department

MS is a chronic demyelinating disorder of the CNS affecting an estimated 2.5 million individuals worldwide.¹ Approximately 80% of individuals with MS initially present with the relapsing-remitting form of the disease, characterized by intermittent episodes of exacerbations of a variety of neurologic symptoms that can reflect underlying acute inflammation (eg, numbness or tingling of the limbs, blurred vision, and weakness).²⁻⁶ Exacerbations are generally not life-threatening, and neurologic recovery can be hastened with high-dose steroids.⁷⁻¹⁰ However, the unpredictable timing of their occurrence and vari-

ability of neurologic deficits may lead patients to present to the emergency department (ED). A 2014 study at the Mount Sinai Hospital ED in New York found an average of 2.5 visits to the ED per patient with MS for neurologic and non-neurologic problems during a 3-year period.¹¹

Currently, MR imaging is the preferred tool for assessing MS disease activity. "MR imaging activity," defined as gadolinium-enhancing lesions and/or lesions with restricted diffusion, is used as a marker of active demyelination (AD) during an exacerbation.¹²⁻¹⁷ New or enlarging T2WI/FLAIR hyperintense lesions can also be used as indicators of disease progression but are generally considered less sensitive for the assessment of acute activity.¹⁵ While MR imaging can therefore be useful for confirming MS exacerbations, it is costly; of long duration when scanning the brain and cervicothoracic spine; technically challenging so as not to miss lesions, particularly in the thoracic spine; and not part of the diagnostic criteria for MS exacerbations.^{7,12-14,18,19} The diagnostic criteria have been defined by the International Panel on the

Received June 10, 2016; accepted after revision August 11.

From the Division of Neuroradiology (J.P., I.I., L.L., D.M.Y.), Russell H. Morgan Department of Radiology and Radiological Science, and Department of Neurology (D.S., E.M.M.), Johns Hopkins Medical Institutions, Baltimore, Maryland.

Please address correspondence to David M. Yousem, MD, MBA, Division of Neuro-radiology, Russell H. Morgan Department of Radiology and Radiological Science, Johns Hopkins Medical Institutions, 600 N Wolfe St, Phipps B100F, Baltimore, MD 21287; e-mail: dyousem1@jh.edu

<http://dx.doi.org/10.3174/ajnr.A4953>

Diagnosis of MS to be neurologic signs typical of an acute inflammatory demyelinating event in the CNS, of at least 24-hour duration.⁸

In April 2012, an MR imaging scanner was installed in the ED of our hospital for use 24 hours per day. The following year saw a 51.4% increase in MR imaging use in the ED for neurology consult patients.²⁰ While this reduced the burden on the inpatient MR imaging scanners, the increased use of ED MR imaging raised the question of its added value to certain patient groups for what is still a limited but heavily used hospital resource. Additionally, the use of emergency imaging has previously been shown to be associated with increased patient length of stay in the ED and downstream ED crowding, reduced patient satisfaction, and negative impacts on the timeliness of patient care.²⁰⁻²⁴ A 2012 study that used ED data from a national data base found MR imaging use to be associated with a 64-minute increase in the length of stay in the ED, second only to blood tests for time-cost among testing modalities.²³

This study aimed to assess the value of using the ED MR imaging scanner for patients with a known diagnosis of MS by evaluating the extent to which it is used as a diagnostic tool for MS exacerbations and its yield of diagnostic findings. On the basis of the anecdotal experience of the radiologist authors, we hypothesized the following: 1) that MS exacerbations identified by AD plaques would occur in less than half (50%) of cases, 2) suggesting an alternative diagnosis to MS exacerbation based on an MR imaging finding would be an uncommon (<10%) occurrence, 3) the management decision of the treating physicians would rarely be affected (<5% of ED presentations), and 4) new enhancing spinal cord lesions would rarely be detected (ie, <5% of patients).

MATERIALS AND METHODS

This study complied with the Health Insurance Portability and Accountability Act and was approved by the institutional review board at our institution. Because of its retrospective nature, informed consent requirements were waived.

Data Collection and Analysis

An automated query of the radiology information system of our institution was used to identify all patients with ED MR imaging encounters in a 2-year period, March 1, 2014, to March 1, 2016, in which at least 1 of the terms “multiple sclerosis,” “MS,” “clinically isolated syndrome,” “demyelination,” “demyelinating,” “myelitis,” or “optic neuritis” appeared anywhere in the ED MR imaging report. The total proportion of ED neuroradiologic MRI requests that were for suspected MS exacerbations was determined by searching the indications of all Current Procedural Terminology codes for neuroradiology procedures in the ED MR scanner during that period. We then limited our study to those patients with a preexisting diagnosis of MS who had presented to the ED and for whom an “MS exacerbation” was part of the differential diagnosis in the patients’ electronic medical records. An MS exacerbation could be indicated by synonymous terminology (eg, “flare-up,” “attack,” or “relapse”). For each encounter, patient demographics, presenting symptoms, imaging protocol used, MR imaging radiology report, final diagnosis, disposition (admission versus discharge), treatment (high-dose steroids or no steroids), and

Table 1: ED MRI requesting patterns by CNS location imaged

Encounter MRI Requests	N = 115	% of Total
Brain	17	14.5%
Brain + orbit	4	3.5%
Brain + C-spine	9	7.8%
Brain + orbit + C-spine	1	0.9%
Brain + C- + T-spine	53	46.1%
Brain + orbit + C- + T-spine	2	1.8%
Brain + C- + T- + L-spine	21	18.3%
Brain + orbit + C- + T- + L-spine	1	0.9%
Orbit	1	0.9%
C-spine	1	0.9%
T- + C-spine	4	3.5%
T- + C- + L-spine	1	0.9%

Note:—C indicates cervical; T, thoracic; L, lumbar.

length of stay (if admitted) were determined. Additionally, we reviewed the electronic medical records to determine the proportion of patients for whom the neurology consult recommended MR imaging.

For comparison, ED admission records were also queried for patients with MS admitted to the neurology department for a suspected MS exacerbation from the ED without obtaining an ED MR image. For these patients, we examined whether they subsequently underwent inpatient MR imaging and their length of stay on admission. Per hospital procedure, it is highly unlikely that a patient with MS presenting to the ED with a suspected MS exacerbation would be discharged from the ED without either admission for management or inpatient or ED imaging; thus such cases were not included in this study.

ED MR Imaging Requests

Of the 115 patients who were scanned in the ED, 93.0% (107/115) had neuroradiological MR imaging through use of the hospital’s MS protocol with and without gadolinium contrast administration (as opposed to the stroke or routine brain protocols). This protocol includes a 6-minute 3D FLAIR whole-brain pulse sequence in the sagittal plane, which could be reconstructed in axial and coronal sections. Of the 115, 69.6% ($n = 80$) had a combination of MR imaging of the brain and spine under the MS protocol. A further 18 patients had only MR imaging of the brain under the MS protocol, and 9 patients had only MR imaging of the spine under the MS protocol. Eight patients had imaging under the routine brain or stroke protocols.

In total, 108 MR images of the brain, 93 of the cervical spine, 82 of the thoracic spine, 22 of the lumbar spine, and 9 orbit examinations were obtained. The CNS locations imaged by using the ED MR imaging scanner and the combinations used for each encounter are represented in Table 1.

Statistical Analyses

We calculated a Pearson χ^2 test of independence, comparing the frequency of identification of MR imaging activity and the diagnosis of an MS exacerbation. A Wilcoxon rank sum test was used to compare the length of stay on admission of patients who had ED MR imaging versus inpatient MR imaging. Statistical significance was defined at $P < .05$. Analyses were performed by using STATA (StataCorp, College Station, Texas).

RESULTS

Between March 1, 2014, and March 1, 2016, 4% of all neuroradiologic ED MR imaging requests (MR imaging of the brain, orbits, cervical, thoracic, and lumbar spine) were for patients with an established MS diagnosis who presented to the ED with a possible MS exacerbation. These represent the 115 ED encounters of patients with MS who made up our study population. Their demographic profiles are shown in Table 2.

For 74.8% (86/115) of patient encounters, it was determined from the patients' electronic medical records that the MR imaging requests were recommended by a neurology resident consult, not solely by the ED service itself.

ED MR Imaging and Diagnosis

Of 115 patients with MS in our study population, 41.7% ($n = 48$) were diagnosed with an MS exacerbation. Their findings at ED MR imaging are shown in Table 3.

Of the 42 patients who were diagnosed with an MS exacerbation and who had MR imaging activity, 37 had gadolinium-enhancing lesions, 3 had diffusion restriction and gadolinium-enhancing lesions, and 2 had only lesions of diffusion restriction. Two patients with alternative clinical diagnoses also had lesions of diffusion restriction.

MR Imaging Activity and CNS Location

The breakdown of the CNS locations where MR imaging activity was identified is shown in Table 4. The 33 patients with demonstrated MR imaging brain activity accounted for 78.6% of the 42 patients who had such activity demonstrated. Three-quarters of encounters (85/115) included both MR imaging studies of the brain and cervical spine, and in only 7.1% (6/85) of these cases did MR imaging of the cervical spine demonstrate MR imaging activity when the MR imaging of the brain did not. Among the 82 cases with thoracic spine MR imaging, it was the only location to demonstrate AD in only 3 cases (3.7%). In total, 20.4% (19/93) of encounters that used any spinal imaging demonstrated MR imaging activity in the spine, but spine imaging demonstrated MR imaging activity in the absence of activity in the brain in <10% (9/93, 9.7%) of cases.

An MS exacerbation was significantly more likely to be diagnosed if the MR imaging showed activity compared with patients in whom this finding was lacking ($P < .001$, odds ratio = 462; 95% confidence interval, 128–1670).

Table 2: Patient demographic profiles

Demographics	
No.	115
Age (yr)	39 ± 12.1
Sex	98 Women, 17 men

In the 67 patients who were not diagnosed with an MS exacerbation, a positive finding other than AD on MR imaging suggested an alternative diagnosis in only 7.5% (5/67) of cases. These were C5 spondyloradiculopathy, tonsillitis, degenerative compressive myelopathy ($n = 2$), and stroke. Final diagnoses in patients not diagnosed with an MS exacerbation varied considerably (Table 5).

Management

Admission and Treatment. In total, 59.1% (68/115) of our study population were recommended for admission, and 91.7% (44/48) of those with a final diagnosis of an MS exacerbation were admitted. All patients admitted with an MS exacerbation were treated with intravenous methylprednisolone except 1 patient who had a previous adverse reaction to high-dose steroids. Of patients not diagnosed with an MS exacerbation, 35.8% (24/67) required admission for their alternative diagnoses. These included neurosurgical intervention for decompression, symptomatic pain relief and fluid management, antibiotics for tonsillitis, and so forth. On the basis of review of the electronic medical records, the decision as to whether to admit the patient correlated with identification or absence of AD lesions in 70% of all encounters (80/115). Neurology consult notes in the medical records of 39% (45/115) of the MS patients in the ED also indicated that MR imaging findings would determine disposition (admission versus discharge) and treatment (high-dose steroids or not).

In the same time period, 19 patients with MS were admitted to the neurology department for a suspected MS exacerbation without having ED MR imaging. Except for 1 patient who refused due to pregnancy, the other 18 had MR imaging as inpatients (Table 6). Eight of these patients were ultimately diagnosed with an MS exacerbation, 3 of whom did not demonstrate MR imaging activity. Eleven were admitted for an MS exacerbation but had an alternative final diagnosis established. The difference in length of stay upon admission between patients with MS admitted following ED MR imaging (median, 3.3 days; interquartile range, 1.9–4.4 days) versus with subsequent inpatient imaging (median, 4.2 days; interquartile range, 2.1–6.4 days) was not statistically significant because of the large SDs ($P > .05$). Nonetheless, the average hospital admission with ED MR imaging was 0.9 days shorter than if admitted without such imaging. In 2 of 11 of these patients who were not given a final diagnosis of an MS exacerbation, a 5-day course of IV methylprednisolone was commenced before the availability of inpatient MR imaging results, and was subsequently stopped midcourse as an alternative diagnosis was made.

No patient with MS with a suspected MS exacerbation who presented to the ED in the 2-year period of the study was admitted

Table 3: Findings at MRI in patients diagnosed with an MS exacerbation or an alternative diagnosis

	MRI Activity Only (with Enhancement or Diffusion Restriction) ^a	MRI Activity + Progressive WM Lesions	Progressive WM Lesions Only (without Enhancement or Diffusion Restriction) ^b	MRI Negative for MS Change	Total
Final clinical diagnosis of MS exacerbation (No.)	15	27	1	5	48
Other final clinical diagnoses (No.)	0	1	12	54	67

^a The presence of a sign of active demyelination (ie, the presence of gadolinium-enhancing lesions and/or diffusion restriction).

^b The reporting of a new or enlarging white matter lesion.

Table 4: CNS location and MRI activity^a

Imaging Section	Cervical			Lumbar	
	Brain	Spine	Thoracic	Spine	Orbit
MRI activity	33 (31%)	13 (14%)	8 (10%)	0 (0%)	4 (44%)
No MRI activity	75 (69%)	80 (86%)	74 (90%)	22 (100%)	5 (56%)
Total	108	93	82	22	9

^aPercentages of column totals are in parentheses.

Table 5: Number of alternative diagnoses made for patients not diagnosed with an MS exacerbation in the study population

Diagnosis
No final diagnosis: 23
Pseudoexacerbation: 18
Neuropathic pain: 5
Musculoskeletal: 5
Migraine: 2
Seizure: 2
Neuralgia: 3
Compressive myelopathy: 2
Arthralgia: 1
Tonsillitis: 1
Avascular necrosis: 1
C5 radiculopathy: 1
Postconcussive syndrome: 1
Stroke: 1
Acute manic bipolar disorder episode: 1

Table 6: MRI findings at inpatient MRI

	Brain	Cervical	Thoracic	Lumbar	Orbit
Total scans (No.)	16	14	14	3	1
MRI activity (No.)	5	0	1	0	0
Progressive WM lesions (No.)	2	0	0	0	0

for IV steroid treatment without an MR imaging study at some point in their hospitalization.

DISCUSSION

A growing number of hospital EDs may be compelled to acquire MR imaging scanners as they strive to meet the requirements of The Joint Commission Standards for Comprehensive Stroke Center certification, which currently necessitate around-the-clock availability of on-site MR imaging.²⁵ It is therefore of increasing relevance to establish the utility of ED MR imaging for various patient groups. In the 2-year period encompassed by our study, patients with MS with suspected MS exacerbations represented 4% of neuroradiologic MR imaging requests that used the ED scanner. Before the introduction of MR imaging in the ED, these and other patients requiring MR imaging during their ED encounter would require the approval of a radiologist and transport to a more remote area of the hospital (estimated travel time, 5–10 minutes). A technologist would be called in emergently between the hours of 11 PM and 6 AM for off-shift scanning.

We found that around one-third (36.5%) of MS encounters in our study population were diagnosed with an MS exacerbation with demonstration of MR imaging activity on ED MR imaging, in keeping with our first hypothesis that MR imaging activity in this patient population would be identified <50% of cases. The presence of gadolinium-enhancing lesions was significantly associated with a diagnosis of an MS exacerbation because these were present in 92.5% of cases diagnosed as such, versus only in 1 case

of a patient with MS with an alternative diagnosis ($P < .001$). Of the diagnosed MS exacerbations, more than half (58.3%) also demonstrated new or enlarging hyperintense lesions at MR imaging to support disease activity. Although we further hypothesized that the likelihood of suggesting an alternative diagnosis to an MS exacerbation based on a positive MR imaging finding would be an uncommon occurrence (ie, less than 10% of encounters), we found that MR imaging findings provided alternative diagnoses in only 7.5% of cases ($n = 5$). Most (60%) encounters not diagnosed as MS exacerbations either had no final diagnosis established or documented (23 encounters) or were diagnosed as pseudoexacerbations (18 encounters). The latter are instances in which heat, stress, or infection can cause a recurrence of MS symptoms from a previous exacerbation without underlying new inflammation or disease progression (as such these have no pathognomonic findings on MR imaging and are not treated with IV steroids).^{26,27}

Our third hypothesis was that the management decision of the treating physician would rarely be affected by MR imaging (<10% of cases). However, in 70% of encounters, the decision as to whether to admit the patient correlated with identification of AD lesions. This is explained by the significant relationship between identification of MRI imaging activity and an MS exacerbation diagnosis. Our findings suggest that while ED MR imaging has a low yield in identifying alternative diagnoses in this patient group, ruling out an MS exacerbation can avoid unnecessary hospitalization for intravenous steroid administration and its associated cost. This finding is supported by the commencement and early termination of IV methylprednisolone treatment in 2 patients in our comparison group who were admitted without ED MR imaging and were subsequently not diagnosed with MS exacerbations after inpatient scans. The difference in the length of stay on admission of patients who had ED MR imaging versus inpatient MR imaging was not statistically significant; however, the difference in the median length of stay was 0.9 days, a notable cost. Furthermore, only 8/19 (42.1%) of those patients admitted without an ED MR imaging for presumed MS exacerbation actually had the diagnosis. This finding contrasts with that in those patients having preceding ED MR imaging: 91.7% (44/48) of those with a final diagnosis of an MS exacerbation were admitted. These 44 patients represent 64.7% (44/68) of admissions in the population examined, much better than without the ED MR imaging.

The significant association between MR imaging activity and the diagnosis of an exacerbation (and therefore subsequent management decisions) appears to suggest that ED MR imaging may be worthwhile from a diagnostic standpoint for suspected MS exacerbations. However, the association raises 2 important issues that warrant further consideration.

The first issue is whether studies of different CNS locations have equal diagnostic value. While the proportion of spinal MRIs that demonstrated enhancing lesions was greater than hypothesized (20.4%), AD shown on MR imaging was limited to the spine in only 9.7% of cases (ie, MR imaging activity was not concomitantly found on MR imaging of the brain). Nonetheless, approximately two-thirds of patients had a combination of MR imaging of the brain and the cervical and thoracic spine ordered as a set from the ED. In only 7% of these instances (6/85) was the cervical spine the only imaging location to show MR imaging activity. The

value of thoracic spine MR imaging was particularly low considering that it was requested for 71% of patients with MS but was the sole MR imaging examination that showed MR imaging activity in only 4% of these encounters. The study of all 3 body parts for nearly three-quarters of our patient group must therefore be questioned in light of the low yield of spinal MR imaging as the only location of MR imaging activity. Our results suggest that a more cost-efficient MR imaging request paradigm may be represented by performing an MR imaging of the brain initially and requesting further spinal images only as needed subsequently. The management of an MS exacerbation in the form of steroid treatment is standard irrespective of the site of the exacerbation. The disadvantage of such a paradigm may be time-cost in the patient potentially requiring multiple separate MR imaging studies. However, having a radiologist review the brain MR imaging while the patient is still in the MR imaging scanner to see if additional imaging is required could avoid this limitation. Although the proportion of requested MR imaging of lumbar spine scans was relatively low (20% of encounters), these identified no findings of diagnostic value in our study population.

The second major issue that arises from these results is whether there is an over-reliance on identification of MR imaging activity as a diagnostic determinant of an MS exacerbation, even though MR imaging findings are not part of the diagnostic criteria for an MS exacerbation. If MR imaging findings are the major determining factor in whether a patient is diagnosed with an MS exacerbation, this would bias our analysis of the utility of ED MR imaging. We found that for 39% of patients (45/115), the electronic medical records explicitly indicated that a management decision to admit and/or administer intravenous steroids for an MS exacerbation was determined by findings of MR imaging activity. For example, documentation from 1 patient's neurology consultation record stated, "Steroids/admission if evidence of enhancement, otherwise discharge with outpatient follow-up." Because MR imaging results were available before neurology consultation for a substantial proportion of the study population, we suspect that our figure of 39% is actually an underestimation of the role of MR imaging in the decision-making process. These findings indicate reliance on demonstration of MR imaging activity to make a diagnosis of an MS exacerbation when patients present to the ED. Further evidence toward reliance on MR imaging is that no (nonpregnant) patient with MS presenting to the ED was admitted for treatment of an MS exacerbation without either an ED MR imaging or inpatient MR imaging, despite the current definition of MS exacerbations as a clinical diagnosis.

The use of brain and spinal ED MR imaging for making the diagnosis of an exacerbation may reflect a lack of experience or confidence among the neurology trainees and non-neurology specialists who perform the initial evaluations of these patients in the ED. In addition, the availability of an MR imaging scanner in the ED itself could be contributing to an unintentional overuse and over-reliance on such imaging. A lack of specialist experience by the physicians, heavy patient loads, staff shortages, and stringent time pressures may provoke the substitution of imaging for other clinical assessments.²⁸⁻³⁰ An over-reliance can be problematic both due to unnecessary use of an expensive resource but also because current imaging methods for detect-

ing AD are not 100% sensitive and thus may result in underdiagnosis of MS exacerbations.⁵

Further research is needed in a prospectively designed study to assess whether physicians would reach the same diagnostic decisions if they did not have access to ED MR imaging. Additionally, research should explore differences in MR imaging use by the level of physician experience, including discrepancies between neurologists, neurology trainees, and MS specialists.

Finally, this study should be viewed in the context of a number of limitations. Variability in note-taking by multiple physicians means that objective measures of MR imaging reliance were limited. This was a single-institution study at an academic medical center, so all of the study patients were initially assessed by physicians-in-training. The ability to perform statistical analyses comparing patients who had an ED MR imaging versus inpatient MR imaging was limited by the small sample size of patients in the latter group, resulting in a skewed dataset and power of only 26% at the 5% significance level. It would be of interest to further analyze discrepancies in a larger patient set. For instance, our results demonstrate that the percentage of patients with positive findings on MR imaging may be higher in patients with ED-versus-inpatient MR imaging.

This study is also limited by its retrospective study design, which means that we cannot determine what the physicians would or would not have done without the availability of MR imaging, and MR imaging results may be biasing the clinical diagnoses. This study only examined use for patients with a known MS diagnosis. The full use of ED MR imaging for MS diagnoses (ie, including for those patients not yet fulfilling the McDonald criteria for MS) was not examined in this cohort.¹⁴ Finally, we were not able to determine retrospectively the downstream impact of ED crowding when the MR imaging scanner was used, such as delays for other patients while the relatively long brain-cervical-thoracic spine MR imaging was taking place. For example, whether this impacts imaging availability for patients presenting with symptoms concerning for an acute stroke is a useful future research area for a prospective study.

CONCLUSIONS

ED MR imaging is a worthwhile endeavor from a diagnostic standpoint to assess for an MS exacerbation and has corresponding downstream impact on management decisions to admit patients and administer intravenous steroids. However, we raise the possibility that physicians may be placing undue weight on MR imaging findings relative to history and physical examination findings in diagnosing MS exacerbations. An examination of this and a full cost-benefit analysis of ED MR imaging for suspected MS exacerbations represent important avenues for future work. We further found that immediate concurrent spinal MR imaging use is a questionable addition to MR imaging of the brain due to its particularly low yield in identifying isolated spinal AD, especially in the thoracic and lumbar spine.

Disclosures: Izlem Izbudak—UNRELATED: Grants/Grants Pending: Siemens*; Other: Biogen, Comments: pending*. Ellen M. Mowry—UNRELATED: Grants/Grants Pending: Biogen, Sun Pharma, Comments: investigator-initiated trial from Biogen, site Principal Investigator of trials from Biogen and Sun Pharma*; Royalties: UptoDate, Comments: chapter editing; Other: Teva Neuroscience, Comments: free medi-

cation for clinical trial, of which I am the Principal Investigator*. David M. Yousem—UNRELATED: Medicolegal neuroradiologist expert testimony. *Payment for Lectures including service on Speakers Bureaus*: American College of Radiology Education Center; *Royalties*: book royalties for 4 books. *Payment for Development of Educational Presentations*: CMEinfo.com*. *Money paid to the institution.

REFERENCES

1. **The National Multiple Sclerosis Society**. <http://www.nmss.org/>. Accessed June 10, 2016
2. Lublin FD, Reingold SC. **Defining the clinical course of multiple sclerosis: results of an international survey—National Multiple Sclerosis Society (USA) Advisory Committee on Clinical Trials of New Agents in Multiple Sclerosis**. *Neurology* 1996;46:907–11 CrossRef Medline
3. Racke MK. **Immunopathogenesis of multiple sclerosis**. *Ann Indian Acad Neurol* 2009;12:215–20 CrossRef Medline
4. Compston A, Coles A. **Multiple sclerosis**. *Lancet* 2008;372:1502–17 CrossRef Medline
5. Lublin FD. **The incomplete nature of multiple sclerosis relapse resolution**. *J Neurol Sci* 2007;256:S14–18 CrossRef Medline
6. Frohman EM, Eagar T, Monson N, et al. **Immunologic mechanisms of multiple sclerosis**. *Neuroimaging Clin N Am* 2008;18:577–88, ix CrossRef Medline
7. Ontaneda D, Rae-Grant AD. **Management of acute exacerbations in multiple sclerosis**. *Ann Indian Acad Neurol* 2009;12:264–72 CrossRef Medline
8. Polman CH, Reingold SC, Banwell B, et al. **Diagnostic criteria for multiple sclerosis: 2010 revisions to the McDonald criteria**. *Ann Neurol* 2011;69:292–302 CrossRef Medline
9. Repovic P, Lublin FD. **Treatment of multiple sclerosis exacerbations**. *Neurol Clin* 2011;29:389–400 CrossRef Medline
10. Burton JM, O'Connor PW, Hohol M, et al. **Oral versus intravenous steroids for treatment of relapses in multiple sclerosis**. *Cochrane Database Syst Rev* 2012;12:CD006921 CrossRef Medline
11. Oynhausen S, Alcauskas M, Hannigan C, et al. **Emergency medical care of multiple sclerosis patients: primary data from the Mount Sinai resource utilization in multiple sclerosis project**. *J Clin Neurol* 2014;10:216–21 CrossRef Medline
12. Arnold DL, Matthews PM. **MRI in the diagnosis and management of multiple sclerosis**. *Neurology* 2002;58:S23–31 CrossRef Medline
13. Karussis D. **The diagnosis of multiple sclerosis and the various related demyelinating syndromes: a critical review**. *J Autoimmun* 2014;48–49:134–42 CrossRef Medline
14. McDonald WI, Compston A, Edan G, et al. **Recommended diagnostic criteria for multiple sclerosis: guidelines from the International Panel on the Diagnosis of Multiple Sclerosis**. *Ann Neurol* 2001;50:121–27 CrossRef Medline
15. Bonzano L, Roccatagliata L, Mancardi GL, et al. **Gadolinium-enhancing or active T2 magnetic resonance imaging lesions in multiple sclerosis clinical trials?** *Mult Scler* 2009;15:1043–47 CrossRef Medline
16. Nusbaum AO, Lu D, Tang CY, et al. **Quantitative diffusion measurements in focal multiple sclerosis lesions: correlations with appearance on T1-weighted MR images**. *AJR Am J Roentgenol* 2000;175:821–25 CrossRef Medline
17. Kornienko VN, Pronin IN. *Diagnostic Neuroradiology*. Berlin: Springer Berlin; 2009
18. Kermode AG, Tofts PS, Thompson AJ, et al. **Heterogeneity of blood-brain barrier changes in multiple sclerosis: an MRI study with gadolinium-DTPA enhancement**. *Neurology* 1990;40:229–35 CrossRef Medline
19. Hyland M, Bermel RA, Cohen JA. **Restricted diffusion preceding gadolinium enhancement in large or tumefactive demyelinating lesions**. *Neurol Clin Pract* 2013;3:15–21 CrossRef Medline
20. Redd V, Levin S, Toerper M, et al. **Effects of fully accessible magnetic resonance imaging in the emergency department**. *Acad Emerg Med* 2015;22:741–49 CrossRef Medline
21. Bernstein SL, Aronsky D, Duseja R, et al; Society for Academic Emergency Medicine, Emergency Department Crowding Task Force. **The effect of emergency department crowding on clinically oriented outcomes**. *Acad Emerg Med* 2009;16:1–10 CrossRef Medline
22. Gardner RL, Sarkar U, Maselli JH, et al. **Factors associated with longer ED lengths of stay**. *Am J Emerg Med* 2007;25:643–50 CrossRef Medline
23. Kocher KE, Meurer WJ, Desmond JS, et al. **Effect of testing and treatment on emergency department length of stay using a national database**. *Acad Emerg Med* 2012;19:525–34 CrossRef Medline
24. Trzeciak S, Rivers EP. **Emergency department overcrowding in the United States: an emerging threat to patient safety and public health**. *Emerg Med J* 2003;20:402–05 CrossRef Medline
25. Advanced Disease-Specific Care Certification Requirements for Comprehensive Stroke Center (CSC). http://www.jointcommission.org/assets/1/18/dsc_csc_chap.pdf. Accessed May 16, 2016
26. Thrower BW. **Relapse management in multiple sclerosis**. *Neurologist* 2009;15:1–5 CrossRef Medline
27. Wingerchuk DM, Rodriguez M. **Premenstrual multiple sclerosis pseudoexacerbations: role of body temperature and prevention with aspirin**. *Arch Neurol* 2006;63:1005–08 CrossRef Medline
28. American Academy of Pediatrics Committee on Pediatric Emergency Medicine. **Overcrowding crisis in our nation's emergency departments: is our safety net unraveling?** *Pediatrics* 2004;114:878–88 CrossRef Medline
29. Derlet RW, Richards JR. **Overcrowding in the nation's emergency departments: complex causes and disturbing effects**. *Ann Emerg Med* 2000;35:63–68 CrossRef Medline
30. Zwemer FL Jr. **Emergency department overcrowding**. *Ann Emerg Med* 2000;36:279–80 Medline

Hippocampal and Deep Gray Matter Nuclei Atrophy Is Relevant for Explaining Cognitive Impairment in MS: A Multicenter Study

 D. Damjanovic,  P. Valsasina,  M.A. Rocca,  M.L. Stromillo,  A. Gallo,  C. Enzinger,  H.E. Hulst,  A. Rovira,  N. Muhlert,  N. De Stefano,  A. Bisecco,  F. Fazekas,  M.J. Arévalo,  T.A. Yousry, and  M. Filippi



ABSTRACT

BACKGROUND AND PURPOSE: The structural MR imaging correlates of cognitive impairment in multiple sclerosis are still debated. This study assessed lesional and atrophy measures of white matter and gray matter involvement in patients with MS acquired in 7 European sites to identify the MR imaging variables most closely associated with cognitive dysfunction.

MATERIALS AND METHODS: Brain dual-echo, 3D T1-weighted, and double inversion recovery scans were acquired at 3T from 62 patients with relapsing-remitting MS and 65 controls. Patients with at least 2 neuropsychological tests with abnormal findings were considered cognitively impaired. Focal WM and cortical lesions were identified, and volumetric measures from WM, cortical GM, the hippocampus, and deep GM nuclei were obtained. Age- and site-adjusted models were used to compare lesion and volumetric MR imaging variables between patients with MS who were cognitively impaired and cognitively preserved. A multivariate analysis identified MR imaging variables associated with cognitive scores and disability.

RESULTS: Twenty-three patients (38%) were cognitively impaired. Compared with those with who were cognitively preserved, patients with MS with cognitive impairment had higher T2 and T1 lesion volumes and a trend toward a higher number of cortical lesions. Significant brain, cortical GM, hippocampal, deep GM nuclei, and WM atrophy was found in patients with MS with cognitive impairment versus those who were cognitively preserved. Hippocampal and deep GM nuclei atrophy were the best predictors of cognitive impairment, while WM atrophy was the best predictor of disability.

CONCLUSIONS: Hippocampal and deep GM nuclei atrophy are key factors associated with cognitive impairment in MS. These MR imaging measures could be applied in a multicenter context, with cognition as clinical outcome.

ABBREVIATIONS: CI = cognitively impaired; CL = cortical lesion; CP = cognitively preserved; DIR = double inversion recovery; EDSS = Expanded Disability Status Scale; HC = healthy controls; LV = lesion volumes; WCST = Wisconsin Card Sorting Test

Cognitive impairment is a frequent finding in patients with multiple sclerosis, with 40%–70% of patients showing cognitive deficits.¹ The most affected domains are attention, information-processing speed, executive functions, and memory and

visuospatial abilities.¹ Given its dramatic effect on the activities of patients' daily lives, there is a critical need to define the pathophysiological mechanisms of cognitive impairment in MS, to develop markers for its monitoring, and to identify valid therapeutic strategies.

Many studies tried to characterize the structural MR imaging correlates of cognitive impairment in patients with MS. T2 and T1 lesion volumes were found to be generally higher in patients with

Received June 8, 2016; accepted after revision August 11.

From the Neuroimaging Research Unit (D.D., P.V., M.A.R., M.F.) and Department of Neurology (M.A.R., M.F.), Institute of Experimental Neurology, Division of Neuroscience, San Raffaele Scientific Institute, Vita-Salute San Raffaele University, Milan, Italy; Center for Radiology and MRI of Clinical Center of Serbia (D.D.), Faculty of Medicine, University of Belgrade, Belgrade, Serbia; Department of Neurological and Behavioural Sciences (M.L.S., N.D.S.), University of Siena, Siena, Italy; MRI Center "SUN-FISM" (A.G., A.B.), Second University of Naples and Institute of Diagnosis and Care "Hermitage-Capodimonte," Naples, Italy; I Division of Neurology (A.G., A.B.), Department of Medical, Surgical, Neurological, Metabolic and Aging Sciences, Second University of Naples, Naples, Italy; Department of Neurology (C.E., F.F.) and Division of Neuroradiology (C.E.), Vascular and Interventional Radiology, Department of Radiology, Medical University of Graz, Graz, Austria; Department of Radiology and Nuclear Medicine (H.E.H.), MS Centre Amsterdam, VU University Medical Centre, Amsterdam, Netherlands; Magnetic Resonance Unit (A.R., M.J.A.), Department of Radiology and MS Centre of Catalonia, Hospital Universitari Vall d'Hebron, Barcelona, Spain; and NMR Research Unit (N.M., T.A.Y.), Queen Square MS Centre, University College London Institute of Neurology, London, UK.

This study has been partially supported by a grant from the Italian Ministry of Health (GR-2009-1529671). The MS Centre Amsterdam is supported by the Dutch MS Research Foundation (grant 09-538d). Dr Damjanovic was supported by an ECTRIMS-MAGNIMS fellowship.

Please address correspondence to Massimo Filippi, MD, Neuroimaging Research Unit, Institute of Experimental Neurology, Division of Neuroscience, San Raffaele Scientific Institute, Vita-Salute San Raffaele University, Via Olgettina, 60, 20132 Milan, Italy; e-mail: filippi.massimo@hsr.it

 Indicates open access to non-subscribers at www.ajnr.org

 Indicates article with supplemental on-line table.

<http://dx.doi.org/10.3174/ajnr.A4952>

MS who were cognitively impaired (CI) than in those who were cognitively preserved (CP),²⁻⁵ and poor performance on a given neuropsychological test correlated with the presence of lesions in relevant WM tracts.^{2,4,6} GM damage was also variously related to cognitive impairment in these patients. In particular, higher cortical lesion (CL) volume on double inversion recovery (DIR) sequences,^{7,8} reduced neocortical and total GM volume,^{7,9} and structural abnormalities within strategic GM regions, such as the thalamus, putamen, and hippocampus, were related to the presence and severity of cognitive symptoms.¹⁰⁻¹³

Despite the clear association between isolated measures of structural CNS damage (eg, WM lesion volume or GM volume) and cognitive performance, when multiparametric models were applied to identify the imaging correlates of cognitive impairment, conflicting results have been obtained, with some studies identifying a prominent contribution of WM damage^{5,14} and others underpinning the relevance of cortical or deep GM nuclei involvement.^{3,9,13} Additionally, composite models explaining cognitive impairment have only been tested at single sites, in selected groups of patients.¹³ Lesional and volumetric MR imaging measures of WM and GM damage might be used as outcome measures for disease-monitoring purposes, both in observational and treatment studies. However, to test the utility of these measures as objective imaging biomarkers of cognitive impairment, a validation of such multiparametric models in a multicenter setting is needed.

Here, we hypothesized that GM loss might be the most relevant contributor of cognitive impairment in MS. To test our hypothesis, we characterized the structural MR imaging correlates of cognitive impairment in a group of patients with MS acquired in 7 European sites by analyzing lesional and atrophy measures of WM and GM involvement, and we identified the set of MR imaging variables most closely associated with cognitive dysfunction.

MATERIALS AND METHODS

Ethics Committee Approval

Local ethics approval was obtained at all sites; all subjects gave written informed consent.

Subjects

Subjects were recruited from January 2009 to May 2012 as part of a project on imaging correlates of cognitive impairment in MS at 7 European centers. The results of regional analysis of GM and WM damage by using surface-based¹⁵ and voxelwise techniques¹⁶ have been previously reported.

All subjects had to be between 20 and 65 years of age. Patients had to have a diagnosis of relapsing-remitting MS,¹⁷ no relapse or corticosteroid treatment within the month before scanning, and no history of psychiatric conditions, including major depression.

The final dataset included 62 patients with MS (22/40 men/women; mean age, 39.5 ± 8.5 years; mean disease duration, 8.2 years [range, 2–33 years]; median Expanded Disability Status Scale [EDSS] score, 2.0 [range, 0.0–6.0]) and 65 healthy controls (HC) (27/38 men/women; mean age, 35.8 ± 9.4 years) (On-line Table). Sex did not differ between HC and patients with MS ($P = .7$), whereas HC were younger than patients with MS ($P = .006$).

Thus, age was included as a nuisance covariate in all statistical models.

Clinical and Neuropsychological Assessment

Within 48 hours from the MR imaging acquisition, patients with MS underwent a neurologic evaluation, with an EDSS rating and a neuropsychological assessment performed at each site by an experienced neuropsychologist unaware of the MR imaging results, using validated translations of the neuropsychological tests. Cognitive performance was assessed by using the Brief Repeatable Battery of Neuropsychological Tests,¹⁸ including the Selective Reminding Test to assess verbal memory; the 10/36 Spatial Recall Test to assess visuospatial memory; the Symbol Digit Modalities Test and the Paced Auditory Serial Addition Test 2 seconds and 3 seconds to assess attention and information processing speed; and the Word List Generation test to assess verbal fluency. As previously described,¹⁹ z scores for each of the previous domains and a global z score of cognitive function (obtained by averaging z scores of all tests) were calculated.

In addition, the Wisconsin Card Sorting Test (WCST) was administered to evaluate executive functions.²⁰ Performance on the WCST was evaluated by computing scores related to the total errors, the number of perseverative errors, and the number of perseverative responses.²⁰ Patients with a score ≥ 2 SDs below normative values in at least 1 of these measures were considered impaired on the WCST.

Patients with at least 2 abnormal test results (defined as a score ≥ 2 SDs below the normative value provided by Boringa et al²¹ for the Brief Repeatable Battery of Neuropsychological Tests and by Heaton²⁰ for the WCST) were considered CI, as previously described.¹⁶

MR Imaging Acquisition

With 3T scanners (Centers I and VI: Signa; GE Healthcare, Milwaukee, Wisconsin; Centers II, III, and IV: Magnetom Trio; Siemens, Erlangen, Germany; Centers V and VII: Intera; Philips Healthcare, Best, the Netherlands), centers performed the following brain sequences: 1) dual-echo TSE: TR = 4000–5380 ms; TE₁ = 10–23 ms; TE₂ = 90–102 ms; echo-train length = 5–11; 44 contiguous, 3-mm-thick axial sections parallel to the anterior/posterior commissure plane; matrix = 256 × 192; FOV = 240 × 180 mm² (rectangular FOV = 75%); 2) 3D T1-weighted scan: TR = 5.5–8.3 ms (for GE Healthcare/Philips Healthcare scanners) or 1900–2300 ms (for Siemens scanners); TE = 1.7–3.0 ms; flip angle = 8°–12°; 176–192 sagittal sections with thickness = 1 mm and in-plane resolution = 1 × 1 mm²; 3) double inversion recovery sequence: TR = 7500–16,000 ms; TE = 25–317 ms; TI₁ = 325–500 ms; TI₂ = 2100–3870 ms; echo-train length = 10–13; 44 contiguous, 3-mm-thick axial sections parallel to the anterior/posterior commissure plane; matrix = 256 × 192; FOV = 240 × 180 mm² (rectangular FOV = 75%), apart from Center I, which performed a 3D acquisition with 140 sagittal sections with thickness = 1.2 mm; matrix = 224 × 224; FOV = 220 × 220 mm².

MR Imaging Analysis

Center V performed central analysis of MR imaging scans. WM and GM lesions were identified by a radiologist (D.D., with 10

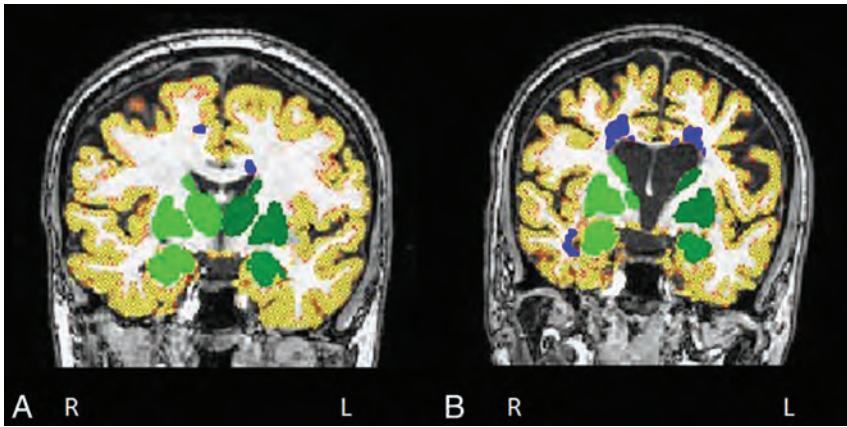


FIG 1. Illustrative examples of segmentation of cortical gray matter volume (in red-yellow), deep gray matter volume (in green), and lesions (in blue) in patients with multiple sclerosis without (A) and with (B) cognitive impairment. Images are in radiologic convention.

years of experience) supervised by a neurologist (M.A.R., with 20 years of experience). Brain T2-hyperintense and T1-hypointense lesion volumes (LV) were measured on dual-echo and 3D T1-weighted scans, respectively, by using a local thresholding segmentation technique (Jim 6.0 software; <http://www.xinapse.com/home.php>). DIR scans from Center I were first reformatted to the axial orientation and resampled to 3-mm section thickness, to standardize evaluation of DIR lesions across sites. Then, DIR images were used to count CLs according to consensus recommendations.²² CLs included the following: 1) lesions confined to the cortical ribbon without involving the underlying subcortical WM (pure intracortical lesions), and 2) mixed WM/GM lesions (type I) with a prominent extension within the GM ($\geq 75\%$). Attention was paid to the exclusion of artifacts. Pure, mixed WM/GM, and total DIR LV were calculated by using Jim software.

Normalized brain volume, normalized GM volume, normalized cortical GM volume, and normalized WM volume were measured on 3D T1-weighted scans by using FSL SIENAX (<http://fsl.fmrib.ox.ac.uk/fsl/fslwiki/SIENA>) after refilling of T1-hypointense lesions.²³ Automatic segmentation of the thalamus, caudate, putamen, pallidum, hippocampus, amygdala, and accumbens was performed on 3D T1-weighted scans by using the FMRIB Integrated Registration and Segmentation Tool (FIRST; <http://fsl.fmrib.ox.ac.uk/fsl/fslwiki/FIRST>) software (Fig 1).²⁴ The volume of these structures was multiplied by the head-normalization factor derived from SIENAX.

Statistical Analysis

Demographic and clinical characteristics, together with lesional and volumetric MR imaging variables, were reported as means and ranges, or frequencies and percentages, for continuous and categorical variables, respectively. Brain T2 and T1 LV were log-transformed due to their skewed distribution. Given the similar behavior of right and left deep GM nuclei, deep GM volumes were averaged across hemispheres before statistical analysis. This process avoided multicollinearity and reduced the number of comparisons. The normalized volume of deep GM nuclei (ie, the sum of the thalamus, caudate, putamen, pallidum, amygdala, and accumbens) was also obtained. Between-center heterogeneity of

MR imaging variables was tested by using ANOVA models for continuous variables and Pearson χ^2 tests for categorical variables (apart from CL numbers, which were entered into negative binomial models).

Comparisons between HC and patients with MS and between HC and patients with MS who were CP and CI of lesional and volumetric MR imaging quantities were performed by using age-adjusted generalized linear random-effect models, accounting for clustering (ie, subjects within the recruitment site) by using random intercepts and an unstructured covariance matrix.

Univariate correlations between clinical, neuropsychological, and lesion/volumetric MR imaging variables were also assessed by using generalized linear random-effects models, accounting for clustering by using random intercepts and an unstructured covariance matrix, adjusting for age. The effect size of correlations was reported by using standardized regression coefficients. The same modeling strategy was used to identify MR imaging variables independently associated with cognitive and EDSS scores by using a stepwise variable selection. Variables were selected by using a significance level of .10 for entry into the model and a significance level of .05 to remain in the multivariate model.

A P value $< .05$ was considered statistically significant (SAS Release 9.1.3 software; SAS Institute, Cary, North Carolina). All results were adjusted for multiple comparisons by using the false discovery rate approach.²⁵

RESULTS

Demographic, Clinical, and Neuropsychological Measures

The On-line Table summarizes the main demographic and clinical characteristics of the study subjects. No site heterogeneity was found for sex and disease duration, while age and EDSS were heterogeneous among sites (On-line Table).

Twenty-three (37%) patients with MS were CI. The domains most frequently involved were the following: attention and information-processing speed (43%), verbal memory (27%), spatial memory (21%), and fluency (16%). All patients impaired on the WCST ($n = 15$) were also classified as CI on the Brief Repeatable Battery of Neuropsychological Tests. Compared with CP patients, those with MS who were CI were significantly older ($P = .007$), whereas no difference was found for sex ($P = .2$), EDSS score ($P = .3$), disease duration ($P = .4$), and education (mean years of education, 13.7 ± 3.1 years in CP MS and 13.5 ± 3.4 years in CI MS, $P = .8$).

Lesion Findings

There was no significant between-site heterogeneity for T2 ($P = .17$), T1 ($P = .22$), and DIR ($P = .09$) LV (Table 1). The number of CLs was significantly heterogeneous among sites ($P < .001$ for total and pure CLs, $P = .07$ for mixed CLs). Compared with CP

Table 1: Lesion and volumetric MRI findings in healthy controls and patients with MS, first considered as a whole and then divided into patients who are cognitively preserved and cognitively impaired

	HC	MS	P ^a	Cognitively Preserved	Cognitively Impaired	P ^a
				Patients	Patients	
T2 LV (mL) (SD)	NA	10.6 (13.9)	NA	7.1 (9.6)	16.5 (17.8)	.01
T1 LV (mL) (SD)	NA	5.5 (5.8)	NA	3.6 (3.5)	8.7 (7.6)	.01
DIR LV (mL) (SD)	NA	0.4 (0.7)	NA	0.4 (0.9)	0.4 (0.4)	.4
Median CL (No.) (range)	NA	3 (0–33)	NA	2.0 (0–33)	6.0 (1–16)	.5 ^b
Median pure CL (No.) (range)	NA	1 (0–14)	NA	0.5 (0–14)	1.5 (0–11)	.8 ^b
Median mixed CL (No.) (range)	NA	2 (0–19)	NA	1.0 (0–19)	4.0 (0–9)	.9 ^b
NBV (mL) (SD)	1533 (79)	1436 (145)	<.001	1460 (98)	1395 (113)	.006
NGMV (mL) (SD)	826 (56)	776 (67)	.0002	793 (68)	748 (57)	.02
NCGMV (mL) (SD)	638 (48)	599 (53)	.0004	612 (55)	578 (43)	.02
NWMV (mL) (SD)	706 (40)	659 (68)	<.001	667 (54)	645 (88)	.03
Total normalized deep GM volume (mL) (SD)	28.1 (1.7)	24.7 (3.1)	<.001	25.8 (2.4)	23.0 (3.5)	<.001
Average normalized thalamus volume (mL) (SD)	11.1 (0.7)	9.7 (1.3)	<.001	10.1 (1.0)	9.0 (1.4)	.0007
Average normalized caudate volume (mL) (SD)	5.0 (0.5)	4.4 (0.7)	<.001	4.5 (0.6)	4.1 (0.7)	.02
Average normalized putamen volume (mL) (SD)	6.8 (0.6)	6.1 (0.9)	<.001	6.5 (0.7)	5.5 (0.9)	<.001
Average normalized pallidum volume (mL) (SD)	2.5 (0.3)	2.2 (0.2)	<.001	2.3 (0.1)	2.1 (0.3)	.05
Average normalized hippocampus volume (mL) (SD)	5.3 (0.4)	4.8 (0.6)	<.001	5.0 (0.5)	4.5 (0.7)	.004
Average normalized amygdala volume (mL) (SD)	1.8 (0.3)	1.6 (0.3)	.001	1.7 (0.3)	1.5 (0.3)	.05
Average normalized accumbens volume (mL) (SD)	0.7 (0.1)	0.6 (0.1)	.004	0.6 (0.1)	0.5 (0.1)	.01

Note:—NA indicates not applicable; NBV, normalized brain volume; NGMV, normalized GM volume; NCGMV, normalized cortical GM volume; NWMV, normalized WM volume.

^a Age- and site-adjusted linear mixed-effect model with random intercept for recruitment site.

^b Age-adjusted negative binomial mixed-effect model with random intercept for recruitment site (false discovery rate–corrected).

Table 2: Correlations between lesion and volumetric MRI measures of WM and GM with clinical and neuropsychological variables (age-adjusted linear mixed-effect model with random intercept for recruitment site, false discovery rate–corrected)^a

MRI Measure	Global Cognitive Z Score	Attention Z Score	Visual Memory Z Score	Executive Functions (WCSTpr)	EDSS
T2 LV	−0.35 (.01)	−0.33 (.008)	−0.34 (.03)	−0.25 (.06)	NS
T1 LV	−0.31 (.02)	−0.31 (.01)	−0.33 (.03)	−0.28 (.05)	NS
NBV	0.44 (.01)	0.44 (.001)	0.35 (.03)	NS	−0.33 (.01)
NGMV	0.36 (.01)	0.31 (.01)	NS	NS	NS
NCGMV	0.42 (.01)	0.36 (.01)	NS	NS	NS
NWMV	0.37 (.01)	0.40 (.004)	0.35 (.03)	NS	−0.35 (.008)
Total normalized deep GM volume	0.40 (.001)	0.47 (<.001)	0.33 (.04)	NS	−0.29 (.03)
Average normalized thalamus volume	0.36 (.002)	0.41 (.0005)	0.30 (.05)	NS	NS
Average normalized caudate volume	0.40 (.001)	0.50 (<.001)	NS	NS	NS
Average normalized putamen volume	0.40 (.001)	0.46 (.0001)	0.37 (.03)	NS	−0.30 (.03)
Average normalized pallidum volume	0.25 (.03)	0.34 (.003)	NS	NS	−0.35 (.01)
Average normalized hippocampus volume	0.39 (.001)	0.34 (.003)	NS	NS	NS
Average normalized amygdala volume	0.33 (.01)	0.33 (.01)	NS	NS	NS
Average normalized accumbens volume	0.32 (.009)	0.36 (.003)	NS	NS	NS

Note:—NS indicates not significant; WCSTpr, Wisconsin Card Sorting Test, number of perseverative responses; NBV, normalized brain volume; NGMV, normalized GM volume; NCGMV, normalized cortical GM volume; NWMV, normalized WM volume.

^a Correlations are reported as standardized coefficients (to include size effect), and P values are reported in parentheses.

patients, those with MS who were CI had higher T2 and T1 LV, whereas DIR LV and the number of CLs did not differ between groups (Table 1).

Volumetric MR Imaging Findings

Normalized brain volume, normalized GM volume, normalized cortical GM volume, and normalized white matter volume were significantly heterogeneous across sites ($P = <.001-.04$), while this was not the case in deep GM nuclei volumes, apart from the amygdala ($P < .001$). Volumes of deep GM nuclei were similar to those obtained in previous studies.^{26,27} All structures were atrophied in patients with MS compared with HC ($P < .001$) and in patients with MS who were CI versus CP (Table 1).

Analysis of Correlation

T2 LV and T1 LV were significantly correlated with global and partial cognitive scores, but not with EDSS (Table 2). Lower nor-

malized brain volume was associated with worse neuropsychological scores and higher disability. When looking at brain tissue compartments (ie, WM and GM), we found that EDSS was correlated with normalized white matter volume, whereas the highest correlation with the global cognitive score was found with decreased normalized cortical GM volume (Table 2). Decreased volumes of all deep GM nuclei and the hippocampus were significantly associated with global and attention neuropsychological scores. Lower putamen and pallidum volumes were correlated with higher EDSS scores. There were no significant correlations between MR imaging measures and disease duration, verbal memory, or fluency z scores. Furthermore, no correlation was found between CLs and clinical/neuropsychological measures.

The multivariate analysis retained average hippocampal volume (explained variance = 15%, $P = .0002$) as the best predictor of global cognitive z scores, normalized volume of deep GM nuclei (explained variance = 19%, $P < .001$) as the best predictor of

attention z scores, normalized brain volume (explained variance = 10%, $P = .006$) as the best predictor of visual memory z scores, and normalized WM volume (explained variance = 8%, $P = .008$) as the best predictor of EDSS scores.

DISCUSSION

This is one of the first multicenter studies characterizing lesion and volumetric MR imaging correlates of cognitive impairment in patients with MS, to our knowledge. More severe damage of both WM and GM compartments was found in patients with MS who were CI compared with CP, despite similar levels of clinical disability. WM lesion volume and GM atrophy were both correlated with the severity of cognitive deficits, supporting the notion that different substrates contribute to cognitive dysfunction. However, on multivariate analysis, measures of GM volume were identified as the best correlate of global cognitive impairment. Overall, our results suggest that volumes of the hippocampus and deep GM nuclei may be reliable biomarkers of cognitive impairment in MS and might be used in multicenter observational or treatment studies.

In agreement with the results of previous studies,^{2-4,18} we found that both T2 and T1 LV were higher in patients with MS who were CI than CP. This finding seems to indicate that disconnection, caused by focal WM damage, may represent one of the factors contributing to the development of cognitive impairment in MS.⁴ Hyperintensities on T2-weighted MR imaging have a relatively low pathologic specificity because they relate to a variety of processes, while T1 hypointensities seem to be more closely associated with severe demyelination and axonal loss.²⁸ The significantly higher T1 LV we found in CI versus CP MS suggest that not only the extent but also the severity of damage within MS lesions might be relevant in determining cognitive decline in these patients.

Contrary to our expectations, we found only a nonsignificant trend toward a higher number of CLs in patients with MS who were CI compared with CP. This is in contrast to results of previous studies,^{7,8} which reported associations between the number and volume of CLs and cognitive impairment. At least 2 factors could help explain this discrepancy. First, DIR sequences can be challenging to standardize across scanners, and in this study, they were acquired with different geometry (3D versus 2D) and parameters across sites. These differences may have contributed to the heterogeneity of CL counts and volumes seen across sites. In comparison, dual-echo and 3D T1-weighted scans were acquired with a relatively standardized protocol, and T2 and T1 LV were accordingly similar among sites. Second, DIR sequences are more prone to artifacts than T2- and T1-weighted sequences, which can impact the detection of CLs.²²

GM atrophy can also contribute to cognitive symptoms in MS. In line with previous studies, we found significantly reduced cortical, hippocampal, and deep GM volumes in patients with MS who were CI compared with CP. Reduced neocortical volume^{2,3,7,9} and a widespread pattern of regional GM atrophy^{15,16,29} have been frequently associated with cognitive impairment in MS, as also shown by a previous investigation of the same patient cohort.¹⁶ GM pathology is known to be substantially present in MS from the earliest stages of the disease and is strongly

associated with CI not only in cross-sectional but also in longitudinal studies.³⁰ GM pathology has traditionally been thought to occur secondary to injury from focal WM lesions (so-called Wallerian degeneration), but recent studies have convincingly shown that cortical inflammatory pathology from subpial demyelination also plays a critical role.^{31,32}

Another interesting result was the widespread volume loss we found in CI compared with CP MS in deep GM nuclei and the hippocampus. This finding confirms a previous voxelwise investigation of the same cohort,¹⁶ which showed that hippocampal atrophy was among the best MR imaging variables discriminating patients with MS who were CI from those who were CP. The thalamus, hippocampus, and striatal structures represent convergence points across multiple cortical, limbic, brain stem, and cerebellar systems and have a key role for efficient information processing.³³ Because a decrease in information-processing speed is one of the main features of cognitive impairment in MS,³⁴ damage to these structures has frequently been linked to cognitive impairment.^{10,11,13} Remarkably, even if we found a significant correlation between thalamic atrophy and CI, our multivariate model indicated a major role of the hippocampus in explaining cognitive deficits. This finding partially conflicts with findings in previous studies.^{10,11} However, these studies did not perform a direct comparison of the relative contribution of thalamic and hippocampal atrophy with cognitive impairment. On the other hand, hippocampal injury has been associated not only with memory deficits^{35,36} but also with impaired visuospatial or verbal memory abilities.^{12,36}

Our results indicated that most cognitive scores were correlated with higher T2 and T1 LV. This result was not the case for the EDSS, which did not correlate with lesion extent in univariate models. Moreover, univariate correlations showed that cognitive and clinical disability scores were associated with decreased global and deep GM volumes. Most interesting, multivariate correlations showed that cognitive scores were best predicted by hippocampal and deep GM loss, whereas WM loss was the most significant contributor to the EDSS score. Although we cannot exclude GM volume loss of critical cortical regions (eg, the motor cortex) also contributing to the EDSS score, the high relevance to clinical disability from normalized WM volume suggests that demyelination and the consequent disruption of WM pathways play an important role in explaining clinical (and in particular, locomotor) disability. Conversely, cortical, hippocampal, and deep GM nuclei atrophy in patients with MS was more closely associated with cognitive scores than WM atrophy. This result is in line with several previous studies,^{2,3,9} including a previous voxelwise investigation of the same cohort.¹⁶ This similarity suggests that the findings hold across a wide spectrum of the MS population. Moreover, because normalized cortical GM volume and normalized volume of deep GM nuclei predict cognitive deterioration with time,^{27,37} they might be used as reliable outcome measures in multicenter observational or treatment studies of cognitive impairment in MS.

Our study has limitations. First, the DIR acquisition protocol was not fully standardized across sites. Second, multicenter, longitudinal observations, including larger cohorts of patients with MS at different stages of the disease, are needed to validate our

findings and to define how the development of GM and WM damage contributes to the evolution of cognitive impairment with time. Third, clinical disability was measured by using the EDSS, which is strongly weighted toward locomotor dysfunction. Composite scores (such as the Multiple Sclerosis Functional Composite) might have provided a more comprehensive evaluation of clinical impairment. Finally, we limited our analysis to a subset of possible MR imaging variables (lesions and atrophy of whole-tissue compartments), which are likely to be sensitive to only some of the pathologic substrates of the disease. Further studies should assess the added contribution of microstructural WM damage or intrinsic damage within lesions, for example, by diffusion tensor imaging or other quantitative MR imaging techniques.

CONCLUSIONS

Our study shows that GM atrophy is critical for explaining cognitive impairment in MS. If an adequate standardization of MR imaging acquisition and analysis is performed, lesional and atrophy measures of GM and WM might be used as biomarkers in future multicenter observational and treatment studies of cognitive impairment in MS.

ACKNOWLEDGMENTS

The authors are grateful to Dr Massimiliano Copetti for assisting in the statistical analysis.

Disclosures: Dusan Damjanovic—RELATED: Dr Damjanovic was supported by an ECTRIMS-MAGNIMS fellowship. Paola Valsasina—UNRELATED: Payment for Lectures including service on Speakers Bureaus: Excellence in Medical Education. Maria A. Rocca—RELATED: Grant: This study has been partially supported by a grant from the Italian Ministry of Health (GR-2009-152967). UNRELATED: Payment for Lectures including service on Speakers Bureaus: Biogen, Novartis, Teva, and Genzyme. Antonio Gallo—UNRELATED: Payment for Lectures including service on Speakers Bureaus: Biogen, Teva, Merck Serono, Novartis, Genzyme. Hanneke E. Hulst—UNRELATED: Consultancy: Merck Serono, Genzyme, Novartis*; Grants/Grants Pending: Dutch MS Research Foundations*; Payment for Lectures including service on Speakers Bureaus: Merck Serono, Genzyme, Roche*. Alex Rovira—UNRELATED: Consultancy: Novartis, Genzyme, Olea, Biogen; Payment for Lectures including service on Speakers Bureaus: Novartis, Teva, Stendhal, Bayer, Bracco, Genzyme, Biogen; Payment for Development of Educational Presentations: Teva, Biogen, Stendhal, Genzyme. Nicola De Stefano—UNRELATED: Consultancy: Schering, Biogen, Teva, Novartis, Genzyme, Roche, and Merck Serono; Grants/Grants Pending: Italian MS Society*; Payment for Lectures including service on Speakers Bureaus: Schering, Biogen, Teva, Novartis, Genzyme, Roche, and Merck Serono; Travel/Accommodations/Meeting Expenses Unrelated to Activities Listed: Schering, Biogen, Teva, Novartis, Genzyme, Roche, and Merck Serono. Tarek A. Youssry—UNRELATED: Board Membership: Biogen*; Consultancy: IXICO*; Grants/Grants Pending: GlaxoSmithKline, Biogen, Novartis*; Payment for Lectures including service on Speakers Bureaus: Novartis. Massimo Filippi—RELATED: Grant: This study has been partially supported by a grant from the Italian Ministry of Health (GR-2009-152967); UNRELATED: Board Membership: Teva; Consultancy: Biogen, Excellence in Medical Education, Novartis, and Teva; Grants/Grants Pending: Biogen, Teva, Novartis*; Payment for Lectures including service on Speakers Bureaus: Biogen, Excellence in Medical Education, Novartis, and Teva. *Money paid to the institution.

REFERENCES

- Chiaravallotti ND, DeLuca J. **Cognitive impairment in multiple sclerosis.** *Lancet Neurol* 2008;7:1139–51 CrossRef Medline
- Lazeron RH, Boringa JB, Schouten M, et al. **Brain atrophy and lesion load as explaining parameters for cognitive impairment in multiple sclerosis.** *Mult Scler* 2005;11:524–31 CrossRef Medline
- Benedict RH, Bruce JM, Dwyer MG, et al. **Neocortical atrophy, third ventricular width, and cognitive dysfunction in multiple sclerosis.** *Arch Neurol* 2006;63:1301–06 CrossRef Medline
- Rossi F, Giorgio A, Battaglini M, et al. **Relevance of brain lesion location to cognition in relapsing multiple sclerosis.** *PLoS One* 2012; 7:e44826 CrossRef Medline
- Hulst HE, Steenwijk MD, Versteeg A, et al. **Cognitive impairment in MS: impact of white matter integrity, gray matter volume, and lesions.** *Neurology* 2013;80:1025–32 CrossRef Medline
- Mesaros S, Rocca MA, Kacar K, et al. **Diffusion tensor MRI tractography and cognitive impairment in multiple sclerosis.** *Neurology* 2012;78:969–75 CrossRef Medline
- Calabrese M, Agosta F, Rinaldi F, et al. **Cortical lesions and atrophy associated with cognitive impairment in relapsing-remitting multiple sclerosis.** *Arch Neurol* 2009;66:1144–50 Medline
- Roosendaal SD, Moraal B, Pouwels PJ, et al. **Accumulation of cortical lesions in MS: relation with cognitive impairment.** *Mult Scler* 2009; 15:708–14 CrossRef Medline
- Amato MP, Bartolozzi ML, Zipoli V, et al. **Neocortical volume decrease in relapsing-remitting MS patients with mild cognitive impairment.** *Neurology* 2004;63:89–93 CrossRef Medline
- Schoonheim MM, Hulst HE, Brandt RB, et al. **Thalamus structure and function determine severity of cognitive impairment in multiple sclerosis.** *Neurology* 2015;84:776–83 CrossRef Medline
- Biseco A, Rocca MA, Pagani E, et al; MAGNIMS Network. **Connectivity-based parcellation of the thalamus in multiple sclerosis and its implications for cognitive impairment: a multicenter study.** *Hum Brain Mapp* 2015;36:2809–25 CrossRef Medline
- Longoni G, Rocca MA, Pagani E, et al. **Deficits in memory and visuospatial learning correlate with regional hippocampal atrophy in MS.** *Brain Struct Funct* 2015;220:435–44 CrossRef Medline
- Daams M, Steenwijk MD, Schoonheim MM, et al. **Multi-parametric structural magnetic resonance imaging in relation to cognitive dysfunction in long-standing multiple sclerosis.** *Mult Scler* 2016;22: 608–19 CrossRef Medline
- Sanfilippo MP, Benedict RH, Weinstock-Guttman B, et al. **Gray and white matter brain atrophy and neuropsychological impairment in multiple sclerosis.** *Neurology* 2006;66:685–92 CrossRef Medline
- Tillema JM, Hulst HE, Rocca MA, et al; MAGNIMS Study Group. **Regional cortical thinning in multiple sclerosis and its relation with cognitive impairment: a multicenter study.** *Mult Scler* 2016;22: 901–09 CrossRef Medline
- Preziosa P, Rocca MA, Pagani E, et al; MAGNIMS Study Group. **Structural MRI correlates of cognitive impairment in patients with multiple sclerosis: a multicenter study.** *Hum Brain Mapp* 2016;37: 1627–44 CrossRef Medline
- Polman CH, Reingold SC, Banwell B, et al. **Diagnostic criteria for multiple sclerosis: 2010 revisions to the McDonald criteria.** *Ann Neurol* 2011;69:292–302 CrossRef Medline
- Rao SM, Leo GJ, Houghton VM, et al. **Correlation of magnetic resonance imaging with neuropsychological testing in multiple sclerosis.** *Neurology* 1989;39:161–66 CrossRef Medline
- Sepulcre J, Vanotti S, Hernández R, et al. **Cognitive impairment in patients with multiple sclerosis using the Brief Repeatable Battery Neuropsychology Test.** *Mult Scler* 2006;12:187–95 CrossRef Medline
- Heaton RK, Chelune GJ, Talley JL, et al. *Wisconsin Card Sorting Test Manual: Revised and Expanded.* Odessa, Florida: Psychological Assessment Resources; 1993
- Boringa JB, Lazeron RH, Reuling IE, et al. **The Brief Repeatable Battery of Neuropsychological Tests: normative values allow application in multiple sclerosis clinical practice.** *Mult Scler* 2001;7:263–67 CrossRef Medline
- Geurts JJ, Roosendaal SD, Calabrese M, et al; MAGNIMS Study Group. **Consensus recommendations for MS cortical lesion scoring using double inversion recovery MRI.** *Neurology* 2011;76:418–24 CrossRef Medline
- Chard DT, Jackson JS, Miller DH, et al. **Reducing the impact of white matter lesions on automated measures of brain gray and white matter volumes.** *J Magn Reson Imaging* 2010;32:223–28 CrossRef Medline
- Patenaude B, Smith SM, Kennedy DN, et al. **A Bayesian model of**

- shape and appearance for subcortical brain segmentation. *Neuroimage* 2011;56:907–22 CrossRef Medline
25. Benjamini Y, Hochberg Y. **Controlling the false discovery rate: a practical and powerful approach to multiple testing.** *J R Stat Soc Ser B* 1995;57:289–300
 26. Debernard L, Melzer TR, Alla S, et al. **Deep grey matter MRI abnormalities and cognitive function in relapsing-remitting multiple sclerosis.** *Psychiatry Res* 2015;234:352–61 CrossRef Medline
 27. Uddin MN, Lebel RM, Seres P, et al. **Spin echo transverse relaxation and atrophy in multiple sclerosis deep gray matter: a two-year longitudinal study.** *Mult Scler* 2016;22:1133–43 CrossRef Medline
 28. van Waesberghe JH, Kamphorst W, De Groot CJ, et al. **Axonal loss in multiple sclerosis lesions: magnetic resonance imaging insights into substrates of disability.** *Ann Neurol* 1999;46:747–54 CrossRef Medline
 29. Riccitelli G, Rocca MA, Pagani E, et al. **Cognitive impairment in multiple sclerosis is associated to different patterns of gray matter atrophy according to clinical phenotype.** *Hum Brain Mapp* 2011;32:1535–43 CrossRef Medline
 30. Rocca MA, Amato MP, De Stefano N, et al; MAGNIMS Study Group. **Clinical and imaging assessment of cognitive dysfunction in multiple sclerosis.** *Lancet Neurol* 2015;14:302–17 CrossRef Medline
 31. Louapre C, Govindarajan ST, Gianni C, et al. **Beyond focal cortical lesions in MS: an in vivo quantitative and spatial imaging study at 7T.** *Neurology* 2015;85:1702–09 CrossRef Medline
 32. Mainero C, Louapre C. **Meningeal inflammation in multiple sclerosis: the key to the origin of cortical lesions?** *Neurology* 2015;85:12–13 CrossRef Medline
 33. Leyden J, Kleinig T. **The role of the basal ganglia in data processing.** *Med Hypotheses* 2008;71:61–64 CrossRef Medline
 34. Denney DR, Lynch SG, Parmenter BA, et al. **Cognitive impairment in relapsing and primary progressive multiple sclerosis: mostly a matter of speed.** *J Int Neuropsychol Soc* 2004;10:948–56 Medline
 35. Sicotte NL, Kern KC, Giesser BS, et al. **Regional hippocampal atrophy in multiple sclerosis.** *Brain* 2008;131:1134–41 CrossRef Medline
 36. Sacco R, Bisecco A, Corbo D, et al. **Cognitive impairment and memory disorders in relapsing-remitting multiple sclerosis: the role of white matter, gray matter and hippocampus.** *J Neurol* 2015;262:1691–97 CrossRef Medline
 37. Amato MP, Portaccio E, Goretti B, et al. **Association of neocortical volume changes with cognitive deterioration in relapsing-remitting multiple sclerosis.** *Arch Neurol* 2007;64:1157–61 CrossRef Medline

Influence of Small Vessel Disease and Microstructural Integrity on Neurocognitive Functioning in Older Individuals: The DANTE Study Leiden

J.E.F. Moonen, J.C. Foster-Dingley, A.A. van den Berg-Huijsmans, W. de Ruijter, A.J.M. de Craen, J. van der Grond, and R.C. van der Mast



ABSTRACT

BACKGROUND AND PURPOSE: Small vessel disease is a major cause of neurocognitive dysfunction in the elderly. Small vessel disease may manifest as white matter hyperintensities, lacunar infarcts, cerebral microbleeds, and atrophy, all of which are visible on conventional MR imaging or as microstructural changes determined by diffusion tensor imaging. This study investigated whether microstructural integrity is associated with neurocognitive dysfunction in older individuals, irrespective of the conventional features of small vessel disease.

MATERIALS AND METHODS: The study included 195 participants (75 years of age or older) who underwent conventional 3T MR imaging with DTI to assess fractional anisotropy, mean diffusivity, axial diffusivity, and radial diffusivity. Cognitive tests were administered to assess cognitive domains, and the Geriatric Depression Scale-15 and Apathy Scale of Starkstein were used to assess symptoms of depression and apathy, respectively. The association between DTI measures and neurocognitive function was analyzed by using linear regression models.

RESULTS: In gray matter, a lower fractional anisotropy and higher mean diffusivity, axial diffusivity, and radial diffusivity were associated with worse executive function, psychomotor speed, and overall cognition and, in white matter, also with memory. Findings were independent of white matter hyperintensities, lacunar infarcts, and cerebral microbleeds. However, after additional adjustment for normalized brain volume, only lower fractional anisotropy in white and gray matter and higher gray matter radial diffusivity remained associated with executive functioning. DTI measures were not associated with scores on the Geriatric Depression Scale-15 or the Apathy Scale of Starkstein.

CONCLUSIONS: Microstructural integrity was associated with cognitive but not psychological dysfunction. Associations were independent of the conventional features of small vessel disease but attenuated after adjusting for brain volume.

ABBREVIATIONS: AD = axial diffusivity; GDS = Geriatric Depression Scale; FA = fractional anisotropy; MD = mean diffusivity; RD = radial diffusivity; SVD = small vessel disease; WMH = white matter hyperintensity

The occurrence of small vessel disease (SVD), seen on conventional MR imaging as white matter hyperintensities (WMHs), lacunar infarcts, cerebral microbleeds, and brain atrophy,¹ increases with advancing age.² SVD is a major cause of cognitive³ and possibly psychological dysfunction.⁴ Nevertheless, the rela-

tionship between these overt signs of SVD and cognitive and psychological dysfunction is modest, and interindividual variability is high. It is suggested that these visible lesions represent only the tip of the iceberg and that SVD may also cause more subtle and diffuse microstructural changes in the brain. Microstructural integrity can be determined with diffusion tensor imaging, which measures the diffusion of cerebral water molecules. Diffusion changes have been observed not only in lesions visible on standard MR imaging but also in the surrounding normal-appearing brain tissue.⁵⁻⁷ The pathologic processes underlying changes in DTI measures include axonal degeneration and

Received December 23, 2015; accepted after revision July 20, 2016.

From the Departments of Psychiatry (J.E.F.M., J.C.F.-D., R.C.v.d.M.), Radiology (A.A.v.d.B.-H., J.v.d.G.), Public Health and Primary Care (W.d.R.), and Gerontology and Geriatrics (A.J.M.d.C.), Leiden University Medical Center, Leiden, the Netherlands; and Department of Psychiatry (R.C.v.d.M.), Collaborative Antwerp Psychiatric Research Institute, University of Antwerp, Antwerp, Belgium.

J.E.F. Moonen and J.C. Foster-Dingley contributed equally.

The authors take full responsibility for the integrity of the data and analyses.

This study was supported by a grant from the Netherlands Organization for Health Research and Development (ZonMW) and Program Priority Medicines for the Elderly (No. 40-41600-98-9014).

The funding organization played no role in the design, conduct, or analysis of the study.

Please address correspondence to Justine E.F. Moonen, MD, Department of Psychiatry, Leiden University Medical Center, PO Box 10392, 2300 WB, Leiden, the Netherlands; e-mail: j.e.f.moonen@lumc.nl

Indicates open access to non-subscribers at www.ajnr.org

Indicates article with supplemental on-line tables.

<http://dx.doi.org/10.3174/ajnr.A4934>

ischemic demyelination,^{7,8} which may lead to disruption of white matter tracts that connect brain regions involved in cognitive functions.

DTI measures of WM microstructural integrity may have additional value in explaining the variance in cognitive function beyond conventional MR imaging features of SVD.⁹ It has also been shown that microstructural integrity is an independent predictor of cognitive function beyond other features of SVD. Cross-sectional studies in older individuals (mean age, 60–70 years) found that diffusion signal abnormality in WMHs, and particularly in normal-appearing white matter, was associated with cognitive dysfunction, irrespective of WMHs, lacunar infarcts, or brain volume.^{10–12} A longitudinal study in older individuals (mean age, 74 years) demonstrated that diffusion signal abnormalities in normal-appearing gray or white brain tissue, rather than in WMHs, predicted faster cognitive decline 3 years later, regardless of conventional SVD features.¹³ Furthermore, a cross-sectional study (mean age, 69 years) found that compared with controls, older individuals with psychological dysfunction had diffusion signal abnormalities, even after the exclusion of WMHs from the DTI measurements.¹⁴

Currently, no data are available for determining the role of microstructural integrity as an independent predictor of neurocognitive function in the oldest elderly individuals, in whom overt features of SVD and, in particular, atrophy are more prevalent. Therefore, this cross-sectional study investigated whether microstructural integrity is independently associated with cognitive and psychological dysfunction in an older population (mean age, 81 years) beyond other features of SVD.

MATERIALS AND METHODS

Participants

Participants for this cross-sectional study were included from the MR imaging substudy of the Discontinuation of Antihypertensive Treatment in Elderly People on Cognitive Functioning (DANTE) Study Leiden.¹⁵ Between June 2011 and August 2013, community-dwelling persons were included when they were 75 years of age or older, had a Mini Mental State Examination score between 21 and 27, were on antihypertensive medication, and had a current systolic blood pressure of ≤ 160 mm Hg. Excluded from the present study were participants with a clinical diagnosis of dementia, current angina pectoris, cardiac arrhythmia, heart failure, myocardial infarction, or a coronary reperfusion procedure ≤ 3 years ago and a history of stroke or transient ischemic attack. A detailed description of the procedures used has been published previously.¹⁵

The Medical Ethical Committee of the Leiden University Medical Center approved the study, and written informed consent was obtained from all participants.

A total of 236 participants underwent MR imaging of the brain, of whom 16 were excluded due to incidental MR imaging findings (cortical infarcts, $n = 8$; aneurysms, $n = 2$; normal pressure hydrocephalus, $n = 2$; meningioma, $n = 1$; cavernoma, $n = 2$; internal carotid artery occlusion, $n = 1$). After an additional 25 were excluded due to DTI of insufficient quality, 195 participants were available for the present analyses.

Data Acquisition

Demographic and Clinical Characteristics. Demographic characteristics were assessed at baseline by using a standardized interview, and blood pressure was measured.¹⁵ General practitioners used structured questionnaires to obtain medical history and medication use.

MR Imaging Acquisition and Processing. All MR images were acquired on a whole-body Achieva MR imaging system operating at a field strength of 3T (Philips Healthcare, Best, the Netherlands), equipped with a 32-channel head coil. DTI was acquired with TR/TE = 9592/56 ms, flip angle = 90°, FOV = 220 × 220 × 128 mm, matrix size = 112 × 110, voxel dimension = 2 mm (isotropic), 64 sections, 32 measurement directions, $b = 1000$. MR images were analyzed with the FMRIB Software Library, Version 5.0.1. (FSL (<http://www.fmrib.ox.ac.uk/fsl>)). With the Diffusion Toolbox in FMRIB (<http://fsl.fmrib.ox.ac.uk/fsl/fslwiki/FDT>), individual fractional anisotropy (FA), mean diffusivity (MD), axial diffusivity (AD), and radial diffusivity (RD) images were created.¹⁶ Using the FMRIB Linear Image Registration Tool (FLIRT; <http://www.fmrib.ox.ac.uk/>) as a non-diffusion-weighted reference volume, we correlated original images for the effects of head movement and eddy currents in the gradient coils. A diffusion tensor model was fitted to the corrected images to create individual FA, MD, AD, and RD images. For global quantification of brain tissue FA, MD, AD, and RD in white or gray brain tissue (which included WMH and other features of SVD), we skull-stripped,¹⁷ segmented,¹⁸ and aligned 3D T1 images into the Montreal Neurological Institute 152 standard space by using FLIRT. Lower FA and higher MD, AD, and RD indicated poorer microstructural integrity.

Microbleeds were assessed by using T2*-weighted MR imaging (TR/TE = 45/31 ms, flip angle = 13°, FOV = 250 × 175 × 112 mm, voxel dimension = 0.8 mm, isotropic) and were defined as focal areas of signal void (on T2-MR imaging), which increased in size on T2*-weighted images (blooming effect) compared with the corresponding T2-weighted images (TR/TE = 4200/80 ms, flip angle = 90°, FOV = 224 × 180 × 144 mm, matrix size = 448 × 320, 40 sections, 3.6 mm thick). Symmetric hypointensities in the basal ganglia, likely representing nonhemorrhagic iron deposits, were disregarded. MR imaging acquisition; image processing; and analysis of WMH volume, brain volume, and lacunar infarcts have been described previously.^{19,20}

Cognitive and Psychological Function

Global cognitive function was assessed with the Mini-Mental State Examination. Scores range from 0 to 30 points with higher scores indicating better performance.²¹ A battery of cognitive tests was administered from which cognitive domain compound scores were calculated.¹⁵ Executive function was assessed with the interference score of the abbreviated Stroop Color and Word Test²² and by the difference between the time to complete the Trail-Making Test A and B.²³ Memory was measured by using the immediate (3 trials) and delayed recall (1 trial) on the 15-Word Verbal Learning Test and the Visual Association Test.²⁴ Psychomotor speed was evaluated with the Letter Digit Substitution Test.²⁵ These 6 tests were combined in the overall cognition com-

pond score. The Geriatric Depression Scale (GDS)-15²⁶ was used to measure symptoms of depression (range, 0–15 points, with higher scores indicating more symptoms), and the Apathy Scale of Starkstein,²⁷ to measure symptoms of apathy (range, 0–42 points, with higher scores indicating more symptoms).

Statistical Analysis

Characteristics of the participants are presented as mean \pm SD, median (interquartile range), or as number (percentage), where appropriate. Education was dichotomized at primary education (6 years of schooling).

The distribution of WMH volume was skewed, which required transformation by a natural logarithm. Linear models were used in which DTI measures in white and gray matter (standardized FA, MD, AD, and RD) were entered as independent variables; and standardized cognitive domain scores or GDS-15 and Apathy Scale of Starkstein scores were entered as dependent variables. In model 1, these analyses were adjusted for age, sex, and education; model 2 included these same variables plus the number of lacunar infarcts and number of microbleeds and WMH volume; and in model 3, normalized brain volume was added.

The *F* test was used to compare the fit (the R^2 ; explained variance) of the different models. Voxelwise statistical analyses of the FA, MD, RD, and AD data were performed by using Tract-Based Spatial Statistics (TBSS; <http://fsl.fmrib.ox.ac.uk/fsl/fslwiki/TBSS>),²⁸ part of FSL. TBSS projects the FA data of all subjects onto a mean FA tract skeleton, before applying voxelwise cross-subject statistics.

Exploratory local DTI analyses were performed in the hippocampus,^{29,30} thalamus,³¹ putamen,^{20,32,33} and pre- and post-central gyrus,^{31,33} because previous studies associated these areas with cognitive dysfunction. To explore the associations between DTI measures in white and gray matter and the features of SVD, we adjusted linear or logistic regression models for age and sex.

The SPSS software for Windows (Version 20.0.0.1; IBM, Armonk, New York) was used for statistical analyses. A *P* value $<$.05 was considered statistically significant.

RESULTS

Demographic and Clinical Characteristics

The Table presents the characteristics of the study population; the mean age was 80.7 \pm 4.1 years, and 41.5% were men.

DTI Measures and SVD

In white matter, the FA, MD, AD, and RD were all related to WMHs, lacunar infarcts, cerebral microbleeds, and normalized brain volume (all $P <$.01) (On-line Table 1). In gray matter, a higher FA was associated with a lower volume of WMH and fewer lacunar infarcts. In addition, in gray matter, higher MD, AD, and RD were associated with the presence of lacunar infarcts and microbleeds and, most strongly, with a lower normalized brain volume.

DTI Measures and Cognitive and Psychological Function

On-line Table 2 presents the associations between DTI measures in white matter and cognitive and psychological function. In model 1, MD, AD, and RD in white matter were associated with

Characteristics of the study population (n = 195)^a

Characteristics	
Demographic and clinical	
Age (yr)	80.7 (4.1)
Male	81 (41.5%)
Education (>6 yr)	137 (70.3%)
Current smoking	13 (6.7%)
Diabetes mellitus	39 (20.0%)
Cardiovascular disease ^b	17 (8.7%)
Systolic blood pressure (mm Hg)	147.5 (20.5)
Diastolic blood pressure (mm Hg)	81.2 (10.5)
Cerebrovascular pathology and brain volumes	
WMH volume (mL)	22.5 (8.1–56.3)
Lacunar infarcts present ^c	52 (26.7%)
Cerebral microbleeds present	50 (26.2%)
Brain volume total (mL)	1000.0 (92.7)
Gray matter volume (mL)	497.2 (48.1)
White matter volume (mL)	502.8 (52.5)
Microstructural integrity in white and gray matter	
Fractional anisotropy	
White matter	0.24 (0.02)
Gray matter	0.17 (0.01)
Mean diffusivity ($\times 10^{-3}$ mm ² /s)	
White matter	1.01 (0.06)
Gray matter	1.15 (0.07)
Axial diffusivity ($\times 10^{-3}$ mm ² /s)	
White matter	1.24 (0.05)
Gray matter	1.34 (0.07)
Radial diffusivity ($\times 10^{-3}$ mm ² /s)	
White matter	0.89 (0.06)
Gray matter	1.05 (0.07)
Cognitive and psychological measures	
Mini-Mental State Examination	26.0 (25.0–27.0)
Executive ^d	
Δ Trail-Making Test (sec) ^e	130.8 (66.6)
Stroop interference score (sec)	39.28 (32.7)
Memory	
15-Word Verbal Learning Test (words remembered)	
Immediate-recall score	16.7 (5.6)
Delayed-recall score	4.8 (2.8)
Visual Association Test (pictures remembered)	12 (10–12)
Psychomotor speed	
Letter Digit Substitution Test (digits coded)	31.0 (9.4)
Geriatric Depression Scale ^d	1.0 (0–3.0)
Apathy Scale of Starkstein ^d	10.7 (4.4)

^a Data are presented as mean \pm SD, median (interquartile range), or as number (percentage) where appropriate.

^b Comprises myocardial infarction or a coronary intervention procedure \geq 3 years ago or peripheral artery disease.

^c Missing for $n = 4$ participants.

^d Higher scores indicate worse functioning.

^e Δ Trail-Making Test denotes difference between Trail-Making Test-B and Trail-Making Test-A.

worse executive function, memory, psychomotor speed, and overall cognition (all, $P <$.05). FA was associated with executive function and overall cognition. To assess the impact of diabetes mellitus and hypertension on our findings, we added these covariates separately to model 1; however, the results remained unchanged (data not shown). In model 2, additional adjustment for conventional features of SVD yielded similar effect estimates. In model 3, after further adjustment for brain volume, all these associations strongly attenuated, with only the association between

FA in white matter and executive functioning remaining. Results for DTI measures in gray matter (On-line Table 3) followed a pattern similar to that of white matter, with the exception of the lack of any association with memory. After adjustment for normalized brain volume, only FA and RD in gray matter remained associated with executive functioning.

To assess the individual contribution of each covariate to overall cognitive functioning, we present the standardized β coefficients for each variable in the fully adjusted model for 1 DTI measure (FA in white matter) in On-line Table 4. The largest effect estimates were found for education and normalized brain volume. Model 3 fit significantly better (F test <0.05) than model 2 for executive function, psychomotor speed, and overall cognition as indicated by footnote *c* in On-line Tables 2 and 3.

TBSS showed no associations between microstructural integrity and cognitive and psychological functioning. On-line Table 5 shows several associations between DTI measures in local brain regions and various cognitive domains. In both white and gray matter, global or local DTI measures were not associated with scores on the GDS-15 or the Apathy Scale of Starkstein.

DISCUSSION

This study shows that in older individuals with mild cognitive deficits, DTI abnormalities in the gray matter were associated with worse executive function, psychomotor speed, and overall cognition, whereas DTI abnormalities in white matter were, in addition, associated with memory. These relationships were independent of WMHs, lacunar infarcts, or cerebral microbleeds, but strongly attenuated after adjusting for brain volume.

In contrast to other studies,^{34,35} no global or local associations between microstructural integrity and symptoms of depression or apathy were found. Also, in contrast to our findings, a 3-year follow-up study in older individuals (mean age, 74 years) showed that DTI abnormalities in normal-appearing brain tissue predicted worse executive function, memory, and psychomotor speed, independent of WMHs, lacunar infarcts, and total brain volume.¹³ In addition, a large cross-sectional study in older individuals (mean age, 67 years) showed that diffusion signal abnormalities were associated with several cognitive domains irrespective of brain volume and other conventional features of SVD.¹² A possible explanation for the differences between these latter study findings and ours is that we used different cognitive tests to assess cognitive function and included older participants, all of whom were using antihypertensive medication. In addition, adjusting for brain volume in populations with different ages (and a different prevalence for brain atrophy) is likely to yield different results.

The present study shows that most of the associations between DTI measures and cognitive dysfunction attenuated after adjusting for brain volume. It is possible that the observed associations were, at least in part, mediated by atrophy. In support of this hypothesis, a longitudinal study reported that midlife white matter diffusion signal abnormalities predicted white matter atrophy.³⁶

However, several DTI measures in global and local brain regions were associated with cognitive functioning, irrespective of brain volume and overt features of SVD. FA in white and gray matter and RD in gray matter remained associated with executive

functioning. Furthermore, FA in the putamen and MD, AD, and RD in the postcentral gyrus remained associated with executive functioning; and MD, AD, and RD in the hippocampus remained associated with memory. These findings might be because microstructural damage to myelin/axons/neurons³⁷ (undetectable on conventional MR imaging) may lead to disruption of neuronal circuits. These microstructural changes are thought to be secondary to SVD and related to vascular risk factors, in particular to hypertension.³⁸ Executive function is known to be the cognitive domain most sensitive to subtle and diffuse deterioration of microstructural integrity of vascular origin.^{9,39}

To investigate to what extent hypertension contributed to our findings, we included blood pressure as an additional covariate in model 1, which did not affect any of the associations. This finding suggests that hypertension is an unlikely etiology for DTI abnormalities and cognitive dysfunction in our population. However, these findings should be interpreted with caution because only participants with a blood pressure of ≤ 160 mm Hg were included, and all participants used antihypertensive treatment, following the strict inclusion criteria from the DANTE study.

Compared with diffusivity measures, FA had a weaker association with brain volume. The disparity in associations suggests that the DTI measures may reflect a different pathophysiology. FA reflects a normalized ratio of diffusion directionality, whereas MD reflects the overall magnitude of water diffusion. Although research on the underlying pathologic substrate is scarce, a lower FA is thought to reflect irreversible structural damage, such as loss of myelin/axons, whereas increased MD may indicate an increase in interstitial or extracellular fluid.⁴⁰

The present results should be interpreted with caution because no causal inference can be made due to the cross-sectional design. Moreover, due to the strict selection criteria of the DANTE trial, the findings are only generalizable to older individuals using antihypertensive treatment without a history of serious cardiovascular disease or dementia. Finally, we performed multiple testing, which can increase the chance of type I errors (wrongfully rejecting the null hypothesis). The Bonferroni correction was not applied because this method is considered too conservative to use in multiple comparisons with outcomes that are correlated.

The strengths of the study include the extensive assessment of cognitive function and of microstructural integrity by using FA, MD, AD, and RD in both white and gray matter. Moreover, in the analyses of the relationship between microstructural integrity and cognitive function, we are the first to adjust for all features of SVD, including the presence of cerebral microbleeds, to our knowledge.

CONCLUSIONS

DTI measures in white and gray matter were associated with worse functioning on several cognitive domains. Associations were independent of WMHs, lacunar infarcts, and cerebral microbleeds but strongly attenuated after adjusting for brain volume. Only white and gray matter fractional anisotropy and gray matter radial diffusivity were associated with executive functioning, irrespective of brain volume. Our findings indicate that the relationship between DTI abnormalities and cognitive function is largely explained by brain volume.

ACKNOWLEDGMENTS

The authors thank all the DANTE participants and the coinvestigators.

Disclosures: Justine E.F. Moonen—RELATED: Grant: Netherlands Organization for Health Research and Development (ZonMW),* Comments: program Priority Medicines for the Elderly, No. 40-41600-98-9014. The funding organization played no role in the design, conduct, or analysis of the study. Wouter de Ruijter—RELATED: Grant: Netherlands Organization for Health Research and Development (ZonMW),* Comments: reference No. 11-31010-03 (ZonMW acts on behalf of the Dutch Ministry of Health, Welfare and Sports). A.J.M. de Craen—RELATED: Grant: Netherlands Organization for Health Research and Development (ZonMW),* *Money paid to the institution.

REFERENCES

1. Wardlaw JM, Smith EE, Biessels GJ, et al; STRIVE v1. **Neuroimaging standards for research into small vessel disease and its contribution to ageing and neurodegeneration.** *Lancet Neurol* 2013;12:822–38 CrossRef Medline
2. Vernooij MW, Ikram MA, Tanghe HL, et al. **Incidental findings on brain MRI in the general population.** *N Engl J Med* 2007;357:1821–28 CrossRef Medline
3. Pantoni L. **Cerebral small vessel disease: from pathogenesis and clinical characteristics to therapeutic challenges.** *Lancet Neurol* 2010;9:689–701 CrossRef Medline
4. Thomas AJ, O'Brien JT, Davis S, et al. **Ischemic basis for deep white matter hyperintensities in major depression: a neuropathological study.** *Arch Gen Psychiatry* 2002;59:785–92 CrossRef Medline
5. Akoudad S, de Groot M, Koudstaal PJ, et al. **Cerebral microbleeds are related to loss of white matter structural integrity.** *Neurology* 2013;81:1930–37 CrossRef Medline
6. Reijmer YD, Freeze WM, Leemans A, et al. **The effect of lacunar infarcts on white matter tract integrity.** *Stroke* 2013;44:2019–21 CrossRef Medline
7. Ropele S, Seewann A, Gouw AA, et al; LADIS study group. **Quantitation of brain tissue changes associated with white matter hyperintensities by diffusion-weighted and magnetization transfer imaging: the LADIS (Leukoaraiosis and Disability in the Elderly) study.** *J Magn Reson Imaging* 2009;29:268–74 CrossRef Medline
8. Schmierer K, Wheeler-Kingshott CA, Boulby PA, et al. **Diffusion tensor imaging of post mortem multiple sclerosis brain.** *Neuroimage* 2007;35:467–77 CrossRef Medline
9. Nitkunan A, Barrick TR, Charlton RA, et al. **Multimodal MRI in cerebral small vessel disease: its relationship with cognition and sensitivity to change over time.** *Stroke* 2008;39:1999–2005 CrossRef Medline
10. Tuladhar AM, van Norden AG, de Laat KF, et al. **White matter integrity in small vessel disease is related to cognition.** *Neuroimage Clin* 2015;7:518–24 CrossRef Medline
11. van Norden AG, de Laat KF, van Dijk EJ, et al. **Diffusion tensor imaging and cognition in cerebral small vessel disease: the RUN DMC study.** *Biochim Biophys Acta* 2012;1822:401–07 CrossRef Medline
12. Vernooij MW, Ikram MA, Vrooman HA, et al. **White matter microstructural integrity and cognitive function in a general elderly population.** *Arch Gen Psychiatry* 2009;66:545–53 CrossRef Medline
13. Jokinen H, Schmidt R, Ropele S, et al; LADIS Study Group. **Diffusion changes predict cognitive and functional outcome: the LADIS study.** *Ann Neurol* 2013;73:576–83 CrossRef Medline
14. Shimony JS, Sheline YI, D'Angelo G, et al. **Diffuse microstructural abnormalities of normal-appearing white matter in late life depression: a diffusion tensor imaging study.** *Biol Psychiatry* 2009;66:245–52 CrossRef Medline
15. Moonen JE, Foster-Dingley JC, de Ruijter W, et al. **Effect of Discontinuation of Antihypertensive Treatment in Elderly People on Cognitive Functioning: the DANTE Study Leiden—a randomized clinical trial.** *JAMA Intern Med* 2015;175:1622–30 CrossRef Medline
16. Behrens TE, Woolrich MW, Jenkinson M, et al. **Characterization and propagation of uncertainty in diffusion-weighted MR imaging.** *Magn Reson Med* 2003;50:1077–88 CrossRef Medline
17. Smith SM. **Fast robust automated brain extraction.** *Hum Brain Mapp* 2002;17:143–55 CrossRef Medline
18. Zhang Y, Brady M, Smith S. **Segmentation of brain MR images through a hidden Markov random field model and the expectation-maximization algorithm.** *IEEE Trans Med Imaging* 2001;20:45–57 CrossRef Medline
19. Foster-Dingley JC, Moonen JE, van den Berg-Huijsmans AA, et al. **Lower blood pressure and gray matter integrity loss in older persons.** *J Clin Hypertens (Greenwich)* 2015;17:630–37 CrossRef Medline
20. Foster-Dingley JC, van der Grond J, Moonen JE, et al. **Lower blood pressure is associated with smaller subcortical brain volumes in older persons.** *Am J Hypertens* 2015;28:1127–33 CrossRef Medline
21. Folstein MF, Folstein SE, McHugh PR. **“Mini-mental state”: a practical method for grading the cognitive state of patients for the clinician.** *J Psychiatr Res* 1975;12:189–98 CrossRef Medline
22. Houx PJ, Jolles J, Vreeling FW. **Stroop interference: aging effects assessed with the Stroop Color-Word Test.** *Exp Aging Res* 1993;19:209–24 CrossRef Medline
23. Arbutnot K, Frank J. **Trail making test, part B as a measure of executive control: validation using a set-switching paradigm.** *J Clin Exp Neuropsychol* 2000;22:518–28 CrossRef Medline
24. Lezak MD, Howieson DB, Loring DW. *Neuropsychological Assessment.* 4th ed. New York: Oxford University Press; 2004
25. Van der Elst W, van Boxtel MP, Van Breukelen GJ, et al. **The Letter Digit Substitution Test: normative data for 1,858 healthy participants aged 24–81 from the Maastricht Aging Study (MAAS)—influence of age, education, and sex.** *J Clin Exp Neuropsychol* 2006;28:998–1009 CrossRef Medline
26. D'Ath P, Katona P, Mullan E, et al. **Screening, detection and management of depression in elderly primary care attenders, I: the acceptability and performance of the 15 item Geriatric Depression Scale (GDS15) and the development of short versions.** *Fam Pract* 1994;11:260–66 CrossRef Medline
27. Starkstein SE, Mayberg HS, Preziosi TJ, et al. **Reliability, validity, and clinical correlates of apathy in Parkinson's disease.** *J Neuropsychiatry Clin Neurosci* 1992;4:134–39 CrossRef Medline
28. Smith SM, Jenkinson M, Johansen-Berg H, et al. **Tract-based spatial statistics: voxelwise analysis of multi-subject diffusion data.** *Neuroimage* 2006;31:1487–505 CrossRef Medline
29. Wessa M, King AV, Meyer P, et al. **Impaired and preserved aspects of feedback learning in aMCI: contributions of structural connectivity.** *Brain Struct Funct* 2016;221:2831–46 CrossRef Medline
30. Brueggen K, Dyrba M, Barkhof F, et al. **Basal forebrain and hippocampus as predictors of conversion to Alzheimer's disease in patients with mild cognitive impairment: a multicenter DTI and volumetry study.** *J Alzheimers Dis* 2015;48:197–204 CrossRef Medline
31. Reginold W, Itorralba J, Tam A, et al. **Correlating quantitative tractography at 3T MRI and cognitive tests in healthy older adults.** *Brain Imaging Behav* 2015 Dec 9. [Epub ahead of print] CrossRef Medline
32. de Jong LW, van der Hiele K, Veer IM, et al. **Strongly reduced volumes of putamen and thalamus in Alzheimer's disease: an MRI study.** *Brain* 2008;131:3277–85 CrossRef Medline
33. Wang Z, Wang J, Zhang H, et al. **Interhemispheric functional and structural disconnection in Alzheimer's disease: a combined resting-state fMRI and DTI study.** *PLoS One* 2015;10:e0126310 CrossRef Medline
34. Ota M, Sato N, Nakata Y, et al. **Relationship between apathy and diffusion tensor imaging metrics of the brain in Alzheimer's disease.** *Int J Geriatr Psychiatry* 2012;27:722–26 CrossRef Medline
35. Reppermund S, Zhuang L, Wen W, et al. **White matter integrity and late-life depression in community-dwelling individuals: diffusion**

- tensor imaging study using tract-based spatial statistics. *Br J Psychiatry* 2014;205:315–20 CrossRef Medline
36. Ly M, Canu E, Xu G, et al. **Midlife measurements of white matter microstructure predict subsequent regional white matter atrophy in healthy adults.** *Hum Brain Mapp* 2014;35:2044–54 CrossRef Medline
37. Peters A. **The effects of normal aging on myelin and nerve fibers: a review.** *J Neurocytol* 2002;31:581–93 CrossRef Medline
38. Muñoz Maniega S, Chappell FM, Valdés Hernández MC, et al. **Integrity of normal-appearing white matter: influence of age, visible lesion burden and hypertension in patients with small-vessel disease.** *J Cereb Blood Flow Metab* 2016 Mar 1. [Epub ahead of print] CrossRef Medline
39. O’Sullivan M, Morris RG, Huckstep B, et al. **Diffusion tensor MRI correlates with executive dysfunction in patients with ischaemic leukoaraiosis.** *J Neurol Neurosurg Psychiatry* 2004;75:441–47 CrossRef Medline
40. Kale RA, Gupta RK, Saraswat VA, et al. **Demonstration of interstitial cerebral edema with diffusion tensor MR imaging in type C hepatic encephalopathy.** *Hepatology* 2006;43:698–706 CrossRef Medline

Measuring Brain Tissue Integrity during 4 Years Using Diffusion Tensor Imaging

 D. Ontaneda,  K. Sakaie,  J. Lin,  X.-F. Wang,  M.J. Lowe,  M.D. Phillips, and  R.J. Fox



ABSTRACT

BACKGROUND AND PURPOSE: DTI is an MR imaging measure of brain tissue integrity. Little is known regarding the long-term longitudinal evolution of lesional and nonlesional tissue DTI parameters in multiple sclerosis and the present study examines DTI evolution over 4 years.

MATERIALS AND METHODS: Twenty-one patients with multiple sclerosis were imaged for up to 48 months after starting natalizumab therapy. Gadolinium-enhancing lesions at baseline, chronic T2 lesions, and normal-appearing white matter were followed longitudinally. T2 lesions were subclassified as black holes and non-black holes. Within each ROI, the average values of DTI metrics were derived by using Analysis of Functional Neuro Images software. The longitudinal trend in DTI metrics was estimated by using a mixed-model regression analysis.

RESULTS: A significant increase was observed for axial diffusivity ($P < .001$) in gadolinium-enhancing lesions and chronic T2 lesions during 4 years. No significant change in radial diffusivity either in normal-appearing white matter or lesional tissue was observed. The evolution of axial diffusivity was different in gadolinium-enhancing lesions ($P < .001$) and chronic T2 lesions ($P = .02$) compared with normal-appearing white matter.

CONCLUSIONS: An increase in axial diffusion in both gadolinium-enhancing lesions and T2 lesions may relate to the complex evolution of chronically demyelinated brain tissue. Pathologic changes in normal-appearing white matter are likely more subtle than in lesional tissue and may explain the stability of these measures with DTI.

ABBREVIATIONS: AD = axial diffusivity; BH = black hole(s); FA = fractional anisotropy; GAD = gadolinium-enhancing lesion; MD = mean diffusivity; NAWM = normal-appearing white matter; NBH = non-black hole(s); RD = radial diffusivity

MS is the leading nontraumatic cause of neurologic disability in young adults in North America. MS pathology is characterized by focal inflammatory demyelinating lesions and diffuse changes in myelin, axon, and neuronal components.¹ Conventional MR imaging in MS has limitations because this technique provides little insight into the underlying pathology of MS lesions, is not sensitive enough to detect tissue changes outside lesions (ie, normal-appearing white matter [NAWM]), and is unable to quantify pathologic substrates of disease such as myelin or axonal

content. Additionally, conventional MR imaging is a relatively insensitive technique in progressive forms of MS in which there is little overt inflammatory activity, and MR imaging–detected lesion burden often does not change despite frequent clear-cut clinical progression.²

DTI is a quantitative MR imaging–based technique that measures the diffusion of water in brain tissue.³ The diffusion properties are thought to reflect the microstructure of the underlying tissue.⁴ DTI metrics include the following: mean diffusivity (MD), fractional anisotropy (FA), radial diffusivity (RD), and axial diffusivity (AD). The different DTI metrics carry a pathologic specificity as well. AD is correlated pathologically with axonal loss in animal models of retinal ischemia.⁵ RD is thought to be a measure of myelin content based on studies examining animal models of demyelination.⁶ DTI may provide a window into the pathologic processes in MS, and through serial imaging studies, it can be used to follow MS lesions in different stages and tissue changes with time.⁷ Additionally, DTI has demonstrated the ability to detect changes in brain tissue that is apparently free of lesions (normal-appearing brain tissue) under standard MR imaging.⁸

Longitudinal studies examining DTI characteristics have typ-

Received May 10, 2016; accepted after revision July 26.

From the Department of Neurology (D.O., R.J.F.), Neurological Institute, Mellen Center for Multiple Sclerosis Treatment and Research; Imaging Institute (K.S., J.L., M.J.L., M.D.P.); and Department of Quantitative Health Sciences (X.-F.W.), Cleveland Clinic Foundation, Cleveland, Ohio.

This work was funded by National Institutes of Health grant KL2 TR000440 to D. Ontaneda and National Multiple Sclerosis Society grants, FP1769-A-1 to D. Ontaneda and RG3548 to R.J. Fox.

Please address correspondence to Daniel Ontaneda, MD, Mellen Center for Multiple Sclerosis Treatment and Research, Cleveland Clinic Foundation, 9500 Euclid Ave, U-10, Cleveland, OH 44195; e-mail: ontaneda@ccf.org; @dxo60_daniel

 Indicates open access to non-subscribers at www.ajnr.org

<http://dx.doi.org/10.3174/ajnr.A4946>

ically only been conducted for 1–2 years with a smaller number of diffusion directions than with currently available high-angular-resolution diffusion imaging. Harrison et al⁸ studied the evolution of white matter tracts based on tractography and found that there was a significant increase in FA and a decrease in RD during a 2-year follow-up period, with most patients in that study being on disease-modifying treatment. Lesional tissue has been studied in acute phases or for short periods of follow-up (1–2 years), and it most consistently has shown increases in MD and RD with a decrease in FA.^{9–12} Diffusion imaging studies have also shown that T1 black holes have higher levels of diffusivity compared with isointense T1 lesions.¹³ There is evidence that radial diffusivity is a strong predictor of T1 black hole conversion.¹¹ Alternatively, longitudinal studies of high-angular-resolution diffusion imaging following lesion evolution with time have not been conducted, to our knowledge.

Natalizumab is a monoclonal antibody directed at the very late antigen-4 receptor on leukocytes.¹⁴ Most patients treated with natalizumab enter a relatively inflammation-free state, which enables the study of the underlying neurodegenerative and reparative aspects of MS, similar to those seen in progressive MS. DTI is a feasible alternative to measure underlying neurodegeneration and to assess the efficacy of potential neuroprotectant medications.

In this study, we aimed to study the evolution of lesional and nonlesional tissue in patients treated with natalizumab during a 4-year period. Previous DTI studies have used low angular resolution and have followed patients for only up to 2 years.⁸ The high-angular-resolution diffusion imaging acquisition¹⁵ reduces the variability and bias found in lower-angular-resolution approaches, allows a more accurate study of DTI metrics with time, and shows advantages over using a small number of diffusion directions.¹⁶

MATERIALS AND METHODS

Participants

Twenty-two patients with relapsing MS starting natalizumab therapy were sequentially enrolled from neurologist referrals at an academic specialty clinical center in an institutional review board–approved longitudinal observational imaging study, as previously described.¹⁷ Inclusion criteria were clinically definite MS by the 2005 Revised McDonald Criteria,¹⁸ age older than 18 years, and the ability to provide informed consent. Exclusion criteria were clinical relapse or steroid treatment in the previous 8 weeks, pregnancy, and contraindications to MR imaging such as severe claustrophobia and implanted devices such as neurostimulators and pacemakers. One patient discontinued imaging follow-up after only 2 months and was removed from the data analysis.

MR Imaging Protocol

MR imaging of the brain was serially performed at time baseline (before natalizumab dosing) and at 1, 2, 6, 12, 18, 24, 36, and 48 months. Images were obtained on a 3T Magnetom Trio scanner (Siemens, Erlangen, Germany). Diffusion-weighted imaging used 71 noncollinear diffusion-weighting gradients ($2.5 \times 2.5 \times 2.5$ mm voxels, $b = 1000$ s/mm², 8 $b = 0$ acquisitions, 260×260 mm FOV, 104×104 matrix, forty-eight 2.5-mm sections, TE = 95 ms, TR = 7300 ms). The b-value of the DTI sequence was reduced at

12 months from $b = 2000$ s/mm² to $b = 1000$ s/mm². This change was implemented to address vibration-related artifacts observed at the higher b-value.¹⁹ Anatomic imaging was performed for lesion detection and coregistration: 3D MPRAGE (256×256 mm FOV, 128×256 matrix, one hundred twenty 1.2-mm sections, TE = 1.71 ms, TR = 1900 ms, T1 = 900 ms, flip angle = 8°); proton density/T2-weighted (230×230 mm FOV, 320×320 matrix, forty-eight 3-mm sections, TE₁ = 20 ms, TE₂ = 91 ms, TR = 3600 ms); and T1 postgadolinium sequences (230×230 mm FOV, 320×320 matrix, forty-eight 3-mm sections, TE = 2.46 ms, TR 300 ms, flip angle = 75°).

Image Analysis

For each subject, ROIs were manually drawn (authors: D.O. and R.J.F.) using Analysis of Functional Neuro Images software (AFNI; <http://afni.nimh.nih.gov/afni>) on all areas with pathologic gadolinium enhancement on T1 postcontrast images at the baseline scan and will be referred to as GAD tissue. Ten ROIs were sequentially drawn in selected chronic lesional tissue (T2 lesions and T1 black holes) also on the baseline scan, and these included 2 lesions in the following locations: periventricular, juxtacortical, corpus callosum, infratentorial, and posterior periaxial (Fig 1). If subjects did not have lesions in the prespecified regions with the required T1/T2 signal characteristics, these regions were ignored. T2 lesions were labeled as black hole (BH) and non-black hole (NBH). T1 black holes were differentiated from NBH by a visible decrease in signal intensity on the T1 sequence compared with normal-appearing adjacent white matter tissue, as has been described previously.²⁰

Images from each time point were coregistered by using the FMRIB Software Library (FSL; <http://fsl.fmrib.ox.ac.uk/>).²¹ The images from the DTI dataset without diffusion weighting, the $b = 0$ images, were coregistered to the baseline T1-weighted images to determine tensor properties in lesional tissues. Inverse transformation was applied to localize ROIs in DTI space. GAD ROIs were observed on FA maps to ensure that these ROIs did not include CSF or CSF volume-averaging artifacts. Lesional ROIs were examined on FA maps and T1 postcontrast images to ensure that ROIs did not include T1 GAD lesions, CSF, or CSF volume-averaging artifacts. FA was used, given the possibility of image warping in DTI space to ensure that ROIs were not in the CSF or voxels adjacent to the CSF.

For each subject, 16 ROIs were also drawn in the normal-appearing white matter bilaterally. These included 2 ROIs (ipsilateral and contralateral) in each of the following regions: corticospinal tracts in the pons, corticospinal tract in the midbrain, anterior limb of the internal capsule, posterior limb of the internal capsule, anterior corpus callosum, posterior corpus callosum, centrum semiovale, and deep white matter of the frontal lobe (Fig 1). ROIs were drawn individually on the coregistered FA maps at each time point with simultaneous observation of the T2 and T1 postcontrast scans to ensure that ROIs did not include T2 lesions, T1 gadolinium-enhancing lesions, CSF, or CSF volume-averaging artifacts and voxels adjacent to CSF. Lesions were shifted within the tract when possible to avoid the above changes, but when this was not possible, these ROIs were eliminated from the analysis.

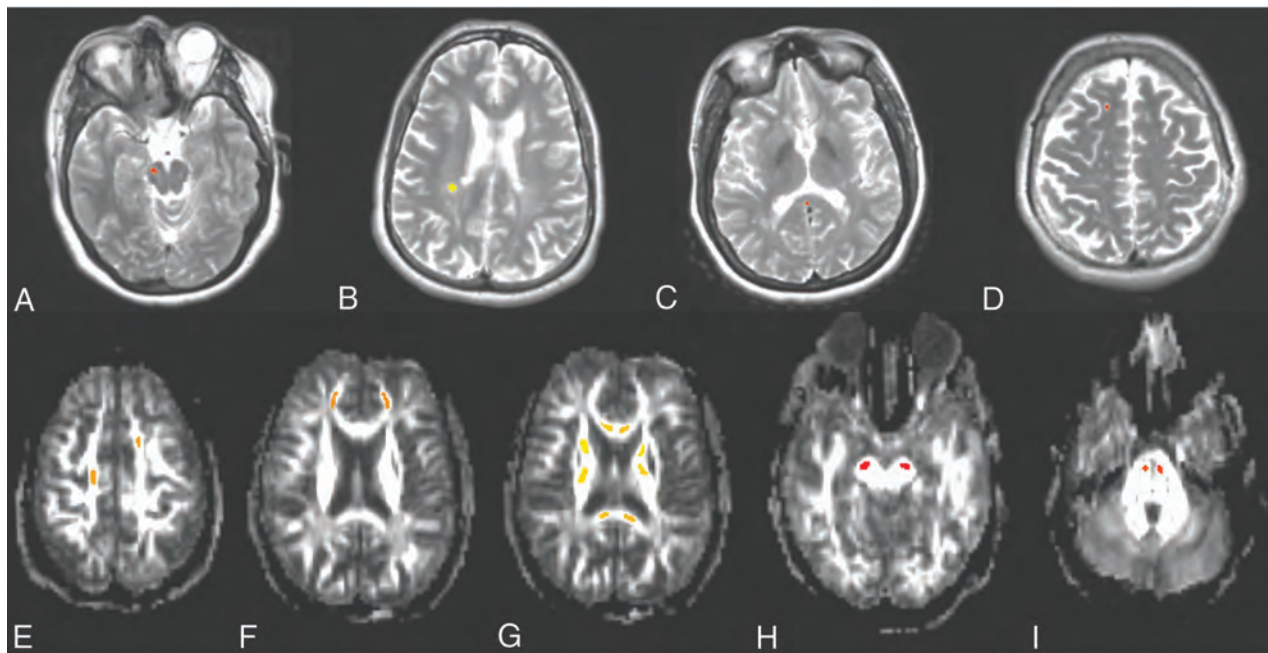


FIG 1. ROIs in infratentorial (A), posterior peritrial (B), corpus callosum (C), and juxtacortical (D) lesional tissues on postcontrast T2-weighted images. Note ROIs in normal-appearing white matter locations (E–I) on fractional anisotropy maps.

Statistical Analysis

The data from each ROI from the FA, MD, RD, and AD maps at all the different time points were extracted. For each subject, distribution plots of the data were created to identify extreme outliers (>2 SDs from the mean). ROI positions of outliers were checked on the different DTI maps and were corrected as needed to ensure that the ROIs did not include CSF, vascular spaces, or lesional tissue (for NAWM). The data were then re-extracted and rechecked.

Statistical testing was directed at demonstrating longitudinal change in DTI metrics among the different tissue types. Hypothesis-driven separate linear mixed models were used to estimate the mean difference in DTI metrics (RD, AD, FA, and MD) with time between NAWM and GAD tissue, NAWM versus T2 lesions, and BH versus NBH. We hypothesized that NAWM would be more stable compared with GAD and that BH would demonstrate more tissue injury than NBH. Each model included fixed effects for the following: 1) tissue type (NAWM and GAD tissue, NAWM and T2 lesions, or BH and NBH), 2) an interaction between tissue type and follow-up time in months (to separately model the DTI evolution in each group with time), and 3) subject age at the time of study initiation (to account for the change observed in DTI metrics with normal aging with time). The model also accounted for the effects of between-lesion variation with time by adding a normal random effect for each ROI to control the heterogeneity over different ROIs. ANOVA tests were used to determine whether the rate of change in DTI measures with time differed between tissue types. All analyses were performed by using the R Statistical Computing Software (Version 3.1.3; <http://www.r-project.org/>). The level of statistical significance was set at $P < .025$ (2-tailed) with a correction for multiple comparisons, to adjust for the 2 independent DTI metrics used in the study (RD, AD). A formal sample size calculation was not conducted, given the exploratory nature of the study.

RESULTS

Twenty-one subjects were recruited into the study. Demographics and baseline clinical/MR imaging characteristics have been previously published in the *American Journal of Neuroradiology*.¹⁷ Seventeen (81.0%) subjects completed the 48-month scan, 1 subject died due to an unrelated cardiac event, and 3 subjects withdrew from the study before completion (at 12, 18, and 24 months). Figure 2 shows AD and RD boxplots for NAWM, GAD, and T2 lesions. Sixty-one GADs were identified at baseline (mean lesion size, 751.3 mm³) along with 141 chronic T2 lesions, of which 90 were BH and 51 were NBH (mean T2 lesion size, 666.8 mm³).

Longitudinal DTI metrics for NAWM, GAD, and T2 lesions are presented in Fig 3. Results of linear mixed-effects models with average yearly changes in DTI metrics are presented in Tables 1 (NAWM, GAD) and 2 (T2 lesions).

DTI Changes in NAWM

No statistically significant changes were observed with time in DTI metrics from NAWM ROIs (all $P > .08$). RD and MD showed an increasing trend with time, while FA and AD showed a trend toward decreases with time.

DTI Changes in GAD

An increase in AD of 1.88×10^{-6} mm²/s per month was observed during 4 years in GAD tissues ($P < .0001$). A nonsignificant increase of 0.66×10^{-6} mm²/s change per month in RD was observed ($P = .037$), which, in combination with AD, resulted in an overall increase of 1.28×10^{-6} mm²/s per month ($P < .0001$) in MD as well.

DTI Changes in T2 Lesions

RD did not significantly change with time in T2 lesions. An increase of 0.54×10^{-6} mm²/s per month in AD ($P = .003$) with a concomitant increase in MD of 0.27×10^{-6} mm²/s per month

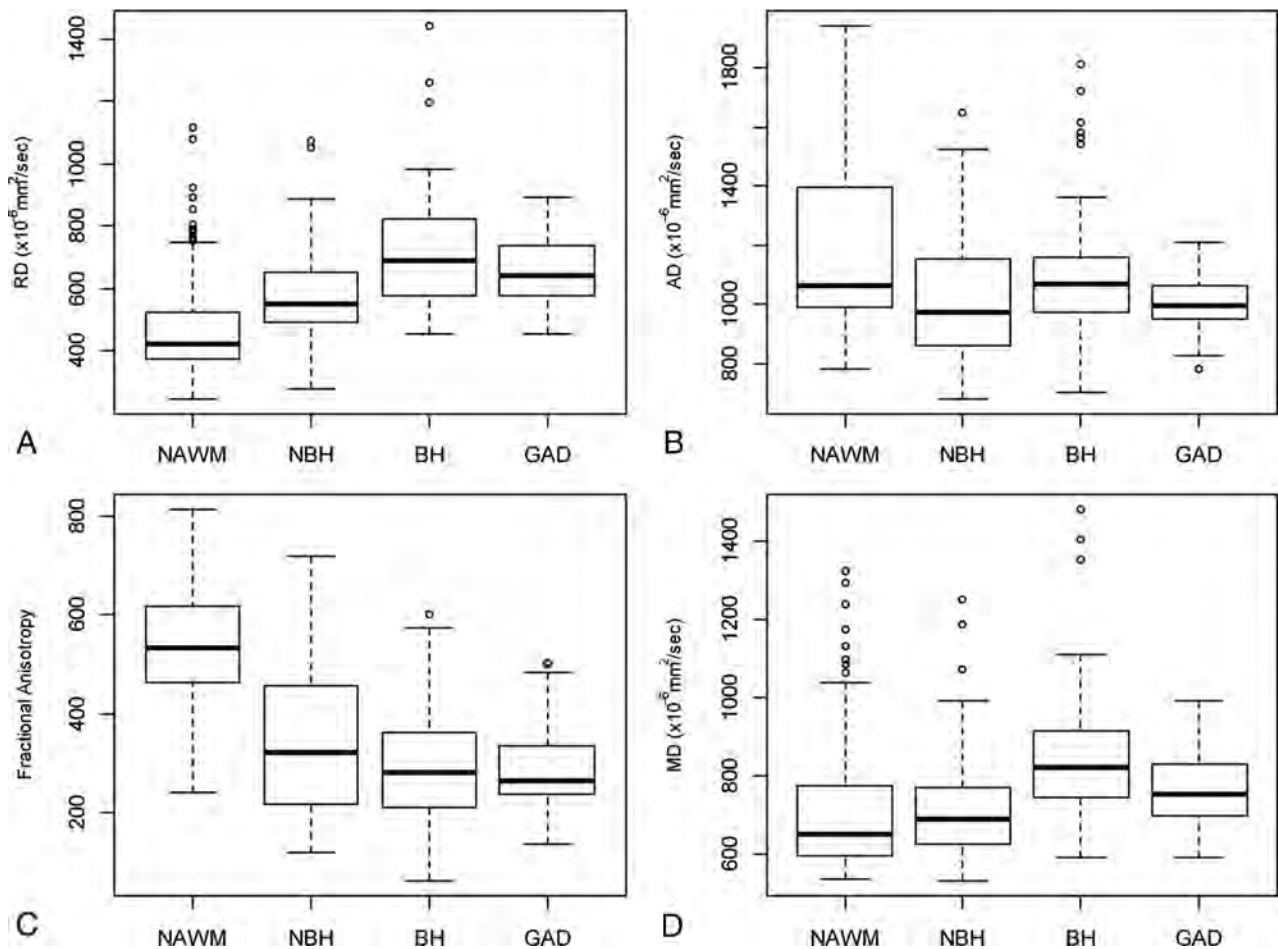


FIG 2. Baseline DTI characteristics of normal-appearing white matter, non-black holes, black holes, and gadolinium-enhancing lesions for radial diffusivity (A), axial diffusivity (B), fractional anisotropy (C), and mean diffusivity (D). Boxplots show median (dark line), upper and lower quartiles (box), maximum and minimum values excluding outliers (whiskers), and outliers (circles).

($P = .021$) was observed. FA increased by $0.16 \times 10^{-6} \text{ mm}^2/\text{s}$ per month, but this increase was not statistically significant ($P = .048$). No significant changes were seen in the evolution of DTI metrics in either BH or NBH when analyzed alone (all $P > .04$). RD increased with time in BH and decreased in NBH, though changes were not significant.

Comparative Evolution of DTI in Different Tissue Types

The tests of fixed effects by ANOVA (Table 3) showed a significant difference between GAD and NAWM in the rate of change with time in AD ($P < .0001$), but not for RD ($P = .111$). AD increased with time in GAD tissue and was stable in NAWM. When we compared T2 lesions and NAWM, a significant difference was detected for AD ($P = .002$), with no significant difference for RD ($P = .86$). When we compared BH and NBH, no differences were observed for RD or AD; however, a significant difference in the evolution of FA was observed between BH and NBH ($P = .012$), showing a decrease in FA in BH and an increase in NBH.

DISCUSSION

At baseline, DTI metrics showed expected differences, with higher RD and MD along with lower FA and AD in gadolinium-enhancing tissue compared with NAWM. This finding suggests the presence of more severe demyelination and axon loss in lesional tissue

compared with NAWM based on the findings in animal models, showing that RD correlates with myelination and AD correlates with axonal injury.^{6,22} It is likely that edema was an additional contributing factor to an increase in RD at the time of acute demyelination.²³ In chronic T2 lesions, DTI metrics at baseline showed higher RD and MD with lower FA and AD compared with NAWM. DTI metrics at baseline were similar in GAD and chronic T2 lesions, but overall GAD tissues had slightly higher RD and slightly lower FA, MD, and AD at baseline. Similar to prior studies,^{24,25} BH showed greater diffusivity at baseline compared with NBH, suggesting greater tissue injury. As would be expected, FA was significantly lower at baseline in BH than in NBH. Alternatively, AD at baseline was similar in BH and NBH. This outcome would not normally be expected because axon loss is a clear histologic feature of BH lesions.^{26,27} Our findings illustrate why equating AD with axonal integrity is an oversimplification of a complex measure. Our findings are similar to previous results showing that AD does not predict BH formation.^{11,17}

No statistically significant changes were observed in the longitudinal evolution of DTI metrics in NAWM. This finding is consistent with the findings of previous groups,²⁸ but it is in contrast to previous shorter term studies that have shown tract-specific longitudinal changes in NAWM DTI values.⁸ The trends observed

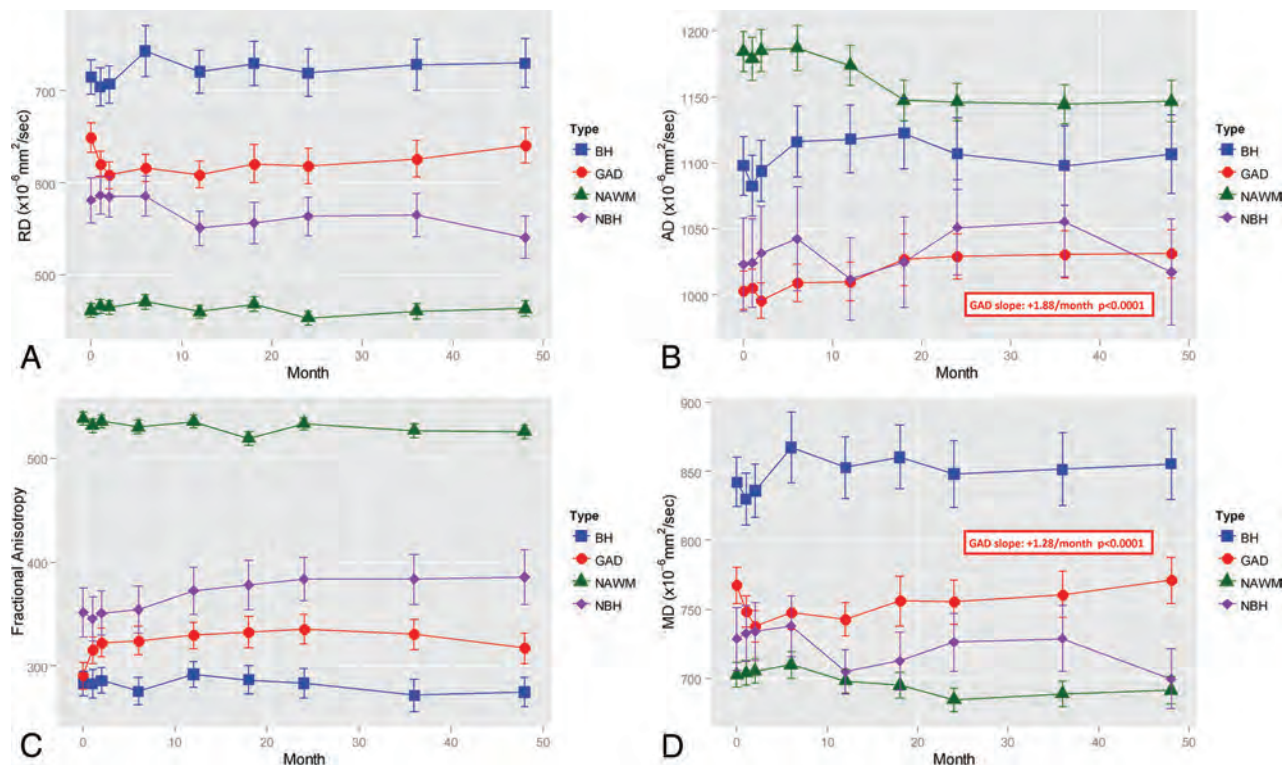


FIG 3. Longitudinal evolution of DTI metrics during 4 years for non-black holes, black holes, and gadolinium-enhancing lesions for radial diffusivity (A), axial diffusivity (B), fractional anisotropy (C), and mean diffusivity (D). Mean values (symbol) and 95% confidence intervals (error bars) are presented. Statistical significance and effect from the mixed-model effect are presented in boxes.

Table 1: Longitudinal DTI changes in NAWM and GAD

	Change/ Month	95% CI	% Annualized Change	P Value
NAWM				
RD $\times 10^{-6}$ mm ² /s	0.2193	-0.187 to 0.625	0.57%	.2898
AD $\times 10^{-6}$ mm ² /s	-0.2109	-0.614 to 0.192	-0.21%	.3052
FA $\times 10^{-3}$	-0.2572	-0.551 to 0.037	-0.57%	.0865
MD $\times 10^{-6}$ mm ² /s	0.03209	-0.331 to 0.396	0.05%	.8626
GAD				
RD $\times 10^{-6}$ mm ² /s	0.6107	0.039 to 1.285	1.22%	.0374
AD $\times 10^{-6}$ mm ² /s	1.8831	1.135 to 2.631	2.25%	<.0001 ^a
FA $\times 10^{-3}$	0.5074	0.031 to 0.984	2.10%	.037
MD $\times 10^{-6}$ mm ² /s	1.2788	0.695 to 1.863	2.00%	<.0001 ^a

^aP < .05.

in NAWM changes with time in our study were similar to what would be pathophysiologically expected, with an increase in RD and decrease in AD with time indicating progressive demyelination with ongoing axonal loss. One explanation for the absence of statistical significance is the relative lack of inflammatory activity seen in our patient population. Highly effective treatment may mitigate longitudinal changes in DTI. Anti-inflammatory therapies are likely to limit the amount of demyelination and secondary axon loss, making differences more difficult to observe.²⁹ A second explanation may relate to technical differences between our study and that of Harrison et al.⁸ In our study, ROIs in the NAWM were individually drawn and voxel volume was relatively small compared with a tractography-based technique. A larger sample size of voxels may have shown statistically significant results in the trends described above.

In gadolinium-enhancing tissue, significant changes were ob-

served in AD and MD during the study period. A progressive increase in AD was observed during 4 years and is similar to prior findings. Naismith et al¹¹ did not find significant changes in AD at the time of gadolinium-enhancement, but in their data, AD also appeared to increase during 1 year of follow-up. The longitudinal increase in AD may have been partially driven by the increase in AD observed in the first month following lesion formation; however, inspection of the trend of AD shows that this was only a marginal

contribution. Given similar results observed in T2 lesions (see below), we conclude that the change in AD is likely a biologic effect in lesional tissue. An alternate explanation may relate to the severity of axon loss in acute lesions. Postmortem analyses have shown that axon loss is maximal at the time of gadolinium-enhancement and that with time, axonal loss becomes less prevalent.³⁰ It is hypothesized that the initial injury causes an acute and severe loss of axons, which is detected by a marked drop in AD. The subsequent increase in AD might be a reflection of a secondary process occurring during chronic lesion evolution. The increase in AD may be due to a partial repair mechanism or may represent chronic lesion changes with scar formation or replacement by CSF/glial tissue.

When comparing the longitudinal evolution of DTI in GAD tissue and NAWM, significant differences were found for AD but not RD. This finding may indicate that distinct processes

Table 2: Longitudinal DTI changes in chronic lesional tissue

	Change/Month	95% CI	% Annualized Change	P Value
All T2 lesions				
RD × 10 ⁻⁶ mm ² /s	0.05683	-0.181 to 0.295	0.11%	.6401
AD × 10 ⁻⁶ mm ² /s	0.5411	0.251 to 0.831	0.62%	.0003 ^a
FA × 10 ⁻³	0.163	0.001 to 0.324	0.61%	.0482 ^a
MD × 10 ⁻⁶ mm ² /s	0.2695	0.040 to 0.499	0.41%	.0211 ^a
BH				
RD × 10 ⁻⁶ mm ² /s	0.3392	-0.028 to 0.706	0.57%	.0701
AD × 10 ⁻⁶ mm ² /s	0.1967	-0.200 to 0.593	0.22%	.331
FA × 10 ⁻³	-0.2137	-0.422 to -0.005	-0.91%	.0444
MD × 10 ⁻⁶ mm ² /s	0.2919	-0.059 to 0.643	0.42%	.1026
NBH				
RD × 10 ⁻⁶ mm ² /s	-0.4137	-0.967 to 0.140	-0.85%	.1432
AD × 10 ⁻⁶ mm ² /s	-0.2392	-0.838 to 0.360	-0.28%	.434
FA × 10 ⁻³	0.2907	-0.025 to 0.606	0.99%	.0708
MD × 10 ⁻⁶ mm ² /s	-0.355	-0.174 to 0.884	-0.58%	.1883

^aP < .05.**Table 3: Analysis of variance of fixed effects on longitudinal changes comparing evolution of DTI metrics from different tissue types during 4 years**

	P Value
NAWM vs GAD	
RD	.11
AD	<.001 ^a
FA	.004 ^a
MD	<.001 ^a
NAWM vs T2 lesions	
RD	.15
AD	.002 ^a
FA	.09
MD	.037
BH vs NBH	
RD	.36
AD	.39
FA	.01 ^a
MD	.07

^aP < .05.

outside demyelination are occurring in lesional tissue that can alter AD but not RD. The absence of changes in RD may represent the abrogation of demyelination induced by natalizumab and may explain differences with prior studies.³¹ The exact changes that drive the change in AD in lesional tissue are not clearly understood and will require further study, including an analysis of the different enhancement patterns within the gadolinium-enhancing lesions and pathologic correlation with DTI measures.

Similar to what was found in GAD tissue, a progressive increase in AD was observed during the 4-year study period in T2 lesions. This finding is of unclear significance, but similar changes have been previously reported as described above. The lack of any inflammatory-driven changes in these lesions along with the similar changes in GAD tissue suggests that the increase in AD is a real phenomenon and not a spurious result. The pathologic significance of this change is more difficult to determine. The correlation of AD with axonal integrity may be different in brain and optic nerve tissues,⁵ where fibers are more-or-less homogeneous in direction. Conversely, brain lesions may contain various different fibers, and an increase in AD may be due to selective loss of certain fibers, resulting in counterintuitive changes in DTI measures.³²

Our study also showed no significant difference in the evolution of RD or AD in BH and NBH. Regarding AD, it appears that the overall progressive increase in T2 lesions was likely determined by changes in BH, and this possibility supports a biologic gradient among NAWM, NBH, and finally BH. While changes were not significant, RD progressively increased in BH and decreased in NBH; these findings suggest ongoing demyelination in BH and possible remyelination in NBH lesions. Remyelination is a well-described phenomenon in NBH and has been demonstrated with magnetization transfer ratio imaging previously.^{33,34}

Our study was limited due to the absence of a control arm treated with something other than natalizumab. We aimed to study MS in a population with little inflammatory disease activity to minimize the effects of ongoing tissue inflammation on DTI measures. Our study was also limited by patients who dropped out of the study. However, it is likely that these drop-outs were patients who did not tolerate natalizumab or who stayed on the medication for only a short time, thus limiting the overall effect on the study.

An additional area of concern is the difficulty in delineating specific lesional tissue with time. Changes in the tissue architecture with time related to gliosis, resolution of edema, and brain atrophy complicate following lesions longitudinally. We used the T2 ROIs at baseline as a guide to follow the extent of the lesion on follow-up scans, but this method did not take into account areas where brain tissue remyelinate and lesions essentially resolve. This limitation is implicit in any study dealing with dynamic tissue changes. The stability of DTI measures in the first 3 time points from chronic lesion tissue and NAWM along with significant variability in GAD tissue demonstrates that DTI measures are quite sensitive to inflammatory changes. NAWM and chronic lesion measures showed good reliability during short imaging intervals (1 month).

A change to the b-value in the DTI sequence was required at month 12 due to vibration-related artifacts. ROI placement avoided regions affected by the vibration artifacts. Noise floor effects can result in systematic bias among measurements taken at different b-values. With a sufficiently low signal-to-noise ratio and in regions of high anisotropy, a reduction in b-value can result in an artifactual increase in diffusivity.³⁵ However, if the effects were substantial, we would expect an increase in diffusivity in all tissue types. Decreases in diffusivity values in normal-appearing white matter and lesional tissue, while not statistically significant, suggest that the impact of bias with the change in b-value did not have a meaningful impact on our data.

The use of DTI in clinical trials has significant promise; however, the DTI outcomes to be used should be tailored depending on the therapeutic mechanism of action and MS disease type. The selection of both the DTI metrics and the tissue from which these metrics are obtained is of importance when considering outcomes for clinical trials. For trials of agents that promote remyelination,

RD is a natural choice because it is thought to be a marker of myelin content. In NAWM, RD shows a tendency to increase with time. Although in our study, this increase was not statistically significant, therapies that promote remyelination may show a progressive decrease in RD. The study of RD in NAWM is advantageous because the cellular architecture is preserved and there is no confounding inflammatory activity, making the interpretation of DTI measures more straightforward. These advantages make RD within NAWM a good potential outcome for primary neuroprotection.

Although AD has been purported as a measure of axonal integrity, our results suggest that lesional AD is not likely correlated to axonal content because AD was not significantly different in BH and NBH. AD may provide a sensitive measure of ongoing disease processes in lesional tissue; however, the pathologic significance of this new finding remains unclear and will have to be studied in the future. The summary measures FA and MD are difficult to interpret as stand-alone measures, so they are less attractive as clinical trial outcomes. FA appears to be a good marker of acute lesion formation; however, the longitudinal evolution of FA did not show statistically significant changes in NAWM and only marginal changes in lesional tissue. In summary, our data suggest that DTI holds promise in trials that promote remyelination and tissue repair within lesions and to a lesser extent in NAWM.

CONCLUSIONS

Lesional tissue demonstrated higher values of RD and lower values of AD compared with NAWM, likely representing demyelination with a component of axon loss. No statistically significant changes were observed with time in NAWM. A progressive increase in AD was also observed in GAD tissues and chronic T2 lesions; however, the significance of this change remains unclear from a pathologic standpoint. Our findings suggest that AD from lesional tissue may be a more sensitive metric than RD from lesions or DTI measures from NAWM. The description of AD in lesional tissue as a surrogate of axon content in MS should be revisited, given its poor ability to differentiate BH and NBH.

ACKNOWLEDGMENTS

We acknowledge the assistance of our research support staff, radiology technicians, and information technology staff at the Melten Center.

Disclosures: Daniel Ontaneda—*RELATED: Grants/Grants Pending:* Dr Ontaneda is supported by a National Institutes of Health (Clinical and Translational Science Collaborative of Cleveland, KL2TR000440) KL2 Award and a National Multiple Sclerosis Clinical Fellowship Award (FP 1769-A-1); *UNRELATED: Consultancy:* Dr Ontaneda has received consulting fees from Acorda Therapeutics, Alkermes, Biogen Idec, Genzyme, Genentech, Mallinckrodt, and Novartis; *OTHER:* research support from Novartis and Genzyme. Ken Sakaie—*UNRELATED: Grants/Grants Pending:* National Institutes of Health,* National Multiple Sclerosis Society,* Department of Defense,* American Heart Association,* the Chiari and Syringomyelia Foundation,* Novartis,* Genzyme,* Biogen.* Jian Lin—*RELATED: Grant:* National Multiple Sclerosis Society*; *UNRELATED: Grants/Grants Pending:* Novartis.* Mark J. Lowe—*UNRELATED: Consultancy:* Siemens. Michael D. Phillips—*UNRELATED: Payment for Lectures (including service on Speakers Bureaus):* Siemens, *Comments:* honorarium for speaking, Robert J. Fox—*RELATED: Grant:* National Multiple Sclerosis Society (RG3546)*; *UNRELATED: Board Membership:* MedDay, *Comments:* Scientific Advisory Board; *Consultancy:* Avanir Pharmaceuticals, Allozyne, Biogen Idec, Novartis, Questcor Pharma-

ceuticals, Teva Neuroscience; *Research Support:* Novartis. *Money paid to the institution.

REFERENCES

- Lassmann H. **Models of multiple sclerosis: new insights into pathophysiology and repair.** *Curr Opin Neurol* 2008;21:242–47 CrossRef Medline
- Ontaneda D, Fox RJ, Chataway J. **Clinical trials in progressive multiple sclerosis: lessons learned and future perspectives.** *Lancet Neurol* 2015;14:208–23 CrossRef Medline
- Fox RJ. **Picturing multiple sclerosis: conventional and diffusion tensor imaging.** *Semin Neurol* 2008;28:453–66 CrossRef Medline
- Beaulieu C, Allen PS. **Determinants of anisotropic water diffusion in nerves.** *Magn Reson Med* 1994;31:394–400 CrossRef Medline
- Song SK, Sun SW, Ju WK, et al. **Diffusion tensor imaging detects and differentiates axon and myelin degeneration in mouse optic nerve after retinal ischemia.** *Neuroimage* 2003;20:1714–22 CrossRef Medline
- Song SK, Sun SW, Ramsbottom MJ, et al. **Dysmyelination revealed through MRI as increased radial (but unchanged axial) diffusion of water.** *Neuroimage* 2002;17:1429–36 CrossRef Medline
- Budde MD, Kim JH, Liang HF, et al. **Toward accurate diagnosis of white matter pathology using diffusion tensor imaging.** *Magn Reson Med* 2007;57:688–95 CrossRef Medline
- Harrison DM, Caffo BS, Shiee N, et al. **Longitudinal changes in diffusion tensor-based quantitative MRI in multiple sclerosis.** *Neurology* 2011;76:179–86 CrossRef Medline
- Goodkin DE, Rooney WD, Sloan R, et al. **A serial study of new MS lesions and the white matter from which they arise.** *Neurology* 1998; 51:1689–97 CrossRef Medline
- Werring DJ, Brassat D, Drogen AG, et al. **The pathogenesis of lesions and normal-appearing white matter changes in multiple sclerosis: a serial diffusion MRI study.** *Brain* 2000;123(pt 8):1667–76 CrossRef Medline
- Naismith RT, Xu J, Tutlam NT, et al. **Increased diffusivity in acute multiple sclerosis lesions predicts risk of black hole.** *Neurology* 2010;74:1694–701 CrossRef Medline
- Rocca MA, Cercignani M, Iannucci G, et al. **Weekly diffusion-weighted imaging of normal-appearing white matter in MS.** *Neurology* 2000;55:882–84 CrossRef Medline
- Filippi M, Iannucci G, Cercignani M, et al. **A quantitative study of water diffusion in multiple sclerosis lesions and normal-appearing white matter using echo-planar imaging.** *Arch Neurol* 2000;57: 1017–21 CrossRef Medline
- Ransohoff RM. **Natalizumab for multiple sclerosis.** *N Engl J Med* 2007;356:2622–29 CrossRef Medline
- Tuch DS, Reese TG, Wiegell MR, et al. **High angular resolution diffusion imaging reveals intravoxel white matter fiber heterogeneity.** *Magn Reson Med* 2002;48:577–82 CrossRef Medline
- Landman BA, Farrell JA, Jones CK, et al. **Effects of diffusion weighting schemes on the reproducibility of DTI-derived fractional anisotropy, mean diffusivity, and principal eigenvector measurements at 1.5T.** *Neuroimage* 2007;36:1123–38 CrossRef Medline
- Fox RJ, Cronin T, Lin J, et al. **Measuring myelin repair and axonal loss with diffusion tensor imaging.** *AJNR Am J Neuroradiol* 2011;32: 85–91 CrossRef Medline
- Polman CH, Reingold SC, Edan G, et al. **Diagnostic criteria for multiple sclerosis: 2005 revisions to the “McDonald criteria.”** *Ann Neurol* 2005;58:840–46 CrossRef Medline
- Hiltunen J, Hari R, Jousmäki V, et al. **Quantification of mechanical vibration during diffusion tensor imaging at 3 T.** *Neuroimage* 2006; 32:93–103 CrossRef Medline
- Brex PA, Parker GJ, Leary SM, et al. **Lesion heterogeneity in multiple sclerosis: a study of the relations between appearances on T1 weighted images, T1 relaxation times, and metabolite concentrations.** *J Neurol Neurosurg Psychiatry* 2000;68:627–32 CrossRef Medline
- Smith SM, Jenkinson M, Woolrich MW, et al. **Advances in functional**

- and structural MR image analysis and implementation as FSL. *Neuroimage* 2004;2(suppl 1):S208–19 Medline
22. Wang S, Wu EX, Tam CN, et al. **Characterization of white matter injury in a hypoxic-ischemic neonatal rat model by diffusion tensor MRI.** *Stroke* 2008;39:2348–53 CrossRef Medline
 23. Kim JH, Loy DN, Liang HF, et al. **Noninvasive diffusion tensor imaging of evolving white matter pathology in a mouse model of acute spinal cord injury.** *Magn Reson Med* 2007;58:253–60 CrossRef Medline
 24. Castriota Scanderbeg A, Tomaiuolo F, Sabatini U, et al. **Demyelinating plaques in relapsing-remitting and secondary-progressive multiple sclerosis: assessment with diffusion MR imaging.** *AJNR Am J Neuroradiol* 2000;21:862–68 Medline
 25. Nusbaum AO, Lu D, Tang CY, et al. **Quantitative diffusion measurements in focal multiple sclerosis lesions: correlations with appearance on T1-weighted MR images.** *AJR Am J Roentgenol* 2000;175:821–25 CrossRef Medline
 26. Bitsch A, Kuhlmann T, Stadelmann C, et al. **A longitudinal MRI study of histopathologically defined hypointense multiple sclerosis lesions.** *Ann Neurol* 2001;49:793–96 CrossRef Medline
 27. Brück W, Bitsch A, Kolenda H, et al. **Inflammatory central nervous system demyelination: correlation of magnetic resonance imaging findings with lesion pathology.** *Ann Neurol* 1997;42:783–93 CrossRef Medline
 28. Rashid W, Hadjiprocopis A, Davies G, et al. **Longitudinal evaluation of clinically early relapsing-remitting multiple sclerosis with diffusion tensor imaging.** *J Neurol* 2008;255:390–97 CrossRef Medline
 29. Boretius S, Escher A, Dallenga T, et al. **Assessment of lesion pathology in a new animal model of MS by multiparametric MRI and DTI.** *Neuroimage* 2012;59:2678–88 CrossRef Medline
 30. Kuhlmann T, Lingfeld G, Bitsch A, et al. **Acute axonal damage in multiple sclerosis is most extensive in early disease stages and decreases over time.** *Brain* 2002;125:2202–12 CrossRef Medline
 31. Moll NM, Rietsch AM, Thomas S, et al. **Multiple sclerosis normal-appearing white matter: pathology-imaging correlations.** *Ann Neurol* 2011;70:764–73 CrossRef Medline
 32. Roosendaal SD, Geurts JJ, Vrenken H, et al. **Regional DTI differences in multiple sclerosis patients.** *Neuroimage* 2009;44:1397–403 CrossRef Medline
 33. Zivadinov R, Hussein S, Bergsland N, et al. **Magnetization transfer imaging of acute black holes in patients on glatiramer acetate.** *Front Biosci (Elite Ed)* 2012;4:1496–504 Medline
 34. Chen JT, Kuhlmann T, Jansen GH, et al; Canadian MS/BMT Study Group. **Voxel-based analysis of the evolution of magnetization transfer ratio to quantify remyelination and demyelination with histopathological validation in a multiple sclerosis lesion.** *Neuroimage* 2007;36:1152–58 CrossRef Medline
 35. Jones DK, Basser PJ. **“Squashing peanuts and smashing pumpkins”: how noise distorts diffusion-weighted MR data.** *Magn Reson Med* 2004;52:979–93 CrossRef Medline

Clinicoradiologic Correlations of Cerebral Microbleeds in Advanced Age

I. Barnaure, M.-L. Montandon, C. Rodriguez, F. Herrmann, K.O. Lövblad, P. Giannakopoulos, and S. Haller



ABSTRACT

BACKGROUND AND PURPOSE: The presence of cerebral microbleeds has been associated with dementia and cognitive decline, although studies report conflicting results. Our aim was to determine the potential role of the presence and location of cerebral microbleeds in early stages of cognitive decline.

MATERIALS AND METHODS: Baseline 3T MR imaging examinations including SWI sequences of 328 cognitively intact community-dwelling controls and 72 subjects with mild cognitive impairment were analyzed with respect to the presence and distribution of cerebral microbleeds. A neuropsychological follow-up of controls was performed at 18 months post inclusion and identified cases with subtle cognitive deficits were referred to as controls with a deteriorating condition. Group differences in radiologic parameters were studied by using nonparametric tests, 1-way analysis of variance, and Spearman correlation coefficients.

RESULTS: Cerebral microbleed prevalence was similar in subjects with mild cognitive impairment and controls with stable and cognitively deteriorating conditions (25%–31.9%). In all diagnostic groups, lobar cerebral microbleeds were more common. They occurred in 20.1% of all cases compared with 6.5% of cases with deep cerebral microbleeds. None of the investigated variables (age, sex, microbleed number, location and depth, baseline Mini-Mental State Examination score, and the Fazekas score) were significantly associated with cognitive deterioration with the exception of education of >12 years showing a slight but significant protective effect (OR, 0.44; 95% CI, 0.22–0.92; $P = .028$). The Mini-Mental State Examination and the Buschke total score were correlated with neither the total number nor lobar-versus-deep location of cerebral microbleeds.

CONCLUSIONS: Cerebral microbleed presence, location, and severity are not related to the early stages of cognitive decline in advanced age.

ABBREVIATIONS: CDR = Clinical Dementia Rating scale; CMB = cerebral microbleed; dCON = control with a deteriorating condition; sCON = control with a stable condition; MCI = mild cognitive impairment; MMSE = Mini-Mental State Examination

Cerebral microbleeds (CMBs) are small, round, or ovoid lesions of the cerebral parenchyma of low signal intensity on T2*-weighted and susceptibility-weighted sequences, with a max-

imal diameter of 5–10 mm,¹ corresponding histologically to focal accumulations of hemosiderin-containing macrophages.² They can be found in healthy subjects, their prevalence increasing with age,^{3–5} but are more frequent in patients with hypertensive encephalopathy and cerebral amyloid angiopathy.^{1,2} Microbleeds have been considered markers of small-vessel disease and are strongly associated with white matter hyperintensities.^{3,6,7} Both hypertensive small-vessel disease and cerebral amyloid angiopathy contribute to the formation of lobar CMBs, while CMBs located in the basal ganglia or infratentorial brain regions are mainly associated with hypertensive vasculopathy.^{8–11}

Their impact on cognition is still a matter of debate. Several studies supported a deleterious effect of CMBs, including increased prevalence in vascular dementia but also in Alzheimer disease,^{3,12–14} associations with poorer cognitive function in cross-sectional studies of patients with dementia,¹⁵ lower A β 42 levels in the CSF in Alzheimer disease and vascular dementia,¹⁶

Received March 15, 2016; accepted after revision August 15.

From the Division of Neuroradiology (I.B., K.O.L.), Department of Mental Health and Psychiatry (M.-L.M., C.R., P.G.), and Departments of Internal Medicine, Rehabilitation, and Geriatrics (F.H.), Geneva University Hospitals, Geneva, Switzerland; Affidea Centre de Diagnostique Radiologique de Carouge CDRC (S.H.), Geneva, Switzerland; Departments of Surgical Sciences and Radiology (S.H.), Uppsala University, Uppsala, Sweden; Department of Neuroradiology (S.H.), University Hospital Freiburg, Germany; and Faculty of Medicine (S.H.), University of Geneva, Geneva, Switzerland.

This study was partially funded by grants from the Swiss National Foundation (grant Nos. SNF 3200B0-1161193, SPUM 33CM30-124111).

Please address correspondence to Sven Haller, MD, MSc, Affidea Centre de Diagnostique Radiologique de Carouge CDRC, Clos de la Fonderie 1, 1227 Carouge, Switzerland; e-mail: sven.haller@me.com

Indicates open access to non-subscribers at www.ajnr.org

Indicates article with supplemental on-line appendix.

<http://dx.doi.org/10.3174/ajnr.A4956>

and decreased frontal-executive performances at 5-year follow-up in patients with stroke.¹⁷ However, negative data were also reported with no or marginal impact of CMBs in early Alzheimer disease (for a review see van der Flier¹⁸ and Heringa et al¹⁹) and in subjects with subcortical vascular cognitive impairment²⁰ and symptomatic small-vessel disease.²¹

Data on mild cognitive impairment (MCI) are even more ambiguous. This entity was initially used to denote a functionally nondisabling amnesic disorder, but its definition has been recently expanded to include any form of cognitive problem that may increase the risk of clinically overt dementia. Certain studies postulated that CMBs are significantly associated with both MCI and the risk of conversion to Alzheimer disease (for a review see Loitfelder et al⁸ and Lei et al²²). Other authors reported a significant association between amyloid deposition and lobar CMB occurrence in patients with MCI but without any relationship between their presence and early cognitive decline.²³ Similarly, substantial formation of lobar but not deep and infratentorial microbleeds was associated with worse cognition in the Rotterdam Scan Study.²⁴ The latter is a population-based study on age-related changes on brain MR imaging. Cross-sectional analysis of 3979 individuals without dementia from this cohort revealed that subjects with higher numbers of lobar microbleeds performed worse in tests exploring various cognitive domains, even after adjustments for vascular risk factors and brain atrophy.²⁴

Most of the previous studies concerned cross-sectional case-control comparisons and did not explore whether CMBs may predict very early phases of cognitive deterioration in healthy controls. Furthermore, the location of CMBs that may be associated with the disruption of brain networks was rarely taken into account.¹⁹ The current investigation is based on the assumption that if CMBs reflect structural damage, their location should have an impact on the corresponding function affected. To determine the potential role of CMBs in early stages of cognitive decline before MCI, we evaluated both the number and location of CMBs in a large sample of 328 community-dwelling healthy controls who were cognitively intact. Imaging was performed at baseline, and cognitive status was determined on the basis of extensive neuropsychological testing both at baseline and at 18-month follow-up. The results were compared with a group of 72 fully documented patients with MCI recruited in the same geographic area.

MATERIALS AND METHODS

Participants

Participants were contacted via advertisements in local media to guarantee a community-based sample. After detailed information about the research was provided, telephone screening was performed with the following inclusion criteria: normal or corrected-to-normal visual acuity; no history of major medical disorders (neoplasm, cardiovascular disorders, infectious diseases), sustained head injury, or psychiatric or neurologic disorders; no alcohol or drug abuse; and no regular use of neuroleptics, antidepressants, mood stabilizers, anticonvulsant drugs, or psychostimulants. To control for the confounding effect of cerebrovascular diseases, we did not include patients with subtle cardiovascular symptoms, severe hypertension, and a history of

stroke or transient ischemic episodes in the present study. Mild hypertension was present at baseline in 27% of the entire sample. The local ethics committee approved this prospective study, and all participants gave written informed consent before inclusion. The inclusion period for controls and those with MCI was from October 2010 to January 2011, when the present cohort was established in the context of a federally funded research project for identifying functional imaging and electroencephalography markers predicting subtle cognitive deficits in a community-dwelling sample of healthy controls. A relatively small number of patients with MCI were recruited as an additional control group.

Neuropsychological Assessment

All participants underwent extensive neuropsychological testing, as described in detail in the On-line Appendix. Briefly, all participants underwent neuropsychological testing and MR imaging at baseline. Participants classified as controls at baseline additionally underwent neuropsychological testing at 18-month follow-up. Those whose cognitive scores remained unchanged were classified as controls with a stable condition (sCON). Those whose performance at follow-up was at least 0.5 SDs lower compared with the first evaluation on at least 2 cognitive tests were classified as controls with a deteriorating condition (dCON). All individuals were also evaluated with the Clinical Dementia Rating scale (CDR).²⁵ Only those with a CDR score of 0 and scores within 1.5 SDs of the age-appropriate mean in all other tests were included in the control group. In agreement with the Petersen criteria,²⁶ participants having a CDR score of 0.5 but no dementia and a score exceeding 1.5 SDs below the age-appropriate mean in any of the above tests were confirmed as to their MCI status.

Two neuropsychologists clinically assessed all individuals independently with high interrater agreement ($\kappa = 0.92$). The final classification of sCON versus dCON was made by a trained neuropsychologist, who took into account both the neuropsychological test results and overall clinical assessment.²⁷

MR Imaging

MR imaging was performed with a routine 3T scanner (Magnetom Trio; Siemens, Erlangen, Germany) and included a standard susceptibility-weighted sequence (matrix, 192 × 256 × 128; voxel size, 0.98 × 0.98 × 1.1 mm; TE/TR, 20/28 ms; number of signals acquired, 1; flip angle, 15°; parallel imaging factor, 2; acquisition time, 6 minutes 1 second). In addition, standard DTI, T2-weighted, T1-weighted, and fluid-attenuated inversion recovery sequences were performed and analyzed to exclude anomalies such as ischemic lesions, parenchymal macrobleeds, extra-axial hematomas, or space-occupying lesions.

Image Analysis

Cerebral microbleeds were defined as focal areas (<10 mm) of very low signal intensity. Two independent readers (1 board-certified neuroradiologist and 1 trained neuropsychologist with 7 and 3 years of experience, respectively) analyzed SWI to define the presence, number, and location of CMBs. In cases of discordant findings, a senior third reader (a board-certified neuroradiologist with 16 years of experience) reviewed the images and determined

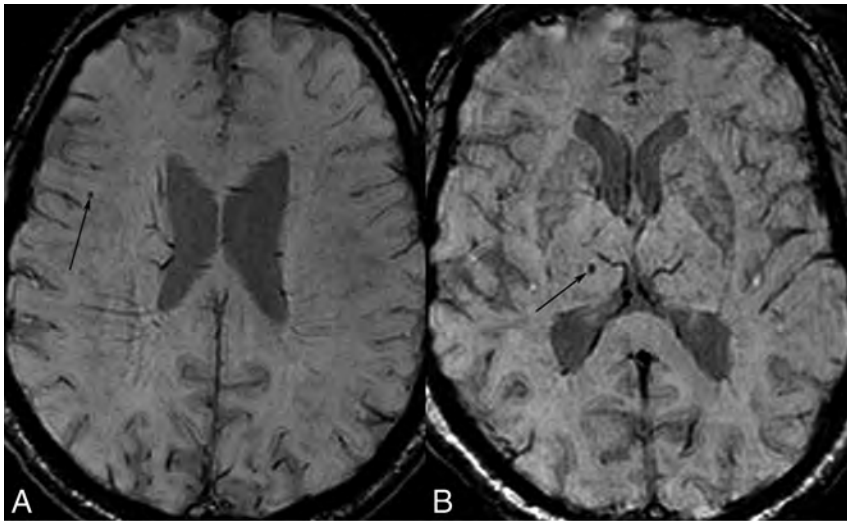


FIGURE. Cerebral microbleeds. Axial SWI of 2 subjects. A, Lobar CMB. Right inferior frontal CMB (arrow) close to the corticomedullary junction. B, Right thalamic CMB (arrow).

Table 1: Demographic data for sCON, dCON, and MCI

	sCON (n = 152)	dCON (n = 176)	MCI (n = 72)	P Value
Females (%)	93 (61.2)	111 (63.1)	25 (34.7)	<.001
Age (M, SD)	73.8 (3.9)	74.5 (4.1)	74 (6.2)	.372
Education ^a				.070
<9 (%)	24 (15.8)	31 (17.6)	8 (11.1)	
9–12 (%)	62 (40.8)	93 (52.8)	37 (51.4)	
>12 (%)	66 (43.4)	52 (29.6)	27 (37.5)	

Note:—M indicates mean.

^a Education in years of schooling.

the final rating. CMB “mimics” such as signal voids caused by vessels or basal ganglia calcification were excluded.

CMBs were classified according to 2 different categories (Figure): lobar versus deep (including the basal ganglia, thalamus, deep white matter, and infratentorial structures) and with further classification of lobar microbleeds according to the cerebral lobe involved (frontal, parietal, temporal, or occipital).

In addition to the analysis of CMBs, microvascular burden in the form of white matter lesions was analyzed on T2-/FLAIR-weighted images according to the established Fazekas scale.²⁸

Statistical Analysis

χ^2 tests, Kruskal-Wallis nonparametric tests, and 1-way ANOVA were used to compare binary/nominal, ordinal, and continuous Gaussian variables, respectively, among the 3 groups. The Cuzick nonparametric test for trend across ordered groups was used to compare the lobar distribution of microbleeds. A *t* test and the Mann-Whitney *U* test were applied to compare ordinal and continuous variables between 2 groups. Moreover, the number and location of CMBs were correlated with neuropsychological data at baseline by using the Spearman rank correlation. A multiple logistic regression model was built with sCON/dCON distinction as the dependent variable and age, sex, CMB location and depth, baseline Mini-Mental State Examination (MMSE) score, education, and Fazekas scale score as independent variables.

A multiple linear regression model was built to determine whether CMBs predict longitudinal changes in cognitive scores. Because cognitive performances at follow-up are expressed on

different scales, which are often discrete, they cannot be linearly combined by adding the individual scores to a unique composite cognitive score. We converted all results to *z* scores; then, we summed the number of cognitive tests at follow-up with performances at least 0.5 SDs higher compared with the first evaluation, leading to the number of tests with improved performances (range, 0–14). Similarly, we summed the number of cognitive tests at follow-up with performances at least 0.5 SDs lower compared with the first evaluation, leading to the number of tests with decreased performances (range, 0–14). Finally, we computed the number of tests with improved minus the number of tests with decreased performances to obtain a continuous cognitive score and built a multiple linear regression model with this score as the dependent variable and age, sex, CMB location and depth, baseline MMSE score, education, and Fazekas scale score as independent variables.

All statistics were performed by using the STATA statistical software, Version 14.1 (StataCorp, College Station, Texas).

RESULTS

Demographic Data

Demographic data of the cohort are shown in Table 1. There were no significant differences among the 3 groups (sCON, dCON, and MCI) regarding age (the mean age was 74 years) and education level. However, a significant difference was evident for sex with a male predominance in the MCI group ($P < .001$).

Neuropsychological Data

Neuropsychological data are presented in Table 2. As expected, there were group differences at follow-up, with worse cognitive performances of dCON for the Shapes test (3 immediate recalls [$P = .004$] and delayed recall [$P = .024$]), Digit Symbol Coding ($P < .001$), and ideomotor transitive praxis ($P = .008$). The Shapes test assesses visual memory (immediate and delayed) via the reproduction of simple designs. Digit Symbol Coding (time-monitored copy of symbols) explores perceptual-motor speed mostly related to attention. Ideomotor transitive praxis refers to the ability to perform transitive movements demonstrating the use of tools.

Number of CMBs

Eleven subjects were excluded due to a presumed (incidental) diagnosis of amyloid angiopathy (based on the observation of multiple microbleeds at the corticomedullary junction in association with signs of superficial siderosis or sequelae of lobar hemorrhage) or hypertensive encephalopathy (based on the observation of microbleeds in association with extensive white matter signal anomalies and infarctions).

Most subjects had no CMBs: 75.0% of sCON, 72.7% of dCON,

Table 2: Neuropsychological data of control subjects

	sCON (n = 152)		dCON (n = 176)		P Value
	M	SD	M	SD	
MMSE	28.6	1.2	28.4	1.5	.439
IADL	8.3	0.82	8.3	1.1	.933
HADS total	5.7	3.5	6.2	3.9	1.000
Anxiety	4.3	2.6	4.5	2.7	1.000
Depression	1.4	1.6	1.8	1.9	.248
Digit Span Forward	5.6	1.1	5.8	0.96	.386
Visual Memory Span Forward (Corsi)	5.1	0.97	5.1	0.89	.876
RI-48 Cued Recall Test					
Delayed cued recall	27.3	5.0	26.8	5.1	1.000
Shapes test					
Total score (3 immediate recalls)	33.9	3.2	32.7	4.3	.004 ^a
Delayed recall	11.7	0.74	11.4	1.3	.024 ^a
Boston Naming Test	19.3	1.0	19.2	1.2	.680
Digit Symbol Coding	56.1	11.8	50.8	11.0	<.001 ^a
Trail-Making Test A					
Time (s)	42.1	16.0	42.0	11.4	1.000
Error	0.05	0.25	0.07	0.31	1.000
Trail-Making Test B					
Time (s)	98.7	41.9	105.7	43.0	.667
Error	0.51	0.73	0.48	0.75	1.000
Verbal Fluency	22.0	5.6	22.5	6.5	1.000
Wisconsin Card Sorting Test					
No. of categories completed	4.6	2.1	4.3	2.2	.223
Praxis					
Constructional	10.9	0.48	10.7	0.77	.032
Ideomotor transitive	9.4	0.81	9.1	1.2	.008 ^a
Ideomotor intransitive	19.5	1.1	19.5	1.0	.686
Reflexive	7.0	0.98	6.9	1.1	.665
Visual gnosis (Ghent Overlapping Figures)	5.0	0.08	5.0	0.08	.917

Note:—IADL indicates Lawton Instrumental Activities of Daily Living scale; HADS, Hospital Anxiety and Depression Scale; M, mean.

^a Significant.

Table 3: Microbleed numbers in the present series^a

Microbleeds	sCON (n = 152)		dCON (n = 176)		MCI (n = 72)	
	No.	%	No.	%	No.	%
0	114	75.0	128	72.7	49	68.1
1	25 (25)	16.5	30 (30)	17.1	21 (21)	29.2
2	9 (18)	5.9	12 (24)	6.8	2 (4)	2.8
3	3 (9)	2.0	6 (18)	3.4	0 (0)	0.00
4	1 (4)	0.66	0 (0)	0.00	0 (0)	0.00
Total ^b	152 (56)	100	176 (72)	100	72 (25)	100

^a Number and proportion of subjects with x numbers of CMB in each group. Number of CMBs is in parentheses.

^b The total number of microbleeds for the 3 groups was 153.

and 68.1% of MCI. Although the prevalence of at least 1 CMB increased from 25.0% in those with sCON to 28.3% in those with dCON and 31.9% in patients with MCI, group differences were not significant. There was no significant difference in the number of CMBs among the 3 groups (Table 3).

Location of CMBs

Lobar versus Deep. Overall, lobar CMBs were more common and occurred in 20.1% of all cases compared with only 6.5% of cases with deep CMBs. There was no significant difference in the number of cases with lobar or deep CMBs among the 3 groups (Table 4).

Lobar Distribution. There was no lobar predilection specific to 1

Table 4: Microbleed distribution^a

Microbleed	sCON (n = 152)		dCON (n = 176)		MCI (n = 72)	
	No.	%	No.	%	No.	%
Location						
None	114	75.0	128	72.7	49	68.1
Lobar	31	20.4	34	19.3	18	25.0
Deep	7	4.6	14	8.0	5	6.9
Lobes						
Frontal	17	11.2	19	10.8	9	12.5
Parietal	5	3.3	11	6.3	5	6.9
Temporal	5	3.3	6	3.4	3	4.2
Occipital ^b	15	9.9	9	5.1	2	2.8

^a Number and proportion of subjects with CMBs for each location.

^b $P = .03$ (between sCON and MCI).

Table 5: Multivariate logistic regression to predict progression (sCON/dCON distinction)

	OR	95% CI	P Value
Male	1.11	(0.68–1.81)	.687
Age (yr)	1.03	(0.97–1.10)	.289
MMSE	0.89	(0.74–1.07)	.216
Education (yr)			
<9	1.00	–	–
9–12	0.76	(0.38–1.50)	.427
>12	0.44	(0.22–0.92)	.028
Fazekas score			
Absent	1.00	–	–
Mild	0.69	(0.41–1.18)	.176
Moderate	0.50	(0.24–1.04)	.062
Severe	1.30	(0.51–3.31)	.586
No. of microbleeds	2.14	(0.70–6.48)	.180
Microbleed lobar location			
Frontal	0.41	(0.07–2.58)	.343
Parietal	1.18	(0.22–6.17)	.847
Temporal	0.63	(0.08–5.13)	.667
Occipital	0.26	(0.05–1.28)	.098
Other	8.09	(0.73–89.20)	.088
Microbleed depth			
Absent	1.00	–	–
Lobar	0.85	(0.21–3.46)	.825
At least 1 deep	0.18	(0.02–2.09)	.171

group. The highest prevalence of CMBs was found in the frontal lobe (11.3% of subjects having frontal lobe CMBs), followed by the occipital, parietal, and temporal lobes (6.5%, 5.3%, and 3.5%, respectively). There was no significant difference in the percentage of cases with CMBs among the 3 groups for any of these lobes, with the exception of the occipital lobe. The groups with more cognitive deficits had significantly fewer occipital lesions than those in the sCON group (P for trend = .0261) (Table 4).

Correlation of CMBs with Neurocognitive Testing

There was no significant correlation between the scores of the neurocognitive testing and the number or location of CMBs. For instance, the MMSE and the Buschke total score were correlated with neither the total number (Spearman $\rho = -0.023$, $P = .653$; $\rho = -0.065$; $P = .213$, respectively) nor the lobar-versus-deep location of CMBs (Spearman $\rho = -0.013$, $P = .790$; $\rho = -0.064$, $P = .219$, respectively). This finding was also the case for lobar distribution (data not shown).

A multiple logistic regression model (Table 5) showed that none of the investigated variables (age, sex, CMB number, loca-

Table 6: Multivariate linear regression to predict the number of cognitive tests ($n = 14$) that showed improvement minus the number of tests in which scores declined >0.5 SDs

	Coefficient	95% CI	P Value
Male	-0.39	(-1.29-0.51)	.391
Age (yr)	-0.06	(-0.18-0.05)	.260
MMSE	-0.35	(-0.68-0.01)	.042
Education (yr)			
<9	1.00	-	-
9-12	0.21	(-1.02-1.44)	.739
>12	0.76	(-0.54-2.07)	.252
Fazekas score			
Absent	1.00	-	-
Mild	0.57	(-0.40-1.55)	.247
Moderate	0.71	(-0.63-2.05)	.298
Severe	0.18	(-1.44-1.81)	.826
No. of microbleeds	-0.36	(-2.27-1.54)	.707
Microbleed lobar location			
Frontal	0.58	(-2.56-3.72)	.716
Parietal	-0.89	(-3.81-2.02)	.546
Temporal	0.80	(-2.91-4.50)	.672
Occipital	1.78	(-0.98-4.55)	.205
Other	-2.01	(-6.12-2.09)	.336
Microbleed depth			
Absent	1.00	-	-
Lobar	-1.39	(-3.93-1.16)	.284
At least 1 deep	1.11	(-3.18-5.40)	.612

tion and depth, baseline MMSE score, and Fazekas score) were significantly associated with deterioration among controls as expressed by the dCON status, with the exception of education of >12 years showing a slight-but-significant protective effect (OR, 0.44; 95% CI, 0.22-0.92; $P = .028$).

Overall, 26% of the sample had a resulting decline in ≥ 2 cognitive tests when simultaneously taking into account both improved and decreased performances in the 14 cognitive tests. A multiple linear regression model (Table 6) predicting the number of cognitive tests ($n = 14$) with improved minus the number of tests with decreased performances by more than 0.5 SDs showed no effect of microbleeds and a protective effect of the MMSE score (coefficient, -0.35; 95% CI, -0.68-0.01; $P = .042$).

DISCUSSION

The current longitudinal, community-based study addresses the impact of CMBs in the very early stage of cognitive decline. We performed imaging at baseline in 328 elderly individuals with intact cognition at inclusion and determined very early cognitive decline based on neuropsychological follow-up at 18 months. Moreover, we compared these results with a group of 72 patients with fully documented MCI. We found no significant differences in the number or location of CMBs between controls with stable and deteriorating conditions and those with MCI. Moreover, there was no significant association between the number or location of CMBs and neuropsychological testing.

Prevalence of CMBs

Overall, the prevalence of CMBs in the present series varied from 25.0% in sCON to 28.3% in dCON and 31.9% in MCI. The trend toward increasing prevalence in MCI cases was not significant.

The prevalence in healthy controls (25.0%-28.3%) was higher

than that reported in earlier studies.^{4,24,29} In particular, the Rotterdam Scan study that focused on elderly controls found a CMB prevalence of 15.3%.^{4,24} Differences in inclusion criteria and imaging techniques may be at the origin of these differences. Notably, our series included elderly individuals with a mean age of 74 years, clearly higher than that in previous reports. Because the prevalence of CMBs increases with age,³⁻⁵ the higher age may partially explain the increased CMB prevalence observed here. In addition, technical differences among the studies, namely examinations at different field strengths (3T versus 1.5T) and with different sequences (SWI versus T2* gradient echo) may contribute to differing results. The present study used an SWI sequence obtained at 3T, while previous reports in controls used 1.5T machines and/or T2* sequences. It has been shown that SWI sequences detect more CMBs than 2D gradient-recalled echo sequences,³⁰⁻³² with an increase in detected lesions of 67% according to Nandigam et al.³⁰

As in our study, the prevalence of CMBs was relatively similar in patients with MCI and controls (14% and 11%, respectively) in the cohort of Ayaz et al,³³ including 28 healthy controls and 75 subjects with MCI examined at 1.5T with a SWI sequence. Other studies found an association between CMBs and low cognitive performance¹² or cognitive decline.¹³ This variability may be due to differences in study design with varying cohort sizes and composition (eg, absence of a control group, varying exclusion criteria) and variable definitions of cognitive impairment. In the present study, the control group at baseline included only subjects who were cognitively intact confirmed by extensive neuropsychological testing. Moreover, subjects with a presumed (incidental) diagnosis of amyloid angiopathy or hypertensive encephalopathy were excluded to eliminate confounding effects.

CMB-Related Variables in the 3 Diagnostic Groups

The location of CMBs (ie, lobar versus deep and according to cerebral lobes) was not different among the 3 groups in our study with the exception of occipital lobe location. In the present series, subjects with MCI had a strikingly low prevalence of CMBs in the occipital cortex compared with sCON (P for trend = .0261). This latter group showed a similar CMB prevalence in frontal (comparable to MCI) and occipital cortices, excluding the idea of a preferential CMB formation in the visual cortex. Although unclear from a physiologic viewpoint, this finding further points to the dissociation between the formation of these lesions and cognitive decline.

In contrast, previous reports showed a strong association of CMB location with performance on cognitive tasks both in cross-sectional and longitudinal studies, though with conflicting results. Qiu et al¹² found that deep hemispheric and infratentorial CMBs were associated with low performance, while in the Rotterdam Scan Study, strictly lobar CMB had the strongest impact on cognition.²⁴ In a longitudinal study by Miwa et al,³⁴ multiple CMBs or the presence of both deep and lobar CMBs (but not only strictly lobar CMBs) was associated with an increased risk for dementia, whereas Chiang et al³⁵ found that lobar CMBs were associated with accelerated cognitive decline in their cohort. One could speculate that because CMBs reflect structural damage in a given region, their formation locally may affect the corresponding

cognitive functions (eg, executive impairment in a frontal location). This was clearly not the case in the present series.

In fact, CMB presence and number did not correlate with neuropsychological variables in our cohort.

CMB-Based Prediction of Cognitive Decline in Healthy Elderly

In previous studies, greater or increasing numbers of CMBs with time were related to impaired cognitive functioning, in both cross-sectional^{12,24} and longitudinal analyses^{13,33-36} in different types of cohorts (eg, population-based or in a memory clinic setting). The nature of the associations between CMBs and cognitive performance was, however, variable and not necessarily independent. While the presence of CMBs was predictive of progression from MCI to dementia in the cohort of Kirsch et al,¹³ this association did not persist when adjusting for age. We found no association between cognitive decline at 18-month follow-up and CMB burden or location at baseline.

Several reasons may explain this clinicoradiologic dissociation. The low number of microbleeds in this community-based sample may prevent establishing valid correlations with clinical variables. Such correlations may become obvious at later time points at further follow-up; the absence of follow-up imaging constitutes one of the limitations of the present investigation. Similarly, the short clinical follow-up interval may have masked potential associations. Kirsch et al¹³ noted that during the 50-month follow-up of their study, only 5% of the subjects initially classified as healthy controls progressed to MCI or dementia. In the cohort of Miwa et al,³⁴ 8% of subjects developed dementia during a median follow-up of 7.5 years. Most of the prior studies did not investigate very early cognitive decline longitudinally. While 26% of controls in the present study showed deteriorating performance in an 18-month period, the investigated changes may have been too subtle, leading to the absence of an association with CMB observed here. In fact, we cannot formally exclude cognitive restoration possibly occurring at later time points in some of our subjects with dCON. One could speculate that a more prominent decline at later follow-up could allow identifying a cognitive impact of CMBs. However, this is unlikely because no difference in CMB prevalence was found between subjects with MCI with stable and deteriorating conditions in a prior study.³⁶

Alternatively, structural damage reflected by isolated CMBs may not be important enough to impair clinically apparent locally associated functions, in contrast to the larger number of CMBs in vascular dementia and cerebral amyloid angiopathy (and Alzheimer disease).^{1,3,4}

In contrast to CMB, there has been rising interest in the correlation of declining cognitive function and another possible marker of small (and large) vessel disease in dementia, cortical microinfarcts. This entity consists of lesions barely visible at conventional imaging but demonstrated at pathology and 7T MR imaging, with the lesions visible on imaging (especially at 3T) representing only a small fraction of the actual lesional burden.³⁷ Future radiologic studies with new-generation MRIs may lead to better insight into the deleterious effects of widely disseminated microvascular changes in advanced age.

CONCLUSIONS

Ultimately, in this large extensively tested cohort of subjects with MCI and controls having undergone MR imaging at 3T with a SWI sequence, there was no group-level difference in microbleed prevalence or distribution or a correlation with neuropsychological test results.

Disclosures: Sven Haller—RELATED: Grant: Swiss National Foundation Grant SNF 3200B0-1161193 and SPUM 33CM30-124111.* *Money paid to the institution.

REFERENCES

1. Greenberg SM, Vernooij MW, Cordonnier C, et al; Microbleed Study Group. **Cerebral microbleeds: a guide to detection and interpretation.** *Lancet Neurol* 2009;8:165–74 CrossRef Medline
2. Fazekas F, Kleinert R, Roob G, et al. **Histopathologic analysis of foci of signal loss on gradient-echo T2*-weighted MR images in patients with spontaneous intracerebral hemorrhage: evidence of microangiopathy-related microbleeds.** *AJNR Am J Neuroradiol* 1999;20:637–42 Medline
3. Cordonnier C, van der Flier WM, Sluimer JD, et al. **Prevalence and severity of microbleeds in a memory clinic setting.** *Neurology* 2006;66:1356–60 CrossRef Medline
4. Vernooij MW, van der Lugt A, Ikram MA, et al. **Prevalence and risk factors of cerebral microbleeds: the Rotterdam Scan Study.** *Neurology* 2008;70:1208–14 CrossRef Medline
5. Sveinbjornsdottir S, Sigurdsson S, Aspelund T, et al. **Cerebral microbleeds in the population based AGES-Reykjavik study: prevalence and location.** *J Neurol Neurosurg Psychiatry* 2008;79:1002–06 CrossRef Medline
6. Schmidt R, Berghold A, Jokinen H, et al. **White matter lesion progression in LADIS: frequency, clinical effects, and sample size calculations.** *Stroke* 2012;43:2643–47 CrossRef Medline
7. Del Brutto VJ, Zambrano M, Mera RM, et al. **Population-based study of cerebral microbleeds in stroke-free older adults living in Rural Ecuador: the Atahualpa Project.** *Stroke* 2015;46:1984–86 CrossRef Medline
8. Loitfelder M, Seiler S, Schwingenschuh P, et al. **Cerebral microbleeds: a review.** *Panminerva Med* 2012;54:149–60 Medline Medline
9. Park JH, Seo SW, Kim C, et al. **Pathogenesis of cerebral microbleeds: in vivo imaging of amyloid and subcortical ischemic small vessel disease in 226 individuals with cognitive impairment.** *Ann Neurol* 2013;73:584–93 CrossRef Medline
10. Nagasawa J, Kiyozaka T, Ikeda K. **Prevalence and clinicoradiological analyses of patients with Alzheimer disease coexisting multiple microbleeds.** *J Stroke Cerebrovasc Dis* 2014;23:2444–49 CrossRef Medline
11. Yakushiji Y, Yokota C, Yamada N, et al. **Clinical characteristics by topographical distribution of brain microbleeds, with a particular emphasis on diffuse microbleeds.** *J Stroke Cerebrovasc Dis* 2011;20:214–21 CrossRef Medline
12. Qiu C, Cotch MF, Sigurdsson S, et al. **Cerebral microbleeds, retinopathy, and dementia: the AGES-Reykjavik Study.** *Neurology* 2010;75:2221–28 CrossRef Medline
13. Kirsch W, McAuley G, Holshouser B, et al. **Serial susceptibility weighted MRI measures brain iron and microbleeds in dementia.** *J Alzheimers Dis* 2009;17:599–609 Medline
14. Uetani H, Hirai T, Hashimoto M, et al. **Prevalence and topography of small hypointense foci suggesting microbleeds on 3T susceptibility-weighted imaging in various types of dementia.** *AJNR Am J Neuroradiol* 2013;34:984–89 CrossRef Medline
15. Hilal S, Saini M, Tan CS, et al. **Cerebral microbleeds and cognition: the epidemiology of dementia in Singapore study.** *Alzheimer Dis Assoc Disord* 2014;28:106–12 CrossRef Medline
16. Kester MI, Goos JD, Teunissen CE, et al. **Associations between cerebral small-vessel disease and Alzheimer disease pathology as mea-**

- asured by cerebrospinal fluid biomarkers. *JAMA Neurol* 2014;71:855–62 CrossRef Medline
17. Gregoire SM, Smith K, Jäger HR, et al. **Cerebral microbleeds and long-term cognitive outcome: longitudinal cohort study of stroke clinic patients.** *Cerebrovasc Dis* 2012;33:430–35 CrossRef Medline
 18. van der Flier WM. **Clinical aspects of microbleeds in Alzheimer's disease.** *J Neurol Sci* 2012;322:56–58 CrossRef Medline
 19. Heringa SM, Reijmer YD, Leemans A, et al; Utrecht Vascular Cognitive Impairment (VCI) Study Group. **Multiple microbleeds are related to cerebral network disruptions in patients with early Alzheimer's disease.** *J Alzheimers Dis* 2014;38:211–21 CrossRef Medline
 20. Park JH, Seo SW, Kim C, et al. **Effects of cerebrovascular disease and amyloid beta burden on cognition in subjects with subcortical vascular cognitive impairment.** *Neurobiol Aging* 2014;35:254–60 CrossRef Medline
 21. Patel B, Lawrence AJ, Chung AW, et al. **Cerebral microbleeds and cognition in patients with symptomatic small vessel disease.** *Stroke* 2013;44:356–61 CrossRef Medline
 22. Lei C, Lin S, Tao W, et al. **Association between cerebral microbleeds and cognitive function: a systematic review.** *J Neurol Neurosurg Psychiatry* 2013;84:693–97 CrossRef Medline
 23. Yates PA, Desmond PM, Phal PM, et al; AIBL Research Group. **Incidence of cerebral microbleeds in preclinical Alzheimer disease.** *Neurology* 2014;82:1266–73 CrossRef Medline
 24. Poels MM, Ikram MA, van der Lugt A, et al. **Cerebral microbleeds are associated with worse cognitive function: the Rotterdam Scan Study.** *Neurology* 2012;78:326–33 CrossRef Medline
 25. Hughes CP, Berg L, Danziger WL, et al. **A new clinical scale for the staging of dementia.** *Br J Psychiatry* 1982;140:566–72 CrossRef Medline
 26. Petersen RC. **Mild cognitive impairment as a diagnostic entity.** *J Intern Med* 2004;256:183–94 CrossRef Medline
 27. Deiber MP, Meziane HB, Hasler R, et al. **Attention and working memory-related EEG markers of subtle cognitive deterioration in healthy elderly individuals.** *J Alzheimers Dis* 2015;47:335–49 CrossRef Medline
 28. Fazekas F, Chawluk JB, Alavi A, et al. **MR signal abnormalities at 1.5 T in Alzheimer's dementia and normal aging.** *AJR Am J Roentgenol* 1987;149:351–56 CrossRef Medline
 29. Jeerakathil T, Wolf PA, Beiser A, et al. **Cerebral microbleeds: prevalence and associations with cardiovascular risk factors in the Framingham Study.** *Stroke* 2004;35:1831–35 CrossRef Medline
 30. Nandigam RN, Viswanathan A, Delgado P, et al. **MR imaging detection of cerebral microbleeds: effect of susceptibility-weighted imaging, section thickness, and field strength.** *AJNR Am J Neuroradiol* 2009;30:338–43 Medline
 31. Goos JD, van der Flier WM, Knol DL, et al. **Clinical relevance of improved microbleed detection by susceptibility-weighted magnetic resonance imaging.** *Stroke* 2011;42:1894–900 CrossRef Medline
 32. Shams S, Martola J, Cavallin L, et al. **SWI or T2*: which MRI sequence to use in the detection of cerebral microbleeds? The Karolinska Imaging Dementia Study.** *AJNR Am J Neuroradiol* 2015;36:1089–95 CrossRef Medline
 33. Ayaz M, Boikov AS, Haacke EM, et al. **Imaging cerebral microbleeds using susceptibility weighted imaging: one step toward detecting vascular dementia.** *J Magn Reson Imaging* 2010;31:142–48 CrossRef Medline
 34. Miwa K, Tanaka M, Okazaki S, et al. **Multiple or mixed cerebral microbleeds and dementia in patients with vascular risk factors.** *Neurology* 2014;83:646–53 CrossRef Medline
 35. Chiang GC, Cruz Hernandez JC, Kantarci K, et al. **Cerebral microbleeds, CSF p-tau, and cognitive decline: significance of anatomic distribution.** *AJNR Am J Neuroradiol* 2015;36:1635–41 CrossRef Medline
 36. Haller S, Bartsch A, Nguyen D, et al. **Cerebral microhemorrhage and iron deposition in mild cognitive impairment: susceptibility-weighted MR imaging assessment.** *Radiology* 2010;257:764–73 CrossRef Medline
 37. van Veluw SJ, Hilal S, Kuijff HJ, et al. **Cortical microinfarcts on 3T MRI: clinical correlates in memory-clinic patients.** *Alzheimers Dement* 2015;11:1500–09 CrossRef Medline

Body Temperature Modulates Infarction Growth following Endovascular Reperfusion

 S. Dehkharghani,  M. Bowen,  D.C. Haussen,  T. Gleason,  A. Prater,  Q. Cai,  J. Kang, and  R.G. Nogueira

ABSTRACT

BACKGROUND AND PURPOSE: The neuronal substrate is highly sensitive to temperature elevation; however, its impact on the fate of the ischemic penumbra has not been established. We analyzed interactions between temperature and penumbral expansion among successfully reperfused patients with acute ischemic stroke, hypothesizing infarction growth and worse outcomes among patients with fever who achieve full reperfusion.

MATERIALS AND METHODS: Data from 129 successfully reperfused (modified TICl 2b/3) patients (mean age, 65 ± 15 years) presenting within 12 hours of onset were examined from a prospectively collected acute ischemic stroke registry. CT perfusion was analyzed to produce infarct core, hypoperfusion, and penumbral mismatch volumes. Final DWI infarction volumes were measured, and relative infarction growth was computed. Systemic temperatures were recorded throughout hospitalization. Correlational and logistic regression analyses assessed the associations between fever ($>37.5^\circ\text{C}$) and both relative infarction growth and favorable clinical outcome (90-day mRS of ≤ 2), corrected for NIHSS score, reperfusion times, and age. An optimized model for outcome prediction was computed by using the Akaike Information Criterion.

RESULTS: The median presentation NIHSS score was 18 (interquartile range, 14–22). Median (interquartile range) CTP-derived volumes were: core = 9.6 mL (1.5–25.3 mL); hypoperfusion = 133 mL (84.2–204 mL); and final infarct volume = 9.6 mL (8.3–45.2 mL). Highly significant correlations were observed between temperature of $>37.5^\circ\text{C}$ and relative infarction growth (Kendall τ correlation coefficient = 0.24, $P = .002$). Odds ratios for favorable clinical outcome suggested a trend toward significance for fever in predicting a 90-day mRS of ≤ 2 (OR = 0.31, $P = .05$). The optimized predictive model for favorable outcomes included age, NIHSS score, procedure time to reperfusion, and fever. Likelihood ratios confirmed the superiority of fever inclusion ($P < .05$). Baseline temperature, range, and maximum temperature did not meet statistical significance.

CONCLUSIONS: These findings suggest that imaging and clinical outcomes may be affected by systemic temperature elevations, promoting infarction growth despite reperfusion.

ABBREVIATIONS: AIC = Akaike Information Criterion; AIS = acute ischemic stroke; IQR = interquartile range; mTICl = modified TICl; R = tissue residue function; T_{max} = time-to-maximum of the tissue residue function

The exquisite temperature sensitivity of the neuronal substrate has been detailed extensively since initial reports in canine models in the early 20th century.¹ The development of pyrexia

following acute ischemic stroke (AIS) has been well-documented and has been tied to stroke severity, infarct size, and poor functional outcomes, as well as to both short-term and long-term mortality.^{2–6}

The untoward impact of even small brain temperature elevations during ischemic injury is well-described, with histopathologic evidence of irreversible ischemic injury varying substantially with minor temperature changes, and even across physiologic

Received June 1, 2016; accepted after revision August 23.

From the Department of Radiology and Imaging Sciences (S.D., M.B., T.G., A.P.), Emory University Hospital, Atlanta, Georgia; Department of Neurology (S.D., D.C.H., R.G.N.), Marcus Stroke and Neuroscience Center, Grady Memorial Hospital and Emory University Hospital, Atlanta, Georgia; Department of Biostatistics (Q.C.), Emory University, Atlanta, Georgia; and Department of Biostatistics (J.K.), University of Michigan, Ann Arbor, Michigan.

The corresponding author had full access to the data in the study and maintains final responsibility for the decision to submit for publication.

Paper previously presented at: Annual Meeting of the Radiological Society of North America, November 29 to December 4, 2015; Chicago, Illinois. "Body Temperature Fluctuations Modulate Infarct Expansion, Penumbral Rescue, and Clinical

Outcome in AIS Following Successful Endovascular Reperfusion: Impact of Subclinical Temperature Changes on Ischemic Progression." Paper No. RC305-11.

Please address correspondence to Seena Dehkharghani, MD, New York University, Department of Radiology, Neuroradiology Section, 660 First Ave, New York, NY 10016; e-mail: Seena.Dehkharghani@NYUMC.Org

<http://dx.doi.org/10.3174/ajnr.A4969>

ranges.⁷ It remains unclear, however, whether temperature elevation is associated with poor outcome as a causal factor driving stroke severity and penumbral expansion or as an epiphenomenon to inherently severe or extensive ischemic injury.

The goals of this study were to analyze the impact of temperature elevation on the fate of at-risk tissues as derived from the penumbra paradigm of cerebrovascular ischemia by using CTP. We studied the interaction of systemic temperature fluctuations with expansion of infarcted tissues in a cohort of successfully reperfused patients with AIS, hypothesizing greater relative infarction growth as a function of temperature elevation in the early aftermath of AIS.

MATERIALS AND METHODS

Study Design

We retrospectively reviewed a prospectively collected endovascular stroke therapy registry of 605 consecutive patients at the Marcus Stroke and Neuroscience Center at Grady Memorial Hospital, spanning December 2010 to September 2014, with approval of the institutional review board. Patients were included for analysis if they met all of the following criteria: 1) AIS due to cerebrovascular large-vessel occlusion, including the internal carotid artery, anterior cerebral artery, and/or the middle cerebral artery (M1 and/or M2 segments), or vertebrobasilar circulation on CTA; 2) time from last known well to groin puncture, ≤ 12 hours; 3) successful endovascular reperfusion (mTICI 2b/3); and 4) full CTP datasets obtained and technically adequate for analysis of ischemic core and penumbral volumes.

Imaging Protocol

All patients underwent an institutional imaging protocol, including noncontrast CT, CTA, and CTP. CT was performed on a 40-mm, 64-detector row clinical system (LightSpeed VCT; GE Healthcare, Milwaukee, Wisconsin). Helical noncontrast CT (120 kV, 100–350 auto-mA) was performed from the foramen magnum through the vertex at a 5.0-mm section thickness. In the absence of visible intracranial hemorrhage during real-time evaluation by a radiologist and stroke neurologist, 2 contiguous CTP slabs were obtained for 8-cm combined coverage of the supratentorial brain, obtained at eight 5-mm sections per slab. Cine mode acquisition (80 kV, 100 mA) permitting high-temporal-resolution (1-second sampling interval) dynamic bolus passage imaging was obtained following the administration of 35 mL of iodinated contrast (iopamidol, Isovue 370; Bracco, Princeton, New Jersey), power injected at 5 mL/s through an 18-ga or larger antecubital IV access. Contrast administration was followed by a 25-mL saline flush at the same rate. Lastly, helical CTA (120 kV, 200–350 auto-mA) was performed from the carina to the vertex (section thickness/interval, 0.625/0.375 mm) following IV administration of 70 mL of iodinated contrast injected at 5 mL/s and followed by a 25-mL saline flush. All images were transferred to a separate workstation for analysis (Apple Mac Pro; Apple, Cupertino, California) by using a third-party viewer (OsiriX 64-bit; <http://www.osirix-viewer.com>).

CT Perfusion Analysis

All perfusion imaging was processed by using the fully user- and vendor-independent software platform RAPid processing of Per-

fusIon and Diffusion (RAPID version 4.5; iSchemaView, Stanford, California) to produce irreversible infarction core and total hypoperfused tissue volume estimates, detailed below. Details of the CTP processing pipeline were provided previously.⁸ Briefly, following preprocessing steps correcting rigid body motion, arterial input function selection was performed and deconvolved from the voxel time-attenuation course using a delay-insensitive algorithm for isolation of the tissue residue function (R). Time-to-maximum (T_{max}) of R was determined on a voxelwise basis, with T_{max} maps thresholded at 6 seconds and overlaid on the source CTP data. All analyses and data collection were performed under the direct supervision of a dedicated neuroradiologist (S.D.) with subspecialty certification and >8 years of experience in advanced clinical stroke imaging and research, and blinded to the clinical and outcome data.

CBF expressed in milliliters/100 g/min was computed on a voxelwise basis for estimation of irreversibly infarcted (core) tissues determined at relative CBF $<30\%$ of contralateral normal tissues, as conducted recently in the clinical and stroke trial setting.^{8,9} Processed maps were automatically generated and overlaid on source images for review purposes. A mismatch volume defining the putative ischemic penumbra was calculated as the difference between $T_{max} >6$ volumes and relative CBF core infarction volumes (Fig 1).

Temperature Analysis

Systemic temperatures were recovered from the patient medical record, beginning from the initial presentation and continuously to the time of follow-up MR imaging, up to every 15 minutes, with minima, maxima, and total ranges collected for each patient. Tympanic temperatures were preferentially used for analysis. In addition to maximum temperature, the following temperature-related parameters were determined for each patient: 1) presentation baseline temperature, 2) temperature range (maximum–minimum), and 3) dichotomized fever (defined as a temperature of $>37.5^{\circ}\text{C}$ during the recording period).¹⁰ Patient records were reviewed for positive cultures or other clinical factors indicating the presence of profound systemic infection during hospitalization and up to the time of final follow-up imaging. Antipyretic administration was obtained from the medical record. Data on procedure duration for endovascular thrombectomy and the use of general or monitored anesthesia care were collected from intraoperative reports.

Imaging Outcome

All patients underwent follow-up MR imaging with diffusion-weighted imaging for determination of final infarction volumes before discharge. A semiautomated DWI lesion mask and segmentation methodology were used, with full details of the analysis pipeline elaborated previously.⁸ Final infarct volumes were used to compute relative infarction growth, defined as [(final infarction volume–initial CTP core)/initial CTP mismatch], and were computed for each patient as a measure of the relative expansion of initial infarction core by incorporation of the initial at-risk volume. Imaging analysis and final infarction volume measures were conducted under the direct supervision of the same neuroradiologist (S.D.), again blinded to other clinical, imaging, and outcome data.

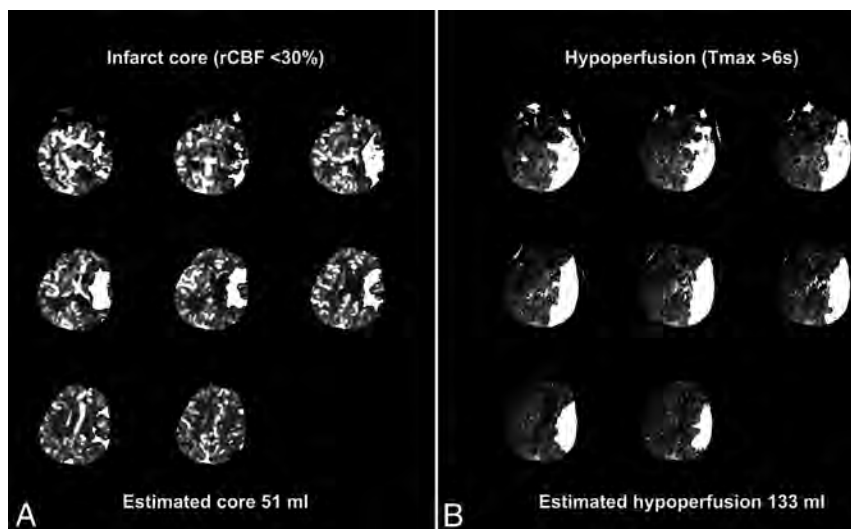


FIG 1. CT perfusion mismatch maps for infarct core and penumbral volume estimates. Representative sample of the CT perfusion analysis pipeline with estimated infarction core (A) determined as relative cerebral blood flow <30% of normal and total hypoperfused tissue volume (B) measured from regions of time-to-maximum of residue function of >6 seconds. Lesion estimates (white overlays) produced from sequential sections obtained from presentation CT perfusion in a 62-year-old woman presenting with acute left MCA syndrome. Segmented lesions are overlaid on raw perfusion images for review purposes, and automated lesion volumes are produced as shown. Penumbral mismatch is computed from the difference between estimated lesion volumes and is summed for each of 2 contiguous perfusion slabs.

Clinical Outcome

Ninety-day mRS was determined by mRS-certified investigators on clinical follow-up or by phone interview. Favorable clinical outcomes were assigned at a 90-day mRS of ≤ 2 .

Statistical Analysis

Continuous variables are reported as mean \pm SD or median and interquartile ranges. The Kendall τ correlation coefficient test (denoted as τ) was applied to assess the nonlinear relationship between temperature-related parameters (baseline temperature, range, maximum, and fever $>37.5^\circ\text{C}$) versus the primary outcome variable of relative infarction growth.

A linear regression model was fitted with relative infarction growth as the response variable and age, presentation NIHSS, last-known-well time to reperfusion, and procedure time to reperfusion as covariates, to establish the correlation of temperature with relative infarction growth, corrected for potentially confounding variables.

The impact of temperature on the likelihood of favorable clinical outcome, mRS ≤ 2 , was secondarily tested. The Kendall τ correlation between the same temperature profiles described above and favorable clinical outcome was computed with statistical significance set to $P < .05$. An additional 2-sample t test was conducted to test the difference in likelihoods of favorable clinical outcome as a function of differences in systemic temperature ranges and fever. Odds ratios for favorable clinical outcome were evaluated in binary logistic regression, with a 90-day mRS of ≤ 2 as the outcome variable, expressed as OR and 95% confidence intervals. Age, presentation NIHSS score, initial core volume, procedure time, time to reperfusion, temperature change from baseline, range, maximum, and fever (temperature of $>37.5^\circ\text{C}$) were assessed in the development of a multivariable model for

prediction of favorable clinical outcome by using the Akaike Information Criterion (AIC) for model selection. Optimal model selection was achieved by minimization of AIC, and the final model was tested by both a goodness-of-fit test and a likelihood ratio to inform the significance of inclusion of temperature in the prediction of favorable clinical outcome. Statistical analysis was performed in R (R statistical and computing software; <http://www.r-project.org/>).

RESULTS

One hundred twenty-nine patients of the 605 consecutive patients with AIS who underwent endovascular therapy during the study period met the inclusion criteria for the current analysis. The main reason for exclusion from the study was the lack of routine CTP preceding thrombectomy early in the study period, before full incorporation of CTP into our stroke imaging protocol, affecting 373 patients. The remainder were excluded due to some combination of unsuccessful reperfusion,

thrombectomy outside the 12-hour window, and isolated extracranial occlusions. Demographic details of the study population are summarized in Table 1. Briefly, among patients meeting all the inclusion criteria, the median age was 65 years (interquartile range [IQR], 18–94 years). Sixty were women (median age, 68.5 years; IQR, 17–94 years); 69 were men (median age, 64 years; IQR, 30–86 years). The median baseline NIHSS score was 18 (IQR, 14–22). The site of vessel occlusion was distributed as follows: intracranial ICA = 17; extracranial ICA = 2; M1 = 63; M2 = 24; anterior cerebral artery = 4; vertebrobasilar = 1; tandem cervical ICA with intracranial ICA or proximal MCA lesions = 18.

Median presentation CTP core infarction volume was 9.6 mL (IQR, 1.5–25.3 mL), and the median hypoperfused volume at Tmax > 6 seconds was 132.6 mL (IQR, 84.2–204 mL). Median procedure time to reperfusion was 58.0 minutes (IQR, 38.5–94.5 minutes). Forty-four patients (34.1%) received general anesthesia. The median time from last known well to reperfusion was 414 minutes (IQR, 294.5–572.3 minutes), and median CTP to reperfusion was 119 minutes (IQR, 84–162.5 minutes). A total of 67 (52.9%) patients achieved modified TICI (mTICI) 2b, and 62 (48.1%) achieved mTICI 3 reperfusion. The median time from CTP to follow-up MR imaging was 26.8 hours (IQR, 20.0–47.2 hours). The median final DWI infarct volume was 19.6 mL (IQR, 8.3–45.2 mL). The mean 90-day mRS score was 2, and 77 (59.7%) patients achieved a favorable clinical outcome as characterized by a 90-day mRS of ≤ 2 . The 90-day mortality was 8.5% (11 patients).

The mean of the population temperature minima was 35.3°C , and maxima, 37.9°C . A median per-patient temperature fluctuation in the population of 2.4°C (IQR, 1.8°C – 3.3°C) was observed.

Table 1: Patient characteristics and temperature profile^a

Characteristics	
Mean age (yr)	65 (range, 18–94)
NIHSS score	18 (14–22)
Women	60 (46.5%)
Presentation core infarction volume ^b	9.6 mL (1.5–25.3)
Hypoperfused volume ^c	132.6 mL (84.2–204)
Occluded vessels	n (%)
Intracranial ICA	17 (13.2%)
Extracranial ICA	2 (1.6%)
M1 MCA	63 (48.8%)
M2 MCA	24 (18.6%)
ACA	4 (3.1%)
Vertebrobasilar	1 (0.8%)
Tandem	18 (14%)
Reperfusion score	
mTICI 2b	67 (52.9%)
mTICI 3	62 (48.1%)
Last known well to reperfusion	414 min (295–572)
CTP to reperfusion	119 min (84–162)
Procedure time to reperfusion	58.0 min (38.5–94.5)
Total procedural duration	77 min (51–118)
CTP-to-MRI time	26.8 hr (20–47.2)
Last known well to MRI	30.6 hr (24.0–51.2)
General anesthesia (No.)	44 (34.1%)
Aspirin therapy (No.)	125 (96.9%)
Received acetaminophen (No.)	91 (70.5%)
Final infarct volume	19.6 mL (8.3–45.2 mL)
Mean 90-day mRS	2
Favorable clinical outcome (mRS ≤2) (No.)	77 (59.7%)
90-day mortality (No.)	11 (8.5%)
Population temperature minima (mean)	35.3°C
Population temperature maxima (mean)	37.9°C
Per-patient temperature fluctuation	2.4°C (1.8°C–3.3°C)
Temperature increase from baseline	1.6°C (1.0°C–2.5°C)

Note:—ACA indicates anterior cerebral artery.

^a Data are reported as proportions and median (IQR), unless otherwise stated.

^b Relative cerebral blood flow <30% of contralateral normal tissues.

^c Tmax of >6 seconds.

The median temperature increase from presentation baseline was 1.6°C (IQR, 1.0°C–2.5°C). Relative infarction growth corresponding to the first and third quartiles of temperature elevation was 19.0% and 66.6%, respectively. Ninety-one patients (70.5%), reached a maximum temperature of >37.5°C. The median infarction expansion was 8.3 mL (IQR, 22.0 mL). Ninety-five patients (73.6%) had expansion of their infarction; of these, 71 (74.7%) also had fever. All except 4 patients (96.9%) received aspirin therapy; 91 patients (70.5%) received at least 1 dose of acetaminophen during hospitalization. No patients were found to have evidence of severe systemic infections or septicemia prior to their final imaging analysis.

Imaging Outcomes

The Kendall τ correlation between fever and relative infarction growth demonstrated significant associations among patients with a temperature of >37.5°C ($\tau = 0.27$, $P < .001$). Fever exceeding 37.5°C did not, however, correlate with the size of the initial core ($P = .14$). Additionally, initial core volume had a small but significant association with relative infarction growth ($\tau = -0.24$, $P < .001$). When corrected for the potential confounders of age, procedure time, onset to reperfusion, initial NIHSS score, initial CTP predicted core volume, and time from symptom on-

Table 2: Optimal model for prediction of favorable clinical outcome: variable selection by Akaike Information Criterion^a

Variable	Odds Ratio	95% CI	P Value
Fever (>37.5°C)	0.31	0.09–0.96	.052
Age	0.96	0.92–0.99	.007
Total procedure time	0.99	0.98–0.995	.003
NIHSS score	0.84	0.75–0.92	<.001

^a Variable selection using Akaike Information Criterion minimization, indicated by the goodness-of-fit test ($P > .05$), and the likelihood ratio test for inclusion of fever ($P = .041$) vs exclusion of fever in the prediction of favorable clinical outcome.

set, the presence of fever (>37.5°C) remained significantly correlated with infarction expansion ($\tau = 0.24$, $P = .002$). By comparison, correlations for baseline temperature at presentation ($\tau = 0.06$, $P = .38$), range ($\tau = 0.01$, $P = .89$), and maximum ($\tau = 0.12$, $P = .053$) did not reach statistical significance when adjusted.

Clinical Outcomes

Similar results were observed in a 2-sample *t* test examining the relationship among fever ($P = .002$), temperature range ($P = .03$), and absolute temperature maximum ($P = .03$) and favorable clinical outcome, while statistical significance was not achieved for baseline temperature or temperature range in relation to favorable clinical outcome.

The results of binary logistic regression with model selection by using AIC produced an optimized model for prediction of favorable clinical outcome, which included variables of age, NIHSS score, procedure time, and fever of >37.5°C, while initial core volume; baseline temperature, range, and maximum; and time from symptom onset to reperfusion did not meet optimization criteria in AIC (Table 2). The likelihood ratio testing confirmed the superiority for model inclusion of fever ($P < .05$) compared with the elimination of fever from the model, and the goodness-of-fit test further supported the robustness of the selected model for prediction of favorable clinical outcome ($P > .05$).

Adjusted odds ratios for favorable clinical outcome were computed, suggesting a possible trend toward significance for fever in the likelihood of 90-day mRS of ≤2 (OR = 0.31; 95% CI, 0.08–0.97; $P = .056$). The remaining temperature-related parameters did not approach statistical significance ($P > .05$).

DISCUSSION

These findings lend further support to the hypothesized, detrimental influence of temperature elevation on the fate of ischemic tissues in the early aftermath of cerebrovascular injury. The sensitivity of the neurovascular unit to potentially subclinical temperature elevations and, conversely, the neuroprotective attributes of therapeutic hypothermia have been observed in humans, as well as in nonhuman experimental animal models.^{11,12} However, this study represents, to our knowledge, the first investigation of the interaction between systemic temperature change and the fate of reperfused tissues following AIS. In this study, reaching febrile temperatures during hospitalization impacted not only relative infarction growth in a cohort of reperfused patients with AIS but moreover suggested a possible negative influence on the likelihood of favorable clinical outcome. This association remained significant even when correcting for known confounders such as age, procedure time, initial stroke severity (NIHSS score), and CTP predicted core size, as well as all reperfusion and proce-

dural times. Although these variables demonstrated significant associations, in the development of a parsimonious and optimized model, only age, procedure time, and initial NIHSS score met inclusion in the final AIC model, in keeping with findings in recent trials reporting that the association between endovascular therapy and good functional outcomes is not strictly time-dependent among patients presenting within 12 hours.¹³

Our findings add to earlier work establishing the association between poor long-term outcome and even small increases in systemic temperatures.^{5,14,15} The influence of systemic temperature changes on the rescue or progression of putatively at-risk brain tissues is likely multifactorial and may be nonlinear; accordingly, within our analysis, the modest but highly significant correlation between elevated temperatures and relative infarction growth may belie the overall complexity of this relationship. Nevertheless, just as therapeutic hypothermia regimens aim for the achievement of a predefined minimum temperature to achieve neuroprotection, the negative influence of temperature elevation in this study was observed at a discrete febrile temperature ($>37.5^{\circ}$) defined a priori.^{16,17} Importantly, admission temperatures were not significantly associated with the measured outcomes, in line with existing studies suggesting that the effects of temperature elevation may more commonly manifest hours after the initial injury.^{14,15}

Pyrexia represents an adaptive response to numerous exogenous or endogenous stimuli, though particular definitions for fever are inconsistent.¹⁸ In the context of neurologic diseases, reported fever thresholds vary, including 37.5°C , which we used in a conservative first approximation of the hypothesized interaction in this study.¹⁰ While other fever thresholds could be used in such investigations, our selection was intended to reasonably represent conventions within the literature. For this study, we examined the influence of systemic temperatures on the expansion of initial infarction estimates relative to predicted penumbral volumes. Systemic modes of thermometry were used, given their nearly universal availability and known association with NIHSS severity and clinical outcome.^{5,6,19,20} More recently, dedicated brain temperature estimates have been achieved noninvasively by MR imaging, expanding the potential for direct brain thermometry beyond the costly and invasive approaches to temperature probe implantation.^{19,21-23} Noninvasive brain thermometry has emphasized the potential for significant differences between brain and body temperatures, decoupling of the brain-systemic temperature gradient during brain injury, and the presence of intracerebral temperature gradients, which may themselves differ between injured and noninjured tissues.^{19,21,22} While the influence of systemic temperature elevations on ischemic expansion is apparent from this and other studies, the impact of more specific signatures of brain spatial and temporal temperature gradients remains uncertain and requires continued investigation.

We acknowledge a number of study limitations, particularly those inherent in the retrospective nature of the analysis. These results were obtained from a single-institution prospectively collected stroke registry. Analysis included primarily objective, quantitative data such as systemic temperatures and a fully automated, user-independent software environment for CT perfusion analysis as reported recently in the clinical and trial setting for stroke imaging analysis.²⁴⁻²⁶ The absolute error of CTP may be

non-negligible. However, we contend that the use of a validated user-independent platform for analysis is in line with contemporary clinical and trial implementations of CTP, and we would not anticipate that potential errors relating to such inaccuracies would impart specific bias significantly affecting the relationship between infarct expansion and temperature.^{8,24,26} Systemic temperatures were primarily tympanic, as detailed in the study "Materials and Methods." Occasional variability in this respect relates to several factors that could not be controlled within the retrospective design, including patient condition, location within the hospital, and nursing-specific variables requiring the use of urinary catheter temperatures in some circumstances. We believe the systematic bias related to temperature acquisition from different sites to be minor because the concordance between temperatures collected from standard locations is high.²⁷

Several potential medications administered during hospitalization may have an impact on systemic temperatures. Principally, antipyretics such as aspirin and acetaminophen and anesthetics administered during the intervention may affect systemic or brain temperature.^{28,29} In this study, most patients received aspirin and acetaminophen, and all received anesthetics during endovascular therapy. Unfortunately, sample size limitations precluded direct analysis of the relationship between antipyretic exposure, fever, and ischemic expansion. While this may affect the temperature profile of an individual patient, the goals of this study were to establish the relationship between febrile temperatures and relative infarction growth, irrespective of external influences on temperature profile.

In this study, we aimed to isolate the impact of temperature elevation on relative infarction growth and, to this end, selected a cohort of revascularized patients (mTICI 2b/3). We acknowledge that heterogeneity in full reperfusion and infarction evolution may exist across this cohort, given the inclusion of mTICI 2b, as well as variability in time to follow-up MR imaging; however, previous studies have indicated generally high accuracy in the ability of DWI obtained in the early stroke aftermath (<5 days) to predict chronic infarction volumes and clinical outcomes.^{30,31}

Last, we acknowledge that the duration of time spent at or above the threshold temperature for fever could influence both the rate and extent of relative infarction growth. Unfortunately, this retrospective investigation was not powered to assess such interactions. Further study of a potential dose- and time-dependent response of infarction expansion and fever in a larger population of matched patients is thus warranted.

CONCLUSIONS

These preliminary findings suggest that temperature dysregulation may potentiate neuronal injury following acute ischemic stroke, compelling further investigation into the mechanistic and temporal relationship in larger cohorts.^{20,29,32,33} Infarction progression despite reperfusion is well-documented and multifactorial and not yet fully understood.³⁴ We propose that the relative contribution of temperature elevation remains a comparatively under-recognized factor potentially modulating infarction expansion despite reperfusion. Viable penumbra can be found up to 48 hours following stroke onset, during which time temperature dysregulation may drive ischemic expansion.³⁵ These findings suggest that neuronal fate may be affected by mild temperature

changes, motivating future work to further elaborate the nature of this relationship and to advance our understanding of temperature as a biomarker in prognostication following ischemic stroke.

Disclosures: Raul G. Nogueira—UNRELATED: Other: Stryker Neurovascular (Thrombectomy Revascularization of large Vessel Occlusions (TREVO) II trial Principal Investigator—modest; Diffusion Weighted Imaging (DWI) or Computerized Tomography Perfusion (CTP) Assessment With Clinical Mismatch in the Triage of Wake Up and Late Presenting Strokes Undergoing Neurointervention (DAWN) Trial Principal Investigator—no compensation), Medtronic (Solitaire With the Intention For Thrombectomy (SWIFT) Trial Steering Committee—modest; Solitaire With the Intention For Thrombectomy as PRiMary Endovascular Treatment Trial Steering Committee—no compensation; Solitaire FR Thrombectomy for Acute Revascularisation (STAR) Trial Angiographic Core Laboratory—significant), Penumbra (3D Separator Trial Executive Committee—no compensation), Editor-in-Chief of *Interventional Neurology Journal* (no compensation).

REFERENCES

1. Wolfe KB. **Effect of hypothermia on cerebral damage resulting from cardiac arrest.** *Am J Cardiol* 1960;6:809–12 CrossRef Medline
2. Azzimondi G, Bassein L, Nonino F, et al. **Fever in acute stroke worsens prognosis: a prospective study.** *Stroke* 1995;26:2040–43 CrossRef Medline
3. Castillo J, Davalos A, Marrugat J, et al. **Timing for fever-related brain damage in acute ischemic stroke.** *Stroke* 1998;29:2455–60 CrossRef Medline
4. Hajat C, Hajat S, Sharma P. **Effects of poststroke pyrexia on stroke outcome: a meta-analysis of studies in patients.** *Stroke* 2000;31:410–14 CrossRef Medline
5. Kammersgaard LP, Jorgensen HS, Rungby JA, et al. **Admission body temperature predicts long-term mortality after acute stroke: the Copenhagen Stroke Study.** *Stroke* 2002;33:1759–62 CrossRef Medline
6. Reith J, Jorgensen HS, Pedersen PM, et al. **Body temperature in acute stroke: relation to stroke severity, infarct size, mortality, and outcome.** *Lancet* 1996;347:422–25 CrossRef Medline
7. Busto R, Dietrich WD, Globus MY, et al. **Small differences in intrischemic brain temperature critically determine the extent of ischemic neuronal injury.** *J Cereb Blood Flow Metab* 1987;7:729–38 Medline
8. Dehkharghani S, Bammer R, Straka M, et al. **Performance and predictive value of a user-independent platform for CT perfusion analysis: threshold-derived automated systems outperform examiner-driven approaches in outcome prediction of acute ischemic stroke.** *AJNR Am J Neuroradiol* 2015;36:1419–25 CrossRef Medline
9. Straka M, Albers G, Bammer R. **Real-time diffusion-perfusion mismatch analysis in acute stroke.** *J Magn Reson Imaging* 2010;1024–37 CrossRef Medline
10. Axelrod YK, Diringner MN. **Temperature management in acute neurologic disorders.** *Neurol Clin* 2008;26:585–603, xi CrossRef Medline
11. Dumitrascu OM, Lamb J, Lyden PD. **Still cooling after all these years: meta-analysis of pre-clinical trials of therapeutic hypothermia for acute ischemic stroke.** *J Cereb Blood Flow Metab* 2016;36:1157–64 CrossRef Medline
12. Hong JM, Lee JS, Song HJ, et al. **Therapeutic hypothermia after recanalization in patients with acute ischemic stroke.** *Stroke* 2014;45:134–40 CrossRef Medline
13. Lansberg MG, Cereda CW, Mlynash M, et al; Diffusion and Perfusion Imaging Evaluation for Understanding Stroke Evolution 2 (DEFUSE 2) Study Investigators. **Response to endovascular reperfusion is not time-dependent in patients with salvageable tissue.** *Neurology* 2015;85:708–14 CrossRef Medline
14. Boysen G, Christensen H. **Stroke severity determines body temperature in acute stroke.** *Stroke* 2001;32:413–17 CrossRef Medline
15. Kim Y, Busto R, Dietrich WD, et al. **Delayed postischemic hyperthermia in awake rats worsens the histopathological outcome of transient focal cerebral ischemia.** *Stroke* 1996;27:2274–80; discussion 2281 CrossRef Medline
16. Krieger DW, De Georgia MA, Abou-Chebl A, et al. **Cooling for acute ischemic brain damage (COOL AID): an open pilot study of induced hypothermia in acute ischemic stroke.** *Stroke* 2001;32:1847–54 CrossRef Medline
17. De Georgia MA, Krieger DW, Abou-Chebl A, et al. **Cooling for Acute Ischemic Brain Damage (COOL AID): a feasibility trial of endovascular cooling.** *Neurology* 2004;63:312–17 CrossRef Medline
18. Aiyagari V, Diringner MN. **Fever control and its impact on outcomes: what is the evidence?** *J Neurol Sci* 2007;261:39–46 CrossRef Medline
19. Karaszewski B, Carpenter TK, Thomas RG, et al. **Relationships between brain and body temperature, clinical and imaging outcomes after ischemic stroke.** *J Cereb Blood Flow Metab* 2013;33:1083–89 CrossRef Medline
20. Whiteley WN, Thomas RG, Lowe G, et al. **Do acute phase markers explain body temperature and brain temperature after ischemic stroke?** *Neurology* 2012;79:152–58 CrossRef Medline
21. Cady EB, D'Souza PC, Penrice J, et al. **The estimation of local brain temperature by in vivo 1H magnetic resonance spectroscopy.** *Magn Reson Med* 1995;33:862–67 CrossRef Medline
22. Dehkharghani S, Mao H, Howell L, et al. **Proton resonance frequency chemical shift thermometry: experimental design and validation toward high-resolution noninvasive temperature monitoring and in vivo experience in a nonhuman primate model of acute ischemic stroke.** *AJNR Am J Neuroradiol* 2015;36:1128–35 CrossRef Medline
23. Marshall I, Karaszewski B, Wardlaw JM, et al. **Measurement of regional brain temperature using proton spectroscopic imaging: validation and application to acute ischemic stroke.** *Magn Reson Imaging* 2006;24:699–706 CrossRef Medline
24. Lansberg MG, Straka M, Kemp S, et al; DEFUSE 2 study investigators. **MRI profile and response to endovascular reperfusion after stroke (DEFUSE 2): a prospective cohort study.** *Lancet Neurol* 2012;11:860–67 CrossRef Medline
25. Campbell BC, Mitchell PJ, Yan B, et al; EXTEND-IA investigators. **A multicenter, randomized, controlled study to investigate EXTending the time for Thrombolysis in Emergency Neurological Deficits with Intra-Arterial therapy (EXTEND-IA).** *Int J Stroke* 2014;9:126–32 CrossRef Medline
26. Saver JL, Goyal M, Bonafe A, et al; SWIFT PRIME Investigators. **Stent-retriever thrombectomy after intravenous t-PA vs. t-PA alone in stroke.** *N Engl J Med* 2015;372:2285–95 CrossRef Medline
27. Christensen H, Boysen G. **Acceptable agreement between tympanic and rectal temperatures in acute stroke patients.** *Int J Clin Pract* 2002;56:82–84 Medline
28. den Hertog HM, van der Worp HB, van Gemert HM, et al. **An early rise in body temperature is related to unfavorable outcome after stroke: data from the PAIS study.** *J Neurol* 2011;258:302–07 CrossRef Medline
29. Zhu M, Nehra D, Ackerman JH, et al. **On the role of anesthesia on the body/brain temperature differential in rats.** *J Therm Biol* 2004;29:599–603
30. Ritzl A, Meisel S, Wittsack HJ, et al. **Development of brain infarct volume as assessed by magnetic resonance imaging (MRI): follow-up of diffusion-weighted MRI lesions.** *J Magn Reson Imaging* 2004;20:201–07 CrossRef Medline
31. Kim SM, Kwon SU, Kim JS, et al. **Early infarct growth predicts long-term clinical outcome in ischemic stroke.** *J Neurol Sci* 2014;347:205–09 CrossRef Medline
32. Parry-Jones AR, Liimatainen T, Kauppinen RA, et al. **Interleukin-1 exacerbates focal cerebral ischemia and reduces ischemic brain temperature in the rat.** *Magn Reson Med* 2008;59:1239–49 CrossRef Medline
33. Karaszewski B, Wardlaw JM, Marshall I, et al. **Early brain temperature elevation and anaerobic metabolism in human acute ischaemic stroke.** *Brain* 2009;132:955–64 Medline
34. Haussen DC, Nogueira RG, Elhammady MS, et al. **Infarct growth despite full reperfusion in endovascular therapy for acute ischemic stroke.** *J Neurointerv Surg* 2016;8:117–21 CrossRef Medline
35. Schlaug G, Benfield A, Baird AE, et al. **The ischemic penumbra operationally defined.** *Neurology* 1999;53

Collateral Assessment by CT Angiography as a Predictor of Outcome in Symptomatic Cervical Internal Carotid Artery Occlusion

S. Sundaram, S. Kannoth, B. Thomas, P.S. Sarma, and P.N. Sylaja



ABSTRACT

BACKGROUND AND PURPOSE: Cervical internal carotid artery occlusion can present with varied clinical manifestations such as transient ischemic attack, stroke, and chronic ocular ischemia, or can be asymptomatic. The outcome in these patients is considerably influenced by cerebral hemodynamic compensatory adaptation of the intracranial collateral pathways. Our aim was to study whether collateral circulation as assessed by CT angiography can predict 3-month outcome and initial stroke severity in patients with symptomatic cervical ICA occlusion.

MATERIALS AND METHODS: This was a retrospective study of 65 patients with symptomatic cervical ICA occlusion from January 2011 to December 2013. The collateral vessels (anterior and posterior communicating arteries, ophthalmic artery, and leptomeningeal arteries) were assessed by CTA. The outcome at 3 months was defined as poor if the modified Rankin Scale score was ≥ 3 .

RESULTS: The mean age of subjects was 57 ± 11.6 years (range, 32–80 years), and 92% were men. Thirty-three (50.8%) patients had poor outcome. Absence of the ipsilateral ophthalmic artery, poor leptomeningeal collaterals, and < 2 collaterals were predictors of stroke severity at onset and poor 3-month outcome in univariate analysis. In the multiple logistic regression analysis, inadequate flow through the secondary collaterals (ipsilateral ophthalmic artery or leptomeningeal collaterals; OR, 4.5; 95% CI, 1.4–14.9; $P = .01$) and higher NIHSS score at stroke onset (OR, 19.2; 95% CI, 2.2–166.2; $P = .007$) independently predicted poor outcome at 3 months.

CONCLUSIONS: Assessment of collateral circulation with CTA can be a useful predictor of 3-month outcome in patients with symptomatic cervical ICA occlusion.

ABBREVIATIONS: AcomA = anterior communicating artery; LC = leptomeningeal collaterals; OA = ophthalmic artery; PcomA = posterior communicating artery

Cervical ICA occlusion can present with varied clinical manifestations such as transient ischemic attack, stroke, and chronic ocular ischemia, or can be asymptomatic. The outcome in these patients is influenced by cerebral hemodynamic compensatory adaptation, with the intracranial collateral pathways playing an important role in maintaining adequate perfusion to the ischemic zone.¹

In large-artery occlusion, the primary collaterals (anterior and posterior communicating arteries) act as the immediate flow diverters and the secondary collaterals (leptomeningeal and oph-

thalmic arteries [OAs]) further enhance the cerebral perfusion.² The role of collaterals as predictors of stroke severity, response to thrombolysis, and outcome in patients with acute stroke and large-vessel occlusion has been investigated in multiple studies.^{3–5} Good leptomeningeal collateral circulation and the presence of ≥ 2 collaterals were found to be associated with good outcome in patients with cervical large-vessel occlusion.^{6,7}

Most of the earlier studies on collaterals have focused on the prognostic implications of primary collateral circulation and cerebrovascular autoregulation in patients with stroke. Only a very few of them have explored the clinical significance of secondary collaterals, especially the ophthalmic artery, in ICA occlusion. The earlier studies were also limited by the nonuniformity of study protocols, especially the imaging technique with a combination of either MRA, DSA, CTA, or transcranial Doppler for assessing the cerebral collaterals. We analyzed both primary and secondary collaterals by using CTA, which is a noninvasive technique currently recommended for the evaluation of vascular anatomy in stroke. The main objective of our study was to determine whether collateral circulation as assessed by CTA helps in predict-

Received May 29, 2016; accepted after revision August 14.

From the Department of Neurology (S.S., P.N.S.), Comprehensive Stroke Care Program; Department of Imaging Sciences and Interventional Radiology (S.K., B.T.); and Achutha Menon Centre for Health Science Studies (P.S.S.), Sree Chitra Tirunal Institute for Medical Sciences and Technology, Trivandrum, India.

Please address correspondence to P.N. Sylaja, MD, Department of Neurology, Comprehensive Stroke Care Program, Sree Chitra Tirunal Institute for Medical Sciences and Technology, Trivandrum 695011, Kerala, India; e-mail: sylajapn@hotmail.com

Indicates article with supplemental on-line table.

<http://dx.doi.org/10.3174/ajnr.A4957>

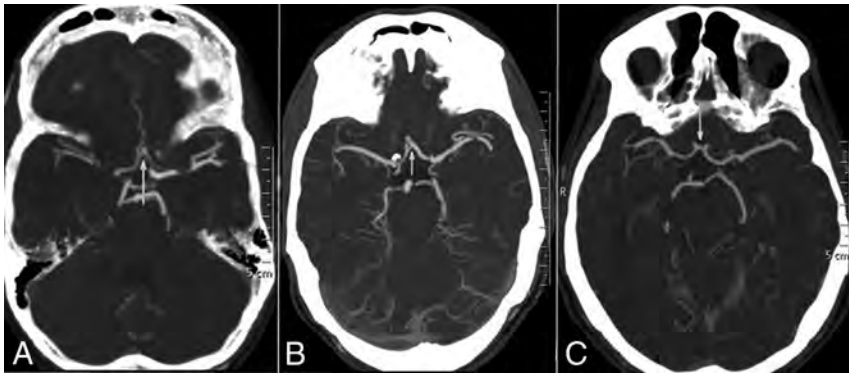


FIG 1. CT angiographic grading of the anterior communicating artery shows a hairline AcomA (A), definitely present AcomA (B), and robust AcomA (C).

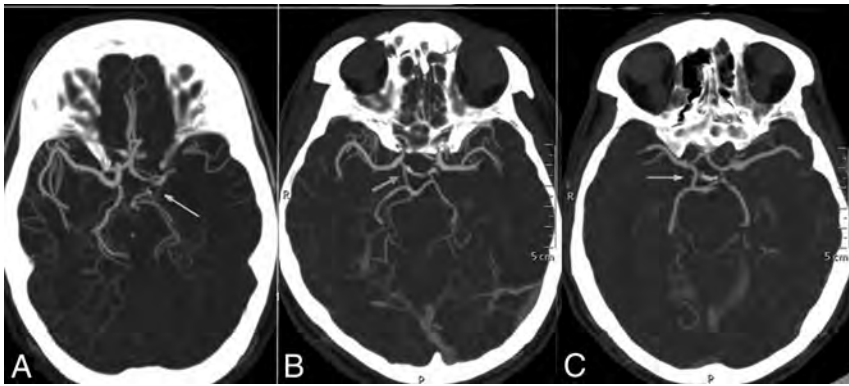


FIG 2. CT angiographic grading of the posterior communicating artery shows a hairline PcomA (A), definitely present PcomA (B), and robust PcomA (C).

ing the 3-month outcome and initial stroke severity in patients with symptomatic cervical ICA occlusion.

MATERIALS AND METHODS

Subjects

This was a retrospective study, conducted in the Comprehensive Stroke Care unit of a tertiary care center. All patients with symptomatic cervical ICA occlusion who presented to the unit from January 2011 to December 2013 satisfying the selection criteria were included in the study. Patients older than 18 years of age who had a TIA (hemispheric/retinal) or stroke with ipsilateral extracranial ICA occlusion who underwent CTA of the cerebral circulation within 3 weeks of symptom onset were included. Those with intracranial ICA occlusion, asymptomatic ICA occlusion, tandem MCA occlusion, and ICA occlusion due to Moyamoya disease and patients who underwent revascularization therapy were excluded. The study had the approval of the institutional ethics committee.

Assessment of Subjects

The demographic and clinical profiles of patients, including vascular risk factors, were extracted from the patient records. Stroke severity at the initial presentation was expressed by the NIHSS score. CT, MR imaging, and CTA were reviewed independently by an interventional neuroradiologist and stroke neurologist. The 2 CTA readers were blinded to the clinical information and outcome.

The baseline CT scan was used for assessing the ASPECTS, and a score of ≥ 8 was considered good. The type of infarct was classified into territorial (involving >1 subdivision of the MCA), hemodynamic (watershed or border-zone infarcts), or other (small infarcts of <1 cm located in the cortex or centrum semiovale or no infarct).⁸

Collateral Assessment by CTA

CTA is routinely used for the evaluation of all patients with stroke for delineating the vascular anatomy in our center if there is no contraindication. CTA was obtained with z-axis coverage from the arch of the aorta to the vertex. All the imaging studies were acquired in a 256-section CT scanner (Brilliance iCT; Philips Healthcare, Best, the Netherlands) with the following technical parameters: section thickness, 0.9 mm (pitch, 0.6); collimation, 0.625 mm; gantry rotation speed, -500 ms; 120 kV-peak; 450 mAs; FOV, 200–250 mm; and 512×512 matrix. Angiography was performed by using bolus tracking by placing a region of threshold (ROI) in the upper descending thoracic aorta, triggering the acquisition beyond the threshold of 150 HU. A total of 50–60

mL of low-osmolar contrast medium (iohexol, 320 mg/mL, or iodixanol, 270 mg/mL) was administered through an 18-ga cannula secured in the right antecubital vein at the rate of 5 mL/s followed by a saline chase of 40 mL at 5 mL/s. The images were later transferred to a dedicated vendor workstation for detailed interpretation. MIP images of 5-mm thickness were created from CTA source imaging for the assessment of the collateral circulation.

The grading system of Maas et al⁹ was adopted in this study for the flow through the anterior communicating artery (AcomA), posterior communicating artery (PcomA), and the leptomeningeal collaterals (LC). A 5-point grading system was used for the assessment of flow through the AcomA (Fig 1) and the ipsilateral PcomA (Fig 2): Grade 1 denoted absent flow; grade 2, probably present; grade 3, hairline; grade 4, definitely present; and grade 5, robust. LC were graded by comparing the symptomatic hemisphere with opposite side categorized into 5 grades (Fig 3): grade 1, absent; grade 2, less than those on the contralateral side; grade 3, equal to those on the contralateral side; grade 4, greater than those on the contralateral side; and grade 5, exuberant.⁹ Because the number of patients in each group was not enough for any statistical analysis to be relevant, the grades were collapsed into 2 grades. LC were dichotomized into poor (grades 1 and 2) and good (grades 3, 4, and 5) collaterals. Similarly, the AcomA and PcomA were dichotomized into poor (grades 1, 2, and 3) and good (grades 4 and 5) flow. Grading of the leptomeningeal and com-

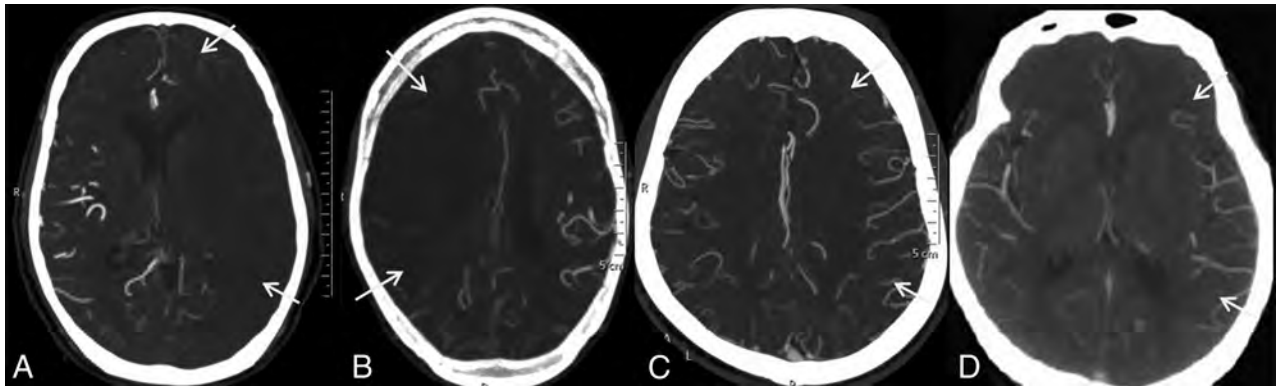


FIG 3. CT angiographic grading of leptomeningeal collaterals compared with the side contralateral to the symptomatic cervical ICA occlusion shows absent leptomeningeal collaterals (A), reduced leptomeningeal collaterals (B), equal leptomeningeal collaterals (C), and leptomeningeal collaterals more than on the opposite side (D).

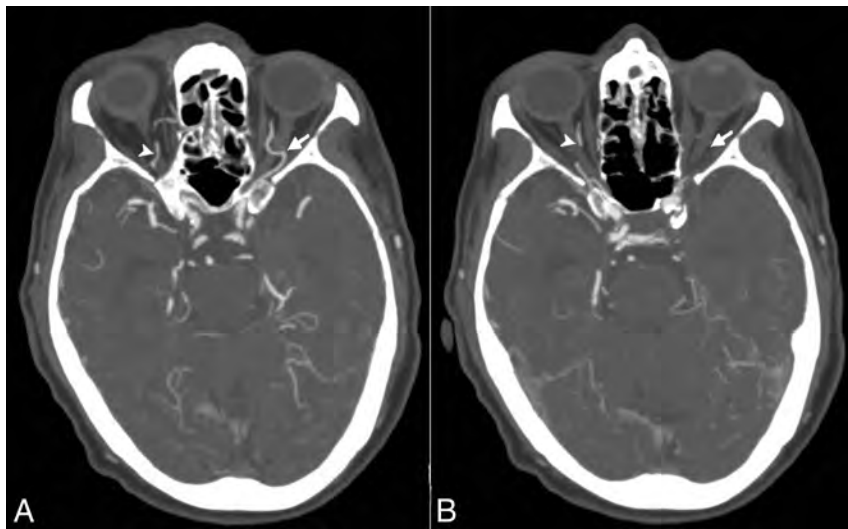


FIG 4. CT angiographic axial images showing the presence (A) and absence (B) of the ophthalmic artery on the side of the symptomatic cervical ICA occlusion (arrow) and the presence of the ophthalmic artery on the opposite side (arrowhead).

municating arteries were not similar. Absent, probably present, and hairline communicating arteries may not contribute significantly to collateral circulation; hence, grades 1–3 were taken together as the poor-flow group, whereas in LC, either absent or less than those in the opposite hemisphere, constituted poor flow. The OA on the ipsilateral side of the ICA occlusion was graded as present or absent on the basis of its perceptibility on CTA (Fig 4).

Outcome Assessment

All patients received standard care as per the current stroke guidelines, with the best medical management and control of modifiable vascular risk factors. Patients with large-vessel atherosclerotic disease and dissection received antiplatelet agents and high-dose statins, while the 2 patients with cardioembolic ICA occlusion received anticoagulation. The functional outcome at 3 months was assessed by the mRS, and poor outcome was defined as $mRS \geq 3$. The mortality and recurrent ischemic events were recorded during follow-up.

Statistical Analysis

Continuous variables were reported as means or as median \pm interquartile range. Categorical variables were reported as propor-

tions. Differences in continuous variables and proportions were assessed by ANOVA and the χ^2 /Fisher exact test, respectively. Interobserver agreement for the status of collaterals was assessed with κ statistics, and in cases in which there was divergence between the 2 assessors, a consensus decision was reached.

Baseline characteristics (age, sex, vascular risk factors, and prior neurologic events), NIHSS score at stroke onset, type of infarct, ASPECTS, and collaterals were compared between excellent ($mRS \leq 2$) and poor ($mRS \geq 3$) outcome groups. On the basis of initial stroke severity, patients were grouped into mild ($NIHSS < 5$) and moderate-to-severe ($NIHSS \geq 5$) stroke. The baseline characteristics and collaterals were also compared between these 2 groups.

Among the predictors of 3-month outcome significant in univariate analysis ($P < .05$), highly correlated variables were excluded while retaining 1 of them that was clinically relevant for multiple logistic regression analysis. Two models were included for multivariable analysis of 3-month outcome based on the results from univariate analysis. In model 1 of multiple logistic regression analysis, the ipsilateral OA and LC were independently analyzed along with the NIHSS score, and in model 2, both the ipsilateral OA and LC were analyzed together as secondary collaterals along with the NIHSS score for predicting 3-month outcome. Due to small cell values (zero) for a few parameters, multivariable analysis was not attempted for assessing the predictors of stroke severity. The results of multivariable analysis were expressed as ORs with 95% CI. All statistical analyses were performed by using SPSS 21 software for Windows (IBM, Armonk, New York).

RESULTS

Sixty-five patients were identified from 73 with symptomatic ICA occlusion. Five patients with intracranial ICA occlusion and 3 with ipsilateral MCA occlusion were excluded.

The mean age of subjects was 57 ± 11.6 years (range, 32–80 years), with 60 (92%) men. Sixty-one patients (93.8%) had stroke, and 4 patients (6.2%) had transient ischemic attack as the initial presentation. The median NIHSS score at presentation was 10 (interquartile range, 4–18). Territorial infarcts were seen in 24 (36.9%), hemodynamic infarcts in 23 (35.4%), and small cortical or superficial infarcts or no infarct, in 18 (27.7%) patients. Poor ASPECTS was seen in 23 patients (35.38%). Atherosclerosis was the most common cause of ICA occlusion observed in 43 patients (66.2%), followed by arterial dissection in 20 (30.8%) and cardio-embolic stroke in 2 (3%) patients.

The median time interval from the onset of symptoms to the acquisition of CTA was 74.0 hours (range, 2–504 hours). Interobserver agreement for the status of collaterals by using κ statistics showed good agreement ($\kappa = 0.89$). Good flow through the AcomA, ipsilateral PcomA, and LC was seen in 34 (52.3%), 26 (40%), and 47 patients (72.3%), respectively. The ipsilateral OA was not visualized in 26 patients (40%).

All patients had 3-month follow-up, and 33 patients (50.8%) had poor outcome. The presence of an MCA territory infarct ($P = .002$), poor ASPECTS ($P < .001$), higher NIHSS score at stroke onset ($P < .001$), absent ipsilateral OA ($P = .02$), poor flow through the LC ($P = .001$), and no or only 1 collateral ($P = .005$) were significant univariate predictors of poor outcome at 3 months (Table 1). The role of the AcomA and PcomA was not significant in determining outcome. In patients with an absent ipsilateral OA, 18 (69.2%) had poor outcome, and 15 of the 18 patients (83.3%) with poor flow through the LC had poor outcome. Patients with either no or only 1 collateral had poor outcome compared with patients with ≥ 2 collaterals (76.2% versus 38.6%; $P = .005$).

In multiple logistic regression analysis of 3-month outcome, highly correlated variables were excluded by retaining one of them that was clinically relevant (Table 2). In model 1, only the NIHSS score was found to be a significant predictor of 3-month outcome (OR, 16.5; 95% CI, 1.9–142.2; $P = .01$). In model 2 of multivariable analysis, absence of either of the secondary collaterals (ipsilateral OA or LC; OR, 4.5; 95% CI, 1.4–14.9; $P = .01$) and higher initial NIHSS score (OR, 19.2; 95% CI, 2.2–166.2; $P = .007$) were independent predictors of poor outcome at 3 months.

Patients with large territorial infarcts ($P < .001$), an ASPECTS of ≤ 7 ($P < .001$), an absent ipsilateral OA ($P = .04$), poor flow through the LC ($P < .001$), and < 2 collaterals ($P = .01$) were found to have higher NIHSS score at stroke onset (On-line Table). All 18 patients with poor LC had severe stroke. However, multiple logistic regression analysis for stroke severity could not be performed due to the small cell size.

Four patients (6.2%) died, 3 from malignant MCA stroke and 1 patient from myocardial infarction after discharge. Only 2 patients (3.1%) had recurrent vascular events. Age, sex, vascular risk factors, and etiology of the ICA occlusion were not predictive of the 3-month outcome or initial stroke severity.

DISCUSSION

Our study highlights the role of the secondary collaterals (ie, OA on the side of ICA occlusion and LC) in determining stroke outcome. Poor collateral circulation through either the LC or ipsilat-

Table 1: Demographic data, vascular risk factor profile, clinical parameters, and collateral circulation^a

Clinical Imaging Parameters	Excellent Outcome (mRS ≤ 2) (n = 32)	Poor Outcome (mRS ≥ 3) (n = 33)	P Value
Age (yr) (mean)	59.5 \pm 10.84	56.3 \pm 13.2	.200
Male sex	28 (87.5)	32 (94.2)	.400
Hypertension	16 (55)	13 (39.4)	.390
Diabetes mellitus	7 (21.9)	10 (30.3)	.440
Dyslipidemia	4 (12.5)	0 (0)	.053
Current smoking	19 (56.3)	21 (63.6)	.724
Prior ischemic events	8 (25)	6 (18.2)	.504
Atherosclerotic ICA occlusion	23 (71.9)	20 (60.6)	.337
Dissection/embolic ICA occlusion	9 (18.8)	13 (39.4)	
Territorial (MCA) infarct	7 (21.9)	17 (51.5)	.002
Hemodynamic infarct	10 (31.2)	13 (39.4)	
Others small infarcts	15 (46.9)	3 (9.1)	
ASPECTS ≥ 8	28 (87.5)	14 (42.4)	<.001
Median NIHSS (IQR)	0.5 (0–4)	15 (17–19)	
NIHSS < 5	15 (46.9)	1 (3.1)	<.001
AcomA, poor flow	15 (46.9)	16 (48.5)	.897
AcomA, good flow	17 (53.1)	17 (51.5)	
Ipsilateral PcomA, poor flow	16 (50)	23 (69.7)	.105
Ipsilateral PcomA, good flow	16 (50)	10 (30.3)	
Contralateral PcomA, poor flow	21 (65.6)	22 (66.7)	.929
Contralateral PcomA, good flow	11 (34.4)	11 (33.3)	
Ipsilateral OA, absent	8 (25)	18 (54.5)	.015
Ipsilateral OA, present	24 (75)	15 (45.5)	
Contralateral OA, absent	3 (9.4)	4 (12.1)	1.000
Contralateral OA, present	29 (90.6)	29 (87.9)	
LC, poor flow	3 (9.4)	15 (45.5)	.001
LC, good flow	29 (90.6)	18 (54.5)	
No. of collaterals, ≥ 2	27 (84.4)	17 (51.5)	.005

Note.—IQR indicates interquartile range.

^a Data are number and percentage unless otherwise indicated.

Table 2: Multiple logistic regression analyses for predictors of poor 3-month outcome

Variables	OR	95% CI	P Value
Model 1 ^a			
Poor LC flow	0.28	0.07–1.19	.085
Absent ipsilateral OA	0.45	0.13–1.54	.201
NIHSS ≥ 5	16.44	1.90–142.18	.011
Model 2 ^b			
Absent ipsilateral OA or poor LC flow	4.50	1.35–14.93	.014
NIHSS ≥ 5	19.21	2.22–166.19	.007

^a In model 1 of multiple logistic regression analysis, the ipsilateral OA and LC were independently analyzed along with the NIHSS.

^b In model 2, both the ipsilateral OA and LC were analyzed together (presence of both secondary collaterals vs absence of either of them or both) along with the NIHSS for predicting 3-month outcome.

eral OA was a significant predictor of poor outcome at 3 months in patients with symptomatic cervical ICA occlusion.

The presence of reversed OA flow is considered a harbinger of poor cerebral hemodynamics in patients with carotid occlusion, but data regarding its effect on outcome were inconclusive.¹⁰ Tsai et al,⁴ in a retrospective study of patients with severe ICA stenosis or occlusion with transcranial Doppler and MRA, showed that the patients with ICA occlusion had a significantly higher incidence of reversed OA flow compared with patients with unilateral high-

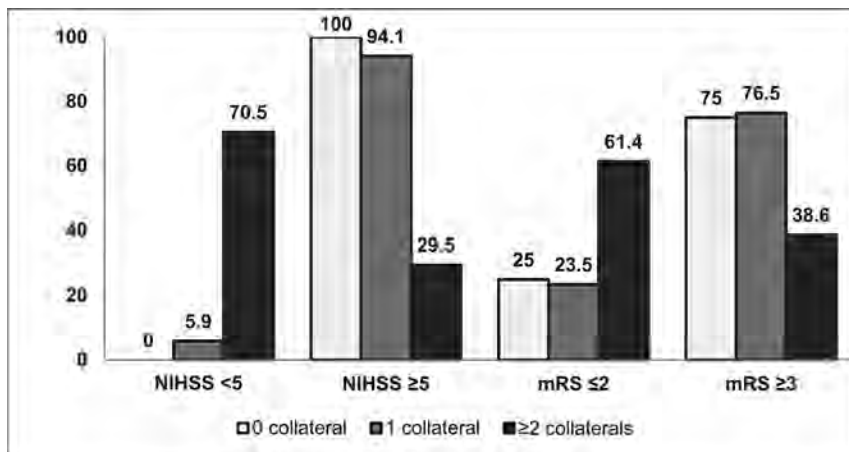


FIG 5. Number of collaterals with initial stroke severity and 3-month outcome.

grade carotid stenosis. Reversed OA flow was considered a marker of impaired cerebral hemodynamics in patients with severe carotid disease because it was associated with poor functional outcome. On the contrary, stroke outcome improved by 10%–20% in the reversed OA flow group compared with the forward OA flow group in subjects with severe intracranial carotid stenosis ($\geq 50\%$).¹¹ This finding is in accord with our study, which showed that most patients with absent ipsilateral OA compared with its presence were associated with poor outcome (69.2% versus 38.5%; $P = .02$). Although the role of the OA as an effective collateral is questionable, owing to its small caliber, the retrograde flow through the OA might compensate for the insufficiency in the anterior portion of Willisian circulation, and its presence may indicate an overall good collateral perfusion.^{12–14}

Previous studies have suggested an important role for LC in determining the extent of infarct, outcome, and response to revascularization therapy in acute stroke.^{5,7,15–17} Similarly, our study showed that 15 of 18 patients with poor flow through the LC had poor outcome, and all of them had moderate-to-severe stroke at onset. The diversion of blood flow through the leptomeningeal vessels provides sufficient oxygenation to the ischemic bed distal to the occlusion. Not only the quantity of collaterals but also the quality of oxygenation through the slow flow along leptomeningeal vessels determines the fate of the ischemic bed.^{2,18}

In our study, patients with ≥ 2 collaterals (ipsilateral OA, ipsilateral PcomA, AcomA, and LC) had excellent outcome, indicating that as more collaterals are recruited, more blood flow is diverted to the ischemic areas, providing an effective compensatory mechanism (Fig 5). A similar finding was observed in ICA dissection in which patients with < 2 collaterals showed a significant increased risk of poor recovery.¹⁹ The annual risk of recurrent ischemic events was also reduced in patients when more collaterals were recruited.⁶ Hence the presence of > 1 major collateral pathway supplying the hemisphere on the side of the occlusion had a positive association with better outcome.

Willisian collateral flow was considered an immediate diverter of blood flow in the event of any large-vessel occlusion.^{2,20,21} However, in this study, the flow through the AcomA and PcomA was not independently predictive of stroke severity or outcome. This may be due to the anatomic variations such as hypoplasia or

atresia of vessels or a fetal posterior cerebral artery, which might reduce their role as a collateral route.^{22,23} Alternatively, their role as a reliable alternative conduit may be questionable. Some patients with severe stroke or mortality due to malignant MCA stroke might not have reached our hospital, and their collateral status, including the communicating arteries, was unknown. More likely, such patients might have had poor collaterals and poor hemodynamic compensation through the communicating arteries, which could have resulted in greater stroke severity.

Our study patients were a homogeneous cohort because we excluded patients with intracranial ICA occlusion and tandem MCA occlusion and those who

underwent revascularization therapy. The key advantage of our study was the uniformity in the study protocol, with a single imaging technique (CTA) for the concurrent assessment of both the primary and secondary collaterals. The images were independently read by an interventional neuroradiologist and a stroke neurologist with reasonable interrater agreement.

A major limitation of the study was the inability to assess the direction of flow in the OA by CTA. Multiphasic CTA was not performed in our patients, and how a vessel is filled (antegrade or retrograde) could not be determined. Although none of the techniques used to study cerebral collaterals have been systematically studied or validated, transcranial Doppler or DSA is generally preferred for the delineation of retrograde-versus-forward flow.^{18,22} We included patients up to 3 weeks after the event, which would have a bearing on the interpretation of the collateral status because time is a critical variable and collateral circulation is dynamic.^{18,24–26} The other limitation was the selection bias in which patients who had severe stroke or who died early are clearly not represented in our sample (not referred to our institution), and obviously they might have had poor collateral circulation, including absent flow through the AcomA and PcomA. Probably this would explain the role of communicating arteries being insignificant in this study. We also did not analyze the role of intracranial ICA stenosis and anomalies of the circle of Willis. A larger sample size could have helped us analyze the factors determining stroke severity, including the role of collaterals, which was another limitation.

CONCLUSIONS

Our study shows that assessment of collateral circulation with CTA is an important tool in predicting 3-month outcome in patients with symptomatic ICA occlusion. Secondary collaterals (leptomeningeal collaterals and ophthalmic artery) rather than Willisian flow might be more influential in determining the outcome in such patients.

ACKNOWLEDGMENTS

The authors acknowledge the contribution of Mr Babunath B, technical assistant (Department of Imaging Sciences and Interventional Radiology), for the processing of CTA images.

REFERENCES

1. Powers WJ. **Cerebral hemodynamics in ischemic cerebrovascular disease.** *Ann Neurol* 1991;29:231–40 CrossRef Medline
2. Liebeskind DS. **Collateral circulation.** *Stroke* 2003;34:2279–84 CrossRef Medline
3. Miteff F, Levi CR, Bateman GA, et al. **The independent predictive utility of computed tomography angiographic collateral status in acute ischaemic stroke.** *Brain* 2009;132:2231–38 CrossRef Medline
4. Tsai CL, Lee JT, Cheng CA, et al. **Reversal of ophthalmic artery flow as a predictor of intracranial hemodynamic compromise: implication for prognosis of severe carotid stenosis.** *Eur J Neurol* 2013;20:564–70 CrossRef Medline
5. Liebeskind DS, Jahan R, Nogueira RG, et al; SWIFT investigators. **Impact of collaterals on successful revascularization in Solitaire FR with the intention for thrombectomy.** *Stroke* 2014;45:2036–40 CrossRef Medline
6. Vernieri F, Pasqualetti P, Matteis M, et al. **Effect of collateral blood flow and cerebral vasomotor reactivity on the outcome of carotid artery occlusion.** *Stroke* 2001;32:1552–58 CrossRef Medline
7. Lima FO, Furie KL, Silva GS, et al. **The pattern of leptomeningeal collaterals on CT angiography is a strong predictor of long-term functional outcome in stroke patients with large vessel intracranial occlusion.** *Stroke* 2010;41:2316–22 CrossRef Medline
8. Bang OY, Lee PH, Heo KG, et al. **Specific DWI lesion patterns predict prognosis after acute ischaemic stroke within the MCA territory.** *J Neurol Neurosurg Psychiatry* 2005;76:1222–28 CrossRef Medline
9. Maas MB, Lev MH, Ay H, et al. **Collateral vessels on CT angiography predict outcome in acute ischemic stroke.** *Stroke* 2009;40:3001–05 CrossRef Medline
10. Hofmeijer J, Klijn CJ, Kappelle LJ, et al. **Collateral circulation via ophthalmic artery or leptomeningeal vessels is associated with impaired cerebral vasoreactivity in patients with symptomatic carotid artery occlusion.** *Cerebrovasc Dis* 2002;14:22–26 CrossRef Medline
11. Sung YF, Tsai CL, Lee JT, et al. **Reversal of ophthalmic artery flow and stroke outcomes in Asian patients with acute ischemic stroke and unilateral severe cervical carotid stenosis.** *PLoS One* 2013;8:e80675 CrossRef Medline
12. Orge F, Harris A, Kagemann L, et al. **The first technique for non-invasive measurements of volumetric ophthalmic artery blood flow in humans.** *Br J Ophthalmol* 2002;86:1216–19 CrossRef Medline
13. Reinhard M, Muller T, Guschlbauer B, et al. **Dynamic cerebral autoregulation and collateral flow patterns in patients with severe carotid stenosis or occlusion.** *Ultrasound Med Biol* 2003;29:1105–13 CrossRef Medline
14. Saqqur M, Demchuk AM, Hill MD, et al. **Bedside emergency transcranial Doppler diagnosis of severe carotid disease using orbital window examination.** *J Neuroimaging* 2005;15:138–43 CrossRef Medline
15. Bang OY, Saver JL, Kim SJ, et al; UCLA-Samsung stroke collaborators. **Collateral flow averts hemorrhagic transformation after endovascular therapy for acute ischemic stroke.** *Stroke* 2011;42:2235–39 CrossRef Medline
16. Bang OY, Saver JL, Buck BH, et al; UCLA collateral investigators. **Impact of collateral flow on tissue fate in acute ischaemic stroke.** *J Neurol Neurosurg Psychiatry* 2008;79:625–29 Medline
17. McVerry F, Liebeskind DS, Muir KW. **Systematic review of methods for assessing leptomeningeal collateral flow.** *AJNR Am J Neuroradiol* 2012;33:576–82 CrossRef Medline
18. Liebeskind DS. **Collaterals in acute stroke: beyond the clot.** *Neuroimaging Clin N Am* 2005;15:553–73, x CrossRef Medline
19. Silvestrini M, Altamura C, Cerqua R, et al. **Early activation of intracranial collateral vessels influences the outcome of spontaneous internal carotid artery dissection.** *Stroke* 2011;42:139–43 CrossRef Medline
20. Miralles M, Dolz JL, Cotillas J, et al. **The role of the circle of Willis in carotid occlusion: assessment with phase contrast MR angiography and transcranial duplex.** *Eur J Vasc Endovasc Surg* 1995;10:424–30 CrossRef Medline
21. Hartkamp MJ, van Der Grond J, van Everdingen KJ, et al. **Circle of Willis collateral flow investigated by magnetic resonance angiography.** *Stroke* 1999;30:2671–78 CrossRef Medline
22. Shuaib A, Butcher K, Mohammad AA, et al. **Collateral blood vessels in acute ischaemic stroke: a potential therapeutic target.** *Lancet Neurol* 2011;10:909–21 CrossRef Medline
23. Riggs HE, Rupp C. **Variation in form of circle of Willis: the relation of the variations to collateral circulation—anatomical analysis.** *Arch Neurol* 1963;8:8–14 CrossRef Medline
24. Widder B, Kleiser B, Krapf H. **Course of cerebrovascular reactivity in patients with carotid artery occlusions.** *Stroke* 1994;25:1963–67 CrossRef Medline
25. Derdeyn CP, Videen TO, Fritsch SM, et al. **Compensatory mechanisms for chronic cerebral hypoperfusion in patients with carotid occlusion.** *Stroke* 1999;30:1019–24 CrossRef Medline
26. Liebeskind DS, Sansing LH. **Willisian collateralization.** *Neurology* 2004;63:344 CrossRef Medline

Acute Ischemic Stroke Infarct Topology: Association with Lesion Volume and Severity of Symptoms at Admission and Discharge

S. Payabvash, S. Taleb, J.C. Benson, and A.M. McKinney



ABSTRACT

BACKGROUND AND PURPOSE: Acute stroke presentation and outcome depend on both ischemic infarct volume and location. We aimed to determine the association between acute ischemic infarct topology and lesion volume and stroke severity at presentation and discharge.

MATERIALS AND METHODS: Patients with acute ischemic stroke who underwent MR imaging within 24 hours of symptom onset or last seen well were included. Infarcts were segmented and coregistered on the Montreal Neurological Institute-152 brain map. Voxel-based analyses were performed to determine the distribution of infarct lesions associated with larger volumes, higher NIHSS scores at admission and discharge, and greater NIHSS/volume ratios.

RESULTS: A total of 238 patients were included. Ischemic infarcts involving the bilateral lentiform nuclei, insular ribbons, middle corona radiata, and right precentral gyrus were associated with larger infarct volumes (average, 76.7 ± 125.6 mL versus 16.4 ± 24.0 mL, $P < .001$) and higher admission NIHSS scores. Meanwhile, brain stem and thalami infarctions were associated with higher admission NIHSS/volume ratios. The discharge NIHSS scores were available in 218 patients, in whom voxel-based analysis demonstrated that ischemic infarcts of the bilateral posterior insular ribbons, middle corona radiata, and right precentral gyrus were associated with more severe symptoms at discharge, whereas ischemic lesions of the brain stem, bilateral thalami, and, to a lesser extent, the middle corona radiata were associated with higher ratios of discharge NIHSS score/infarct volume.

CONCLUSIONS: Acute ischemic infarcts of the insulae, lentiform nuclei, and middle corona radiata tend to have larger volumes, more severe presentations, and worse outcomes, whereas brain stem and thalamic infarcts have greater symptom severity relative to smaller lesion volumes.

ABBREVIATION: VLSM = voxel-based lesion symptom mapping

The primary goal of acute-phase stroke imaging is to exclude intracranial hemorrhage and to estimate the volume of irreversible ischemic infarct, to identify candidates for thrombolytic therapy. Currently, NCCT is the most widely used imaging technique for this purpose, given its availability, speed, and reliability for ruling out intracranial hemorrhage. However, acute stroke imaging could also have the potential to provide additional prog-

nostic information. For example, the DWI infarct volume, ASPECTS, and malignant CTA collateral profile are imaging markers that have shown prognostic value in patients with acute ischemic stroke.¹⁻³

Patients with acute ischemic stroke with larger infarct volumes have a higher risk of developing symptomatic intracranial hemorrhage and worse clinical outcome following intravenous thrombolysis.^{4,5} The presence of ischemic changes of greater than one-third of the MCA territory on noncontrast CT may exclude patients from reperfusion therapy. Certain studies have suggested that a DWI infarct volume of >70 – 100 mL represents a malignant profile that has a higher risk of hemorrhagic transformation and poor outcome.^{4,5} Consequently, the ASPECTS, which has been correlated with outcome, was developed as a means of quantifying ischemic changes on NCCT to identify candidates for thrombolysis.^{6,7}

In addition to volume, the location of an infarct is fundamentally linked to neurologic deficits. There is a limited correlation

Received May 31, 2016; accepted after revision August 22.

From the Department of Radiology, University of Minnesota, Minneapolis, Minnesota.

The data were partially presented at: Annual Meeting of the American Society of Neuroradiology, May 21–26, 2016; Washington, DC.

Please address correspondence to Alexander M. McKinney, MD, Department of Radiology, University of Minnesota, MMC 292, 420 Delaware St SE, Minneapolis, MN 55455; e-mail: mckinrad@umn.edu

 Indicates article with supplemental on-line photos.

<http://dx.doi.org/10.3174/ajnr.A4970>

between the infarct volume and the severity of stroke symptoms; while the infarct volume accounts for 38% of the variation in stroke severity, the combination of both infarct volume and location can account for 62% of the variation in NIHSS scores.⁸ Thus, there has been recent effort to assess the relationship between the infarct topology and outcome in patients with stroke.^{9–12} Specifically, some studies reported that ischemic infarcts in the insular ribbon, lentiform nucleus, and corona radiata are associated with poor prognosis in patients with stroke.^{10,13,14} However, there are limited prior studies on voxel-based evaluation of the relationship between acute infarct location and volume in these patients.

The primary goal of our study was to determine the location of acute ischemic infarcts with larger volumes on admission MR imaging by using a voxel-based analysis. It is likely that the distribution of infarct lesions with larger volumes could, at least in part, explain some of the recent findings on the topographic correlation of admission infarct distribution and clinical presentation, as well as outcome. Also, the present study investigated the interconnection of infarct topology, lesion volume, and severity of symptoms at admission and discharge. Additionally, we evaluated the distribution of infarct lesions with higher ratios of NIHSS-to-infarct volume, which represent worse clinical deficits relative to smaller lesion size. The voxel-based analysis of lesion-location volume or location-symptom relation can search for significant associations between infarct topology and outcome variables without a priori cerebral parcellation, compared with an atlas-based image analysis methodology.^{11,12} Such findings can potentially be the basis for development of a “hazard atlas” of the brain to predict clinical outcome and, perhaps, response to treatment on the basis of infarct distribution and size at the time of admission.

MATERIALS AND METHODS

Patients

This study was approved by the institutional review boards at the University of Minnesota Medical Center, Hennepin County Medical Center. The medical and imaging records of all patients who were admitted with a diagnosis of stroke to those 2 hospitals were reviewed between January 2011 and December 2014. Patients were included in this study if all of the following criteria were present: 1) They underwent MR imaging within 24 hours of symptom onset or, alternatively, at the time last seen well; 2) the patient had a “unilateral” acute ischemic infarct based on DWI; and 3) the patient had no evidence of intracranial hemorrhage on the admission CT or MR imaging examinations. As per the stroke registry protocol of the 2 institutions, the NIHSS score is recorded for all patients presenting with stroke symptoms, as a measure of symptom severity.^{11,12} The demographic data, time to scan, stroke risk factors, and reperfusion therapy data were all extracted from the electronic medical record.

Infarct Lesion Segmentation and Coregistration

Infarct lesions were manually segmented on the admission DWI via the MRICron software (<http://www.mccauslandcenter.sc.edu/crn/>).¹⁵ An intensity filter was used to augment selection and segmentation of the DWI-hyperintense lesions. The lesion volumes were also calculated by using the above-mentioned software. Thereafter, the infarct lesion volumes, along with the cor-

responding DWI scan, were coregistered to the Montreal Neurological Institute-152 brain space by using the FMRI Linear Image Registration Tool (FLIRT; <http://www.fmrib.ox.ac.uk/>).¹⁶ To illustrate the distribution of infarct lesions across this cohort of patients, we created a summation color-coded overlay map with each voxel showing the number of patients with an infarct at that voxel coordinate (On-line Fig 1A).

Voxel-Based Lesion Symptom Mapping

For voxel-based analysis, the nonparametric mapping toolbox included in the MRICron software package was used.^{10,15} Five series of group comparisons were performed for each voxel (infarcted versus noninfarcted) with the following: 1) the admission infarct volume, 2–3) the NIHSS scores at the admission and discharge (if available), and 4–5) the ratio of NIHSS/volume at the admission and discharge. Separate Voxel-Based Lesion Symptom Mapping (VLSM) analyses were also performed for voxel-based topographic association of admission infarct location with component scores of upper extremity motor (question 5), lower extremity motor (question 6), and language functions (sum scores of questions 9 and 10) on the admission NIHSS test. The software uses the Brunner-Munzel rank order test, and the results provide a corresponding *z* score map, in which higher values indicate the association of an infarct at that specific voxel with either larger lesion volume, more severe symptoms, or a higher NIHSS/volume ratio, respectively (Fig 1). To correct for multiple comparisons, we performed a family-wise error Bonferroni correction with 2000 permutations to compensate for the small sample size. To achieve optimal statistical power, we included only voxels affected in at least 10 patients in the voxel-based analysis (On-line Fig 1B), as suggested by prior studies.¹⁷ For each series of analyses, the family-wise error Bonferroni-corrected *z* scores corresponding to .05 and .01 *P* value thresholds are listed with the depiction window narrowed to approximate corresponding levels (Fig 1 and On-line Fig 2).

Statistical Analysis

The data are expressed as mean \pm SD, frequency (percentage) or median (interquartile range) when appropriate. The *z* score maps from the VLSM analysis were used to develop brain masks and dichotomize patients into 2 groups on the basis of whether their infarct lesions overlapped with the brain mask. An independent samples Student *t* test was performed to compare the average lesion volumes between the dichotomized groups; and a Mann-Whitney *U* test was used for comparison of the NIHSS scores. All statistical analyses were performed by using the SPSS for Mac, Version 21.0 (IBM, Armonk, New York). A *P* value $<$.05 was considered statistically significant.

RESULTS

Patient Characteristics

A total of 238 patients were included in this series. The patient characteristics are summarized in the Table. MR imaging was performed at a mean of 13.6 ± 7.1 hours after symptom onset or time last seen well. On-line Fig 1 illustrates the distribution of infarcts among patients. Most infarcts were centered at the insular ribbon and lentiform nuclei, with less frequency at the periphery of the MCA territory and posterior circulation. Overall, 70 (29.4%) pa-

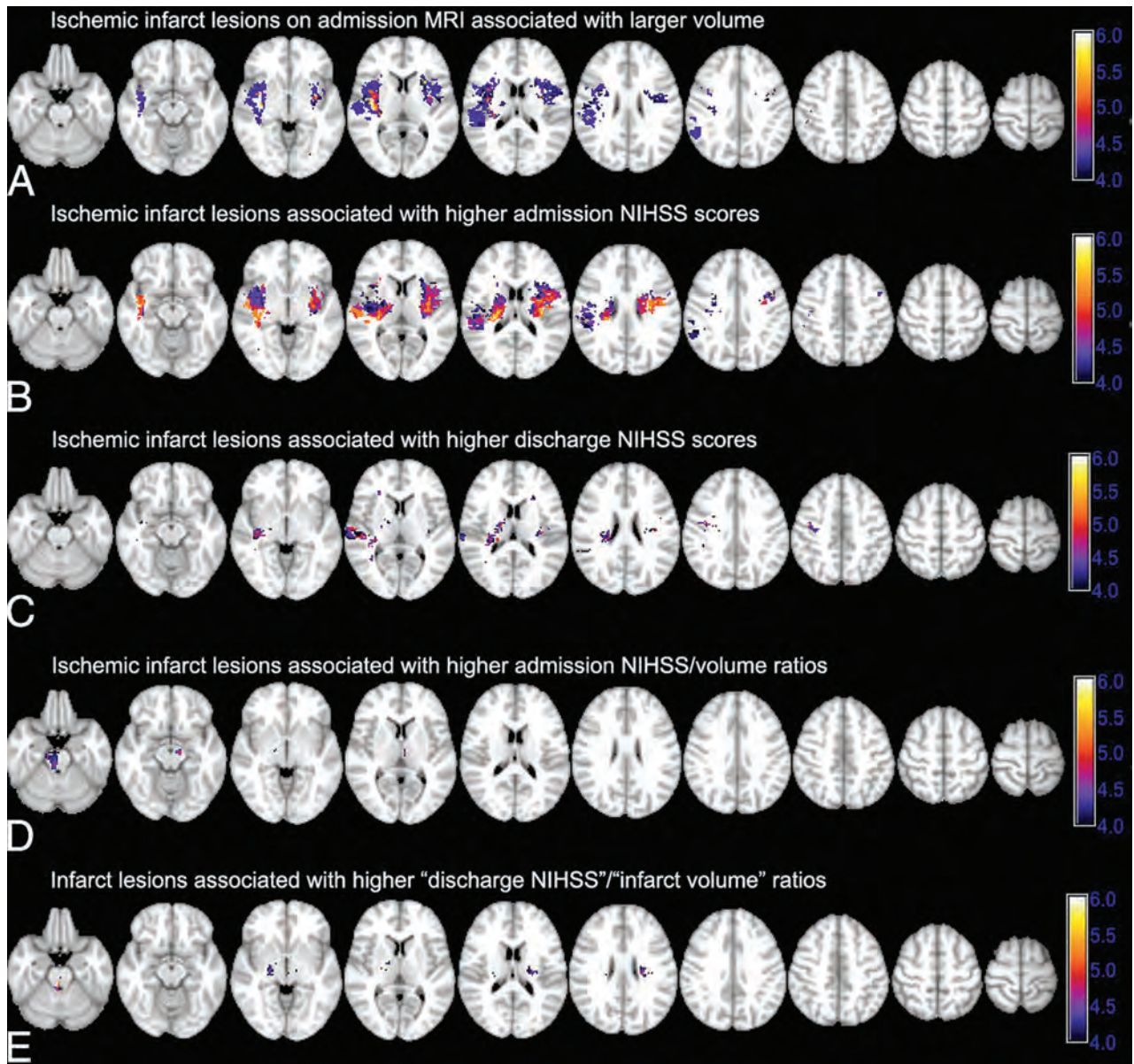


FIG 1. Voxel-based analysis of the association of admission infarct location with infarct volume, admission and discharge NIHSS scores, and NIHSS/volume ratios. The color range shows z scores, and corresponding *P* value thresholds are calculated after family-wise error Bonferroni correction for multiple comparisons and applying 2000 permutations. *A*, Ischemic infarcts are associated with larger admission DWI-lesion volumes. Higher family-wise error scores are associated with larger lesion volumes: z score = 4.27 \rightarrow *P* value = .05; z score = 4.96 \rightarrow *P* value = .01. *B* and *C*, Infarct lesions in voxels with higher z scores are associated with higher admission NIHSS scores (z score = 4.35 \rightarrow *P* value = .05; z score = 4.93 \rightarrow *P* value = .01) and discharge NIHSS scores (z score = 4.23 \rightarrow *P* value = .05; z score = 5.01 \rightarrow *P* value = .01). *D* and *E*, Voxel-based analysis of NIHSS/volume ratio highlights those regions where infarction is associated with a higher ratio of admission (*D*) and discharge (*E*) NIHSS scores per infarct volume, so infarction is associated with worse clinical symptoms despite a smaller volume (for admission ratios: z score = 4.30 \rightarrow *P* value = .05; z score = 4.98 \rightarrow *P* value = .01; for discharge ratios: z score = 4.30 \rightarrow *P* value = .05; z score = 5.15 \rightarrow *P* value = .01).

tients had ischemic infarct lesions within the posterior circulation territory; and 120 (50.4%) had a right-sided stroke.

Topology of Acute Ischemic Infarct Lesions with Larger Volume

The average infarct volume on admission DWI was 39.5 ± 84.9 mL. Fig 1A depicts the VLSM analysis results of lesion volume-location correlation. Infarctions of the bilateral lentiform nuclei, insular ribbons, central corona radiata, and the right precentral gyrus were associated with larger infarct volumes. A brain mask was developed by using the z score map corresponding to a fam-

ily-wise error-corrected *P* value of .05, to dichotomize infarcts into high-versus-low volume (Fig 1A). On average, the volume of ischemic infarcts that involved the highlighted regions in Fig 1A (76.7 ± 125.6 mL) was higher than those that spared these regions (16.4 ± 24.0 mL, $P < .001$).

Topology of Infarcts with Higher NIHSS Scores at Admission and Discharge

Fig 1B highlights the cerebral regions where infarction is associated with higher admission NIHSS scores based on the VLSM analysis. Infarct lesions localized to the insula bilaterally and co-

Patient characteristics (N = 238)^a

Characteristics	
Age at presentation (mean) (yr)	64.4 ± 16.8
NIHSS score at admission	4 (2–8)
Female	92 (38.7%)
Duration of hospital stay (days)	3 (2–5)
Major arterial occlusion	54 (22.7%)
ICA	7 (2.9%)
MCA	30 (12.6%)
ACA	1 (0.4%)
PCA	13 (5.5%)
Basilar artery	3 (1.3%)
IV thrombolytic therapy	56 (23.5%)
IA thrombolysis/thrombectomy	5 (2.1%)
NIHSS score at 24 hr (n = 179)	2 (1–5)
NIHSS score at discharge (n = 218)	2 (0–3)
Stroke risk factors	
Hypertension	184 (77.3%)
Tobacco use	99 (41.6%)
Atrial fibrillation	52 (21.8%)
Diabetes mellitus	67 (28.2%)
Hyperlipidemia	131 (55%)
Coronary artery disease	47 (19.7%)
Prior cerebrovascular accident	63 (26.5%)

Note:—ACA indicates anterior cerebral artery; PCA, posterior cerebral artery; IA, intra-arterial.

^aData are representative of patients' demographic and clinical characteristics.

rona radiata and, to a lesser extent, the right precentral gyrus were associated with higher NIHSS scores at admission. On-line Fig 2 shows the distribution of infarct lesions associated with higher component NIHSS scores for the upper and lower extremity motor deficit and aphasia/dysarthria at the time of admission. Overall, ischemic infarct lesions of the bilateral periventricular white matter and middle corona radiata and the bilateral precentral gyri were associated with higher scores of upper and lower extremity motor deficits—questions 5 and 6, respectively—on the admission NIHSS test (On-line Fig 2A, -B). Higher sum scores on questions 9 (best language) and 10 (dysarthria) were associated with infarct lesions in the left inferior frontal lobe, insular ribbon, and high left precentral gyrus (On-line Fig 2C).

Patients were discharged between 1 and 33 days after stroke onset with 215 (90.3%) discharged within 10 days of admission (Table). The discharge NIHSS scores were available in 218 (91.6%) patients. Ischemic infarct lesions in the bilateral middle corona radiata, posterior insular ribbons, and right precentral gyrus were associated with more severe symptoms at discharge (Fig 1C). Notably, there was no significant difference in admission or discharge NIHSS scores between patients with right-versus-left hemisphere ischemic stroke in univariate analysis (*P* values = 0.569 and 1.000, respectively).

Topology of Infarcts with Higher NIHSS/Volume Ratio

The infarct lesions in the brain stem and, to a lesser extent, the bilateral thalami were associated with higher admission NIHSS/volume ratios (Fig 1D). The patients were then dichotomized into 2 groups: those with infarction within the brain stem (ie, mid-brain, pons, or medulla) and/or thalami versus those with an infarct that spared these regions. The average volume of ischemic infarcts involving the brain stem and/or thalami (21.5 ± 35.1 mL) was less than that of infarcts sparing these regions (43.6 ± 92.1

mL, *P* = .010), whereas, patients with brain stem/thalami infarcts had higher admission NIHSS scores (median, 6; interquartile range, 3–11) compared with the remainder of patients (median, 4; interquartile range, 2–7, *P* = .006). Similar results were found for the topographic distribution of discharge NIHSS score/admission infarct volume ratio (Fig 1E); higher ratios were found in the brain stem, bilateral thalami, and, to an extent, the bilateral middle corona radiata. Among 218 patients with available discharge NIHSS scores, the average volume of ischemic infarcts involving the brain stem and/or thalami (22.6 ± 33.1 mL) was smaller compared with infarcts sparing these regions (39.3 ± 72.6 mL, *P* = .048), with no significant difference in discharge NIHSS scores between these 2 subgroups (*P* = .336).

DISCUSSION

The present study found a topographic overlap in the distribution of acute ischemic infarcts associated with larger lesion volumes, more severe admission symptoms, and worse clinical deficits at discharge. It seems that infarct lesions affecting the insular ribbon, lentiform nuclei, and middle corona radiata in the acute phase represent an ominous sign in terms of clinical presentation and outcome, which could be, at least in part, due to their larger size. On the other hand, those patients with acute ischemic infarcts in the brain stem and thalami had more severe neurologic deficits relative to smaller infarct volumes at presentation and discharge. These findings are in accordance with and can partially explain the mechanism of the recent reports linking acute infarcts of the insula, lentiform nuclei, and periventricular white matter with poor prognosis in anterior circulation stroke.^{9,10,13,14,18} The results suggest that admission infarct topology, possibly along with the integration of clinical findings and lesion volume, can be applied to develop a quantitative population-based probability map for prediction of long-term outcome or assessment of treatment risk versus benefit.

The association between larger infarct volume and involvement of the insular ribbon, lentiform nuclei, and central corona radiata could be due to the spatial location of these regions because extensive ischemic infarcts in the MCA territory would inevitably involve the central portion. However, the topographic distribution of larger infarct lesions may also be secondary to the higher ischemic vulnerability of the insular ribbon and adjacent lentiform nuclei.¹⁶ In addition, proximal MCA occlusion infarcts that involve the insula are more likely to grow into areas of initial perfusion-DWI mismatch.¹⁹ On the other hand, a proximal MCA occlusion stroke sparing the insula may indicate adequate MCA collaterals, given that the insular ribbon arterial supply is almost exclusively from the superior and inferior M2 branches, with a small contribution from the M1 insular branches.²⁰

Regarding outcome prediction, various imaging and clinical variables at stroke presentation have been shown to help predict the clinical outcome. Such predictors described within the literature include the severity of symptoms at presentation (ie, NIHSS score), prestroke mRS score, patient age, and blood glucose level at baseline.^{4,5} As for imaging-based scoring systems proposed for prediction of stroke outcome, ASPECTS is the most widely used tool.¹ However, each DWI-ASPECTS score may represent a wide

range of infarct volumes,²¹ which could be, in part, due to unequal weighing of different MCA regions in ASPECTS, favoring the basal ganglia.²² The results of this study demonstrate that larger infarcts and those associated with more severe symptoms at admission and discharge tend to involve the lentiform nuclei and adjacent insular ribbon, which may explain the prognostic power of the ASPECTS scoring tool despite volumetrically unequal region components.

Recently, there have been growing attempts at prediction of stroke outcome based on the infarct topology.⁹⁻¹⁴ A penalized logistic analysis of ASPECTS component scores on pretreatment CT in the National Institute for Neurological Disorders Tissue Plasminogen Activator trial found that infarction of the lentiform nucleus and parieto-occipital junction (M6 region) predicts poor outcome in older patients.¹³ A voxel-based analysis reported an association between infarction of the central corona radiata, internal capsule, and insular ribbon with higher mRS scores on 1-month follow-up.¹⁰ The current study suggests that admission ischemic infarcts within the insular ribbon, lentiform nuclei, and middle corona radiata are predictors of poor neurologic function at discharge, in part, due to larger lesion volume of infarcts involving these areas and their association with more severe symptoms at presentation. On the other hand, special attention should be paid to the less frequent posterior circulation ischemic infarcts involving the brain stem and thalami, given that such lesions tend to have relatively prominent neurologic deficits at admission and discharge despite their smaller volume.

Although the findings in the current study suggest that infarct topology affects stroke outcome, in part due to lesion volume, the infarct location–outcome correlation persists even after adjustment for infarct volume.¹⁸ Rangaraju et al¹⁸ showed that right parieto-occipital (M6) and left superior frontal (M4) infarctions are associated with poor clinical outcome in patients with stroke with anterior large arterial occlusion over and above the corresponding infarct lesion volume. Timpone et al¹⁴ showed that the percentage of insular ribbon infarction of >50% is an independent predictor of poor clinical outcome despite small admission DWI lesion volumes (<70 mL). Nevertheless, the combination of lesion volume and infarct location results in a stronger correlation with the severity of symptoms at presentation.⁸

Posterior circulation infarcts compose 20%–25% of ischemic strokes.²³ Many prior studies on lesion–function correlation have focused on patients with anterior circulation stroke,^{9,10,18} presumably due to the lower rate of posterior circulation stroke. In the current study, posterior circulation infarcts were not associated with higher NIHSS values on overall VLSM analysis; however, infarctions of the brain stem and thalami were associated with higher ratios of admission and discharge NIHSS scores relative to acute infarct volume. In addition, those patients with ischemic lesions of the brain stem or thalami had higher admission NIHSS scores compared with the remainder of patients. Given the lower rate of posterior circulation infarcts and their smaller volume, it seems pertinent to run a separate analysis for patients with anterior-versus-posterior circulation territory stroke for the development of an inclusive imaging-based prognostic model. Another consideration would be to investigate the relationship of infarct volume in each vascular territory to the territory volume to

demonstrate the relative impact of different infarct lesion volumes in a given arterial territory. However, there is no consensus regarding the precise boundaries of different vascular territories, given the great interpatient variability, which can introduce limitations and bias in calculations.

On separate voxel-based analyses of location–function, this study found a strong association between infarcts of the left inferior frontal gyrus, insular ribbon, and, to a lesser extent, the lower precentral gyrus with aphasia and dysarthria (On-line Fig 2). In addition, infarcts of the precentral primary motor cortex and middle corona radiata along the cerebrospinal tracts were associated with higher degrees of arm and leg paresis at the time of admission. These findings are consistent with prior topographic studies in patients with stroke with CT perfusion and MR imaging.^{11,12,24} Thus, a location-weighted assessment of admission MR imaging can potentially help with the clinical evaluation of stroke patients who have altered mental status by predicting neurologic deficits on the basis of the topology of the infarct lesion.²⁴

One of the limitations of our study is the variability of the onset-to-MR imaging interval gap duration. We tried to minimize such an effect by restricting our inclusion criteria to those patients who underwent MR imaging within 24 hours of stroke. However, the inclusion of patients who had MR imaging within the first 24 hours of stroke might introduce a selection bias because some of the sickest patients with large infarct volumes have only undergone CT. The relatively mild stroke symptoms in our patient cohort were reflected in the median NIHSS scores of 4 at presentation and 2 at 24 hours and discharge, which may limit the extrapolation of these findings to other cohorts. Moreover, some of the vertebrobasilar distribution infarct lesions might be false-negative on early DWI within the first 24 hours of stroke, which might introduce some limitations in our study.²⁵ Also, as an inherent limitation of the current study, the VLSM is affected by the variability in the regional frequency of infarct lesions throughout the brain, so those regions that are scarcely infarcted may not be well-evaluated (eg, anterior cerebral artery, and posterior circulation territory).

In addition, limiting the inclusion criteria to those patients with unilateral infarct lesions might introduce a selection bias by excluding patients with brain stem infarcts that crossed the midline. Thus, the slight asymmetry in lateralization of a higher NIHSS/volume ratio in the right brain stem is most likely secondary to the limited number of patients rather than a true physiologic right-versus-left difference. Additionally, a multivariate voxel-based analysis for correction of findings based on different risk factors or stroke subtypes can further promote our knowledge of the correlation between infarct location and lesion volume and stroke severity. Finally, the follow-up evaluations (namely, the 3-month mRS score) were not available in all patients, and discharge NIHSS scores obtained at variable time points after stroke onset may not provide an accurate and homogeneous measure for early outcome. Nonetheless, the purpose of the current study was not to derive a predictive model for outcome but rather to explore the association between lesion volume and anatomic distribution of infarcts with attention to the severity of symptoms at presentation.

CONCLUSIONS

There has been growing interest in the assessment of infarct location for the prediction of clinical outcome, and some have suggested that the location of cerebral ischemia rather than volume can predict clinical outcome. This study found a topographic overlap between the distribution of infarct lesions with larger volumes and more severe neurologic deficits at admission and discharge. These findings may, in part, explain the underlying mechanism of recent imaging-based predictive models that have noted a poor prognosis of ischemic infarcts involving the insular ribbon, lentiform nuclei, and middle corona radiata, suggesting that such lesions not only affect the eloquent cerebral regions and major white matter neural pathways but also reflect larger infarct sizes. On the other hand, among the less frequent posterior circulation strokes, brain stem and thalamic infarcts were associated with worse symptoms relative to their smaller lesion volumes. Such findings may potentially be the basis of designing a hazard atlas of the brain for prognostication and treatment triage of acute ischemic stroke.

Disclosures: Alexander M. McKinney—UNRELATED: Other Relationships: medicolegal consultation <\$5000 per annum.

REFERENCES

1. Barber PA, Demchuk AM, Zhang J, et al. **Validity and reliability of a quantitative computed tomography score in predicting outcome of hyperacute stroke before thrombolytic therapy: ASPECTS Study Group—Alberta Stroke Programme Early CT Score.** *Lancet* 2000; 355:1670–74 CrossRef Medline
2. Souza LC, Yoo AJ, Chaudhry ZA, et al. **Malignant CTA collateral profile is highly specific for large admission DWI infarct core and poor outcome in acute stroke.** *AJNR Am J Neuroradiol* 2012;33:1331–36 CrossRef Medline
3. Benson J, Payabvash S, Salazar P, et al. **Comparison of CT perfusion summary maps to early diffusion-weighted images in suspected acute middle cerebral artery stroke.** *Eur J Radiol* 2015;84:682–89 CrossRef Medline
4. Lansberg MG, Straka M, Kemp S, et al; DEFUSE 2 Study Investigators. **MRI profile and response to endovascular reperfusion after stroke (DEFUSE 2): a prospective cohort study.** *Lancet Neurol* 2012;11:860–67 CrossRef Medline
5. Mlynash M, Lansberg MG, De Silva DA, et al; DEFUSE-EPITHET Investigators. **Refining the definition of the malignant profile: insights from the DEFUSE-EPITHET pooled data set.** *Stroke* 2011;42:1270–75 CrossRef Medline
6. Demchuk AM, Hill MD, Barber PA, et al; NINDS rtPA Stroke Study Group, NIH. **Importance of early ischemic computed tomography changes using ASPECTS in NINDS rtPA Stroke Study.** *Stroke* 2005; 36:2110–15 CrossRef Medline
7. Pexman JH, Barber PA, Hill MD, et al. **Use of the Alberta Stroke Program Early CT Score (ASPECTS) for assessing CT scans in patients with acute stroke.** *AJNR Am J Neuroradiol* 2001;22:1534–42 Medline
8. Menezes NM, Ay H, Wang Zhu M, et al. **The real estate factor: quantifying the impact of infarct location on stroke severity.** *Stroke* 2007; 38:194–97 CrossRef Medline
9. Beare R, Chen J, Phan TG, et al; VISTA-Acute Collaboration. **Google stroke ASPECTS to determine disability: exploratory analysis from VISTA-Acute Collaboration.** *PLoS One* 2015;10:e0125687 CrossRef Medline
10. Cheng B, Forkert ND, Zavaglia M, et al. **Influence of stroke infarct location on functional outcome measured by the modified Rankin scale.** *Stroke* 2014;45:1695–702 CrossRef Medline
11. Payabvash S, Kamalian S, Fung S, et al. **Predicting language improvement in acute stroke patients presenting with aphasia: a multivariate logistic model using location-weighted atlas-based analysis of admission CT perfusion scans.** *AJNR Am J Neuroradiol* 2010;31:1661–68 CrossRef Medline
12. Payabvash S, Souza LC, Kamalian S, et al. **Location-weighted CTP analysis predicts early motor improvement in stroke: a preliminary study.** *Neurology* 2012;78:1853–59 CrossRef Medline
13. Phan TG, Demchuk A, Srikanth V, et al. **Proof of concept study: relating infarct location to stroke disability in the NINDS rt-PA trial.** *Cerebrovasc Dis* 2013;35:560–65 CrossRef Medline
14. Timpone VM, Lev MH, Kamalian S, et al. **Percentage insula ribbon infarction of >50% identifies patients likely to have poor clinical outcome despite small DWI infarct volume.** *AJNR Am J Neuroradiol* 2015;36:40–45 CrossRef Medline
15. Rorden C, Karnath HO, Bonilha L. **Improving lesion-symptom mapping.** *J Cogn Neurosci* 2007;19:1081–88 CrossRef Medline
16. Payabvash S, Souza LC, Wang Y, et al. **Regional ischemic vulnerability of the brain to hypoperfusion: the need for location specific computed tomography perfusion thresholds in acute stroke patients.** *Stroke* 2011;42:1255–60 CrossRef Medline
17. Reynolds AM, Peters DM, Vendemia JM, et al. **Neuronal injury in the motor cortex after chronic stroke and lower limb motor impairment: a voxel-based lesion symptom mapping study.** *Neural Regen Res* 2014;9:766–72 CrossRef Medline
18. Rangaraju S, Streib C, Aghaebrahim A, et al. **Relationship between lesion topology and clinical outcome in anterior circulation large vessel occlusions.** *Stroke* 2015;46:1787–92 CrossRef Medline
19. Kamalian S, Kemmling A, Borgie RC, et al. **Admission insular infarction >25% is the strongest predictor of large mismatch loss in proximal middle cerebral artery stroke.** *Stroke* 2013;44:3084–89 CrossRef Medline
20. Türe U, Yasargil MG, Al-Mefty O, et al. **Arteries of the insula.** *J Neurosurg* 2000;92:676–87 CrossRef Medline
21. de Margerie-Mellon C, Turc G, Tisserand M, et al. **Can DWI-ASPECTS substitute for lesion volume in acute stroke?** *Stroke* 2013; 44:3565–67 CrossRef Medline
22. Phan TG, Donnan GA, Koga M, et al. **The ASPECTS template is weighted in favor of the striatocapsular region.** *Neuroimage* 2006; 31:477–81 CrossRef Medline
23. Merwick Á, Werring D. **Posterior circulation ischaemic stroke.** *BMJ* 2014;348:g3175 CrossRef Medline
24. Phan TG, Chen J, Donnan G, et al. **Development of a new tool to correlate stroke outcome with infarct topography: a proof-of-concept study.** *Neuroimage* 2010;49:127–33 CrossRef Medline
25. Oppenheim C, Stanescu R, Dormont D, et al. **False-negative diffusion-weighted MR findings in acute ischemic stroke.** *AJNR Am J Neuroradiol* 2000;21:1434–40 Medline

Structural Brain Network Reorganization in Patients with Neuropsychiatric Systemic Lupus Erythematosus

X. Xu, E.S. Hui, M.Y. Mok, J. Jian, C.S. Lau, and H.K.F. Mak

ABSTRACT

BACKGROUND AND PURPOSE: Patients with neuropsychiatric systemic lupus erythematosus have worse outcomes compared with those with systemic lupus erythematosus. A better understanding of the mechanisms of neuropsychiatric systemic lupus erythematosus could potentially improve diagnosis and management. The goal of this study was to investigate the differences in the structural brain network of patients with neuropsychiatric systemic lupus erythematosus compared with patients with systemic lupus erythematosus by using brain connectivity analysis.

MATERIALS AND METHODS: We recruited 20 subjects for each patient cohort and age-matched healthy controls. The topology and efficiency of the network and the characteristics of various brain hubs were investigated by using brain connectivity analysis of diffusion MR imaging data.

RESULTS: There were more extensive reorganizations in the structural brain network of patients with neuropsychiatric systemic lupus erythematosus than in patients with systemic lupus erythematosus. For example, the network of the former had significantly decreased clustering coefficient and local efficiency. They also had significantly lower nodal efficiency in the superior temporal gyrus ($P = .046$) and middle temporal gyrus ($P = .041$).

CONCLUSIONS: Our results hint at a plausible relationship between the neuropsychiatric symptoms and reorganization of the structural brain network of patients with systemic lupus erythematosus. Brain connectivity analysis may be a potential tool to subtype these patients.

ABBREVIATIONS: NPSLE = neuropsychiatric systemic lupus erythematosus; SLE = systemic lupus erythematosus

Patients with systemic lupus erythematosus (SLE) with neuropsychiatric manifestations, known as neuropsychiatric SLE (NPSLE), have significantly worse outcomes than those without these manifestations.¹ The anti-dsDNA antibody is a hallmark serologic biomarker for the definitive diagnosis of SLE. The diagnosis of NPSLE is, on the contrary, challenging and depends largely on the clinical assessment and the appropriate selection of diagnostic investigations.² Gross radiologic abnormalities on

conventional MR imaging are either not often found³ or are not related to neuropsychiatric sequelae.⁴ Nonetheless, recent studies by using diffusion tensor imaging have demonstrated differences in the microstructures of the white matter of patients with NPSLE compared with those with SLE.^{5,6} That the global disease burdens of NPSLE are not well explained by focal brain abnormalities and that brain microstructural alterations may be at play suggest that changes in the architecture of brain wiring, known as the brain network,⁷ may likely underpin the neuropsychiatric deficits.⁸

To better understand and comprehensively characterize a brain network, brain connectivity analysis has been devised.⁹ With such analysis, it has been found that the topology of the normal human brain closely resembles that of a “small-world” network, one that is critical for normal brain functions, and optimizes the cost of information processing in the brain.⁷ Apart from network topology, the relationship between individual brain regions and the rest of the network can also be investigated by using brain connectivity analysis. For instance, the hubs of a brain network, the regions that have the largest number of connections with the rest of the brain, can be identified.¹⁰ The vital roles of

Received February 29, 2016; accepted after revision July 28.

From the Department of Diagnostic Radiology (X.X., E.S.H., H.K.F.M.) and Division of Rheumatology and Clinical Immunology (C.S.L.), Department of Medicine, University of Hong Kong, Pokfulam, Hong Kong Special Administrative Region; Department of Biomedical Sciences (M.Y.M.), City University of Hong Kong, Kowloon Tong, Hong Kong Special Administrative Region; and Radiology Department (J.J.), The First Affiliated Hospital, Nanchang University, Nanchang, Jiangxi China.

This work was supported by the University of Hong Kong Small Project Funding, 200907176197

Please address correspondence to Edward S. Hui, PhD, Department of Diagnostic Radiology, University of Hong Kong, Pokfulam, HKSAR; e-mail: edward.s.hui@gmail.com; Henry K.F. Mak, MD, Department of Diagnostic Radiology, University of Hong Kong, Pokfulam, HKSAR; e-mail: makkf@hku.hk

<http://dx.doi.org/10.3174/ajnr.A4947>

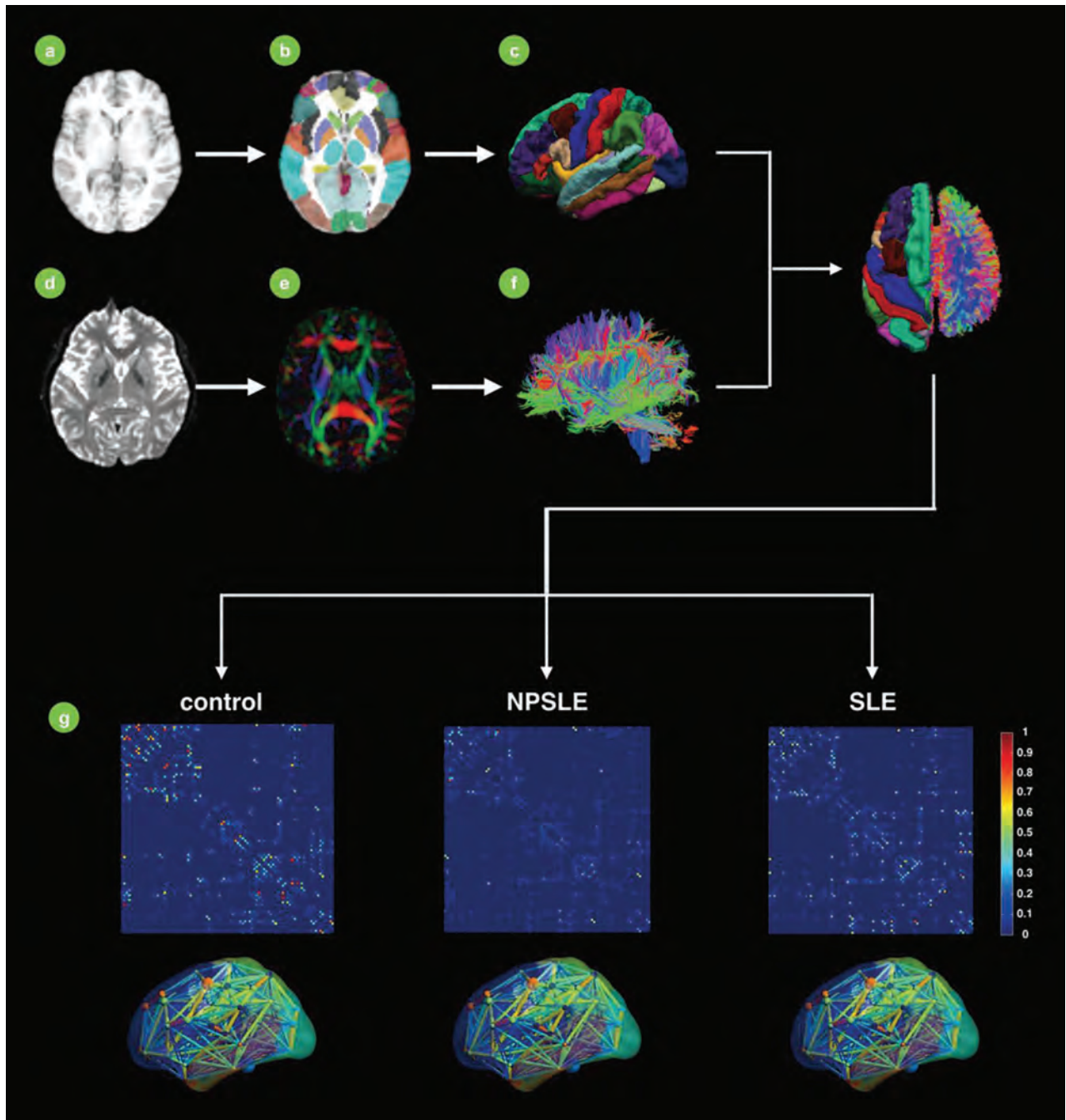


FIG 1. A flowchart of the postprocessing required for brain connectivity analysis. For each subject, T1-weighted anatomic images (A) were registered to non-diffusion-weighted images and subsequently to the International Consortium for Brain Mapping 152 template. The resulting transformation matrix was then used to bring various brain regions or ROIs (B and C) from the Automated Anatomical Labeling atlas into the native anatomic image space. Diffusion tensor was obtained from diffusion-weighted images (D); and its associated diffusion metrics, such as color-coded fractional anisotropy maps (red, left to right; green, anterior to posterior; blue, inferior to superior), were subsequently obtained for constructing the whole-brain white matter tractogram (F). After we combined the tractogram (F) and ROIs (C), the connectivity matrix (G), which records the connections among all ROIs, was obtained for subsequent group analysis.

these hubs have been supported by studies that have demonstrated associations between the change in the properties of brain hubs and behavioral and cognitive deficits for various neuropsychiatric diseases and disorders.^{11,12}

Considering that the diagnosis of NPSLE is far from definitive, it is imperative that a reliable neuroimaging method for subtyping patients with SLE be made available. We hypothesized that brain connectivity analysis could potentially fill this void. The goal of

this study was to investigate the differences in the structural brain networks of patients with NPSLE compared with those with SLE.

MATERIALS AND METHODS

Participants

This retrospective study was approved by the Institutional Review Board of the University of Hong Kong and informed consent was obtained. The inclusion criteria were the following: patients with

SLE who satisfied the revised American College of Rheumatology classification criteria¹³; and patients with NPSLE who fulfilled the case definition of the American College of Rheumatology for neuropsychiatric lupus,¹⁴ with ≥ 1 of the following features: serologic activities, abnormal CSF findings with the exclusion of infection, and abnormal white matter lesions on MR imaging of the brain. Subjects who had obvious dementia and a recent operation were excluded. Patients with SLE and NPSLE were matched by age, sex, and disease duration. Twenty female patients with chronic NPSLE and 20 female patients with SLE were referred from the Rheumatology Clinic of University Hospital, while 20 age-matched healthy female controls without any neurologic or psychological conditions or physical disabilities were recruited.

Image Acquisition

All scans were performed on a 3T MR imaging scanner (Achieva; Philips Healthcare, Best, the Netherlands) with an 8-channel sensitivity encoding head coil for reception. Diffusion MR imaging with non-diffusion-weighted image (B_0) with 4 averaging and diffusion-weighted images along 15 gradient directions with b -values of 1000 s/mm^2 with 2 averaging were acquired by using a single-shot echo-planar imaging sequence with the following parameters: TR/TE = 9150/65 ms, FOV = $225 \times 225 \text{ mm}^2$, reconstruction resolution = $2 \times 2 \text{ mm}^2$, section thickness = 2 mm (no gap), 70 sections, sensitivity encoding factor = 2, scan time = 9 minutes 39 seconds. For anatomic reference, T1-weighted images were acquired by using a 3D-MPRAGE sequence with the following parameters: TR/TE/TI = 15/3.5/800 ms, reconstruction resolution = $1 \times 1 \times 1.5 \text{ mm}^3$, 100 sections, scan time = 6 minutes 1 second. Axial T2-weighted images with the same geometry as that of the DTI acquisition were obtained by using a multishot turbo spin-echo sequence (TR/TE = 3000/80 ms, reconstruction resolution = $0.33 \times 0.33 \text{ mm}^2$, section thickness = 3 mm, 24 sections, total scan time = 1 minute 18 seconds).

Image Processing and Structural Brain Network Construction

The presence of radiologic abnormalities such as lacunar infarct, chronic infarct, and microbleeds were assessed from T2-weighted images by an experienced radiologist. Figure 1 summarizes the postprocessing required for performing brain-connectivity analysis by using diffusion MR imaging data.

Brain Parcellation. An Automated Anatomical Labeling atlas (<http://www.gin.cnrs.fr/AAL-216>) was used to parcellate the brain into 90 cortical and subcortical regions.¹⁵ T1-weighted images were first registered to DTIs by using the FMRIB Linear Image Registration Tool (FLIRT; <http://www.fmrib.ox.ac.uk>).¹⁶ The native space structural images were subsequently registered to the International Consortium for Brain Mapping 152 template (<http://www.bic.mni.mcgill.ca/ServicesAtlases/ICBM152Nlin2009>) by using the FMRIB Nonlinear Registration Tool (FNIRT; <http://fsl.fmrib.ox.ac.uk/fsl/fslwiki/FNIRT>).¹⁶ The inverse of the transformation matrix was subsequently applied to the atlas, thereby bringing all brain ROIs from the Automated Anatomical Labeling atlas into each subject's native structural MR imaging space. Volumetric analysis was subsequently performed by using the UCLA

Multimodal Connectivity Package (http://www.ccn.ucla.edu/wiki/index.php/UCLA_Multimodal_Connectivity_Package).¹⁷

Diffusion MR Imaging Tractography. All DWI was first registered to B_0 images to correct for eddy current distortion and head motion with the FMRIB Diffusion Toolbox (<http://fsl.fmrib.ox.ac.uk/fsl/fslwiki/FDT>).¹⁸ The diffusion tensor and its associated eigenvectors and eigenvalues were obtained with the Diffusion Toolbox.¹⁹ To construct the structural connections among 90 brain regions, we performed DTI-based tractography to track WM fiber tracts by using TrackVis (<http://trackvis.org>) with a fractional anisotropy threshold of 0.2 and a fiber turning angle threshold of 45° .

Brain Network. The connections among all brain regions were computed from the WM tractogram by using the UCLA Multimodal Connectivity Package.¹⁷ The structural connection was estimated by counting the number of WM fiber tracts that originate from 1 region and terminate in another. The fiber count was considered the weight of each edge. After we repeated this step for all regions, an interregional undirected weighted network with weighted connections was constructed.

Brain Connectivity Analysis

The individual's weighted connectivity matrix was normalized to its largest entry to minimize the overall differences in connectivity strength within each subject. Then for each normalized connectivity matrix, measures of small-world properties and network efficiency with the characteristics of each node were computed with the Brain Connectivity Toolbox (<http://www.brain-connectivity-toolbox.net/>).²⁰

Small-World Properties. Measures of the small-world network were first introduced by Watts and Strogatz.²¹ The clustering coefficient of a node refers to how the neighboring nodes and the node itself are connected. The clustering coefficient of the entire network is the average of that of all nodes in the network. The characteristic shortest path length of a node refers to the average shortest travel distance between another node and the node itself. The characteristic shortest path length of the entire network is the average of that of all nodes. The clustering coefficient and characteristic shortest path length of the network are often normalized to those of 100 random networks with a preserved edge number and probability distribution of degree, respectively, to determine how a network is different from a small-world network. A network is considered small-world if the normalized clustering coefficient (γ) is much larger than 1 and the normalized characteristic shortest path length (λ) is close to 1.²¹

Network Efficiencies. The global efficiency of a network is the average of the inverse of the shortest path length of all node pairs in the network²² and usually reflects the ability of the network in parallel information processing. The local efficiency of an entire network is the average of the global efficiency of the community neighboring all nodes in the network and is often considered an indicator of the fault tolerance of a network.²³

Table 1: Demographics

	Control	NPSLE	SLE	P Value
Sample size	20	19	19	—
Age (yr)	40.1 ± 14.6	44.2 ± 13.4	41.9 ± 14.1	.822
Disease duration (yr)	—	18.0 ± 10.1	17.4 ± 9.3	.954
Cumulative prednisolone dosage (g)	—	53.8 ± 39.8	48.9 ± 28.9	.317
Radiologic abnormalities (prevalence) (%)				
Lacunar infarct	—	21	11	.179
Chronic infarct	—	16	11	.350
Microbleeds	—	11	11	1.000
Neuropsychiatric symptoms (prevalence) (%)				
Seizure	—	53	—	—
Confusion	—	21	—	—
Stroke	—	16	—	—
Psychosis	—	11	—	—
Cognitive impairment	—	5	—	—

Note:— indicates not applicable.

Table 2: Volumetric analysis

Brain Regions	P Value	
	NPSLE vs Controls	SLE vs Controls
L. Precentral gyrus	.016 ^a	.007 ^b
L. Middle frontal gyrus	.005 ^b	.001 ^b
R. Middle frontal gyrus, orbital part	.050 ^a	.012 ^a
L. Inferior frontal gyrus, opercular part	.001 ^b	<.001 ^b
L. Inferior frontal gyrus, triangular part	.001 ^b	<.001 ^b
L. Calcarine	.029 ^a	.043 ^a
L. Rolandic operculum	.001 ^b	.001 ^b
L. Insula	.002 ^b	.001 ^b
L. Anterior cingulate and paracingulate gyri	.002 ^b	.001 ^a
R. Anterior cingulate and paracingulate gyri	.046 ^a	.005 ^b
R. Median cingulate and paracingulate gyri	.010 ^a	.006 ^b
L. Amygdala	.013 ^a	.013 ^a
R. Cuneus	.038 ^a	.031 ^a
L. Postcentral gyrus	.004 ^b	.044 ^a
R. Lingual gyrus	.035 ^a	.008 ^b
R. Angular gyrus	.023 ^a	.020 ^a
R. Superior parietal gyrus	.014 ^a	.015 ^a
L. Supramarginal gyrus	.001 ^b	.002 ^b
L. Caudate	.002 ^b	.006 ^b
R. Caudate	.048 ^a	.013 ^a
L. Heschl gyrus	.002 ^b	.001 ^b
L. Superior temporal gyrus	.001 ^b	.001 ^b
R. Superior occipital gyrus	.014 ^a	.023 ^a
R. Middle occipital gyrus	.006 ^b	.015 ^a
R. Inferior occipital gyrus	.024 ^a	.041 ^a

Note:—L indicates left; R, right.

^a $P < .05$.

^b $P < .01$.

Nodal Characteristics. The degree of a node is the number of connections between other nodes and the node and reflects the interaction between the node and its neighbors. Nodal efficiency is the average of the inverse of the shortest path length between the node of interest and all other nodes, and it measures the ability of a node to transmit information to other nodes in the network. The betweenness centrality can quantify how central a node is located within a network and the role it plays in facilitating communication with other nodes.

Identification of Hubs. Brain regions with a large number of connections are considered hubs, characterized by their high degree of connectivity to other regions and small characteristic shortest path lengths. We used betweenness centrality and degree as the hub score for identifying the hubs of a network. All the mea-

sures were averaged between 2 hemispheres. Regions were ranked by nodal betweenness centrality and degree. The top 20% of brain regions were assigned as network hubs.

Statistical Analysis

To determine the between-group difference in all the aforementioned network metrics of all 3 cohorts, we used 1-way ANOVA with 90 regional brain volumes and the absence or presence of lacunar infarcts, chronic infarcts, and microbleeds as covariates. Post hoc analyses were performed with corrections for multiple comparisons by using Bonferroni correction. A significance level of $P < .05$ was set for all statistical tests. The software package SPSS 22.0 (IBM, Armonk, New York) was used for all the statistical analyses.

RESULTS

Demographics

One patients with SLE and 1 with NPSLE were excluded due to imaging artifacts. There was no significant difference in age among all cohorts and no difference in disease duration, total cumulative prednisolone use (from disease onset until the time of study), and the prevalence of radiologic abnormalities of patients with NPSLE compared with those with SLE. All demographics, radiologic abnormalities, prevalence of various neuropsychiatric symptoms, and P values of group comparisons are shown in Table 1.

Volumetric Analysis

There were widespread decreases in regional brain volumes for patients with both NPSLE and SLE compared with controls (Table 2). The differences between patients with NPSLE and those with SLE were not statistically significant.

Small-Worldness

The structural brain network of all cohorts was consistent with the small-world network (γ/λ for NPSLE, $2.91 \pm 0.26/1.30 \pm 0.03$; SLE, $3.01 \pm 0.28/1.29 \pm 0.03$; control, $2.97 \pm 0.38/1.28 \pm 0.03$). Compared with controls, patients with NPSLE had a significantly decreased clustering coefficient ($P = .031$) and increased characteristic shortest path length ($P < .001$), whereas patients with SLE had significantly higher characteristic shortest path length ($P = .012$). Compared with patients with SLE, patients with NPSLE had a significantly lower clustering coefficient ($P = .034$).

Table 3: Hubs identified from each cohort

Regions	Abbreviation	Controls	NPSLE	SLE
Precuneus	PCUN	✓	✓	✓
Insula	INS	✓	✓	✓
Putamen	PUT	✓	✓	✓
Hippocampus	HIP	✓	✓	✓
Caudate nucleus	CAU	✓	✓	✓
Superior frontal gyrus, medial	SFGmed	✓	✓	✓
Thalamus	THA	✓	✓	✓
Median cingulate and paracingulate gyri	DCG	✓	✓	✓
Pallidum	PAL	✓	✓	✓
Superior temporal gyrus	STG	✓	✓	✓
Lingual gyrus	LING	✓	✓	✓
Middle temporal gyrus	MTG	✓	✓	✓
Temporal pole: middle temporal gyrus	TPOmid	✓	✓	✓

Note:—/ indicates identified as hub.

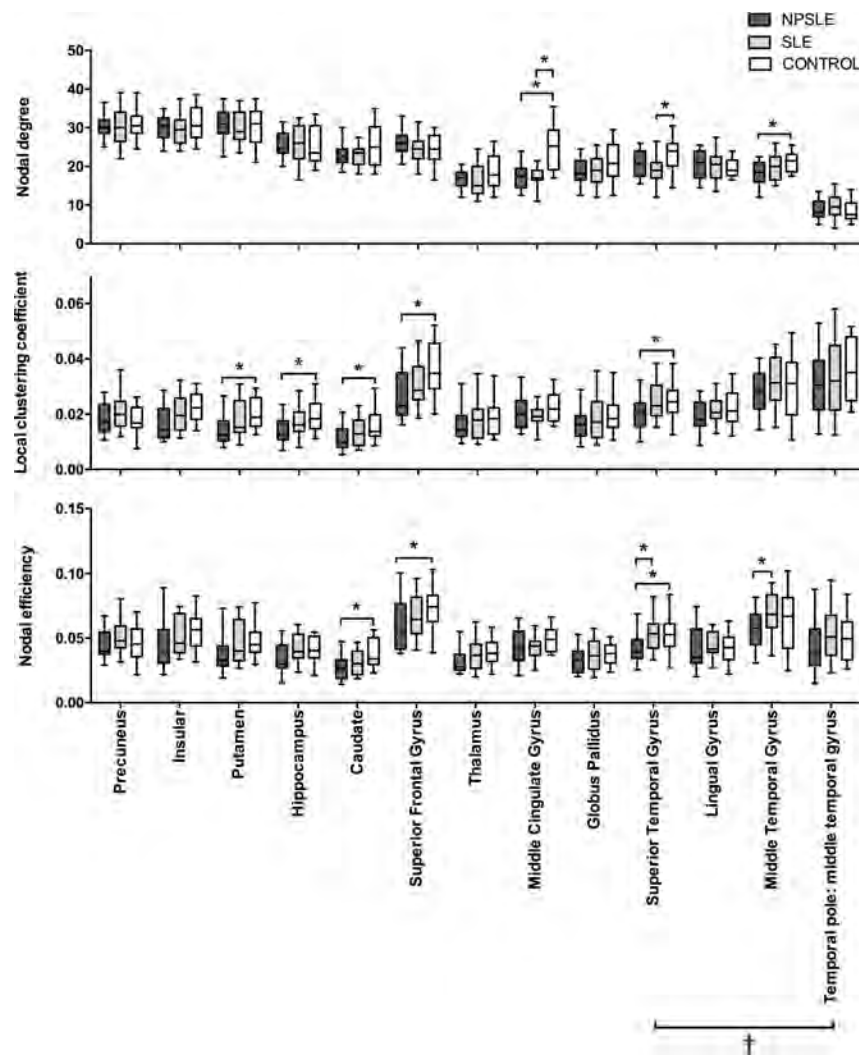


FIG 2. Boxplots showing the group comparisons (median, 50th percentile values, maximum, and minimum) for nodal degree, local clustering coefficient, and nodal efficiency of the 9 network hubs identified from healthy controls and 4 identified from patients with SLE or NPSLE. The nodal degree of the middle cingulate cortex ($P = .005$) was decreased for both patients with NPSLE and those with SLE compared with controls. For patients with NPSLE, the local clustering coefficients of the superior frontal cortex ($P = .003$), hippocampus ($P = .027$), caudate ($P = .018$), and putamen ($P = .010$) were decreased. The nodal efficiency of the superior frontal cortex ($P = .048$) and caudate ($P = .004$) were also decreased. Compared with patients with SLE, patients with NPSLE had significantly lower nodal efficiency in the superior temporal gyrus ($P = .046$) and middle temporal gyrus ($P = .041$). The asterisk indicates $P < .05$; dagger, network hubs identified from patients with SLE or NPSLE.

Network Efficiency

Compared with controls, only patients with NPSLE had significantly lower global efficiency ($P = .010$) and local efficiency ($P = .035$). Compared with patients with SLE, patients with NPSLE had significantly lower local efficiency ($P = .049$).

Nodal Characteristics

From each cohort, 9 of 45 cortical and subcortical regions in each hemisphere were identified as hubs according to the descending order of hub scores (Table 3). Contrary to the controls, the following brain regions were identified as hubs in the NPSLE cohort: the lingual, superior temporal, and middle temporal gyri; and in the SLE cohort: the middle temporal gyrus. The nodal characteristics of the hubs identified from all cohorts were compared and are shown in Fig 2. Compared with controls, patients with SLE ($P = .004$) and NPSLE ($P = .005$) had a significantly decreased nodal degree in the middle cingulate cortex. The local clustering coefficients of the superior frontal cortex ($P = .003$), hippocampus ($P = .027$), caudate ($P = .018$), and putamen ($P = .010$) and the nodal efficiency of the superior frontal cortex ($P = .048$) and caudate ($P = .004$) of patients with NPSLE were also significantly reduced. Compared with patients with SLE, patients with NPSLE had significantly lower nodal efficiency in the superior temporal gyrus ($P = .046$) and middle temporal gyrus ($P = .041$).

DISCUSSION

The coordination and dynamic interactions among different brain regions are critical to normal cognition and behavior.²⁴ Disruption of this complex brain network due to neuropsychiatric disorders, such as Alzheimer disease²⁵ or schizophrenia,²⁶ could lead to cognitive and behavioral deficits in addition to local neurologic sequelae.⁷

In the current study, we have demonstrated that there are more extensive local and global alterations in the structural brain network of patients with NPSLE compared with those with SLE and that the findings thereof were independent of regional brain volumetric changes and hence were likely micro-

structural in nature. In a similar vein, several studies^{6,27,28} have observed a larger extent of focal microstructural alterations in patients with NPSLE than in those with SLE. For instance, Jung et al⁶ demonstrated significant changes in the fractional anisotropy and mean diffusivity of the body of the corpus callosum, left forceps major, and left anterior corona radiata in patients with NPSLE, but not in patients with SLE, compared with controls. Zimny et al²⁸ have shown that the fractional anisotropy of the left inferior longitudinal and inferior fronto-occipital fasciculi of patients with NPSLE was lower compared with patients with SLE.

Together, these findings lead us to believe that there is a likely association between neuropsychiatric symptoms and the extent of alterations in the structural brain network of patients with NPSLE.

Global Network Reorganization

Our results show that the structural brain network of both patient cohorts was consistent with an intact small-world network, albeit a decrease in the clustering coefficient of patients with NPSLE and an increase in the characteristic shortest path length of both patient cohorts compared with controls. The fact that the structural brain network of patients with NPSLE had a lower clustering coefficient compared with patients with SLE suggests that the balance between functional segregation and integration for patients with NPSLE may be compromised.⁷ Thus, their functional brain network may have to reconfigure to meet and compensate for the demand necessary for maintaining the working capacity of the structural brain network in effortful cognitive tasks.²⁹

From the perspective of network efficiency, only the structural brain network of patients with NPSLE had lower global and local efficiencies compared with controls and lower local efficiency than patients with SLE. A decrease in the global efficiency of a brain network suggests a loss of long-range connections, likely as a result of compromised cognitive capacity.³⁰ On the other hand, a decrease in the local efficiency suggests a loss of short-range connections throughout the entire brain network, likely attributable to changes in the modularized information-processing ability and fault tolerance in information transfer of the network.³⁰

Local Network Reorganization

Of the 9 brain regions identified as hubs from controls, the thalamus, middle cingulate cortex, and globus pallidus were replaced by lingual, superior temporal, and middle temporal gyri for patients with NPSLE (Fig 2). That the former 3 brain regions were no longer hubs is largely consistent with the behavioral and cognitive deficits that these patients often endure.³¹⁻³³ On the other hand, the thalamus and middle cingulate cortex were replaced by the middle temporal gyrus for patients with SLE. As is evident from Fig 2, there are more extensive changes in the nodal characteristics of various brain hubs of patients with NPSLE than in those with SLE compared with controls. These results indicate that the role of these hubs was weakened,¹⁰ likely related to the cognitive deficits and emotional instability commonly seen in patients with NPSLE.³⁴

Brain Network Alterations and Neuropsychiatric Manifestations in SLE

The findings from the current study indicate that there were more extensive local and global reorganizations in the structural brain network of patients with NPSLE than in those with SLE and that these changes are the likely attempts of the network to compensate for the neuropsychiatric symptoms commonly seen in the patients with NPSLE. Apart from the structural network, reorganization of the functional brain network of these patients has also been observed in functionally similar brain regions.^{33,35-38} For instance, Fitzgibbon et al³³ demonstrated that patients with NPSLE had larger functional MR imaging activations during working memory tasks compared with controls. Rocca et al³⁶ showed that patients with NPSLE had altered cortical fMRI activation during simple motor tasks. Mak et al³⁵ have shown that additional cortical regions were recruited for the executive function of patients with SLE.³⁵ Differential fMRI activations for the visuoconstructional ability, working memory, and attention of children with childhood-onset SLE were also observed by DiFrancesco et al.³⁷ These functional network reorganizations further supported the notion of increased recruitment of extra cortical pathways to compensate for the cognitive or behavioral deficits of these patients.

CONCLUSIONS

We have demonstrated that there were more extensive local and global alterations in the structural brain network of patients with NPSLE than in those with SLE. Brain connectivity analysis may be a diagnostic tool to subtype these patients, thereby potentially allowing the appropriate therapeutics to be arranged, especially when a more aggressive treatment regimen is necessary for those with NPSLE.

Disclosures: Mo Yin Mok—UNRELATED: Grants/Grants Pending: General Research Fund; Comments: fund in Hong Kong for a basic science project; Payment for Lectures (including service on Speakers Bureaus): Roche, Pfizer, and Janssen; Comments: honorarium given as speakers for isolated educational events organized by pharmaceutical companies. Wallace Chak Sing Lau—UNRELATED: Consultancy: Pfizer (as advisor to their Asia Rheumatology Expert Advisory Council for Health program); Employment: the University of Hong Kong (as clinical professor of medicine); Grants/Grants Pending: General Research Fund, Hong Kong; Health and Medical Research Fund, Hong Kong; Payment for Lectures (including service on Speakers Bureaus): honorarium given as speaker for Asia Rheumatology Expert Advisory Council for Health.

REFERENCES

1. Jeltsch-David H, Muller S. **Neuropsychiatric systemic lupus erythematosus: pathogenesis and biomarkers.** *Nat Rev Neurol* 2014; 10:579–96 CrossRef Medline
2. Hanly JG. **Diagnosis and management of neuropsychiatric SLE.** *Nat Rev Rheumatol* 2014;10:338–47 CrossRef Medline
3. Luyendijk J, Steens SCA, Ouwendijk WJ, et al. **Neuropsychiatric systemic lupus erythematosus: lessons learned from magnetic resonance imaging.** *Arthritis Rheum* 2011;63:722–32 CrossRef Medline
4. Bosma GPT, Middelkoop HA, Rood MJ, et al. **Association of global brain damage and clinical functioning in neuropsychiatric systemic lupus erythematosus.** *Arthritis Rheum* 2002;46:2665–72 CrossRef Medline
5. Lee SP, Wu CS, Hsieh LC, et al. **Efficacy of magnetic resonance diffusion tensor imaging and three-dimensional fiber tractography in the detection of clinical manifestations of central nervous system lupus.** *Magn Reson Imaging* 2014;32:598–603 CrossRef Medline

6. Jung RE, Caprihan A, Chavez RS, et al. **Diffusion tensor imaging in neuropsychiatric systemic lupus erythematosus.** *BMC Neurol* 2010; 10:65 CrossRef Medline
7. Bullmore E, Sporns O. **The economy of brain network organization.** *Nat Rev Neurosci* 2012;13:336–49 CrossRef Medline
8. Gratton C, Nomura EM, Pérez F, et al. **Focal brain lesions to critical locations cause widespread disruption of the modular organization of the brain.** *J Cogn Neurosci* 2012;24:1275–85 CrossRef Medline
9. Bullmore E, Sporns O. **Complex brain networks: graph theoretical analysis of structural and functional systems.** *Nat Rev Neurosci* 2009;10:186–98 CrossRef Medline
10. van den Heuvel MP, Sporns O. **Network hubs in the human brain.** *Trends Cogn Sci* 2013;17:683–96 CrossRef Medline
11. Shi F, Wang L, Peng Z, et al. **Altered modular organization of structural cortical networks in children with autism.** *PLoS One* 2013;8: e63131 CrossRef Medline
12. de Haan W, Mott K, van Straaten EC, et al. **Activity dependent degeneration explains hub vulnerability in Alzheimer's disease.** *PLoS Comput Biol* 2012;8:e1002582 CrossRef Medline
13. Hochberg MC. **Updating the American College of Rheumatology revised criteria for the classification of systemic lupus erythematosus.** *Arthritis Rheum* 1997;40:1725–25 CrossRef Medline
14. **The American College of Rheumatology nomenclature and case definitions for neuropsychiatric lupus syndromes.** *Arthritis Rheum* 1999;42:599–608 Medline
15. Fischl B, Salat DH, Busa E, et al. **Whole brain segmentation: automated labeling of neuroanatomical structures in the human brain.** *Neuron* 2002;33:341–55 CrossRef Medline
16. Smith SM, Jenkinson M, Woolrich MW, et al. **Advances in functional and structural MR image analysis and implementation as FSL.** *Neuroimage* 2004;23(suppl 1):S208–19 CrossRef Medline
17. Brown JA, Rudie JD, Bandrowski A, et al. **The UCLA multimodal connectivity database: a web-based platform for brain connectivity matrix sharing and analysis.** *Front Neuroinform* 2012;6:28 CrossRef Medline
18. Woolrich MW, Jbabdi S, Patenaude B, et al. **Bayesian analysis of neuroimaging data in FSL.** *Neuroimage* 2009;45:S173–86 CrossRef Medline
19. Wang R, Benner T. **Diffusion toolkit: a software package for diffusion imaging data processing and tractography.** In: *Proceedings of the European Society for Magnetic Resonance in Medicine and Biology and the International Society for Magnetic Resonance in Medicine Joint Annual Meeting.* Berlin, Germany; May 19–25, 2007;15:3720
20. Rubinov M, Sporns O. **Complex network measures of brain connectivity: uses and interpretations.** *Neuroimage* 2010;52: 1059–69 CrossRef Medline
21. Watts DJ, Strogatz SH. **Collective dynamics of “small-world” networks.** *Nature* 1998;393:440–42 CrossRef Medline
22. Latora V, Marchiori M. **Economic small-world behavior in weighted networks.** *Eur Phys J B* 2003;32:249–63 CrossRef
23. Latora V, Marchiori M. **Efficient behavior of small-world networks.** *Phys Rev Lett* 2001;87:198701 CrossRef Medline
24. Pessoa L. **On the relationship between emotion and cognition.** *Nat Rev Neurosci* 2008;9:148–58 CrossRef Medline
25. Lo CC, Wang PP, Chou KH, et al. **Diffusion tensor tractography reveals abnormal topological organization in structural cortical networks in Alzheimer's disease.** *J Neurosci* 2010;30:16876–85 CrossRef Medline
26. Wang Q, Su T-P, Zhou Y, et al. **Anatomical insights into disrupted small-world networks in schizophrenia.** *Neuroimage* 2012;59: 1085–93 CrossRef Medline
27. Schmidt-Wilcke T, Cagnoli P, Wang P, et al. **Diminished white matter integrity in patients with systemic lupus erythematosus.** *Neuroimage Clin* 2014;5:291–97 CrossRef Medline
28. Zimny A, Szmyrka-Kaczmarek M, Szewczyk P, et al. **In vivo evaluation of brain damage in the course of systemic lupus erythematosus using magnetic resonance spectroscopy, perfusion-weighted and diffusion-tensor imaging.** *Lupus* 2014;23:10–19 CrossRef Medline
29. Bassett DS, Wymbs NF, Porter MA, et al. **Dynamic reconfiguration of human brain networks during learning.** *Proc Natl Acad Sci U S A* 2011;108:7641–46 CrossRef Medline
30. Achard S, Bullmore E. **Efficiency and cost of economical brain functional networks.** *PLoS Comput Biol* 2007;3:e17 CrossRef Medline
31. Mittal M, Khan S. **Starvation causes acute psychosis due to anterior thalamic infarction.** *South Med J* 2010;103:701–03 CrossRef Medline
32. Ren T, Ho RC-M, Mak A. **Dysfunctional cortico-basal ganglia-thalamic circuit and altered hippocampal-amygdala activity on cognitive set-shifting in non-neuropsychiatric systemic lupus erythematosus.** *Arthritis Rheum* 2012;64:4048–59 CrossRef Medline
33. Fitzgibbon BM, Fairhall SL, Kirk IJ, et al. **Functional MRI in NPSLE patients reveals increased parietal and frontal brain activation during a working memory task compared with controls.** *Rheumatology* 2008;47:50–53 CrossRef Medline
34. Goldin PR, McRae K, Ramel W, et al. **The neural bases of emotion regulation: reappraisal and suppression of negative emotion.** *Biol Psychiatry* 2008;63:577–86 CrossRef Medline
35. Mak A, Ren T, Fu EH, et al. **A prospective functional MRI study for executive function in patients with systemic lupus erythematosus without neuropsychiatric symptoms.** *Semin Arthritis Rheum* 2012; 41:849–58 CrossRef Medline
36. Rocca MA, Agosta F, Mezzapesa DM, et al. **An fMRI study of the motor system in patients with neuropsychiatric systemic lupus erythematosus.** *Neuroimage* 2006;30:478–84 CrossRef Medline
37. DiFrancesco MW, Gitelman DR, Klein-Gitelman MS, et al. **Functional neuronal network activity differs with cognitive dysfunction in childhood-onset systemic lupus erythematosus.** *Arthritis Res Ther* 2013;15:R40 CrossRef Medline
38. Mikdashi JA. **Altered functional neuronal activity in neuropsychiatric lupus: a systematic review of the fMRI investigations.** *Semin Arthritis Rheum* 2016;45:455–62 CrossRef Medline

Intracranial Arteriovenous Shunting: Detection with Arterial Spin-Labeling and Susceptibility-Weighted Imaging Combined

J. Hodel, X. Leclerc, E. Kalsoum, M. Zuber, R. Tamazyan, M.A. Benadjaoud, J.-P. Pruvo, M. Piotin, H. Baharvahdat, M. Zins, and R. Blanc



ABSTRACT

BACKGROUND AND PURPOSE: Arterial spin-labeling and susceptibility-weighted imaging are 2 MR imaging techniques that do not require gadolinium. The study aimed to assess the accuracy of arterial spin-labeling and SWI combined for detecting intracranial arteriovenous shunting in comparison with conventional MR imaging.

MATERIALS AND METHODS: Ninety-two consecutive patients with a known ($n = 24$) or suspected arteriovenous shunting ($n = 68$) underwent digital subtraction angiography and brain MR imaging, including arterial spin-labeling/SWI and conventional angiographic MR imaging (3D TOF, 4D time-resolved, and 3D contrast-enhanced MRA). Arterial spin-labeling/SWI and conventional MR imaging were reviewed separately in a randomized order by 2 blinded radiologists who judged the presence or absence of arteriovenous shunting. The accuracy of arterial spin-labeling/SWI for the detection of arteriovenous shunting was calculated by using the area under receiver operating curve with DSA as reference standard. κ coefficients were computed to determine interobserver and intermodality agreement.

RESULTS: Of the 92 patients, DSA showed arteriovenous shunting in 63 (arteriovenous malformation in 53 and dural arteriovenous fistula in 10). Interobserver agreement was excellent ($\kappa = 0.83$ – 0.95). In 5 patients, arterial spin-labeling/SWI correctly detected arteriovenous shunting, while the conventional angiographic MR imaging did not. Compared with conventional MR imaging, arterial spin-labeling/SWI was significantly more sensitive (0.98 versus 0.90, $P = .04$) and equally specific (0.97) and showed significantly higher agreement with DSA ($\kappa = 0.95$ versus 0.84, $P = .01$) and higher area under the receiver operating curve (0.97 versus 0.93, $P = .02$).

CONCLUSIONS: Our study showed that the combined use of arterial spin-labeling and SWI may be an alternative to contrast-enhanced MRA for the detection of intracranial arteriovenous shunting.

ABBREVIATIONS: ASL = arterial spin-labeling; AUC = area under the receiver operating curve; AVS = arteriovenous shunting; DAVF = dural arteriovenous fistula; ICH = intracranial hemorrhage

Intracranial arteriovenous shunting (AVS) related to dural arteriovenous fistulas (DAVFs) or AVMs may lead to several neurologic complications, including acute intracranial hemorrhage (ICH).^{1–3} DSA remains the reference standard to confirm AVS and assess its angioarchitecture. However, conventional brain MR imaging, including time-of-flight and contrast-enhanced MR angiography, is commonly performed in patients with suspected

AVS, particularly in the setting of acute ICH. Time-resolved (4D) contrast-enhanced MRA is routinely performed in patients suspected of having AVS or for characterizing a known AVM or DAVF.^{4–6} Limitations of this approach include low spatial resolution, incomplete brain coverage, and technical difficulties.^{4–7}

Recently, 2 noncontrast MR imaging techniques, namely SWI and arterial spin-labeling (ASL), were also reported useful for the detection of intracranial AVS. SWI can demonstrate the venous drainage as high signal intensity because of increased blood flow and the presence of a large amount of oxyhemoglobin,^{8–11} while ASL can improve the detection of AVS by showing venous ASL signal.^{12–16} To our knowledge, no previous study has yet compared the accuracy for detecting AVS of these noncontrast techniques with the conventional MR imaging protocol, including contrast-enhanced MRA. During a 4-year period, we have systematically performed 3T MR imaging, including SWI, ASL, and conventional angiographic MR imaging (ie, TOF-MRA, 3D and 4D contrast-enhanced MRA), in all consecutive patients referred

Received May 13, 2016; accepted after revision August 16.

From the Departments of Radiology (J.H., M.Z.) and Neurology (M.Z., R.T.), Saint Joseph Hospital, Paris, France; Department of Neuroradiology (J.H., E.K.), Centre-Hospitalier-Universitaire Henri Mondor, Créteil, France; Department of Neuroradiology (X.L., J.-P. P.), Roger Salengro Hospital, Lille, France; Department of Radiobiology and Epidemiology (M.A.B.), Institute for Radiological Protection and Nuclear Safety (IRSN), Fontenay-Aux-Roses, France; and Department of Interventional Neuroradiology (M.P., H.B., R.B.), Rothschild Foundation Hospital, Paris, France.

J. Hodel and X. Leclerc are co-first authors.

Please address correspondence to Jérôme Hodel, MD, PhD, Department of Neuro-radiology, CHU Henri Mondor, Créteil, France; e-mail: jerome.hodel@gmail.com

<http://dx.doi.org/10.3174/ajnr.A4961>

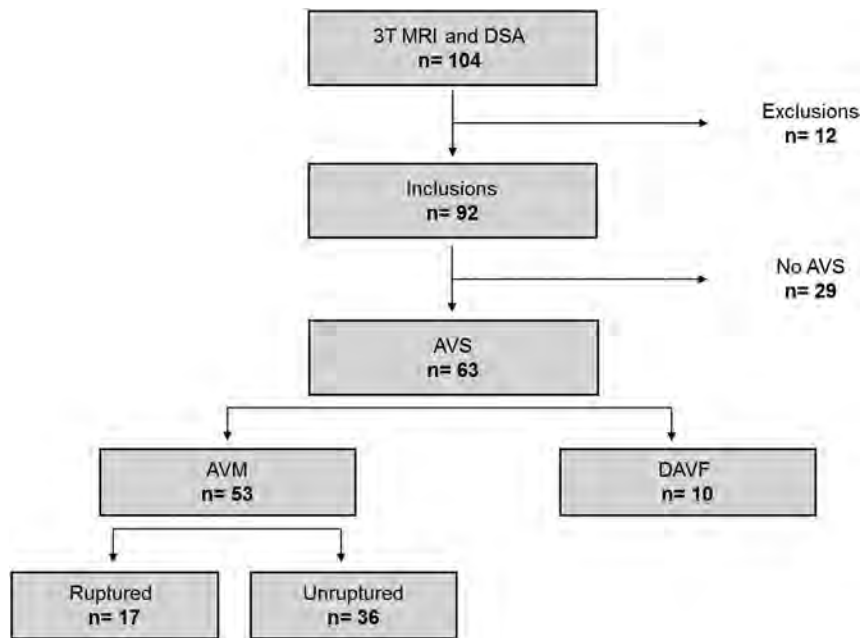


FIG 1. Flow chart illustrating patient selection.

for DSA (considered the reference standard in the present study) for known or suspected AVS. This study sought to determine the accuracy of the combined use of ASL and SWI (ASL/SWI) for the detection of AVS in comparison with conventional MR imaging, including contrast-enhanced MRA.

MATERIALS AND METHODS

Patients and Brain Imaging

This study was approved by the Rothschild Foundation Hospital institutional review board, and written informed consent was obtained from all subjects. From September 1, 2011, to August 31, 2015, 104 consecutive patients (45 females and 59 males; mean age, 48.3 years; range, 11–81 years) underwent DSA for a known ($n = 26$) or suspected ($n = 78$) AVS. Known AVS included brain AVM previously treated by embolization and/or radiosurgery. In this patient group, DSA was performed to evaluate nidus reduction or detect a potential residual shunting, DAVF or brain AVM was suspected in patients with brain hematoma (according to clinical status, patient age, medical history, and location of hemorrhage), pulsatile tinnitus, and suggestive findings on brain MR imaging/CT. In these patients, DSA was performed to confirm AVS and to analyze its location and angioarchitecture.

DSA was performed on a flat panel biplane system (Allura; Philips Healthcare, Best, the Netherlands) and included a selective injection in both the internal and external carotid arteries and vertebral arteries with at least 2 intracranial views (frontal and sagittal). When necessary, 3D rotational angiography with MIP reconstructions and additional oblique views was performed. Each angiogram was acquired at 2 frames per second with a 1024×1024 matrix size and a 20-cm or 27-cm FOV.

In all 104 consecutive patients, we systematically performed 3T MR imaging (Discovery MR750; GE Healthcare, Milwaukee, Wisconsin) once per patient as required by the institutional review board and within the 3 weeks following DSA. Patients were excluded from the study on the basis of at least 1 of the following

conditions: 1) The time interval between MR imaging and DSA was >4 weeks; 2) an endovascular or a radiosurgical procedure was performed in the interval between MR imaging and DSA; and 3) image artifacts prevented accurate analysis of the MR images. Among the 104 consecutive patients, 12 were excluded from the study because of major artifacts on MR imaging. Finally, the study group consisted of 92 patients (40 females and 52 males; mean age, 47.4 years; range, 11–81 years) with a mean time interval between MR imaging and DSA of 13 days (range, 2–21 days). A flow chart illustrating the patient characteristics is shown in Fig 1.

The conventional MR imaging protocol included 2D diffusion-weighted imaging, 2D gradient-echo T2*, 3D FLAIR, 3D TOF MRA, 4D contrast-enhanced MRA (TR, 2.6 ms; TE, 1.1 ms; temporal resolution, 1 second; voxel

size, $1 \times 1 \times 1$ mm) directly followed by a 3D high-resolution contrast-enhanced MRA (TR, 3.6 ms; TE, 1.5 ms; voxel size, $0.6 \times 0.6 \times 0.6$ mm), and postcontrast 3D gradient-echo T1WI sequences (voxel size, $1 \times 1 \times 1$ mm). In addition, SWI (TR, 40 ms; TE, 25 ms; voxel size, $1 \times 1 \times 2$ mm) and ASL (3D FSE; pseudocontinuous; postlabel delay, 1525 ms; section thickness, 4 mm) were performed in each subject before gadolinium administration.

4D contrast-enhanced MRA covered a half-brain that was chosen according to DSA results to optimize temporal and spatial resolution. Intravenous gadobutrol (Gadovist; Bayer Schering Pharma, Berlin, Germany) was administered at a concentration of 0.1 mmol/kg during the acquisition of 4D contrast-enhanced MRA.

Image Analysis

DSA examinations were interpreted by 2 interventional neuroradiologists (X.L., J.-P.P.) together, with >20 years of experience. They reviewed the DSA images of all 92 patients to determine the presence or absence of AVS. In case of AVS, they assigned the vascular malformation as DAVF or AVM. A lesion was considered consistent with a DAVF if meningeal arterial feeders and a fistulous point on the dura mater were identified. A lesion was considered consistent with AVM if arterial feeders and a complex AVS (nidus) located in the brain were identified. Developmental venous anomaly was also located by using DSA, if present.

MR images were first anonymized and randomly mixed. Two experienced neuroradiologists with 14 (R.B.) and 10 (J.H.) years of experience, blinded to the results of DSA and clinical data, independently reviewed all the MR imaging datasets for the presence of AVS. Four independent readings took place 2 weeks apart to avoid recall bias with the following sequences available: 1) ASL alone, 2) SWI alone, 3) ASL/SWI, and 4) the “conventional MR

imaging protocol,” including diffusion-weighted imaging, T2*, 3D FLAIR, TOF MRA, 4D and 3D contrast-enhanced MRA, and postcontrast 3D T1WI MR imaging. Criteria for the presence of AVS on MR images were defined as follows:

With ASL, the presence of an intracranial venous hypersignal within the dural sinuses or cortical veins.

With SWI, a hyperintense venous structure and/or direct visualization of the nidus/fistulous point.

With 4D contrast-enhanced MRA, visualization of the venous drainage at the arterial phase.

With TOF and 3D contrast-enhanced MRA, enlarged and dilated serpiginous vessels and/or direct visualization of the fistulous point/nidus.

For each patient, all the MR images were assessed by using a dedicated workstation (Advantage Windows Workstation; GE Healthcare) with multiplanar reformations available. With SWI, axial 10-mm-thick maximum intensity projections were systematically reconstructed as well as raw data and CBF color maps of ASL. With 4D contrast-enhanced MRA, a time-resolved MIP sagittal view was available as well as each of the 3D MRA volumes generated. When assessing combined MR images, the readers had the ability to merge MR images from different sequences, with or without manual thresholding, by using the available fusion software (3D synchroview, Advantage Windows Workstation; GE Healthcare). Discrepancies between readers were resolved by con-

sensus by using a panel, including an additional board-certified neuroradiologist (X.L.). In each patient, signal abnormalities previously detected on MR images by the blinded readers were correlated with the presence or absence of AVS on DSA. Medical records were also systematically reviewed for acute ICH and previous surgical or endovascular AVS treatments.

Statistical Analysis

Statistical analysis was performed by using SAS software, Version 9.3 (SAS Institute, Cary, North Carolina). Interobserver and intermodality agreement was calculated by using the Cohen κ test. κ values were interpreted as follows: κ value of 0 indicates poor agreement; κ values of 0.01–0.20 indicate minor agreement; κ values of 0.21–0.40, fair agreement; κ values of 0.41–0.60, moderate agreement; κ values of 0.61–0.80, good agreement; and κ values of 0.81–1, excellent agreement. For each of the 4 independent readings, we calculated standard diagnostic accuracy parameters (ie, sensitivity, specificity, and positive and negative predictive values) for the detection of AVS in the whole cohort ($n = 92$), by using DSA as a reference standard. Diagnostic accuracy was also determined by calculating the area under the receiver operating curve (AUC), which equals 0.5 and 1 for models with random and perfect discrimination, respectively. In addition, sensitivity and specificity were calculated in the 2 subgroups: the patients with ICH ($n = 24$) and those previously treated for AVS ($n = 24$). The McNemar test was used to compare measures of diagnostic accuracy. The confidence intervals were calculated by using normal based approximation and were truncated to avoid values of >1 .

RESULTS

DSA Findings

Among the 92 included patients, 68 underwent DSA for a suspected AVS, and 24, for a known AVS previously treated (including 14 without AVS on DSA and 10 with angiographically proved residual AVS related to an AVM). Of these 92 patients, DSA was consistent with AVS in 63 patients (68.5%; 23 females, 40 males; mean age, 45.8 years; range, 11–81 years), including DAVFs in 10 and AVMs in 53. DAVFs were confined to the sinus with antegrade flow (type I according to the Cognard classification) in 2 patients; confined to the sinus with reflux into the sinus (type IIa) in 1 patient; with reflux into the cortical veins (type IIb) in 1 patient; directly draining into the cortical veins (type III) in 4 patients; and with venous ectasia (type IV) in 2 patients. In the 53 patients with AVMs, the Spetzler-Martin classification ranged from I to V (grade I in 14, grade II in 13, grade III in 15, grade IV in 8, and grade V in 3); and the nidus size was <3 cm in 37 (including 13 patients with a nidus size ≤ 1 cm), between 3 and 6 cm in 13, and >6 cm in 3.

The remaining 29 patients without AVS (17 females; mean age, 45.8 years; range, 11–81 years) consisted of 7 patients with no lesion detected by DSA, 14 with a previously treated and completely cured AVS (AVM in 8 and DAVF in 6), and 8 with developmental venous anomalies. In 24 patients with acute

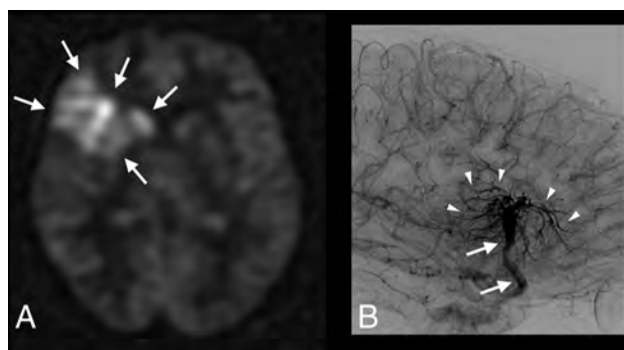


FIG 2. Patient 62 with a complex developmental venous anomaly. ASL raw data (A) and right internal carotid artery angiogram, venous phase, lateral view (B). Increased signal-intensity is visible on ASL images within the right frontal lobe and deep brain nuclei (A, arrows). ASL images were considered suggestive of AVS by 1 blinded reader. Developmental venous anomaly was correctly diagnosed (and thus absence of AVS) by using SWI and a combination of SWI and ASL (not shown). DSA confirms the diagnosis of developmental venous anomaly by revealing a classic umbrella-shaped aspect at the venous phase with medullary veins (B, arrowheads) draining into an enlarged collector (B, arrows), which further drains into the superficial Sylvian vein and cavernous sinus.

Table 1: Diagnosis of AVS (number of patients correctly diagnosed) using ASL, SWI, and conventional MRI

MRI Sequences	DSA			
	No AVS ($n = 29$)	AVS ($n = 63$)	DAVF ($n = 10$)	AVM ($n = 53$)
SWI	28 (97%)	55 (87%)	8 (80%)	47 (89%)
ASL	26 (90%)	60 (95%)	8 (80%)	52 (98%)
ASL/SWI	28 (97%)	62 (98%)	9 (90%)	53 (100%)
Conventional MRI	28 (97%)	57 (90%)	9 (90%)	48 (91%)

Note.—ASL/SWI indicates ASL and SWI combined; conventional MRI, conventional MRI protocol (including diffusion-weighted imaging, gradient-echo T2*, 3D FLAIR, TOF MRA, 4D and 3D contrast-enhanced MRA, and postcontrast 3D T1WI sequences).

Table 2: Diagnostic accuracy parameters using ASL, SWI, and conventional MRI

MRI Sequences	Diagnostic Accuracy Parameters				
	Se (95% CI)	Sp (95% CI)	PPV (95% CI)	NPV (95% CI)	AUC (95% CI)
SWI	0.87 (0.79–0.96)	0.97 (0.90–1)	0.98 (0.90–1)	0.78 (0.61–0.90)	0.92 (0.85–0.96)
ASL	0.95 (0.90–1)	0.90 (0.78–1)	0.95 (0.87–0.99)	0.90 (0.73–0.98)	0.92 (0.84–0.97)
ASL/SWI	0.98 (0.95–1)	0.97 (0.90–1)	0.98 (0.95–1)	0.97 (0.90–1)	0.97 (0.90–1)
Conventional MRI	0.90 (0.83–0.98)	0.97 (0.90–1)	0.98 (0.91–1)	0.92 (0.65–0.93)	0.93 (0.87–0.97)

Note:—Se indicates sensitivity; Sp, specificity; PPV, predictive positive value; NPV, negative predictive value.

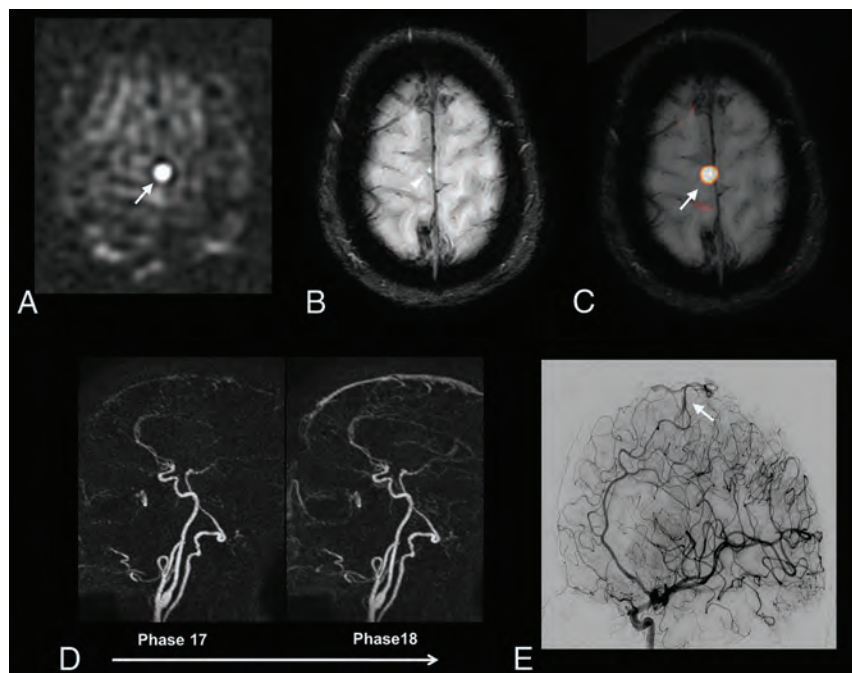


FIG 3. A 60-year-old patient with a right paracentral AVM. ASL raw data (A) demonstrates a strong hypersignal at the anterior part of the right paracentral region (A, arrow). The slight venous hypersignal related to AVS was initially missed by the blinded readers by using SWI alone (B, arrowhead) but was correctly identified by using ASL and SWI combined (C, ASL/SWI merged image, arrow). Findings of time-resolved 4D contrast-enhanced MRA (D) were considered negative by the blinded readers. DSA reveals a small pial AVM in the right paracentral region (E, arrow).

ICH, DSA revealed AVS in 17, including 7 with AVMs under treatment and 10 with an untreated AVM.

Interobserver Agreement

Interobserver agreement (κ value, 95% CI) between both blinded readers was the following: 0.83 (0.78–0.98) for SWI; 0.91 (0.82–1) for conventional MR imaging protocol; and 0.95 (0.88–1) for ASL and ASL/SWI. There were 2 disagreements with ASL: 1 hyperintensity judged as too faint by 1 reader to be related to AVS and 1 other suggestive of developmental venous anomaly for reader 1 and AVS according to reader 2 (Fig 2). Disagreements between readers were observed in 5 cases with SWI.

Detection of AVS by Using MR Imaging

Results are summarized in Tables 1 and 2. ASL and SWI used in combination correctly demonstrated AVS in 5 patients in whom the conventional MR imaging protocol had failed (Figs 3–5). These patients presented with small AVMs, with a nidus size of <1 cm, associated with acute ICH in 1 subject and previously treated in another.

To detect AVS, ASL/SWI was significantly more sensitive than

(0.98 versus 0.90, $P = .04$) and as specific as (0.97) the conventional MR imaging protocol and had a significantly higher agreement with DSA ($\kappa = 0.95$ versus 0.83, $P = .01$) and higher AUC (0.97 versus 0.93, $P = .02$). Considering the agreement with DSA or AUC, ASL and SWI did not differ significantly ($\kappa = 0.85$ versus 0.79, $P = .5$, and AUC = 0.92, $P = .9$, respectively).

Within the subgroups of patients with ICH ($n = 24$) and those with a previously treated AVS ($n = 24$), ASL/SWI was the most sensitive approach for detecting AVS. In patients with ICH, ASL/SWI was 100% sensitive and 86% specific, while conventional MR imaging protocol was 82% sensitive and 86% specific. In patients previously treated, ASL/SWI was 100% sensitive and specific, while the conventional MR imaging protocol was 90% sensitive and 100% specific.

DISCUSSION

Our study showed that 2 noncontrast MR imaging techniques used in combination, namely ASL and SWI, may offer a noninvasive and practical alternative to contrast-enhanced MRA for the detection of intracranial AVS. Such a finding is of clinical relevance if one considers the risk of nephrogenic systemic fibrosis in patients with renal insufficiency.¹⁷ Other limitations of the use of gadolinium chelate are related to age, pregnancy or lactation, and the recent data regarding gadolinium retention in deep brain nuclei.^{18,19} Indeed, patients with AVM or DAVF frequently undergo repeated MR imaging examinations during their follow-up to rule out residual AVS.

In the present study, we assumed that the combined use of ASL and SWI (ASL/SWI) could be as successful as contrast-enhanced MR imaging to detect intracranial AVS. This explains why we separately interpreted contrast-enhanced MR images and ASL/SWI. The excellent negative predictive value of ASL/SWI suggests that such an approach may be of use in ruling out AVS in patients with acute ICH and/or equivocal conventional MR imaging findings, potentially sparing them from invasive DSA evaluation. Conversely, considering the high positive predictive value of ASL/SWI, DSA should also be performed in patients with suggestive signal abnormalities to confirm and characterize the AVS. Several

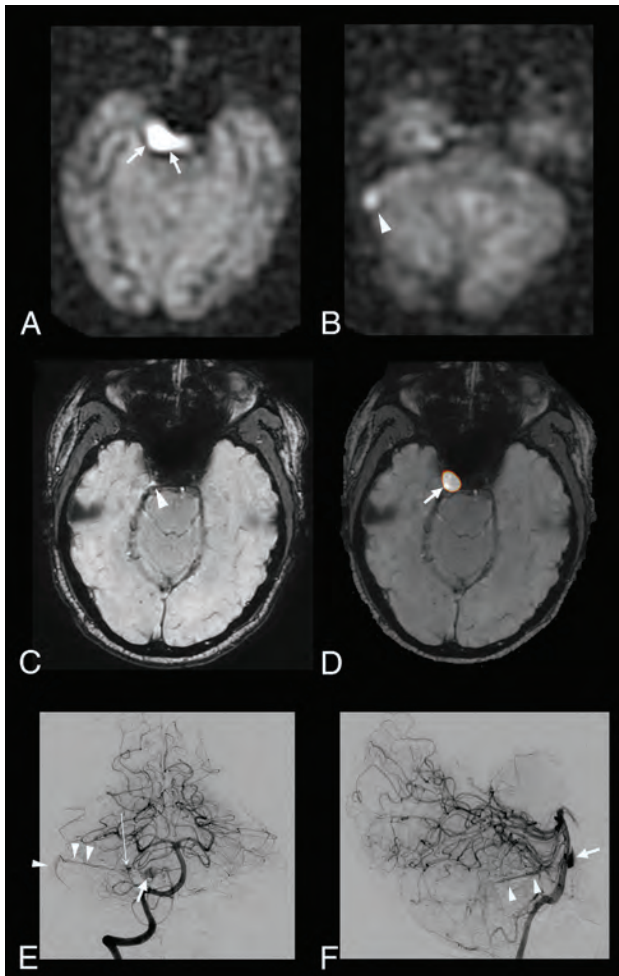


FIG 4. A 52-year-old patient with a right cerebellar AVM draining into the right transverse sinus and the right periclavicular plexus. ASL raw data demonstrate a strong hypersignal within the right periclavicular plexus (A, arrows) and the right lateral sinus (B, arrowhead). With SWI alone, the slight venous hypersignal within the right periclavicular plexus and related to AVS was initially missed by the blinded readers (C, arrowhead) but correctly identified by using ASL and SWI combined (D, ASL/SWI merged image, arrow). Findings of time-resolved and high-resolution contrast-enhanced MRA were negative. Anteroposterior (E) and lateral (F) views from the right vertebral conventional angiograms show a small nidus (E, long arrow) draining into the right lateral sinus through the right superior petrosal sinus (E and F, arrowheads) and into the periclavicular plexus through a lateropontine vein (E and F, arrow).

advantages of the combined use of SWI and ASL may be stressed. First, SWI and ASL provide full-brain coverage, while 4D contrast-enhanced MRA is frequently performed with half-brain coverage to optimize spatial and temporal resolution. Second, the detection of AVS on SWI and ASL images is simple (with a strong hypersignal related to AVS, easily recognizable from the background) and reproducible as suggested by the excellent interobserver agreement, while imaging findings on postcontrast MR imaging may be less specific because dilated intracranial veins may be found in a wide range of conditions.

Our results were in agreement with previous studies showing that SWI and ASL are 2 effective techniques to detect intracranial AVS.⁸⁻¹⁵ Jagadeesan et al¹⁰ demonstrated that SWI was 93% sensitive and 98% specific for the detection of AVS in patients with AVM. SWI was also found to accurately differentiate between

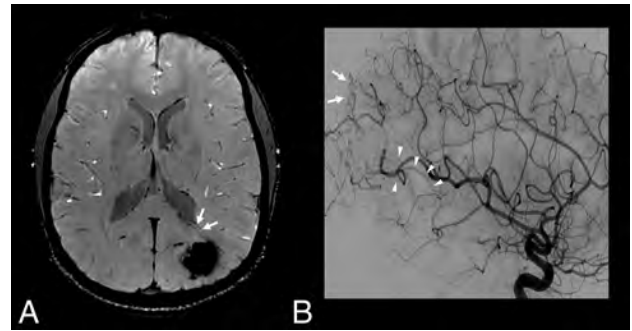


FIG 5. Patient 26 with a previously treated AVM and residual AVS according to DSA. SWI (A) and left internal carotid artery angiogram, arterial phase, lateral view (B). An increased signal intensity is visible with SWI within a deep vein adjacent to the treated nidus (A, arrows), suggestive of AVS. Of note, findings of ASL and contrast-enhanced MR images were considered negative (not shown). DSA confirms the presence of dysplastic vessels around the cast of the embolic agent (B, arrows) and an early opacification of venous drainage (B, arrowheads) coursing toward the deep venous system at the anterior and inferior pole of the embolized AVM.

high-flow and low-flow abnormalities of the vein of Galen in children.⁹ The high sensitivity of ASL for the diagnosis of AVS was also previously reported.^{13,15,16} Similar to the previous study of Le et al,¹² we have included patients with small AVMs or DAVFs for whom the diagnosis of AVS remains challenging. In comparison with this previous study, we found a higher sensitivity of ASL for detecting AVS (95% versus 78%), which may be partly explained by the higher field strength we used, with the signal-to-noise ratio of the ASL sequence being markedly improved at 3T.

ASL/SWI provided a high diagnostic performance by detecting all the AVMs in our cohort and diagnosing significantly more patients with AVS in comparison with the conventional MR imaging protocol. While ASL is highly sensitive for detecting AVS, SWI appears more specific in providing anatomic details of the whole-brain vasculature and differentiating arteries from veins. Merged images between ASL and SWI also appeared particularly useful for precisely locating the ASL signal inside or outside a venous structure, further improving the detection of AVS. Most interesting, in our study, ASL/SWI correctly demonstrated AVS in 5 patients with small AVMs, while the conventional MR imaging protocol did not.

In patients with AVMs previously treated, contrast-enhanced MR images may be misleading.²⁰ Specifically, dilated draining veins or enlarged arteries might persist in the absence of AVS because the decrease of vessel caliber after AVS occlusion often takes time to reverse.⁴ Likewise, contrast enhancement may occur in the treated nidus due to reactive gliosis.²¹ Our results suggest that ASL/SWI could be particularly effective in the specific setting of AVS under treatment. Indeed, the ASL fast spin-echo readout appears very suitable in patients with ICH or with previous embolization, for whom susceptibility artifacts are both common and widespread on MR images.

There are several limitations to our study. First, the diagnostic performance of SWI and/or ASL in case of slow-blood-flow AVS remains unclear, even if we investigated a large cohort of patients with various AVS. The high diagnostic performance of ASL/SWI in patients with treated AVMs, and thus with reduced blood-flow, suggests that this approach remains effective. Second, in our

study, ASL was performed by using a postlabel delay of 1525 ms, whereas it would have been useful to evaluate the accuracy of ASL by using shorter or higher values. The use of multiple postlabel delays may further improve locating the AVS. Further studies are required to test this hypothesis. Third, we did not evaluate the accuracy of ASL/SWI for the assessment of AVM or DAVF angio-architecture. Indeed, we focused our study on the detection of AVS with MR imaging, considering that DSA will be systematically performed in all patients with a high suspicion of AVS. Finally, while a wide range of conditions such as hypervascular tumors, luxury perfusion, reperfusion, or seizures²² may induce ASL hyperintensity, we did not include patients with etiologies other than AVS.

CONCLUSIONS

Our study showed that the combined use of ASL and SWI may be an alternative to contrast-enhanced MRA for the detection of intracranial AVS. Special attention should also be given to hyperintense signal in venous structures on merged ASL/SWI because it appears highly correlated with AVS.

ACKNOWLEDGMENTS

We thank Rachid Mahdjoub, Guillermo Zanolli, and Bastien Perez from GE Healthcare for their support.

Disclosures: Ruben Tamazyán—UNRELATED: Travel/Accommodations/Meeting Expenses Unrelated to Activities Listed: Boehringer Ingelheim France, Comments: European School of Oncology Meeting in 2015. Michel Piotin—UNRELATED: Consultancy: Stryker, Medtronic, MicroVention, Balt, Penumbra*; Payment for Development of Educational Presentations: Stryker, Medtronic, MicroVention, Balt*. Raphael Blanc—UNRELATED: Payment for Development of Educational Presentations: Medtronic, MicroVention, Stryker.* *Money paid to the institution.

REFERENCES

- Hofmeister C, Stapf C, Hartmann A, et al. **Demographic, morphological, and clinical characteristics of 1289 patients with brain arteriovenous malformation.** *Stroke* 2000;31:1307–10 CrossRef Medline
- Gandhi D, Chen J, Pearl M, et al. **Intracranial dural arteriovenous fistulas: classification, imaging findings, and treatment.** *AJNR Am J Neuroradiol* 2012;33:1007–13 CrossRef Medline
- Alexander MD, Cooke DL, Nelson J, et al. **Association between venous angioarchitectural features of sporadic brain arteriovenous malformations and intracranial hemorrhage.** *AJNR Am J Neuroradiol* 2015;36:949–52 CrossRef Medline
- Hadizadeh DR, von Falkenhausen M, Gieseke J, et al. **Cerebral arteriovenous malformation: Spetzler-Martin classification at subsecond-temporal-resolution four-dimensional MR angiography compared with that at DSA.** *Radiology* 2008;246:205–13 CrossRef Medline
- Taschner CA, Gieseke J, Le Thuc V, et al. **Intracranial arteriovenous malformation: time-resolved contrast-enhanced MR angiography with combination of parallel imaging, keyhole acquisition, and k-space sampling techniques at 1.5 T.** *Radiology* 2008;246:871–79 CrossRef Medline
- Nishimura S, Hirai T, Sasao A, et al. **Evaluation of dural arteriovenous fistulas with 4D contrast-enhanced MR angiography at 3T.** *AJNR Am J Neuroradiol* 2010;31:80–85 CrossRef Medline
- Eddleman CS, Jeong HJ, Hurley MC, et al. **4D radial acquisition contrast-enhanced MR angiography and intracranial arteriovenous malformations: quickly approaching digital subtraction angiography.** *Stroke* 2009;40:2749–53 CrossRef Medline
- Hodel J, Blanc R, Rodallec M, et al. **Susceptibility-weighted angiography for the detection of high-flow intracranial vascular lesions: preliminary study.** *Eur Radiol* 2013;23:1122–30 CrossRef Medline
- Jagadeesan BD, Cross DT 3rd, Delgado Almandoz JE, et al. **Susceptibility-weighted imaging: a new tool in the diagnosis and evaluation of abnormalities of the vein of Galen in children.** *AJNR Am J Neuroradiol* 2012;33:1747–51 CrossRef Medline
- Jagadeesan BD, Delgado Almandoz JE, Moran CJ, et al. **Accuracy of susceptibility-weighted imaging for the detection of arteriovenous shunting in vascular malformations of the brain.** *Stroke* 2011;42:87–92 CrossRef Medline
- Letourneau-Guillon L, Krings T. **Simultaneous arteriovenous shunting and venous congestion identification in dural arteriovenous fistulas using susceptibility-weighted imaging: initial experience.** *AJNR Am J Neuroradiol* 2012;33:301–07 CrossRef Medline
- Le TT, Fischbein NJ, André JB, et al. **Identification of venous signal on arterial spin labeling improves diagnosis of dural arteriovenous fistulas and small arteriovenous malformations.** *AJNR Am J Neuroradiol* 2012;33:61–68 CrossRef Medline
- Wolf RL, Wang J, Detre JA, et al. **Arteriovenous shunt visualization in arteriovenous malformations with arterial spin-labeling MR imaging.** *AJNR Am J Neuroradiol* 2008;29:681–87 CrossRef Medline
- Yu SL, Wang R, Wang R, et al. **Accuracy of vessel-encoded pseudo-continuous arterial spin-labeling in identification of feeding arteries in patients with intracranial arteriovenous malformations.** *AJNR Am J Neuroradiol* 2014;35:65–71 CrossRef Medline
- Nabavizadeh SA, Edgar JC, Vossough A. **Utility of susceptibility-weighted imaging and arterial spin perfusion imaging in pediatric brain arteriovenous shunting.** *Neuroradiology* 2014;56:877–84 CrossRef Medline
- Lüdemann L, Jedrzejewski G, Heidenreich J, et al. **Perfusion imaging of cerebral arteriovenous malformations: a study comparing quantitative continuous arterial spin labeling and dynamic contrast-enhanced magnetic resonance imaging at 3 T.** *Magn Reson Imaging* 2011;29:1157–64 CrossRef Medline
- Ramalho J, Semelka RC, Ramalho M, et al. **Gadolinium-based contrast agent accumulation and toxicity: an update.** *AJNR Am J Neuroradiol* 2016;37:1192–98 CrossRef Medline
- Adin ME, Kleinberg L, Vaidya D, et al. **Hyperintense dentate nuclei on T1-weighted MRI: relation to repeat gadolinium administration.** *AJNR Am J Neuroradiol* 2015;36:1859–65 CrossRef Medline
- Kanda T, Ishii K, Kawaguchi H, et al. **High signal intensity in the dentate nucleus and globus pallidus on unenhanced T1-weighted MR images: relationship with increasing cumulative dose of a gadolinium-based contrast material.** *Radiology* 2014;270:834–41 CrossRef Medline
- Cashen TA, Carr JC, Shin W, et al. **Intracranial time-resolved contrast-enhanced MR angiography at 3T.** *AJNR Am J Neuroradiol* 2006;27:822–29 Medline
- Yamamoto M, Ide M, Jimbo M, et al. **Neuroimaging studies of postobliteration nidus changes in cerebral arteriovenous malformations treated by gamma knife radiosurgery.** *Surg Neurol* 1996;45:110–19; discussion 119–22 CrossRef Medline
- Deibler AR, Pollock JM, Kraft RA, et al. **Arterial spin-labeling in routine clinical practice, part 3: hyperperfusion patterns.** *AJNR Am J Neuroradiol* 2008;29:1428–35 CrossRef Medline

Diagnostic Value of Brain Calcifications in Adult-Onset Leukoencephalopathy with Axonal Spheroids and Pigmented Glia

T. Konno, D.F. Broderick, N. Mezaki, A. Isami, D. Kaneda, Y. Tashiro, T. Tokutake, B.M. Keegan, B.K. Woodruff, T. Miura, H. Nozaki, M. Nishizawa, O. Onodera, Z.K. Wszolek, and T. Ikeuchi



ABSTRACT

SUMMARY: Adult-onset leukoencephalopathy with axonal spheroids and pigmented glia is a rare neurodegenerative disease resulting from mutations in the *colony stimulating factor 1 receptor* gene. Accurate diagnosis can be difficult because the associated clinical and MR imaging findings are nonspecific. We present 9 cases with intracranial calcifications distributed in 2 brain regions: the frontal white matter adjacent to the anterior horns of the lateral ventricles and the parietal subcortical white matter. Thin-section (1-mm) CT scans are particularly helpful in detection due to the small size of the calcifications. These calcifications had a symmetric “stepping stone appearance” in the frontal pericallosal regions, which was clearly visible on reconstructed sagittal CT images. Intrafamilial variability was seen in 2 of the families, and calcifications were seen at birth in a single individual. These characteristic calcification patterns may assist in making a correct diagnosis and may contribute to understanding of the pathogenesis of leukoencephalopathy.

ABBREVIATIONS: ALSP = adult-onset leukoencephalopathy with axonal spheroids and pigmented glia; *CSF1R* = *colony stimulating factor 1 receptor*; TORCH syndrome = Toxoplasmosis, Other agents, Rubella, Cytomegalovirus, and Herpes simplex

Adult-onset leukoencephalopathy with axonal spheroids and pigmented glia (ALSP) is a rare inheritable neurodegenerative disease caused by a mutation in the *colony stimulating factor 1 receptor* (*CSF1R*) gene. Before discovery of the causative gene, the term “hereditary diffuse leukoencephalopathy with spheroids or pigmented orthochromatic leukodystrophy” was used to describe patients with the clinical and neuropathologic phenomena, which

are now associated with ALSP. ALSP has been proposed to encompass both of these diseases because of the clinical and pathologic overlap between them^{1,2} and because *CSF1R* mutations have been identified in families with both of these diseases.^{3,4} Although ALSP may be observed anywhere in the world, it seems to be relatively common in Japan.⁵

The clinical presentation of ALSP is heterogeneous. Some patients show parkinsonian features,⁶ while others, particularly young women, are sometimes misdiagnosed as having multiple sclerosis.^{7,8} Imaging findings may be helpful to distinguish these differential diagnoses. Patients with ALSP have several characteristic white matter findings that can be seen on MR imaging, including patchy and later diffuse nonenhancing lesions predomi-

Received May 20, 2016; accepted after revision July 20.

From the Departments of Neurology (T.K., Z.K.W.) and Radiology (D.F.B.), Mayo Clinic Florida, Jacksonville, Florida; Departments of Neurology (T.K., N.M., A.I., T.T., T.M., M.N., O.O.), Molecular Genetics (T.I.), Brain Research Institute, and Medical Technology (H.N.), School of Health Sciences Faculty of Medicine, Niigata University, Niigata, Japan; Department of Neurology (D.K.), Tokyo Metropolitan Geriatric Hospital, Tokyo, Japan; Department of Neurology (D.K.), Osaka Red Cross Hospital, Osaka, Japan; Department of Neurology (Y.T.), National Hospital Organization Tokyo Medical Center, Ibaraki, Japan; Department of Neurology (B.M.K.), Mayo Clinic Rochester, Rochester, Minnesota; and Department of Neurology (B.K.W.), Mayo Clinic Arizona, Scottsdale, Arizona.

Author Contributions: Takuya Konno: drafting the manuscript; design and conceptualization of the study; acquisition, analysis, and interpretation of the data; and final approval of the manuscript. Daniel F. Broderick: reviewing the manuscript, conceptualization of the study, acquisition and interpretation of the data, and final approval of the manuscript. Naomi Mezaki: reviewing the manuscript, acquisition and analysis of the data, and final approval of the manuscript. Aiko Isami: reviewing the manuscript, acquisition and analysis of the data, and final approval of the manuscript. Daita Kaneda: reviewing the manuscript, acquisition of the data, and final approval of the manuscript. Yuichi Tashiro: reviewing the manuscript, acquisition of the data, and final approval of the manuscript. Takayoshi Tokutake: reviewing the manuscript, acquisition of the data, and final approval of the manuscript. B. Mark Keegan: reviewing the manuscript, acquisition of the data, and final approval of the manuscript. Bryan K. Woodruff: reviewing the manuscript, acquisition of the data, and final approval of the manuscript. Takeshi Miura: reviewing the manuscript, acquisition of the data, and final approval of the manuscript. Hiroaki Nozaki: reviewing the manuscript, acquisition of the data, and final approval of the manuscript. Masatoyo Nishizawa: reviewing the manuscript,

conceptualization of the study, interpretation of the data, and final approval of the manuscript. Osamu Onodera: reviewing the manuscript, conceptualization of the study, interpretation of the data, and final approval of the manuscript. Zbigniew K. Wszolek: reviewing the manuscript, conceptualization of the study, interpretation of the data, and final approval of the manuscript. Takeshi Ikeuchi: reviewing the manuscript, design and conceptualization of the study, interpretation of the data, and final approval of the manuscript.

This study was supported by a grant from the Ministry of Health, Labour and Welfare, and Grant-in-Aid for Scientific Research (26117506 and 16H01331), Japan, and was partially supported by the National Institutes of Health grant P50 NS072187.

Paper previously presented in the form of poster at: Keystone Symposia, June 14, 2016; Keystone, Colorado.

Please address correspondence to Takeshi Ikeuchi, MD, PhD, Department of Molecular Genetics, Brain Research Institute, Niigata University, 1-757 Asahimachi, Niigata, 951-8585, Japan; e-mail: ikeuchi@bri.niigata-u.ac.jp

Indicates open access to non-subscribers at www.ajnr.org

Indicates article with supplemental on-line photos.

<http://dx.doi.org/10.3174/ajnr.A4938>

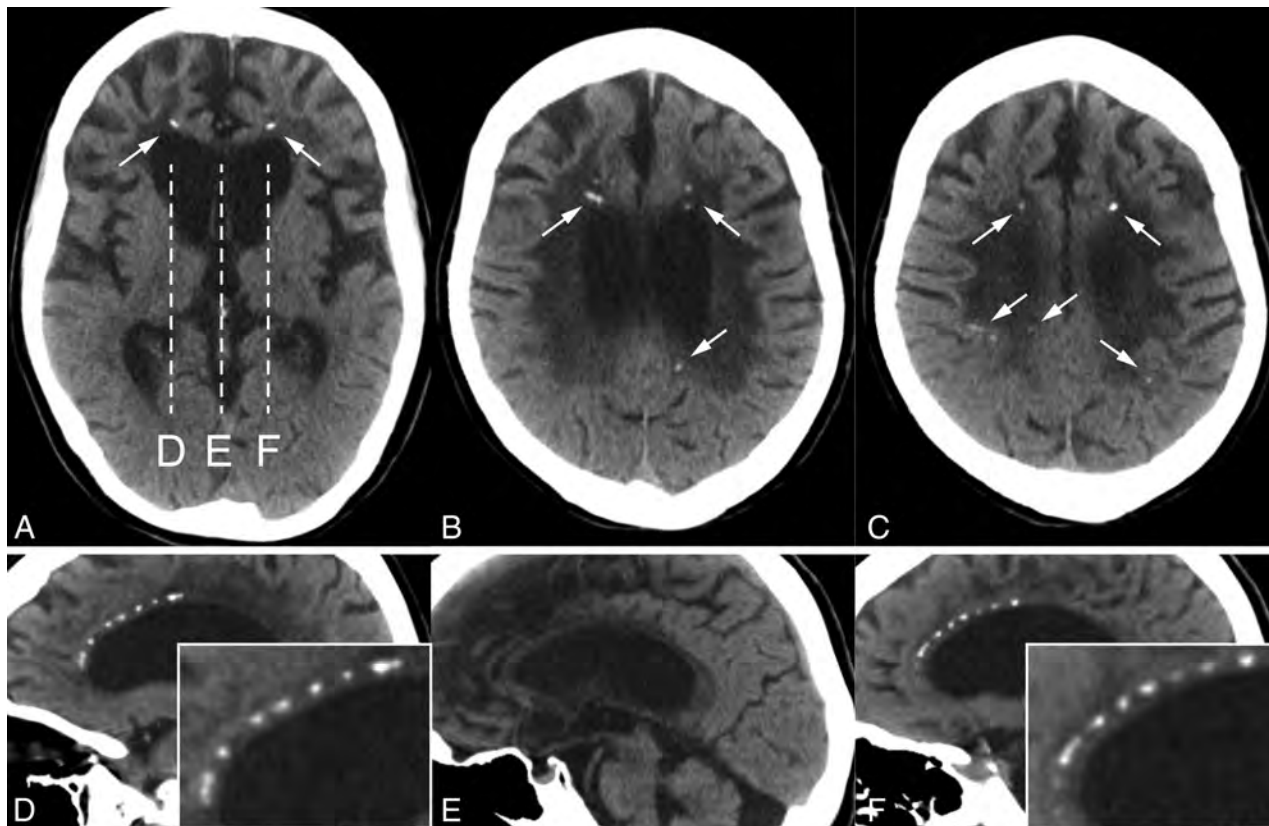


FIG 1. A–C, Case 1. Small bilateral calcifications in the frontal and parietal subcortical white matter on axial CT images (arrows). D–F, Sagittal CT images corresponding to the *dashes* in A show pericallosal calcifications. Note that these calcifications symmetrically aligned with the upper edges of the lateral ventricles have a stepping stone appearance (enlarged images are inserted); no calcifications are seen in the midline (E).

nantly in the frontal and parietal regions, a thinning of the corpus callosum accompanied by abnormal signal intensity, lesions in the pyramidal tracts, and foci of restricted diffusion on DWI, which persists at least for months.^{5,9–11} Patients can also show disproportionately large lateral ventricles for their age and cortical atrophy as the disease progresses. These findings are commonly seen in patients with ALSP but are not specific. Furthermore, calcifications in the white matter can be detected in some patients with ALSP by CT.^{5,12} However, the clinical significance and pathogenesis of the calcifications remain unclear. Here we describe 9 cases of ALSP with a characteristic distribution of white matter calcifications on head CT. These calcifications allow correct and timely diagnosis of ALSP.

CASE SERIES

Clinical Presentations and Brain CT Findings

Due to the retrospective nature of the study, the acquisition criteria for the CT scans were variable. The sagittal and coronal images were reconstructed with MPR methods.

Case 1

A 37-year-old woman noticed that the slipper on her right foot came off while walking. She developed difficulties with writing and speaking, motor aphasia, general spasticity, gait disturbances, and increasing micturition frequency. She was diagnosed with MS and treated with steroid therapy and interferon β -1b without any benefit. The disease progressed rapidly. Cognitive impair-

ment, tremor, and right-sided hemiconvulsion appeared; she required a gastrostomy due to severe dysphagia. She was bedridden at 41 years of age. Her family history was not notable.

A brain CT scan showed punctate calcifications in the frontal and parietal subcortical white matter bilaterally (Fig 1A–C). On sagittal images, these calcifications had a symmetric “stepping stone appearance” in the frontal pericallosal regions (Fig 1D–F).

Case 2

A 30-year-old woman initially presented with gait disturbances followed by cognitive impairment and personality changes, which rapidly progressed. A year later, she had severe dementia. She was found to have total aphasia, indifference, abnormal eating behavior, hyperreflexia, and ataxic gait. A demyelinating disorder was suspected; steroid therapy resulted in no benefit. None of her family members had any similar symptoms.

A CT scan showed brain calcifications predominantly in the bilateral parietal subcortical white matter (Fig 2A–C). Some of them appeared to be located in the cortex on axial images; however, they could definitely be seen in the white matter on coronal images (Fig 2D). She also had very small bilateral calcifications in the frontal white matter.

Cases 3 and 4

A 27-year-old woman had difficulty releasing items she was holding in her left hand. Subsequently, she developed gait dis-

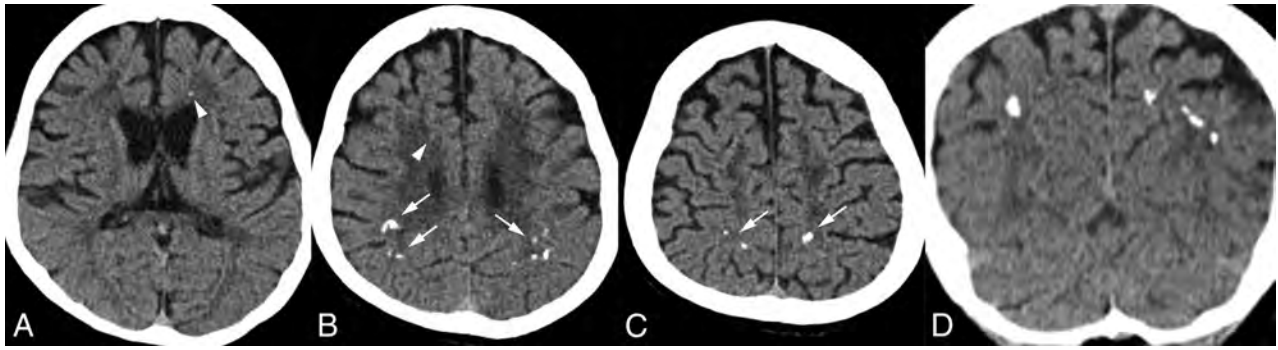


FIG 2. A–C, Case 2. Bilateral, scattered calcifications in the parietal subcortical white matter on axial CT images (arrows in B and C). There are also very tiny calcifications in the bilateral frontal white matter (arrowheads in A and B). D, Coronal CT imaging reveals that the parietal calcifications are located in the subcortical white matter, not in the cortex.

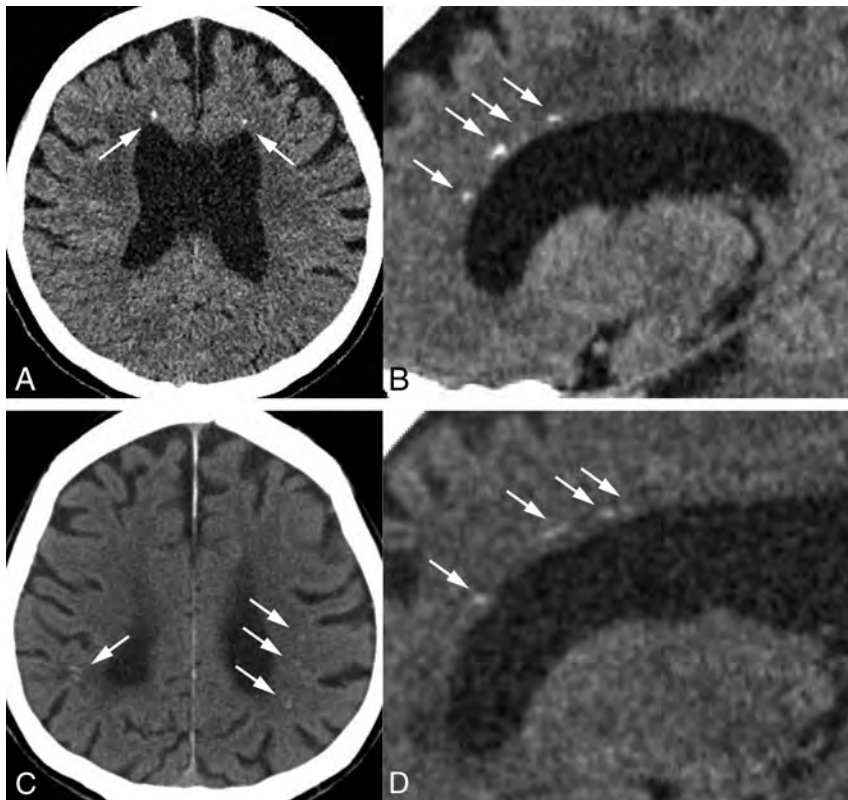


FIG 3. A, Case 3. Small bilateral calcifications in the frontal white matter adjacent to the anterior horns of the lateral ventricles on an axial CT image (arrows). B, Sagittal view represents the symmetric and characteristic stepping stone appearance (arrows). C, Case 4. Small bilateral calcifications in the parietal subcortical white matter on an axial CT image (arrows), but there are no calcifications in the frontal area. D, Sagittal CT image displays subtle calcifications in the anterior pericallosal region bilaterally (arrows).

turbances, tremor, micrographia, postural instability, urge incontinence, and constipation. She was euphoric and had frontal lobe dysfunction. She also had apraxia, left alien hand syndrome, forced grasping, and spastic gait by 28 years of age. She was treated with steroid therapy, which did not benefit her condition.

Her father (case 4) insidiously developed cognitive impairment and personality changes around 58 years of age. He became irritable and could not do simple calculations or 2 different tasks at the same time. He did not think that his daughter's condition was serious. He mainly had cognitive and frontal lobe dysfunctions.

He did not have any parkinsonian symptoms, but he did have truncal imbalance and hyperreflexia in his lower limbs.

A brain CT scan of case 3 showed bilateral punctate calcifications in the frontal white matter adjacent to the anterior horns of the lateral ventricles (Fig 3A). On sagittal CT images, these calcifications had a characteristic symmetric stepping stone appearance (Fig 3B). The brain CT scan of case 4 displayed small bilateral calcifications in the parietal subcortical white matter, but we could not see any frontal calcifications on 4-mm-thick axial images (Fig 3C). However, on the 1-mm-thick sagittal images, we observed the characteristic stepping stone appearance of calcifications on the anterior part of pericallosal regions (Fig 3D).

Case 5

The clinical and MR imaging findings of case 5 have already been reported.^{3,10} In brief, this woman exhibited cognitive decline, psychiatric symptoms, apraxia, and spastic-ataxic gait impairment when she was 24 years of age. She was born prematurely but had essentially normal development until disease onset. She had no family history of neurodegenerative disease.

Several calcified lesions were detected in the frontal and parietal white matter on a CT scan obtained 1 month after birth (Fig 4A–C). Toxoplasmosis, Other agents, Rubella (also known as German measles), Cytomegalovirus, and Herpes simplex (TORCH) syndrome had been suspected at that time, but she had not been definitively diagnosed. The calcifications remained visible when she was 24 years of age (Fig 4D–H). Most interesting, some of them, especially the ones in the frontal white matter, seemed to have decreased in size. The calcifications were symmetric and had the characteristic stepping stone appearance on sagittal imaging (Fig 4G, -H).

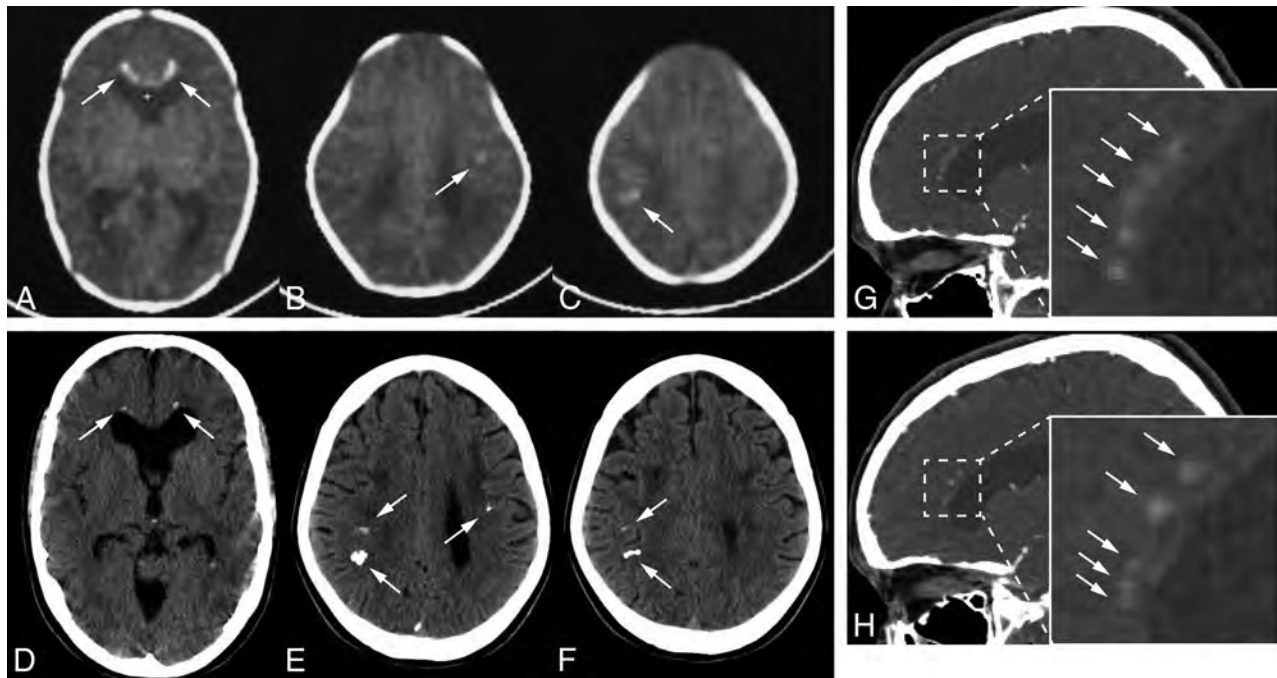


FIG 4. A–C, Case 5. Axial CT images at 1 month after birth show bilateral frontal and parietal calcifications (arrows). D–F, These calcifications still exist when the patient is 24 years of age, but they are somewhat smaller, especially those in the frontal regions (arrows). The white cursor inside the anterior horn is included (A) because this is a captured image. G and H, Sagittal views show symmetric frontal pericallosal calcifications in the characteristic stepping stone appearance (arrows; enlarged images in the inserts: G is the right hemisphere, and H is the left hemisphere).

Case 6

This case has been included in previous reports.^{3,6,9} The female patient exhibited cognitive impairment and depression from 18 years of age. Subsequently, parkinsonian signs such as hypomimia, bradykinesia, and rigidity developed. Her symptoms gradually worsened. Her mother, who died at the 30 years of age, had similar symptoms and seizures. The mother was diagnosed as having ALSP by postmortem examination.

Small calcifications were observed bilaterally in the frontal white matter on CT (On-line Fig 1A, -B). The stepping stone appearance was seen on the sagittal view (On-line Fig 1C, -D).

Cases 7 and 8

Some of the clinical findings of case 7 have been previously reported.^{3,6,12} The male patient's initial symptoms were forgetfulness and difficulty finding words at 58 years of age. His cognitive function deteriorated rapidly. He had depression, apraxia, aphasia, agrapahia, parkinsonian symptoms, hyperreflexia, myoclonus, seizure, and urinary incontinence during his disease course. He died at 62 years of age and was diagnosed as having ALSP by postmortem examination and genetic testing.

It was previously reported that there was no evidence of brain calcifications on either CT scans or pathologic analysis.¹² However, when his brain CT images were reviewed, we identified extremely small calcifications in the bilateral frontal white matter (On-line Fig 2A).

His sister (case 8), whose clinical features have also been previously reported,¹¹ had genetically confirmed ALSP and brain calcifications. Her calcifications were scattered and distributed predominantly in the parietal subcortical white matter, particularly on the right side.¹² There was clear intrafamilial variability of the pattern of calcifications.

Case 9

A 67-year-old man initially presented with balance difficulties and multiple falls at 57 years of age. Cognitive impairment and speech problems began around 63 years of age. On neurologic examination, he showed ideomotor apraxia, vertical gaze limitations, frequent stammer, dysarthria, dysphagia, unusual flexor posturing of his fingers and wrists, reduced arm swing, diffuse rigidity, subtle action tremor in his right upper arm, difficulty in initiating gait, small steps with postural instability, and urinary incontinence. In addition, he had depression with occasional suicidal thoughts. He was clinically suspected of having corticobasal syndrome. He died at 68 years of age. Postmortem findings were comparable with those for ALSP.

The brain CT showed very small bilateral calcifications in the frontal white matter adjacent to the anterior horns (On-line Fig 2B–D). This case only had axial images available, and we could not identify any parietal calcifications on the available 3-mm axial images.

Brain MR Images

Although the degree of lesions was variable for each case, all except 1 case (case 9) showed typical findings consistent with ALSP (Fig 5). The MR images of cases 5 and 6 have been presented previously.^{9,10} Unfortunately, we did not have MR images of case 9. Of note, there was intrafamilial variability between cases 3 and 4. The calcifications in cases 2, 3, and 6 were not apparently recognized by T2* at 5-mm section thickness.

Genetic and Functional Analyses of CSFIR

All genetic studies were conducted with approval by the institutional review board of Niigata University School of Medicine and Mayo Clinic Florida. We identified 3 novel heterozygous muta-

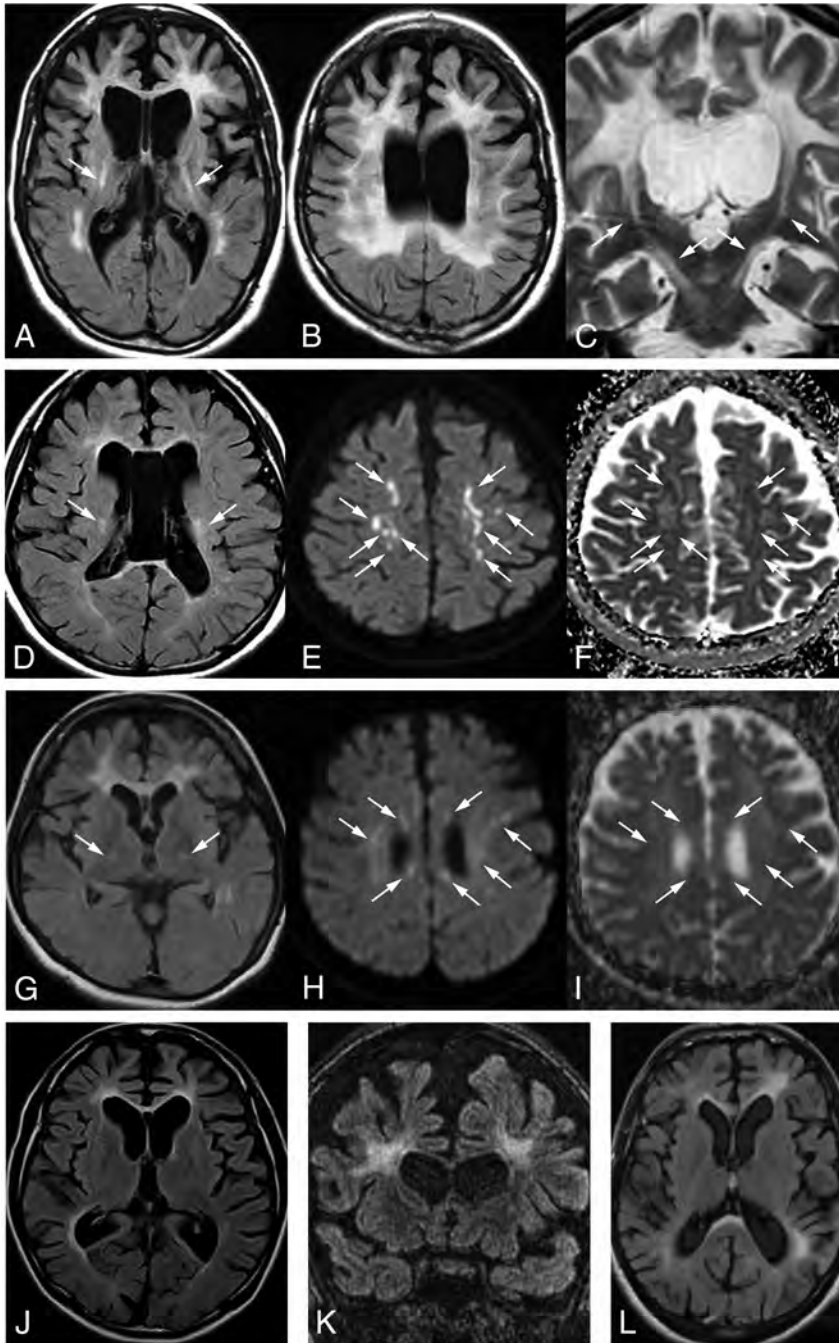


FIG 5. A–C, Case 1. Typical white matter changes involving the corpus callosum and the pyramidal tracts (A and C, *arrows*), dilation of the lateral ventricles and cortical atrophy seen on FLAIR axial (A and B) and T2-weighted coronal imaging (C). D–F, Case 2. Abnormal signaling in the white matter, corpus callosum, and bilateral pyramidal tracts (D, *arrows*) and enlarging of the lateral ventricles on FLAIR (D). Several diffusion-restricted lesions with low ADC values in the white matter on DWI (E, *arrows*) and ADC maps (F, *arrows*). G–I, Case 3. FLAIR image shows frontal-dominant white matter changes bilaterally as well as in the internal capsules (G, *arrows*). The genu of the corpus callosum is also involved. Several diffusion-restricted lesions in the subcortical white matter can be seen around the lateral ventricles on DWI (H, *arrows*). These lesions demonstrate decreased signals on ADC maps (I, *arrows*). J, Case 4. The severity of the white matter changes is less evident than in case 3, the daughter of case 4, on the FLAIR axial image. K, Case 6. Bifrontal white matter lesions, thinning of the corpus callosum, dilation of the lateral ventricles, and cortical atrophy on FLAIR coronal image. L, Case 7. Left-side predominant white matter changes in the frontal and parietal regions and involvement in the corpus callosum on a FLAIR axial image.

tions in 4 cases (Table): 2 missense mutations, p.Gly589Arg (case 1) and p.Ala652Pro (case 2), and 1 splice-site mutation, c.2442+5G>A (cases 3 and 4). The mutations in cases 5, 6, 7, and 8 have already been reported elsewhere, c.2442+5G>C (case 5), p.Met766Thr (case 6), and p.Gly589Glu (cases 7 and 8).³ We could not analyze case 9 because the samples were not available.

We also showed that the novel missense mutant *CSFIRs* were not auto-phosphorylated after treatment with *CSFIR* ligands (colony stimulating factor 1 and interleukin-34) and that abnormal splicing was induced by the novel splice-site mutation by using functional and splicing assays as previously described (On-line Fig 3).⁵ A sub-cloning analysis revealed that these aberrant splice variants were identical to those of a previously reported case carrying a c.2442+1G>T.⁵

DISCUSSION

While most genetic and metabolic brain calcifications are usually observed in the basal ganglia, thalamus, and cerebellum,^{13,14} these regions are not typically affected in ALSP. The calcifications seen in these 9 cases of ALSP were distributed mainly in 2 regions: the frontal white matter adjacent to the anterior horns of the lateral ventricles as described previously⁵ (all cases) and the parietal subcortical white matter (cases 1, 2, 4, 5, and 8). Parietal calcifications were larger than frontal calcifications in some cases (cases 2, 5). The calcifications were usually symmetric, but some level of laterality may exist. The calcifications could often be overlooked because they were extremely small; thus, thin-section CT scans would be preferable for detecting them. Indeed, no calcifications were identified during the initial evaluation of cases 7 and 9. In addition, calcifications were not identified at 4-mm section thickness, but they were visible on 1-mm sections in a previously reported case.⁵ MRI T2* and/or susceptibility-weighted images that are calcium-sensitive can be used as an alternative to CT scans, but T2* imaging apparently failed to detect the calcifications in cases 2, 3, and 6, probably because of the section thickness. Given that relatively young female patients tended to be misdiagnosed

Case series of ALSP with brain calcifications

Case	Sex	CSFIR Mutation	Origin	FH	Age at Onset (yr)	Age at CT (yr)	Section Thickness (mm)	Location of Calcifications		Stepping Stone Appearance on Sagittal CT
								Frontal	Parietal	
1	F	c.1765G>A/p.G589R ^a	Japan	—	37	44	5	+	+	+
2	F	c.1954G>C/p.A652P ^a	Japan	—	30	31	2	+	+	NA
3	F	c.2442+5G>A ^a	Japan	+	27	28	1	+	—	+
4	M	c.2442+5G>A ^a	Japan	+	58	61	4 (1) ^c	+	+	+
5	F	c.2442+5G>C	US	—	23	0, 24	6, 5	+	+	+
6	F	c.2297T>C/p.M766T	US	+	18	30	1.3 (1) ^c	+	—	+
7	M	c.1766G>A/p.G589E	US	+	58	60	3	+	—	NA
8	F	c.1766G>A/p.G589E	US	+	47	52	7	+	+	NA
9	M	Untested ^b	US	—	57	67	3	+	—	NA

Note:—FH indicates family history; NA, not available for sagittal images.

^a Novel mutations.

^b This case was diagnosed by pathologic analysis. We could not conduct genetic testing because of a lack of samples.

^c For axial images, 4 or 1.3 mm and 1 mm for reconstructed sagittal images.

as having demyelinating disorders, such as MS (cases 1–3), brain CT scans could be useful for the differential diagnosis.

The appearance of the frontal calcifications can be clearly demonstrated on the reconstructed sagittal view. They had a stepping stone appearance (Figs 1, 3, 4, and On-line Fig 1). Most interesting, they seemed to line up along a structure running anterior to posterior through the pericallosal region of the brain. While brain calcifications in other diseases often were observed in small vessels,^{15,16} there was no evidence of an association between these calcifications and the vessels in 1 postmortem case.⁵

There was phenotypic variability seen in the families with c.2442+5G>A and p.Gly589Glu mutations. In the family with the c.2442+5G>A mutation, case 3 showed a young-onset spastic gait and fewer cognitive deficits in the early disease course, while her father (case 4) presented with dementia as an initial symptom at 58 years of age. Not only the MR imaging findings (Fig 5) but also the predominant area of calcifications was also different in both cases (Fig 3). However, the degree of aberrant splicing was not apparently different in the 2 cases (On-line Fig 3). In the family with the p.Gly589Glu mutation, case 7 mainly presented with cognitive decline, but pyramidal dysfunction was the most prominent feature in his sister. In addition, her disease began >10 years earlier than his.¹² The distribution of calcifications also differed. These findings suggest that the phenotype might be determined by not only a CSFIR mutation but potentially other genetic, environmental, or biologic factors, such as sex.

The most interesting finding was that case 5 had calcifications present at birth. This case indicated that ALSP should be considered in the differential diagnosis for TORCH syndrome. Furthermore, some of these calcifications seemed to decrease in size as she grew older. Given that the CSFIR is required for microglial differentiation, proliferation, and migration into the brain during embryogenesis,¹⁷ a loss of function of CSFIR due to a CSFIR mutation might induce developmental problems in the microglia. In the fetal brain, microglia are clustered in the frontal crossroads that intersect callosal, associative, and thalamocortical fibers.^{18,19} These microglia organize axonal projections in the prospective white matter.¹⁸ This microglial accumulation spreads along the rostrocaudal axis above the immature anterior horn of the lateral ventricles.^{18,19} Because these embryonic microglial distributions are similar to those of the calcifications presented here, we assume that microglial dysfunction has a causal relationship with the de-

velopment of calcifications. In addition, microglial dysfunction might lead to incomplete white matter integrity. However, the patients who had CSFIR mutations were asymptomatic until they were adults. This finding suggests that the residual wild-type CSFIR should be sufficient for function until adulthood. It also suggests that neurodegeneration of the white matter may insidiously begin and progress, but symptom onset may not occur until the middle of life. Indeed, white matter changes have been observed in elderly asymptomatic mutation carriers.^{20,21} Additionally, the calcifications may diminish while white matter pathology progresses. However, to elucidate the mechanism by which CSFIR mutations cause such unique calcifications, further investigation is still required.

CONCLUSIONS

We demonstrated a characteristic distribution of intracranial calcifications in 9 cases of ALSP. The unique distribution of the calcifications may make it possible to diagnose ALSP correctly.

ACKNOWLEDGMENTS

We thank Ms Kelly Viola, ELS, for her assistance with the technical preparation of this manuscript.

Disclosures: Takuya Konno—OTHER: Received research support from the Japan Society for the Promotion of Science Postdoctoral Fellowships for Research Abroad and is partially supported by a gift from Carl Edward Bolch Jr, and Susan Bass Bolch. B. Mark Keegan—UNRELATED: Grants/Grants Pending: Terumo BCT*; Payment for Development of Educational Presentations: American Academy of Neurology, Consortium of MS Centers meeting, Masatoyo Nishizawa—UNRELATED: Consultancy: Kissei Pharmaceuticals, Comments: an adviser for the development of a new disease-modifying drug for cerebellar ataxia; OTHER: supported by Grants-in-Aid (A) for Scientific Research from Japan Society of Promotion of Science and a grant-in-aid from the Ministry of Health, Labour and Welfare, Japan. Zbigniew K. Wszolek—RELATED: Grant: National Institutes of Health/National Institute of Neurological Disorders and Stroke P50 NS072187; UNRELATED: Grants/Grants Pending: National Institutes of Health/National Institute of Aging (primary) and National Institutes of Health/National Institute of Neurological Disorders and Stroke (secondary) 1U01AG045390-01A1, Mayo Clinic Center for Regenerative Medicine, Mayo Clinic Center for Individualized Medicine, Mayo Clinic Neuroscience Focused Research Team (Cecilia and Dan Carmichael Family Foundation and the James C. and Sarah K. Kennedy Fund for Neurodegenerative Disease Research at Mayo Clinic in Florida), and The Sol Goldman Charitable Trust; Employment: Mayo Clinic Foundation (salary); Patents (planned, pending or issued): Mayo Clinic and I have a financial interest in technologies entitled "Identification of Mutations in PARK8, a Locus for Familial Parkinson's Disease" and "Identification of a Novel LRRK2 Mutation, 6055G>A (G2019S), Linked to Autosomal Dominant Parkinsonism in Families from Several European Populations"; these technologies have been licensed to a commercial entity, and to date, I have received royalties of <\$1500 through Mayo Clinic in accordance

with its royalty-sharing policies.* Takeshi Ikeuchi—RELATED: Grant: grants from the Ministry of Health, Labour and Welfare,* and KAKENHI (26117506 and H16H01331), a grant-in-aid from the Ministry of Health, Labour and Welfare of Japan, and a grant-in-aid from Japan Agency for Medical Research and Development. *Money paid to the institution.

REFERENCES

1. Marotti JD, Tobias S, Fratkin JD, et al. **Adult onset leukodystrophy with neuroaxonal spheroids and pigmented glia: report of a family, historical perspective, and review of the literature.** *Acta Neuropathol* 2004;107:481–88 CrossRef Medline
2. Wider C, Van Gerpen JA, DeArmond S, et al. **Leukoencephalopathy with spheroids (HDLS) and pigmentary leukodystrophy (POLD): a single entity?** *Neurology* 2009;72:1953–59 CrossRef Medline
3. Rademakers R, Baker M, Nicholson AM, et al. **Mutations in the colony stimulating factor 1 receptor (CSF1R) gene cause hereditary diffuse leukoencephalopathy with spheroids.** *Nat Genet* 2012;44:200–05 CrossRef Medline
4. Nicholson AM, Baker MC, Finch NA, et al. **CSF1R mutations link POLD and HDLS as a single disease entity.** *Neurology* 2013;80:1033–40 CrossRef Medline
5. Konno T, Tada M, Tada M, et al. **Haploinsufficiency of CSF-1R and clinicopathologic characterization in patients with HDLS.** *Neurology* 2014;82:139–48 CrossRef Medline
6. Sundal C, Fujioka S, Van Gerpen JA, et al. **Parkinsonian features in hereditary diffuse leukoencephalopathy with spheroids (HDLS) and CSF1R mutations.** *Parkinsonism Relat Disord* 2013;19:869–77 CrossRef Medline
7. Saitoh BY, Yamasaki R, Hayashi S, et al. **A case of hereditary diffuse leukoencephalopathy with axonal spheroids caused by a de novo mutation in CSF1R masquerading as primary progressive multiple sclerosis.** *Mult Scler* 2013;19:1367–70 CrossRef Medline
8. Granberg T, Hashim F, Andersen O, et al. **Hereditary diffuse leukoencephalopathy with spheroids: a volumetric and radiological comparison with multiple sclerosis patients and healthy controls.** *Eur J Neurol* 2016;23:817–22 CrossRef Medline
9. Sundal C, Van Gerpen JA, Nicholson AM, et al. **MRI characteristics and scoring in HDLS due to CSF1R gene mutations.** *Neurology* 2012;79:566–74 CrossRef Medline
10. Mateen FJ, Keegan BM, Krecke K, et al. **Sporadic leucodystrophy with neuroaxonal spheroids: persistence of DWI changes and neurocognitive profiles: a case study.** *J Neurol Neurosurg Psychiatry* 2010;81:619–22 CrossRef Medline
11. Bender B, Klose U, Lindig T, et al. **Imaging features in conventional MRI, spectroscopy and diffusion weighted images of hereditary diffuse leukoencephalopathy with axonal spheroids (HDLS).** *J Neurol* 2014;261:2351–59 CrossRef Medline
12. Fujioka S, Broderick DF, Sundal C, et al. **An adult-onset leukoencephalopathy with axonal spheroids and pigmented glia accompanied by brain calcifications: a case report and a literature review of brain calcifications disorders.** *J Neurol* 2013;260:2665–68 CrossRef Medline
13. Klünemann HH, Ridha BH, Magy L, et al. **The genetic causes of basal ganglia calcification, dementia, and bone cysts: DAP12 and TREM2.** *Neurology* 2005;64:1502–07 CrossRef Medline
14. Baba Y, Broderick DF, Uitti RJ, et al. **Heredofamilial brain calcinosis syndrome.** *Mayo Clin Proc* 2005;80:641–51 CrossRef Medline
15. Linnankivi T, Valanne L, Paetau A, et al. **Cerebroretinal microangiopathy with calcifications and cysts.** *Neurology* 2006;67:1437–43 CrossRef Medline
16. Miklossy J, Mackenzie IR, Dorovini-Zis K, et al. **Severe vascular disturbance in a case of familial brain calcinosis.** *Acta Neuropathol* 2005;109:643–53 CrossRef Medline
17. Saijo K, Glass CK. **Microglial cell origin and phenotypes in health and disease.** *Nat Rev Immunol* 2011;11:775–87 CrossRef Medline
18. Judas M, Rados M, Jovanov-Milosevic N, et al. **Structural, immunocytochemical, and MR imaging properties of periventricular crossroads of growing cortical pathways in preterm infants.** *AJNR Am J Neuroradiol* 2005;26:2671–84 Medline
19. Monier A, Adle-Biassette H, Delezoide AL, et al. **Entry and distribution of microglial cells in human embryonic and fetal cerebral cortex.** *J Neuropathol Exp Neurol* 2007;66:372–82 CrossRef Medline
20. Karle KN, Biskup S, Schüle R, et al. **De novo mutations in hereditary diffuse leukoencephalopathy with axonal spheroids (HDLS).** *Neurology* 2013;81:2039–44 CrossRef Medline
21. La Piana R, Webber A, Guiot MC, et al. **A novel mutation in the CSF1R gene causes a variable leukoencephalopathy with spheroids.** *Neurogenetics* 2014;15:289–94 CrossRef Medline

Endovascular Therapy of M2 Occlusion in IMS III: Role of M2 Segment Definition and Location on Clinical and Revascularization Outcomes

T.A. Tomsick, J. Carrozzella, L. Foster, M.D. Hill, R. von Kummer, M. Goyal, A.M. Demchuk, P. Khatri, Y. Palesch, J.P. Broderick, S.D. Yeatts, and D.S. Liebeskind, for the IMS III Investigators



ABSTRACT

BACKGROUND AND PURPOSE: Uncertainty persists regarding the safety and efficacy of endovascular therapy of M2 occlusions following IV tPA. We reviewed the impact of revascularization on clinical outcomes in 83 patients with M2 occlusions in the Interventional Management of Stroke III trial according to specific M1-M2 segment anatomic features.

MATERIALS AND METHODS: Perfusion of any M2 branch distinguished M2-versus-M1 occlusion. Prespecified modified TIC1 and arterial occlusive lesion revascularization and clinical mRS 0–2 end points at 90 days for endovascular therapy–treated M2 occlusions were analyzed. Post hoc analyses of the relationship of outcomes to multiple baseline angiographic M2 and M1 subgroup characteristics were performed.

RESULTS: Of 83 participants with M2 occlusion who underwent endovascular therapy, 41.0% achieved mRS 0–2 at 90 days, including 46.6% with modified TIC1 2–3 reperfusion compared with 26.1% with modified TIC1 0–1 reperfusion (risk difference, 20.6%; 95% CI, –1.4%–42.5%). mRS 0–2 outcome was associated with reperfusion for M2 trunk ($n = 9$) or M2 division ($n = 42$) occlusions, but not for M2 branch occlusions ($n = 28$). Of participants with trunk and division occlusions, 63.2% with modified TIC1 2a and 42.9% with modified TIC1 2b reperfusion achieved mRS 0–2 outcomes; mRS 0–2 outcomes for M2 trunk occlusions (33%) did not differ from distal (38.2%) and proximal (26.9%) M1 occlusions.

CONCLUSIONS: mRS 0–2 at 90 days was dependent on reperfusion for M2 trunk but not for M2 branch occlusions. For M2 division occlusions, good outcome with modified TIC1 2b reperfusion did not differ from that in modified TIC1 2a. M2 segment definition and occlusion location may contribute to differences in revascularization and good outcome between Interventional Management of Stroke III and other endovascular therapy studies.

ABBREVIATIONS: ATA = anterior temporal artery; EVT = endovascular therapy; IMS = Interventional Management of Stroke; MID = distal M1; MIP = proximal M1; mTIC1 = modified TIC1

Recent analysis of M2 occlusions treated by IV tPA and endovascular therapy (EVT) in the Interventional Management of Stroke (IMS) I and II trials and by EVT in the Prolyse in Acute Cerebral Thromboembolism (PROACT) II study failed to dem-

onstrate an association between reperfusion and good outcome.^{1–4} Other recent publications are more optimistic regarding outcome with EVT for M2 occlusion.^{5–7} Uncertainty arises regarding not only patient selection and the utility of EVT for M2 occlusions identified on digital subtraction angiography (DSA-M2),^{8,9} but also of the M1-M2 occlusion designation. More recent trials with positive EVT outcomes included very few DSA-M2 occlusions, and some specifically excluded them.^{10–12}

We herein summarize the efficacy and safety outcomes of combined IV-EVT in DSA-M2 occlusions in the Interventional Management of Stroke III trial as originally reported,¹³ and we also report post hoc subgroup analyses that explored the hypoth-

Received June 17, 2016; accepted after revision August 1.

From the Department of Radiology (T.A.T., J.C.), University of Cincinnati Academic Health Center, University Hospital, Cincinnati, Ohio; Department of Biostatistics, Bioinformatics, and Epidemiology (L.F., Y.P., S.D.Y.), Medical University of South Carolina, Charleston, South Carolina; Calgary Stroke Program (M.D.H., A.M.D.), Department of Clinical Neurosciences, Medicine, Community Health Sciences, Hotchkiss Brain Institute, University of Calgary, Foothills Hospital, Calgary, Alberta, Canada; Department of Neuroradiology (R.v.K.), Dresden University Stroke Center, Universitätsklinikum Carl Gustav Carus an der Technischen Universität Dresden, Dresden, Germany; Department of Radiology and Clinical Neurosciences (M.G.), University of Calgary, Calgary, Alberta, Canada; Department of Neurology (P.K., J.P.B.), University of Cincinnati Academic Health Center, Cincinnati, Ohio; and University of California Los Angeles Stroke Center (D.S.L.), Los Angeles, California.

The work was supported by grants from the National Institutes of Health and the National Institute of Neurological Disorders and Stroke (UC U01NS052220, MUSC U01NS054630 and U01NS077304) and by Genentech, EKOS, Concentric Medical, Cordis Neurovascular, and Boehringer Ingelheim.

Please address correspondence to Thomas A. Tomsick, MD, University of Cincinnati, UC Health, Department of Radiology, 231 Albert Sabin Way, Cincinnati, OH 45267-0762; e-mail: Thomas.Tomsick@UCHealth.com

Indicates open access to non-subscribers at www.ajnr.org

Indicates article with supplemental on-line tables.

<http://dx.doi.org/10.3174/ajnr.A4979>



FIG 1. A, Right M1 trunk gives rise to the ATA with the posterior temporal branch filling on microcatheter injection. B, Lateral view baseline common carotid arteriogram confirms mid- and posterior temporal lobe cortical supply from the patent posterior temporal artery.

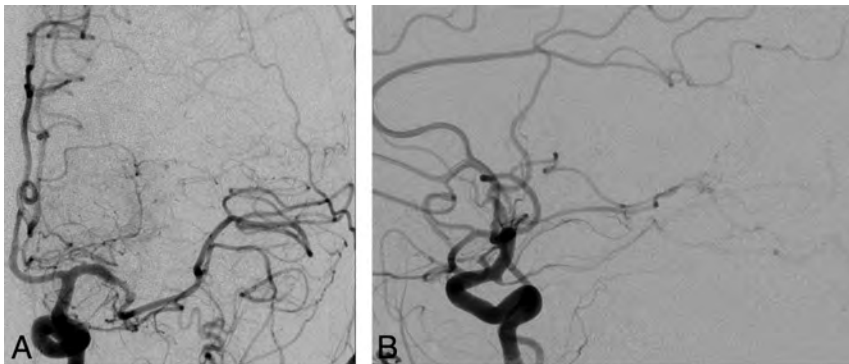


FIG 2. A, Anteroposterior: short M1 trunk with no ATA arising is shown. An isolated M2 holotemporal branch originates, simulating and giving origin to the ATA. It then exits the insular cistern, with multiple middle and posterior temporal arteries draping over and supplying the remainder of the temporal lobe (B). B, Lateral view common carotid arteriogram confirms filling of the holotemporal branch, with no other MCA branches filling.

esis that anatomic heterogeneity, operational definitions, and the affected M2 segment location have an effect on outcome in the reperfusion of M2 occlusion.

MATERIALS AND METHODS

IMS III eligibility and exclusion criteria, randomization and statistical methods, and results have been previously reported.¹³⁻¹⁵ CT angiography, CT perfusion, and MR angiography and/or perfusion were allowed in centers where they were established as a local standard of evaluation and care.

The IMS III primary outcome measure was a modified Rankin Scale score of 0–2 at 90 days. Secondary efficacy end points were angiographic reperfusion defined as modified Thrombolysis in Cerebral Infarction (mTICI) 2–3 (minimum arteriographic reperfusion <50% of the occluded territory at risk) and mTICI 2b–3 ($\geq 50\%$ reperfusion), and recanalization defined as an arterial occlusive lesion recanalization score of 2–3 (partial or complete recanalization with flow). In addition to standard microcatheter thrombolysis, 4 thrombectomy methods were allowed for EVT of M2 occlusions.¹⁶⁻¹⁹

DSA was reviewed by the angiographic core lab (T.A.T., D.S.L.), and M2 segment and revascularization scores were determined by consensus. mRS 0–2 outcomes were analyzed according to mTICI reperfusion results. The relationship of reperfusion to mRS 0–2 and 0–1 outcomes was determined. As in the Emergency Management of Stroke and IMS I and II trials, the opera-

tional definition of M1 occlusion was that 100% of the MCA cortical distribution was at risk, less anterior temporal artery (ATA) supply, with no antegrade M2 branch filling.²⁰⁻²² The corollary of this physiologic definition of M1 occlusion is that filling of ≥ 1 classic M2 branch then represents M2 occlusion.

Baseline clinical characteristics of 83 evaluable M2 and 135 M1 occlusions proximal (M1P) or distal (M1D) to the lenticulostriate origins were excerpted from case report forms and compared for differences.

Multiple secondary observations of M1 and M2 anatomic features were derived post hoc from baseline and/or posttreatment DSA and recorded, to identify similarities or differences that might discriminate revascularization and clinical outcome.

An isolated branch arising from M1, adjacent to and with a similar course to the ATA but larger and distributing to the mid- and posterior temporal lobe supply, was termed a “posterior temporal M2 branch” (Fig 1). An isolated branch arising from M1 simulating the ATA but giving origin to the ATA and the mid- and posterior temporal lobes

was termed a “holotemporal” M2 branch (Fig 2). The isolated holotemporal or posterior temporal branch might also variously supply portions of the inferior parietal lobe or temporo-occipital region via distal M3 and M4 cortical arteries. The single vessel continuation of M1 beyond the isolated patent posterior temporal or holotemporal branches is termed the “M2 trunk,” which simulates the distal M1 trunk (Fig 3).

A functional IMS M1-M2 anatomic classification, based on pretreatment and posttreatment angiographic findings and relevant clinical correlates, is detailed in On-line Table 1. Occlusion proximal to the lenticulostriate arteries was termed a “proximal M1 occlusion,” and occlusion beyond the lenticulostriate arteries, “a distal M1 occlusion.” M2 segment occlusions were categorized as trunk, division, division-branch, and/or branch occlusion. M2 trunk occlusion was occlusion of the single large segment beyond the posterior temporal or holotemporal branch (Fig 3). Occlusion of an M2 segment giving rise to ≥ 2 classic M2 branches was termed “M2 division occlusion.” Occlusion of M2 branches arising from divisions was termed “division-branch occlusion.” Occlusion of isolated, individual, classic M2 branches arising from the distal M1 (eg, orbitofrontal, operculofrontal, central or Rolondic, angular, parietal, or posterior temporal branches) was termed “M2 branch occlusion.”

Post hoc secondary subgroup analyses in 79 evaluable cases,

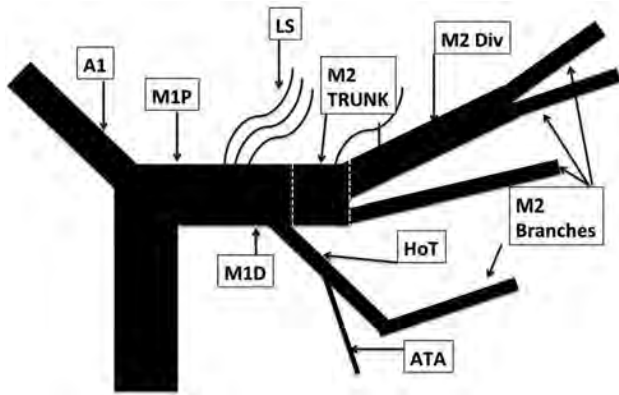


FIG 3. Composite diagram of M1-M2 trunk anatomy based on IMS III post hoc analysis. The M1 trunk proximal to the lenticulostriate arteries (LS) is termed "M1P." The anterior temporal artery arises from the holotemporal M2 branch (HoT). The M2 trunk is a continuation of the distal M1 trunk, beyond a holotemporal (HoT) or posterior temporal M2 branch. The M2 trunk divides into M2 divisions (M2 Div) or branches. M2 divisions divide further into M2 branches.

including review of revascularization and clinical outcome, were also performed, including analysis of the following: 1) occluded segment description (trunk, division, division-branch, branch); 2) estimated percentage MCA distribution of the region at risk according to the occluded segment anatomy; 3) M2 occlusion location (proximal, mid, or distal) and number (single or multiple) on revascularization and outcome; and 4) the presence of isolated holotemporal and posterior temporal lobe branch supply and M2 trunk occlusion on day-2 CTP core infarct and penumbra volumes.

Primary safety end points recorded were mortality and symptomatic intracranial hemorrhage, defined as any intracranial hemorrhage associated with neurologic deterioration within the first 30 hours of IV tPA initiation. Secondary end points included parenchymal hematoma types 1 and 2; asymptomatic intracranial hemorrhage; subarachnoid hemorrhage or intraventricular hemorrhage; angiographically identified vessel dissection or perforation; and DSA-identified emboli into a new (previously unoccluded) arterial territory.

Twenty-six M2 and 45 M1 occlusions from IMS I and II were reviewed post hoc for confirmation of reporting reproducibility and the effect of anatomic characteristics on outcome compared with IMS III.

Differences in reperfusion and mRS 0–2 outcomes between M2 occlusion subgroups were analyzed with the χ^2 test, and differences in percentage MCA distribution at risk between subgroups, via the *t* test.

RESULTS

Complete patient accountability, clinical, revascularization, and safety results have been previously reported for the entire EVT and IV rtPA groups.^{13,20} No differences in baseline clinical characteristics of 83 subjects with M2 occlusion and 135 previously reported M1 occlusions treated with EVT were identified (On-line Table 2). ASPECTS of 8–10 was significantly lower with M1

occlusion proximal to the striate arteries ($P = .02$). The proportion of subjects with a baseline NIHSS score of ≥ 20 was not.

Overall, 34/83 (41%) mRS 0–2 outcomes occurred with M2 EVT. Reperfusion trended ($P = .09$) toward an association with good outcome (46.7% mRS 0–2 for mTICI 2–3 compared with 26.1% for mTICI 0–1; risk difference, 20.6%; 95% CI -1.4% – 42.5%). M2 occlusions were treated predominantly by standard microcatheter thrombolysis ($n = 54$, 65.1%), with 5 sonography-assisted thrombolysis, 13 Merci retriever (Concentric Medical, Mountain View, California), 10 Penumbra System (Penumbra, Alameda, California), and 1 Solitaire Stent (Covidien, Irvine, California) thrombectomy procedures. mTICI 2–3 reperfusion was achieved in 66% (39/59) of thrombolysis-only treatments and in 88% (21/24) of thrombectomy-device procedures ($P = .048$).

The Table summarizes M2-segment-occlusion mRS 0–2 outcomes according to mTICI reperfusion results for not only each mTICI grade but also grouped as mTICI 0–1 versus 2–3 and as 0–2a versus 2b–3. Good outcome for trunk occlusion required mTICI 2b–3 reperfusion. No mRS 0–2 outcome differences were identified for mTICI 2a-versus-2b reperfusion for division occlusion. M2 branch occlusions achieved numerically poorer mTICI 2b–3 reperfusion (28.6%) and mRS 0–2 outcomes overall (32.1%) compared with trunk and division occlusions.

On post hoc review of M2 occlusions, ATAs were identified arising from 42 (53.2%) M1 and 34 (43.0%) M2 vessels in 79 evaluable subjects, either before or after revascularization. Eighteen (22.8%) holotemporal ($n = 10$) and posterior temporal ($n = 8$) branches arising from M1 and simulating the ATA were identified on baseline DSA, half with other patent M2 segments. Seven holotemporal and 2 posterior temporal branches were the only M2 branches patent, defining M2 trunk occlusion and closely simulating M1 trunk occlusion in appearance. Lenticulostriate arteries arose from 16 (20.3%) M2 segments overall, but in association with 5 (50%) patent holotemporal arteries and 3 (33.3%) M2 trunk occlusions.

On the basis of these anatomic features and the IMS III definitions, the core lab estimated that 30.4% of M2 occlusions could have been termed M1 occlusion, predominantly where posterior temporal or holotemporal branches simulated the ATA (10/18 versus 14/61, $P = .008$). One instance of patency of an orbito-operculo-frontal division as the only patent segment, without ATA, was classified as an M2 division occlusion, with no ATA or other M2 segments filling from a large trunklike segment.

Post hoc analysis of revascularization and clinical outcomes for trunk, division, division-branch, and branch occlusions and for proximal and distal M1 occlusion is detailed in On-line Table 3. mRS outcome 0–2 for M2 occlusion was similar to that for M1D, despite numerically lower mTICI 2–3 and 2b–3 reperfusion. M2-plus-M1D occlusions combined had a higher proportion of mRS 0–1 and 0–2 outcomes compared with proximal M1 occlusion ($P = .06$ and 0.07 , respectively). Good outcome for M2 trunk occlusion (33.3%) was numerically greater than for M1P occlusion (26.9%, $P > .05$), but not for M1D (38.2%, $P > .05$).

M2 trunk occlusions were associated with a greater percentage area distribution at risk for infarction compared with division and branch occlusions combined ($P = .0012$), as were division occlusions compared with branch occlusions ($P < .0001$). No differ-

mRS 0–2 outcomes for 79 evaluable M2 trunk, division, and branch occlusion grouped according to mTICI 0–1, 2a, 2b–3 reperfusion grade^a

mTICI Grade	M2 Trunk (n = 9)		M2 Division (n = 42)		M2 Branch (n = 28)	
	N	% mRS 0–2	N	% mRS 0–2	N	% mRS 0–2
0–1	2	0	6	0	11	36.4
2a	1	0	18	66.7	9	22.2
2b–3	6 ^b	50	18 ^b	44.4	8	37.5

^a This table uses only the evaluable sample.

^b mTICI 3: n = 1.

ence in MCA distribution at risk was estimated between 16 division-branch and 12 branch occlusions, but excellent and good outcomes were numerically fewer for division-branch occlusions.

Fifty-four of 79 (69.1%) DSA-M2 occlusions were proximal, with greater estimated percentage MCA distribution at risk compared with mid- or distal occlusions ($P = .0001$). Ten (12.7%) multiple M2 occlusions included 6 divisions with additional branch occlusions and 4 multiple branch occlusions. The estimated percentage MCA at risk was greater for multiple M2 occlusions than for single ones ($P = .05$).

Post hoc review of anatomic features of 27 M2 and 45 M1 previously treated IMS I and II occlusions confirmed classification consistency with IMS III, including patent holotemporal branches in 3 M2 trunk occlusions (11.1%). Fifty percent of division-branch or branch occlusions were confirmed in IMS I and II, compared with 37.1%, in IMS III. In the 3 IMS studies, 5/12 (41.6%) M2 trunk occlusions achieved mRS 0–2 outcomes.

Symptomatic intracranial hemorrhage occurred in 7.2% (6/83) of subjects with IMS III M2 occlusions. One (1.2%) arterial perforation and 3 (3.6%) emboli into a new (previously unoccluded) arterial territory were identified by the core lab. Ten deaths (12.0%) occurred.

DISCUSSION

In IMS III, as in IMS I and II, among DSA-defined M2 occlusions, independent functional outcome (mRS 0–2) was not associated with mTICI 2b–3 reperfusion compared with EVT of the more proximal intracranial ICA or M1 occlusions.²⁰ No good outcomes for trunk occlusion occurred in the absence of mTICI 2b–3 reperfusion. No differences in good outcome were identified for mTICI 2a-versus-2b reperfusion for division occlusion. Good outcome was not associated with reperfusion in branch occlusions; this finding may be due to the small sample size ($n = 29$), limited amount of at-risk tissue, or recanalization spontaneously or by IV rtPA alone after completion of EVT. While IMS III M2 mTICI 2–3 reperfusion was better than that in IMS I and II (72.3% versus 60.9%), mRS 0–2 outcomes were poorer (40.9% versus 69.6%).^{1,4,9} Good outcomes for M2 occlusion with mTICI 0–1 reperfusion were more frequent in IMS I and II (26.1% versus 77.7%), all occurring with branch occlusions.

In addition to differences in M2 segment occlusion types treated, differences in the definition of M1 and M2 occlusion may contribute to reported outcome differences.^{23,24} A similar ratio of M2-to-M1 occlusion in IMS I and II (64.4%) and IMS III (60.7%) suggests comparable general definition application. Whereas PROACT II had a similar percentage ratio (62.2%), the ratio was lower (40.7%) in the Middle Cerebral Artery Embolism Local Fibrinolytic Intervention Trial (MELT).²⁵ The definition of M1 versus M2 has historically been based on anatomic criteria, with the hori-

zontal sphenoidal MCA segment in the stem of the Sylvian fissure, proximal to the insula, termed M1, irrespective of the at-risk proportion of the brain supplied by the occluded segment.²⁶ The IMS operational functional definition of M1 occlusion places virtually its entire cortical distribution at risk and allows confident comparability of baseline occlusion and

outcome data among the IMS studies.

The classic clinicoanatomic model of 2 M2 divisions (superior/anterior or inferior/posterior) occurs in approximately 50% of instances of M1 trunk branching, pseudo-bifurcations, and -trifurcations, each in approximately 25% of patients.^{27,28} The description of postdivision branching has not been uniform historically. Where M2 “division” occlusion therapy in PROACT II included treatment of not only divisions that will branch but also branches from divisions and individual branches, potential confusion in terminology exists. Standard arteriographic references avoid “division” entirely, refer to groups or complexes, mix “branch” and “artery” somewhat interchangeably, and have used the term “trunk” to vaguely describe a large Sylvian segment beyond an operculofrontal branch terminating in parietal and angular branches.²⁹ Muddled terminology risks including, lumping, equating, and then comparing occluded classic M2 division occlusions (53.1%) with smaller, single, even distal M2 division-branch (19.8%) or branch occlusions (16.0%) or major trunks beyond a single patent, classic M2 branch (11.1%) in stroke-treatment studies.

Two nomenclature adaptations are used here for post hoc description and analysis of observations initially made on primary core lab reporting. The holotemporal branch supplying the entire temporal lobe was linked to M2 “trunk” occlusion when no other M2 branches were filling, simulating M1 occlusion. Designation of any M2 branch patency determining the occluded segment is also termed “M2” as either trunk, single or multiple divisions, division-branches, or branches.

If IMS M2 trunk occlusion is attributed to the M1 rather than M2 group, 9.0% good outcome difference between IMS M2 trunk and IMS III M1 occlusion (5/12, 41.6% versus 44/135, 32.6%) would increase reported good outcomes for M1 compared with M2 occlusion. Ascribing an M1 occlusion instead of an M2 trunk occlusion may falsely reduce anticipated brain volume at risk, erroneously increase the expected risk of temporal lobe edema and herniation, and underestimate available collateral flow while overestimating collateral need, thereby predisposing to a higher percentage of good outcome compared with M1 occlusion as defined in IMS. A single branch supplying the entire temporal lobe has been suggested by Gibo et al²⁷ to occur anatomically in 2% but was identified in 10 (13.6%) in our DSA cohort. Alexandrov has identified a prominent ATA acting as a collateral with transcranial Doppler (A. Alexandrov, MD, personal oral communication, International Stroke Conference, February 12, 2014). Menon et al³⁰ identified a patent “prominent anterior temporal artery” on 102 (19.6%) CTAs in patients with M1 occlusion. Survival was better in the presence of its demonstration (18/20, 90%) than in its absence (66/82, 80.4%). While the relationship of their demonstration of a prominent ATA to our holotemporal/posterior

temporal branch designation is uncertain, it is reasonable to hypothesize that the assignment of the latter as a marker of the functional M1-M2 junction has some relevance as EVT refines its methods and metrics beyond revascularization alone in exploring differences in outcomes in EVT. Post hoc blinded review of limited CT perfusion studies in IMS III found that mean core and penumbra volumes were numerically lowest in M2 trunk versus M2 division versus M1 trunk occlusions: 4.0 versus 17.2 versus 18.6 mL for core, and 27.8 versus 62.3 versus 85.7 mL for penumbra, respectively.³¹

The percentage MCA at risk was greater with M2 trunk occlusion than in its absence, as was division occlusion with division-branch and branch occlusion. However, the percentage MCA at risk, mTICI 2–3, and mRS 0–1 and 0–2 were lower with branch than division trunk occlusion. This contradiction requires further analysis of baseline CT and CTA imaging findings to determine whether more proximal occlusions may have already futilely recanalized, leaving only residual branch occlusion before DSA.

Limitations exist in these observations and analyses. Data on M2 occlusion here are based on EVT following IV rtPA administration. Results were obtained with thrombectomy technology and thrombolytic methods not commonly used currently. Whereas up to 20% of initially occluded arteries may have recanalized before angiography, clinical outcomes may relate more to the original occlusion than to the arteriographic occlusion.^{20,32} In subjects with M2 occlusion on baseline CTA, no significant difference in patency was identified on 24-hour CTA (88.5% in the EVT arm versus 76.5% in the IV tPA arm), but 90-day mRS 0–2 outcomes were greater with EVT ($n = 31$) than IV tPA alone ($n = 15$) in M2 subjects with no ICA occlusion/stenosis, 51.6% versus 33.4%.³³

Reperfusion results were preliminarily reported here variously as mTICI 2–3 and/or 2b–3 to allow comparison with IMS I and II results of failed reperfusion versus outcome. Neither interobserver agreement in distinguishing 2a versus 2b reperfusion nor mTICI 2b–3 reperfusion as a predictor of good outcome for M2 occlusion had yet been shown. The latter is not confirmed here for division or branch occlusion, and no difference in mRS 0–2 outcome between mTICI 2a versus 2b for division occlusion was identified with reperfusion methods used (Table).

The major limitation of the data and explorative analysis presented here may be perceived in its derivation within the futile IMS IV-EVT treatment paradigm and the treatment methods used. Although thrombectomy devices may be more effective than thrombolysis alone across the M2 group, larger studies with newer devices are indicated for M2 occlusion. Emphasizing terms such as “M2 trunk” and “holotemporal artery” would be irrelevant had not retrospective analyses demonstrated that the unique anatomic features might confer potential relevant differences in brain at risk and/or outcome. Comparisons of small subgroup numbers here, such as the M2 trunk group, are subject to error. Uncommon occlusions beyond the patency of other single segments (such as orbitofrontal or operculofrontal branches) may also be classified as trunk occlusions in the future.

However, the operational IMS occlusion model, excluding M1 occlusion if any M2 branch is filling, reduces the subjectivity of vessel orientation/course, eliminates dilemmas in identifying and classifying major branch points, and becomes one approach to

assuring uniformity in outcome analysis for not only M1 occlusion primarily but also M2 segment occlusion secondarily.

CONCLUSIONS

In IMS III, revascularization rates were higher but mRS 0–2 outcomes were lower for combined IV rtPA–EVT for M2 occlusion than those measured in IMS I and II. mRS 0–2 outcomes differed according to the involved segment, dependent on mTICI 2b reperfusion for trunk occlusion, with no difference between mTICI 2a and 2b reperfusion for division occlusion. mRS 0–2 outcome was not dependent on reperfusion for M2 branch occlusion. Differences in good outcome between the M2 trunk in IMS I, II, and III (41.6%) versus M1 occlusion (32.6%) suggest that failing to distinguish between them could influence reported outcome differences in EVT studies. M2 trunk occlusion, simulating M1 trunk occlusion, is proposed as an M2 occlusion subgroup for closer analysis in EVT studies.

Disclosures: Thomas A. Tomsick—RELATED: Grant: National Institutes of Health*; Support for Travel to Meetings for the Study or Other Purposes: IMS III; UNRELATED: Expert Testimony: medicolegal consultations (no travel). Janice Carrozzella—RELATED: Grant: National Institutes of Health–National Institute of Neurological Disorders and Stroke, Comments: IMS III trial*; Support for Travel to Meetings for the Study or Other Purposes: IMS III; UNRELATED: Employment: Department of Radiology, University of Cincinnati. Lydia Foster—RELATED: Grant: National Institute of Neurological Disorders and Stroke.* Michael D. Hill—RELATED: Grant: National Institute of Neurological Disorders and Stroke grant for the IMS III trial*; UNRELATED: Consultancy: for Merck for an advisory panel for clinical trials; Grants/Grants Pending: Medtronic, Bayer Canada, Boehringer Ingelheim, Comments: grants for clinical trials*; Payment for Lectures including Service on Speakers Bureaus: Boehringer Ingelheim, Bayer Canada, Bristol-Myers Squibb-Pfizer, Comments: honoraria for Continuing Medical Education lectures; Patents (Planned, Pending, or Issued): patent for stroke imaging, Comments: patent pending; Stock/Stock Options: Calgary Scientific Inc, Comments: stock ownership in imaging software company. Mayank Goyal—RELATED: Grant: Medtronic, Comments: part funding for the ESCAPE trial, funding for HERMES collaboration*; Consulting Fee or Honorarium: Medtronic, Stryker, Microvention, Comments: education and advice related to acute stroke treatment and products; UNRELATED: Patents (Planned, Pending, or Issued): GE Healthcare, Comments: licensing agreement for Systems of Stroke Diagnosis. R. von Kummer—RELATED: Support for Travel to Meetings for the Study or Other Purposes: National Institutes of Health; UNRELATED: Consultancy: Lundbeck A/S, Covidien, Synarc Inc, BrainsGate, Boehringer Ingelheim, Comments: Steering Committee for Desmoteplase in Acute Ischemic Stroke 3/4, Data and Safety Monitoring Board for SWIFT PRIME, Adjudication Committee for Desmoteplase in Acute Ischemic Stroke 3/4, Data and Safety Monitoring Board for IMPact, Data and Safety Monitoring Board for ReSPECT ESUS. Andrew M. Demchuk—RELATED: Grant: National Institutes of Health–National Institute of Neurological Disorders and Stroke, Comments: The IMS III trial was funded by National Institutes of Health–National Institute of Neurological Disorders and Stroke. The CT imaging core lab was supported by funds from the National Institutes of Health–National Institute of Neurological Disorders and Stroke*; UNRELATED: Payment for Lectures including Service on Speakers Bureaus: Medtronic, Comments: honoraria for Continuing Medical Education events. Pooja Khatri—RELATED: Grant: National Institutes of Health–National Institute of Neurological Disorders and Stroke U01 for IMS III*; UNRELATED: Consultancy: Grand Rounds Experts, Comments: On-line clinical consultation; Expert Testimony: medicolegal consultations; Royalties: UpToDate, Comments: On-line publication; Other: Genentech, Penumbra, and Biogen, Comments: Genentech pays my salary for my effort as Lead Principal Investigator of the PRISMS trial. Penumbra has paid my salary for my effort as the Lead Neurology Principal Investigator of the THERAPY trial. Biogen has paid my institution and now pays me for effort as a Data and Safety Monitoring Board member.* Yuko Palesch—RELATED: Grant: National Institutes of Health–National Institute of Neurological Disorders and Stroke, Comments: U01 grant support for IMS III*; UNRELATED: Travel/Accommodations/Meeting Expenses Unrelated to Activities Listed: 13th International Symposium on Thrombolysis Thrombectomy and Acute Stroke Therapy, Comments: travel/accommodation expenses to be a speaker; Other: BrainsGate, Comments: statistical member of the Data and Safety Monitoring Board for their clinical trials. Joseph P. Broderick—RELATED: Support for Travel to Meetings for the Study or Other Purposes: Boehringer Ingelheim*; Fees for Participation in Review Activities such as Data Monitoring Boards, Statistical Analysis, Endpoint Committees, and the Like: IMS III; Other: Ge-

nentech, study medication; EKOS, Concentric Inc, and Cordis Neurovascular supplied study catheters in early phase of the IMS III trial; *UNRELATED: Other:* Genentech, financial support paid to the department for role on Steering Committee for PRISMS Trial. Sharon D. Yeatts—*RELATED: Grant:* National Institute of Neurological Disorders and Stroke, *Comments:* IMS III*; *UNRELATED: Consultancy:* Genentech, *Comments:* I received consultant fees for my role on the PRISMS Trial Steering Committee. David S. Liebeskind—*UNRELATED: Consultancy:* Stryker, Medtronic, *Comments:* imaging core lab. *Money paid to the institution.

REFERENCES

- Rahme R, Yeatts SD, Abruzzo T, et al. **Early reperfusion and clinical outcome in patients with M2 occlusion: pooled analysis of the PROACT II, IMS, and IMS II studies.** *J Neurosurg* 2014;121:1354–58 CrossRef Medline
- IMS Study Investigators. **Combined intravenous and intra-arterial recanalization for acute ischemic stroke: the Interventional Management of Stroke Study.** *Stroke* 2004;35:904–11 CrossRef Medline
- The IMS II Trial Investigators. **The Interventional Management of Stroke (IMS) II study.** *Stroke* 2007;38:2127–35 CrossRef Medline
- Tomsick TA, Broderick J, Carrozella J, et al; Interventional Management of Stroke II Investigators. **Revascularization results in the Interventional Management of Stroke II Trial.** *AJNR Am J Neuroradiol* 2008;29:582–87 CrossRef Medline
- Galimanis A, Jung S, Mono ML, et al. **Endovascular therapy of 623 patients with anterior circulation stroke.** *Radiology* 2012;43:1052–57 CrossRef Medline
- Sheth S, Saver J, Jahan R, et al; UCLA Comprehensive Stroke Center. **M2 occlusions as targets for endovascular therapy: comprehensive analysis of diffusion/perfusion MRI, angiography, and clinical outcomes.** *J Neurointerv Surg* 2015;7:478–83 CrossRef Medline
- Flores A, Tomasello A, Cardona P, et al; Catalan Stroke Code and Reperfusion Consortium Cat-SCR. **Endovascular treatment for M2 occlusions in the era of stentrievers: a descriptive multicenter experience.** *J Neurointerv Surg* 2015;7:234–37 CrossRef Medline
- Tomsick TA, Khatri P, Jovin T, et al; IMS III Executive Committee. **Equipoise among recanalization strategies.** *Neurology* 2010;74:1069–76 CrossRef Medline
- Rahme R, Abruzzo T, Martin RH, et al. **Is intra-arterial thrombolysis beneficial for M2 Occlusions? Subgroup analysis of the PROACT II Trial.** *Stroke* 2013;44:240–42 CrossRef Medline
- Goyal M, Demchuk AM, Menon BK, et al; ESCAPE Trial Investigators. **Randomized assessment of rapid endovascular treatment of acute stroke.** *N Engl J Med* 2015;372:1019–30 CrossRef Medline
- Campbell BC, Mitchell PJ, Kleinig TJ, et al; EXTEND-IA Investigators. **Endovascular therapy for ischemic stroke with perfusion-imaging selection.** *N Engl J Med* 2015;372:1009–18 CrossRef Medline
- Berkheimer OA, Fransen PS, Beumer D, et al; MR CLEAN Investigators. **A randomized trial of intraarterial treatment for acute stroke.** *N Engl J Med* 2015;372:11–20 CrossRef Medline
- Broderick JP, Palesch YY, Demchuk AM, et al; Interventional Management of Stroke (IMS) III Investigators. **Endovascular therapy after intravenous rt-PA alone for stroke.** *N Engl J Med* 2013;368:893–903 CrossRef Medline
- Khatri P, Hill M, Palesch Y, et al; Interventional Management of Stroke III Investigators. **Methodology of the Interventional Management of Stroke III trial.** *Int J Stroke* 2008;3:130–37 CrossRef Medline
- Yeatts SD, Martin RH, Foster LD, et al. **Challenges of decision-making regarding futility in a randomized trial: the IMS III experience.** In: *Proceedings of the International Stroke Conference*, Honolulu, Hawaii. February 6–8, 2013
- Smith WS, Sung G, Starkman S, et al; MERCI Trial Investigators. **Safety and efficacy of mechanical embolectomy in acute ischemic stroke: results of the MERCI trial.** *Stroke* 2005;36:1432–38 CrossRef Medline
- Smith WS, Sung G, Saver J, et al. **Mechanical thrombectomy for acute ischemic stroke: final results of the Multi MERCI trial.** *Stroke* 2008;39:1205–12 CrossRef Medline
- Penumbra Pivotal Stroke Trial Investigators. **The Penumbra Pivotal Stroke Trial: safety and effectiveness of a new generation of mechanical devices for clot removal in intracranial large vessel occlusive disease.** *Stroke* 2009;40:2761–68 CrossRef Medline
- Dávalos A, Pereira VM, Chapot R, et al. **Retrospective multicenter study of Solitaire FR for revascularization in the treatment of acute ischemic stroke.** *Stroke* 2012;43:2699–705 CrossRef Medline
- Tomsick T, Yeatts SD, Liebeskind D, et al; IMS III Investigators. **Endovascular revascularization results in IMS III: intracranial ICA and M1 occlusions.** *J Neurointerv Surg* 2015;7:795–802 CrossRef Medline
- Morris PP, Choi IS. **Cerebral vascular anatomy.** *Neuroimaging Clin N Am* 1996;6:541–60 Medline
- Ring BA. **The middle cerebral artery.** In: Newton TH, Potts DG, eds. *Radiology of the Skull and Brain: Angiography*. Vol 2. Great Neck: CV Mosby; 1974:1442–78
- Appireddy RM, Menon BK, Horn M, et al. **Using the M2 vessel diameter and baseline NIHSS to identify which M2 occlusions should be treated endovascularly.** *Stroke* 2015;46:AWP56
- Gulati D, Ducruet A, Aghaebrahim A, et al. **Impact of differences in definition of M1 and M2 segment of middle cerebral artery on acute stroke endovascular therapy.** *Stroke* 2015; 46:AWMP22
- Ogawa A, Mori E, Minematsu K, et al. **Randomized trial of intra-arterial infusion of urokinase within 6 hours of middle cerebral artery stroke: the middle cerebral artery embolism local fibrinolytic intervention trial (MELT) Japan.** *Stroke* 2007;38:2633–39 CrossRef Medline
- Zaidat OO, Yoo AJ, Khatri P, et al; Cerebral Angiographic Revascularization Grading (CARG) Collaborators, STIR Revascularization Working Group, STIR Thrombolysis in Cerebral Infarction (TICI) Task Force. **Recommendations on angiographic revascularization standards for acute ischemic stroke: a consensus statement.** *Stroke* 2013;44:2650–63 CrossRef Medline
- Gibo H, Carver CC, Rhoton AL Jr, et al. **Microsurgical anatomy of the middle cerebral artery.** *J Neurosurg* 1981;54:151–69 CrossRef Medline
- Krayenbuhl HA, Yasargil MG. *Cerebral Angiography*. 2nd ed. Philadelphia; Lippincott; 1968
- Ring BA. **The middle cerebral artery.** In: Newton TH, Potts DG, eds. *Radiology of the Skull and Brain: Angiography*. Vol 2. Great Neck; CV Mosby; 1974:1459
- Menon BK, Bal S, Modi J, et al. **Anterior temporal artery sign in CT angiography predicts fatal brain edema and mortality in acute M1 middle cerebral artery occlusion.** *J Neuroimaging* 2012;22:145–48 CrossRef Medline
- Livorine A, Vagal A, Shu J, et al. **Anatomical variation of M2 occlusions and tissue at risk in IMS III trial: an exploratory analysis.** In: *Proceedings of the Annual Meeting of American Roentgen Ray Society*, Toronto, Ontario, Canada. April 19–24, 2015
- Von Kummer R, Demchuk AM, Foster LD, et al. **Early arterial recanalization after intra-venous tissue-plasminogen-activator treatment in the Interventional Management of Stroke-3 study.** *Stroke* 2014;45:A74
- Demchuk AM, Goyal M, Yeatts SD, et al; IMS III Investigators. **Recanalization and clinical outcome of occlusion sites at baseline CT angiography in the Interventional Management of Stroke III trial.** *Radiology* 2014;273:202–10 CrossRef Medline

Impact of Modified TICI 3 versus Modified TICI 2b Reperfusion Score to Predict Good Outcome following Endovascular Therapy

C. Dargazanli, A. Consoli, M. Barral, J. Labreuche, H. Redjem, G. Ciccio, S. Smajda, J.P. Desilles, G. Taylor, C. Preda, O. Coskun, G. Rodesch, M. Piotin, R. Blanc, and B. Lapegue

ABSTRACT

BACKGROUND AND PURPOSE: The TICI score is widely used to evaluate cerebral perfusion before and after the endovascular treatment of stroke. Recent studies showing the effectiveness and safety of mechanical thrombectomy combine modified TICI 2b and modified TICI 3 to assess the technical success of endovascular treatment. The purpose of this study was to determine how much clinical outcomes differ between patients achieving modified TICI 2b and modified TICI 3 reperfusion.

MATERIALS AND METHODS: We analyzed 222 consecutive patients with acute large intracranial artery occlusion of the anterior circulation having achieved modified TICI 2b or modified TICI 3 reperfusion after thrombectomy. The primary end point was the rate of favorable outcome defined as the achievement of a modified Rankin Scale score of 0–2 at 3 months.

RESULTS: Patients with modified TICI 3 more often had favorable collateral circulation and atherosclerosis etiology, with a shorter time from onset to reperfusion than patients with modified TICI 2b (all $P < .05$). The number of total passes to achieve reperfusion was higher in the modified TICI 2b group (median, 2; interquartile range, 1–3, 1–9) versus (median, 1; interquartile range, 1–2, 1–8) in the modified TICI 3 group ($P = .0002$). Favorable outcome was reached more often for patients with modified TICI 3 than for those with modified TICI 2b (71.7% versus 50.5%, $P = .001$), with a similar difference when considering excellent outcome. In addition, patients with modified TICI 3 had a lower intracerebral hemorrhage rate (23.0% versus 45.0%, $P < .001$).

CONCLUSIONS: Patients with modified TICI 3 reperfusion have better functional outcomes than those with modified TICI 2b. Given the improving reperfusion rates obtained with thrombectomy devices, future thrombectomy trials should consider modified TICI 2b and modified TICI 3 status separately.

ABBREVIATIONS: ADAPT = A Direct Aspiration First-Pass Technique; ICH = intracranial hemorrhage; IQR = interquartile range; mTICI = modified TICI

Thrombectomy is now recommended as the standard of care for acute ischemic stroke with proximal large-vessel occlusion in the anterior circulation,¹ and successful revascularization is a major predictor of good outcome following endovascular therapy for acute large-vessel occlusions.² The Thrombolysis in Cerebral Infarction score is currently used to assess cerebral perfusion be-

fore and after endovascular stroke treatment.³ Recent studies demonstrating the effectiveness of intracranial large-vessel reperfusion by using mechanical thrombectomy considered modified TICI (mTICI) 2b and mTICI 3 (complete reperfusion) to represent technical success,⁴ though some researchers have suggested that patients with mTICI 2b reperfusion have a poorer outcome than patients with complete reperfusion.^{5–7} Thus, the aim of our study was to determine how much functional outcome differed between patients achieving mTICI 2b and those with mTICI 3 reperfusion after thrombectomy for acute stroke in the anterior circulation.

MATERIALS AND METHODS

Inclusion Criteria

In this retrospective study, data were extracted from a bicentric prospective clinical registry (EFFECTS registry, Endovascular Treatment at Foch Hospital–Rothschild Foundation for Ischemic Stroke) of consecutive patients treated by mechanical thrombectomy for acute cerebral infarct between January 2012 and Novem-

Received April 27, 2016; accepted after revision August 18.

From the Departments of Interventional Neuroradiology (C.D., M.B., H.R., G.C., S.S., J.P.D., M.P., R.B.) and Anesthesiology and Reanimation (G.T.), Rothschild Foundation, Paris, France; Department of Diagnostic and Interventional Neuroradiology (A.C., O.C., G.R.) and Division of Neurology, Stroke Center (B.L.), Foch Hospital, Université Versailles Saint Quentin en Yvelines, Suresnes, France; Department of Biostatistics (J.L.), University of Lille, Epidémiologie et Qualité des Soins, Lille, France; and Laboratoire de Mathématiques Paul Painlevé (C.P.), Lille, France.

R.B. and M.P. received institutional grants from Stryker, Medtronic, Microvention and Balt. B.L. received travel funding from Medtronic and speaker honoraria from Penumbra. Drs Piotin and Blanc are proctors for a Medtronic Pipeline case.

Please address correspondence to Cyril Dargazanli, MD, MSc, Department of Interventional Neuroradiology, Rothschild Foundation, 25–29 Rue Manin, 75019 Paris, France; e-mail: c.dargazanli@gmail.com

<http://dx.doi.org/10.3174/ajnr.A4968>

ber 2015. The local ethics committees approved the use of patient data for this retrospective analysis.

All patients referred for endovascular treatment of acute intracranial large-vessel occlusion involving the anterior circulation, with the exception of tandem and multifocal occlusions, were potentially included. Inclusion criteria were the following: 1) middle cerebral artery M1 or M2 segment and/or intracranial internal carotid artery occlusion; 2) intracranial artery occlusion and acute stroke confirmed on cerebral MRA and DWI, respectively; and 3) achievement of mTICI 2b or mTICI 3 reperfusion status after endovascular treatment by mechanical thrombectomy. Exclusion criteria were the following: 1) patients without baseline functional independence (modified Rankin Scale score of >2), and 2) patients with tandem occlusions, with >1 cerebral territory involved or a large ischemic score (DWI-ASPECTS < 6).

Patient Characteristics

Patient demographics, vascular risk factors, imaging findings, vital signs before treatment, severity of ischemic stroke, and clinical outcomes were collected prospectively with a structured questionnaire. Data on age, sex, cardiovascular risk factors (hypertension, dyslipidemia, diabetes, and smoking habits), time of symptom onset, National Institutes of Health Stroke Scale score at baseline and day 1, use of IV thrombolytics, and time of IV thrombolysis were collected. The Alberta Stroke Program Early CT Score on diffusion-weighted MR imaging was calculated by a neuroradiologist blinded to the results of the endovascular procedure. For each patient, the final mTICI score was retrospectively assessed by a neurointerventionalist (C.D.) blinded to both the first reader's scoring and the clinical outcome. A consensus was reached with an additional reader (M.P.) for cases with discrepant judgments. After an in-hospital work-up, stroke etiology was defined, according to the Trial of ORG 10172 in Acute Stroke Treatment classification.⁸

Endovascular Procedure

All patients were treated in a dedicated neuroangiography suite under general anesthesia or conscious sedation, after evaluation by a dedicated anesthesiology team. The thrombectomy device was chosen at the interventionalist's discretion, by using a stent retriever or A Direct Aspiration First-Pass Technique (ADAPT) in the first instance. Arterial occlusion site, time from symptom onset to groin puncture, procedure time, and time to reperfusion were recorded. Reperfusion results were reported by using the mTICI score and were defined as ranging from no reperfusion (mTICI 0) to complete reperfusion (mTICI 3), including partial reperfusion (mTICI 2). Partial reperfusion occurs when the iodine contrast medium passes beyond the obstruction, opacifying the distal arterial bed but with a rate of entry of contrast material and/or its rate of clearance from the vascular bed slower than that in comparable areas not perfused by the previously occluded vessel. The contralateral cerebral angiography, often available for T-carotid occlusions, was used for comparison. In other cases, the arterial bed proximal to the occlusion could be used for comparisons. mTICI 2 was further divided into 2a and 2b as less than and greater than 50%, respectively.⁹ This definition is

different from the original TICI score in which 2a was defined as less than two-thirds perfusion of the distal territory, and 2b, as greater than two-thirds perfusion.¹⁰ Collateral arterial supply was assessed by using the capillary index score,¹¹ and patients were dichotomized into favorable and unfavorable collateral flow groups (capillary index score 2 or 3 and capillary index score 0–1, respectively). Periprocedural complications (embolization in a new territory, defined as an angiographic occlusion in a previously unaffected vascular territory observed on the angiogram after clot removal; arterial dissection or perforation; vasospasm; and subarachnoid hemorrhage) were also noted.

A Direct Aspiration First-Pass Technique Group

Patients in this treatment arm received aspiration thrombectomy by ADAPT by using the 5MAX ACE Reperfusion Catheter (Penumbra, Alameda, California) as frontline therapy. The detailed technical procedure has been published previously.¹² In brief, access was achieved through the femoral artery in compliance with the standard of care. A large-bore catheter was placed distally into the internal carotid artery to provide access for the 5MAX ACE aspiration catheter. Adhering to the instructions for use, we then performed aspiration by using the Penumbra Aspiration Pump (Penumbra, Alameda, California) in all cases. Angiography was performed following recovery to evaluate the flow rate. Steps were repeated if necessary until successful reperfusion to mTICI 2b–3 was achieved. The interventional neuroradiologist could, in case of reperfusion failure (mTICI < 2b) with ADAPT, use another thrombectomy device of the operator's choice (rescue therapy).

Stent-Retriever Group

Procedures were performed by using the Solitaire FR (Covidien, Irvine, California) or the Trevo device (Stryker, Kalamazoo, Michigan) via the femoral artery approach. Following the instructions for use of the stent retriever, we positioned a balloon catheter within the internal carotid artery to allow flow arrest during thrombus retrieval. The stent retriever was delivered through a microcatheter and deployed inside the thrombus. A control angiogram was performed to determine the immediate reperfusion status, and the device was left deployed for a minimum of 3 minutes. Subsequently, the device and microcatheter were slowly retrieved. A control angiogram was obtained to assess recanalization and reperfusion.^{13,14} This sequence was repeated until mTICI 2b or 3 flow (defined as successful reperfusion) was established. The interventional neuroradiologist could, in the case of reperfusion failure (mTICI < 2b) with the stent retriever, use another thrombectomy device of the operator's choice (rescue therapy).

Adjunctive Therapies

Use of complementary mechanical (intracranial angioplasty or stent placement) and/or pharmacologic treatment was recorded. Complementary pharmacologic treatments used were intra-arterial fibrinolysis (alteplase) or intravenous administration of abiximab (Reopro).

Table 1: Baseline characteristics, procedure details, and complications according to reperfusion status^a

	Successful Reperfusion Status		P Value
	(mTICI 2b)	Complete (mTICI 3)	
No. of patients	109	113	
Age (mean) (yr)	69.0 ± 15.9	68.9 ± 14.7	.95
Men	41 (37.6)	55 (48.7)	.096
Medical history			
Hypertension	63 (57.8)	70 (62.0)	.53
Diabetes	18 (16.5)	21 (18.6)	.69
Dyslipidemia	32 (29.4)	37 (32.7)	.59
Current smoking ^b	20 (20.0)	22 (20.4)	.95
NIHSS score (mean)	14.6 ± 6.3	13.7 ± 6.7	.30
Prestroke mRS ≥1	11 (10.1)	12 (10.6)	.90
ASPECTS (median) (IQR)	8 (7–8)	8 (7–9)	.32
Occlusion site			
ICA	27 (24.8)	18 (15.9)	.18
MCA-M1	66 (60.5)	81 (71.7)	
MCA-M2	16 (14.7)	14 (12.4)	
TICI initial (1 vs 0)	10 (9.2)	9 (8.0)	.75
Favorable collateral flow ^c	79 (77.5)	97 (91.5)	.005
Etiology			
Cardioembolism	73 (67.0)	64 (56.7)	.020
Large-artery atherosclerosis	5 (4.6)	18 (15.9)	
Other or undetermined	31 (28.4)	31 (27.4)	
Previous use of IV thrombolysis	77 (70.6)	73 (64.6)	.34
General anesthesia	36 (33.0)	34 (30.1)	.64
Onset to reperfusion time (median) (IQR) (min)	310 (260–361)	285 (225–340)	.021
Onset-to-groin puncture	251 (208–300)	237 (191–292)	.11
Groin puncture to reperfusion (median) (IQR) (min)	50 (31–68)	40 (24–58)	.018
Total number of passes (median) (IQR)	2 (1–3)	1 (1–2)	.0002
Periprocedural complication	13 (11.9)	9 (8.0)	.32
Adjunctive treatment	7 (6.4)	3 (2.7)	.21

^a Values expressed as number (percentage) unless otherwise indicated.

^b Fourteen missing data (9 in mTICI 2b and 5 in mTICI 3).

^c Fourteen missing data (7 in mTICI 2b and 7 in mTICI 3).

Follow-Up and Outcome

All patients underwent cross-sectional imaging (CT or MR imaging) within 18–24 hours after the procedure. Intracranial hemorrhage (ICH) was classified according to the European Cooperative Acute Stroke Study (ECASS) criteria.¹⁵ Patients were evaluated 24 hours after the procedure by using the NIHSS, and “symptomatic intracranial hemorrhage” was defined as any intracerebral hemorrhage with an increase of at least 4 NIHSS points within 24 hours, or resulting in death. The mRS at 90 days was assessed by trained research nurses unaware of the study group assignments during face-to-face interviews or via telephone conversations with the patients, their relatives, or their general practitioners.

The primary study outcome was the achievement of an mRS score of 0–2 at 3 months (favorable outcome). Secondary outcomes included excellent outcome (defined as an mRS score of 0–1), any ICH, all-cause mortality at 90 days, and procedural complications. Furthermore, attention was given to the type of endovascular procedure performed for all patients.

Statistical Analysis

Quantitative variables are expressed as means ± SD or medians (interquartile range [IQR]), and categorical variables are expressed as numbers (percentages). Normality of distributions was assessed by using histograms and the Shapiro-Wilk test. Bivariate

comparisons between complete and mTICI 2b reperfusion groups were made by using the χ^2 test or Fisher exact test for categorical variables, the Cochran-Armitage Trend test for ordinal variables, and the Student *t* test or Mann-Whitney *U* test for quantitative variables as appropriate. We assessed the heterogeneity in the relationship between successful reperfusion status and each outcome (excellent outcome, favorable outcome, 90-day mortality, and any ICH) across the 2 centers by using the Breslow-Day test. Comparisons in outcomes between the 2 successful reperfusion groups were further adjusted for the center and prespecified confounders regarding prior evidence of an association with clinical outcome (namely age, diabetes, admission NIHSS score, site of occlusion, collateral flow, etiology, previous IV thrombolysis, and onset to reperfusion time) by using logistic regression models.⁷ An additional adjustment for ICH occurrence was performed for comparison in functional outcomes (excellent and favorable). To avoid case deletion in multivariable analyses due to missing data on the collateral favorable covariate (missing in 14 patients), we imputed missing data under a missing-at-random assumption by using a regression-switching approach

(chained equation with *m* = 10 imputations obtained by using the R statistical software, Version 3.03; <http://www.r-project.org/>).^{16,17} Imputation procedures were performed by using all variables listed in Table 1 and each study outcome. Multiple imputed datasets were combined by using the Rubin rules.¹⁸ Unadjusted and adjusted odds ratios for reaching each outcome were calculated by using mTICI 2b as the reference group. Statistical testing was performed at the 2-tailed α level of .05. Data were analyzed by using SAS software, Version 9.3 (SAS Institute, Cary, North Carolina).

RESULTS

A total of 593 consecutive patients with an acute internal carotid artery or middle cerebral artery occlusion were treated by endovascular therapy at 2 comprehensive stroke centers (Fig 1). Of these, 92 with no baseline MR imaging, 153 with DWI-ASPECTS of <6, 95 with substantial perfusion on the baseline angiogram (mTICI ≥ 2), and 20 with failure of endovascular treatment (final mTICI < 2b) were excluded. Overall, 233 patients achieved successful reperfusion (mTICI ≥ 2b) and were included in the study. Two initially included patients with intracranial stenosis and early arterial reocclusion were excluded, and 9 patients were lost to follow-up, resulting in a final study sample size of 222 patients. Among them, 113 (50.9%) achieved mTICI 3 reperfusion and 109

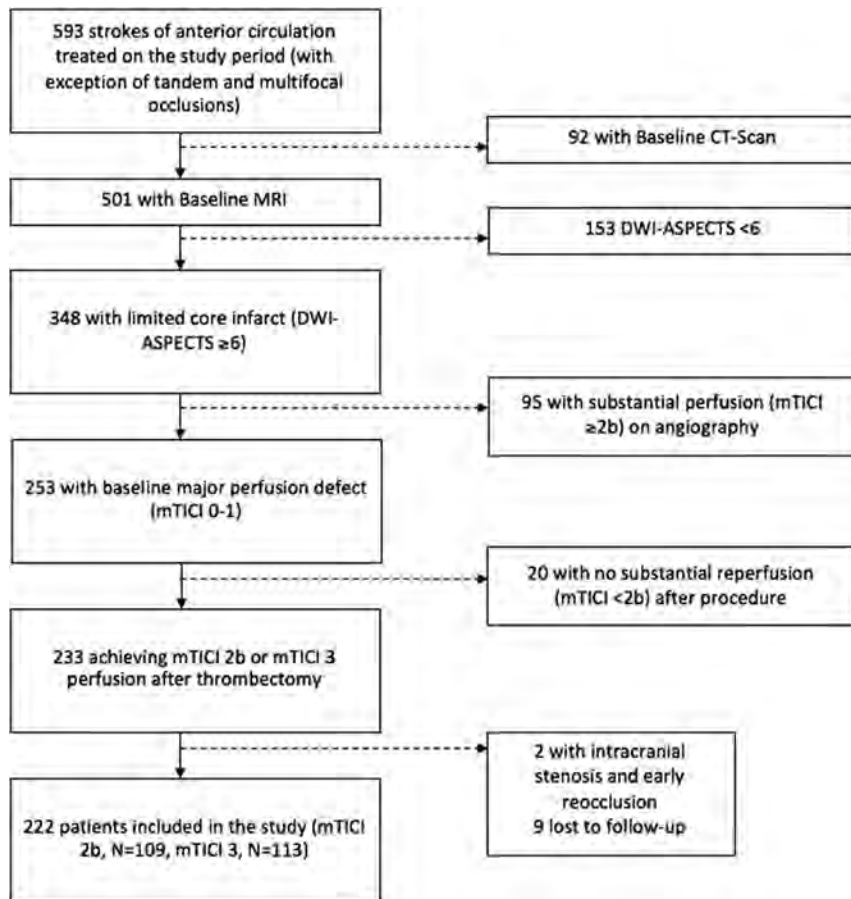


FIG 1. Flow chart of the study.

(49.1%) achieved mTICI 2b reperfusion. The median time of successful reperfusion from symptom onset was 291 minutes (IQR, 240–355).

Baseline characteristics, including time from onset to reperfusion, number of passes to achieve reperfusion, and periprocedural complications are shown in Table 1, according to successful reperfusion status. There was no significant difference in age, vascular risk factors, admission NIHSS score, ASPECTS, or fibrinolytic administration between the 2 reperfusion groups. However, patients with complete reperfusion (mTICI 3) more often had favorable collateral flow and large-artery atherosclerosis etiology, together with a lower onset-to-reperfusion time than patients with mTICI 2b reperfusion (all $P < .05$). The number of total passes to achieve reperfusion was higher in the mTICI 2b group (median, 2; interquartile range, 1–3, 1–9) versus (median, 1; interquartile range, 1–2, 1–8) in the mTICI 3 group ($P = .0002$). Procedural complications (emboli into new territories, procedure-related arterial dissection or perforation, subarachnoid hemorrhage, and vasospasm) occurred in 9 (8%) patients with complete reperfusion and in 13 (11.9%) patients with mTICI 2b reperfusion ($P = .32$).

ADAPT was used in the first instance in 110 patients (49.5%), among whom switching to the stent-retriever technique occurred in 12 patients (11%). The stent-retriever technique was used in the first instance in 112 patients (50.5%), and switching to ADAPT occurred in 3 (11.9%) of these.

No difference was found regarding the use of adjunctive treatment.

The distribution of 90-day mRS according to successful reperfusion status is shown in Fig 2. Favorable outcome (mRS ≤ 2) was achieved more often in patients with complete reperfusion than in those with mTICI 2b reperfusion (71.7% versus 50.5%, $P = .001$). A similar difference was found when considering excellent outcome (mRS < 2 , Table 2). In addition, patients with complete reperfusion had a nonsignificantly lower mortality rate (8.9% versus 16.5%, $P = .086$) and a lower ICH rate (23.0% versus 45.0%, $P < .001$) compared with those with mTICI 2b reperfusion. Regarding the ECASS classification, HI1, HI2, PH1, and PH2 types occurred respectively in 20, 4, 1, and 1 patients with complete reperfusion and 22, 17, 4, and 6 patients with mTICI 2b reperfusion. Symptomatic ICH occurred in only 1 patient (0.9%) with complete reperfusion and in 4 patients (3.7%) with mTICI 2b reperfusion.

We found no significant heterogeneity in the impact of successful reperfusion status on outcomes across the 2 centers (All P values for heterogeneity, $> .26$). After we adjusted for center and baseline between-group differences, mTICI

3 status remained significantly associated with an increased probability of excellent and favorable outcomes and a decreased probability of any ICH (Table 2). When comparison in functional outcomes was further adjusted for ICH, the differences were not modified; the adjusted ORs of excellent and favorable outcomes for complete relative to mTICI 2b reperfusion groups were, respectively, 2.55 (95% CI, 1.23–5.26) and 2.78 (95% CI, 1.28–6.08).

DISCUSSION

Our study shows that patients with complete reperfusion after endovascular treatment by using new-generation mechanical thrombectomy devices have a better outcome than those who achieve a mTICI 2b reperfusion. To our knowledge, this is the first study to specifically compare the impact of mTICI 2b versus mTICI 3 on functional outcome at 3 months, though it has already been shown that patients with TICI 3 have a lower NIHSS score at discharge than those with TICI 2b (the original TICI definition was used in this article).⁶ One recent study also suggested that patients with mTICI 3 had better functional outcomes than those with mTICI 2b, though significance was only achieved in univariate analysis.⁷

Recent controlled trials demonstrating the efficiency and safety of mechanical thrombectomy⁴ consider that technical success of the endovascular procedure is achieved when mTICI 2b or 3 reperfusion is obtained. According to a recent meta-analysis of individual data about endovascular therapy, this threshold is

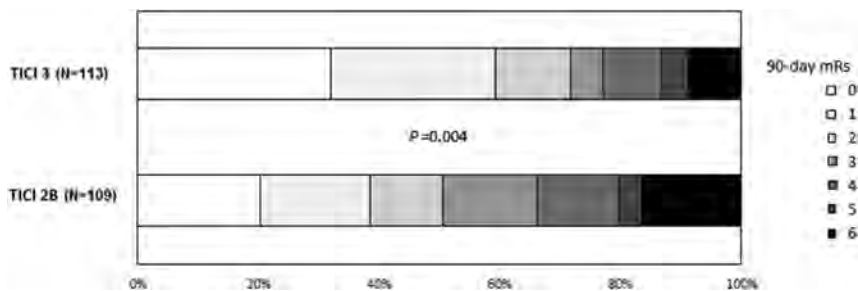


FIG 2. Distribution of modified Rankin Scale scores at 90 days according to successful reperfusion status.

Table 2: Outcomes according to successful reperfusion status^a

	mTICI 2b (n = 109)	Complete mTICI 3 (n = 113)	OR (95% CI)	P	OR (95% CI) ^b	P ^b
Excellent outcome	42 (38.5)	67 (59.3)	2.32 (1.35–3.98)	.002	2.98 (1.46–6.06)	.0037
Favorable outcome	55 (50.5)	81 (71.7)	2.49 (1.42–4.33)	.001	3.34 (1.56–7.11)	.002
90-Day mortality	18 (16.5)	10 (8.9)	0.49 (0.21–1.12)	.086	NR	NR
Any ICH	49 (45.0)	26 (23.0)	0.37 (0.20–0.65)	<.001	0.33 (0.16–0.64)	.001
HI1	22 (20.2)	20 (17.7)	–	–	–	–
HI2	17 (15.6)	4 (3.5)	–	–	–	–
PH1	4 (3.7)	1 (0.9)	–	–	–	–
PH2	6 (5.5)	1 (0.9)	–	–	–	–

Note:—NR indicates not reportable regarding the small number of events; OR, odds ratio.

^a Excellent outcome was defined as 90-day mRS ≤ 1, and favorable outcome, as 90-day mRS ≤ 2. ORs were calculated using mTICI 2b reperfusion as a reference.

^b Adjusted on center, age, diabetes, admission NIHSS score, prior use of IV thrombolysis, site of occlusion, favorable collateral flow, etiology, and onset to reperfusion time using multivariable logistic regression models (after a mean of 10 imputations to handle missing data on favorable collateral flow).

reached in 71% of cases in the trials mentioned above.⁴ After a clinical study showing a trend to more favorable outcomes for patients with mTICI 3 compared with mTICI 2b but with no statistically significant difference,¹³ a consensus statement defined the mTICI 2b threshold as the target angiographic end point for technical success of mechanical thrombectomy.¹⁴ Since the MERCI trials era, it is well-accepted that greater degrees of recanalization are associated with an increased rate of favorable functional outcome.¹⁹ In the Interventional Management of Stroke (IMS) III study,⁵ though performed during the pre-stent-retriever period, the authors reported that the proportions of patients with mRS ≤ 2 at 90 days (primary outcome) increased with greater reperfusion. However, these studies had a lack of distinction between the various degrees of partial recanalization and the use of the Thrombolysis in Myocardial Infarction score. Currently, the mTICI score is widely used in the literature to assess cerebral reperfusion following stroke therapy.³ Indeed, it has been demonstrated to better correlate with clinical outcome than the Thrombolysis in Myocardial Infarction score.¹⁹ The current definition of the mTICI score (the modified mTICI 2b) is the version introduced by the IMS investigators,²⁰ which is simpler and shows better interrater agreement than the original definition.

Etiologies

We observed in our retrospective cohort that patients with a stroke of atherothrombotic origin achieved complete reperfusion with a higher frequency than those with a stroke from other causes (mainly cardioembolism). In the literature or in recent trials demonstrating the efficiency of thrombectomy, limited data are available about recanalization or reperfusion rates according to stroke etiologic sub-

type.² Further studies may explore this concern, and clot composition and mechanical characteristics may be a clue to explain this difference.²¹

Time from Symptom Onset and Procedure Time

Patients achieving mTICI 2b reperfusion had longer times from symptom onset to reperfusion than those achieving mTICI 3 reperfusion. Indeed, the procedure time was longer and the total number of passes to achieve reperfusion was higher in the mTICI 2b group than in the mTICI 3 group. This higher number of passes was not associated with a higher rate of periprocedural complications or adjunctive therapies in this study. After adjustment for differences in time to reperfusion, mTICI 3 remained a predictor of better clinical outcome than mTICI 2b reperfusion. The onset-to-reperfusion time in our study (297.5 minutes) is in accordance with those reported in recent trials evaluating thrombectomy, calculated as 285 minutes in a recent meta-analysis.⁴

Rate of Hemorrhage

In our cohort, ICH was less frequent in patients with mTICI 3 than in those with mTICI 2b (23.0% versus 45.0%, $P < .001$). Both the time from symptom onset to reperfusion (median, 310 versus 285 minutes; $P = .021$) and the procedure time (median, 50 versus 40 minutes; $P = .018$) were longer in the mTICI 2b group. Delayed reperfusion and longer procedural times are independently associated with occurrence of intracranial hemorrhage in patients with large-vessel occlusion undergoing endovascular reperfusion therapy of stroke.²² These data are supported by experimental evidence.²³ Mechanisms involved are multiple, mainly involving blood-brain barrier disruption.²⁴ However, our results may be affected by the low frequency of symptomatic ICH in our study, which can be explained by our inclusion criteria, excluding patients with large-core infarcts, known to have a higher risk of ICH.

Baseline Collateral Status and Reperfusion Rate

Baseline collateral status varies in patients with acute ischemic stroke. Most patients in this study had good collateral flow. This is related to the selection of patients with proximal occlusion and both a limited clinical deficit and limited infarct core who likely have good collateral circulation.²⁵ Nevertheless, we observed that patients achieving complete reperfusion had better collateral flow on baseline angiograms than those who did not. This finding is consistent with the literature, and a recent meta-analysis showed that good pretreatment collateral status may enhance the rate of both recanalization and reperfusion in patients with stroke receiving mechanical revascularization therapy.²⁶ However, mecha-

nisms of the effects of good collateral flow on successful revascularization remain poorly understood. One explanation may be that retrograde filling would allow neuroprotective agents (intrinsic or extrinsic) to access the clot.²⁷ A mechanical effect of collateral flow facilitating clot removal may also provide an explanation.

Limitations

Our study has the limitations inherent in its retrospective design, with a relatively small sample size extracted from 2 centers. Bias related to missing data on collateral flow ($n = 14$) cannot be completely ruled out because multiple imputation procedures replacing missing values with a set of plausible values were performed under a missing-at-random assumption. No core laboratory has adjudicated MR imaging/MRA and angiographic findings, though mTICI, DWI-ASPECTS, and clinical outcomes were all assessed in a blinded manner.

Among baseline characteristics, we observed more terminal carotid occlusion in the mTICI 2b group, though the difference was not significant. Intuitively, thrombus burden may be higher in this group, resulting in a lower complete reperfusion rate. Moreover, mTICI 2b reperfusion occurred in a heterogeneous group of patients with various parenchymal defects regardless of their clinical significance. Indeed, a patient presenting with a defect in the right prefrontal area will be categorized as mTICI 2b, as will be a patient with a defect in the right central area. However, their respective clinical outcomes may not be the same. Similarly, a parenchymal defect in the same area but located in the left or right hemisphere may have a distinct clinical outcome. Further research should be performed to analyze this heterogeneous subgroup of mTICI 2b, regarding the complex anatomy of the MCA and its territories of supply, and to take into account the lateralization of the defect as well.

Second, we did not consider here the TICI 2c subcategory,²⁸ defined by near-complete perfusion except for slow flow or distal emboli in a few distal cortical vessels. However, Almekhlafi et al²⁸ reported similar clinical outcomes between TICI 2c and TICI 3.

CONCLUSIONS

We found that patients with mTICI 3 reperfusion achieve better clinical outcomes and less hemorrhagic transformation than patients achieving mTICI 2b reperfusion. Therefore, mTICI 3 may be considered as representing the optimal technical success in reperfusion and a target end point for the neurointerventionalist. Future thrombectomy devices or techniques should focus on achieving mTICI 3 reperfusion. Our results, though requiring confirmation in further studies, suggest considering patients with mTICI 2b and mTICI 3 separately in future prospective studies evaluating the effectiveness of mechanical thrombectomy. Moreover, other potential areas for future research could include a subgroup analysis of the recent major stroke trials or an analysis of one of the major stroke data bases (such as Get With The Guidelines Stroke Registry of the American Heart Association), with comparison of mRS outcomes between patients with mTICI 2b versus mTICI 3 reperfusion.

ACKNOWLEDGMENTS

We thank Mary Osborne-Pellegrin for help in editing the final draft of the manuscript.

Disclosures: Guillaume Taylor—UNRELATED: Payment for Lectures including service on Speakers Bureaus: Stryker, Medtronic, Comments: lectures regarding intracranial stenting for aneurysm treatment*; Travel/Accommodations/Meeting Expenses Unrelated to Activities Listed: Astra Zeneca, Medtronic, Comments: meeting on antiplatelet treatment protocols for a stroke course. Michel Piotin—UNRELATED: Consultancy: Medtronic, Stryker, MicroVention, Penumbra, Balt*; Payment for Development of Educational Presentations: Medtronic, Stryker, MicroVention, Balt.* *Money paid to the institution.

REFERENCES

1. Powers WJ, Derdeyn CP, Biller J, et al; American Heart Association Stroke Council. 2015 American Heart Association/American Stroke Association Focused Update of the 2013 Guidelines for the Early Management of Patients With Acute Ischemic Stroke Regarding Endovascular Treatment: a guideline for healthcare professionals from the American Heart Association/American Stroke Association. *Stroke* 2015;46:3020–35 CrossRef Medline
2. Rha JH, Saver JL. The impact of recanalization on ischemic stroke outcome: a meta-analysis. *Stroke* 2007;38:967–73 CrossRef Medline
3. Fugate JE, Klunder AM, Kallmes DF. What Is meant by “TICI”? *AJNR Am J Neuroradiol* 2013;34:1792–97 CrossRef Medline
4. Goyal M, Menon BK, van Zwam WH, et al; HERMES collaborators. Endovascular thrombectomy after large-vessel ischaemic stroke: a meta-analysis of individual patient data from five randomised trials. *Lancet* 2016;387:1723–31 CrossRef Medline
5. Broderick JP, Palesch YY, Demchuk AM, et al; Interventional Management of Stroke (IMS) III Investigators. Endovascular therapy after intravenous t-PA versus t-PA alone for stroke. *N Engl J Med* 2013;368:893–903 CrossRef Medline
6. Kleine JF, Wunderlich S, Zimmer C, et al. Time to redefine success? TICI 3 versus TICI 2b recanalization in middle cerebral artery occlusion treated with thrombectomy. *J NeuroInterventional Surg* 2016 Feb 17. [Epub ahead of print] CrossRef Medline
7. Linfante I, Starosciak AK, Walker GR, et al. Predictors of poor outcome despite recanalization: a multiple regression analysis of the NASA registry. *J Neurointerv Surg* 2016;8:224–29 CrossRef Medline
8. Adams HP Jr, Bendixen BH, Kappelle LJ, et al. Classification of subtype of acute ischemic stroke: definitions for use in a multicenter clinical trial—TOAST. Trial of Org 10172 in Acute Stroke Treatment. *Stroke* 1993;24:35–41 CrossRef Medline
9. Tomsick T, Broderick J, Carrozella J, et al; Interventional Management of Stroke II Investigators. Revascularization results in Interventional Management of Stroke II Trial. *AJNR Am J Neuroradiol* 2008;29:582–87 CrossRef Medline
10. Higashida RT, Furlan AJ, Roberts H, et al; Technology Assessment Committee of the American Society of Interventional and Therapeutic Neuroradiology; Technology Assessment Committee of the Society of Interventional Radiology. Trial design and reporting standards for intra-arterial cerebral thrombolysis for acute ischemic stroke. *Stroke* 2003;34:e109–37 CrossRef Medline
11. Al-Ali F, Jefferson A, Barrow T, et al. The capillary index score: rethinking the acute ischemic stroke treatment algorithm—results from the Borgess Medical Center Acute Ischemic Stroke Registry. *J Neurointerv Surg* 2013;5:139–43 CrossRef Medline
12. Turk AS, Frei D, Fiorella D, et al. ADAPT FAST study: a direct aspiration first pass technique for acute stroke thrombectomy. *J Neurointerv Surg* 2014;6:260–64 CrossRef Medline
13. Yoo AJ, Simonsen CZ, Prabhakaran S, et al; Cerebral Angiographic Revascularization Grading Collaborators. Refining angiographic biomarkers of revascularization: improving outcome prediction after intra-arterial therapy. *Stroke* 2013;44:2509–12 CrossRef Medline
14. Zaidat OO, Yoo AJ, Khatri P, et al; Cerebral Angiographic Revascularization Grading (CARG) Collaborators, STIR Revascularization

- working group, STIR Thrombolysis in Cerebral Infarction (TICI) Task Force. **Recommendations on angiographic revascularization grading standards for acute ischemic stroke: a consensus statement.** *Stroke* 2013;44:2650–63 CrossRef Medline
15. Hacke W, Kaste M, Fieschi C, et al. **Intravenous thrombolysis with recombinant tissue plasminogen activator for acute hemispheric stroke: the European Cooperative Acute Stroke Study (ECASS).** *JAMA* 1995;274:1017–25 CrossRef Medline
 16. Buuren S, Groothuis-Oudshoorn K. **Mice: multivariate imputation by chained equations in R.** *J Stat Softw* 2011;45:1–67
 17. R Core Team. *R Language and Environment for Statistical Computing.* R Foundation for Statistical Computing:Vienna, Austria, 2013. <http://www.R-project.org>
 18. Rubin DB. *Multiple Imputation for Nonresponse in Surveys.* New York: Wiley; 1987
 19. Fields JD, Lutsep HL, Smith WS, et al; MERCI Multi MERCI Investigators. **Higher degrees of recanalization after mechanical thrombectomy for acute stroke are associated with improved outcome and decreased mortality: pooled analysis of the MERCI and Multi MERCI trials.** *AJNR Am J Neuroradiol* 2011;32:2170–74 CrossRef Medline
 20. Khatri P, Hill MD, Palesch YY, et al; Interventional Management of Stroke III Investigators. **Methodology of the Interventional Management of Stroke (IMS) III Trial.** *Int J Stroke* 2008;3:130–37 CrossRef Medline
 21. Dargazanli C, Rigau V, Eker O, et al. **High CD3+ cells in intracranial thrombi represent a biomarker of atherothrombotic stroke.** *PLoS One* 2016;11:e0154945 CrossRef Medline
 22. Kass-Hout T, Kass-Hout O, Sun CH, et al. **Longer procedural times are independently associated with symptomatic intracranial hemorrhage in patients with large vessel occlusion stroke undergoing thrombectomy.** *J Neurointerv Surg* 2016 Feb 1. [Epub ahead of print] CrossRef Medline
 23. Jickling GC, Liu D, Stamova B, et al. **Hemorrhagic transformation after ischemic stroke in animals and humans.** *J Cereb Blood Flow Metab* 2014;34:185–99 CrossRef Medline
 24. Mokin M, Kan P, Kass-Hout T, et al. **Intracerebral hemorrhage secondary to intravenous and endovascular intraarterial revascularization therapies in acute ischemic stroke: an update on risk factors, predictors, and management.** *Neurosurg Focus* 2012;32:E2 CrossRef Medline
 25. Hakimelahi R, Vachha BA, Copen WA, et al. **Time and diffusion lesion size in major anterior circulation ischemic strokes.** *Stroke* 2014;45:2936–41 CrossRef Medline
 26. Leng X, Fang H, Leung TWH, et al. **Impact of collateral status on successful revascularization in endovascular treatment: a systematic review and meta-analysis.** *Cerebrovasc Dis* 2016;41:27–34 CrossRef Medline
 27. Caplan LR, Hennerici M. **Impaired clearance of emboli (washout) is an important link between hypoperfusion, embolism, and ischemic stroke.** *Arch Neurol* 1998;55:1475–82 CrossRef Medline
 28. Almekhlafi MA, Mishra S, Desai JA, et al. **Not all “successful” angiographic reperfusion patients are an equal validation of a modified TICI scoring system.** *Interv Neuroradiol* 2014;20:21–27 CrossRef Medline

Emergent Endovascular Management of Long-Segment and Flow-Limiting Carotid Artery Dissections in Acute Ischemic Stroke Intervention with Multiple Tandem Stents

S.A. Ansari, A.L. Kühn, A.R. Honarmand, M. Khan, M.C. Hurley, M.B. Potts, B.S. Jahromi, A. Shaibani, M.J. Gounis, A.K. Wakhloo, and A.S. Puri



ABSTRACT

BACKGROUND AND PURPOSE: Although most cervical dissections are managed medically, emergent endovascular treatment may become necessary in the presence of intracranial large-vessel occlusions, flow-limiting and long-segment dissections with impending occlusion, and/or hypoperfusion-related ischemia at risk of infarction. We investigated the role of emergent endovascular stenting of long-segment carotid dissections in the acute ischemic stroke setting.

MATERIALS AND METHODS: We retrospectively studied long-segment carotid dissections requiring stent reconstruction with multiple tandem stents (≥ 3 stents) and presenting with acute (< 12 hours) ischemic stroke symptoms (NIHSS score, ≥ 4). We analyzed patient demographics, vascular risk factors, clinical presentations, imaging/angiographic findings, technical procedures/complications, and clinical outcomes.

RESULTS: Fifteen patients (mean age, 51.5 years) with acute ischemic stroke (mean NIHSS score, 15) underwent endovascular stent reconstruction for vessel and/or ischemic tissue salvage. All carotid dissections presented with $> 70\%$ flow limiting stenosis and involved the distal cervical ICA with a minimum length of 3.5 cm. Carotid stent reconstruction was successful in all patients with no residual stenosis or flow limitation. Nine patients (60%) harbored intracranial occlusions, and 6 patients (40%) required intra-arterial thrombolysis/thrombectomy, achieving 100% TIC1 2b–3 reperfusion. Two procedural complications were limited to thromboembolic infarcts from in-stent thrombus and asymptomatic hemorrhagic infarct transformation (7% morbidity, 0% mortality). Angiographic and ultrasound follow-up confirmed normal carotid caliber and stent patency, with 2 cases of $< 20\%$ in-stent stenosis. Early clinical improvement resulted in a mean discharge NIHSS score of 6, and 9/15 (60%) patients achieved a 90-day mRS of ≤ 2 .

CONCLUSIONS: Emergent stent reconstruction of long-segment and flow-limiting carotid dissections in acute ischemic stroke intervention is safe and effective, with favorable clinical outcomes, allowing successful thrombectomy, vessel salvage, restoration of cerebral perfusion, and/or prevention of recurrent thromboembolic stroke.

ABBREVIATIONS: AIS = acute ischemic stroke; ELVO = emergent large-vessel occlusion; IA = intra-arterial

Cervical carotid or vertebral artery dissections are a common cause of acute ischemic stroke (AIS) in middle-aged and young adults.^{1–3} The prognosis of cervical dissections is favorable,

with the standard of care being medical management as the majority of patients respond to anticoagulation/antiplatelet therapy.^{4,5} Delayed endovascular stenting of cervical dissections is reserved for patients presenting with recurrent ischemic symptoms and/or thromboembolic strokes refractory to medical management, progression of dissection-related stenosis, or symptomatic/enlarging dissecting pseudoaneurysms. Emergent endovascular treatment may also be required for cervical dissections presenting with concomitant intracranial thromboemboli/emergent large-vessel occlusion (ELVO), flow-limiting and long-segment lesions with impending occlusion, and/or hypoperfusion-related ischemia at risk of cerebral infarction.

Multiple randomized controlled trials have proved endovascular thrombectomy the standard of care in the treatment of ELVO.^{6–8} Since superimposed extracranial carotid or intracranial

Received July 7, 2016; accepted after revision August 18.

From the Departments of Radiology, Neurology, and Neurological Surgery (S.A.A., A.R.H., M.C.H., M.B.P., B.S.J., A.S.), Northwestern University Feinberg School of Medicine, Chicago, Illinois; Division of Neuroimaging and Intervention (A.L.K., M.J.G., A.K.W., A.S.P.), Department of Radiology and New England Center for Stroke Research, University of Massachusetts, Worcester, Massachusetts; and Department of Neurology (M.K.), Brown University, Providence, Rhode Island.

Please address correspondence to Sameer A. Ansari, MD, PhD, Departments of Radiology, Neurology, and Neurological Surgery, Northwestern University, Feinberg School of Medicine, 676 N St. Clair St, Suite 800, Chicago, IL 60611-2927; e-mail: s-ansari@northwestern.edu

Indicates open access to non-subscribers at www.ajnr.org

Indicates article with supplemental on-line table.

<http://dx.doi.org/10.3174/ajnr.A4965>

atherosclerotic disease and dissections are often an etiology of ELVO, recent studies have evaluated endovascular angioplasty/stenting techniques combined with intracranial thrombectomy. Adjunctive angioplasty/stenting techniques may be valuable in tandem carotid-intracranial occlusions secondary to acutely ruptured carotid atherosclerotic plaques, underlying intracranial atherosclerotic disease at risk for rethrombosis, or severe flow-limiting cervical/intracranial dissections. Furthermore, extracranial carotid stent placement may be necessary in emergent settings to provide distal access for intracranial thrombectomy, vessel salvage, or revascularization in hypoperfusion ischemic syndromes without sufficient intracranial collaterals. Several investigators have demonstrated the feasibility of emergency ICA stenting combined with intracranial thrombectomy for tandem ICA-MCA occlusions with acceptable rates of successful recanalization, complications, and clinical outcomes.⁹⁻¹⁴ In two of the recent multicenter trials that demonstrated a benefit of endovascular thrombectomy for AIS, carotid artery stent placement was necessary in 8.6%–12.9% of patients.^{6,7}

Few studies have focused on the endovascular management of spontaneous cervical dissections with or without tandem intracranial ELVOs in the AIS setting, often limited to small sample sizes because most dissections can be managed medically post-thrombectomy.¹⁵⁻¹⁷ We report on a unique cohort presenting for AIS intervention secondary to long-segment and flow-limiting carotid dissections requiring multiple tandem stents for endovascular reconstruction, irrespective of intracranial ELVO or successful thrombolysis/thrombectomy.

MATERIALS AND METHODS

Patients

Patients presenting with spontaneous carotid artery dissections that underwent stent reconstruction between January 2011 and January 2015 were identified at the University of Massachusetts Medical Center or Northwestern University affiliated hospitals by using their neurointerventional databases. Institutional review board (IRB) approvals were acquired for a collaborative retrospective study. Emergent off-label use of Humanitarian Device Exemption (HDE) intracranial stents for the treatment of carotid dissections was reported to the respective IRBs and manufacturers as required. Medical record and PACS imaging data sharing was conducted under Health Insurance Portability and Accountability Act (HIPAA) guidelines. We included patients who were treated emergently in the AIS intervention window (<12 hours from symptom onset) with symptomatic (NIHSS \geq 4) and long-segment carotid dissections requiring multiple tandem stents (\geq 3 stents) for endovascular reconstruction.

All patients had baseline CT/CTA and/or MRI/MRA available as components of AIS imaging protocols to exclude patients with intracranial hemorrhage and large ischemic infarcts of more than one-third of the MCA distribution and to identify suspected intracranial thromboembolic occlusions. CT/MR perfusion and MR diffusion-weighted imaging were not uniformly used, but were performed in 6/15 patients to estimate salvageable ischemic tissue and infarction volumes before intervention. If eligible, patients received IV tPA prior to attempted intra-arterial (IA)

thrombolysis/mechanical thrombectomy of ELVOs and/or stent reconstruction of carotid dissections.

Procedures

All endovascular procedures were performed with the patient under monitored anesthesia care ($n = 4$) or general anesthesia ($n = 11$) with hemodynamic monitoring. Transfemoral access and retrograde advancement of 6F guide sheaths into the common carotid arteries, proximal to the dissections, provided guide sheath support. Microcatheter/microwire access was obtained across the dissection flaps with contrast injections confirming true lumen catheterization and opacification of the distal intracranial vasculature. Intravenous heparin anticoagulation was used in 14/15 cases with activated clotting time (ACT) monitoring (200–250 seconds). ELVOs were targeted with intra-arterial thrombolysis by using tPA and/or mechanical thrombectomy via direct aspiration or stent-retriever techniques. Due to persisting neurologic symptoms and/or severe flow limitations into the anterior circulation, carotid dissections were repaired using tandem stent reconstruction with partial overlapping techniques to prevent uncovered gaps across the stent constructs. Self-expanding or balloon-expanding stents were advanced and deployed over 0.014-inch exchange microwires, maintaining distal access across the length of the carotid dissections. Specific types of intracranial/carotid self-expanding stents (Wingspan/Neuroform intracranial stents; Stryker Neurovascular, Kalamazoo, Michigan; Precise carotid stent; Cordis, Fremont, California; Xact carotid stent; Abbott Laboratories, Abbott Park, Illinois) or peripheral/coronary balloon-expanding stents (Xience everolimus-eluting coronary stent; Abbott Laboratories; Express SD; Boston Scientific, Natick, Massachusetts; Resolute Integrity zotarolimus-eluting coronary stent; Medtronic, Minneapolis, Minnesota) were used at the discretion of the treating neurointerventionalist. Carotid stent reconstruction was performed serially to secure the distal intimal flap and proximal dissection inflow zone.

During carotid stent-placement procedures, intraoperative antiplatelet loading doses were administered with either orogastric/rectal aspirin 325–650 mg ($n = 5$), dual aspirin 325–650 mg, and clopidogrel 300–600 mg ($n = 5$), or intravenous glycoprotein IIb/IIIa inhibitors (eptifibatid 0.18 mg/kg, $n = 3$). The remaining two patients previously on dual aspirin/clopidogrel or warfarin/aspirin therapy were bridged to aspirin/clopidogrel. Patients who received intraoperative IIb/IIIa inhibitors or aspirin-only loading doses were subsequently loaded with clopidogrel 300–600 mg, within 12 hours postprocedure. All patients remained on dual aspirin 81–325 mg/clopidogrel 75 mg antiplatelet therapy for >6 months.

Clinical and Imaging Data Analysis

We studied patient demographics, vascular risk factors, presentations, NIHSS scores on admission, initial and follow-up imaging/angiographic findings, technical efficacy and safety, procedural complications, and clinical outcomes at discharge (NIHSS and mRS scores) and at 90 days (mRS). All carotid dissections were classified according to the Modified Carotid Artery Injury Grading Scale on DSA and were measured for the length of vessel involvement on initial CTA/MRA studies.¹⁸ Final post-proce-

Patient demographics and presentations

Demographics/Presentations	
Age (mean) (yr)	51.5 (range 37–79 years)
Sex (F/M)	4/11
Presenting symptoms (No.) (%)	
Hemiplegia/hemiparesis	12 (80)
Aphasia	6 (40)
Headache	4 (26.7)
Facial droop	4 (26.7)
Sensory deficit	3 (20)
Hemineglect	2 (13.3)
Visual deficit	2 (13.3)
Risk factors (No.) (%)	
Hypertension	7 (46.7)
Dyslipidemia	5 (33.3)
Diabetes mellitus	1 (6.7)
Fibromuscular dysplasia	1 (6.7)
No significant risk factor	6 (40)

dural DSA studies after carotid stent reconstruction and adjunctive IA thrombolysis/thrombectomy techniques were evaluated for residual cervical segmental stenosis (significance >50% by NASCET criteria),¹⁹ flow limitation, and cerebral reperfusion according to the modified TIC1 scale.

Follow-up imaging with noncontrast CT head studies post-procedure and at 24–72 hours was assessed for any intracranial hemorrhagic (reperfusion or infarct transformation) complications according to the European Cooperative Acute Stroke Study (ECASS) criteria²⁰ and evolving infarction. Symptomatic intracranial hemorrhage was defined as an association with any clinical deterioration or increase in the NIHSS score of >4. Delayed carotid Doppler ultrasound and CTA and/or conventional angiographic follow-up studies at 3–6 months post-procedure were evaluated to assess midterm carotid and stent patency.

All retrospective clinical and imaging data analysis was agreed upon by two senior neurointerventionalists at each site. Statistical analysis was limited to mean and standard deviation calculations for patient age, NIHSS score, and mean dissection lengths, and median calculations for the number of stent constructs and mRS scores.

RESULTS

We retrospectively identified 15 patients (11 men: 4 women; mean age 51.5 years) who underwent endovascular stent reconstruction with ≥ 3 stents for long-segment and symptomatic (mean NIHSS score 15) carotid dissections in the AIS setting (<12 hours from symptom onset). Baseline demographics data, presenting signs and symptoms, and precipitating risk factors are presented in the Table. Procedural data regarding pretreatment IV tPA thrombolysis, IA recanalization of concurrent intracranial occlusion, anatomic extent of dissections, length and degree of flow limitation, number/type of stents for carotid reconstruction, complications, and clinical outcomes are noted in the On-line Table.

All carotid dissections were classified as at least grade 2b lesions (>70% stenosis with flow limitation) per the Modified Carotid Artery Injury Grading Scale¹⁸ with a minimum lesion length of 3.5 cm (mean 6.7 cm; range 3.5–9 cm) and involved the distal cervical segment; 10/15 dissections extended past the skull base

into the petrous-cavernous segments of the ICA without intracranial extension. Additionally, 5 (33%) patients presented with associated dissecting pseudoaneurysms (grade 3b), and 4 (27%) patients had progressed to an acute cervical carotid occlusion (grade 4), requiring extracranial thromboaspiration in a single case for revascularization across the occluded vessel. Multiple stents were utilized, with a median of 5 stent constructs per patient, including self-expanding peripheral/carotid stents (13/15 patients), coronary balloon-expanding stents (4/15 patients), and self-expanding intracranial stents (12/15 patients) for distal cervical and skull base pathology. Long-segment carotid stent reconstruction was technically successful in all patients with no significant (>50%) residual stenosis/occlusion or flow limitation, immediate reduction in subintimal inflow, and contrast stasis visualized in associated pseudoaneurysms on post-procedure DSA analysis.

Nine patients (60%) also presented with intracranial thromboemboli, either proximal large-vessel ($n = 5$) or distal small-vessel ($n = 4$) occlusions. Additional endovascular intracranial interventions were performed in 6/15 (40%) patients, consisting of IA tPA thrombolysis ($n = 3$) and/or thrombectomy with thromboaspiration ($n = 1$) or stent-retriever ($n = 3$) techniques. TIC1 2b/3 reperfusion was achieved in all patients (100%) post-thrombolysis/thrombectomy and carotid stent reconstruction.

Interventions were relatively safe with procedural complications limited to a single patient (patient 6) developing multifocal thromboembolic infarcts in the left middle cerebral artery distribution secondary to in-stent thrombus. Subsequent clinical deterioration and a poor clinical outcome at discharge resulted in overall procedural morbidity of 1/15 (7%). Although no symptomatic intracranial hemorrhages occurred to suggest reperfusion complications, a left temporal lobe intraparenchymal hemorrhage without neurologic sequelae was consistent with hemorrhagic infarct conversion (HI-2 grade by ECASS criteria) on follow-up CT head studies. There was no procedure-related mortality at discharge or at 90-day follow-up.

Rapid improvement in post-procedural clinical outcomes was observed from a mean NIHSS score of 15 ± 8 on admission to NIHSS 6 ± 5 on discharge. On clinical follow-up, most patients obtained further functional independence from a median mRS of 2 at discharge to an mRS 1 at 90-day follow-up, with 9/15 patients (60%) achieving an mRS of ≤ 2 at discharge and 90-day follow-up as noted in the On-line Table. There were no interval recurrent ischemic symptoms, TIAs, or strokes during the course of clinical follow-up.

Follow-up carotid Doppler ultrasound and CTA/DSA studies at 3–6 months were available in 14/15 patients, with 12 patients demonstrating stent patency, complete restoration of carotid artery caliber, and no evidence of in-stent thrombosis or significant stenosis. Two patients exhibited either mild persisting vessel irregularity/tapering or intimal hyperplasia causing <20% segmental in-stent stenosis. In addition, no new or persisting carotid pseudoaneurysms were identified, with interval thrombolysis/healing of dissecting aneurysms in all 5 patients, suggesting successful stent-associated flow diversion and intimal flap reconstruction.

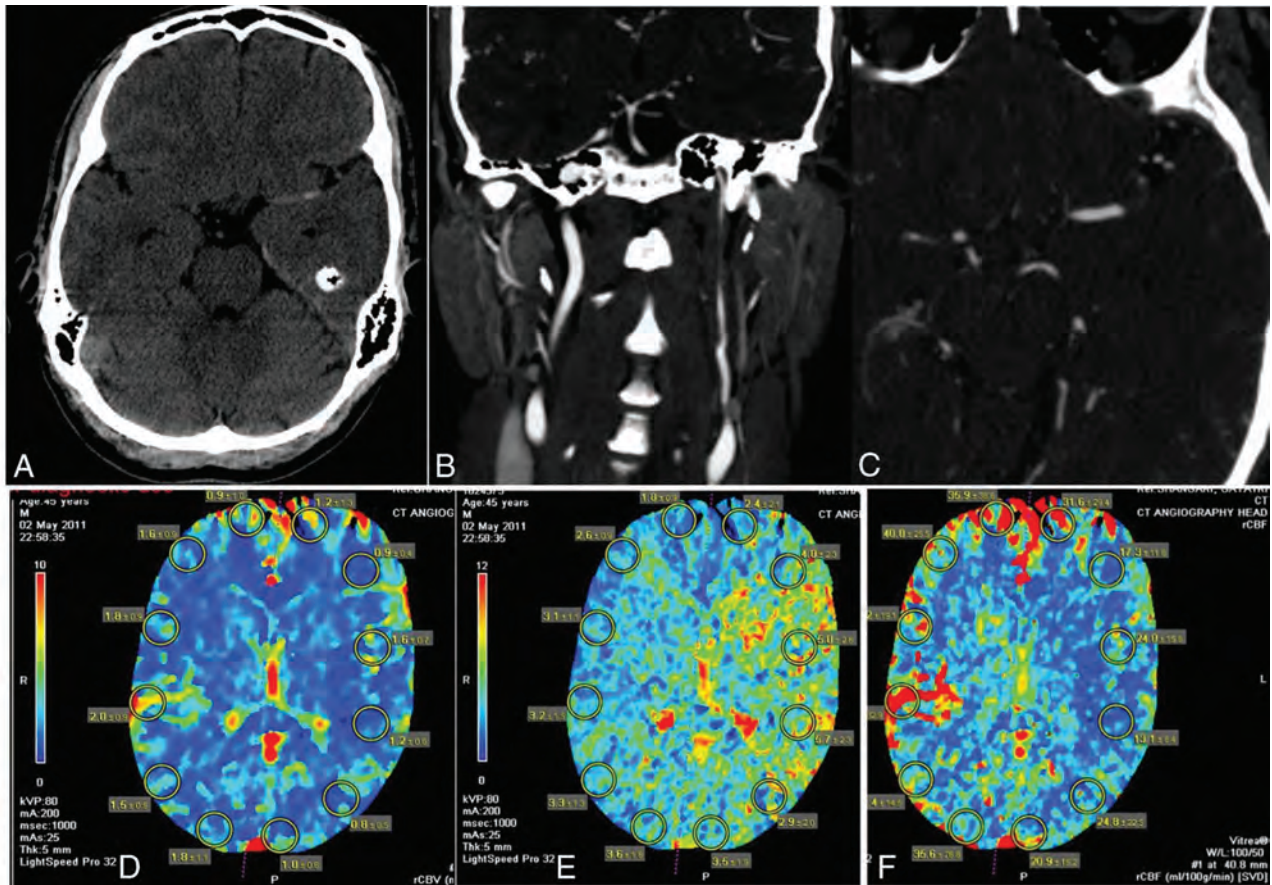


FIG 1. Illustrative case (patient 13). A, NCCT axial image demonstrates no large regional infarction or intracranial hemorrhage, but a hyperdense left MCA sign suggestive of a large vessel occlusion. Coronal (B) and axial (C) CTA head/neck images demonstrate a long-segment left ICA dissection involving the proximal cervical-to-horizontal petrous segment with an associated distal M1 segment left MCA occlusion. D, CT brain perfusion study with preserved relative cerebral blood volume, markedly elevated relative mean transit time (E), and mildly decreased relative cerebral blood flow (F), consistent with severe hemodynamic impairment and hypoperfusion-related ischemia in the left cerebral hemisphere.

Illustrative Case

A 45-year-old man (patient 13) presented to the emergency department with acute onset of aphasia, right hemineglect, hemiparesis, and left-sided gaze deviation with an NIHSS score of 20. CT/CTA studies identified a 9-cm-long-segment left ICA dissection from the carotid bifurcation to the petrous segment and a distal thromboembolic occlusion of the left M1 segment (Fig 1A–C). CT brain perfusion studies confirmed a large left hemispheric perfusion abnormality, suggesting an ischemic penumbra and salvageable tissue (Fig 1D, –F). Following IV tPA infusion with no neurologic improvement, the patient was placed under general anesthesia in the neurointerventional suite with hemodynamic vasopressor support to augment pial collaterals. Following 6F guide sheath placement in the left common carotid artery, DSA studies confirmed a severe >80% flow-limiting cervical left ICA dissection and distal M1 segment thromboembolus/ELVO (Fig 2A, –B). A Penumbra aspiration coaxial catheter system (Penumbra, Alameda, California) was advanced over a Transend EX 0.014-inch microwire (Stryker), which enabled access across the true lumen of the ICA dissection into the M1 segment of the left MCA, confirmed on intermittent microcatheter angiograms (Fig 2C). Intra-arterial tPA (5 mg) infusion and mechanical thrombectomy with vacuum aspiration techniques resulted in complete recanalization of the left MCA distribution

consistent with TIC1 2b reperfusion. Since the long-segment left ICA dissection remained at risk for re-thrombosis/occlusion due to persisting flow limitation despite intracranial thrombectomy (Fig 2D), we initiated tandem and partially overlapping stent reconstruction of the left ICA from the petrocavernous junction to the proximal cervical segment (Fig 2E–G).

The patient received eptifibatid 10.8 mg intravenously during carotid vessel wall reconstruction. With deployment of multiple tandem intracranial and carotid stents, the left ICA normalized in caliber with no evidence of a residual intimal flap, pseudoaneurysm, in-stent thrombosis/stenosis, or flow limitation into the intracranial circulation, consistent with TIC1 3 reperfusion. After a post-procedure CT head study excluded reperfusion hemorrhage or hemorrhagic infarct conversion, the patient was loaded with dual-antiplatelet therapy (aspirin 325 mg and clopidogrel 600 mg). The patient made an excellent neurologic recovery with a discharge NIHSS score of 0 and functionally independent clinical outcome with a discharge and 90-day mRS 0.

DISCUSSION

We present a rare series of long-segment and flow-limiting carotid artery dissections with or without associated ELVO, presenting as a primary AIS etiology and requiring endovascular stent reconstruction with multiple stents due to hemodynamic

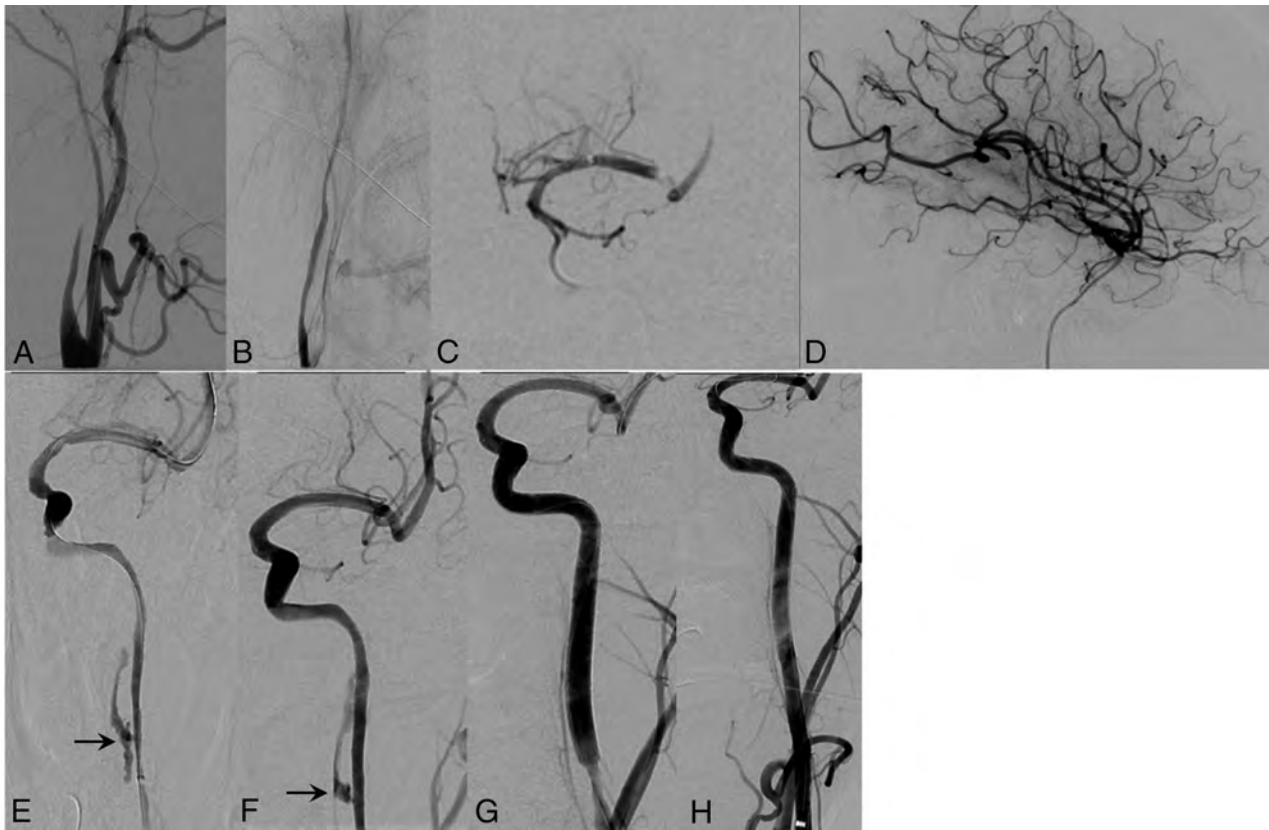


FIG 2. Illustrative case (patient 13). *A* and *B*, Lateral DSA images demonstrate a tapered and severely narrowed left ICA dissection with flow limitation that extends across the cervical segment into the skull base. *C*, Anteroposterior DSA image of an aspiration thrombectomy catheter navigated across the left ICA cervical dissection and placed just proximal to the M1 segment thromboembolus. *D*, Lateral DSA image demonstrates successful thrombolysis/thrombectomy, resulting in complete recanalization and eventual TICI 3 reperfusion of the left MCA distribution. *E–H*, Serial anteroposterior DSA images demonstrate stent reconstruction of the long-segment left ICA dissection after MCA thrombectomy, distal to the petrocavernous junction into the proximal cervical left ICA, resulting in near-normal vessel caliber, with no residual stenosis or flow limitation. Note spontaneous thrombosis of the carotid pseudoaneurysm (*arrow*) and no residual subintimal contrast in the midcervical segment after stent-induced apposition of the intimal flap.

insufficiency. We performed adjunctive IA thrombolysis/thrombectomy in 40% of patients with tandem intracranial ELVO, and all patients achieved >TICI 2b reperfusion on the final angiographic assessment. Low complication, symptomatic intracranial hemorrhage, and morbidity (7%) rates translated into favorable clinical outcomes (60%, mRS \leq 2). Although not always necessary as noted in prior studies,^{15,16} stent reconstruction can salvage acutely occluded carotid dissections and confer an ability to navigate larger guide or intermediate catheters for the management of associated extra- and intracranial ELVOs. Moreover, re-establishing robust cervical antegrade flow can be inherently thrombolytic for small-vessel intracranial occlusions, prevent recurrent thromboemboli or reocclusion after successful cervical recanalization/intracranial thrombectomy, and provide hemodynamic augmentation to pial collaterals supplying any residual ischemic tissue. Even in the absence of ELVO or distal small intracranial thromboemboli (40% of patients in our study), severe flow-limiting cervical dissections without adequate circle of Willis or pial collateral supply can present with profound hypoperfusion-related ischemia, requiring emergent endovascular stent reconstruction and cerebral reperfusion to salvage the ischemic penumbra.

Multiple published studies have described internal carotid ar-

tery stent placement for the endovascular management of complicated dissections for various indications and using multiple stents to treat long-segment cervical dissections,^{21–23} but the maximum number of stents or the length of the dissection pathology was not reported. Biondi et al²⁴ and Coric et al²⁵ also had individual case reports about treating complicated long-segment carotid dissections with multiple stents, presenting with refractory ischemic symptoms after the failure of medical management. In our series, we did not use a precise definition of “long-segment” but included dissections that required the use of multiple (\geq 3) tandem stents to cover the entire dissection flap, which nearly always involved the distal cervical segment of the ICA. Therefore, we selected severely symptomatic, flow-limiting dissections (>2b Modified Carotid Artery Injury Grading Scale) that required emergent intervention. Additionally, these lesions presented with characteristic long-segment (>3.5 cm) and distal cervical/skull base involvement of the vessel wall, perhaps due to unrestrained subintimal extension or spiral dissection. Recent developments in intravascular ultrasound optical coherence tomography, and high-resolution, vessel wall MR imaging techniques may improve the cross-sectional assessment of intramural pathology for more accurate diagnosis and treatment planning.^{26,27}

Furthermore, we limited our study to flow-limiting carotid

dissections that presented with severe, acute ischemic symptoms (mean NIHSS score of 15) within <12 hours from symptom onset, requiring emergent multiple tandem stent reconstructions with or without adjunctive IA thrombolysis/thrombectomy. Other than a few case reports,^{28,29} limited series have been published to suggest the technical and clinical efficacy of stent placement in cervical dissections in the AIS setting. In the larger traumatic carotid dissection series by Cohen et al,²³ 14/23 patients presented with AIS and underwent carotid stent placement with 16/23 patients having severe or flow-limiting dissections (subocclusive grade IV/occlusive grade V). Although they reported excellent clinical outcomes (92.3%, mRS 0–3 at 90 days), this series focused on traumatic carotid dissections, a separate pathology with often delayed presentations, unclear intervention times from symptom onset (<17 hours) in the AIS subgroup, and only 2 patients with ELVO that required tandem IA thrombolysis/thrombectomy.²³ Lavallée et al¹⁷ compared 6 patients with tandem ICA/MCA occlusions who underwent endovascular stent placement of underlying carotid dissections and intracranial mechanical thrombectomy versus 4 patients who received IV tPA alone. Endovascular treatment was associated with markedly improved ICA/MCA recanalization rates and correlated directly with independent functional outcomes, mRS 0–2 (100% versus 25%). Fields et al¹⁶ reported a small cohort of 8 ICA and 1 vertebral artery dissections and tandem intracranial occlusions from the mechanical thrombectomy Merci registry, but carotid/vertebral stent placement was needed in only 5/9 patients. This relatively young cohort (mean age, 48 years) obtained 60% TIC1 >2b reperfusion rates, without significant complications or symptomatic intracerebral hemorrhage, and excellent clinical outcomes (80%, mRS ≤ 2). More recently, Marnat et al¹⁵ reported their experience with 20/258 patients (7.6%) from the prospective RECAST (Prognostic Factors Related to Clinical Outcome Following Thrombectomy in Ischemic Stroke) Study, who presented with tandem carotid artery dissections and anterior circulation ELVOs with severe AIS (mean NIHSS score 17) within 6 hours of symptom onset. In comparison to patients with isolated ELVO, they identified a statistically younger population; prolonged interventional procedure times; no difference in TIC1 2b/3 recanalization, complications, or symptomatic intracerebral hemorrhage rates; and equivalent-to-better clinical outcomes (70%, mRS ≤ 2) in this cohort. However, 15/20 (75%) carotid dissections were managed medically in this series with no need for endovascular stent reconstruction after angiographic confirmation of an adequate circle of Willis (anterior/posterior communicating arteries) and <2-second venous phase delay in the affected cerebral hemisphere.¹⁵

Multiple case reports and case series have demonstrated the successful technical use of self-expanding carotid or peripheral stents and covered stent grafts in the endovascular reconstruction of cervical dissections and dissecting aneurysms. In fact, after stent realignment of the intimal flap, acute dissecting aneurysms will often undergo spontaneous thrombosis due to flow diversion and reduced inflow into the false aneurysm lumen, as observed in all 5 associated pseudoaneurysms in our series. Long-segment carotid dissections may extend into the distal cervical, petrocavernous, and even intracranial segments, requiring off-label applica-

tions of lower profile balloon-expanding coronary stents or flexible/navigable self-expanding intracranial stents, as seen in nearly all our patients.³⁰ Although intracranial stents are highly trackable and accommodating to the tortuous distal cervical vasculature with adequate radial force for the treatment of cervical dissections, this application is considered an off-label use of an HDE device, requiring institutional review board and manufacturer notification. Alternatively, balloon-expanding coronary stents can be advantageous in severe dissection-related stenoses with focal intramural hemorrhage, spiral dissections, or in the constrained osseous compartment of the petrous carotid canal, provide greater angioplasty-dependent radial force and precise placement for vessel reconstruction. Mechanical thrombectomy of tandem ICA–MCA occlusions has been described by several authors, including a proximal-to-distal approach with carotid stent placement to re-establish antegrade flow and access to the intracranial circulation for thrombectomy.^{9–14} Despite this being necessary in acutely occluded or severe atherosclerotic carotid stenoses, acute cervical dissections can usually be traversed with distal-access catheter technology to target distal ELVOs, first with either direct aspiration and/or stent-retriever thrombectomy for rapid cerebral reperfusion. In our experience, the use of proximal balloon-guide catheters was deferred in preference to lower profile and distal-access aspiration catheters with or without stent retrievers to prevent further injury to the cervical carotid wall during thrombectomy. Subsequently, tandem stent reconstruction of cervical dissections was performed as described from a distal-to-proximal approach, maintaining access across the true lumen and securing the distal extension of the flap to the proximal inflow zone.

Although stent reconstruction of long-segment cervical lesions avoids anticoagulation use in the AIS setting, dual antiplatelet therapy is mandatory with preoperative or intraoperative loading preferred to prevent intraprocedural in-stent thromboembolic/occlusion complications. Deployment of multiple tandem stents with extensive vessel wall exposure to foreign metallic material increases the risk of platelet aggregation and thromboemboli. However, even antiplatelets may be contraindicated or used with trepidation in the AIS setting after IV tPA thrombolysis and/or mechanical thrombectomy, especially if there is a high risk of reperfusion hemorrhage or hemorrhagic infarct transformation. We used several different antiplatelet strategies in this precarious setting, but in a few patients, we provided an intravenous glycoprotein IIb/IIIa inhibitor (eptifibatide, 0.18 mg/kg) during carotid stent reconstruction. Several advantages of IIb/IIIa inhibitors include immediate antiplatelet protection without the need for oral aspirin/clopidogrel loading and a reduced time to reach peak platelet inhibition (minutes versus hours depending on dose and class of oral thienopyridines). As a reversible competitive inhibitor with a short half-life, eptifibatide rapidly decays with normalizing platelet function over hours, providing time to initiate aspirin/clopidogrel loading or terminate antiplatelet therapy if hemorrhagic complications are suspected. If CT head findings are equivocal or concerning, clopidogrel loading can be delayed until a repeat follow-up CT head study definitively excludes evolving intracranial hemorrhage. New dual-energy CT applications may assist with the ear-

lier diagnosis of contrast staining versus hemorrhagic infarct transformation after endovascular stroke interventions; hence, allowing confident initiation of dual-antiplatelet therapy and protection from stent-related thromboembolic complications in the AIS setting.³¹

Our study had several limitations as a retrospective and non-randomized study of a small cohort that lacked a control population for comparison. Variable carotid stent placement protocols, equipment preferences, and antiplatelet management could not be standardized in our study design. However, severe flow-limiting and long-segment carotid dissections are rare pathologies in the setting of AIS, and it would be difficult to conduct a large cohort study without multicenter involvement. Even the Merci registry of 980 patients yielded only 5 patients with cervical dissections requiring stent reconstruction with intracranial thrombectomy.¹⁶ Furthermore, severe acute presentations in this population warrant intervention, at least for associated intracranial ELVO and hypoperfusion-related ischemia at risk for infarction in the absence of sufficient intracranial collaterals. However, if sufficient flow across an acute cervical dissection is re-established after ELVO thrombectomy or adequate intracranial collaterals are present with a neurologic response and symptomatic improvement, this population could potentially be studied, comparing emergent stent reconstruction versus conservative medical management using an early transition to anticoagulation therapy.

CONCLUSIONS

In this series, we demonstrate the technical feasibility, safety, and clinical efficacy of multiple tandem stents to reconstruct long-segment and flow-limiting carotid dissections presenting in the AIS setting. As an independent or adjunctive methodology to IA thrombolysis/thrombectomy, it is a valuable technique in AIS intervention. Carotid stent reconstruction of severe flow-limiting dissections may prevent further dissection propagation, carotid occlusion, recurrent thromboembolic complications, and/or perfusion-dependent ischemia/infarction. Although midterm technical and clinical efficacy is promising, diligent antiplatelet management and further validation with larger multicenter studies and long-term outcome assessment are required.

Disclosures: Muhib Khan—UNRELATED: Other: Women's Health Initiative, Comments: stroke-outcome adjudication. Michael C. Hurley—UNRELATED: Payment for Lectures including Service on Speakers Bureaus: Penumbra. Matthew J. Gounis—UNRELATED: Consultancy: Codman Neurovascular, Stryker Neurovascular; Grants/Grants Pending: National Institutes of Health, Asahi Intecc, Blockade Medical, CereVasc LLC, Codman Neurovascular, Cook, Gentuity LLC, Fraunhofer Institute, InNeuroCo Inc, Lazarus Effect, Medtronic Neurovascular, MicroVention/Terumo, Neuravi, Philips Healthcare, Stryker Neurovascular, Wyss Institute for Biologically Inspired Engineering*; Stock/Stock Options: InNeuroCo. Ajay K. Wakhloo—UNRELATED: Consultancy: Stryker Neurovascular, Codman Neurovascular, Philips Healthcare; Expert Testimony: McCoy LLC, Coral Gables, Florida, Comments: expert testimony for defendant physician; Grants/Grants Pending: Philips Healthcare, Comments: equipment grant*; Payment for Lectures including Service on Speakers Bureaus: Harvard Postgraduate Course, Miami Vascular Institute; Stock/Stock Options: InNeuroCo, Penumbra; Other: Pulsar Vascular Comments: bridge loan. Ajit S. Puri—UNRELATED: Consultancy: Stryker Neurovascular, Medtronic, Codman, Comments: proctor for Stryker and Medtronic; Grants/Grants Pending: Stryker Neurovascular and Medtronic*; Stock/Stock Options: InNeuroCo. *Money paid to the institution.

REFERENCES

1. Bogousslavsky J, Regli F. Ischemic stroke in adults younger than 30 years of age. Cause and prognosis. *Arch Neurol* 1987;44:479–82 CrossRef Medline
2. Schievink WI. Spontaneous dissection of the carotid and vertebral arteries. *N Engl J Med* 2001;344:898–906 CrossRef Medline
3. Lucas C, Moulin T, Deplanque D, et al. Stroke patterns of internal carotid artery dissection in 40 patients. *Stroke* 1998;29:2646–48 CrossRef Medline
4. Engelter ST, Lyrer PA, Kirsch EC, et al. Long-term follow-up after extracranial internal carotid artery dissection. *Eur Neurol* 2000;44:199–204 CrossRef Medline
5. Schievink WI. The treatment of spontaneous carotid and vertebral artery dissections. *Curr Opin Cardiol* 2000;15:316–21 CrossRef Medline
6. Berkhemer OA, Fransen PS, Beumer D, et al. A randomized trial of intraarterial treatment for acute ischemic stroke. *N Engl J Med* 2015;372:11–20 CrossRef Medline
7. Jovin TG, Chamorro A, Cobo E, et al; REVASCAT Trial Investigators. Thrombectomy within 8 hours after symptom onset in ischemic stroke. *N Engl J Med* 2015;372:2296–306 CrossRef Medline
8. Goyal M, Demchuk AM, Menon BK, et al; ESCAPE Trial Investigators. Randomized assessment of rapid endovascular treatment of ischemic stroke. *N Engl J Med* 2015;372:1019–30 CrossRef Medline
9. Stampfl S, Ringleb PA, Möhlenbruch M, et al. Emergency cervical internal carotid artery stenting in combination with intracranial thrombectomy in acute stroke. *AJNR Am J Neuroradiol* 2014;35:741–46 CrossRef Medline
10. Cohen JE, Gomori JM, Rajz G, et al. Extracranial carotid artery stenting followed by intracranial stent-based thrombectomy for acute tandem occlusive disease. *J Neurointerv Surg* 2015;7:412–17 CrossRef Medline
11. Matsubara N, Miyachi S, Tsukamoto N, et al. Endovascular intervention for acute cervical carotid artery occlusion. *Acta Neurochir (Wien)* 2013;155:1115–23 CrossRef Medline
12. Papanagiotou P, Roth C, Walter S, et al. Carotid artery stenting in acute stroke. *J Am Coll Cardiol* 2011;58:2363–69 CrossRef Medline
13. Malik AM, Vora NA, Lin R, et al. Endovascular treatment of tandem extracranial/intracranial anterior circulation occlusions: preliminary single-center experience. *Stroke* 2011;42:1653–57 CrossRef Medline
14. Spiotta AM, Lena J, Vargas J, et al. Proximal to distal approach in the treatment of tandem occlusions causing an acute stroke. *J Neurointerv Surg* 2015;7:164–69 CrossRef Medline
15. Marnat G, Mourand I, Eker O, et al. Endovascular management of tandem occlusion stroke related to internal carotid artery dissection using a distal to proximal approach: insight from the RECAST Study. *AJNR Am J Neuroradiol* 2016;37:1281–88 CrossRef Medline
16. Fields JD, Lutsep HL, Rymer MR, et al; Merci Registry Investigators. Endovascular mechanical thrombectomy for the treatment of acute ischemic stroke due to arterial dissection. *Interv Neuroradiol* 2012;18:74–79 Medline
17. Lavallée PC, Mazighi M, Saint-Maurice JP, et al. Stent-assisted endovascular thrombolysis versus intravenous thrombolysis in internal carotid artery dissection with tandem internal carotid and middle cerebral artery occlusion. *Stroke* 2007;38:2270–74 CrossRef Medline
18. Seth R, Obuchowski AM, Zoarski GH. Endovascular repair of traumatic cervical internal carotid artery injuries: a safe and effective treatment option. *AJNR Am J Neuroradiol* 2013;34:1219–26 CrossRef Medline
19. North American Symptomatic Carotid Endarterectomy Trial Collaborators. Beneficial effect of carotid endarterectomy in symptomatic patients with high-grade carotid stenosis. *N Engl J Med* 1991;325:445–53 CrossRef Medline
20. Larrue V, von Kummer RR, Müller A, et al. Risk factors for severe hemorrhagic transformation in ischemic stroke patients treated with recombinant tissue plasminogen activator: a secondary anal-

- ysis of the European-Australasian Acute Stroke Study (ECASS II). *Stroke* 2001;32:438–41 Medline
21. Bejjani GK, Monsein LH, Laird JR, et al. **Treatment of symptomatic cervical carotid dissections with endovascular stents.** *Neurosurgery* 1999;44:755–60; discussion 760–61 CrossRef Medline
 22. Malek AM, Higashida RT, Phatouros CC, et al. **Endovascular management of extracranial carotid artery dissection achieved using stent angioplasty.** *AJNR Am J Neuroradiol* 2000;21:1280–92 Medline
 23. Cohen JE, Gomori JM, Itshayek E, et al. **Single-center experience on endovascular reconstruction of traumatic internal carotid artery dissections.** *J Trauma Acute Care Surg* 2012;72:216–21 CrossRef Medline
 24. Biondi A, Katz JM, Vallabh J, et al. **Progressive symptomatic carotid dissection treated with multiple stents.** *Stroke* 2005;36:e80–82 CrossRef Medline
 25. Coric D, Wilson JA, Regan JD, et al. **Primary stenting of the extracranial internal carotid artery in a patient with multiple cervical dissections: technical case report.** *Neurosurgery* 1998;43:956–59 CrossRef Medline
 26. Swartz RH, Bhuta SS, Farb RI, et al. **Intracranial arterial wall imaging using high-resolution 3-Tesla contrast-enhanced MRI.** *Neurology* 2009;72:627–34 CrossRef Medline
 27. Xu P, Lv L, Li S, et al. **Use of high-resolution 3.0-T magnetic resonance imaging to characterize atherosclerotic plaques in patients with cerebral infarction.** *Exp Ther Med* 2015;10:2424–28 Medline
 28. Chen M. **Mechanical recanalization of acute carotid terminus occlusion from traumatic arterial dissection.** *Front Neurol* 2010;1:123 CrossRef Medline
 29. Yu W, Binder D, Foster-Barber A, et al. **Endovascular embolectomy of acute basilar artery occlusion.** *Neurology* 2003;61:1421–23 CrossRef Medline
 30. Ansari SA, Thompson BG, Gemmete JJ, et al. **Endovascular treatment of distal cervical and intracranial dissections with the Neuroform stent.** *Neurosurgery* 2008;62:636–46; discussion 636–46 CrossRef Medline
 31. Phan CM, Yoo AJ, Hirsch JA, et al. **Differentiation of hemorrhage from iodinated contrast in different intracranial compartments using dual-energy head CT.** *AJNR Am J Neuroradiol* 2012;33:1088–94 CrossRef Medline

Treatment of Intra- and Extracranial Aneurysms Using the Flow-Redirection Endoluminal Device: Multicenter Experience and Follow-Up Results

F. Drescher, W. Weber, A. Berlis, S. Rohde, A. Carolus, and S. Fischer

ABSTRACT

BACKGROUND AND PURPOSE: Flow diversion emerged as a crucial treatment option for intracranial aneurysms. We report a multicenter retrospective analysis of the safety and efficacy in the treatment of intracranial aneurysms with the Flow-Redirection Endoluminal Device (FRED) flow diverter, a dual-layer flow-modulation device.

MATERIALS AND METHODS: All intracranial aneurysms treated with the FRED between March 2013 and February 2016 at 4 neurovascular centers were included. Angiographic and clinical results were retrospectively analyzed, including all follow-up examinations. Aneurysms were unruptured in 44 cases, whereas 8 treatments were due to an acute SAH from the target aneurysm.

RESULTS: Successful implantation of the FRED was possible in 96.2% (50/52) of cases. At 3-month follow-up, complete occlusion was determined in 58.1% (25/43) and near-complete in 25.6% (11/43). At 12-month follow-up, aneurysm occlusion was complete in 75.0% (27/36) and near-complete in 22.2% (8/36). The overall acute and late thromboembolic and hemorrhagic complication rate was 17.3% (9/52), with a permanent treatment-related morbidity and mortality of 4.0% (2/50) and 2.0% (1/50), respectively, to date.

CONCLUSIONS: The FRED device offers an effective tool in the treatment of intracranial aneurysms. The dual-layer design promotes contemporary and stable long-term occlusion rates. Sufficient device expansion should be documented by angiographic CT. Further studies might help to identify a more optimal antiplatelet regimen to avoid thromboembolic complications during the follow-up period.

ABBREVIATIONS: FRED = Flow-Redirection Endoluminal Device; PED = Pipeline Embolization Device

The concept of flow diversion has been proved an effective method in the treatment of broad-based, fusiform, and small intracranial aneurysms.¹⁻⁴ The most common flow diverters, such as the Pipeline Embolization Device (PED/PED flex; Covidien, Irvine, California), the Silk/Silk+ (Balt Extrusion, Montmorency, France), or the Surpass stent (Stryker Neurovascular, Kalamazoo, Michigan) are single-layer self-expanding devices

with low porosity (proportion of metal-free area to total surface area) compared with conventional stents.

In this retrospective study, we analyzed the clinical and angiographic results of 52 intra- and extracranial aneurysms treated with the only available dual-layer flow diverter (Flow-Redirection Endoluminal Device [FRED]; MicroVention, Tustin, California) at 4 neurovascular centers.

MATERIALS AND METHODS

Flow-Redirection Endoluminal Device

The FRED is a braided stent-in-stent device composed of an inner closed-cell stent (48 nitinol wires) with low porosity and an outer mesh with higher porosity (16 nitinol wires). The proximal and distal ends of the device are composed of the single-layer mesh of the outer stent, whereas the middle part of the device (80%) consists of the dual-layer structure. The fluoroscopic visibility results from 4 radiopaque markers at the distal and proximal ends and 2 interwoven helical marker strands delineating the dual-layer section of the device (Fig 1). The FRED is available in 5 nominal diameters (3.5, 4.0, 4.5, 5.0, and 5.5 mm) recommended for vessel diameters from 3.0 to 5.5 mm. It is mounted on a microwire with a distal and proximal radiopaque marker. A resheathing of the

Received May 31, 2016; accepted after revision August 16.

From the Knappschafts Krankenhaus Bochum (F.D., W.W., S.F.), Universitätsklinik, Institut für Diagnostische und Interventionelle Radiologie, Neuroradiologie, Nuklearmedizin, Bochum, Germany; Knappschafts Krankenhaus Recklinghausen Klinik für Radiologie Neuroradiologie und Nuklearmedizin (W.W.), Recklinghausen, Germany; Klinikum Augsburg (A.B.), Klinik für Diagnostische Radiologie und Neuroradiologie, Augsburg, Germany; Klinikum Dortmund (S.R.), Klinik für Radiologie und Neuroradiologie, Dortmund, Germany; and Knappschafts Krankenhaus Bochum (A.C.), Universitätsklinik, Klinik für Neurochirurgie, Bochum, Germany.

Preliminary data from this series was previously presented at: Annual Meeting of the German Society of Neuroradiology, October 15–17, 2015; Cologne, Germany.

Please address correspondence to Sebastian Fischer, MD, Knappschafts Krankenhaus Bochum, Universitätsklinik, Institut für Diagnostische und Interventionelle Radiologie, Neuroradiologie, Nuklearmedizin, In der Schornau 23–25, 44892 Bochum, Germany; e-mail: sebif101@googlemail.com

<http://dx.doi.org/10.3174/ajnr.A4964>

Table 1: Inclusion and exclusion criteria for treatment with FRED

Criteria
In favor of treatment with FRED
Intradural incidental aneurysm
Intradural or extradural symptomatic aneurysm (mass effect)
Supposed difficulty for coil treatment alone (dome-to-neck ratio of <1.2, broad-based aneurysm, fusiform morphology, blisterlike shape)
Difficulty or impossibility of neurosurgical clip placement due to aneurysm morphology or anatomic location
Acutely ruptured aneurysms without any alternative neurosurgical or endovascular treatment option
Aneurysm remnant or reperfusion after endovascular or microsurgical treatment
Documented response to medicamentous platelet function inhibition
Exclusion for treatment with FRED
Intradural aneurysm with a definable neck
Intradural bifurcation aneurysm
Documented nonresponse to medicamentous platelet function inhibition
Patient preference for alternative treatment options
Patient preference against any treatment

Table 2: Summary of the locations of the treated aneurysms

Location	Aneurysms (No.)	Ratio
Anterior circulation (<i>n</i> = 39; 75.0%)		
ICA cervical	8	15.4%
ICA cavernous	3	5.8%
ICA paraophthalmic	21	40.5%
ICA Pcom	3	5.8%
ACA	2	3.8%
MCA	2	3.8%
Posterior circulation (<i>n</i> = 13; 25.0%)		
BA	2	3.8%
VA V4	9	17.3%
PCA	2	3.8%
Total	52	100.0%

Note:—ACA indicates anterior cerebral artery; BA, basilar artery; VA, vertebral artery; PCA, posterior cerebral artery; Pcom, posterior communicating; MCA, middle cerebral artery.

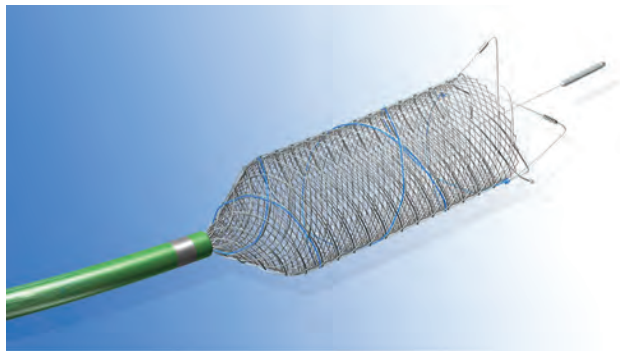


FIG 1. Dual-layer structure of the FRED. The fluoroscopic visibility results from 2 interwoven helical marker strands delineating the dual-layer section (working length) and 4 radiopaque markers at the flared ends.

device is possible as long as 20% of the device remains unsheathed from the 0.027-inch microcatheter (point of no return). An undersized device results in an abatement of porosity with a distinct shortening and insufficient coverage of the vessel wall. An oversized device decreases the hemodynamic effect correspondingly.

Selection Criteria, Patient Population, and Clinical Presentation

This retrospective study was approved by the institutional ethics committee. All patients, apart from those with an acute SAH, were

informed of the treatment strategy, including all potential alternatives.

The decision for the endovascular treatment with the FRED resulted from a constantly performed interdisciplinary neurovascular conference at the participating centers. Table 1 summarizes the inclusion and exclusion criteria. On the basis of these criteria, 50 patients (40 women, 10 men; mean age, 56 years; range, 20–80 years) with 52 aneurysms were included. The clinical condition of each patient was measured according to the mRS before the procedure, at discharge, and after 3 and 12 months.⁵ Thirty patients were asymptomatic before the procedure, 12 patients had an mRS of 1 or 2 caused by the target aneurysm, and 8 patients had an mRS of >2 caused by an acute rupture from the aneurysm.

and 8 patients had an mRS of >2 caused by an acute rupture from the aneurysm.

Aneurysm Characteristics, Morphology, and Location

Of the 52 aneurysms included, 23 were incidental findings, 8 were ruptured (SAH within 5 days before the procedure), and 12 caused symptoms of mass effect. Three were remnants of clipped or wrapped aneurysms, 2 were previously coiled, and 4 were pretreated with other devices (p64; phenox, Bochum, Germany, *n* = 2; Woven EndoBridge [WEB] aneurysm embolization system; Sequent Medical, Aliso Viejo, California, *n* = 1; stent-assisted coiling, *n* = 1). The series comprises 30 saccular and 21 fusiform aneurysms and 1 blisterlike aneurysm. Forty-four aneurysms were located intradurally compared with 8 extradural locations. Table 2 indicates the locations of the treated aneurysms in detail.

The median fundus size of all saccular aneurysms was 5.0 mm (range, 2.0–35.0 mm) with a median neck width of 4.0 mm (range, 2.0–20.0 mm).

Endovascular Procedure

All procedures were performed by 5 experienced operators on a biplane DSA unit. A coaxial 8F/6F guiding/intermediate catheter system was navigated into the target artery. The microcatheter was placed distal to the aneurysm at the intended distal landing zone.

Size selection of the flow diverter was based on calibrated measurements of the artery distal and proximal to the aneurysm. The largest diameter of the landing zones was used as a direct reference for the nominal diameter of the device. Once the flow diverter was pushed through the microcatheter to a position appropriate to cover the aneurysm, deployment resulted from a combination of careful retraction of the microcatheter and adjusted backpressure of the delivery wire (push and pull technique). Proper expansion, sufficient apposition to the vessel wall, and the correct position of the device were monitored under continuous fluoroscopy.

If the treatment was combined with coils, a microcatheter was placed initially (jailing).

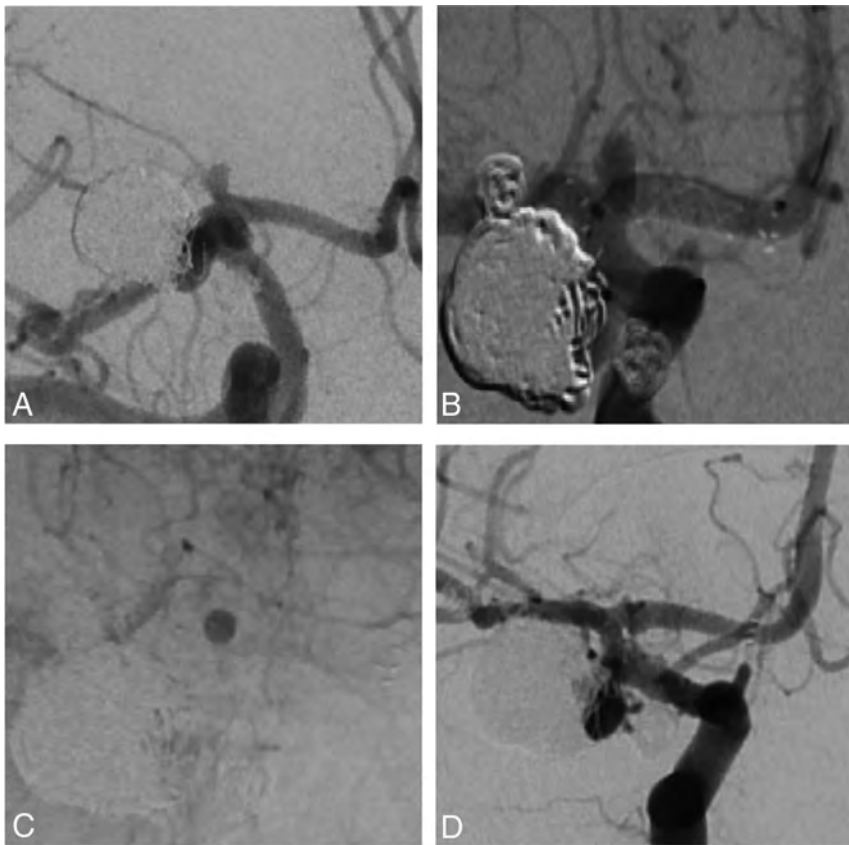


FIG 2. A, A male patient with multiple asymptomatic intracranial aneurysms with a small proximal aneurysm of the A1 segment status post stent-assisted coil occlusion of a distal ICA aneurysm, right oblique and cranial views. B, Placement of a 3.5-/13/7-mm FRED with its flared ends extending toward the ICA bifurcation to cover the aneurysm with the dual-layer part of the device, right oblique and cranial views. C, Stasis of contrast material up to the venous phase, right oblique and cranial views. D, 4-month follow-up angiography with complete occlusion of the aneurysm, right oblique and cranial views.

Anticoagulation/Antiplatelet Regimen

All patients, except for those with ruptured aneurysms, were placed on dual-antiplatelet medication with 100 mg of acetylsalicylic acid and 75 mg of clopidogrel daily at least 5 days before the treatment. Clopidogrel was continued for at least 3 months followed by life-long continuation of acetylsalicylic acid.

The sufficiency was tested by an impedance aggregometry testing method (Multiplate; Roche, Basel, Switzerland). Clopidogrel nonresponders were changed to a loading dose of 180 mg of ticagrelor followed by 90 mg twice daily. The Multiplate test was repeated with rescheduling of the intervention if necessary until a dual-platelet inhibition was clearly ascertained.

Eptifibatide was administered intravenously with a bolus followed by continuous intravenous application for at least 12 hours bridged with a loading dose of 500 mg of acetylsalicylic acid and 300 mg of clopidogrel in ruptured aneurysms. All procedures were performed with the patient under systemic heparinization.

Follow-Up

Clinical and angiographic follow-up examinations were planned after 3 and 12 months according to the institutional standards. The angiographic results were classified as the following: complete occlusion, minor neck remnant, major residual filling, or

unchanged aneurysm filling. The results were independently analyzed by 2 interventional neuroradiologists.⁶

RESULTS

Technical and Immediate

Angiographic Results

Overall, 52 cases were included within the sample period (March 2013 to February 2016) at the participating centers. Centers 1 and 3 included 19 cases, whereas 5 cases were included at center 2, and 9 were from center 4.

Implantation of the FRED was performed as intended in 50/52 cases (96.2%) and failed in 2 cases of ICA aneurysms due to a severe elongation of the target vessel. Although placement of the microcatheter distal to the aneurysm was possible without difficulty, a sufficient opening of the flow diverter was not achieved despite several repositioning maneuvers. Both aneurysms were finally treated by stent-assisted coiling.

In 44 cases, a single device was used (Fig 2). Two were coaxially implanted in 2 cases. In 1 case of a large cavernous ICA aneurysm, a single FRED was combined with 3 Silk flow diverters and 5 Pipeline Embolization Devices (case 26). Arguments in favor of >1 device included an unchanged aneurysm perfusion after the first device or a large incorporation of the

vessel in cases of very wide-neck or fusiform aneurysms.

An incomplete expansion occurred in 4 cases requiring balloon angioplasty. The treatment was combined with coils in 8 cases with the objective of accelerating the process of thrombus formation (Fig 3).

Angiographic Follow-Up Results

The first follow-up angiography was performed in 41/48 patients with 43/50 aneurysms after a median of 3.0 months (range, 1.0–12.0 months). Of the remaining 7 patients, 2 patients died during the early follow-up period as consequence of their preexisting SAH, 4 patients were lost to follow-up, and 1 patient died due to a delayed aneurysm rupture (case 49). To date, a second follow-up angiography is available for 34/48 patients with 36/50 aneurysms, after a median of 12.0 months (range, 2.0–24.0 months).

The complete occlusion rate improved from 58.1% (25/43 cases) at the first angiography to 75.0% (27/36 cases) at the second follow-up examination. A detailed illustration of the results is given in Table 3.

Three cases of asymptomatic moderate-grade in-stent stenosis without hemodynamic relevance were observed during the early follow-up period. Two of these findings remained unchanged during the observational period, whereas the third patient developed an acute in-stent thrombosis 5 months later (case 25).

Clinical Results and Complications

Complications were analyzed at discharge and after 3 and 12 months according to their underlying pathomechanism (thromboembolic or hemorrhagic) and their clinical relevance. Asymptomatic complications were those without any worsening on the mRS grading scale; those with an increase on the mRS scale related to the complication were classified as symptomatic. A summary

of the complications encountered in this series, including the mortality and morbidity, is given in Tables 4 and 5.

The overall mortality and morbidity related to the treatment in the entire series is 2.0% (1/50 patients) and 4.0% (2/50 patients) to date. The mRS score improved or remained unchanged in 94.0% (47/50 patients) and worsened in 6.0% (3/50 patients), related to the treatment.

The overall complication rate most probably related to the treatment was 17.3% (9/52 cases) during the median follow-up of 12 months; 15.4% (8/52) were thromboembolic compared with 1.9% (1/52) hemorrhagic complications. Fortunately, only 2 of the thromboembolic complications resulted in a permanent neurologic deterioration (cases 13 and 25). Both were paraophthalmic ICA aneurysms in patients previously placed on ticagrelor due to a nonresponder status to clopidogrel. One patient experienced a parent artery thrombosis 3 weeks after the intervention with ongoing dual-antiplatelet inhibition, whereas the second thrombosis occurred 5 months after cessation of ticagrelor. These 2 patients were discharged with a clinical deterioration to an mRS of 4.

The remaining 6 cases of parent vessel thrombosis remained clinically asymptomatic or caused transient clinical deficits due to a sufficient collateralization via the circle of Willis in 4 and a successful recanalization in the remaining 2 cases (intra-arterial thrombolysis and balloon angioplasty) (Fig 4). These findings were in patients with continued dual-antiplatelet medication except case 25. All were carotid artery aneurysms treated with 1 FRED, except case 26. This patient was previously treated with 3 Silk and 5 PED flow diverters.

One fatal SAH occurred 19 days after treatment of a large paraophthalmic aneurysm of the ICA with 1 FRED and additional coiling (case 49).

One management-related adverse event without clinical impairment was encountered. This was a mild dissection



FIG 3. A, Finding of a large irregularly shaped aneurysm of the right ICA (posterior communicating segment) in a woman, causing symptoms of mass effect, 3D rotational angiography. B, Placement of a 4.0-/18/12-mm FRED after jailing of a microcatheter. Intra-aneurysmal stasis of contrast material, lateral view. C, Loose coil occlusion of the aneurysm, lateral view. D, Complete occlusion of the aneurysm on 3-month follow-up angiography, lateral view.

Table 3: Occlusion rates at 3- and 12-month follow-up

Occlusion	3-Month Follow-Up	Ratio	12-Month Follow-Up	Ratio
Complete occlusion	25	58.1%	27	75.0%
Minor neck remnant	11	25.6%	8	22.2%
Major residual filling	3	7.0%	1	2.8%
Unchanged filling	4	9.3%	0	0.0%
Total	43	100.0%	36	100.0%

Table 4: Summary of complications during the follow-up period

Adverse Events	At Discharge (n = 52 cases)		3-Month Follow-Up (n = 43 cases)		12-Month Follow-Up (n = 36 cases)	
		Ratio		Ratio		Ratio
Hemorrhagic	0	0.0%	1	2.3%	0	0.0%
Thromboembolic, symptomatic	1	1.9%	0	0.0%	1	2.8%
Thromboembolic, asymptomatic	3	5.7%	2	4.7%	1	2.8%
Total	4	7.6%	3	7.0%	2	5.6%

of the V2 segment of the vertebral artery in a female patient with a fusiform aneurysm of the V4 segment, probably caused by a guidewire injury. The intimal disruption was covered with an Enterprise self-expanding stent (Codman & Shurtleff, Raynham, Massachusetts) without technical difficulty. The patient remained clinically unchanged.

DISCUSSION

In this retrospective multicenter series, we present the angiographic and clinical results with the FRED in the treatment of 52 extra- and intracranial aneurysms. The series comprises ruptured and unruptured aneurysms of different subgroups (eg, saccular, fusiform, and anterior and posterior circulation). The technical success rate of 96.2% and the angiographic results with a complete and near-complete occlusion rate of 97.2% during a median follow-up period of 12.0 months are comparable with or partly superior to those of previously published series concerning flow diversion.^{1-4,7,8}

The rate of morbidity and mortality is within the range

known from previous series. Overall our results demonstrate that FRED is a useful and effective device in the treatment of complex aneurysms. Several technical and clinical aspects require detailed consideration.

Technical Factors of Flow Diversion

The effectiveness of flow diverters depends on 2 characteristics: the porosity, which is defined as the ratio of the metal-free surface to the total surface area, and the pore density, which describes the number of pores per unit of surface area.⁹ The porosity of the FRED is sectionalized due to its dual-layer design in the middle part, with a comparatively low porosity compared with the proximal and distal overlap of the outer stent. This design offers the possibility of placing maximum coverage above the aneurysm with low coverage at the landing zones to preserve side branches. The hemodynamic impact of this design is similar and probably more effective compared with the available single-layer flow diverters.

The flow-diverting effect can be increased by the implantation of multiple flow diverters in a telescoping manner. The initial implantation of >1 device will increase the risk of complications, especially with regard to side branch occlusions and an extended procedure time.¹⁰ Our angiographic results

Table 5: Morbidity and mortality during the follow-up period

	At Discharge (n = 50 patients)		3-Month Follow-Up (n = 41 patients)		12-Month Follow-Up (n = 34 patients)	
		Ratio		Ratio		Ratio
Morbidity	1	2.0%	0	0.0%	1	2.0%
Mortality	0	0.0%	1	2.0%	0	0.0

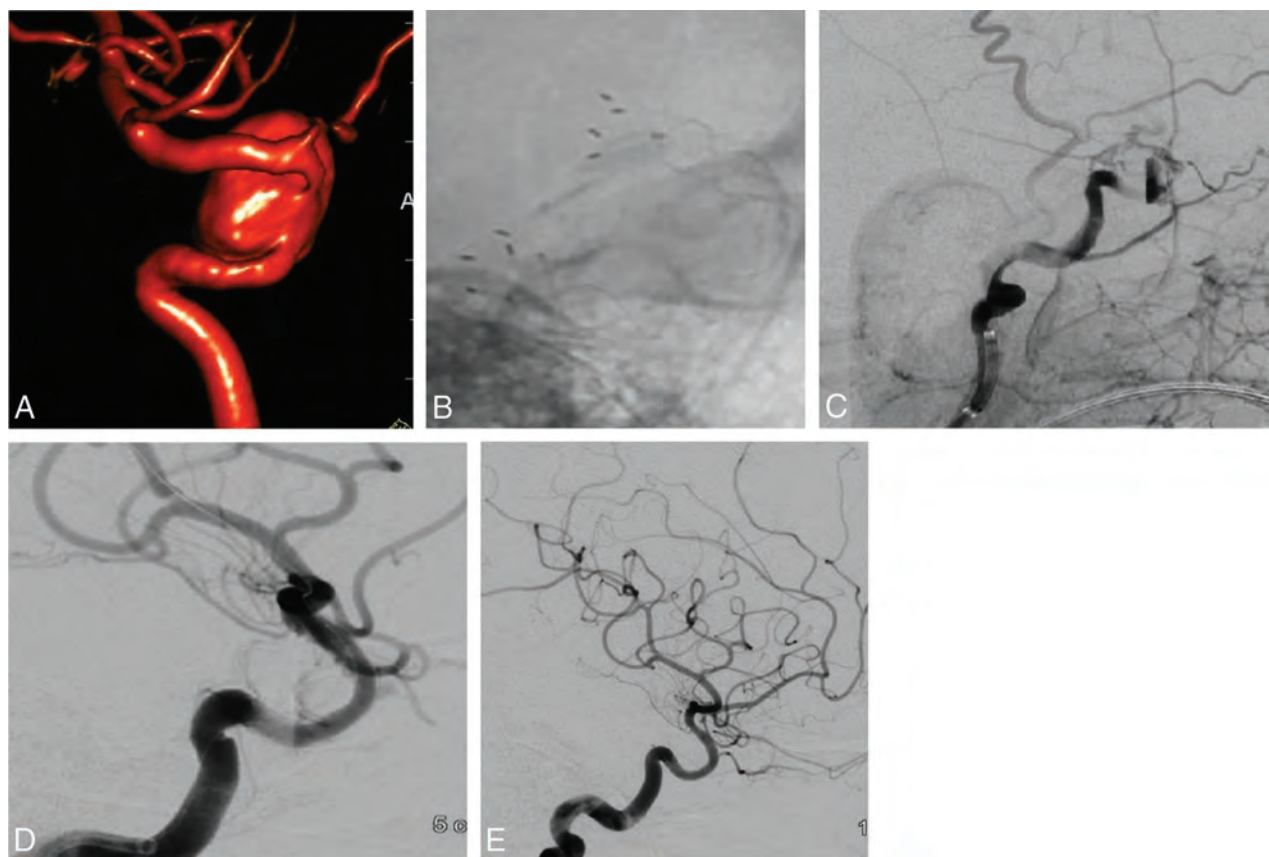


FIG 4. A, Incidental finding of a cavernous ICA aneurysm in a female patient, 3D rotational angiography. B, Placement of a 3.5-/22/16-mm FRED with incomplete expansion in the midsection of the flow diverter, recorded with fluoroscopy. C, Acute thrombotic occlusion of the ICA caused by the incompletely expanded flow diverter, right anterior oblique view. D, Status post dilation of the FRED with a coronary percutaneous transluminal angioplasty balloon (Sequent Medical, 2.75 × 10 mm), right anterior oblique view. E, 3-month follow-up angiography demonstrates complete occlusion of the cavernous aneurysm with regular opacification of the ICA, lateral view.

Table 6: Complication rates with different flow diverters including the period under review

Author	Year	Flow Diverter	No. of Patients	Thromboembolic Complications	Hemorrhagic Complications	Median Follow-Up Time (mo)
Möhlenbruch et al ⁸	2015	FRED	29	14.0%	3.0%	6
Poncyłysz et al ¹¹	2013	FRED	6	17.0%	0.0%	3
Briganti et al ¹²	2016	FRED	20	0.0%	0.0%	12
Lubicz et al ¹³	2015	Silk	26	23.1%	11.5%	6
Briganti et al ⁴	2012	Silk + Pipeline	273	4.8%	5.5%	3
Colby et al ⁷	2016	Pipeline Flex	44	2.0%	0.0%	Not applicable
De Vries et al ¹⁴	2013	Surpass	37	13.5%	5.4%	12
Fischer et al ¹⁵	2015	p64	130	3.0%	0.0%	9
Our data	2016	FRED	48	15.4%	1.9%	12

underline the efficiency of a single FRED. A further advantage of the dual-layer design apart from the potential improvement of flow diversion might be found in a strengthened radial force. The radial force vectors of the outer stent might lead to a higher safety of opening, especially when using long devices.

Thromboembolic Complications

Thromboembolic complications play an important role in the context of flow diversion. Table 6 gives a summary of thromboembolic and hemorrhagic complication rates in preexisting series with flow diverters, including the period under review. The rate of thromboembolic complications is comparatively high in the present series. The underlying factors are presumably multifactorial because we failed to identify a distinct similarity.

The risk of thrombus formation and parent artery occlusion is higher with suboptimal wall apposition as discussed by Möhlenbruch et al⁸ in their series of 29 patients with 34 aneurysms treated with the FRED. They observed 2 patients (6.9%) with in-stent thrombosis and performed an in-stent percutaneous transarterial angioplasty of the flow diverter in 17% (5/29) of their aneurysms exclusively located at the sharp angulation of the carotid siphon. They stressed the importance of a slow and well-controlled push-and-pull technique with the microcatheter held in the central position of the vessel to achieve an optimal opening and apposition of the flow diverter to the vessel wall. They recommended resheathing the flow diverter if the slightest suspicion of incomplete wall apposition occurs.

Buyukkaya et al,¹⁶ in their series of 34 aneurysms treated with the Silk flow diverter, observed a thromboembolic complication rate of 12.1%. They discussed the difficulty of deployment as indirectly associated with thromboembolic events. A successful deployment is clearly dependent on the personal experience of the interventionalist and becomes more complex in highly curved anatomies such as the carotid siphon. Most interesting, the rate of aneurysms located at the paraophthalmic highly curved segment of the ICA was comparatively high in their series (58.8%), which was rather similar in our series (40.5%). This might be a possible explanation for the thromboembolic complications in our series because a suboptimal expansion is more likely in tortuous vessels. This context is underlined by the illustrative case given (Fig 4), which documents an incomplete expansion of the FRED in the curved anatomy of the ICA, which resulted in an immediate in-stent thrombosis.

In some cases, fluoroscopy alone is inappropriate for proving the sufficient expansion of flow-modulation devices. Advanced

techniques such as rotational angiography without subtraction and angiographic CT are helpful in the final assessment after implantation of flow diverters. On the basis of our results, we decided to include angiographic CT (DynaCT; Siemens, Erlangen, Germany) in our routine institutional standard to detect minor device malpositions and irregular expansions.¹⁷

A further source of thromboembolic complications might be found in the duration and monitoring of the antiplatelet medication. Several studies showed a significant individual variation in the response to clopidogrel.^{18,19} Patients with high platelet reactivity despite clopidogrel treatment are exposed to a higher risk of thromboembolic events.²⁰ Factors influencing the responsiveness to clopidogrel and acetylsalicylic acid, such as drug interactions, bioavailability, diabetes, smoking, age, and drug compliance, are clearly identified in the literature.²¹ These conditions are inconsistent among patients and change during the follow-up interval.

Routine platelet function testing during the follow-up interval with a precise analysis of the relevant concomitant circumstances might help to identify patients with a de novo resistance to their antiplatelet therapy. The therapy should be tailored and individualized to those findings by a dose modification or changeover to another P2Y₁₂ antagonist as suggested by Oran et al.²²

The optimal duration of dual-antiplatelet medication after flow-diverter treatment is still controversial. A continuation of the dual-antiplatelet medication during the process of neoendothelialization up to 12 months might help to decrease the incidence of late thromboembolic events. In the series of Kocer et al²³ with 37 aneurysms treated with the FRED, the dual antiplatelet medication was used for at least 6 months, and in cases of in-stent stenosis, the medication was maintained.

The standard duration of dual-antiplatelet medication was comparatively short in our series (3 months), which might serve as an explanation for the delayed thromboembolic complications. However, only 1 thromboembolic complication occurred with acetylsalicylic acid alone.

As described above, our retrospective study protocol did not include platelet-activation testing during the follow-up period, resulting in a failure to identify patients with a recent nonresponder status. This could explain the occurrence of thromboembolic complications in patients believed to be on sufficient dual-antiplatelet therapy. We plan to modify our institutional follow-up standards accordingly.

Hemorrhagic Complications

As described above, 1 delayed rupture of a large ICA aneurysm occurred in this series. Several studies identified larger aneurysms as being more prone to delayed aneurysm ruptures.^{24,25} An inflammatory reaction by lytic enzymes such as metalloproteinases might promote degradation of the aneurysmal wall during thrombus formation. Potential strategies to minimize the risk of delayed aneurysm ruptures after flow diversion might aim for an acceleration of intra-aneurysmal thrombus formation and an attenuation of the inflammatory reaction. A combination with additional coiling in large aneurysms might accelerate the process of thrombus formation, though delayed ruptures are reported in cases with additional coiling.^{4,26,27} The positive effect of a concomitant anti-inflammatory medication on the stability of the aneurysmal wall remains unproven. Thielen et al²⁸ could not prove a significant change in the level of lytic enzymes such as metalloproteinase induced by cyclosporine. However, the basic approach of an inflammatory modulation possibly managed with cortisone appears promising and deserves further investigation.

Limitations

Our study has several limitations. The retrospective analysis of the data might cause inhomogeneity because the standards differ slightly among the centers. However, all cases were performed according to a consistent study protocol.

Further limitations are the wide range of different aneurysm types (ruptured, fusiform, saccular, and blister) included in this series and the lack of comparability with conventional treatment strategies. The entire cohort is too small for a significant analysis of the safety and efficacy of the different subtypes of aneurysms treated with the FRED.

Regarding the late thromboembolic events in this series, an analysis of the dual-antiplatelet response during the follow-up period would have been of major interest to identify the proportion of subjects resistant to dual antiplatelet medication and to verify the individual compliance.

Nevertheless, to the best of our knowledge, this is the largest series of aneurysms treated with the FRED comprising a long-term follow-up evaluation of the angiographic and clinical course.

CONCLUSIONS

The technical and angiographic success rate with the FRED is compelling. Contemporary aneurysm occlusion can be accomplished with a single device in most cases. The dual-layer design promotes contemporary and stable occlusion rates. Exact sizing of the device with a consistent expansion and a sufficient wall apposition ideally documented with angiographic CT and rotational angiography without subtraction are essential factors in the management of aneurysms treated with FRED.

Routine platelet-activation testing during the follow-up period might help to decrease the incidence of late thromboembolic events. Further prospective studies may evaluate the implementation of an idealized, individually tailored long-term antiplatelet strategy.

Disclosures: Werner Weber—RELATED: Other: proctor for MicroVention Terumo. Ansgar Berlis—RELATED: Consulting Fee or Honorarium: MicroVention/Terumo. Comments: proctor; Support for Travel to Meetings for the Study or Other Pur-

poses: MicroVention/Terumo. Comments: invited lectures at meetings, arranged by MicroVention/Terumo; UNRELATED: Consultancy: Sequent Medical, Covidien, Stryker; Comments: proctor contract; Payment for Lectures including Service on Speakers Bureaus: Sequent Medical, Covidien, Stryker, Penumbra; Comments: invited lectures at meetings, arranged by MicroVention/Terumo. Stefan Rohde—UNRELATED: Payment for Lectures including Service on Speakers Bureaus: <€1000, MicroVention, ev3; Travel/Accommodations/Meeting Expenses Unrelated to Activities Listed: <€1000, MicroVention, Stryker Neurovascular. Sebastian Fischer—UNRELATED: Board Membership: advisory board member for Codman Neurovascular.

REFERENCES

1. Fischer S, Vajda Z, Aguilar Perez M, et al. **Pipeline embolization device (PED) for neurovascular reconstruction: initial experience in the treatment of 101 intracranial aneurysms and dissections.** *Neuroradiology* 2012;54:369–82 CrossRef Medline
2. Brinjikji W, Murad MH, Lanzino G, et al. **Endovascular treatment of intracranial aneurysms with flow diverters: a meta-analysis.** *Stroke* 2013;44:442–47 CrossRef Medline
3. D'Urso PI, Lanzino G, Cloft HJ, et al. **Flow diversion for intracranial aneurysms: a review.** *Stroke* 2011;42:2363–68 CrossRef Medline
4. Briganti F, Napoli M, Tortora F, et al. **Italian multicenter experience with flow-diverter devices for intracranial unruptured aneurysm treatment with periprocedural complications: a retrospective data analysis.** *Neuroradiology* 2012;54:1145–52 CrossRef Medline
5. Rankin J. **Cerebral vascular accidents in patients over the age of 60, II: prognosis.** *Scott Med J* 1957;2:254–68 Medline
6. Joshi MD, O'Kelly CJ, Krings T, et al. **Observer variability of an angiographic grading scale used for the assessment of intracranial aneurysms treated with flow-diverting stents.** *AJNR Am J Neuroradiol* 2013;34:1589–92 CrossRef Medline
7. Colby GP, Lin LM, Caplan JM, et al. **Immediate procedural outcomes in 44 consecutive Pipeline Flex cases: the first North American single-center series.** *J Neurointerv Surg* 2016;8:702–09 CrossRef Medline
8. Möhlenbruch M, Herweh C, Jestaedt L, et al. **The FRED flow-diverter stent for intracranial aneurysms: clinical study to assess safety and efficacy.** *AJNR Am J Neuroradiol* 2015;36:1155–61 CrossRef Medline
9. Sadasivan C, Cesar L, Seong J, et al. **An original flow diversion device for treatment of intracranial aneurysms: evaluation in the rabbit elastase-induced model.** *Stroke* 2009;40:952–58 CrossRef Medline
10. Tan LA, Keigher KM, Munich SA, et al. **Thromboembolic complications with Pipeline Embolization Device placement: impact of procedure time, number of stents and pre-procedure P2Y12 reaction unit (PRU) value.** *J NeuroIntervent Surg* 2015;7:217–21 CrossRef Medline
11. Poncyłjusz W, Sagan L, Safranow, et al. **Initial experience with implantation of a novel dual layer-flow diverter FRED.** *Wideochir Inne Tech Maloinwazyjne* 2013;8:258–64 CrossRef Medline
12. Briganti F, Leone G, Ugga G, et al. **Safety and efficacy of flow redirection endoluminal device (FRED) in the treatment of cerebral aneurysms: a single center experience.** *Acta Neurochir* 2016;158:1745–55 CrossRef Medline
13. Lubicz B, Van der Elst O, Collignon L, et al. **Silk flow-diverter stent for the treatment of intracranial aneurysms: a series of 58 patients with emphasis on long-term results.** *AJNR Am J Neuroradiol* 2015;36:542–46 CrossRef Medline
14. De Vries J, Boogarts J, Van Norden A, et al. **New generation of flow diverter (Surpass) for unruptured intracranial aneurysms: a prospective single-center study in 37 patients.** *Stroke* 2013;44:1567–77 CrossRef Medline
15. Fischer S, Aguilar-Pérez M, Henkes E, et al. **Initial experience with p64: a novel mechanically detachable flow diverter for the treatment of intracranial saccular sidewall aneurysms.** *AJNR Am J Neuroradiol* 2015;36:2082–89 CrossRef Medline
16. Buyukkaya R, Kocaeli H, Yildirim N, et al. **Treatment of complex intracranial aneurysms using flow diverting Silk® stents: an analy-**

- sis of 32 consecutive patients. *Interv Neuroradiol* 2014;20:729–35 CrossRef Medline
17. Faragò G, Caldiera V, Tempa G, et al. **Advanced digital subtraction angiography and MR fusion imaging protocol applied to accurate placement of flow diverter device.** *J NeuroInterv Surg* 2016;8:e5 CrossRef Medline
 18. Gurbel PA, Bliden KP, Hiatt BL, et al. **Clopidogrel for coronary stenting: response variability, drug resistance, and the effect of pretreatment platelet reactivity.** *Circulation* 2003;107:2908–13 CrossRef Medline
 19. Petricevic M, Milicic D, White A, et al. **Development of a concept for a personalized approach in the perioperative antiplatelet therapy administration/discontinuation management based on multiple electrode aggregometry in patients undergoing coronary artery surgery.** *J Thromb Thrombolysis* 2015;40:383–91 CrossRef Medline
 20. Fifi JT, Brockington C, Narang J, et al. **Clopidogrel resistance is associated with thromboembolic complications in patients undergoing neurovascular stenting.** *AJNR Am J Neuroradiol* 2013;34:716–20 CrossRef Medline
 21. Nakagawa I, Park HS, Yokoyama S, et al. **Influence of diabetes mellitus and cigarette smoking on the variability of the clopidogrel-induced antiplatelet effect and efficacy of active management of the target P2Y12 reaction unit range in patients undergoing neurointerventional procedures.** *J Stroke Cerebrovasc Dis* 2016;25:163–71 CrossRef Medline
 22. Oran I, Cinar C, Bozkaya H, et al. **Tailoring platelet inhibition according to multiple electrode aggregometry decreases the rate of thromboembolic complications after intracranial flow-diverting stent implantation.** *J NeuroInterv Surg* 2015;7:357–62 CrossRef Medline
 23. Kocer N, Islak C, Kizilkilic O, et al. **Flow Re-direction Endoluminal Device in treatment of cerebral aneurysms: initial experience with short-term follow-up results.** *J Neurosurg* 2014;120:1158–71 CrossRef Medline
 24. Rouchaud A, Brinjikji W, Lanzino G, et al. **Delayed hemorrhagic complications after flow diversion for intracranial aneurysms: a literature overview.** *Neuroradiology* 2016;58:171–77 CrossRef Medline
 25. Kulcsár Z, Houdart E, Bonafé A, et al. **Intra-aneurysmal thrombosis as a possible cause of delayed aneurysm rupture after flow-diversion treatment.** *AJNR Am J Neuroradiol* 2011;32:20–25 CrossRef Medline
 26. Kallmes DF, Hanel R, Lopes D, et al. **International retrospective study of the Pipeline Embolization Device: a multicenter aneurysm treatment study.** *AJNR Am J Neuroradiol* 2015;36:108–15 CrossRef Medline
 27. Turowski B, Macht S, Kulcsar Z, et al. **Early fatal hemorrhage after endovascular cerebral aneurysm treatment with a flow diverter (SILK-Stent): do we need to rethink our concepts?** *Neuroradiology* 2011;53:37–41 CrossRef Medline
 28. Thielen E, McClure M, Rauchaud A, et al. **Concomitant coiling reduces metalloproteinase levels in flow-diverter treated aneurysms but anti-inflammatory treatment has no effect.** *J Neurointervent Surg* 2016 Mar 14. [Epub ahead of print] Medline

Flow Diverters in the Treatment of Pediatric Cerebrovascular Diseases

M. Barbuoglu and A. Arat



ABSTRACT

BACKGROUND AND PURPOSE: There is very limited data concerning utilization of flow diverters in children. Our aim is to report results for the treatment of complex intracranial aneurysms and carotid cavernous fistulas by using flow diverters in children.

MATERIALS AND METHODS: Retrospective review of children (17 years of age or younger) treated with flow diverters between May 2011 and July 2014 was performed. Clinical and laboratory data and angiographic findings were extracted. Seven patients (6 males, 1 female; mean age, 12.7 years; range, 3–16 years) were included. Two presented with posttraumatic fistulas. The remaining patients presented with traumatic aneurysms of the cavernous carotid artery or fusiform aneurysms of the distal vertebral artery, M1, or A2 segments. All patients were premedicated with clopidogrel (75 mg daily for patients with body weights of >45 kg, 37.5 mg daily for 1 small child with a body weight of <45 kg) and aspirin (300 mg daily for \geq 45 kg, 100 mg daily for smaller children).

RESULTS: VerifyNow and Multiplate Analyzer values were higher than expected. No clinical complications were noted. Imaging performed at 7–52 months after the procedure (mean/median, 22.3/14 months) revealed occlusions of all aneurysms and fistulas. One patient had an asymptomatic occlusion of the parent artery; otherwise, no hemodynamically significant parent artery stenosis was observed. There were no clinically significant neurologic events during follow-up.

CONCLUSIONS: Although flow-diverter placement appears to be safe and effective on midterm follow-up in children, longer follow-up is critical. The current sizes of flow diverter devices and delivery systems cover the pediatric size range, obviating developing flow diverters specific to children.

ABBREVIATIONS: APT = antiplatelet therapy; CCF = carotid cavernous fistula; PRU = P2Y12 receptor reaction unit

The introduction of flow diverters into endovascular practice has been defined by some authors as a paradigm shift.¹ Currently, a significant proportion of intracranial aneurysms in adults are successfully treated with flow diverters. However, there are few case reports on the use of flow diverters in the pediatric population.^{2–11} In this retrospective study, we report our experience with of flow diverters in 5 children with intracranial aneurysms and 2 children with carotid cavernous fistulas (CCFs). Through a review of our patient data and the relevant literature, we also summarize the current antiplatelet regimens used for chil-

dren undergoing cerebrovascular interventions involving the placement of stents and flow diverters. There is a need for the development of a standardized antiplatelet therapy protocol for children undergoing cerebrovascular interventions involving the placement of permanent vascular scaffolds.

MATERIALS AND METHODS

Patient Population

We retrospectively reviewed our records to identify patients 17 years of age or younger who were treated by the senior author with implantation of a flow-diverter stent between May 2011 and July 2014. Clinical findings, angiographic findings, and follow-up data were extracted from our electronic hospital information system.

General Description of the Endovascular Procedure

All endovascular procedures were performed with the patients under general anesthesia. A 6F 90-cm-long sheath introducer was inserted through the common femoral artery for patients older than 4 years (6 patients), and a 5F long sheath introducer was used only for patients younger than 4 years of age. After insertion of the

Received May 25, 2016; accepted after revision August 8.

From the Department of Radiology (M.B.), Istanbul University Medical School, Istanbul, Turkey; and Department of Radiology (A.A.), School of Medicine, Hacettepe University, Ankara, Turkey.

Please address correspondence to Anil Arat, MD, Department of Radiology, School of Medicine, Hacettepe University, Sıhhiye, Ankara, Turkey; e-mail: anilarat@hotmail.com

Indicates open access to non-subscribers at www.ajnr.org

Indicates article with supplemental on-line tables.

<http://dx.doi.org/10.3174/ajnr.A4959>

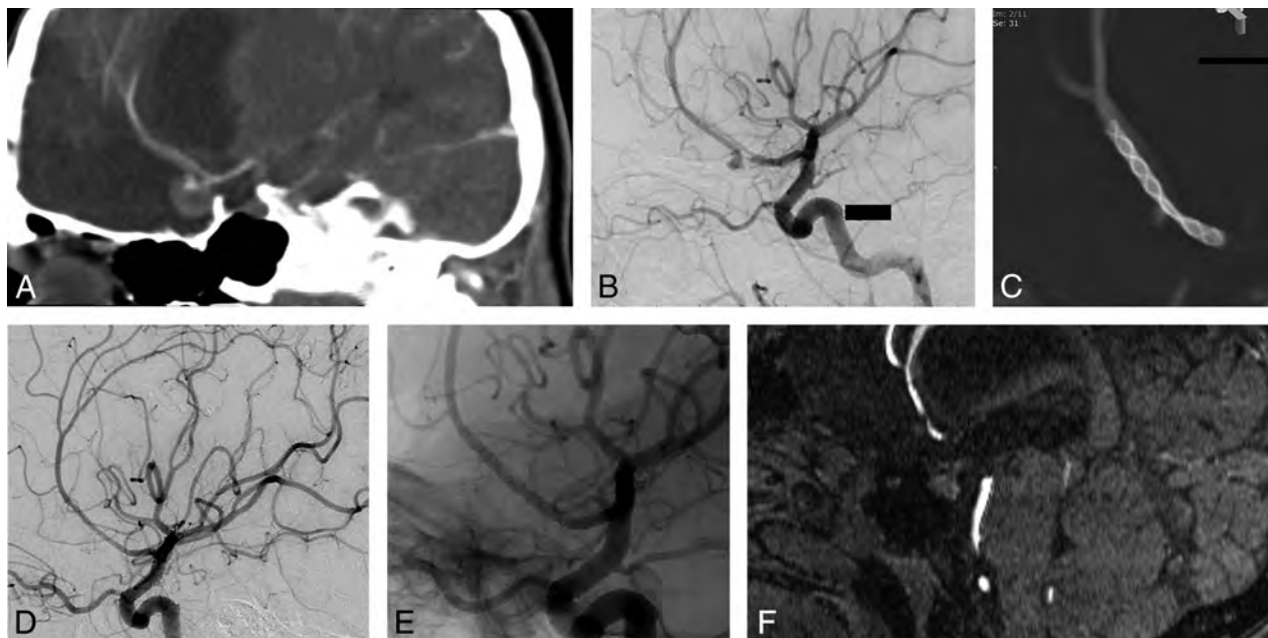


FIG 1. A, An aneurysm of the A2 segment of the right anterior cerebral artery is demonstrated on sagittal reformations of a cranial CT angiogram in a 14-year-old girl who sustained a traumatic brain injury approximately 10 years ago. The aneurysm is partially clotted and measures 10 mm in its largest dimension. B, Lateral view of the right common carotid arteriogram verifies partial opacification of the aneurysm dome. There is a stenosis of the parent artery proximal to the aneurysm, suggesting that the aneurysm is dissecting/traumatic in nature. C, Flat panel CT scan obtained during administration of diluted contrast medium intra-arterially shows that the Silk flow diverter (Balt Extrusion, Montmorency, France) totally covers the aneurysmal segment, and it is constrained at the level of the stenosis of the proximal A2 segment. D and E, Subtracted and native views of a 6-month follow-up angiogram reveal that the aneurysm is no longer opacified, the parent artery is patent, and the stenosis of the parent artery has disappeared. F, A noncontrast MRA of the head obtained at 42 months shows that the patency of the parent artery is maintained and the size of the aneurysm has decreased significantly, consistent with the healing of the aneurysm.

introducer, 100 IU/kg of heparin was intravenously administered in a bolus dose; then, a heparin infusion was initiated to maintain an activated clotting time of around twice the baseline value. In all cases, a long introducer sheath was used to catheterize the common carotid or subclavian artery. A distal access catheter was placed through this sheath into the petrous segment of the targeted internal carotid arteries or the V2 segment of the vertebral artery.

For aneurysm treatment, flow diverters were deployed using previously described techniques¹²⁻¹⁴ after meticulous measurement of the parent artery size at the proximal and distal segments of the aneurysm. These measurements were made on DSA images and 3D images reconstructed from rotational angiograms on workstations of biplane angiography units (Artis zee; Siemens, Erlangen, Germany). Scaffolding stents were used for ideal placement of the flow diverters and to prevent overexpansion/shortening in fusiform giant aneurysms. The devices were optimally apposed to the vessel wall by using hypercompliant intracranial balloons if necessary after deployment. Follow-up imaging included DSA at 6 months, noncontrast MRA at 12 months, and yearly MRA thereafter. In 1 patient, a 1-month DSA was obtained to rule out residual fistula.

Antiplatelet Treatment and Anticoagulation

All patients were premedicated with clopidogrel (75 mg per day for patients weighing >45 kg, 37.5 mg per day for the 1 child of <45 kg) and aspirin (300 mg per day for children weighing ≥45 kg, 100 mg per day for smaller children) at least 5 days before endovascular treatment. Platelet reactivity to clopidogrel based on VerifyNow (Accumetrics, San Diego, California) and results of

ADP and TRAP assays (Multiplate Analyzer; Roche Diagnostics, Mannheim, Germany) were available for 6 of the 7 treatments performed. During the procedure, an intravenous bolus dose of heparin (100 IU/Kg) was administered and heparinization was continued to maintain an activated clotting time at 2–3 times the baseline value throughout the procedure. After the procedure, dual antiplatelet treatment was continued for at least 6 months. At the 6-month DSA follow-up, clopidogrel was stopped, and aspirin was maintained. In 1 patient, both clopidogrel and aspirin were discontinued after 6 months without clinical sequelae.

Statistical Analysis

All statistical analyses were performed by using SPSS software, Version 22.0 (IBM, Armonk, New York). Categorical variables were compared using the Fisher exact test. The test was used to compare the occurrence of significant adverse events in children treated for CCF versus aneurysm.

RESULTS

Seven children (6 males and 1 female; mean age, 12.7 years; range, 3–16 years) were treated with flow diverters. Two of the patients presented with posttraumatic CCFs. The CCFs were treated by using transarterial deployment of a flow diverter with coil and/or Onyx (Covidien, Irvine, California) embolization of the fistula from the venous side. Of the remaining 5 patients, 2 presented with posttraumatic aneurysms: 1 at the origin of the A2 segment of the anterior cerebral artery (Fig 1) and 1 at the M1 segment of the middle cerebral artery. Two patients presented with recurrent cavernous segment aneurysms following endovascular treatment

of posttraumatic CCFs. Finally, 1 patient presented with a giant right vertebral artery V4 segment aneurysm.

Scaffolding stents were placed during the same endovascular session in 2 aneurysms. Additionally, 1 stent was placed within the flow diverter 1 month after the endovascular procedure to prevent further fish mouting (ie, a pencil tip-like narrowing of the distal tip of the device to form a so-called “womble-nose appearance”),¹⁵ which was evident on early follow-up on MRA and plain radiographs.

Navigation of the flow diverter to the targeted arterial segment was successful in all cases, and no problems were encountered during deployment. All the procedures were well-tolerated by the patients in the postoperative period. No clinically significant complications were noted during the follow-up period. Control cerebral angiograms or MRAs performed at 7–52 months (mean/median, 22.3/14 months) revealed occlusion of all aneurysms and fistulas. One patient had an asymptomatic occlusion of the parent artery incidentally noted on 7-month follow-up angiography. A detailed clinical inquiry revealed that contrary to our recommendations, the patient had chosen to stop his antiplatelet medications for approximately 2 weeks following a 3-month CT angiogram that had revealed obliteration of the aneurysm and patency of the parent artery. There was no hemodynamically significant stenosis of the parent artery in any of the remaining patients. Data on patient characteristics and antiplatelet agents are provided in detail in On-line Table 1. Three of 7 patients were hyper-responders to clopidogrel (P2Y₁₂ receptor reaction unit [PRU] of <60; On-line Table 1). In these patients, aspirin was stopped and patients were maintained on only clopidogrel for 6 months. After the follow-up angiogram, aspirin was restarted and clopidogrel was discontinued. There were no children with clopidogrel resistance (PRU of >240).

There was no significant difference in the occurrence of significant adverse effects in patients treated for CCF compared with those with aneurysms ($P = 1.0$; OR, 4; 95% confidence interval, 0.11–136.95).

DISCUSSION

Pediatric intracranial aneurysms are uncommon (0.5%–4.6% of all intracranial aneurysms), and there are limited data regarding the optimal treatment method.^{16–18} Saraf et al¹⁹ reported that endovascular management is a safe, durable, and effective treatment for pediatric intracranial aneurysms.

Considering the substantial rise in the use of flow diverters among all contemporary endovascular devices in adults, it is expected that these devices will be used with increasing frequency in the pediatric population. There are higher incidences of fusiform and giant aneurysms in the pediatric population.^{12,18,20} Hence, pediatric aneurysms are more likely to be suitable for flow diversion compared with those in adults. However, because there are fundamental differences between intracranial aneurysms in adults and children, it has been proposed that the results of cerebral flow diversion may not be readily applicable to children.¹¹ Although endovascular treatment with flow diverters has shown good angiographic results, high complete occlusion rates,^{21–23} and acceptable overall procedure-related morbidity/mortality²¹ in adults, there is a higher risk of unfavorable outcomes in poste-

rior circulation aneurysms and large/giant aneurysms, which are more frequently encountered in the pediatric population.^{21,24}

The current series is the largest one of pediatric patients treated with flow diverters reported to date. To the best of our knowledge, 15 cases (16 aneurysms) of flow-diverter implantation in children have been reported in the literature, including case reports and 2 series with 3 patients each.^{2–11} The current study reports the youngest patient treated with a flow diverter and reports the use of these devices for the treatment of noniatrogenic intracranial fistula in children for the first time, to our knowledge.

Data on the results of the use of flow diverters in children have been considered positive, and potential pitfalls have been overlooked. All of the previously reported cases, except a case described by Abla et al,⁹ were technically successful and produced good clinical outcomes, and all devices except 1 were patent on follow-up. These reports suggest that flow diversion can be a good alternative for the treatment of challenging pediatric cerebral aneurysms. On the basis of our results, we believe that flow diverters are associated with significant improvement in the endovascular treatment of cerebrovascular diseases. However, several issues still require further clarification.

The first issue is children's growth. The ongoing growth of cerebral vessels in children has been suggested as a potential pitfall by some authors^{11,25} or even as a contraindication for cerebral stent placement or flow diversion in this age group.²⁶ Waitzman et al²⁷ showed that cranial growth is rapid during the first year of life, slows markedly in later years, and is almost complete by age 6. Arat et al²⁸ showed that by 48 months of life, 81%–99% of adult diameters were attained in intracranial arteries; however, only 59% of adult diameters were attained for the common iliac artery. Later, similar findings regarding children were also reported by He et al.²⁹ From a morphometric standpoint, these studies suggest the following: The size range of current intracranial stents or flow diverters is sufficient to cover the pediatric population, and intracranial arterial diameters in children do not undergo striking growth, especially after early childhood. Thus, the implication that stent placement may result in intracranial stenosis or similar effects later in life is not supported by the current literature. Problems associated with femoral access through the significantly smaller iliac/femoral artery diameters in children can be minimized by using long 4F introducer sheaths or by direct groin access with 4F diagnostic catheters. In one of the patients in the current report, we were able to place a flow diverter through a direct femoral access by using a 4F catheter, which is remarkably smaller than a 3F sheath.³⁰

The second, and more important, issue is our concern about pre-/postprocedural antiplatelet medication protocols used for flow diverters. There is no standard antiplatelet/anticoagulant therapy for children undergoing intracranial placement of vascular scaffolds (ie, stents, stent grafts, or flow diverters). Analyzing the 35 cases reported in the literature in which there is a somewhat detailed description of the placement of cerebral vascular scaffolds in children, we found that antiplatelet administration for endovascular treatment was extremely variable (On-line Table 2).^{2–11,25,31–43} There are neither guidelines published on antiplatelet therapy (APT) in children with cerebrovascular diseases²⁵ nor conclusive trials on pediatric APT regimens.^{44,45} Weight-

based dose calculations extrapolated from an adult dosing of 75 mg per day are not only misleading but also may lead to life-threatening consequences.^{45,46} A randomized study in children with heart disease showed that clopidogrel doses as low as 0.2 mg/kg may be enough to achieve a sufficient therapeutic effect in infants and young children (compared with the approximate dose of 1 mg/kg used for adults).⁴⁶ Furthermore, the need for age-specific reference ranges for children has been discussed.⁴⁷ On the basis of the referenced reports, we modified our adult regimen of APT (75 mg per day of clopidogrel daily and 300 mg of aspirin daily for 6 months, cessation of clopidogrel at 6 months, and administration of 300 mg of aspirin indefinitely). We chose to premedicate our patients with clopidogrel (75 mg per day for patients of >45 kg, 37.5 mg per day for patients of <45 kg) and aspirin (300 mg per day for patients of ≥45 kg, 100 mg per day for smaller children) before endovascular treatment. This regimen was based on the assumption that older children would respond to aspirin and clopidogrel as safely as our low-weight adult patients who weigh around 45 kg. For young children, we wanted to reduce the dose.

We had 2 options for clopidogrel dose reduction: giving clopidogrel every other day or breaking the tablet into 2 or 4 pieces. We did not favor the “every-other-day” type of regimen because we were not able to predict the pharmacokinetics with this approach and there was a risk of lower efficacy and stent thrombosis. Instead, we took a risk of a hyper-response and decided to administer a fraction of a tablet. Because breaking the tablet into 4 parts proved unreliable with families, we asked them to give half a tablet per day. For adjusting the aspirin dose, our thinking was similar. We chose to start the older children on a higher dose to avoid thromboembolic events. If the PRU levels were <60 on the day of the procedure, aspirin was discontinued for 6 months (until follow-up angiography); it was then restarted as clopidogrel was discontinued. Point-of-care test results for the evaluation of clopidogrel resistance were available for all our patients except 1 (On-line Table 1), compared with 4/35 children with the placement of some form of intracranial stent reported in the literature (On-line Table 2) showing the effectiveness of this protocol. However, the level of antiplatelet response as determined by point-of-care testing was higher than the response reported in adults⁴⁸ and was indicative of lower doses of APT possibly being used to more safely produce the desired antiaggregation.

Routine testing of platelet function has been recommended for APT in children with cardiac disease,⁴⁹ and it may help to prevent excessive platelet inhibition in pediatric cerebrovascular diseases as well. In the pediatric population, aspirin should be used cautiously because of its association with Reye syndrome, which can be life-threatening.⁵⁰ The American Heart Association recommends that aspirin be withheld in children during influenza and chicken pox infections.⁵¹ The need for life-long antiplatelet therapy is a drawback of flow diverters. We were able to discontinue both aspirin and clopidogrel in one of our patients after 6 months on the basis of the large size of the stented artery (cavernous ICA), enabling complete thrombosis of the aneurysm and patency of the parent artery without any clinical consequences. Bioabsorbable stents have been used for neurovascular diseases to address this problem.^{52,53}

Another drawback is related to the delayed events that can occur after the placement of flow diverters. Abila et al⁹ described the failure of 7 telescopically placed flow diverters in a child; because further endovascular options were diminished, their patient had to undergo a surgical parent artery occlusion with a superficial temporal artery–middle cerebral artery bypass. In addition to this patient, we report a child presenting with occlusion of a giant middle cerebral artery aneurysm and the parent artery at 7-month follow-up. This patient admitted that he discontinued clopidogrel for several weeks between his 3- and 7-month follow-up studies. Similar occlusions have been reported in pediatric patients after intracranial placement of flow diverters or stent grafts.^{11,54} Another child in this study as well as 1 patient who underwent treatment of a giant basilar artery aneurysm with a Pipeline Embolization Device (PED; Covidien, Irvine, California) (this patient was not included in our analysis because he was not previously treated by us; however, he is currently under our follow-up) had TIA-like symptoms and no abnormalities on diffusion-weighted MR imaging performed just after the event. These symptoms occurred after short-term interruption of antiplatelet medications and resolved after the medications were resumed. Additionally, one of our patients showed a delayed spontaneous change in the configuration of his flow diverter, necessitating a second endovascular intervention. These cases suggest that delayed findings or events may be observed in children after flow diversion, similar to those observed in adults. Children will have to live with the consequences of these delayed events for the remainder of their lives.

Fortunately, the treatment of aneurysms with flow diverters results in reduced total radiation doses, fluoroscopy time, and contrast medium administration with respect to standard coiling techniques.⁵⁵ Follow-up imaging after flow diversion can be performed without radiation by MR imaging to rule out aneurysm recurrence.⁵⁶ The reduction of the radiation dose is critical in pediatric interventional procedures.^{25,55,57}

Our results point to problems associated with the use of flow diverters in the pediatric population and antiplatelet regimens for children. However, there are limitations to our study. The main limitations of this series are the low number patients, the heterogeneity of pathologic conditions (fistulas and aneurysms), and the variations in technique (such as placement of different flow diverters, placement of scaffolding stents). In addition, a longer follow-up duration is preferable in children. Because the number of pediatric patients amenable to flow diverters is limited, it is not possible to draw firm conclusions on pediatric flow diversion based on single-center studies. Multicenter studies and registries may be helpful in addressing the benefits and limitations of flow diverters in children more reliably.

CONCLUSIONS

In this study, we retrospectively analyzed our data to identify pediatric patients who were treated with the implantation of flow-diverter stents. Five patients with aneurysms and 2 patients with CCFs were successfully treated with flow diverters. This case series suggests that treatment with flow diverters is an option for complex pediatric intracranial aneurysms and CCFs; however, the long-term efficacy, patency, and risk of long-term APT are yet to be clarified through additional studies. With further refinement

in flow-diverter technology, flow diversion is very likely to be used more frequently in children.

REFERENCES

1. D'Urso PI, Lanzino G, Cloft HJ, et al. **Flow diversion for intracranial aneurysms: a review.** *Stroke* 2011;42:2363–68 CrossRef Medline
2. Takemoto K, Tateshima S, Golshan A, et al. **Endovascular treatment of pediatric intracranial aneurysms: a retrospective study of 35 aneurysms.** *J Neurointerv Surg* 2014;6:432–38 CrossRef Medline
3. Appelboom G, Kadri K, Hassan F, et al. **Infectious aneurysm of the cavernous carotid artery in a child treated with a new-generation of flow-diverting stent graft: case report.** *Neurosurgery* 2010;66:E623–24 CrossRef Medline
4. Burrows AM, Zipfel G, Lanzino G. **Treatment of a pediatric recurrent fusiform middle cerebral artery (MCA) aneurysm with a flow diverter.** *J Neurointerv Surg* 2013;5:e47 CrossRef Medline
5. Lubicz B, Collignon L, Raphaeli G, et al. **Flow-diverter stent for the endovascular treatment of intracranial aneurysms: a prospective study in 29 patients with 34 aneurysms.** *Stroke* 2010;41:2247–53 CrossRef Medline
6. Zarzecka A, Gory B, Turjman F. **Implantation of two flow diverter devices in a child with a giant, fusiform vertebral artery aneurysm: case report.** *Pediatr Neurol* 2014;50:185–87 CrossRef Medline
7. Navarro R, Brown BL, Beier A, et al. **Flow diversion for complex intracranial aneurysms in young children.** *J Neurosurg Pediatr* 2015;15:276–81 CrossRef Medline
8. Ikeda DS, Marlin ES, Shaw A, et al. **Successful endovascular reconstruction of a recurrent giant middle cerebral artery aneurysm with multiple telescoping flow diverters in a pediatric patient.** *Pediatr Neurosurg* 2015;50:88–93 CrossRef Medline
9. Abila AA, Zaidi HA, Crowley RW, et al. **Optic chiasm compression from mass effect and thrombus formation following unsuccessful treatment of a giant supraclinoid ICA aneurysm with the Pipeline device: open surgical bailout with STA-MCA bypass and parent vessel occlusion.** *J Neurosurg Pediatr* 2014;14:31–37 CrossRef Medline
10. Kan P, Mokin M, Puri AS, et al. **Successful treatment of a giant pediatric fusiform basilar trunk aneurysm with Surpass flow diverter.** *J Neurointerv Surg* 2016;8:e23 CrossRef Medline
11. Vargas SA, Diaz C, Herrera DA, et al. **Intracranial aneurysms in children: the role of stenting and flow-diversion.** *J Neuroimaging* 2016;26:41–45 CrossRef Medline
12. Lonjon M, Pennes F, Sedat J, et al. **Epidemiology, genetic, natural history and clinical presentation of giant cerebral aneurysms.** *Neurochirurgie* 2015;61:361–65 CrossRef Medline
13. Gurkas E, Kaya T, Daglioglu E, et al. **Silk device for the treatment of intracranial aneurysms, part 1: periprocedural results, technical aspects and learning curve.** *Turk Neurosurg* 2016;26:525–32 CrossRef Medline
14. De Vries J, Boogaarts J, Van Norden A, et al. **New generation of flow diverter (Surpass) for unruptured intracranial aneurysms: a prospective single-center study in 37 patients.** *Stroke* 2013;44:1567–77 CrossRef Medline
15. Derakhshani S, Rosa S, Low S, et al. **Early and late postoperative changes in the flow diverter's intra arterial morphology that can have significant consequences (the womble nose effect).** *Interv Neuroradiol* 2013;19(suppl 1):185–87
16. Hettis SW, Narvid J, Sanai N, et al. **Intracranial aneurysms in childhood: 27-year single-institution experience.** *AJNR Am J Neuroradiol* 2009;30:1315–24 CrossRef Medline
17. Mehrotra A, Nair AP, Das KK, et al. **Clinical and radiological profiles and outcomes in pediatric patients with intracranial aneurysms.** *J Neurosurg Pediatr* 2012;10:340–46 CrossRef Medline
18. Jian BJ, Hettis SW, Lawton MT, et al. **Pediatric intracranial aneurysms.** *Neurosurg Clin N Am* 2010;21:491–501 CrossRef Medline
19. Saraf R, Shrivastava M, Siddhartha W, et al. **Intracranial pediatric aneurysms: endovascular treatment and its outcome.** *J Neurosurg Pediatr* 2012;10:230–40 CrossRef Medline
20. Krings T, Geibprasert S, terBrugge KG. **Pathomechanisms and treatment of pediatric aneurysms.** *Childs Nerv Syst* 2010;26:1309–18 CrossRef Medline
21. Brinjikji W, Murad MH, Lanzino G, et al. **Endovascular treatment of intracranial aneurysms with flow diverters: a meta-analysis.** *Stroke* 2013;44:442–47 CrossRef Medline
22. Shankar JJ, Tampieri D, Iancu D, et al. **SILK flow diverter for complex intracranial aneurysms: a Canadian registry.** *J Neurointerv Surg* 2016;8:273–78 CrossRef Medline
23. Chalouhi N, Tjoumakaris S, Starke RM, et al. **Comparison of flow diversion and coiling in large unruptured intracranial saccular aneurysms.** *Stroke* 2013;44:2150–54 CrossRef Medline
24. Kaya T, Daglioglu E, Gurkas E, et al. **Silk device for the treatment of intracranial aneurysms, part 2: factors related to clinical and angiographic outcome.** *Turk Neurosurg* 2016;26:533–37 CrossRef Medline
25. Requejo F, Lipsich F, Jaimovich R, et al. **Neurovascular stents in pediatric population.** *Childs Nerv Syst* 2016;32:505–09 CrossRef Medline
26. Arnold M, Steinlin M, Baumann A, et al. **Thrombolysis in childhood stroke: report of 2 cases and review of the literature.** *Stroke* 2009;40:801–07 Medline
27. Waitzman AA, Posnick JC, Armstrong DC, et al. **Craniofacial skeletal measurements based on computed tomography, part II: normal values and growth trends.** *Cleft Palate Craniofac J* 1992;29:118–28 Medline
28. Arat YO, Arat A, Aydin K. **Angiographic morphometry of internal carotid artery circulation in Turkish children.** *Turk Neurosurg* 2015;25:608–16 CrossRef Medline
29. He L, Ladner TR, Pruthi S, et al. **Rule of 5: angiographic diameters of cervicocerebral arteries in children and compatibility with adult neurointerventional devices.** *J Neurointerv Surg* 2015 Nov 6. [Epub ahead of print] Medline
30. Sanon S, Gulati R. **Slender approach and sheathless techniques.** *Intervent Cardiol Clin* 2015;4:161–66 CrossRef
31. Cohen JE, Ferrario A, Ceratto R, et al. **Reconstructive endovascular approach for a cavernous aneurysm in infancy.** *Neurol Res* 2003;25:492–96 Medline
32. Chandela S, Alzate J, Sen C, et al. **Treatment of a complex posterior fossa aneurysm in a child using side-to-side posterior inferior cerebellar artery-posterior inferior cerebellar artery bypass.** *J Neurosurg Pediatr* 2008;1:79–82 Medline
33. Crowley RW, Evans AJ, Kassell NF, et al. **Endovascular treatment of a fusiform basilar artery aneurysm using multiple “in-stent stents”: technical note.** *J Neurosurg Pediatr* 2009;3:496–500 Medline
34. Wilms G, Buyse G, van Loon J, et al. **Treatment of a giant basilar artery aneurysm with a bridging stent and subsequent coil occlusion of the stent: case report.** *Neurosurgery* 2010;67:E510–11 CrossRef Medline
35. Fontela PS, Tampieri D, Atkinson JD, et al. **Posttraumatic pseudoaneurysm of the intracavernous internal carotid artery presenting with massive epistaxis.** *Pediatr Crit Care Med* 2006;7:260–62 Medline
36. Gupta V, Jain V, Mathuria SN, et al. **Endovascular treatment of a mycotic intracavernous carotid artery aneurysm using a stent graft.** *Interv Neuroradiol* 2013;19:313–19 Medline
37. Gralla J, Brekenfeld C, Schmidli J, et al. **Internal carotid artery aneurysm with life-threatening hemorrhages in a pediatric patient: endovascular treatment options.** *J Endovasc Ther* 2004;11:734–38 Medline
38. Komiyama M, Yoshimura M, Honnda Y, et al. **Acute basilar artery dissection treated by emergency stenting in a 13-year-old boy.** *Pediatr Neurosurg* 2005;41:318–22 Medline
39. Lai YJ, Chang FC, Lin CJ, et al. **Endovascular therapy in pediatric intracranial carotid artery dissection.** *Pediatr Neurol* 2010;42:291–94 CrossRef Medline
40. Lee JY, Kwon BJ, Kang HS, et al. **Subarachnoid hemorrhage from a dissecting aneurysm of the posterior cerebral artery in a child: re-**

- bleeding after stent-assisted coiling followed by stent-within-stent technique. *J Korean Neurosurg Soc* 2011;49:134–38 CrossRef Medline
41. Binning MJ, Khalessi AA, Siddiqui AH, et al. **Stent placement for the treatment of a symptomatic intracranial arterial dissection in an adolescent.** *J Neurosurg Pediatr* 2010;6:154–58 CrossRef Medline
 42. Ogilvy CS, Tawk RG, Mokin M, et al. **Stent-assisted coiling treatment of pediatric traumatic pseudoaneurysm resulting from tumor surgery.** *Pediatr Neurosurg* 2011;47:442–48 CrossRef Medline
 43. Savastano LE, Chaudhary N, Gemmete JJ, et al. **Stent-assisted coil embolization of a symptomatic middle cerebral artery aneurysm in an infant.** *J Neurosurg Pediatr* 2014;14:550–54 CrossRef Medline
 44. Bassareo PP, Fanos V, Iacovidou N, et al. **Antiplatelet therapy in children: why so different from adults?** *Curr Pharm Des* 2012;18:3019–33 CrossRef Medline
 45. Mertens L, Eyskens B, Boshoff D, et al. **Safety and efficacy of clopidogrel in children with heart disease.** *J Pediatr* 2008;153:61–64 Medline
 46. Li JS, Yow E, Berezny KY, et al; PICOLO Investigators. **Dosing of clopidogrel for platelet inhibition in infants and young children: primary results of the platelet inhibition in children on clopidogrel (PICOLO) trial.** *Circulation* 2008;117:553–59 CrossRef Medline
 47. Yip C, Linden MD, Attard C, et al. **Platelets from children are hyper-responsive to activation by thrombin receptor activator peptide and adenosine diphosphate compared to platelets from adults.** *Br J Haematol* 2015;168:526–32 CrossRef Medline
 48. Delgado Almandoz JE, Kadkhodayan Y, Crandall BM, et al. **Variability in initial response to standard clopidogrel therapy, delayed conversion to clopidogrel hyper-response, and associated thromboembolic and hemorrhagic complications in patients undergoing endovascular treatment of unruptured cerebral aneurysms.** *J Neurointerv Surg* 2014;6:767–73 CrossRef Medline
 49. Hanke CA, Stiller B, Nakamura L, et al. **Prophylactic use of clopidogrel in paediatric cardiac patients.** *Klin Padiatr* 2012;224:166–69 CrossRef Medline
 50. Selves A, Ruiz S, Crognier L, et al. **Aspirin and its danger: Reye syndrome in young adult** [in French]. *Ann Fr Anesth Reanim* 2013;32:814–16 CrossRef Medline
 51. Giglia TM, Massicotte MP, Tweddell JS, et al; American Heart Association Congenital Heart Defects Committee of the Council on Cardiovascular Disease in the Young, Council on Cardiovascular and Stroke Nursing, Council on Epidemiology and Prevention, and Stroke Council. **Prevention and treatment of thrombosis in pediatric and congenital heart disease: a scientific statement from the American Heart Association.** *Circulation* 2013;128:2622–703 CrossRef Medline
 52. Arat A, Daglioglu E, Akmangit I. **Neurovascular applications of bio-absorbable stents.** *Interv Neuroradiol* 2015;21;(suppl 1):181
 53. Wang K, Yuan S, Zhang X, et al. **Biodegradable flow-diverting device for the treatment of intracranial aneurysm: short-term results of a rabbit experiment.** *Neuroradiology* 2013;55:621–28 CrossRef Medline
 54. Özkan Arat Y, Arat A, Aydın K. **Cerebrovascular complications of transorbital penetrating intracranial injuries.** *Ulus Travma Acil Cerrahi Derg* 2015;21:271–78 CrossRef Medline
 55. Colby GP, Lin LM, Nundkumar N, et al. **Radiation dose analysis of large and giant internal carotid artery aneurysm treatment with the Pipeline embolization device versus traditional coiling techniques.** *J Neurointerv Surg* 2015;7:380–84 CrossRef Medline
 56. Attali J, Benaissa A, Soize S, et al. **Follow-up of intracranial aneurysms treated by flow diverter: comparison of three-dimensional time-of-flight MR angiography (3D-TOF-MRA) and contrast-enhanced MR angiography (CE-MRA) sequences with digital subtraction angiography as the gold standard.** *J Neurointerv Surg* 2016;8:81–86 CrossRef Medline
 57. Johnson C, Martin-Carreras T, Rabinowitz D. **Pediatric interventional radiology and dose-reduction techniques.** *Semin Ultrasound CT MR* 2014;35:409–14 CrossRef Medline
 58. Halimeh S, Angelis G, Sander A, et al. **Multiplate whole blood impedance point of care aggregometry: preliminary reference values in healthy infants, children and adolescents.** *Klin Padiatr* 2010;222:158–63 CrossRef Medline

Flow Conditions in the Intracranial Aneurysm Lumen Are Associated with Inflammation and Degenerative Changes of the Aneurysm Wall

J. Cebal, E. Ollikainen, B.J. Chung, F. Mut, V. Sippola, B.R. Jahromi, R. Tulamo, J. Hernesniemi, M. Niemelä, A. Robertson, and J. Frösen



ABSTRACT

BACKGROUND AND PURPOSE: Saccular intracranial aneurysm is a common disease that may cause devastating intracranial hemorrhage. Hemodynamics, wall remodeling, and wall inflammation have been associated with saccular intracranial aneurysm rupture. We investigated how saccular intracranial aneurysm hemodynamics is associated with wall remodeling and inflammation of the saccular intracranial aneurysm wall.

MATERIALS AND METHODS: Tissue samples resected during a saccular intracranial aneurysm operation (11 unruptured, 9 ruptured) were studied with histology and immunohistochemistry. Patient-specific computational models of hemodynamics were created from preoperative CT angiographies.

RESULTS: More stable and less complex flows were associated with thick, hyperplastic saccular intracranial aneurysm walls, while slower flows with more diffuse inflow were associated with degenerated and decellularized saccular intracranial aneurysm walls. Wall degeneration ($P = .041$) and rupture were associated with increased inflammation (CD45+, $P = .031$). High wall shear stress ($P = .018$), higher vorticity ($P = .046$), higher viscous dissipation ($P = .046$), and high shear rate ($P = .046$) were associated with increased inflammation. Inflammation was also associated with lack of an intact endothelium ($P = .034$) and the presence of organized luminal thrombosis ($P = .018$), though overall organized thrombosis was associated with low minimum wall shear stress ($P = .034$) and not with the flow conditions associated with inflammation.

CONCLUSIONS: Flow conditions in the saccular intracranial aneurysm are associated with wall remodeling. Inflammation, which is associated with degenerative wall remodeling and rupture, is related to high flow activity, including elevated wall shear stress. Endothelial injury may be a mechanism by which flow induces inflammation in the saccular intracranial aneurysm wall. Hemodynamic simulations might prove useful in identifying saccular intracranial aneurysms at risk of developing inflammation, a potential biomarker for rupture.

ABBREVIATIONS: max = maximum; OSI = oscillatory shear index; sIA = saccular intracranial aneurysm; VO = vorticity; WSS = wall shear stress

Saccular intracranial aneurysm (sIA) is a relatively common disease (estimated prevalence, 2%–3%¹), which is often undiagnosed because of a lack of symptoms but may cause a devastating intracranial hemorrhage. Some patients die immediately after sIA rupture, and of those patients who make it to the hospital after

sIA rupture, 27% die despite neurosurgical intensive care.² Because of the sinister outcome of sIA rupture, many diagnosed unruptured sIAs are treated to prevent rupture. However, many, if not most, sIAs do not rupture during life-long follow-up.³ Moreover, currently, sIA rupture can be prevented only by invasive procedures (endovascular or microsurgical occlusion) with a significant risk of morbidity and even mortality.⁴ It is therefore extremely important to distinguish rupture-prone sIAs from those that will never rupture, especially because unruptured sIAs are being diagnosed with increasing frequency due to improved access to MR imaging and other imaging studies of the brain.

Received May 10, 2016; accepted after revision July 22.

From the Bioengineering Department (J.C., B.J.C., F.M.), Volgenau School of Engineering, George Mason University, Fairfax, Virginia; Neurosurgery Research Group (E.O., V.S., B.R.J., R.T., J.H., M.N., J.F.), Biomedicum Helsinki and Helsinki University Central Hospital, Helsinki, Finland; Mechanical Engineering and Materials Science and Department of Bioengineering (A.R.), Swanson School of Engineering, University of Pittsburgh, Pittsburgh, Pennsylvania; Department of Vascular Surgery (R.T.), Helsinki University Central Hospital, Helsinki, Finland; and Department of Neurosurgery and Hemorrhagic Brain Pathology Research Group (J.F.), Neurocenter, Kuopio University Hospital, Kuopio, Finland.

This work was supported by National Institutes of Health grant R21 NS080031-01A1, Helsinki University Central Hospital research grants TYH2012201 and TYH2014236, Kuopio University Hospital research grants, Helsinki Biomedical Graduate Program funding, the Orion Research Foundation, and the Finnish Medical Foundation.

Please address correspondence to Juhana Frösen, MD PhD, Department of Neurosurgery and Hemorrhagic Brain Pathology Research Group, Puijonlaaksontie 2, Kuopio University Hospital 70029, Kuopio, Finland; e-mail: juhana.frosen@kuh.fi

Indicates open access to non-subscribers at www.ajnr.org

Indicates article with supplemental on-line tables.

<http://dx.doi.org/10.3174/ajnr.A4951>

An aneurysm wall ruptures when the wall strength is exceeded by the mechanical stress imposed on it. Wall strength depends on wall structure, which is dependent on the cellular and extracellular composition of the sIA wall. The characteristics of the cellular and extracellular composition of the ruptured or rupture-prone sIA wall, mainly damage to the endothelium, inflammation, and loss of mural cells, have been previously reported by us and others.⁵⁻⁸ The cause of these histologic changes, which we refer to as “degenerative remodeling” remains unknown.

We have previously described the potential mechanism by which nonphysiologic flow conditions can trigger degenerative remodeling of the sIA wall via damage to the endothelium.^{10,11} In addition, we and others have previously shown that flow and wall shear stress (WSS) differ in ruptured and unruptured sIAs¹²⁻¹⁴ and that these flows are associated with changes in sIA morphology.¹⁵ The association of flow and WSS with sIA rupture suggests that they affect sIA wall structure, the main determinant of rupture risk.

Here we studied the possible association of hemodynamics with the histologic changes of the sIA wall. We focused especially on wall degeneration, inflammatory cell infiltration, and damage to the endothelium.

MATERIALS AND METHODS

Patients and Tissue Samples of Intracranial Aneurysms

Patients with intracranial aneurysms that underwent surgical clipping were considered for the study. Twenty patients with preoperative 3D imaging necessary for computational fluid dynamics analysis were included (On-line Table 1). During the surgical intervention, after placement of the clip, a tissue sample was harvested from the aneurysm dome for histology and immunohistochemical analysis. The size of the tissue sample excised from the aneurysm wall varied depending on the size of the aneurysm and how the aneurysm was clipped (Fig 1). Of these 20 patients, 10 were included in a prior histopathologic study by our group.¹⁷ The study was approved by the ethics committee of Helsinki University Central Hospital, and patients gave informed consent to participate to the study.

Histology and Immunohistochemistry

The 20 aneurysm tissue samples underwent immunostaining against CD45 (pan-leukocyte marker, clone 2B11 + PD7/26, dilution 1:400; DAKO, Glostrup, Denmark; Fig 1). The degree of inflammation in the sIA wall was quantified by calculating the number of CD45-positive cells per standardized surface area (0.613 mm²) under a $\times 20$ magnification from 1 to 3 hotspots in the intracranial aneurysm wall. Degenerative remodeling of the sIA wall was scored from hematoxylin-eosin staining by using a previously described scale based on the cellular composition of the sIA wall and the structure of the sIA wall extracellular matrix.⁶ This scale is associated with the rupture rate.⁶ The presence of fresh or organized luminal thrombus was assessed from hematoxylin-eosin staining. The presence of endothelium on the luminal surface was scored from CD31 immunostainings according to the morphology of the cell and positivity to CD31 (Fig 1, CD31 data available for only a subset of 10 aneurysms) as described previously by Ollikainen et al.¹⁷

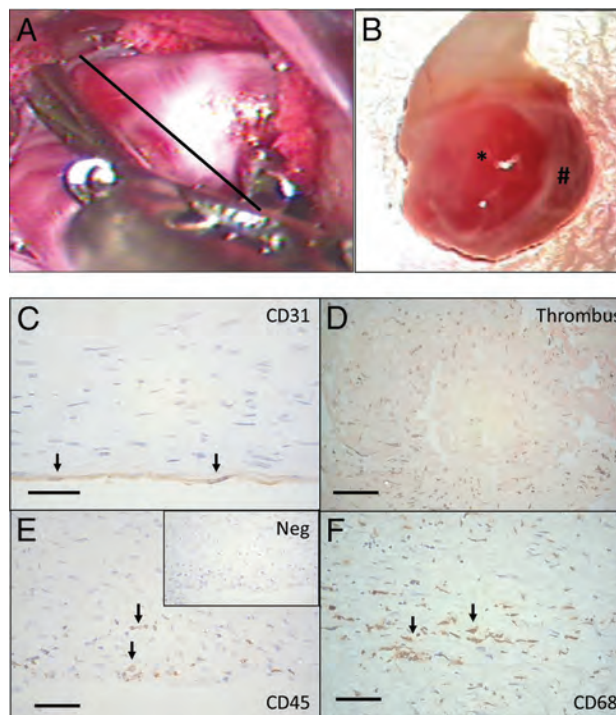


FIG 1. Tissue samples were harvested after aneurysm clipping by cutting through the aneurysm dome distal to the clip, as demonstrated in A (black line represents the estimated site of cut). B, The tissue samples obtained varied significantly in size (from small, approximately 2×1 mm tissue samples to half domes with a >10 -mm radius). In addition to variation in size, many of the aneurysm samples had local variation in the appearance of the wall (B) with translucent areas (asterisk) and thicker wall regions (hash tag). C, In histology, endothelium (CD31+ luminal cells with endothelial cells morphology) was present in only 3/10 of the studied aneurysm walls. D, In 8/20 aneurysms, the luminal surface was instead covered by thrombus, and in 7/20 aneurysms, some degree of thrombus organization was observed (hematoxylin-eosin staining). E, Loss of endothelium and organizing luminal thrombosis were associated with inflammatory cell infiltration (CD45+) in the aneurysm wall. F, Many of the inflammatory cells were macrophages (CD68+). Immunostaining protocol for CD68 is described by Ollikainen et al.¹⁷ Scale bars represent a 50- μ m scale. Negative control for immunostaining is given for CD45 staining (Neg). The black arrows indicate positive cells.

Computational Flow Analysis

Image-based computational fluid dynamics models were constructed from preoperative 3D CT angiography images.¹⁸ CTA images consisted of approximately 250 axial sections with 512×512 pixels and a typical voxel resolution of $0.4 \times 0.4 \times 0.6$ mm. Pulsatile flow simulations were performed by solving the 3D incompressible Navier-Stokes equations by using finite elements on unstructured grids.¹⁹ The computational meshes had a resolution of 200 μ m and contained between 2 and 5 million elements. Inflow boundary conditions were prescribed by using the Womersley velocity profile²⁰ and flow waveforms derived from flow measurements in healthy subjects.^{21,22} Inflow rates were scaled with the inlet area according to the Murray law,²³ and mean flows ranged from approximately 1.2 to 4.1 mL/s. Outflow conditions were prescribed by splitting the outflow rates according to the principle of minimum work (Murray law).²³ Vessel walls were assumed rigid, and blood was approximated as a Newtonian fluid with a density of $\rho = 1.0$ g/cm³ and a viscosity of 0.04- μ m poise. Numeric solutions were obtained for 2 cardiac cycles by using 100

time-steps per cycle. Flow fields corresponding to the second cycle were saved for analysis.

To characterize the aneurysm hemodynamic environment, we computed a number of flow variables over the aneurysm region (On-line Table 2). Exact mathematic definitions of these quantities are given by Mut et al.²⁴ Our choice of mesh resolution and time-step size has been shown to be adequate for accurate quantification of the spatial and time-averaged quantities considered in this work.²⁵

Geometric Analysis

The geometry of the aneurysm (ie, its size and shape) was characterized by automatically computing several geometric variables by using 3D vascular reconstruction (On-line Table 3). Definitions of these quantities and a physical explanation of their meaning can be found in Ma et al²⁶ and Raghavan et al.²⁷

Statistical Analysis

Because our hypothesis was that it is the nonphysiologic WSS (whether too high or too low) but not the physiologic WSS that triggers the degenerative remodeling and inflammation of the sIA wall,¹⁰ we classified our aneurysms accordingly into groups of low, mid-, or high WSS instead of directly comparing WSS with wall remodeling or inflammation. Because there is no clear definition for what constitutes the physiologic range of WSS, especially in a saccular intracranial aneurysm, we classified our aneurysms according to the median of the time and sac-averaged WSS magnitude (8.9 dyne/cm²) and its SD (12.6 dyne/cm²). These groups were the following: 1) low WSS: aneurysms with $WSS < WSS_0$; 2) mid-WSS: aneurysms with $WSS_0 < WSS < WSS_1$; and 3) high WSS: aneurysms with $WSS > WSS_1$. The WSS_0 and WSS_1 were calculated as one-half and twice the WSS median over the 20 aneurysms ($WSS_0 = 4.5$ dyne/cm² and $WSS_1 = 18.0$ dyne/cm²). The number of inflammatory cells was then compared as a continuous variable among these 3 groups.

Next, to compare the hemodynamic and geometric characteristics between aneurysms with little inflammation or substantial inflammation, the samples were classified as the following: group 1: little inflammation if the number of CD45+ was less than the median of CD45+ counts for all samples, and group 2: substantial inflammation if the number of CD45+ was larger than the median of CD45+ counts for all samples. The hemodynamic and geometric indices were then compared as continuous variables between the groups.

The flow-related parameters are given as time-averaged (over systole-diastole) and space-averaged (over aneurysm volume including the neck) values, unless otherwise defined. To study the potential effect of focal variations in the wall shear stress distribution and in inflammation, we categorized both according to their heterogeneity and compared the scores. Flow was defined as homogeneous if the mean over time of the spatial SD/mean over time of the spatial average was <0.5 or the average was <3 dyne/cm². All other flows were defined as heterogeneous. Heterogeneity of the CD45 count was considered in the context of the heterogeneity in the reported values for CD45 hotspots. The number of hotspots ranged from 1 to 3. Samples with only 1 spot were removed from analysis; 18 were assessed for wall heterogeneity. The

wall was considered homogeneous if all values in the sample were less than a threshold of 10 or greater than a threshold of 200. For those between these threshold values, a value of $(\text{maximum} - \text{minimum})/\text{SD} < 1.0$ was considered homogeneous.

Overall, proportions and frequencies were calculated for categorical variables; and for continuous variables, median and range were used because the distributions of the continuous variables deviated from normal distribution. The Fisher exact test was used to compare categorical variables. The nonparametric Spearman rank correlation test was used for correlations between 2 continuous variables; and the Mann-Whitney *U* test, for comparison of continuous and categorical variables. The Mann-Whitney *U* test was used as a one-sided test due to our limited statistical power (≤ 20 cases). Statistical analyses were performed by using Python scripts and the SciPy package (<http://www.scipy.org/>) or SPSS statistical software (IBM, Armonk, New York). *P* values $< .05$ were considered significant.

RESULTS

Factors Associated with Wall Degeneration and Rupture: Inflammation

In this series, flow-related hemodynamic variables did not significantly differ between ruptured and unruptured sIAs (On-line Table 3). Of the studied geometric variables, only the ellipticity index ($P = .047$) and Gaussian curvature ($P = .047$) were associated with rupture (On-line Table 4).

Compared with sIAs with walls that have a histology most resembling the composition of the normal arterial wall (A type, $n = 2$), sIAs with both thick walls and hyperplasia of mural cells (B-type walls, $n = 10$) as well as degenerated walls with loss of mural cells (C type, $n = 8$) had less oscillatory flows (lower oscillatory shear index [OSI] and maximum oscillatory shear index [OSImax], Table 1). Interestingly, thick hyperplastic walls were also associated with simpler and more stable flows (lower corelen, vortex core line length, a measure of flow complexity; and lower podent, proper orthogonal decomposition entropy, a measure of flow instability; Table 1), whereas loss of mural cells was associated with slower and more diffuse inflows (Table 1).

Degenerated walls characterized by loss of mural cells were associated with increased infiltration of inflammatory cells (wall types B versus C, $P = .011$; A versus C, $P = .041$). In addition to wall degeneration, inflammation was associated with rupture ($P = .031$, Fig 2A).

Factors Associated with Aneurysm Wall Inflammation: High Flow Conditions and Endothelial Damage

Inflammation was associated with WSS (Figs 2B and 3). The degrees of wall inflammation (CD45+ cells) in each WSS group are presented in Fig 2B. Aneurysms with high WSS ($n = 4$) had larger numbers of inflammatory cells than sIAs with mid-WSS levels ($n = 9$, $P = .018$). Also sIAs with low WSS ($n = 7$) had somewhat higher numbers of inflammatory cells than sIAs with mid-WSS levels, though the difference did not reach statistical significance. Other flow characteristics associated with increased inflammation were higher vorticity (VO, $P = .046$), higher viscous dissipation ($P = .046$), and higher shear rate ($P = .046$). Heterogeneity in the distribution of WSS across a single aneurysm sac was associ-

Table 1: Associations between flow characteristics and composition of the sIA wall^a

Hemodynamic Variable	Wall Type			P Values
	A	B	C	
ICI	2.24 (1.92–2.56)	0.62 (0.11–2.91)	0.36 (0.22–1.67)	$p_{AB} = .119, p_{AC} = .04, p_{BC} = .334$
Q	1.71 (1.22–2.19)	0.67 (0.52–2.32)	0.52 (0.31–0.95)	$p_{AB} = .081, p_{AC} = .041, p_{BC} = .291$
Corelen	5.56 (4.31–6.81)	1.48 (0.00–3.11)	0.46 (0.03–4.80)	$p_{AB} = .021, p_{AC} = .088, p_{BC} = .476$
Podent	0.55 (0.37–0.74)	0.24 (0.13–0.54)	0.19 (0.13–0.44)	$p_{AB} = .034, p_{AC} = .088, p_{BC} = .334$
OSImax	0.47 (0.46–0.49)	0.36 (0.26–0.46)	0.28 (0.10–0.44)	$p_{AB} = .034, p_{AC} = .041, p_{BC} = .213$
OSI	0.044 (0.03–0.05)	0.02 (0.01–0.03)	0.01 (0.00–0.03)	$p_{AB} = .021, p_{AC} = .041, p_{BC} = .427$

Note:—ICI indicates inflow concentration index; Q, inflow rate into the aneurysm; corelen, vortex core line length, a measure of flow complexity; podent, proper orthogonal decomposition entropy, a measure of flow instability.

^aMedian and range are given for the hemodynamic variables in each wall type group, and corresponding P values for comparisons between groups are given. p_{AB} = P value (A vs B), p_{AC} = P value (A vs C), p_{BC} = P value (B vs C). Group A is defined by an intact-looking wall with linearly organized smooth muscle cells and intact endothelium; group B, by smooth muscle cell hyperplasia; and group C, by loss of smooth muscle cells and endothelial cells complemented by degeneration of the extracellular matrix and luminal thrombosis.

^bSignificant.

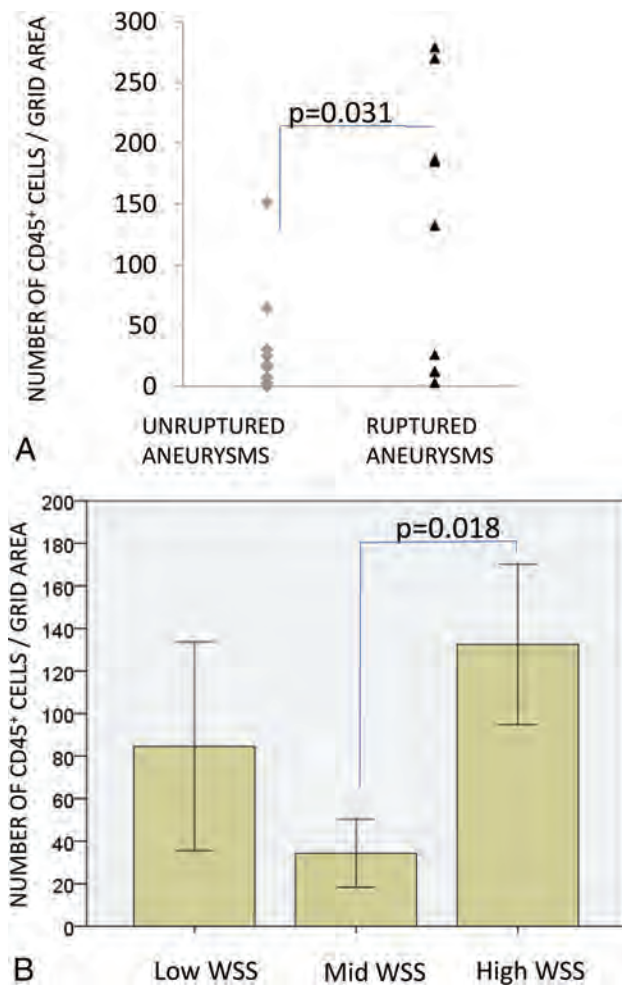


FIG 2. A, Infiltration of inflammatory cells (CD45+) associated with rupture and high mean wall shear stress. B, WSS grouping is as follows: mean WSS of < 4.5 dyne/cm² = low; $4.5 < \text{mean WSS} < 18$ dyne/cm² = mid; mean WSS > 18 dyne/cm² = high. Bars display means, and error bars, standard error of mean.

ated with heterogeneity in the number of CD45+ cells across the wall ($P = .035$), suggesting that interactions leading to the association of high WSS and inflammation might happen focally at the wall. More inflammatory cells (CD45+) were found in sIA walls that lacked an intact endothelium ($P = .034$, Table 2), as well as in sIAs with organized thrombus ($P = .018$), suggesting that

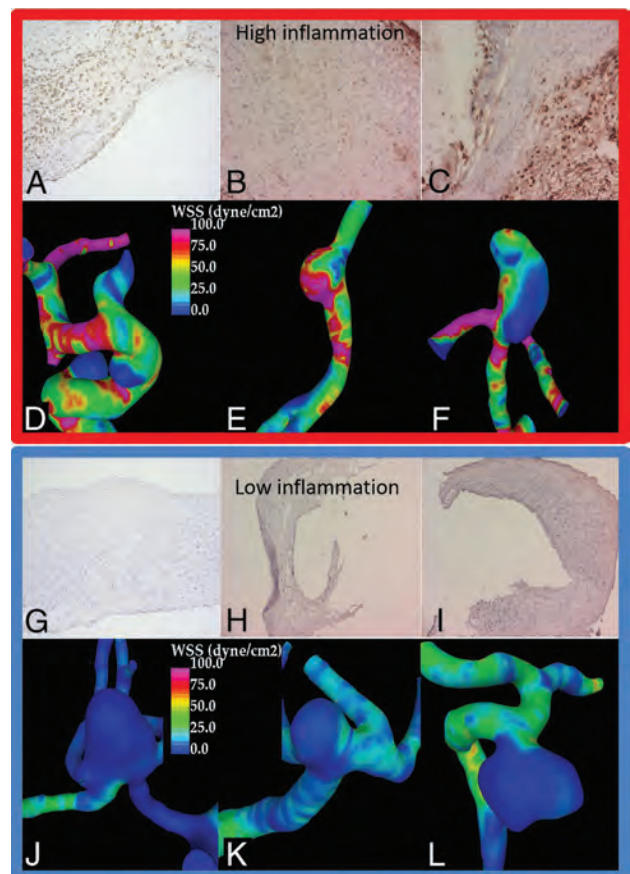


FIG 3. A–F, Three aneurysms from the high WSS group with substantial wall inflammation. A–C, CD45 immunostaining and inflammatory cells in brown along with 3 aneurysms from the low WSS group (G–L) with little wall inflammation (J–L, negative CD45 immunostaining).

damage to the endothelium may mediate the association of flow and inflammation.

Factors Associated with Endothelial Damage: High Flow Conditions

Lack of an intact endothelium was associated with higher vorticity ($P = .034$), higher viscous dissipation ($P = .020$), and higher shear rate ($P = .034$), similar to inflammation. In addition, lack of an endothelium was associated with lower OSImax ($P = .034$), similar to wall remodeling (B- and C-type walls compared with A-type walls). In this series, the sIAs that lacked an intact endo-

Table 2: Association of damage to the sIA wall endothelium (assessed through presence of CD31+ luminal cells with endothelial cell morphology) with wall inflammation (CD45+ cells), hemodynamics, and geometry of the sIA^a

Variables	Condition of the Endothelium		P Value
	Intact	Damaged	
Histology			
CD45+ cells	13 (7–8)	30 (12–279)	.034 ^b
Hemodynamics			
VO	41.2 (38.9–72.3)	191.8 (47.3–317.8)	.034 ^b
VD	23.2 (15.9–45.6)	291.1 (35.0–1027.6)	.020 ^b
SR	28.2 (27.7–51.3)	129.1 (41.5–231.9)	.034 ^b
OSImax	0.30 (0.04–0.41)	0.18 (0.01–0.47)	.034 ^b
Geometry			
Size	15 mm (10–21 mm)	7 mm (4–12 mm)	.020 ^b
Nsize	9 mm (7–13 mm)	5 mm (4–9 mm)	.020 ^b
UI	0.13 (0.04–0.13)	0.25 (0.10–0.35)	.034 ^b
EI	0.24 (0.24–0.24)	0.26 (0.25–0.30)	.011 ^b

Note:—VD indicates viscous dissipation; SR, shear rate; Nsize, neck size; UI, increased undulation; EI, ellipticity index.

^a Values are given as median and range.

^b Significant.

thelium were smaller ($P = .020$), had smaller necks ($P = .020$), and had increased undulation ($P = .034$) and ellipticity ($P = .011$, Table 2).

DISCUSSION

Degenerative wall remodeling, inflammation, and nonphysiologic flow conditions have been previously shown to be associated with sIA rupture.^{6,13,14,28} Although we and others have suggested possible mechanisms by which pathologic flow conditions may lead to degenerative wall remodeling,^{10,12,16,29} this is the first study that compares in vivo flow conditions with the histology of human intracranial aneurysms.

Flow Conditions Associated with Degenerative Wall Remodeling and Inflammation

We have previously shown that loss of mural smooth muscle cells leads to aneurysm growth and rupture in experimental models⁹ and is associated with rupture in human sIAs.³⁰ The cause of smooth muscle cell loss and the degenerative remodeling in human aneurysms is still unknown, but inflammation of the sIA wall has been suggested as a potential cause of the degenerative remodeling that predisposes to rupture.³¹ Moreover, even if not the cause of wall degeneration, inflammation modulates the remodeling of the sIA wall.^{7,10}

In this series, proliferative (hyperplasia) wall remodeling was associated with simple, stable flows, whereas degenerative remodeling (loss of cells and damage to the extracellular matrix) was associated with slower and diffuse inflows. Whether simple, stable flows are needed for the proliferative remodeling, whereas slower and diffuse inflows trigger degenerative processes leading to cell death in the sIA wall remains to be determined. Inflammation of the sIA wall was significantly associated with high flow conditions (Figs 3 and 4), but not with flow conditions that were associated with degenerative remodeling and loss of mural cells (C-type walls). This finding could suggest that flow patterns and hemodynamic stress may affect sIA wall remodeling, including mural smooth muscle cell proliferation and cell death, independent of

wall inflammation. Moreover, it suggests that part of the inflammatory cell response in the sIA wall may be induced by high flow conditions, independent of the wall remodeling.

Flow-Mediated Endothelial Damage as the Trigger of Wall Remodeling and Inflammation?

Endothelial cells are sensors of WSS in the arterial wall.³² They contribute to the control of blood flow in the vessel by regulating muscle tone in the vessel wall and subsequently vessel diameter.³² Endothelial cells also maintain a very important barrier function between the bloodstream and the vessel wall^{32–34} and actively prevent luminal thrombosis.³⁵

The proper function of endothelial cells is very easily disturbed by nonphysiologic (either too high or too low) WSS.^{32–34}

In our series, sIAs that lacked an intact endothelium had more inflammation, and lack of an endothelium was associated with flow conditions similar to those of inflammation. These similar associations among flow conditions, wall inflammation, and loss of endothelial cells suggest that endothelial damage caused by nonphysiologic flow conditions can be a mechanism by which flow conditions trigger or modulate inflammation in the sIA wall.

Although this is the first study to demonstrate associations with sIA wall degeneration and flow conditions in vivo in true sIAs in patients, aberrant flow conditions have been suspected as promoters of sIA wall degeneration, growth, and rupture before.^{10,16,31} Loss of an intact endothelium is characteristic of ruptured sIAs and of degenerated sIA walls.^{5,6} Loss of endothelium exposes thrombogenic matrix surfaces³⁵ and thus predisposes to thrombus formation, which is also characteristic of ruptured sIAs and of degenerated sIA walls.^{5,6} Thrombus can trigger and promote wall degeneration via several mechanisms that cause cell death and proteolytic injury.^{10,16,38} In this series, high inflammation (CD45+) was found in sIAs with organized thrombus (older thrombus) but not in sIAs with only fresh thrombus, suggesting that the prolonged presence of thrombus or degradation of the thrombus with time is what increases inflammation in the sIA wall.

Clinical Implications

Both high and low WSS have previously been implicated as promoters of sIA wall degeneration.^{12–14,39} Most interesting, in this series, high WSS and conditions of high flow in general (high shear rate, high vorticity, high viscous dissipation) were associated with inflammation, whereas low flow was associated with a degenerated wall that had lost mural cells. The observation that different types of flow were associated with distinct histologic changes suggests that flow may affect sIA wall remodeling via several mechanisms and that flow conditions can induce different changes in the sIA wall at different time points during the remodeling of the sIA wall.⁴⁰

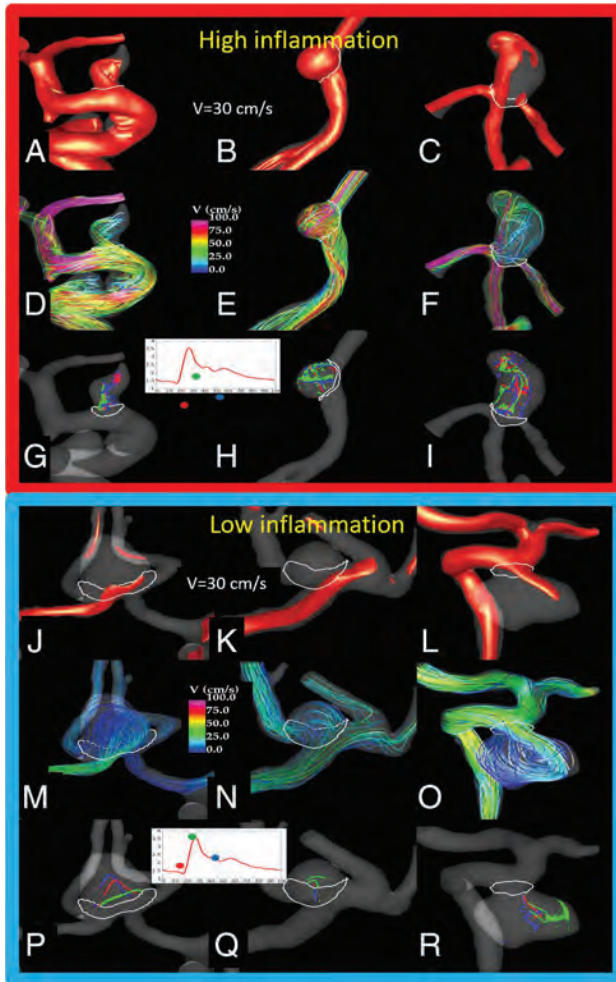


FIG 4. Flow conditions in the 6 sample aneurysms (Fig 3) with high or no inflammation in the wall. The visualizations show the following: the inflow jet at peak systole (A–C, J–L), the flow pattern at peak systole (D–F, M–O), and vortex core lines at 3 instances during the cardiac cycle (G–I, P–R), to illustrate both the complexity of the flow pattern and its change during the cycle (instability). An aneurysm with inflammation (upper panel) had a strong inflow jet impacting the aneurysm dome and producing complex (but somewhat stable) flow structures and associated WSS distributions with regions of high WSS and regions of low WSS near the outflow. In contrast, aneurysms with no inflammation had more diffuse inflows entering the aneurysms at lower velocity and diffusing into a simpler but more variable (unstable) flow pattern, with associated WSS distribution characterized by a fairly uniformly low WSS.

Although it is still unclear whether inflammation is the cause of sIA rupture or a reaction to the cause of the degenerative remodeling that predisposes to rupture, inflammation is clearly an indicator of a degenerated, rupture-prone sIA wall, as demonstrated by histopathologic studies^{5,6,28} and by ferumoxytol-based MR imaging of inflammatory cells in the sIA wall in patients.⁴¹ We now demonstrate that flow conditions determined with patient-specific computational fluid dynamics simulations are associated with the presence of inflammation in the sIA wall. This finding supports the concept that patient-specific flow simulations could be used to distinguish those sIAs that will develop wall inflammation and thus would require either more frequent follow-up imaging or perhaps even more active treatment. Most important, our results also show that computerized geometric

indexes are not similarly associated with wall inflammation and cannot replace flow simulations, even if sIA and parent artery geometry are some of the main determinants of flow conditions in the aneurysm.

In this series, flow dynamics was associated with wall inflammation and with other histologic changes in the sIA wall in small sIAs. Because it is well-established that risk of sIA rupture increases with sIA size^{42,43} but that many of the sIAs that do rupture are small,⁴⁴ it is particularly useful to develop novel diagnostic tools that would predict rupture risk in small sIAs that otherwise would be mistaken for benign, low risk lesions.

Limitations of the Study and Topics for Further Studies

Our series is a highly selected one, with bias in sIA size and clinical risk factors. This kind of selection bias is unavoidable in any kind of study that uses patient-derived tissue samples collected intraoperatively. Moreover, because not all sIAs undergo an operation and not all of those that do are suitable for the acquisition of tissue samples, our series is somewhat limited in number of samples and statistical power. Computational fluid dynamics models make several assumptions and are constructed from CTA images with limited resolution, which could affect the representation of the intrasaccular flows, especially for aneurysms with narrow necks. Our findings need to be replicated in other, similar or larger patient series and in experimental models. Experimental models and computer simulations with cell-cell interaction are needed to establish causality between the different associations and to provide mechanistic insight.

Most interesting, in this series that focused on the time- and space-averaged flow conditions in the whole sIA, heterogeneity in the distribution of WSS across the aneurysm sac was associated with heterogeneity in the number of CD45+ cells in the wall. This finding suggests that the flow-induced cellular interactions that lead to increased inflammation (eg, loss of endothelial cells) might happen focally at the wall. Further studies should include histologic data from different regions of the sIA wall and spatial registration of these histologic changes with focal flow conditions. These studies are also needed to confirm our findings because sIA walls are highly heterogeneous in structure (Fig 1) and this local variation in the aneurysm wall may have biased our results because we were not able to analyze the histology of the whole sIA wall.

In addition, flow simulations need to be correlated with the biology of the sIA wall and the structural strength of the aneurysm wall, to develop a diagnostic tool from computational fluid dynamics models.^{8,35} This requirement is paramount to understand how different kinds of flow patterns affect the sIA wall, which is critical to properly use this technology in diagnostics.

CONCLUSIONS

We show that flow conditions in saccular intracranial aneurysms are associated with inflammation and other histologic changes in the aneurysm wall. In particular, high- and low-flow conditions are associated with different wall changes. This study suggests that computational simulations that determine patient-specific flow conditions could be used to identify aneurysms at risk for devel-

oping inflammation and other rupture-associated changes in their walls.

Degenerative wall remodeling, inflammation, and nonphysiologic flow conditions have been previously shown to be associated with sIA rupture.^{6,13,14,28} Although we and others have suggested possible mechanisms by which pathologic flow conditions may lead to degenerative wall remodeling,^{10,12,16,29} this is the first study that compares in vivo flow conditions with the histology of human intracranial aneurysms.

Disclosures: Juan Cebral—RELATED: Grant: National Institutes of Health*; UNRELATED: Grants/Grants Pending: National Institutes of Health, Philips Healthcare. Eliisa Ollikainen—RELATED: Grant: Helsinki University Central Hospital Engineering Virtual Organization grants, Helsinki Biomedical Graduate Program Funding, Orion Research Foundation, and the Finnish Medical Foundation; UNRELATED: Employment: Helsinki City Hospital and Helsinki University Central Hospital. Fernando Mut—RELATED: Grant: National Institutes of Health.* Visa Sippola—UNRELATED: Employment: Helsinki and Uusimaa Hospital District, Aalto University, Comments: employment as a researcher, no conflicts of interest concerning the study topic. Mika Niemelä—RELATED: TYH2014236.* Comments: research grant by the state. Anne Robertson—RELATED: Grant: National Institutes of Health National Institute of Neurological Disorders and Stroke (R2INS080031).* Juhana Frösen—RELATED: Grant: Finnish Medical Foundation.* *Money paid to the institution.

REFERENCES

1. Vlak MH, Algra A, Brandenburg R, et al. **Prevalence of unruptured intracranial aneurysms, with emphasis on sex, age, comorbidity, country, and time period: a systematic review and meta-analysis.** *Lancet Neurol* 2011;10:626–36 CrossRef Medline
2. Karamanakos PN, von Und Zu Fraunberg M, Bendel S, et al. **Risk factors for three phases of 12-month mortality in 1657 patients from a defined population after acute aneurysmal subarachnoid hemorrhage.** *World Neurosurg* 2012;78:631–39 CrossRef Medline
3. Korja M, Lehto H, Juvela S. **Lifelong rupture risk of intracranial aneurysms depends on risk factors: a prospective Finnish cohort study.** *Stroke* 2014;45:1958–63 CrossRef Medline
4. Kotowski M, Naggara O, Darsaut TE, et al. **Safety and occlusion rates of surgical treatment of unruptured intracranial aneurysms: a systematic review and meta-analysis of the literature from 1990 to 2011.** *J Neurol Neurosurg Psychiatry* 2013;84:42–48 CrossRef Medline
5. Kataoka K, Taneda M, Asai T, et al. **Structural fragility and inflammatory response of ruptured cerebral aneurysms: a comparative study between ruptured and unruptured cerebral aneurysms.** *Stroke* 1999;30:1396–401 CrossRef Medline
6. Frösen J, Piippo A, Paetau A, et al. **Remodeling of saccular cerebral artery aneurysm wall is associated with rupture: histological analysis of 24 unruptured and 42 ruptured cases.** *Stroke* 2004;35:2287–93 CrossRef Medline
7. Tulamo R, Frösen J, Hernesniemi J, et al. **Inflammatory changes in the aneurysm wall: a review.** *J Neurointerv Surg* 2010;2:120–30 CrossRef Medline
8. Robertson AM, Duan X, Aziz KM, et al. **Diversity in the strength and structure of unruptured cerebral aneurysms.** *Ann Biomed Eng* 2015; 43:1502–15 CrossRef Medline
9. Marbacher S, Marjamaa J, Bradacova K, et al. **Loss of mural cells leads to wall degeneration, aneurysm growth, and eventual rupture in a rat aneurysm model.** *Stroke* 2014;45:248–54 CrossRef Medline
10. Frösen J, Tulamo R, Paetau A, et al. **Saccular intracranial aneurysm: pathology and mechanisms.** *Acta Neuropathol* 2012;123:773–86 CrossRef Medline
11. Sforza D, Putman CM, Cebral JR. **Hemodynamics of cerebral aneurysms.** *Annu Rev Fluid Mech* 2009;41:91–107 CrossRef Medline
12. Shojima M, Oshima M, Takagi K, et al. **Magnitude and role of wall shear stress on cerebral aneurysm: computational fluid dynamic study of 20 middle cerebral artery aneurysms.** *Stroke* 2004;35: 2500–05 CrossRef Medline
13. Cebral JR, Mut F, Weir J, et al. **Quantitative characterization of the hemodynamic environment in ruptured and unruptured brain aneurysms.** *AJNR Am J Neuroradiol* 2011;32:145–51 CrossRef Medline
14. Xiang J, Natarajan SK, Tremmel M, et al. **Hemodynamic-morphologic discriminants for intracranial aneurysm rupture.** *Stroke* 2011; 42:144–52 CrossRef Medline
15. Castro MA, Putman CM, Radaelli A, et al. **Hemodynamics and rupture of terminal cerebral aneurysms.** *Acad Radiol* 2009;16:1201–07 CrossRef Medline
16. Ujiie H, Tachibana H, Hiramatsu O, et al. **Effects of size and shape (aspect ratio) on the hemodynamics of saccular aneurysms: a possible index for surgical treatment of intracranial aneurysms.** *Neurosurgery* 1999;45:119–29; discussion 129–30 CrossRef Medline
17. Ollikainen E, Tulamo R, Frösen J, et al. **Mast cells, neovascularization, and microhemorrhages are associated with saccular intracranial artery aneurysm wall remodeling.** *J Neuropathol Exp Neurol* 2014;73:855–64 CrossRef Medline
18. Cebral JR, Castro MA, Appanaboyina S, et al. **Efficient pipeline for image-based patient-specific analysis of cerebral aneurysm hemodynamics: technique and sensitivity.** *IEEE Trans Med Imaging* 2005;24:457–67 CrossRef Medline
19. Mut F, Aubry R, Löhner R, et al. **Fast numerical solutions of patient-specific blood flows in 3D arterial systems.** *Int J Num Meth Biomed Eng* 2010;26:73–85 CrossRef Medline
20. Taylor CA, Hughes TJ, Zarins CK. **Finite element modeling of blood flow in arteries.** *Comp Meth App Mech Eng* 1998;158:155–96 CrossRef
21. Ford MD, Alperin N, Lee SH, et al. **Characterization of volumetric flow rate waveforms in the normal internal carotid and vertebral arteries.** *Physiol Meas* 2005;26:477–88 CrossRef Medline
22. Cebral JR, Castro MA, Putman CM, et al. **Flow-area relationship in internal carotid and vertebral arteries.** *Physiol Meas* 2008;29:585–94 CrossRef Medline
23. Murray CD. **The physiological principle of minimum work, II: oxygen exchange in capillaries.** *Proc Natl Acad Sci U S A* 1926;12: 207–14 Medline
24. Mut F, Löhner R, Chien A, et al. **Computational hemodynamics framework for the analysis of cerebral aneurysms.** *Int J Numer Method Biomed Eng* 2011;27:822–39 CrossRef Medline
25. Cebral JR, Duan X, Gade PS, et al. **Regional mapping of flow and wall characteristics of intracranial aneurysms.** *Ann Biomed Eng* 2016 Jun 27. [Epub ahead of print] Medline
26. Ma B, Harbaugh RE, Raghavan ML. **Three-dimensional geometrical characterization of cerebral aneurysms.** *Ann Biomed Eng* 2004;32: 264–73 CrossRef Medline
27. Raghavan ML, Ma B, Harbaugh RE. **Quantified aneurysm shape and rupture risk.** *J Neurosurg* 2005;102:355–62 CrossRef Medline
28. Tulamo R, Frösen J, Junnikkala S, et al. **Complement activation associates with saccular cerebral artery aneurysm wall degeneration and rupture.** *Neurosurgery* 2006;59:1069–76; discussion 1076–77 Medline
29. Cebral JR, Castro MA, Burgess JE, et al. **Characterization of cerebral aneurysms for assessing risk of rupture by using patient-specific computational hemodynamics models.** *AJNR Am J Neuroradiol* 2005;26:2550–59 Medline
30. Frösen J. **Smooth muscle cells and the formation, degeneration, and rupture of saccular intracranial aneurysm wall: a review of current pathophysiological knowledge.** *Transl Stroke Res* 2014;5:347–56 CrossRef Medline
31. Chalouhi N, Hoh BL, Hasan D. **Review of cerebral aneurysm formation, growth, and rupture.** *Stroke* 2013;44:3613–22 CrossRef Medline
32. Tarbell JM, Simon SI, Curry FR. **Mechanosensing at the vascular interface.** *Annu Rev Biomed Eng* 2014;16:505–32 CrossRef Medline
33. Tarbell JM. **Shear stress and the endothelial transport barrier.** *Cardiovasc Res* 2010;87:320–30 CrossRef Medline
34. Pan S. **Molecular mechanisms responsible for the atheroprotective effects of laminar shear stress.** *Antioxid Redox Signal* 2009;11: 1669–82 CrossRef Medline

35. Aksu K, Donmez A, Keser G. **Inflammation-induced thrombosis: mechanisms, disease associations and management.** *Curr Pharm Des* 2012;18:1478–93 CrossRef Medline
36. Cebal JR, Duan X, Chung BJ, et al. **Wall mechanical properties and hemodynamics of unruptured intracranial aneurysms.** *AJNR Am J Neuroradiol* 2015;36:1695–703 CrossRef Medline
37. Kallmes DF. **Point: CFD—computational fluid dynamics or confounding factor dissemination.** *AJNR Am J Neuroradiol* 2012;33:396–98 CrossRef Medline
38. Cebal JR, Meng H. **Counterpoint: realizing the clinical utility of computational fluid dynamics—closing the gap.** *AJNR Am J Neuroradiol* 2012;33:396–98 CrossRef Medline
39. Meng H, Tutino VM, Xiang J, et al. **High WSS or low WSS? Complex interactions of hemodynamics with intracranial aneurysm initiation, growth, and rupture—toward a unifying hypothesis.** *AJNR Am J Neuroradiol* 2014;35:1254–62 CrossRef Medline
40. Robertson AM, Watton PN, **Computational fluid dynamics in aneurysm research: critical reflections, future directions.** *AJNR Am J Neuroradiol* 2012;33:992–95 CrossRef Medline
41. Hasan D, Chalouhi N, Jabbour P, et al. **Early change in ferumoxytol-enhanced magnetic resonance imaging signal suggests unstable human cerebral aneurysm: a pilot study.** *Stroke* 2012;43:3258–65 CrossRef Medline
42. Wiebers DO, Whisnant JP, Huston J 3rd, et al; International Study of Unruptured Intracranial Aneurysms Investigators. **Unruptured intracranial aneurysms: natural history, clinical outcome, and risks of surgical and endovascular treatment.** *Lancet* 2003;362:103–10 CrossRef Medline
43. Morita A, Kirino T, Hashi K, et al; UCAS Japan Investigators. **The natural course of unruptured cerebral aneurysms in a Japanese cohort.** *N Engl J Med* 2012;366:2474–82 CrossRef Medline
44. Huttunen T, von und zu Fraunberg M, Frösen J, et al. **Saccular intracranial aneurysm disease: distribution of site, size, and age suggests different etiologies for aneurysm formation and rupture in 316 familial and 1454 sporadic eastern Finnish patients.** *Neurosurgery* 2010;66:631–38; discussion 638 CrossRef Medline

Embolization of Intracranial Dural Arteriovenous Fistulas Using PHIL Liquid Embolic Agent in 26 Patients: A Multicenter Study

S. Lamin, H.S. Chew, S. Chavda, A. Thomas, M. Piano, L. Quilici, G. Pero, M. Holtmannspolter, M.E. Cronqvist, A. Casasco, L. Guimaraens, L. Paul, A. Gil Garcia, A. Aleu, and R. Chapot

ABSTRACT

BACKGROUND AND PURPOSE: The introduction of liquid embolic agents has revolutionized endovascular approach to cranial vascular malformations. The aim of the study was to retrospectively assess the efficacy and safety of Precipitating Hydrophobic Injectable Liquid (PHIL), a new nonadhesive liquid embolic agent, in the treatment of patients with cranial dural arteriovenous fistulas. The primary end point was the rate of complete occlusion of dural arteriovenous fistulas. Secondary end points included the incidence of adverse events and clinical status at 3-month follow-up.

MATERIALS AND METHODS: This was a retrospective multicenter study. Twenty-six consecutive patients with dural arteriovenous fistulas (de novo or previously treated) treated by injection of PHIL only or with PHIL in combination with other embolization products (such as Onyx or detachable coils) were included in the study. Recruitment started in August 2014 and ended in September 2015.

RESULTS: Twenty-two (85%) patients were treated with PHIL only, with 3 patients treated with both PHIL and Onyx, and 1, with both PHIL and coils. Immediate complete angiographic occlusion was achieved in 20 (77%) patients. Of the 6 patients with residual fistulas, 3 were retreated with PHIL and 1 achieved angiographic cure. An adverse event was seen in 1 patient who developed worsening of preexisting ataxia due to acute thrombosis of the draining vein.

CONCLUSIONS: PHIL appears to be safe and effective for endovascular treatment of cranial dural arteriovenous fistulas. Short-term angiographic and clinical results are comparable with those of Onyx, with the added advantage of easier preparation and improved homogeneous cast visualization. The use of iodine as a radio-opacifier also produces considerably less artifacts on CT compared with tantalum-based embolic materials.

ABBREVIATIONS: DAVF = dural arteriovenous fistula; DMSO = dimethyl-sulfoxide; PHIL = Precipitating Hydrophobic Injectable Liquid

Dural arteriovenous fistulas (DAVFs) are a rare type of acquired intracranial vascular malformation consisting of a pathologic shunt located within the dura mater of the brain.¹⁻³ These lesions have been categorized by Awad et al,⁴ Borden et al,⁵ and Cognard et al⁶ according to their locations and patterns of venous drainage. Acute presentation with intracranial hemorrhage occurs in up to 65% of patients,⁶ and patients with a previ-

ous intracranial hemorrhage may have up to a 35% risk of another neurologic event within 2 weeks.⁷

Endovascular embolization has become the primary treatment approach for DAVFs.^{1,8,9} The goal of endovascular therapy is to achieve complete obliteration of the fistulous point between the feeding arteries and the draining veins. This can be safely accomplished by occluding the draining veins, which often results in complete closure of the lesion, unlike in cerebral arteriovenous malformations.

The introduction of liquid embolic agents has a significant impact on the endovascular approach to DAVFs. Precipitating Hydrophobic Injectable Liquid (PHIL; MicroVention, Tustin, California) is a new nonadhesive liquid embolic agent comprising a copolymer dissolved in dimethyl-sulfoxide (DMSO). It is delivered by slow and controlled injection through a DMSO-compatible microcatheter under fluoroscopic control. An iodine component is chemically bonded to the copolymer to provide homogeneous radio-opacity during fluoroscopic visualization. When it comes in contact with human blood, the DMSO solvent

Received April 25, 2016; accepted after revision July 24.

From the Department of Neuroradiology (S.L., H.S.C., S.C., A.T.), University Hospitals Birmingham National Health Service Foundation Trust, Queen Elizabeth Hospital Birmingham, UK; Neuroradiologia Department (M.P., L.Q., G.P.), Ospedale Niguarda Ca' Granda, Milan, Italy; Department of Neuroradiology, Section 3023 (M.H., M.E.C.), University of Copenhagen, Rigshospitalet, Copenhagen, Denmark; Instituto de Neurociencias Avanzadas de Madrid (A.C., L.G., L.P., A.G.G., A.A.), Hospital Nuestra Señora del Rosario, Madrid, Spain; and Klinik für Radiologie und Neuroradiologie (R.C.), Alfried Krupp Krankenhaus, Essen, Germany.

Please address correspondence to Saleh Lamin, MD, Department of Neuroradiology, Queen Elizabeth Hospital Birmingham, Mindelsohn Way, Edgbaston, B15 2GW Birmingham, United Kingdom; e-mail: Saleh.Lamin@uhb.nhs.uk

<http://dx.doi.org/10.3174/ajnr.A5037>

dissipates, causing the copolymer to precipitate in situ into a coherent embolus. The PHIL liquid embolic system is available in 3 formulations: 25%, 30%, and 35%. PHIL 25% will travel more distally and penetrate deeper into the fistula due to its lower viscosity compared with PHIL 30% or 35%. The latter 2 are more appropriate for use in high-flow arteriovenous shunts with ≥ 1 direct fistula. Higher strength formulations are also preferred when increased fluoroscopic visibility is desirable.

The aim of our study was to assess the efficacy and safety of PHIL in the treatment of patients with cranial DAVFs.

MATERIALS AND METHODS

Study Design and Setting

This was a retrospective multicenter study. Five European institutions with experience with the PHIL embolic agent for DAVF treatment participated in the study: Queen Elizabeth Hospital Birmingham (United Kingdom), Copenhagen Righospitalet (Denmark), Alfried Krupp Krankenhaus in Essen (Germany), Hospital Rosario in Madrid (Spain), and Ospedale Niguarda Ca' Granda in Milan (Italy).

Participants

Twenty-six consecutive patients with DAVFs (de novo or previously treated) treated by embolization with PHIL only or PHIL used in combination with other embolization products such as Onyx (Covidien, Irvine, California) or detachable coils were included in the study. Recruitment started in August 2014 and ended in September 2015.

Study End Points

The primary end point was the rate of complete angiographic occlusion of the DAVF. Secondary end points included the incidence of adverse events and clinical status at 3-month follow-up.

Data Collection

Patient information including sociodemographic data, medical history, description of the DAVF, procedure details, procedure-related adverse events, and follow-up angiographic and clinical results were collected by the participating investigators, by using an electronic case report form developed specifically for the evaluation. The principal investigator reviewed all reported data for inconsistencies/missing information and sought clarification with individual investigators when needed.

Data Analysis

Only descriptive analyses were performed.

RESULTS

Patient Details

From August 2014 to September 2015, 26 consecutive patients (13 men and 13 women) with cranial DAVFs were treated with the PHIL embolic agent. Among the 26 patients, 30 total procedures were performed, with an average of 1.15 procedures per patient. The mean age of these patients was 60 ± 13 years (median, 57 years; range, 43–90 years).

Seven patients presented acutely, with intracranial hemorrhage (2 patients), hydrocephalus, seizure, venous sinus thrombosis, lower limb monoparesis, and visual loss. The remaining 19

Table 1: Baseline characteristics of patients

	Patients (No.)
Clinical status	
mRS	
Scale 0	9 (34%)
Scale 1	14 (54%)
Scale 2	1 (4%)
Scale 4	1 (4%)
Unknown	1 (4%)
DAVF type	
Cognard classification	
Type I	2 (7%)
Type IIa	3 (12%)
Type IIa + IIb	2 (7%)
Type IIb	3 (12%)
Type III	9 (33%)
Type IV	5 (19%)
Type V	1 (4%)
Unknown	1 (4%)

Table 2: Immediate posttreatment angiographic results by DAVF type

	DAVF Type (No.)			
	\leq Type IIa	$>$ Type IIa	Unknown Type	All Types
Complete occlusion	5 (100%)	14 (70%)	1 (100%)	20 (77%)
Partial occlusion	0	6 (30%)	0	6 (23%)

patients (73%) were asymptomatic. Most (17/26, 65%) of the DAVFs were de novo lesions; while 8/26 (30%) DAVFs had been previously embolized with Onyx. Information regarding previous treatment was not available for 1 patient.

The locations of DAVFs were the transverse sinus (8/26), vein of Galen (7/26), superior sagittal sinus (4/26), and others (7/26). Most patients (20/26, 77%) presented with aggressive DAVFs (type IIb or higher), with $>50\%$ of cases being types III and IV. Five of 26 (19%) patients had type I or IIa DAVFs. The DAVF grade was not reported in 1 patient (Tables 1 and 2).

Procedure Description

Twenty-two (85%) patients were treated with PHIL only, 3 patients were treated with PHIL and Onyx, and 1, with PHIL and detachable coils. Commonly used microcatheters for injection were Headway Duo (10/26; MicroVention), Apollo (7/26; Covidien), and Marathon (4/26; Covidien). Treatment was performed through the injection of the middle meningeal (19/26), occipital (1/26), and vertebral (1/26) arteries and others (5/26). Remodeling balloon catheters were used for venous sinus protection in 7 patients. PHIL 25% was used in most patients (29/30, 90%). The mean duration of the injection was 32 minutes, and the mean volume injected was 1.25 mL. The extent of reflux along the catheter tip was <1 cm in 10/30 procedures, between 1 and 2 cm in 7/30 procedures, and >2 cm in 11/30 procedures. In 2 procedures, the severity of reflux was not reported.

Postprocedure Results

Posttreatment control runs demonstrated complete occlusion of the DAVF in 20/26 patients (77%), including all 5 patients with DAVF types \leq IIa and 14/20 (70%) patients with DAVF types $>$ IIa (Table 2). The results by location showed a higher rate of

complete occlusion in those with vein of Galen (86%) and superior sagittal sinus (100%) lesions (Table 3). Three of 6 patients with partial occlusion underwent additional embolization with PHIL: One of them achieved an angiographic cure, but the other 2 still have a residual shunt.

We had 1 adverse event in our series. This involved a patient with a complex type III vein of Galen DAVF who developed worsening of ataxia after initial embolization due to acute thrombosis of the draining vein.

Follow-Up Results

A follow-up assessment of angiographic occlusion and clinical outcome (mRS) was conducted for 11/26 (42%) patients at 3 months. The mean duration between the final embolization procedure and the follow-up visit was 89 days. The mRS score was evaluated in 10 patients, and angiographic assessment was performed in all 11 patients (9 DSAs and 2 MRAs). Seven of 10 patients had not experienced a change in the mRS score since the postprocedure visit, while 3/10 patients reported an improvement in the mRS score from grade 1 to 0.

Angiographic controls showed 9/11 patients with complete DAVF occlusion at 3 months. Two patients with residual shunts received additional treatment with the PHIL, and 1 of them was successfully occluded. Of the 9 patients with complete angiographic occlusion at 3 months, 2 underwent follow-up angiography at 1 year, which confirmed persistent DAVF occlusion.

DISCUSSION

The objective of endovascular treatment of DAVFs is to completely obliterate the fistulous point between the feeding arteries and draining veins. In our study of 26 consecutive patients treated with PHIL, 20/26 (77%) achieved complete angiographic oc-

clusion at the end of the initial embolization. We identified 1 procedure-related adverse event in a patient who developed worsening of preexisting ataxia due to acute thrombosis of the draining vein.

Our study is, however, limited by the relatively low number of short-term angiographic and clinical follow-ups. Persistent occlusion was observed in 9/11 (82%) patients who had a 3-month follow-up visit, 3 patients showed improved clinical status, and the remaining patients reported stable neurologic functions at 3-month follow-up.

Similar results in terms of complete occlusion and the rate of adverse events were observed in studies conducted in patients treated with Onyx. The largest retrospective study reviewed 53 DAVFs embolized with *n*-BCA or Onyx from November 2003 to November 2008 in the Massachusetts General Hospital (Boston).¹⁰ In this study, 83% (29/35) of DAVFs treated with Onyx showed complete occlusion at the 3-month postprocedure visit, while only 33% (7/21) of patients treated with *n*-BCA had complete occlusion. Three patients treated with Onyx experienced major neurologic adverse events, including 2 facial nerve palsies and an asymptomatic clot formation in the external carotid artery.

Cognard et al¹¹ included 30 patients with cranial DAVFs treated with Onyx in a prospective study between July 2003 and November 2006. Twenty-four of 30 (80%) patients who underwent treatment were found to have complete closure of the fistula on the immediate posttreatment angiographic control. They reported 2 adverse events: One patient woke up with third and fourth cranial nerve palsies as well as fifth cranial nerve territory pain; the other patient developed acute cerebellar syndrome.

Nogueira et al¹² performed a retrospective analysis of 12 consecutive patients with intracranial DAVFs who were treated with Onyx as the only embolic agent between March 2006 and February 2007. Seventeen procedures were performed in 12 patients. Complete angiographic cure on immediate posttreatment angiography was achieved in 10 patients (80%). There was 1 technical complication that resulted in asymptomatic extracranial vertebral artery dissection.

Lv et al¹³ reported 31 cases of patients with DAVFs treated by embolization with Onyx between February 2005 and February

Table 3: Immediate posttreatment angiographic results by location of the DAVF

	DAVF Location (No.)			
	Transverse Sinus	Vein of Galen	Superior Sagittal Sinus	Others
Complete occlusion	5 (63%)	6 (86%)	4 (100%)	5 (71%)
Partial occlusion	3 (37%)	1 (14%)	0	2 (29%)

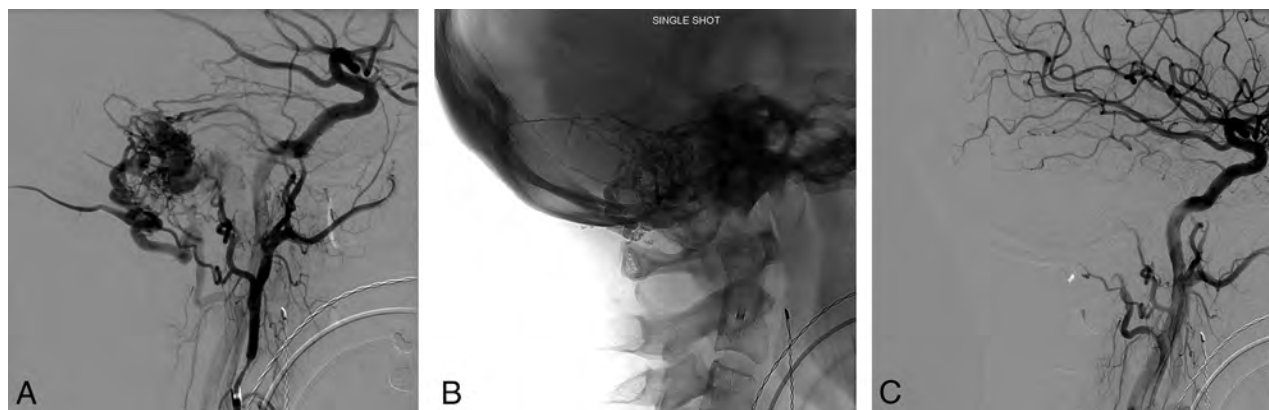


FIG 1. A, Right sigmoid sinus DAVF receives arterial supply from branches of the right occipital, posterior auricular, and middle meningeal arteries as demonstrated on the pre-embolization DSA. B, Posttreatment unsubtracted single-shot image demonstrates the PHIL cast. C, Control run confirms complete angiographic occlusion of the DAVF.

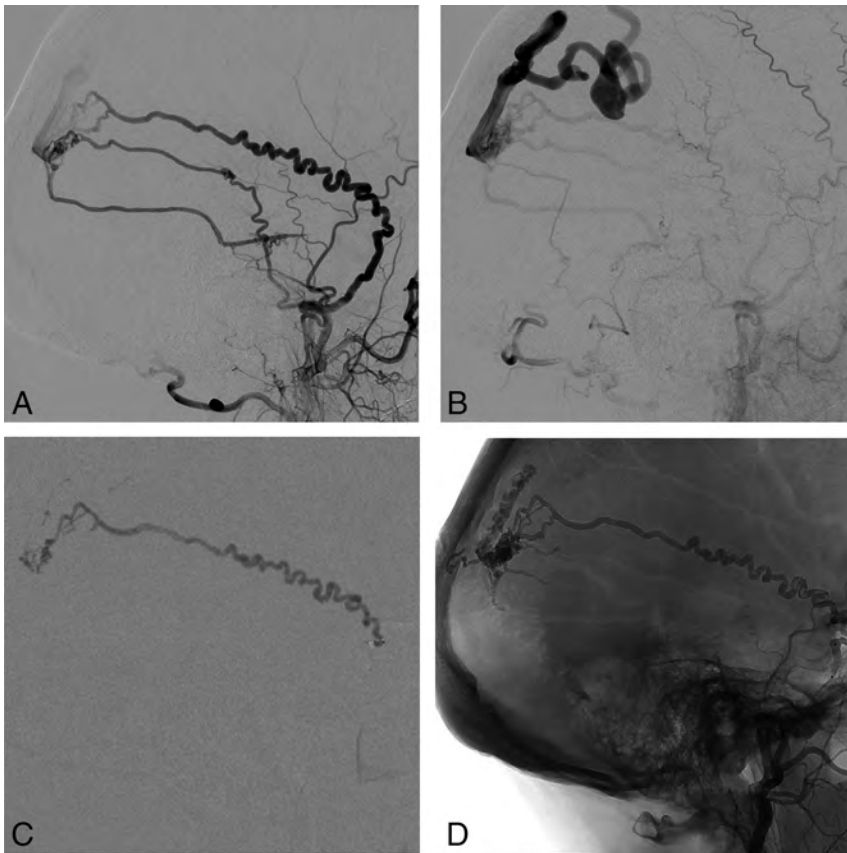


FIG 2. A and B, Initial DSA showing a high-grade right parietal DAVF supplied by a markedly tortuous petrosquamosal branch of the right middle meningeal artery. C, PHIL injection through the Scepter XC balloon (MicroVention) in the proximal middle meningeal artery demonstrates good penetration of the DAVF. D, Unsubtracted image showing the PHIL cast in the draining vein, middle meningeal artery, and other arterial feeders filled in a retrograde manner.

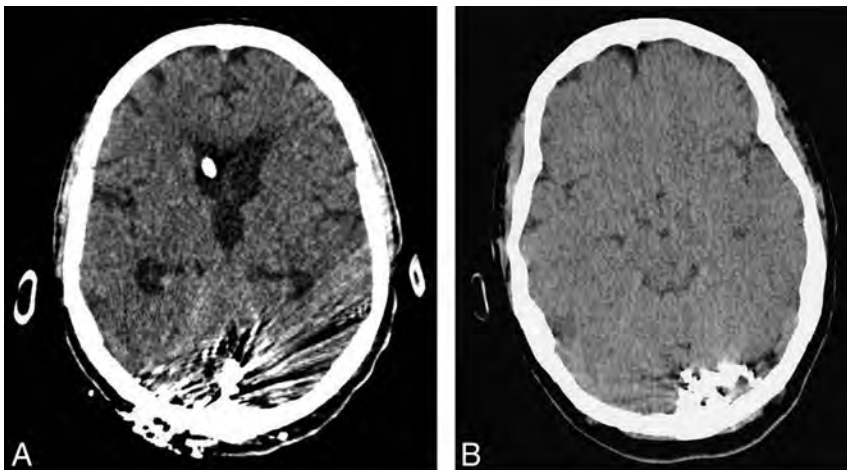


FIG 3. Plain CT images comparing CT artifacts associated with a tantalum-based embolic agent (A) and PHIL (B) casts.

2007 at Beijing Tiantan Hospital. There was angiographic evidence of complete shunt elimination and symptomatic resolution in 19 patients (61.3%). Adverse events occurred in 5/31 patients (16%), including hemifacial palsy, jaw pain, and posterior fossa infarction.

The new-generation nonadhesive liquid embolic agents such as Onyx and PHIL have been described as having advantages

over *n*-BCA. These agents are cohesive and less thrombogenic, allowing deeper and more controlled penetration of the fistulas.

The use of PHIL requires no prior preparation. PHIL 25%, used in most of the cases, is less radiopaque compared with Onyx 18, allowing better visualization through the copolymer cast (Figs 1 and 2) but has the drawback of reduced visibility in case of small-vessel penetration. Operators with experience in both liquid embolic agents often notice the difference in fluoroscopic visibility. In our experience, the risk of inadvertent embolization of potentially dangerous collaterals is not increased compared with other liquid embolic agents.

Due to its iodine-based composition, which is chemically bonded to the copolymer, PHIL is also believed to produce a more homogeneous fluoroscopic appearance, eliminating the risk of tantalum precipitation seen during prolonged Onyx injections. In addition, the use of iodine as a radio-opacifier produces significantly less beam-hardening artifacts on CT compared with tantalum-based embolic agents. As a consequence, more information can be obtained from the postoperative CT scan (Fig 3).

There is no significant technical difference between PHIL and Onyx in terms of reflux control and prevention of catheter retention. In our experience, PHIL appears less adhesive and therefore offers slightly better forward penetration, which probably explains the shorter mean injection time in our study compared with other published results conducted with Onyx injections.¹¹

In high-flow fistulas, PHIL casts have the tendency to fragment and move to the venous side, as opposed to streaming as one would expect with Onyx. Both embolic agents otherwise behave similarly in the treatment of all DAVF types.

CONCLUSIONS

PHIL appears to be a safe and effective option for endovascular treatment of cranial DAVFs. Postembolization short-term angiographic and clinical results are comparable with those of Onyx, with the added advantage of easier preparation and improved homogeneous cast visualization. In our experience, the use of iodine as a radio-opacifier also produces significantly

less artifacts on CT compared with tantalum-based embolic materials.

Disclosures: Saleh Lamin—**RELATED:** *Provision of Writing Assistance, Medicines, Equipment, or Administrative Support:* assistance from MicroVention (assisted in coordinating between the various centers and finalizing the manuscript); **UNRELATED:** *Payment for Lectures including Service on Speakers Bureaus:* Microvention; *Travel/Accommodations/Meeting Expenses Unrelated to Activities Listed:* MicroVention (support to attend World Federation of Interventional and Therapeutic Neuroradiology, Australia); *Other:* proctoring fees, Microvention. Swarupsinh Chavda—**RELATED:** *Provision of Writing Assistance, Medicines, Equipment, or Administrative Support:* Microvention facilitated communication among institutions involved in the study; **UNRELATED:** *Travel/Accommodations/Meeting Expenses Unrelated to Activities Listed:* Microvention provided sponsorship to a meeting of the American Society of Neuroradiology, Montreal. Allan Thomas—**RELATED:** *Support for Travel to Meetings for the Study or Other Purposes:* MicroVention (assistance to attend the annual meeting of the Society of NeuroInterventional Surgery, 2015); **UNRELATED:** *Consultancy:* Sequent Medical (physician proctor for use of the Woven EndoBridge); *Payment for Lectures including Service on Speakers Bureaus:* MicroVention (payment for speaking at the Society of NeuroInterventional Surgery industry evening on the use of the Woven EndoBridge). Mats E. Cronqvist—**RELATED:** *Other:* MicroVention, *Comment:* I was 1 author/physician writing the "Instruction for Use" of the PHIL liquid embolic agent. However, there has been no payment or any financial or other compensation for this work per my request. I am employed as a MD, PhD, at the Section of Neuroradiology, Department of Radiology, Rigshospitalet University Hospital Copenhagen, Denmark. Markus Holtmannspolter—**UNRELATED:** *Consultancy:* MicroVention, Covidien, Sequent Medical (irregular activities as proctor and consultant); *Payment for Lectures including Service on Speakers Bureaus:* MicroVention, Covidien, Sequent Medical (irregular activities as a proctor and consultant); *Travel/Accommodations/Meeting Expenses Unrelated to Activities Listed:* MicroVention, Covidien, Sequent Medical (irregular activities as a proctor and consultant). Alfredo Casasco—**RELATED:** *Support for Travel to Meetings for the Study or Other Purposes:* Microvention. Rene Chapot—**UNRELATED:** *Consultancy:* MicroVention*; *Payment for Lectures including Service on Speakers Bureaus:* Microvention.* *Money paid to the institution.

REFERENCES

1. Gandhi D, Chen J, Pearl M, et al. **Intracranial dural arteriovenous fistulas: classification, imaging findings, and treatment.** *AJNR Am J Neuroradiol* 2012;33:1007–13 CrossRef Medline
2. Kim MS, Han DH, Kwon OK, et al. **Clinical characteristics of dural arteriovenous fistula.** *J Clin Neurosci* 2002;9:147–55 CrossRef Medline
3. Sarma D, ter Brugge K. **Management of intracranial dural arteriovenous shunts in adults.** *Eur J Radiol* 2003;46:206–20 Medline
4. Awad IA, Little JR, Akarawi WP, et al. **Intracranial dural arteriovenous malformations: factors predisposing to an aggressive neurological course.** *J Neurosurg* 1990;72:839–50 CrossRef Medline
5. Borden JA, Wu JK, Shucart WA. **A proposed classification for spinal and cranial dural arteriovenous fistulous malformations and implications for treatment.** *J Neurosurg* 1995;82:166–79 Medline
6. Cognard C, Gobin YP, Pierot L, et al. **Cerebral dural arteriovenous fistulas: clinical and angiographic correlation with a revised classification of venous drainage.** *Radiology* 1995;194:671–80 CrossRef Medline
7. Duffau H, Lopes M, Janosevic V, et al. **Early rebleeding from intracranial dural arteriovenous fistulas: report of 20 cases and review of the literature.** *J Neurosurg* 1999;90:78–84 CrossRef Medline
8. Chung SJ, Kim JS, Kim JC, et al. **Intracranial dural arteriovenous fistulas: analysis of 60 patients.** *Cerebrovasc Dis* 2002;13:79–88 CrossRef Medline
9. Rammos S, Bortolotti C, Lanzino G. **Endovascular management of intracranial dural arteriovenous fistulae.** *Neurosurg Clin N Am* 2014;25:539–49 CrossRef Medline
10. Rabinov J, Yoo AJ, Ogilvy CS, et al. **ONYX versus n-BCA for embolization of cranial dural arteriovenous fistulas.** *J Neurointerv Surg* 2013;5:306–10 CrossRef Medline
11. Cognard C, Januel AC, Silva NA Jr, et al. **Endovascular treatment of intracranial dural arteriovenous fistulas with cortical venous drainage: new management using Onyx.** *AJNR Am J Neuroradiol* 2008;29:235–41 CrossRef Medline
12. Nogueira RG, Dabus G, Rabinov JD, et al. **Preliminary experience with Onyx embolization for the treatment of intracranial dural arteriovenous fistulas.** *AJNR Am J Neuroradiol* 2008;29:91–97 CrossRef Medline
13. Lv X, Jiang C, Li Y, et al. **Results and complications of transarterial embolization of intracranial dural arteriovenous fistulas using Onyx-18.** *J Neurosurg* 2008;109:1083–90 CrossRef Medline

Quantifying the Cerebral Hemodynamics of Dural Arteriovenous Fistula in Transverse Sigmoid Sinus Complicated by Sinus Stenosis: A Retrospective Cohort Study

W.-Y. Guo, C.-C.J. Lee, C.-J. Lin, H.-C. Yang, H.-M. Wu, C.-C. Wu, W.-Y. Chung, and K.-D. Liu

ABSTRACT

BACKGROUND AND PURPOSE: Sinus stenosis occasionally occurs in dural arteriovenous fistulas. Sinus stenosis impedes venous outflow and aggravates intracranial hypertension by reversing cortical venous drainage. This study aimed to analyze the likelihood of sinus stenosis and its impact on cerebral hemodynamics of various types of dural arteriovenous fistulas.

MATERIALS AND METHODS: Forty-three cases of dural arteriovenous fistula in the transverse-sigmoid sinus were reviewed and divided into 3 groups: Cognard type I, type IIa, and types with cortical venous drainage. Sinus stenosis and the double peak sign (occurrence of 2 peaks in the time-density curve of the ipsilateral drainage of the internal jugular vein) in dural arteriovenous fistula were evaluated. "TTP" was defined as the time at which a selected angiographic point reached maximum concentration. TTP of the vein of Labbé, TTP of the ipsilateral normal transverse sinus, trans-fistula time, and trans-stenotic time were compared across the 3 groups.

RESULTS: Thirty-six percent of type I, 100% of type IIa, and 84% of types with cortical venous drainage had sinus stenosis. All sinus stenosis cases demonstrated loss of the double peak sign that occurs in dural arteriovenous fistula. Trans-fistula time (2.09 seconds) and trans-stenotic time (0.67 seconds) in types with cortical venous drainage were the most prolonged, followed by those in type IIa and type I. TTP of the vein of Labbé was significantly shorter in types with cortical venous drainage. Six patients with types with cortical venous drainage underwent venoplasty and stent placement, and 4 were downgraded to type IIa.

CONCLUSIONS: Sinus stenosis indicated dysfunction of venous drainage and is more often encountered in dural arteriovenous fistula with more aggressive types. Venoplasty ameliorates cortical venous drainage in dural arteriovenous fistulas and serves as a bridge treatment to stereotactic radiosurgery in most cases.

ABBREVIATIONS: CVD = cortical venous drainage; DAVF = dural arteriovenous fistula; SRS = stereotactic radiosurgery; SS = sinus stenosis; TFT = trans-fistula time; TST = trans-stenotic time; TTP_{PV} = TTP for the parietal vein; TTP_{VL} = TTP of the vein of Labbé

Dural arteriovenous fistulas (DAVFs) account for 10%–15% of intracranial vascular malformations.^{1,2} The most common location of an intracranial DAVF is the cavernous sinus, followed by the transverse-sigmoid sinus.^{1–3} Major DAVF classification systems, such as the Cognard and Borden systems, grade DAVFs on the basis of venous drainage patterns, in which the

presence of retrograde cortical venous drainage (CVD) indicates a higher risk of hemorrhage.^{4–7} Cases of venous outlet obstruction playing a role in transforming benign (without CVD) into malignant DAVFs (with CVD) have been reported in the literature.⁸ Sinus stenosis (SS) is frequently associated with idiopathic intracranial hypertension.^{9,10} Nevertheless, the incidence of SS and its association with DAVFs have not been thoroughly explored. SS can be found in DAVFs with retrograde or antegrade sinus flow, but its impact on cerebral hemodynamics has rarely been discussed. Theoretically, stenotic and thrombosed sinuses impede the venous outflow, and a DAVF itself increases overall blood volume in the affected sinus; the combination of the 2 hemodynamic disorders adversely affects venous flow and subsequently increases intracranial pressure and the risk of intracranial hemorrhage.

Current treatment strategies for DAVFs in the transverse sinus include microsurgery, endovascular treatment, stereotactic radiosurgery (SRS), or their combinations.^{11–13} Endo-

Received April 1, 2016; accepted after revision August 18.

From the Department of Radiology (W.-Y.G., C.-J.L., H.-M.W., C.-C.W.) and Department of Neurosurgery (C.-C.J.L., H.-C.Y., W.-Y.C., K.-D.L.), Neurological Institute, Taipei Veterans General Hospital, Taipei, Taiwan; and School of Medicine (W.-Y.G., C.-C.J.L., C.-J.L., H.-C.Y., H.-M.W., C.-C.W., W.-Y.C., K.-D.L.), National Yang-Ming University, Taipei, Taiwan.

Dr Chung-Jung Lin is supported by the Taipei Veterans General Hospital (No. V104-C-012), and Dr Wan-Yuo Guo receives a collaboration grant from Siemens and Taipei Veterans General Hospital (No. T1100200).

Please address correspondence to Chung-Jung Lin, MD, Department of Radiology, Taipei Veterans General Hospital, No. 201, Section II, Shipai Rd, Taipei, 11217 Taiwan; e-mail: bcjlin@gmail.com; @ChungJungLin

<http://dx.doi.org/10.3174/ajnr.A4960>

vascular treatment has been the treatment of choice for DAVFs with CVD because it provides immediate curative results and minimizes the risk of hemorrhage.^{14–16} Nevertheless, the complication rate of endovascular treatment is higher than that of SRS.^{14,17,18} By contrast, SRS has hardly any periprocedural risks and achieves DAVF cure rates of between 58% and 73%. Although SRS can reduce the bleeding rate from 20% to 2% after shunting has been totally closed,¹⁹ the latent period for SRS ranges from 1 to 3 years and carries a 4.1% hemorrhagic rate in DAVFs with CVD.^{3,20} Therefore, SRS is usually preferred for cases without CVD, and endovascular treatment is more suitable for immediately minimizing the risk of hemorrhage.

Several studies have proposed a reconstructive method by using venoplasty and stent placement in combination with transarterial embolization to ameliorate or even cure DAVFs with venous outlet obstruction.^{21–23} We wondered whether this approach could downgrade DAVFs with CVD—that is, to restore their normal cortical venous drainage and make them eligible for SRS, thereby minimizing the risk of hemorrhage during the latent period. Therefore, the purpose of the current study was to clarify the following: 1) the incidence of SS in different grades of DAVF in the transverse sigmoid sinus, 2) the impact of SS on DAVF hemodynamics by using quantitative DSA, and 3) the initial treatment results of venoplasty and/or stent placement followed by SRS.

MATERIALS AND METHODS

Patient Population

The institutional review board of Taipei Veterans General Hospital approved this study. From January 2011 to December 2015, we consecutively recruited cases of angiography-proved DAVFs from the angiography logbook. In terms of our inclusion and exclusion criteria, DAVFs involving either side of the transverse-sigmoid sinus were included, while cases already treated before visiting our hospital, DAVFs located elsewhere, and those that did not receive SRS as treatment at all were excluded.

Clinical Presentation, Treatment, and Follow-Up

Data for symptoms at initial presentation, such as tinnitus, bruit, headaches, previous hemorrhage, and neurologic deficits (ie, visual disturbance, seizure, ataxia, and memory decline), and treatment results during follow-up were based on chart review. There were no missing data for the initial presentation. All patients received SRS and the same follow-up protocol: outpatient department visit and MR imaging at 6-month intervals. Adjunctive endovascular treatment was also recorded. The “primary end point” was complete regression, defined as disappearance of abnormal vasculature on follow-up MR imaging with or without additional angiography.²⁰ “Partial regression” was defined as decreased abnormal vascularity compared with the baseline imaging. “Hemorrhage” was defined as any new hemorrhage in the follow-up MR imaging. The “composite end point” (ie, favorable outcome) was defined as complete regression without hemorrhage radiologically. We used the Kaplan-Meier method to handle missing data, treating it as censored. “Restenosis”

was defined as a 50% narrowing of the immediate postvenoplasty sinus diameter during MR imaging follow-up.

Imaging Protocol and Data Analysis

DSA acquisition with a standard, clinically routine protocol was performed in all 43 cases. A power injector (Liebel-Flarsheim Angiomatic; Illumena, San Diego, California) created a contrast bolus by placing a 4F angiocatheter in the common carotid artery at the C4 vertebral body level. A bolus of 12–14 mL of 60% diluted contrast medium (340 mg I/mL) was administered within 1.5 seconds. Neither extra contrast medium nor extra radiation was used. The acquisition parameters were 7.5 frames/s for the first 5 seconds, followed by 4 frames/s for 3 seconds, 3 frames/s for 2 seconds, and finally 2 frames/s for 2 seconds. The entire DSA acquisition process thus normally lasted for 12 seconds, although it was manually prolonged in cases of slow intracranial circulation to allow visualization of internal jugular vein opacification.²⁴ All DSAs were performed with the same biplane angiography scanner (Axiom Artis; Siemens, Erlangen, Germany). “SS” was defined as the diameter at the stenotic site <50% of that of the proximal normal sinus in the lateral view.²⁵ All DSA analyses were performed on a workstation equipped with the software syngo iFlow (Siemens). On the basis of the time-density curve, syngo iFlow extracts the time-to-peak of user-selected vascular ROIs on DSA. With the internal carotid artery as a reference, “TTP” was defined as the time point at which the ROI reached the maximum concentration. The “difference in TTP between 2 ROIs” was defined as the time for blood flow to travel between the 2 ROIs; this measure has been validated as a successful surrogate for the pathologic hemodynamics of cerebrovascular disease.^{24,26–28}

Definition of Different Time Parameters

ROIs were placed on the internal carotid artery, ipsilateral transverse sinus, internal jugular vein in the anteroposterior view and the parietal vein, vein of Labbé, and prestenotic and the poststenotic segments of the sinus on lateral views for circulation-time analysis (Fig 1). “Trans-fistula time” (TFT) was defined as the time difference of TTPs between the ICA and internal jugular vein (ie, TTP_{JV}). “Trans-stenotic time” (TST) was defined as the time difference between the TTPs of pre- and poststenotic ROIs. The TTP for the parietal vein (TTP_{PV}) indicated the normal circulation time of normal brain parenchyma.²⁹ The TTP for the vein of Labbé (TTP_{VL}) indicated the drainage function of the transverse-sigmoid sinus. The ROI placement was standardized to avoid overlapping anatomic structures and inhomogeneous areas. The caliber of the target vessel was used as the diameter for the ROIs.²⁴ The determination of ROIs was performed by a neuroradiologist with 10 years’ experience (reader A) and an angiographic technician with 30 years’ experience (reader B) who were unaware of the condition of sinus stenosis and clinical features.

Definition of Angiographic Signs

We modified the method of Riggeal et al⁹ and defined “venous stenosis” as a diameter <50% of the diameter of the normal sigmoid sinus at the stenotic segment. The “double peak sign” refers to the occurrence of 2 peaks in the time-density curve of the ipsi-

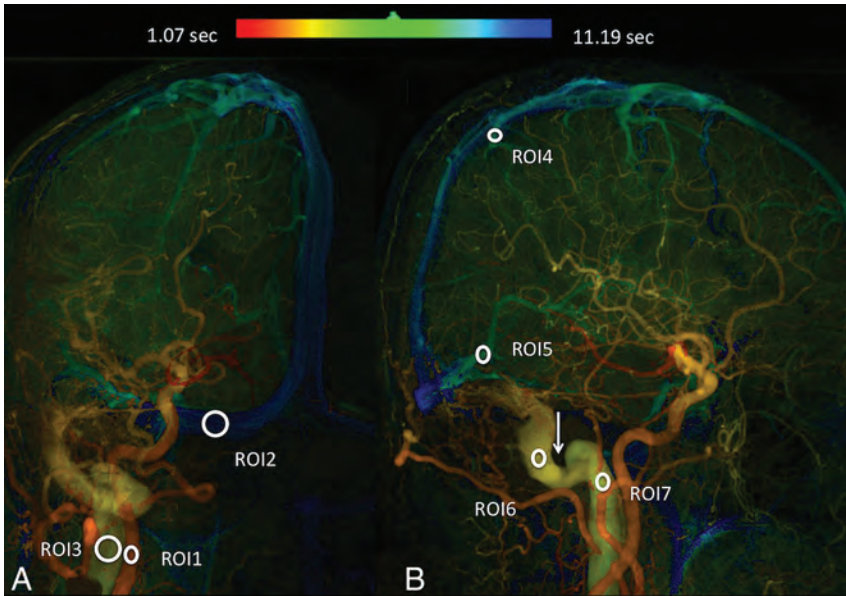


FIG 1. Quantitative color-coded digital subtraction angiography of the anteroposterior (A) and lateral (B) views of a Cognard type I DAVF. ROI1: internal carotid artery; ROI2: ipsilateral normal transverse sinus; ROI3: internal jugular vein; ROI4: parietal vein; ROI5: vein of Labbé; ROI6: prestenotic segment; ROI7: poststenotic segment. The Arrow indicates the stenotic sinus segment.

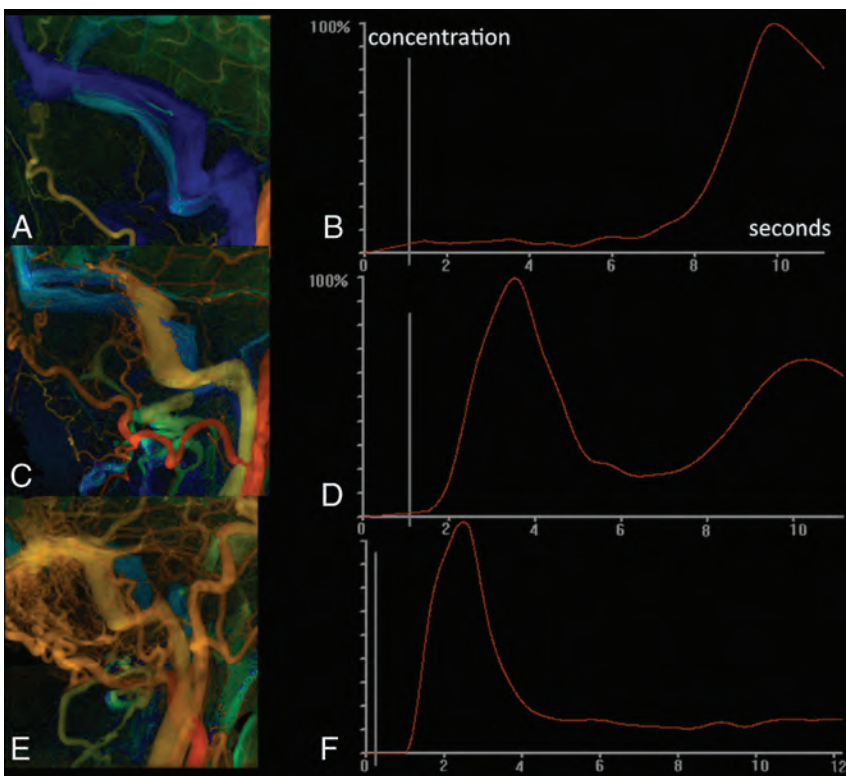


FIG 2. A, Quantitative digital subtraction angiography of a healthy subject. B, One single peak appears at 9.87 seconds (venous phase) in the internal jugular vein. C, Quantitative digital subtraction angiography of a Cognard type I DAVF in the left transverse sinus in a 50-year-old woman. D, Time-density curve of the internal jugular vein demonstrates 2 peaks. The first peak comes from arterial flow from the DAVF shunt; the second peak comes from blood flow from normal brain parenchyma. E, Quantitative digital subtraction of a case of Cognard type IIa+b in the left transverse sigmoid sinus in a 73-year-old man. F, Only a single peak can be depicted in a time-density curve of the ipsilateral jugular vein, indicating that it lacks the drainage function of the normal brain.

lateral drainage internal jugular vein of the DAVF (Fig 2). The first peak indicates shunting arterial blood from the arteriovenous fistula, and the second peak indicates the returning venous blood flows from brain parenchyma. Loss of a double peak with a solitary early peak in cases of DAVF suggests a dysfunction of venous drainage stagnation and may cause venous congestion or venous hypertension. Determinations of sinus stenosis and the double peak sign were made by reader A 1 month after ROI measurement.

Statistical Analysis

All statistical analyses were performed by using SPSS 20 (2010; IBM, Armonk, New York). The differences in various clinical symptoms, incidences of venous stenosis, and loss of the double peak sign among different DAVF types were compared by using a χ^2 test; differences in age and various time parameters among different DAVF types were compared by using an ANOVA test. Inter- and intraobserver variations were evaluated by intraclass classification. The complete regression rate and favorable outcomes were estimated via the Kaplan-Meier method with a log-rank test. Bonferroni adjustment was applied for post hoc intergroup difference analysis. Significance was set at $P < .018$ for all statistical tests except intraclass classification ($P < .05$).

RESULTS

One hundred twenty-six intracranial DAVFs were initially identified from the angiosuite logbook. After excluding 5 patients treated in other hospitals before visiting our hospital, 70 cases of DAVFs in locations other than the transverse-sigmoid sinus, and 8 patients who had undergone endovascular treatment as the sole treatment, there were 43 DAVFs available for analysis (Fig 3). The cohort consisted of 23 men and 18 women (mean, 56.7 years of age); there were 22 Cognard type I, 8 Cognard type IIa, and 13 Cognard types IIa+b or higher DAVFs. Two patients presented with simultaneous cases of bilateral DAVF IIa+b with SS. CVD occurred in all 8 patients who had previous hemorrhage or neurologic deficits other than tinnitus and bruit. No previous hemorrhage

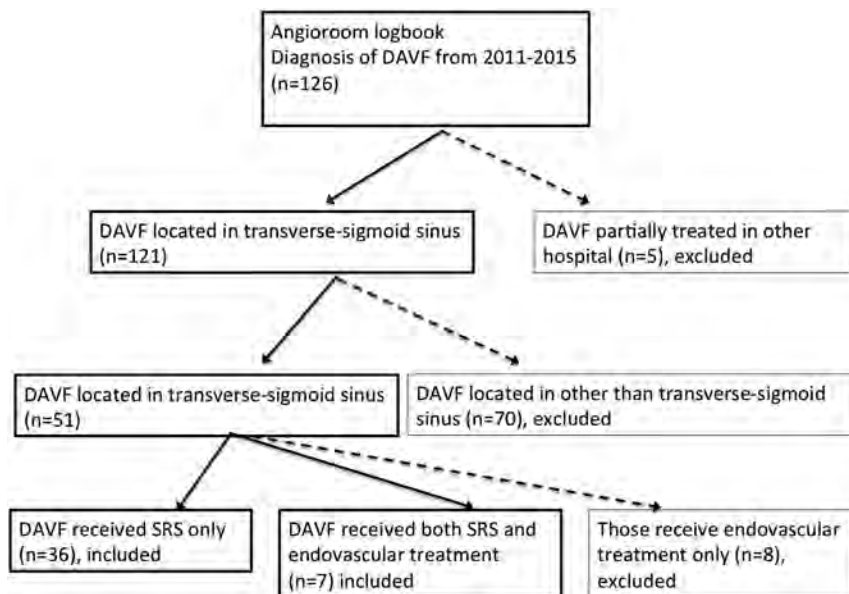


FIG 3. The process of case selection from the angiogram logbook for our study cohort.

Table 1: Comparison of patient characteristics in 3 different groups: type I, type IIa, and types with CVD^a

	Type I	Type IIa	Types with CVD
No.	22	8	13
Age (yr)	58 (52.8–64.2)	54 (35.5–73.7)	52 (41.3–63.8)
Headaches	4 (18.2; 2.1–34.3)	3 (37.5; 6.2–79.5)	4 (30.8; 5.7–55.9)
Hemorrhage/neurologic deficits	0	0	8 (61.5; 35.1–88.0) ^b
Venous stenosis	8 (36.4; 16.3–56.5) ^b	8 (100%)	11 (84.6; 65–100)
Loss of double peak	7 (31.8; 12.4–51.3) ^c	8 (100%) ^c	9 (69.2; 44.1–94.3) ^c

^a The numbers inside the parentheses for age indicate the 95% confidence intervals. The numbers inside the parentheses for headaches, hemorrhage/neurologic deficits, venous stenosis, and loss of double peak indicate the percentage of the observed variable in the group with 95% confidence intervals.

^b Significant difference compared with the other 2 groups.

^c Significant difference across the 3 groups.

Table 2: Intra- and interobserver variability in different time parameters^a

	Reader A	Reader B	Interobserver
TFT	0.98 (0.96–0.99)	0.97 (0.96–0.98)	0.94 (0.90–0.97)
TST	0.97 (0.95–0.99)	0.96 (0.94–0.99)	0.93 (0.90–0.96)
TTP _{PV}	0.98 (0.96–0.99)	0.95 (0.90–0.97)	0.91 (0.86–0.94)
TTP _{VL}	0.98 (0.96–0.99)	0.92 (0.89–0.96)	0.92 (0.87–0.94)
TTP _{TS}	0.95 (0.97–0.91)	0.96 (0.93–0.99)	0.94 (0.90–0.98)

Note:—TTP_{TS} indicates TTP of the ipsilateral normal transverse sinus.

^a Data are 95% CI.

Table 3: Comparison of different time parameters among the 3 groups^a

	Type I	Type IIa	Types with CVD
TFT	1.04 (0.80–1.00)	0.42 (0.27–0.4)	2.09 (1.06–2.26) ^b
TST	0.03 (0–0)	0.34 (0.3–0.53) ^b	0.67 (–0.54–0.8) ^b
TTP _{PV}	4.57 (4.14–5.60)	4.25 (3.20–4.94)	5.6 (4.13–6.26)
TTP _{VL}	4.20 (4.26–5.20)	4.40 (3.50–6.00)	1.4 (0.93–3.46) ^b
TTP _{TS}	6.01 (4.93–7.47) ^b	1.17 (1.06–3.6)	1.1 (1.06–1.86)

Note:—TTP_{TS} indicates TTP of the ipsilateral normal transverse sinus.

^a Data are 95% CI.

^b Significant difference compared with the other 2 groups.

or other neurologic deficits occurred in any of the patients with type I and type IIa. Headaches were observed significantly more often in type IIa and types with CVD (Table 1). Previous hemor-

rhage was significantly more frequent in patients with SS. However, neither headaches nor neurologic deficits differed significantly between patients with and without SS.

SS occurred least in Cognard type I ($n = 8$, 36%), followed by types with CVD ($n = 11$, 85%) and type IIa ($n = 8$, 100%). Seven of 8 patients (88%) with type I and SS demonstrated a loss of double peaks in their time-density curves. All patients with type IIa and SS had a loss of double peaks. Nine of 13 patients with CVD had a loss of double peaks (Table 1). The other 2 patients with CVD and SS showing double peaks were classified as having types III and IV, respectively, indicating that their venous outlets were still functioning.

The intraclass classification of reader A in different time parameters ranged from 0.95 to 0.98; the intraclass classification of reader B ranged from 0.92 to 0.97. The interobserver variation ranged from 0.91 to 0.94 (Table 2). TFT was significantly prolonged in cases with CVD. Trans-stenotic time differed significantly across the 3 groups: longest in types with CVD (2.09 seconds), followed by type IIa (0.42 seconds), with type I (1.04 seconds) having the shortest times. TTP_{VL} was significantly reduced in types with CVD (1.4 seconds) compared with type IIa (4.40 seconds) and type I (4.20 seconds). There was no significant difference in TTP_{PV} among the 3 groups. TTP of the ipsilateral transverse sinus was significantly shortened in type IIa and types with CVD (Table 3).

Six of 13 patients with CVD underwent venoplasty with ($n = 4$) or without ($n = 2$) stent placement before SRS. Peri-stent placement medication consisted of aspirin, 300 mg, and clopidogrel, 100 mg daily for 3 days before the procedure and life-long after stent implantation. For those who underwent angioplasty only, the medication was the same as with stent implantation except that the duration of after-procedure medication was shortened to 3 months. Two received post-SRS transarterial embolization due to the presence of new hemorrhage. Only 1 patient received adjunct transarterial embolization before SRS due to existing hemorrhage. Otherwise, transarterial embolization was not performed before SRS in the remaining 12 patients not showing aggressive clinical symptoms and signs.⁴ One type I patient and 2 patients with CVD did not return for follow-up; these 3 patients were not included in subsequent analyses. The average follow-up time of the SRS was 34 ± 11.5 months. The complete regression rate was 54.5% (12/22) in type I, 38% (3/8) in type IIa, and 23% (3/13) in types with CVD. There was no significant difference in complete regres-

sion ($P = .176$) and favorable outcomes ($P = .079$) among type I, type IIa, type IIa+b, or higher (Fig 4).

All patients experienced improvement of existing pulsatile tinnitus and headaches. Four of the 6 were downgraded to type IIa after combined venoplasty and/or stent placement before SRS treatment. Only 1 patient experienced asymptomatic hemorrhage after the combined treatment, resulting in an annual hemorrhagic rate of 4.0% after treatment. Follow-up DSA of this patient showed reocclusion of the draining sinus. MR imaging detected 2 cases of restenosis in 4 patients undergoing venoplasty and SRS (Table 4). We kept the 2 patients with restenosis under observation due to their asymptomatic clinical course.

DISCUSSION

Sinus stenosis is a common associated finding in DAVF in the transverse sigmoid sinus, especially in Cognard types IIa and IIa+b. The venous-return from normal parenchyma is predominantly drained via the contralateral normal transverse-sigmoid sinus in all patients with type I with SS. Those patients failed to demonstrate passage of normal brain parenchymal returning blood flow in their ipsilateral jugular veins, which makes them distinct from patients with type I without SS, in which the normal brain parenchyma was still drained via the ipsilateral “healthy”

sinus. This finding appears to favor the hypothesis that the stenotic venous outlet plays a role in the progressive development of CVD, pathophysiologically. The hypothesis is supported by Satomi et al,⁸ who reported 2 DAVFs that were longitudinally deteriorated by the development of CVD and venous thrombosis.

In general, the faster the intravascular flow, the shorter the TTT will be. The prolonged TTT in types with CVD in the current study was due to stenotic-induced stagnant flow. In type I, the venous outlet received arterialized antegrade flow and showed no time difference in the peristenotic segment. When the flow reversed in Cognard type II, the TST was prolonged. As SS progressed and CVD developed, the TST was further prolonged (Fig 5). The significantly shorter TTP_{VL} in patients with CVD compared with patients with types I and IIa DAVFs without CVD quantitatively reflects the severity of refluxed arterialized venous flow. It could serve as a real-time quantitative regional hemodynamic surrogate marker for treatment strategies used inside the angiosuite. In other words, normalization of TTP_{VL} after successful venoplasty and/or stent placement in SS indicates that CVD was caused by sinus outlet obstruction before treatment and was relieved after the interventional procedures.

Several previous reports also described symptomatic relief after venoplasty or stent placement to recanalize the stenotic venous

outlets in patients with sinus thrombosis and/or tumor compression.^{23,30-32} The exact etiology of DAVF remains an enigma and might be multifactorial, though most hypotheses hold that it is an acquired disease.³³ The first hypothesis suggests that DAVF develops from reopening of the existing potential arteriovenous communication due to an increment of sinus pressure.³⁴ The second hypothesis asserts that de novo shunts (ie, angiogenesis) develop in response to the stimulation of vascular growth factors in the presence of hypoxia, trauma, or otitis.^{35,36} Venous hypertension induced by an obstruction of the venous

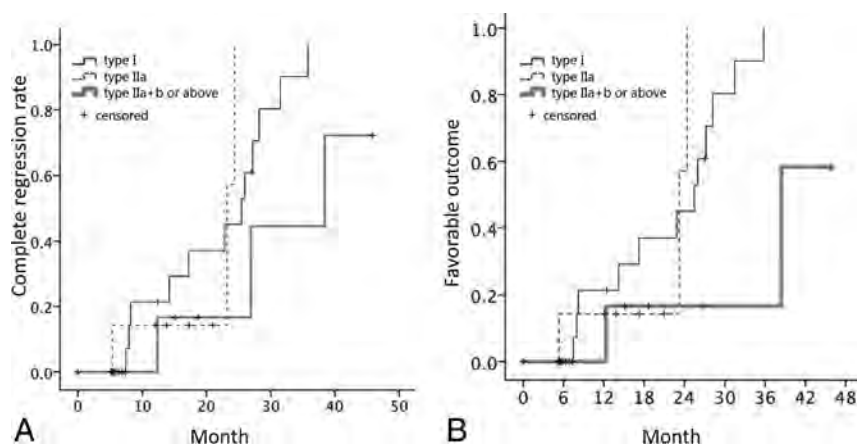


FIG 4. Kaplan-Meier analysis of complete regression (A) and favorable outcomes (B) among types I, IIa, and IIa+b or higher.

Table 4: Clinical characteristics, treatment strategy, and response in 13 patients with DAVF types with CVD

Case No.	Sex	Age (yr)	Cognard Type before SRS	Treatment	Cognard Type		Treatment after SRS	Follow-Up Duration (mo)	Response
					after Venoplasty/	Stent			
1	F	41	IIa+b	Venoplasty/stent	IIa	—	46	PR	
2	M	63	IIa+b	Venoplasty	IIa	—	38	CR	
3	M	56	IIa+b	Venoplasty/stent	IIa	—	19	PR ^a	
4	M	45	IIa+b	—	NA	—	15	CR	
5	F	63	IIa+b	Venoplasty/stent	IIa+b	—	10	PR ^a	
6	M	73	IIa+b	—	NA	—	10	PR	
7	M	17	IIa+b	Venoplasty/stent	IIa+b	—	6	PR	
8	M	55	IIb	—	NA	—	5.6	PR	
9	M	19	III	—	NA	TAE twice	17	PR	
10	M	27	III	Venoplasty	IIa	—	27	CR ^b	
11	M	12	III	—	—	—	13	CR	
12	M	27	IV	—	—	—	27.6	PR	
13	M	55	IV	—	—	—	NA	NA	

Note:—TAE indicates transarterial embolization; CR, complete regression; PR, partial regression; —, no adjunct treatment was performed; NA, not available.

^aRestenosis of sinus after venoplasty and stenting.

^bAsymptomatic intracranial hemorrhage on MR imaging.

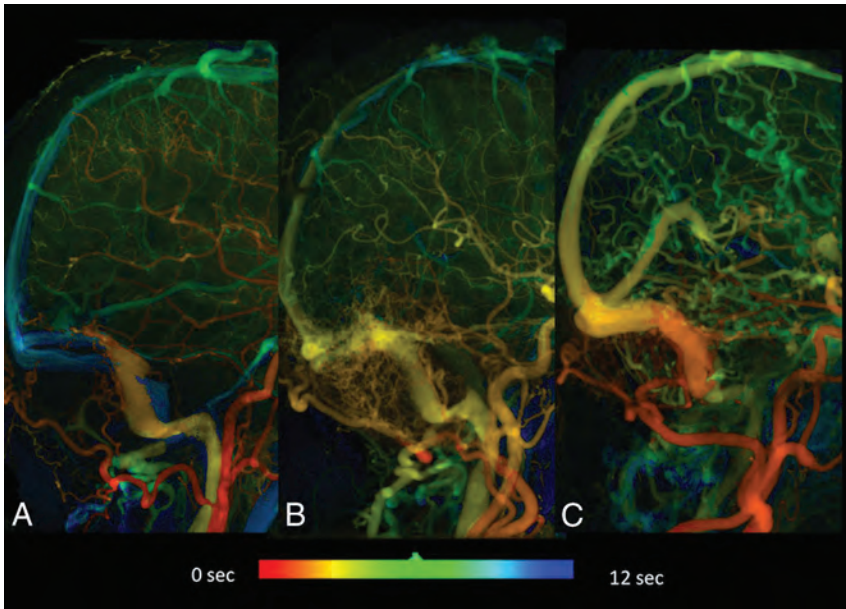


FIG 5. Quantitative DSA of cases of Cognard type I (A), Cognard type IIa (B), and Cognard type IIa+b (C). Severe sinus stenosis is more commonly encountered in more aggressive DAVF types. The TTP (TTP of the internal jugular vein) was largest in type IIa+b (green), followed by types IIa (yellow-green) and I (yellow). Progressive shortening of the TTP in the superior sagittal sinuses in type IIa and type IIa+b is also depicted.

outflow may reduce cerebral perfusion and lead to hypoxia with de novo formation of a DAVF. On the basis of these theories, a correction of the venous hypertension in the sinus should reduce cerebral venous edema and reverse the vicious cycle of creating DAVFs.

None of our patients had a cure of DAVFs by venoplasty and/or stent placement alone. We hypothesize that the application of overlapping stents or stents with a finer network may result in completely blocking the arterial-venous shunts that occur on the sinus wall.^{21,22} Embolization or resection of the sinus is conventionally an option for DAVF types with CVD. The obliteration rate of transarterial embolization in DAVF is 80%.³⁷ If the arterial route to embolize the DAVF also supplies cranial nerves or is technically inaccessible, transvenous embolization might be an option for curing DAVFs.^{38,39} However, sacrifice of a sinus is reserved for cases of an isolated (nonfunctioning) sinus, because sacrificing a functioning sinus might cause deterioration of the CVD and hemorrhage.³⁶ We preferred venoplasty and/or stent placement to transarterial embolization followed by SRS because embolizing agents such as Onyx would likely make optimal targeting challenging in both MR imaging and DSA and because tissue ischemia may render the vascular bed less sensitive to radiation and stimulate angiogenesis leading to lesion growth.^{40,41}

Nevertheless this multidisciplinary treatment approach will potentially increase the number of unfavorable outcomes in patients before SRS takes effect if a hemorrhage were to occur in the unprotected timeframe. The relative risks of curative embolization attempts alone versus venoplasty and stent placement adjunctive to SRS should be very thoroughly weighed because the latent hemorrhage risk for this combined approach was 4.0% according to our study. There are several options when facing restenosis: If patients are asymptomatic, they can be kept under obser-

vation. If the symptoms persist or are aggravated, then re-stent placement in the sinus, a transarterial approach, or microsurgery can be tried.⁴² In our case, we managed to achieve the benefits of both SRS and endovascular treatment without increasing the periprocedural risks of treating DAVFs with CVD.

There were several limitations to the current study. First, because ours is a tertiary referral medical center for neurologic vascular disorders, the incidences of sinus stenosis might be unusually high due to referring bias. Second, the overall efficacy of combined treatments of venoplasty and/or stent placement followed by SRS warrant a larger scale study with a longer follow-up. Moreover, the aggressiveness of DAVF may also serve as an indicator of response to SRS and warrants individualization of dose selection in SRS. Currently, 2D quantitative DSA merely provides time-based parameters such as time-to-peak to reflect intravascular

flow changes. Genuine velocity estimation in DSA relies on 3D acquisitions with an iterative reconstruction algorithm and therefore is not ready for a clinical scenario.⁴³ 3D quantitative assessment of angiographic morphology and DAVF hemodynamics might further improve the accuracy, whatever treatment strategy is taken.⁴³

CONCLUSIONS

Sinus stenosis is present in nearly one-third of cases of Cognard type I DAVF in the transverse-sigmoid sinus and is more frequently encountered in patients with more aggressive types. Loss of the double peak time-density curve of ipsilateral sinus flow in a DAVF suggests dysfunction of venous drainage and warrants urgent treatment. Venoplasty and/or stent placement of the dysfunctional sinus may downgrade the DAVF and make it amenable to SRS with less risk of hemorrhage in the latent period in most cases.

ACKNOWLEDGMENTS

We thank Chung-Hsien Lin for his assistance with the statistical analysis.

Disclosures: Wan-Yuo Guo—RELATED: Grant: Siemens, Comments: This work is supported in part by a collaboration contract between Taipei Veterans General Hospital and Siemens.* Chung-Jung Lin—RELATED: Grant: Taipei Veterans General Hospital (No. V104-C-012).* *Money paid to the institution.

REFERENCES

1. Piippo A, Niemelä M, van Popta J, et al. **Characteristics and long-term outcome of 251 patients with dural arteriovenous fistulas in a defined population.** *J Neurosurg* 2013;118:923–34 CrossRef Medline
2. Kim MS, Han DH, Kwon O-K, et al. **Clinical characteristics of dural arteriovenous fistula.** *J Clin Neurosci* 2002;9:147–55 CrossRef Medline
3. Chen CJ, Lee CC, Ding D, et al. **Stereotactic radiosurgery for intracranial dural arteriovenous fistulas: a systematic review.** *J Neurosurg* 2015;122:353–62 CrossRef Medline

4. Söderman M, Pavic L, Edner G, et al. **Natural history of dural arteriovenous shunts.** *Stroke* 2008;39:1735–39 CrossRef Medline
5. Davies MA, Ter Brugge K, Willinsky R, et al. **The natural history and management of intracranial dural arteriovenous fistulae: part 2, aggressive lesions.** *Interv Neuroradiol* 1997;3:303–11 Medline
6. van Rooij WJ, Sluzewski M, Beute GN. **Dural arteriovenous fistulas with cortical venous drainage: incidence, clinical presentation, and treatment.** *AJNR Am J Neuroradiol* 2007;28:651–55 Medline
7. van Dijk JM, ter Brugge KG, Willinsky RA, et al. **Clinical course of cranial dural arteriovenous fistulas with long-term persistent cortical venous reflux.** *Stroke* 2002;33:1233–36 CrossRef Medline
8. Satomi J, van Dijk JM, Terbrugge KG, et al. **Benign cranial dural arteriovenous fistulas: outcome of conservative management based on the natural history of the lesion.** *J Neurosurg* 2002;97:767–70 CrossRef Medline
9. Riggeal BD, Bruce BB, Saindane AM, et al. **Clinical course of idiopathic intracranial hypertension with transverse sinus stenosis.** *Neurology* 2013;80:289–95 CrossRef Medline
10. Degnan AJ, Levy LM. **Pseudotumor cerebri: brief review of clinical syndrome and imaging findings.** *AJNR Am J Neuroradiol* 2011;32:1986–93 CrossRef Medline
11. Vanlandingham M, Fox B, Hoit D, et al. **Endovascular treatment of intracranial dural arteriovenous fistulas.** *Neurosurgery* 2014;74(suppl 1):S42–49 CrossRef Medline
12. Söderman M, Dodoo E, Karlsson B. **Dural arteriovenous fistulas and the role of gamma knife stereotactic radiosurgery: the Stockholm experience.** *Prog Neurol Surg* 2013;27:205–17 CrossRef Medline
13. Yang H, Kano H, Kondziolka D, et al. **Stereotactic radiosurgery with or without embolization for intracranial dural arteriovenous fistulas.** *Prog Neurol Surg* 2013;27:195–204 CrossRef Medline
14. van Rooij WJ, Sluzewski M. **Curative embolization with Onyx of dural arteriovenous fistulas with cortical venous drainage.** *AJNR Am J Neuroradiol* 2010;31:1516–20 CrossRef Medline
15. Stiefel MF, Albuquerque FC, Park MS, et al. **Endovascular treatment of intracranial dural arteriovenous fistulae using Onyx: a case series.** *Neurosurgery* 2009;65:132–39; discussion 139–40 Medline
16. Macdonald JH, Millar JS, Barker CS. **Endovascular treatment of cranial dural arteriovenous fistulae: a single-centre, 14-year experience and the impact of Onyx on local practise.** *Neuroradiology* 2010;52:387–95 CrossRef Medline
17. Yoshida K, Melake M, Oishi H, et al. **Transvenous embolization of dural carotid cavernous fistulas: a series of 44 consecutive patients.** *AJNR Am J Neuroradiol* 2010;31:651–55 CrossRef Medline
18. Zenteno M, Santos-Franco J, Rodríguez-Parra V, et al. **Management of direct carotid-cavernous sinus fistulas with the use of ethylene-vinyl alcohol (Onyx) only: preliminary results.** *J Neurosurg* 2010;112:595–602 CrossRef Medline
19. Plasencia AR, Santillan A. **Embolization and radiosurgery for arteriovenous malformations.** *Surg Neurol Int* 2012;3(suppl 2):S90–S104 CrossRef Medline
20. Pan DH, Chung WY, Guo WY, et al. **Stereotactic radiosurgery for the treatment of dural arteriovenous fistulas involving the transverse-sigmoid sinus.** *J Neurosurg* 2002;96:823–29 CrossRef Medline
21. Liebig T, Henkes H, Brew S, et al. **Reconstructive treatment of dural arteriovenous fistulas of the transverse and sigmoid sinus: transvenous angioplasty and stent deployment.** *Neuroradiology* 2005;47:543–51 CrossRef Medline
22. Levrier O, Métellus P, Fuentes S, et al. **Use of a self-expanding stent with balloon angioplasty in the treatment of dural arteriovenous fistulas involving the transverse and/or sigmoid sinus: functional and neuroimaging-based outcome in 10 patients.** *J Neurosurg* 2006;104:254–63 CrossRef Medline
23. Xu K, Yu T, Yuan Y, et al. **Current status of the application of intracranial venous sinus stenting.** *Int J Med Sci* 2015;12:780–89 CrossRef Medline
24. Lin CJ, Hung SC, Guo WY, et al. **Monitoring peri-therapeutic cerebral circulation time: a feasibility study using color-coded quantitative DSA in patients with steno-occlusive arterial disease.** *AJNR Am J Neuroradiol* 2012;33:1685–90 CrossRef Medline
25. Lin CJ, Chang FC, Tsai FY, et al. **Stenotic transverse sinus predisposes to poststenting hyperperfusion syndrome as evidenced by quantitative analysis of peritherapeutic cerebral circulation time.** *AJNR Am J Neuroradiol* 2014;35:1132–36 CrossRef Medline
26. Levitt MR, Morton RP, Haynor DR, et al. **Angiographic perfusion imaging: real-time assessment of endovascular treatment for cerebral vasospasm.** *J Neuroimaging* 2014;24:387–92 CrossRef Medline
27. Göllitz P, Struffert T, Lücking H, et al. **Parametric color coding of digital subtraction angiography in the evaluation of carotid cavernous fistulas.** *Clin Neuroradiol* 2013;23:113–20 CrossRef Medline
28. Strother CM, Bender F, Deuerling-Zheng Y, et al. **Parametric color coding of digital subtraction angiography.** *AJNR Am J Neuroradiol* 2010;31:919–24 CrossRef Medline
29. Greitz T. **A radiologic study of the brain circulation by rapid serial angiography of the carotid artery.** *Acta Radiol Suppl* 1956;140:1–123 Medline
30. Tsumoto T, Miyamoto T, Shimizu M, et al. **Restenosis of the sigmoid sinus after stenting for treatment of intracranial venous hypertension: case report.** *Neuroradiology* 2003;45:911–15 CrossRef Medline
31. Ganesan D, Higgins JN, Harrower T, et al. **Stent placement for management of a small parasagittal meningioma: technical note.** *J Neurosurg* 2008;108:377–81 CrossRef Medline
32. Hirata E, Higashi T, Iwamura Y, et al. **Angioplasty and stent deployment in acute sinus thrombosis following endovascular treatment of dural arteriovenous fistulae.** *J Clin Neurosci* 2009;16:725–27 CrossRef Medline
33. Gupta A, Periakaruppan A. **Intracranial dural arteriovenous fistulas: a review.** *Indian J Radiol Imaging* 2009;19:43–48 CrossRef Medline
34. Houser OW, Campbell JK, Campbell RJ, et al. **Arteriovenous malformation affecting the transverse dural venous sinus: an acquired lesion.** *Mayo Clin Proc* 1979;54:651–61 Medline
35. Tirakotai W, Bertalanffy H, Liu-Guan B, et al. **Immunohistochemical study in dural arteriovenous fistulas and possible role of local hypoxia for the de novo formation of dural arteriovenous fistulas.** *Clin Neurol Neurosurg* 2005;107:455–60 CrossRef Medline
36. Lasjaunias P, Brenstein A, ter Brugge KG. *Surgical Neuroangiography.* Berlin: Springer; 2004:565–607
37. Cognard C, Januel AC, Silva NA Jr, et al. **Endovascular treatment of intracranial dural arteriovenous fistulas with cortical venous drainage: new management using Onyx.** *AJNR Am J Neuroradiol* 2008;29:235–41 CrossRef Medline
38. Natarajan SK, Ghodke B, Kim LJ, et al. **Multimodality treatment of intracranial dural arteriovenous fistulas in the Onyx era: a single center experience.** *World Neurosurg* 2010;73:365–79 CrossRef Medline
39. Lekkhong E, Pongpech S, Ter Brugge K, et al. **Transvenous embolization of intracranial dural arteriovenous shunts through occluded venous segments: experience in 51 patients.** *AJNR Am J Neuroradiol* 2011;32:1738–44 CrossRef Medline
40. Akakin A, Ozkan A, Akgun E, et al. **Endovascular treatment increases but gamma knife radiosurgery decreases angiogenic activity of arteriovenous malformations: an in vivo experimental study using a rat cornea model.** *Neurosurgery* 2010;66:121–29; discussion 129–30 CrossRef Medline
41. Mullan S, Mojtahedi S, Johnson DL, et al. **Embryological basis of some aspects of cerebral vascular fistulas and malformations.** *J Neurosurg* 1996;85:1–8 CrossRef Medline
42. Choi BJ, Lee TH, Kim CW, et al. **Reconstructive treatment using a stent graft for a dural arteriovenous fistula of the transverse sinus in the case of hypoplasia of the contralateral venous sinuses: technical case report.** *Neurosurgery* 2009;65:E994–96; discussion E996 CrossRef Medline
43. Chen GH, Li Y. **Synchronized multiartifact reduction with tomographic reconstruction (SMART-RECON): a statistical model based iterative image reconstruction method to eliminate limited-view artifacts and to mitigate the temporal-average artifacts in time-resolved CT.** *Med Phys* 2015;42:4698–707 CrossRef Medline

The Effects of Acetazolamide on the Evaluation of Cerebral Hemodynamics and Functional Connectivity Using Blood Oxygen Level–Dependent MR Imaging in Patients with Chronic Steno-Occlusive Disease of the Anterior Circulation

J. Wu, S. Dehkharghani, F. Nahab, J. Allen, and D. Qiu



ABSTRACT

BACKGROUND AND PURPOSE: Measuring cerebrovascular reactivity with the use of vasodilatory stimuli, such as acetazolamide, is useful for chronic cerebrovascular steno-occlusive disease. The purpose of this study was to evaluate the effects of acetazolamide on the assessment of hemodynamic impairment and functional connectivity by using noninvasive resting-state blood oxygen level–dependent MR imaging.

MATERIALS AND METHODS: A 20-minute resting-state blood oxygen level–dependent MR imaging scan was acquired with infusion of acetazolamide starting at 5 minutes after scan initiation. A recently developed temporal-shift analysis technique was applied on blood oxygen level–dependent MR imaging data before and after acetazolamide infusion to identify regions with hemodynamic impairment, and the results were compared by using contrast agent–based DSC perfusion imaging as the reference standard. Functional connectivity was compared with and without correction on the signal by using information from temporal-shift analysis, before and after acetazolamide infusion.

RESULTS: Visually, temporal-shift analysis of blood oxygen level–dependent MR imaging data identified regions with compromised hemodynamics as defined by DSC, though performance deteriorated in patients with bilateral disease. The Dice similarity coefficient between temporal-shift and DSC maps was higher before (0.487 ± 0.150 by using the superior sagittal sinus signal as a reference for temporal-shift analysis) compared with after acetazolamide administration (0.384 ± 0.107) ($P = .006$, repeated-measures ANOVA). Functional connectivity analysis with temporal-shift correction identified brain network nodes that were otherwise missed. The accuracy of functional connectivity assessment decreased after acetazolamide administration ($P = .015$ for default mode network, repeated-measures ANOVA).

CONCLUSIONS: Temporal-shift analysis of blood oxygen level–dependent MR imaging can identify brain regions with hemodynamic compromise in relation to DSC among patients with chronic cerebrovascular disease. The use of acetazolamide reduces the accuracy of temporal-shift analysis and network connectivity evaluation.

ABBREVIATIONS: ACZ = acetazolamide; BOLD = blood oxygen level–dependent MR imaging; DMN = default mode network; SMN = sensorimotor network; SSS = superior sagittal sinus; T_{\max} = time-to-maximum of the residue function; TS = temporal-shift

The measurement of cerebral perfusion can aid in the characterization of patients with cerebral ischemic diseases.^{1,2} Recent studies have demonstrated that the determination of diffusion-perfusion mismatch provides a valuable paradigm for selecting a subpopulation of patients with acute stroke most likely

to benefit from reperfusion therapies.^{3–8} However, MR perfusion imaging is typically based on DSC with bolus injection of a gadolinium-based contrast agent.^{5,8–10} Although the risk of nephrogenic systemic fibrosis associated with the use of gadolinium-based contrast agents may be minimized through renal function screening, there are recent concerns about chronic deposition of gadolinium in the brain.¹¹ The use of a contrast agent may furthermore preclude repeat perfusion scans in the same session,¹² which are needed in clinical settings such as the evaluation of cerebrovascular reactivity.

The development of noninvasive approaches without the need for contrast agent administration can provide useful alternatives. Although arterial spin-labeling is a noninvasive method for measuring CBF, it is prone to errors in regions with a long arterial

Received May 24, 2016; accepted after revision August 20.

From the Departments of Radiology and Imaging Sciences (J.W., S.D., J.A., D.Q.) and Neurology (F.N.), Emory University School of Medicine, Atlanta, Georgia.

Please address correspondence to Deqiang Qiu, PhD, Department of Radiology and Imaging Sciences, Emory University School of Medicine, 1364 Clifton Rd, Atlanta, GA 30322; e-mail: dqiu3@emory.edu

 Indicates article with supplemental on-line table.

 Indicates article with supplemental on-line photos.

<http://dx.doi.org/10.3174/ajnr.A4973>

transit time of blood,¹²⁻¹⁴ which is particularly problematic in patients with steno-occlusive disease. Recently, temporal-shift (TS) analysis of the resting-state blood oxygen level-dependent MR imaging (BOLD) signal, which is sensitive to local blood flow and oxygen metabolism,¹⁵ has been shown to depict regions with cerebrovascular impairment in acute stroke and chronic cerebral hypoperfusion.¹⁶⁻¹⁸ In addition, compared with the measurement of hemodynamic parameters, the assessment of the functional status of such hypoperfused brain is underinvestigated. A growing body of work supports resting-state BOLD signal possibly being used to evaluate functional brain networks.¹⁹⁻²³ Leveraging different aspects of the same BOLD acquisition, simultaneous assessment of cerebral hemodynamics and functional connectivity therefore becomes an attractive application of resting-state BOLD.

Traditionally, cerebrovascular reactivity has been an important measure in patients with chronic steno-occlusive disease. The measurement of cerebrovascular reactivity is performed by quantifying cerebrovascular responses to vasodilatory stimuli, such as the administration of acetazolamide (ACZ) or inhalation of air with increased CO₂ concentration (eg, 5%).²⁴⁻²⁶ Examining the effects of vasodilatory stimuli on TS and functional connectivity analyses may shed light on their physiologic basis and allow development of an operationalized approach to their evaluation. In this study, we aimed to assess the effects of ACZ on the evaluations of hemodynamic impairment and functional brain connectivity by using resting-state BOLD in patients with chronic steno-occlusive disease of the anterior circulation. We hypothesized that TS analysis of BOLD data could identify regions with hemodynamic compromise in patients with chronic cerebrovascular disease, similar to those shown in acute stroke and Moyamoya disease. We further hypothesized that the use of ACZ would affect the results of TS and functional connectivity analyses due to its alteration in neurovascular coupling.

MATERIALS AND METHODS

Participants

Fourteen patients with chronic steno-occlusive disease of the anterior circulation (mean age, 48 years; range, 31–70 years; 3 men, 11 women) were included in this study. These included 4 patients with idiopathic Moyamoya disease (3 with bilateral disease), 7 patients with atherosclerotic occlusion of the MCA or ICA (2 with bilateral disease), and 3 patients with unilateral atherosclerotic high-grade stenosis of the ICA (see the On-line Table for details). The study was approved by our institutional review board; and all patients underwent specialized acetazolamide-challenge MR imaging. Ten had follow-up scans the next day without ACZ administration.

Data Acquisition and Preprocessing

MR imaging was performed at 3T (Tim Trio; Siemens, Erlangen, Germany). BOLD images were acquired by using a gradient-echo EPI sequence: TR/TE = 2000/30 ms, flip angle = 78°, FOV = 220 × 220 mm², matrix = 64 × 64, section thickness = 4 mm, 30 sections. The entire BOLD scan spanned 20 minutes. At 5 minutes after the initiation of the scan, 1 g of ACZ dissolved in 10 mL of

normal saline was slowly infused intravenously for 3–5 minutes without interruption of the scanning session.

At the conclusion of the BOLD acquisition, DSC imaging was performed by using a gradient-echo EPI sequence (TR = 1500 ms, TE = 40 ms, flip angle = 60°, FOV = 240 × 240 mm², matrix = 128 × 128, section thickness = 5 mm, 19 sections) with the injection of 0.1 mmol/kg of gadobenate dimeglumine (MultiHance; Bracco Diagnostics, Princeton, New Jersey) delivered by a power injector at 4 mL/s through an antecubital intravenous access and followed by a normal saline flush at the same rate. Automated arterial input function and venous output function detection, followed by a delay-insensitive deconvolution with a regularization threshold of 15% of the maximum singular value,²⁷ were implemented to generate perfusion maps, including CBF, CBV, MTT, and the time-to-maximum of the residue function (T_{max}). The perfusion maps were further spatially normalized to standard Montreal Neurological Institute space.

Additionally, T1-weighted MPRAGE imaging (TR = 1900 ms, TE = 3.52 ms, flip angle = 9°, FOV = 216 × 256 mm², matrix = 216 × 256, section thickness = 1 mm, 176) was performed for anatomic localization.

Preprocessing of BOLD images was performed by using SPM8 software (<http://www.fil.ion.ucl.ac.uk/spm/software/spm8>). The first and last 5 minutes of data (150 volumes) were used for analysis, representing data acquired before (pre-ACZ) and after (post-ACZ) administration of ACZ, respectively. The last 5 minutes of images were used for post-ACZ assessment because we found that the ACZ effect plateaued approximately 10 minutes after the initiation of infusion. For both pre-ACZ and post-ACZ data, after removal of the first 10 volumes, BOLD images were corrected for the timing of the section acquisition, realigned to the mean image, normalized to the Montreal Neurological Institute space, resampled to 3-mm isotropic voxel size, and spatially smoothed with a Gaussian kernel of 6-mm full width at half maximum. After removal of the linear temporal trend from the processed images, we regressed out the effects of head motion by using estimates (6 parameters) from the above realignment step as confounding factors. Last, the data were bandpass-filtered to retain signal components with temporal frequency between 0.01 and 0.1 Hz.

Temporal-Shift Maps

TS maps were calculated from the BOLD data by determining, for each voxel, the temporal offset that maximizes the correlation coefficient between the time-shifted (–6 TR to +6 TR; ie, –12 seconds to +12 seconds) reference signal and the temporal signal of each voxel (On-line Fig 1). The temporal offset was then assigned as the value of the respective voxel in the TS map. We considered 2 options of reference signals: the global mean signal and the average time-series over an ROI within the superior sagittal sinus (SSS). The global mean signal was obtained by calculating the mean temporal signal across the entire brain, including contributions from GM, WM, and CSF. To obtain the SSS reference signal, we calculated a temporal SD map of the BOLD signal to reflect the magnitude of spontaneous signal fluctuation in each voxel. Because the SSS has 100% blood volume compared with a maximum of 5% blood volume in brain tissue, the BOLD signal of the SSS has a large variance compared with other regions. An ROI was therefore

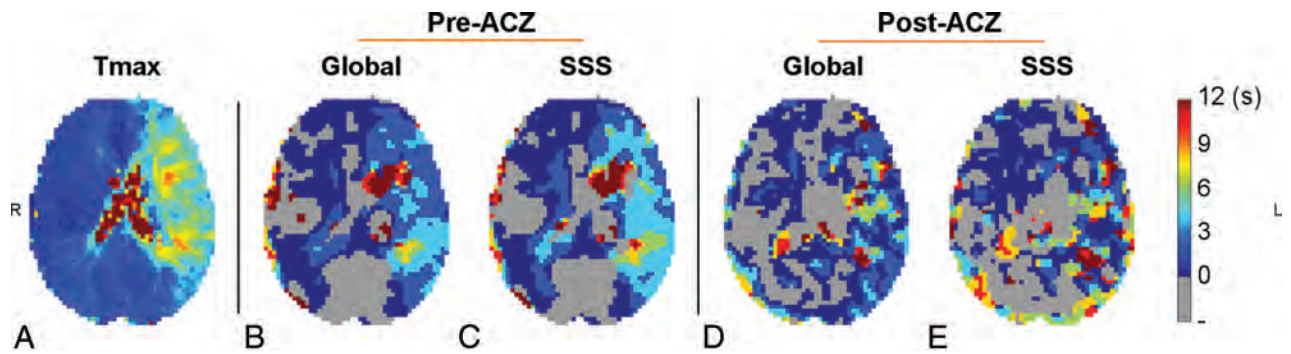


FIG 1. DSC T_{\max} (A) and temporal-shift maps (B–E) derived from resting-state BOLD data by using the global mean signal (B and D) and the superior sagittal sinus (C and E) as references, as well as before (B and C) and after (D and E) acetazolamide administration in a patient with occlusion of the left ICA. Visually, TS maps exhibited a global resemblance to T_{\max} maps. This agreement decreased after ACZ administration. Compared with using the global signal as reference, TS maps generated by using the SSS signal as the reference signal showed a better agreement with T_{\max} maps. The images are in radiologic convention.

manually placed in a brain area with a high SD in the SSS without including adjacent brain tissues (4 voxels for each subject).

While the success of TS analysis depends on the optimal selection of a reference signal (ie, the identification of “normal” tissues), this information could, in turn, be provided by the results of TS analysis. We therefore proposed an iterative approach to optimize the computation of TS maps by improving estimation of the reference signal as shown below. The average time-series of all voxels with a zero time delay (offset = 0 second) from the previous iteration was calculated and used as the new reference signal for the next iteration. The mean TS value over the whole brain was also calculated. The iteration was repeated until convergence in that the absolute difference of mean values between the TS maps in the successive iterations was lower than 0.001 second.

Functional Connectivity Analysis

The default mode network (DMN) and sensorimotor network (SMN) were identified and evaluated by using a seed-based functional connectivity analysis method on the BOLD data.^{19,21,28} Using a functional ROI atlas,²⁹ we defined the seed region for the DMN in the precuneus/posterior cingulate cortex: Montreal Neurological Institute coordinate = (0, -56, 28), radius = 10 mm. The seed ROI for the SMN was placed in the precentral gyrus of the unaffected or less affected hemisphere: Montreal Neurological Institute coordinate = (± 44 , -16, 46), radius = 6 mm. For each network, the average temporal signal in the seed ROI of the pre-processed images was calculated, and then the Pearson correlation coefficient r with this seed temporal signal was calculated for all brain voxels to generate the functional connectivity maps. To evaluate the effect of correction by using temporal-shift information from the TS analysis on functional connectivity analysis, we shifted the temporal signal of each voxel according to the value in the TS map; the functional connectivity analysis was then repeated. This correction is termed “TS correction.”

Image and Statistical Analysis

A mixed-effects model was used to study the correlation between the TS and T_{\max} maps and the effect of ACZ administration (pre-ACZ versus post-ACZ) on this correlation. The mean values of BOLD TS and T_{\max} were calculated in regions with T_{\max} values binned in different ranges (0–1 second, 1–2 seconds, 2–3 seconds,

3–4 seconds, 4–5 seconds, 5–6 seconds, and >6 seconds). The linear relationship between the mean TS and T_{\max} was estimated by modeling subject-specific slope as a random effect.

To further assess the potential clinical value of the TS map, we evaluated the spatial overlap between regions with perfusion deficits as defined by the TS and DSC T_{\max} maps by using the Dice similarity coefficient.¹⁸ The Dice coefficient between regions A and B was defined as the following: Similarity = $2|A \cap B|/(|A| + |B|)$, where $|A \cap B|$ represents the area of the overlapped region between A and B and $|A|$ and $|B|$ represent the areas of A and B, respectively. Because the threshold of T_{\max} for quantifying pathologic tissue volumes is yet to be established in patients with chronic cerebrovascular disease, we used 4 seconds as the threshold, which was an established threshold for estimating hypoperfused tissue volumes in patients with acute stroke.^{27,30} Additional analysis by using $T_{\max} > 3$ seconds as a threshold was also performed to improve the sensitivity for identifying areas with hemodynamic compromise. The optimal threshold for a TS map that maximized its Dice similarity with its respective T_{\max} map was derived by varying the threshold from -12 to 12 seconds with increments of 2 seconds (ie, TR). The values of the Dice similarity were compared by using 2-way repeated-measures ANOVA to test the effect of ACZ administration (pre-ACZ versus post-ACZ) and the choice of reference signal (the global signal versus the SSS signal) on TS analysis.

The Dice similarity coefficient between patient functional networks and templates of brain networks derived from healthy-subject resting-state BOLD data²⁹ was calculated to assess the effects of TS correlation and ACZ on functional connectivity assessment. Two-way repeated-measures ANOVA was performed to test whether ACZ administration (pre-ACZ versus post-ACZ) and TS correction (original versus TS-corrected analysis) influenced the assessment of functional connectivity.

RESULTS

The mixed-effects model showed significant correlation between the TS and T_{\max} maps when using either the global signal or the SSS as the reference signal for calculating TS maps ($P < .001$ for both tests). The slopes of change in TS with respect to T_{\max} were significantly lower after ACZ administration when using the

global signal ($P = .001$) and SSS ($P = .026$) as the reference signal, respectively (On-line Fig 2).

Figure 1 and On-line Fig 3 show the comparison of resting-state BOLD TS maps and DSC T_{max} maps in representative patients. Brain regions with a long T_{max} were associated with a positive TS value in the temporal-shift analysis (a delay in the time course with respect to the reference signal). The On-line Table shows the Dice similarity coefficient between the T_{max} and TS maps in defining brain regions with compromised perfusion for each patient. Using $T_{max} > 4$ seconds as a threshold for compro-

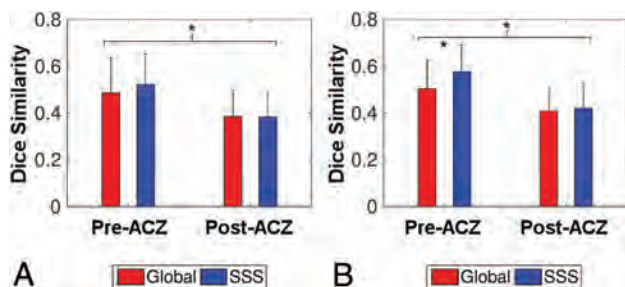


FIG 2. The mean Dice similarity coefficient between temporal-shift and T_{max} maps by using $T_{max} > 4$ seconds (A) and $T_{max} > 3$ seconds (B) as criteria for defining hemodynamic compromise, respectively. TS maps were derived from resting-state BOLD by using either the global signal (red bars) or the superior sagittal sinus signal (blue bars) as the reference. When we used $T_{max} > 4$ seconds as the threshold, a lower Dice similarity between T_{max} and TS maps was found after acetazolamide administration (post-ACZ) compared with that before acetazolamide (pre-ACZ). When using $T_{max} > 3$ seconds as the threshold, TS maps obtained with the SSS signal as the reference showed greater similarity to T_{max} maps than those using the global signal in the pre-ACZ condition. Compared with the pre-ACZ results, the post-ACZ results demonstrated lower similarity. Error bars represent the SD of the mean. Asterisks indicate significant differences as determined by 2-way repeated-measures ANOVA with a post hoc Bonferroni-corrected paired t test.

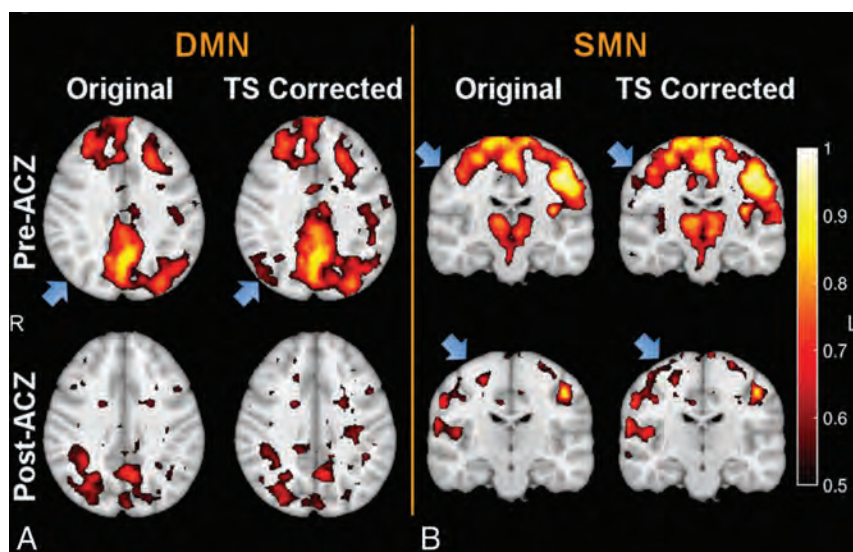


FIG 3. The default mode network (A) and the sensorimotor network (B) overlaid on T1-weighted images before (upper row) and after (lower row) acetazolamide administration, as well as without and with temporal-shift correction in a patient with occlusion of the right MCA. Although functional connectivity changed after ACZ challenge, the DMN and SMN could be still identified. New network nodes were uncovered in the hypoperfused areas after the correction of time delay derived from TS analysis (see the blue arrows in the original and TS-corrected networks). In general, these regions could be observed in the corresponding networks of healthy subjects. The images are in radiologic convention.

mised perfusion, 2-way repeated-measures ANOVA showed that after ACZ administration, the Dice similarity coefficient between TS and T_{max} maps was significantly reduced compared with that before ACZ administration ($P = .006$) (Fig 2A; see the On-line Table for detailed statistics).

When we used $T_{max} > 3$ seconds as a threshold for compromised perfusion, significant effects were found related to the choice of different reference signals ($P = .008$), ACZ administration ($P = .003$), and the interaction between them ($P = .020$) on the similarity coefficient between TS and T_{max} maps (Fig 2B and On-line Table). Post hoc Bonferroni-corrected paired t tests showed the following: 1) before ACZ administration, TS maps derived by using SSS as the reference signal demonstrated higher similarity with T_{max} maps, compared with those using the global signal as the reference signal ($P < .001$); and 2) lower similarity between T_{max} and TS maps was found after ACZ administration compared with before ACZ administration when using either the global signal ($P = .011$) or SSS ($P = .002$) as the reference signal (Fig 2B and On-line Table). For the above analysis, the DSC perfusion after ACZ administration was used. The same analysis was repeated in a subset of 10 patients who underwent a second-day MR imaging examination without the administration of ACZ, and in these cases, the pre-ACZ second-day T_{max} was used. Similar results were obtained (On-line Fig 4).

The default mode network and sensorimotor network of representative patients are shown in Fig 3 and On-line Fig 5. Although the results of functional connectivity changed after ACZ administration, both the DMN and SMN remained identifiable. TS correction uncovered new network nodes in areas with hemodynamic compromise in some patients. In general, these emerged nodes could be observed in the corresponding functional networks of healthy subjects. Temporal-shift information obtained from TS analysis by using

the SSS signal as the reference was used to correct the BOLD signal for functional connectivity analysis because of its better performance in delineating regions with hemodynamic impairment.

Two-way repeated-measures ANOVA showed significant effects of TS correction on the functional connectivity assessment of the DMN ($P < .001$) and the SMN ($P = .024$) (Fig 4). Accuracy in the assessment of both functional networks (as measured by the overlap with template network masks) increased after correction of the signal by using time-shift estimates from the TS analysis. Assessment accuracy decreased after ACZ administration, with statistically significant effects for the DMN ($P = .015$) and a trend toward significance for the SMN ($P = .080$).

DISCUSSION

The present study demonstrated that temporal-shift maps derived from noninvasive resting-state BOLD scans could identify brain regions with abnormal per-

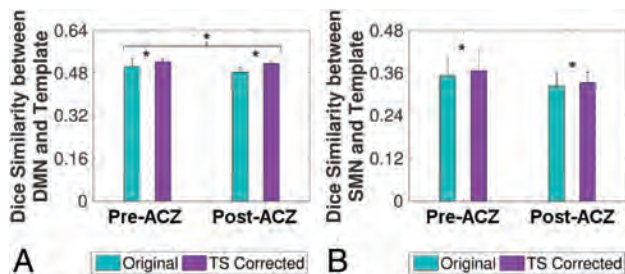


FIG 4. The accuracy of functional connectivity assessment, measured by the Dice similarity coefficient between functional networks and network templates, for default mode (A) and sensorimotor (B) networks. The assessment accuracy of both functional networks increased after temporal-shift correction. The assessment accuracy decreased after acetazolamide administration for the DMN, while a trend toward significance was found for the SMN. Error bars represent the SD of the mean. Asterisks indicate significant differences as determined by 2-way repeated-measures ANOVA.

fusion in patients with chronic steno-occlusive disease of the anterior circulation. The computed temporal-shift maps qualitatively and quantitatively resembled T_{\max} maps derived from contrast agent–based DSC perfusion imaging. Acetazolamide administration reduced the similarity between temporal-shift maps and T_{\max} maps. The performance of temporal-shift analysis in identifying regions with hemodynamic impairment deteriorated in patients with bilateral disease. Functional connectivity analysis on the default mode and sensorimotor networks showed impaired diminished connectivity in some patients, possibly due to impaired neural activity or compromised neurovascular coupling. The correction of temporal signals by using information derived from temporal-shift analysis showed mixed results, with recovery of otherwise missing network nodes in some but not all patients. The use of ACZ reduced the overall accuracy in the identification of resting-state networks.

The evaluation of cerebral perfusion plays an important role in identifying patients with acute stroke who are most likely to benefit from perfusion restoration to ischemic tissues³⁻⁵ and has traditionally relied on MR imaging or CT perfusion imaging with the use of a contrast agent. Although the quantitative value of DSC in evaluating patients with chronic cerebrovascular disease remains to be established, it is qualitatively useful in forming an overall impression of the pathologic status. The requirement of exogenous contrast agent application could be a limitation due to the potential for adverse effects in patients with severe renal impairment as well as recent concerns about gadolinium deposition in the brain and other tissues; this therefore potentially precludes the use of DSC perfusion imaging in applications in which repeated scans are needed. The development of noninvasive methods free of contrast agent provides an alternative in situations in which the use of contrast agent is contraindicated. Our results showed that maps from temporal-shift analysis resembled DSC perfusion T_{\max} maps both visually and quantitatively. This finding provides corroborative evidence that spontaneous fluctuations in the BOLD signal contain information that can be isolated to approximate cerebral perfusion impairment, in addition to neuronal activity, as demonstrated in other patient populations.¹⁶⁻¹⁸ However, differences between TS and T_{\max} maps were also observed. The exact mechanism for potential discrepancies is not completely

understood, but the differences are not surprising because TS analysis and DSC perfusion imaging likely reflect different aspects of the same pathophysiologic process. Further development of the technique and validation within larger cohorts are necessary to further establish the nature of this relation and to further assess TS maps as an adjunct or potential alternative to DSC perfusion imaging in patients with neurovascular disease.

Two options of the reference signals were considered in the temporal-shift analysis: the global mean signal and the signal from the SSS. While both approaches produced TS maps comparable with T_{\max} maps, a higher similarity was observed between T_{\max} maps and TS maps obtained by using the SSS signal as the reference. This suggests that the largely fluctuating signal in the venous sinus and the iterative strategy ensured a better assessment of hemodynamic compromise. Furthermore, while global signal can be easily calculated even without operator input, the accuracy of the reference may be contaminated by inclusion of neural activity³¹ and the hypoperfused brain regions. The problem became particularly apparent when hypoperfused regions were large, such as in patients with bilateral steno-occlusive disease. We also found that the time delay evaluated by using the global signal as a reference tended to be smaller compared with that calculated with the SSS as reference. This finding could be because the global signal showed a time lag from normal areas because of the contribution from the hypoperfused areas, which is weighted by the volumes of these areas. In contrast, although the SSS receives blood from hypoperfused areas as well, the contribution from these areas is weighted by their blood flow; and because of the reduced blood flow in these areas, the contribution from them is smaller.

When we used the temporal delay information calculated from resting-state BOLD data to correct for the functional connectivity analysis of the DMN and the SMN, new areas of both functional networks were found, particularly in regions with hemodynamic compromise. Such areas generally emerged in locations where brain networks of healthy participants typically reside. These findings suggest caution when evaluating functional connectivity in patients with cerebrovascular compromise. For example, an apparent reduction in connectivity could be recovered by TS correction and might not be caused by changes in the underlying neuronal activity but rather by changes in neurovascular coupling.

It has been reported that neuronal function and underlying neurovascular coupling could not be correctly evaluated by BOLD MR imaging in the setting of neurovascular ischemia, purportedly due to the uncoupling of the positive relationship between CBF and BOLD responses under physiologic baseline conditions.^{26,32,33} In this study, changes in the detected DMN and SMN were observed after ACZ administration, though spontaneous neural activity should be unaltered without explicit external neural stimuli. Our finding consequently provides further evidence for the altered assessment of neuronal function of BOLD MR imaging after a vasodilatory challenge. Also, TS analysis needs to be applied to evaluate neuronal activity by using BOLD MR imaging in patients with steno-occlusive disease, due to the possibility of compromised neurovascular coupling. Moreover, we found that TS maps exhibited a decreased similarity with T_{\max} after ACZ administration. This is consistent with previous findings showing that BOLD responses are reduced in task-based

fMRI after ACZ challenge.^{26,33} Although ACZ is useful for interrogating cerebrovascular reactivity, there should be caution in interpreting the results of functional connectivity and TS analyses in BOLD studies after ACZ administration.

Several issues remain to be addressed in future studies. First, while the SSS reference approach provided a good estimate of hemodynamic compromise, the selection of ROIs within the SSS could affect the results. An algorithm for automatic determination of the SSS ROI is required to derive optimal results. Second, a relatively low spatial (voxel size = $3.4 \times 3.4 \times 4 \text{ mm}^3$) and temporal resolution (TR = 2 seconds) BOLD sequence was used in the current study. Higher spatial and temporal resolutions can be achieved via multiband acquisitions, thereby improving the accuracy of the assessment of hemodynamic compromise, similar to that found in resting-state fMRI.^{34,35} Third, although there is variability in the TS correction in unveiling otherwise occult nodes in functional networks, whether this reflects the severity of functional compromise is not clear. Further studies are required to systematically investigate whether functional connectivity with temporal-shift correction is associated with functional/cognitive symptoms and whether this information can be used to better predict functional recovery among these patients.

CONCLUSIONS

Temporal-shift analysis of non-contrast agent–based resting-state BOLD data can delineate brain areas with hemodynamic compromise as measured by DSC T_{max} maps in patients with chronic cerebrovascular disease, though the performance of temporal-shift analysis deteriorates in patients with bilateral disease. Temporal-shift correction recovers nodes of functional brain networks in some hypoperfused areas. The use of ACZ changes the effectiveness of temporal-shift analysis in evaluating cerebral hemodynamic compromise as well as functional connectivity analysis from resting-state BOLD data.

Disclosures: Fadi Nahab—UNRELATED: Employment: The Joint Commission; Expert Testimony: provided legal counsel as an expert witness on cases involving stroke patients; Payment for Lectures including Service on Speakers Bureaus: Medtronic, Genzyme; Payment for Development of Educational Presentations: Imedex. Deqiang Qiu—UNRELATED: Grants/Grants Pending: Siemens.* *Money paid to the institution.

REFERENCES

- Merino JG, Warach S. **Imaging of acute stroke.** *Nat Rev Neurol* 2010; 6:560–71 CrossRef Medline
- Dani KA, Thomas RGR, Chappell FM, et al; Translational Medicine Research Collaboration Multicentre Acute Stroke Imaging Study. **Computed tomography and magnetic resonance perfusion imaging in ischemic stroke: definitions and thresholds.** *Ann Neurol* 2011; 70:384–401 CrossRef Medline
- Latchaw RE, Yonas H, Hunter GJ, et al; Council on Cardiovascular Radiology of the American Heart Association. **Guidelines and recommendations for perfusion imaging in cerebral ischemia: a scientific statement for healthcare professionals by the writing group on perfusion imaging, from the Council on Cardiovascular Radiology of the American Heart Association.** *Stroke* 2003;34:1084–104 CrossRef Medline
- Marks MP, Lansberg MG, Mlynash M, et al; DEFUSE Investigators. **Angiographic outcome of endovascular stroke therapy correlated with MR findings, infarct growth, and clinical outcome in the DEFUSE 2 trial.** *Int J Stroke* 2014;9:860–65 CrossRef Medline
- Lansberg MG, Straka M, Kemp S, et al; DEFUSE 2 study investigators. **MRI profile and response to endovascular reperfusion after stroke (DEFUSE 2): a prospective cohort study.** *Lancet Neurol* 2012;11: 860–67 CrossRef Medline
- Saver JL, Goyal M, Bonafe A, et al; SWIFT PRIME Investigators. **Stent-retriever thrombectomy after intravenous t-PA vs. t-PA alone in stroke.** *N Engl J Med* 2015;372:2285–95 CrossRef Medline
- Jovin TG, Chamorro A, Cobo E, et al; REVASCAT Trial Investigators. **Thrombectomy within 8 hours after symptom onset in ischemic stroke.** *N Engl J Med* 2015;372:2296–306 CrossRef Medline
- Campbell BCV, Christensen S, Levi CR, et al. **Comparison of computed tomography perfusion and magnetic resonance imaging perfusion-diffusion mismatch in ischemic stroke.** *Stroke* 2012;43: 2648–53 CrossRef Medline
- Saver JL, Goyal M, Bonafe A, et al; SWIFT PRIME Investigators. **Solitaire™ with the Intention for Thrombectomy as Primary Endovascular Treatment for Acute Ischemic Stroke (SWIFT PRIME) trial: protocol for a randomized, controlled, multicenter study comparing the Solitaire revascularization device with IV tPA with IV tPA alone in acute ischemic stroke.** *Int J Stroke* 2015;10:439–48 CrossRef Medline
- Østergaard L. **Principles of cerebral perfusion imaging by bolus tracking.** *J Magn Reson Imaging* 2005;22:710–17 CrossRef Medline
- McDonald RJ, McDonald JS, Kallmes DF, et al. **Intracranial gadolinium deposition after contrast-enhanced MR imaging.** *Radiology* 2015;275:772–82 CrossRef Medline
- Ovadia-Caro S, Margulies DS, Villringer A. **The value of resting-state functional magnetic resonance imaging in stroke.** *Stroke* 2014;45: 2818–24 CrossRef Medline
- Petersen ET, Zimine I, Ho YC, et al. **Non-invasive measurement of perfusion: a critical review of arterial spin labelling techniques.** *Br J Radiol* 2006;79:688–701 CrossRef Medline
- Bokkers RP, Hernandez DA, Merino JG, et al; National Institutes of Health Stroke Natural History Investigators. **Whole-brain arterial spin labeling perfusion MRI in patients with acute stroke.** *Stroke* 2012;43:1290–94 CrossRef Medline
- Villringer A, Dirnagl U. **Coupling of brain activity and cerebral blood flow: basis of functional neuroimaging.** *Cerebrovasc Brain Metab Rev* 1995;7:240–76 Medline
- Christen T, Jahanian H, Ni WW, et al. **Noncontrast mapping of arterial delay and functional connectivity using resting-state functional MRI: a study in Moyamoya patients.** *J Magn Reson Imaging* 2015;41:424–30 CrossRef Medline
- Amemiya S, Kunimatsu A, Saito N, et al. **Cerebral hemodynamic impairment: assessment with resting-state functional MR imaging.** *Radiology* 2014;270:548–55 CrossRef Medline
- Lv Y, Margulies DS, Cameron Craddock R, et al. **Identifying the perfusion deficit in acute stroke with resting-state functional magnetic resonance imaging.** *Ann Neurol* 2013;73:136–40 CrossRef Medline
- Fox MD, Raichle ME. **Spontaneous fluctuations in brain activity observed with functional magnetic resonance imaging.** *Nat Rev Neurosci* 2007;8:700–11 CrossRef Medline
- Smith SM, Fox PT, Miller KL, et al. **Correspondence of the brain's functional architecture during activation and rest.** *Proc Natl Acad Sci U S A* 2009;106:13040–45 CrossRef Medline
- van den Heuvel MP, Hulshoff Pol HE. **Exploring the brain network: a review on resting-state fMRI functional connectivity.** *Eur Neuropsychopharmacol* 2010;20:519–34 CrossRef Medline
- Chang TY, Huang KL, Ho MY, et al. **Graph theoretical analysis of functional networks and its relationship to cognitive decline in patients with carotid stenosis.** *J Cereb Blood Flow Metab* 2016;36: 808–18 Medline
- Cheng HL, Lin CJ, Soong BW, et al. **Impairments in cognitive function and brain connectivity in severe asymptomatic carotid stenosis.** *Stroke* 2012;43:2567–73 CrossRef Medline
- Gupta A, Chazen JL, Hartman M, et al. **Cerebrovascular reserve and stroke risk in patients with carotid stenosis or occlusion: a systematic review and meta-analysis.** *Stroke* 2012;43:2884–91 CrossRef Medline

25. Vagal AS, Leach JL, Fernandez-Ulloa M, et al. **The acetazolamide challenge: techniques and applications in the evaluation of chronic cerebral ischemia.** *AJNR Am J Neuroradiol* 2009;30:876–84 CrossRef Medline
26. Siero JC, Hartkamp NS, Donahue MJ, et al. **Neuronal activation induced BOLD and CBF responses upon acetazolamide administration in patients with steno-occlusive artery disease.** *Neuroimage* 2015;105:276–85 CrossRef Medline
27. Straka M, Albers GW, Bammer R. **Real-time diffusion-perfusion mismatch analysis in acute stroke.** *J Magn Reson Imaging* 2010;32:1024–37 CrossRef Medline
28. Biswal B, Yetkin FZ, Haughton VM, et al. **Functional connectivity in the motor cortex of resting human brain using echo-planar MRI.** *Magn Reson Med* 1995;34:537–41 CrossRef Medline
29. Shirer WR, Ryali S, Rykhlevskaia E, et al. **Decoding subject-driven cognitive states with whole-brain connectivity patterns.** *Cereb Cortex* 2012;22:158–65 CrossRef Medline
30. Albers GW, Thijs VN, Wechsler L, et al; DEFUSE Investigators. **Magnetic resonance imaging profiles predict clinical response to early reperfusion: the diffusion and perfusion imaging evaluation for understanding stroke evolution (DEFUSE) study.** *Ann Neurol* 2006;60:508–17 CrossRef Medline
31. Amemiya S, Takao H, Hanaoka S, et al. **Global and structured waves of rs-fMRI signal identified as putative propagation of spontaneous neural activity.** *Neuroimage* 2016;133:331–40 CrossRef Medline
32. Blicher JU, Stagg CJ, O’Shea J, et al. **Visualization of altered neurovascular coupling in chronic stroke patients using multimodal functional MRI.** *J Cereb Blood Flow Metab* 2012;32:2044–54 CrossRef Medline
33. Brown GG, Eyler Zorrilla LT, Georgy B, et al. **BOLD and perfusion response to finger-thumb apposition after acetazolamide administration: differential relationship to global perfusion.** *J Cereb Blood Flow Metab* 2003;23:829–37 Medline
34. Preibisch C, Castrillón G JG, Bührer M, et al. **Evaluation of multi-band EPI acquisitions for resting state fMRI.** *PLoS One* 2015;10:e0136961 CrossRef Medline
35. Feinberg DA, Moeller S, Smith SM, et al. **Multiplexed echo planar imaging for sub-second whole brain FMRI and fast diffusion imaging.** *PLoS One* 2010;5:e15710 CrossRef Medline

Impact of Neuroradiology-Based Peer Review on Head and Neck Radiotherapy Target Delineation

 S. Braunstein,  C.M. Glastonbury,  J. Chen,  J.M. Quivey, and  S.S. Yom

ABSTRACT

BACKGROUND AND PURPOSE: While standard guidelines assist in target delineation for head and neck radiation therapy planning, the complex anatomy, varying patterns of spread, unusual or advanced presentations, and high risk of treatment-related toxicities produce continuous interpretive challenges. In 2007, we instituted weekly treatment planning quality assurance rounds as a joint enterprise of head and neck radiation oncology and neuroradiology. Here we describe its impact on head and neck radiation therapy target delineation.

MATERIALS AND METHODS: For 7 months, treatment planning quality assurance included 80 cases of definitive (48%) or postoperative (52%) head and neck radiation therapy. The planning CT and associated target volumes were reviewed in comparison with diagnostic imaging studies. Alterations were catalogued.

RESULTS: Of the 80 cases, 44 (55%) were altered, and of these, 61% had clinically significant changes resulting in exclusion or inclusion of a distinct area or structure. Reasons for alteration included the following: gross or extant tumor, 26/44 (59%); elective or postoperative coverage, 25/44 (57%); lymph nodes, 13/44 (30%); bone, 7/44 (16%); skull base, 7/44 (16%); normal organs, 5/44 (11%); perineural, 3/44 (7%); distant metastasis, 2/44 (5%); and eye, 1/44 (2%). Gross tumor changes ranged from 0.5% to 133.64%, with a median change in volume of 5.95 mm³ (7.86%). Volumes were more likely to be increased (73%) than decreased (27%).

CONCLUSIONS: A collaborative approach to head and neck treatment planning quality assurance has an impact. Cases likely to have challenging patterns of infiltrative, intracranial, nodal, orbital, or perineural spread warrant intensive imaging-based review in collaboration with a diagnostic neuroradiologist.

ABBREVIATIONS: CTV = clinical tumor volume; GTV = gross tumor volume; HN = head and neck; IMRT = intensity-modulated radiation therapy; PTV = planning target volume; TPQA = treatment planning quality assurance

Retrospective and prospective studies demonstrate increased efficacy from multidisciplinary physician interaction,^{1,2} and team-based approaches to patient care are routine within radiation oncology. However, the process of radiation therapy target delineation remains an essentially solitary activity, and the impact of collaborative peer review is a contested issue. One survey suggested that major alterations from this type of process were rare, occurring in <6% of head and neck (HN) plans, though the extent

of alterations was noted to be dependent on the reviewing peer's subsite experience level.³

The weakness of these studies as applied to HN cancer stems from a tendency to underestimate the specialized nature of anatomically defined HN radiation therapy and its unique interdependence with neuroradiology. Head and neck malignancies comprise a heterogeneous group of neoplasms characterized by complex local and regional anatomy, varying patterns of spread, and frequent occurrence of unusual and/or advanced presentations. Acquiring proficiency in the interpretation of HN imaging is difficult due to the subtlety of the characteristics that may suggest benign or malignant disease and distinguishing them from normal or inflamed tissue. Because management frequently consists of staged, multimodal combinations of surgery, systemic therapy, and/or radiation therapy, the interpretation of sequential image sets is exceptionally challenging, particularly the discrimination of posttreatment changes from residual disease.⁴ Previous studies have found that after re-interpretation by a specialist head

Received November 17, 2014; accepted after revision August 17, 2016.

From the Departments of Radiation Oncology (S.B., C.M.G., J.C., J.M.Q., S.S.Y.) and Radiology (C.M.G.), University of California, San Francisco, San Francisco, California.

Paper previously presented in part at: Annual Meeting of the American Society of Radiation Oncology, October 2–6, 2011; Miami, Florida.

Please address correspondence to Sue S. Yom, MD, PhD, UCSF Radiation Oncology, 1600 Divisadero St, Suite H-1031, San Francisco, CA 94143-1708; e-mail: yoms@radonc.ucsf.edu

<http://dx.doi.org/10.3174/ajnr.A4963>

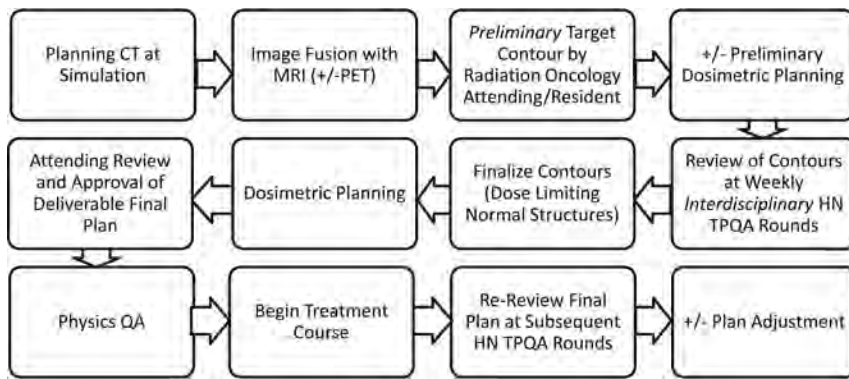


FIG 1. Treatment planning workflow for head and neck radiation oncology.

and neck neuroradiologist, changes in staging or management occur in 38%–56% of cases.^{5,6}

Beginning in 2007, diagnostic neuroradiology participation was included as part of weekly HN treatment planning quality assurance (TPQA) rounds at our institution. The format includes diagnostic imaging review for new and follow-up patients, as well as the highly prioritized review of proposed radiation therapy target volumes and normal organ delineations, which are peer-reviewed by HN radiation oncology and neuroradiology physicians. As of June 2010, electronic documentation was prepared pre- and post-TPQA. This study characterizes the impact of diagnostic neuroradiology involvement on the radiation therapy planning process.

MATERIALS AND METHODS

HN TPQA Workflow

The HN TPQA team consists of radiation oncologists (including S.S.Y., J.M.Q.); diagnostic neuroradiologists (including C.M.G.); neuroradiology and radiation oncology students, residents, and fellows; and members of the dosimetry and physics teams (including J.C.). Review includes plans intended for treatment of the upper aerodigestive tract, and thyroid and HN soft-tissue and lymphatic and cutaneous regions. Pediatrics, spine, mediastinal, and lung cancer cases are occasionally reviewed, but these were excluded from this report. Figure 1 describes the treatment planning workflow.

Before TPQA, radiation planning CT scans are acquired with 3-mm section resolution; 1.5-mm section thickness is acquired for stereotactic cases. The planning CT is fused in multiple orientations with all available imaging studies, including MR imaging, diagnostic CT, and PET/CT. Target volumes and pertinent normal organ structures are delineated in advance by the radiation oncology team, reviewed and approved by the attending radiation oncologist who is designated by identifying first and last initials, and saved as a “Pre-TPQA” file.

Per the International Commission on Radiation Units and Measurements report 50,⁷ targets are designated as gross tumor volume (GTV), which includes all gross tumor appreciated on clinical examinations or visualized on imaging; clinical tumor volume (CTV), denoting regions of clinical risk outside the GTV, which include both areas considered at highest risk for involvement (CTV1) and those considered at lesser risk such as prophylactically included elective nodal basins (CTV2); and planning

target volume (PTV), which adds a small margin to each CTV to account for uncertainties of daily patient and machine setup. A dose range of 6000–7400 cGy is designated for the highest dose target and/or involved or high-risk nodal volumes (GTV, CTV1); and typically 4500–6000 cGy is designated for CTV2 (elective CTV). In the practice of our institution, CTV1 and CTV2 volumes are frequently subdivided (eg, CTV1 could be subdivided into CTV₆₉₉₆ and CTV₆₆₀₀, to clarify relative levels of highest risk by using the radiation dose as the suffix [given in units of centigray]

and to enable “dose painting” when creating the radiation therapy plan). PTV volumes are created as a 2- to 3-mm expansion from the CTV; PTVs are prescribed at the dose of their corresponding CTVs and are used in the final development, optimization, and evaluation of the computerized radiation plan. Image fusion and delineations are usually performed on MIM (MIM Software, Cleveland, Ohio), though stereotactic cases are reviewed on a Multiplan (Accuray, Sunnyvale, California) station. Dosimetry is performed on Pinnacle (Phillips Healthcare, Best, the Netherlands), TomoTherapy (Accuray), or Multiplan systems. An example of image fusion is shown in Fig 2.

TPQA occurs at a workstation complex that includes juxtaposed Pinnacle, TomoTherapy, MIM, and PACS terminals, enabling a parallel display of all imaging and target delineation data. Following review of the clinical, surgical, and pathologic details of the case, the neuroradiologists review all available diagnostic imaging. Preliminary target volumes are then reviewed on the MIM, Pinnacle, or TomoTherapy station, superimposed on the radiation planning CT and all fused diagnostic imaging studies. This process is characterized by interactive discussion and repeat viewing of the diagnostic imaging. The primary focus is on delineation of gross disease and areas of high clinical risk but also includes consideration of sparing adjacent uninvolved and/or critical structures. Any proposed changes are carried out in consultation with the neuroradiologist. After collaborative target volumes are created, a postreview structure set is saved as “Post-TPQA.” A description of alterations is catalogued in the electronic medical record (MOSAIQ; Elekta, Stockholm, Sweden).

Sample Population and Statistical Analysis

Approval was granted for review of demographic and radiographic data by the Committee on Human Research. A primary set of 80 HN consecutive treatment plans was reviewed at TPQA from August 2010 to February 2011; this era was selected for study as quality assurance documentation was consistent by this time point and it was approximately at the midpoint of our quality assurance experience. Descriptive information regarding the type of change by anatomic compartment was documented at the time of review. Volumetric information was later quantitatively compared between the Pre-TPQA and Post-TPQA files. Alterations in major disease-related targets (GTVs, CTVs) and anatomic compartments (soft tissue, lymph nodes, perineural invasion, bone invasion) were recorded. The significance of the frequency and

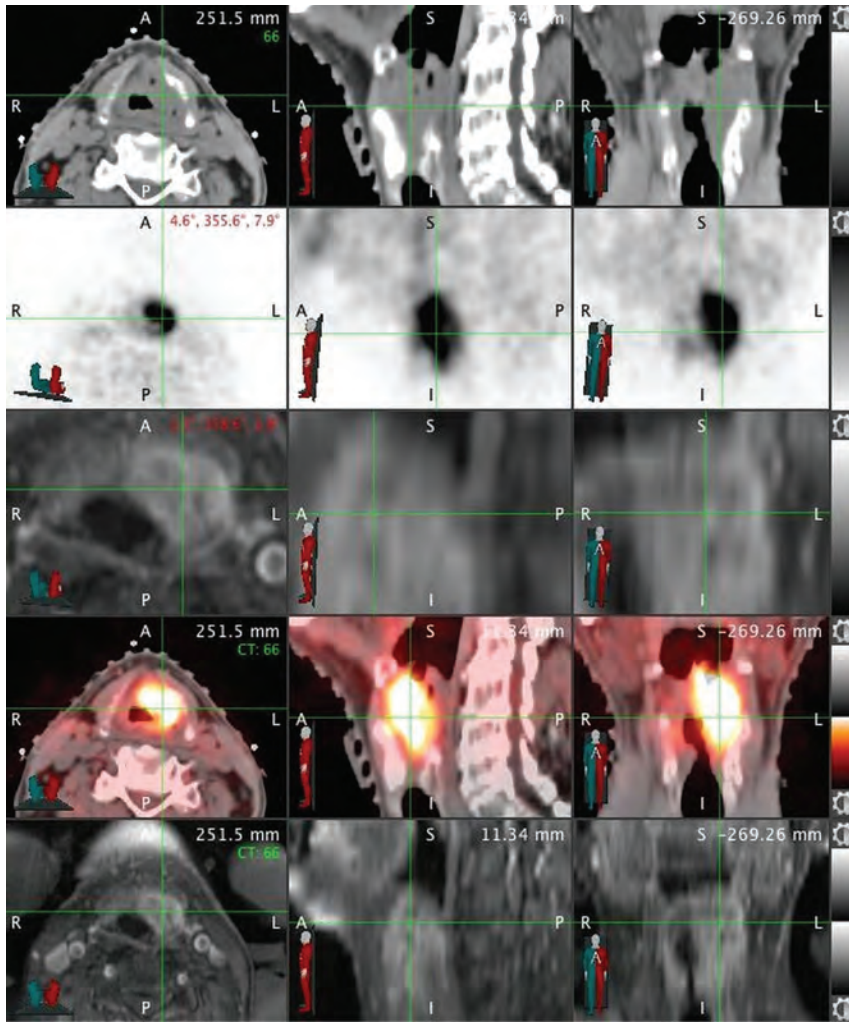


FIG 2. Example of image fusion performed at TPQA. *Green crosshairs* intersect over the laryngeal tumor. Rows represent the following: radiation oncology treatment planning CT scan, diagnostic PET, diagnostic MR imaging, fusion of treatment planning CT with PET, and fusion of treatment planning CT with MR imaging.

volume of change among HN subsites was analyzed by χ^2 contingency analysis and 1-tailed analysis of variance, respectively.

To rule out the presence of a “learning curve,” we similarly reviewed a second set of 40 HN consecutive treatment plans (August 2011 to November 2011). A 2-tailed Fisher exact test was used to compare the extent of target changes between the 2 sets.

RESULTS

Case Characteristics

Demographic and histopathologic information for the 80 consecutive cases is presented in Table 1. Patient median age was 49 years (range, 29–89 years). Predominant subsites included the oral cavity (24%), oropharynx (18%), sinonasal region (11%), and nasopharynx (10%). Additional subsites were skin (9%), salivary gland (9%), hypopharynx (6%), and larynx (5%). “Other” (9%) subsites included the orbit, lacrimal gland, maxilla, and neck (Table 1). Squamous cell carcinoma was the dominant histology (76%), followed by adenocarcinoma (5%) and lymphoma (4%). Other (15%) histologies included sarcoma, esthesioneuroblastoma, neuroendocrine and mucoepidermoid carcinoma,

and ameloblastoma (Table 1). Most cases were advanced-stage (60% stage IV, 19% stage III). Forty-eight percent of patients had definitive radiation-based treatment, and 52% had adjuvant radiation therapy following surgery.

Types of Change during TPQA

Overall, 55% (44/80) of Pre-TPQA structure sets were changed. The frequency of changes across subsites is shown in Fig 3A, from the hypopharynx altered in 80% (4/5) of cases to “other” with 29% (2/7) altered. Alterations were considered “clinically significant” if they resulted in exclusion or inclusion of a distinct area or structure and would change the radiation therapy plan with potential impact on disease control or toxicity. Sixty-one percent of altered plans (34% of all cases) had clinically significant changes, as shown in Fig 3B. Thirty-two percent (26/80) of cases had changes in the GTV, and 31% (25/80) had changes in the elective CTV (Fig 3B). Only 10 of 44 altered cases (23%) had changes in both the GTV and elective CTV. Other changes included addition or subtraction of lymph nodes (16%, 13/80), delineation of perineural pathways of spread (4%, 3/80), or reassessment of cancerous bone invasion (9%, 7/80). Specific forms of perineural and bony/cartilaginous target volume alteration most frequently involved the inclusion or exclusion of branches of the trigeminal and facial cranial nerves and

skull base perineural invasion, such as minor branches around the pterygopalatine fossa and cavernous sinus or Meckel cave, and fine editing of structures such as the clivus, mandible, sinuses, hyoid, laryngeal cartilages, and trachea. For postoperative cases, detailed editing was frequently performed around the areas of reconstruction and flap placement. Frequency and general categorization of types of changes were similar among definitive and postoperative patients.

Volumetric Assessment of Alterations during TPQA

GTV and elective CTV changes are presented in Table 2. For altered plans, the mean absolute volume change for GTV was 14.88 mm³ (19.75%), and for CTV, it was 14.63 mm³ (21.83%). As shown in Fig 4A, most changes were increases in GTV and elective CTV (approximately two-thirds of changed plans). As shown in Fig 4B, both GTV and CTV changes were heterogeneous, ranging from <1% to >100% (up to 275% for elective CTV changes). Furthermore, there was no difference by subsite in the frequency of overall ($n = 80$) volumetric changes in GTV or CTV (1-tailed

Table 1: Patient demographic and histopathologic information

	No. (%)
Total No. of patients	80 (100)
Sex	
M	59 (74)
F	21 (26)
Mean/median age (range) (yr)	51/49 (29–89)
Anatomic subsite	
Oral cavity	19 (24)
Oropharynx	14 (18)
Sinonasal	9 (11)
Nasopharynx	8 (10)
Skin	7 (9)
Salivary gland	7 (9)
Other	7 (9)
Hypopharynx	5 (6)
Larynx	4 (5)
Histology	
Squamous cell carcinoma	61 (76)
Adenocarcinoma	4 (5)
Lymphoma	3 (4)
Other	12 (15)
Stage	
I	4 (5)
II	13 (16)
III	15 (19)
IV	48 (60)
Radiotherapy intent	
Definitive	38 (48)
Postoperative	42 (52)

ANOVA, $P = .64$ and $P = .74$, respectively). Examples of alterations are shown in Fig 5.

In the 40-patient follow-up set, the frequency of change remained stable at 45% (18/40) compared with 55% in the initial cohort (Fisher exact test, $P = .34$). As shown in Fig 6, the categorization of changes was extremely similar to that of the earlier cohort.

DISCUSSION

In this report, approximately half of all radiation therapy plans were edited during neuroradiology-based peer review, and clinically significant changes were seen across all anatomic subsites and in both definitive and postoperative patients. The level of change averaged approximately 25% in volume but varied widely by patient, with reduction of target volumes (and presumably toxicity) in one-third of patients. Small GTV changes were sometimes highly clinically significant, especially for cases of lymph node involvement, osseous infiltration, or perineural extension. In postoperative patients, neuroradiologist input was valuable in identifying areas of close margin or routes of microscopic disease potentially underappreciated at the time of surgery. Because volumes at risk for microscopic disease were reviewed for all definitive and postoperative cases, the CTVs had a high frequency of change.

These findings confirm the impact that neuroradiology-based peer review has on the delineation of HN radiation therapy target volumes. Previous studies of collaboration between subsite-specific radiation oncologists and radiologists have suggested similar findings. In 1 study, a panel reviewed tumor delineations of 10 patients with non-small cell lung cancer.⁸ The radiation

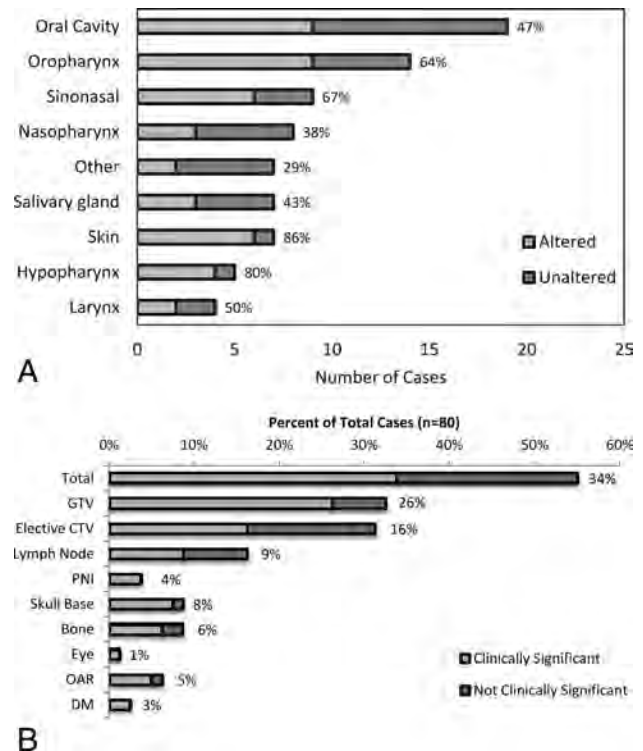


FIG 3. A, Alterations by subsite following HN TPQA. Light gray bars represent cases that were altered after review. Dark gray bars represent cases that were reviewed without subsequent alterations. Percentages to the right of the bars represent the fraction of cases with alterations. B, Types of treatment plan alterations. Light gray bars and data labels represent the percentage of total plans ($n = 80$) found to have changes by listed category. Dark gray bars represent the fraction of total plans with nonsignificant changes. PNI indicates perineural invasion; OAR, organs at risk; and DM, distant metastases. Note that x-axes were broken to reduce the width of the figure while maintaining a display of low and high values.

Table 2: Absolute volumetric changes in GTV and CTV from pre-TPQA to post-TPQA in altered plans

	Volume (mm ³)	Percentage Change
GTV ($n = 26$ cases)		
Mean	14.88	+19.75
Median	5.95	+7.86
Abs. range	1.95–130.59	0.50–133.64
CTV ($n = 25$ cases)		
Mean	14.63	+21.83
Median	10.34	+2.50
Abs. range	1.84–112.70	0.5–275.68

Note:—Abs. indicates absolute.

oncologists' average GTVs were >33% larger and more heterogeneous, outcomes resulting from a lower level of proficiency in applying window settings, discriminating tumor from consolidation, identifying involved lymph nodes, recognizing partial volume effects, and identifying pleural and chest wall involvement.^{8,9} Similarly, Horan et al¹⁰ reported GTV delineation for 10 patients with cancer by a radiologist and 2 radiation oncologists. Two of 5 cases of HN cancer showed major discordance. Discrepancy was attributed to disparate access to clinical information and diagnostic imaging expertise. A follow-up prospective study of non-small cell lung cancer radiation therapy plans included a formal collaborative session to finalize target volumes.¹¹ Changes occurred in

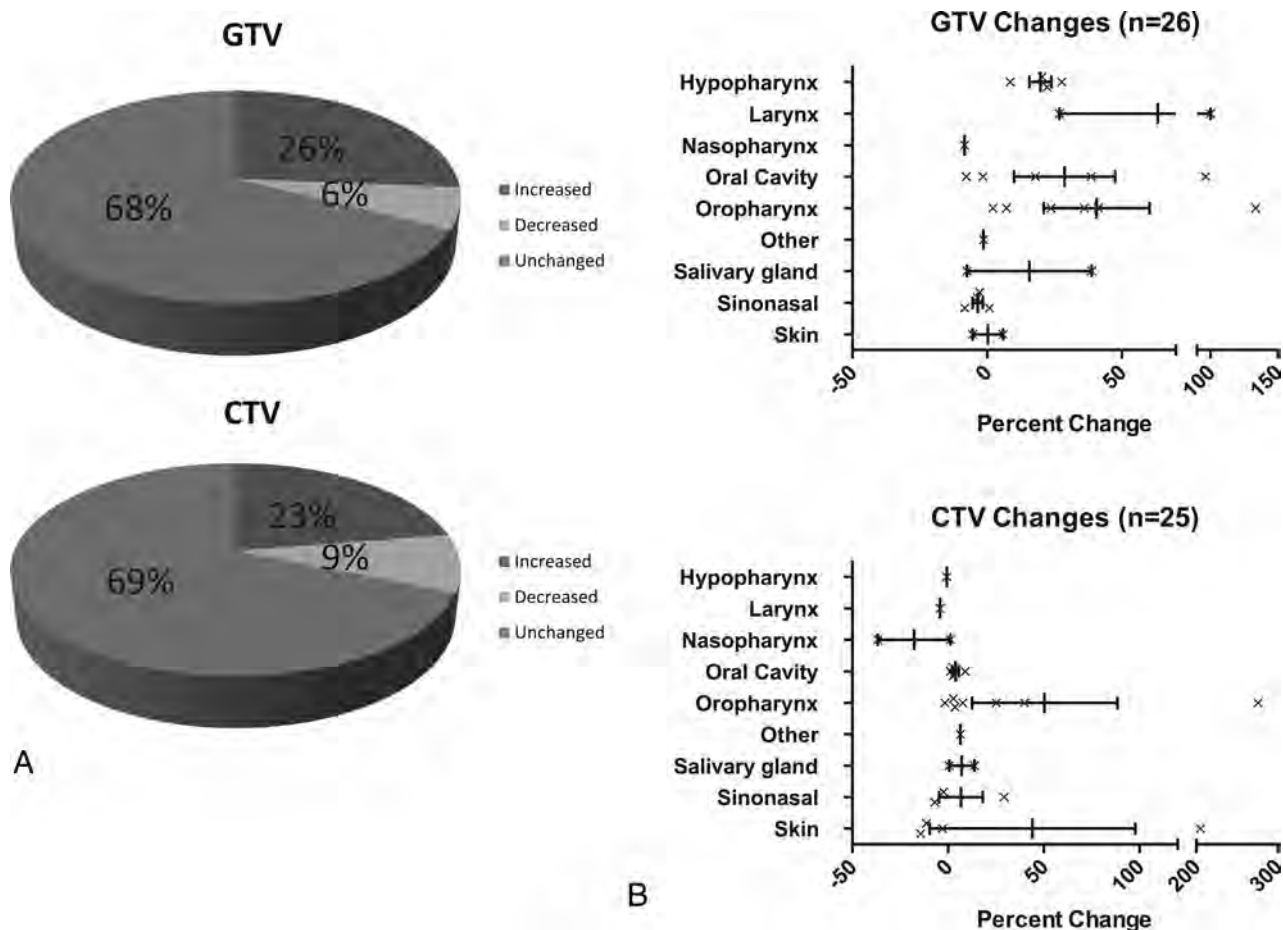


FIG 4. A, Volumetric changes in Pre-TPQA plans compared with Post-TPQA. Overall direction of GTV and CTV change. B, Volumetric changes in Pre-TPQA plans compared with Post-TPQA. Percentage of volume changes by subsite.

19 of 20 cases, with radiation oncologists reporting greater confidence in the resultant GTVs.

The introduction of highly conformal treatments such as intensity-modulated radiation therapy (IMRT) has increased the anatomic specificity of HN radiation therapy targeting, with the potential to decrease toxicities and adverse events.^{12,13} However, because of this increased precision, small errors in treatment design and delivery can affect clinical outcomes.¹⁴ Thus, major societies have issued guidelines enumerating aspects of the quality assurance process for IMRT,¹⁵ and most academic radiation oncology institutions use peer review to improve planning consistency.¹⁶ While textbooks, anatomic atlases,^{17,18} and evolving auto-segmentation tools¹⁹ are available to assist the individual practitioner, process studies have demonstrated a continuing need for multidisciplinary integration to assure effective radiation therapy planning.²⁰

Even among diagnostic neuroradiologists, interpretation of HN imaging is recognized as a challenging area that requires special effort in education and secondary consultation.²¹ Regarding radiation oncology, while it developed as a subspecialty of radiology in the first half of the 20th century,²² the residency now includes no formal diagnostic radiologic education. Meanwhile, developments in imaging acquisition and manipulation have led to increasing complexity and specificity of HN target delineation. Notably, the development of novel MR imaging and PET se-

quences has produced increasingly sophisticated imaging data for review.^{23,24} Integrating these sequences requires fusion to the radiation-planning CT for maximal utility, and thus many radiation oncologists now oversee complex workflows involving multimodality imaging fusion. These processes may require oversight and adjustment, but quality assurance of these procedures is not routine.^{25,26}

Radiation oncologists collaborate with urologists in prostate brachytherapy delivery²⁷ and with neurosurgeons in designing stereotactic radiosurgery for the brain.²⁸ However, while the benefits of collaboration with diagnostic radiology have been promoted for both external beam⁸ and brachytherapy²⁹ treatment planning, there is little evidence of formal inclusion in these spheres.⁹ Cited barriers include distinct workflows, separate locations, independent computer systems, and lack of defined billing mechanisms.³⁰ Nonetheless, rigorously reviewed treatment planning is an essential component of care for patients with HN cancer because salvage options after inadequate radiation therapy are limited. Our experience documents the impact of collaboration across these formidable logistical barriers.

There are limitations to this study. Because of uncertainty independent of the target delineation process (patient setup, machine-based physical uncertainties, multidirectional misalignments), CTVs are further expanded during radiation therapy planning to create planning treatment volumes (PTVs), which are

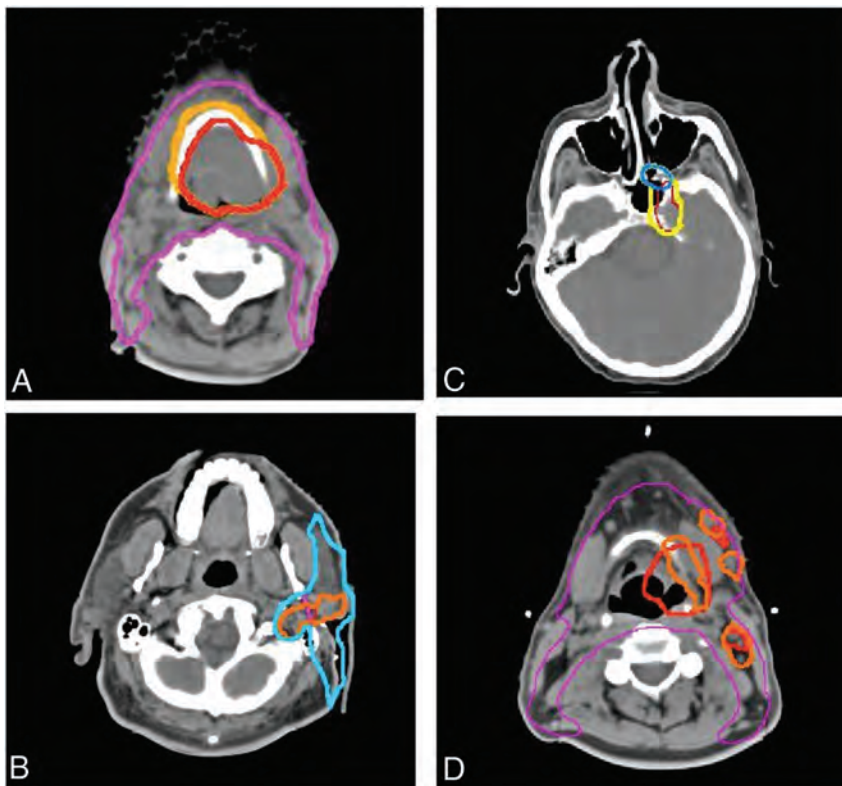


FIG 5. Treatment planning examples of TPQA changes. Red represents the pre-TPQA GTV or CTV1, and orange represents the altered post-TPQA GTV or CTV1. Yellow represents the pre-TPQA or CTV2, and blue represents the altered post-TPQA or CTV2. Changes include the following: increase in GTV for suspicion of gross disease involving the hyoid bone (A), increased GTV and CTV for pre-mastoid disease (B), expansion of CTV to include suspected PNI within the pterygo-palatine fossa (C), and additional nodal GTV but decreased primary tumor GTV to spare additional laryngeal toxicity (D). PNI indicates perineural invasion.

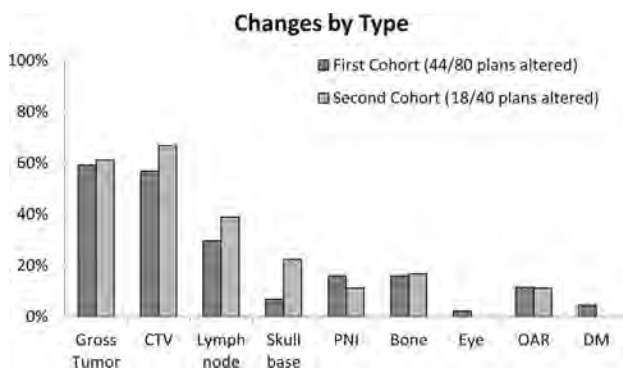


FIG 6. Comparison of TPQA results from 2 different time points. There is an extremely similar frequency of types of changes in the initial cohort ($n = 80$) and the follow-up cohort a year later ($n = 40$). PNI indicates perineural invasion; OAR, organs at risk; and DM, distant metastases.

used to design the final delivered plan and may suppress the effect of small changes in GTVs and CTVs.^{31,32} However, increasingly advanced radiation therapy delivery that decreases these uncertainties has led many practitioners to reduce PTV margins, amplifying the impact of small changes in tumor delineation.¹⁰ Furthermore, we designated clinically significant changes as those that would have resulted in omission or inclusion of an anatomically distinct area; this level of difference would not necessarily be remedied by PTV expansions.

Another limitation may relate to the expectation of scheduled

review, with the possibility that the radiation oncologists postponed decisions on difficult questions until TPQA, resulting in many changes. This phenomenon probably did occur to some extent, but we chose to incorporate these tendencies. Changes reflecting questioning or uncertainty are as important in their need for review as areas of unrecognized error. We believe these “gray areas” are better included than excluded from TPQA.

Third, because of the fluid nature of TPQA, we could not isolate changes made at the discretion of the neuroradiologists versus those suggested by other participants. In fact, the presence of trainees often led to explanations of clinical insights with ramifications for target delineation. A less easily quantified value of TPQA is the educational and team-building function, which increases the capacities of the group as a whole across time. This is a by-product uniquely stemming from the involvement of neuroradiology in the target delineation process.

Finally, it is possible that TPQA was evolutionary and the frequency of alterations changed with time. However, a review of cases from a later period yielded a similar frequency of changes,

suggesting that the impact of the review did not diminish. Informally, we note that approximately half of our cases continue to be altered in some manner at TPQA rounds to this day.

The intensity with which our process is conducted, in a concentrated, uninterrupted period of dedicated time each week, differentiates TPQA from informal arrangements and enabled a concrete documentation of the benefits of collaboration. At many high-volume HN programs, radiation oncologists may query a neuroradiologist about a specific aspect causing concern or confusion. In our TPQA process, neuroradiology is intricately involved in the inspection of targets through their superior-to-inferior extent by using comprehensive pre-prepared image fusion sets with targets overlaid on them. Inevitably, novel questions are raised by this convergence of information. Due to this sort of repeat exposure, our neuroradiology team is now experienced in the challenges of the radiation oncology decision-making process (because describing a tumor is not at all the same as drawing it), and they can understand and discuss the clinical trade-offs that are incurred related to specific targets of high- and low-dose prescription. The repeat synergy of experts at TPQA creates a network of knowledge that incorporates not only purely radiologic viewpoints but others that uniquely arise from the convergence of radiation therapy and radiology. While aspects of this level of teamwork may be replicated in ad hoc arrangements, we believe that structured interactions enabled this synergy at the highest level.

As a by-product of this process, there are some additional clinical benefits of interdisciplinary case review. Occasionally, further evolution or early recurrence of disease was identified on planning CT scans, leading to changes in management.¹⁰ Diagnostic MR images and PET/CT scans were sometimes obtained elsewhere, and TPQA helped overcome the limitations of suboptimal imaging and provided education for participants about appropriate imaging protocols. Last, within the TPQA framework, selected patients' imaging changes could be reviewed during a radiation therapy course which lasts several weeks, with the opportunity to re-plan the radiation treatment due to changes in anatomy or setup.³³ For the neuroradiologists, TPQA provided a focused exposure to imaging correlates of radiation therapy treatment response and sequelae³⁴ and a repertoire of pertinent information to include in reports to assist with radiation therapy target delineation.^{9,35,36}

CONCLUSIONS

Structured collaborative review of radiation therapy target delineation promotes the most effective use of diagnostic imaging in head and neck radiation oncology treatment planning. Interactions with diagnostic neuroradiology should be maximized, to promote a high level of treatment quality in the face of a proliferating array of complex imaging tools.

Disclosures: Sue S. Yom—UNRELATED: Grants/Grants Pending: Genentech, National Comprehensive Cancer Network Foundation, Comments: funding for clinical trials*; Other: American Society for Radiation Oncology, Comments: honoraria for journal editorship. *Money paid to the institution.

REFERENCES

1. Wheless SA, McKinney KA, Zanation AM. **A prospective study of the clinical impact of a multidisciplinary head and neck tumor board.** *Otolaryngol Head Neck Surg* 2010;143:650–54 CrossRef Medline
2. Nguyen NP, Vos P, Lee H, et al. **Impact of tumor board recommendations on treatment outcome for locally advanced head and neck cancer.** *Oncology* 2008;75:186–91 CrossRef Medline
3. Lefresne S, Olivetto IA, Joe H, et al. **Impact of quality assurance rounds in a Canadian radiation therapy department.** *Int J Radiat Oncol Biol Phys* 2013;85:e117–21 CrossRef Medline
4. Saito N, Nadgir RN, Nakahira M, et al. **Posttreatment CT and MR imaging in head and neck cancer: what the radiologist needs to know.** *Radiographics* 2012;32:1261–82; discussion 1282–84 CrossRef Medline
5. Loevner LA, Sonners AI, Schulman BJ, et al. **Reinterpretation of cross-sectional images in patients with head and neck cancer in the setting of a multidisciplinary cancer center.** *AJNR Am J Neuroradiol* 2002;23:1622–26 Medline
6. Lysack JT, Hoy M, Hudon ME, et al. **Impact of neuroradiologist second opinion on staging and management of head and neck cancer.** *J Otolaryngol Head Neck Surg* 2013;42:39 CrossRef Medline
7. Jones D. **ICRU Report 50—Prescribing, Recording and Reporting Photon Beam Therapy.** *Med Phys* 1994;21:833 CrossRef
8. Giraud P, Elles S, Helfre S, et al. **Conformal radiotherapy for lung cancer: different delineation of the gross tumor volume (GTV) by radiologists and radiation oncologists.** *Radiother Oncol* 2002;62:27–36 CrossRef Medline
9. Roy AE, Wells P. **Volume definition in radiotherapy planning for lung cancer: how the radiologist can help.** *Cancer Imaging* 2006;6:116–23 CrossRef Medline
10. Horan G, Roques TW, Curtin J, et al. **“Two are better than one”: a pilot study of how radiologist and oncologists can collaborate in**

- target volume definition. *Cancer Imaging* 2006;6:16–19 CrossRef Medline
11. Hollingdale AE, Roques TW, Curtin J, et al. **Multidisciplinary collaborative gross tumour volume definition for lung cancer radiotherapy: a prospective study.** *Cancer Imaging* 2011;11:202–08 CrossRef Medline
12. Lee N, Xia P, Fischbein NJ, et al. **Intensity-modulated radiation therapy for head-and-neck cancer: the UCSF experience focusing on target volume delineation.** *Int J Radiat Oncol Biol Phys* 2003;57:49–60 CrossRef Medline
13. O'Neill M, Heron DE, Flickinger JC, et al. **Posttreatment quality-of-life assessment in patients with head and neck cancer treated with intensity-modulated radiation therapy.** *Am J Clin Oncol* 2011;34:478–82 CrossRef Medline
14. Ohri N, Shen X, Dicker AP, et al. **Radiotherapy protocol deviations and clinical outcomes: a meta-analysis of cooperative group clinical trials.** *J Natl Cancer Inst* 2013;105:387–93 CrossRef Medline
15. Hartford AC, Galvin JM, Beyer DC, et al. American College of Radiology, American Society for Radiation Oncology, **Practice guideline for intensity-modulated radiation therapy (IMRT).** *Am J Clin Oncol* 2012;35:612–17 CrossRef Medline
16. Lawrence YR, Whiton MA, Symon Z, et al. **Quality assurance peer review chart rounds in 2011: a survey of academic institutions in the United States.** *Int J Radiat Oncol Biol Phys* 2012;84:590–95 CrossRef Medline
17. Grégoire V, Levendag P, Ang KK, et al. **CT-based delineation of lymph node levels and related CTVs in the node-negative neck: DAHANCA, EORTC, GORTEC, NCIC, RTOG consensus guidelines.** *Radiother Oncol* 2003;69:227–36 CrossRef Medline
18. Poon I, Fischbein N, Lee N, et al. **A population-based atlas and clinical target volume for the head-and-neck lymph nodes.** *Int J Radiat Oncol Biol Phys* 2004;59:1301–11 CrossRef Medline
19. Qazi AA, Pekar V, Kim J, et al. **Auto-segmentation of normal and target structures in head and neck CT images: a feature-driven model-based approach.** *Med Phys* 2011;38:6160–70 CrossRef Medline
20. Rosenthal DI, Asper JA, Barker JL Jr, et al. **Importance of patient examination to clinical quality assurance in head and neck radiation oncology.** *Head Neck* 2006;28:967–73 CrossRef Medline
21. Ginsberg LE. **Reinterpretation of head and neck scans: massive can of worms or call to action?** *AJNR Am J Neuroradiol* 2002;23:1617–18 Medline
22. Zietman A. **The future of radiation oncology: the evolution, diversification, and survival of the specialty.** *Semin Radiat Oncol* 2008;18:207–13 CrossRef Medline
23. Chung NN, Ting LL, Hsu WC, et al. **Impact of magnetic resonance imaging versus CT on nasopharyngeal carcinoma: primary tumor target delineation for radiotherapy.** *Head Neck* 2004;26:241–46 CrossRef Medline
24. Wang D, Schultz CJ, Jursinic PA, et al. **Initial experience of FDG-PET/CT guided IMRT of head-and-neck carcinoma.** *Int J Radiat Oncol Biol Phys* 2006;65:143–51 CrossRef Medline
25. Kovalchuk N, Jalisi S, Subramaniam RM, et al. **Deformable registration of preoperative PET/CT with postoperative radiation therapy planning CT in head and neck cancer.** *Radiographics* 2012;32:1329–41 CrossRef Medline
26. Hwang AB, Bacharach SL, Yom SS, et al. **Can positron emission tomography (PET) or PET/computed tomography (CT) acquired in a nontreatment position be accurately registered to a head-and-neck radiotherapy planning CT?** *Int J Radiat Oncol Biol Phys* 2009;73:578–84 CrossRef Medline
27. Sylvester JE, Grimm PD, Eulau SM, et al. **Permanent prostate brachytherapy preplanned technique: the modern Seattle method step-by-step and dosimetric outcomes.** *Brachytherapy* 2009;8:197–206 CrossRef Medline
28. Barnett GH, Linskey ME, Adler JR, et al; American Association of Neurological Surgeons; Congress of Neurological Surgeons Washington Committee Stereotactic Radiosurgery Task Force. **Stereotactic**

- radiosurgery: an organized neurosurgery-sanctioned definition.** *J Neurosurg* 2007;106:1–5 CrossRef Medline
29. Erickson B. **Image-based brachytherapy: a forum for collaboration between radiation oncologists and diagnostic radiologists.** *J Am Coll Radiol* 2005;2:753–58 CrossRef Medline
30. Terezakis SA, Heron DE, Lavigne RF, et al. **What the diagnostic radiologist needs to know about radiation oncology.** *Radiology* 2011; 261:30–44 CrossRef Medline
31. Astreinidou E, Bel A, Raaijmakers CP, et al. **Adequate margins for random setup uncertainties in head-and-neck IMRT.** *Int J Radiat Oncol Biol Phys* 2005;61:938–44 CrossRef Medline
32. Siebers JV, Keall PJ, Wu Q, et al. **Effect of patient setup errors on simultaneously integrated boost head and neck IMRT treatment plans.** *Int J Radiat Oncol Biol Phys* 2005;63:422–33 CrossRef Medline
33. Hansen EK, Bucci MK, Quivey JM, et al. **Repeat CT imaging and replanning during the course of IMRT for head-and-neck cancer.** *Int J Radiat Oncol Biol Phys* 2006;64:355–62 CrossRef Medline
34. Glastonbury CM, Parker EE, Hoang JK. **The postradiation neck: evaluating response to treatment and recognizing complications.** *AJR Am J Roentgenol* 2010;195:W164–71 CrossRef Medline
35. Sharma N, Neumann D, Macklis R. **The impact of functional imaging on radiation medicine.** *Radiat Oncol* 2008;3:25 CrossRef Medline
36. Newbold K, Partridge M, Cook G, et al. **Advanced imaging applied to radiotherapy planning in head and neck cancer: a clinical review.** *Br J Radiol* 2006;79:554–61 CrossRef Medline

Performance of CT in the Preoperative Diagnosis of Cervical Lymph Node Metastasis in Patients with Papillary Thyroid Cancer: A Systematic Review and Meta-Analysis

C.H. Suh, J.H. Baek, Y.J. Choi, and J.H. Lee



ABSTRACT

BACKGROUND AND PURPOSE: Ultrasound has become widely accepted as the first imaging technique used for the assessment of cervical lymph node metastasis in patients with papillary thyroid cancer. In this systematic review and meta-analysis, we evaluate the performance of CT for the preoperative diagnosis of cervical lymph node metastasis in patients with papillary thyroid cancer compared with ultrasound.

MATERIALS AND METHODS: Ovid-MEDLINE and EMBASE data bases were searched for studies regarding the use of CT to diagnose cervical lymph node metastasis. The diagnostic performance of CT, ultrasound, and combined CT/ultrasound was assessed by using level-by-level and patient-based analyses. We also performed meta-analyses on the basis of the central and lateral neck levels.

RESULTS: Nine eligible studies, including a total sample size of 1691 patients, were included. CT showed a summary sensitivity of 62% (95% CI, 52%–70%) and specificity of 87% (95% CI, 80%–92%) for diagnosing cervical lymph node metastasis when using level-by-level analysis. There was a positive correlation between the sensitivity and the false-positive rate (correlation coefficient, 0.807) because of the threshold effect. The summary sensitivity of combined CT/ultrasound (69%; 95% CI, 61%–77%) was significantly higher than ultrasound (51%; 95% CI, 42%–60%), though the summary specificity did not differ.

CONCLUSIONS: The diagnostic performances of CT and ultrasound are similar, though CT and ultrasound combined are superior to ultrasound only. CT may be used as a complementary diagnostic method in addition to ultrasound for diagnosing cervical lymph node metastasis in patients with papillary thyroid cancer.

ABBREVIATIONS: HSROC = hierarchic summary receiver operating characteristic; QUADAS-2 = Quality Assessment of Diagnostic Accuracy Studies-2; US = ultrasound

Papillary thyroid cancer involves metastasis to cervical lymph nodes in up to 60%–70% of patients.^{1,2} The presence of cervical lymph node metastasis is also highly associated with local recurrence and cancer-specific mortality.^{3,4} Several studies have demonstrated that cervical lymph node metastasis had an unfavorable prognostic effect on survival in patients 45 years of age and older.^{5,6} According to the new American Thyroid Association guidelines,⁷ ultrasound (US) has become widely accepted as the first imaging technique used for the assessment of cervical lymph

node metastasis in patients with papillary thyroid cancer. A recent meta-analysis demonstrated that the sensitivity of US was 63% (95% CI, 47%–76%), the specificity was 93% (95% CI, 73%–99%), and the area under the curve was 0.81 (95% CI, 0.77–0.84) by level-by-level analysis.⁸

However, because US is an operator-dependent technique, it is often difficult to evaluate the entire neck. Several US studies have reported variable and relatively low sensitivity for the assessment of central cervical lymph node metastasis.^{9–11} Normal anatomic structures, including the larynx, trachea, and areas deep in the clavicles, jaw, and sternum, cause significant acoustic shadowing.¹² This results in limited US evaluation of the mediastinum and retropharyngeal area, regardless of clinical experience of the operator.

Contrast-enhanced CT is a standard imaging technique used for the assessment of cervical lymph node metastasis in head and neck cancer; however, CT was not recommended as a routine imaging technique for patients with papillary thyroid cancer.¹³ Nevertheless, several recent studies have reported the possibility

Received April 1, 2016; accepted after revision August 22.

From the Department of Radiology and Research Institute of Radiology (C.H.S., J.H.B., Y.J.C., J.H.L.), University of Ulsan College of Medicine, Asan Medical Center, Seoul, Republic of Korea; and Department of Radiology (C.H.S.), Namwon Medical Center, Namwon-Si, Republic of Korea.

Please address correspondence to Jung Hwan Baek, MD, PhD, Department of Radiology and Research Institute of Radiology, University of Ulsan College of Medicine, Asan Medical Center, 86 Asanbyeongwon-Gil, Songpa-Gu, Seoul 138-736, Republic of Korea; e-mail: radbaek@naver.com

Indicates article with supplemental on-line table.

<http://dx.doi.org/10.3174/ajnr.A4967>

of the complementary role of CT for the preoperative evaluation of cervical lymph node metastasis.¹⁴⁻²² According to the new American Thyroid Association guidelines,⁷ CT is currently recommended as an adjunct to US for patients with clinical suspicion of advanced disease, such as invasive primary tumor or clinically apparent, multiple, or bulky lymph node metastasis. Because the US examination is operator-dependent and it is difficult to evaluate deep anatomic structures, CT with contrast enhancement may be useful in delineating the extent of tumor involvement in the airway or esophagus as well as delineating extranodal tumor extension. Preoperative knowledge of these features of the primary tumor or metastases could significantly influence the surgical plan.^{7,23} Therefore, it is timely and necessary to collect currently available data regarding the diagnostic performance of CT in the preoperative diagnosis of cervical lymph node metastasis.

A meta-analysis is part of the systematic review and uses statistical methods to integrate the results of multiple original studies.²⁴ Recently, the use of systematic review with meta-analyses is increasing in the field of radiology academic research (ie, diagnostic test accuracy). The main objectives of systematic review with meta-analyses are to obtain more valid, generalizable summary estimates and to identify and provide information on covariates that affect diagnostic accuracy tests.²⁵⁻²⁷ To the best of our knowledge, no systematic review with meta-analyses has assessed the role of using CT to diagnose cervical lymph node metastasis in patients with papillary thyroid cancer. Therefore, this systematic review with a meta-analysis evaluates the diagnostic performance of CT in the preoperative diagnosis of cervical lymph node metastasis in patients with papillary thyroid cancer compared with US.

MATERIALS AND METHODS

Literature Search Strategy

A computerized search of the MEDLINE and EMBASE data bases was performed to find relevant, original literature reports on the use of CT to diagnose cervical lymph node metastasis in patients with papillary thyroid cancer. We used the following search terms: (“thyroid cancer” OR “thyroid cancers” OR “thyroid carcinoma” OR “thyroid carcinomas”) AND (cervical lymph node metastasis OR cervical metastatic lymph node OR cervical metastatic lymphadenopathy) AND (ultrasonography OR sonography OR US OR “CT” OR CT). The beginning search date was not limited. Our search was limited to human patients and English language studies. We continued updating the literature search until November 29, 2015. To expand the search, we perused the bibliographies of the articles to identify other appropriate articles.

Inclusion Criteria

Studies that investigated the performance of CT in the preoperative diagnosis of cervical lymph node metastasis in patients with papillary thyroid cancer were eligible for inclusion. We included studies that satisfied all of the following criteria:

Population. Studies included >10 patients who underwent CT for papillary thyroid cancer before surgery. None of these patients had undergone previous operations of the head and neck.

Reference Standard. The level of cervical lymph nodes was determined according to the *American Joint Committee on Cancer Cancer Staging Manual*.²⁸ Assignment of cervical lymph nodes was based on compartments, including the lateral compartment (levels I–V) and the central compartment (level VI). The CT criteria for cervical lymph node metastasis were as follows: strong enhancement without hilar vessel enhancement, heterogeneous enhancement, calcification, and cystic or necrotic change.²⁹ The US criteria for cervical lymph node metastasis were as follows: focal or diffuse hyperechogenicity, micro- or macrocalcification, cystic change; an abnormal vascular pattern (a chaotic or peripheral vascular pattern), and a round shape (long-transverse diameter ratio, <1.5).³⁰⁻³² The final diagnoses of lymph nodes at each level were determined on the basis of the pathology reports regarding surgical specimens.

Study Design. Observational studies (retrospective or prospective) were included.

Outcomes. Results were reported in sufficient detail to evaluate the diagnostic performance of CT.

Exclusion Criteria

The exclusion criteria were the following: 1) case reports and series with a sample size of <10 patients and studies with a potential selection bias (eg, nonconsecutive series); 2) review articles, editorials, letters, comments, and conference proceedings; 3) studies on topics other than using CT to diagnose cervical lymph node metastasis in patients with papillary thyroid cancer; 4) studies with insufficient data to construct a 2 × 2 table; and 5) studies with overlapping patients and data. Two reviewers (C.H.S. and J.H.B.) independently selected the studies from the literature.

Data Extraction

We extracted the following data from the selected literature studies onto standardized data forms: 1) study characteristics: authors, year of publication, hospital or medical school, duration of patient recruitment, study design, and sample size; 2) demographic and clinical characteristics of the patients: mean age, analysis methods, and criteria of CT and US for diagnosing cervical lymph node metastasis; and 3) the diagnostic performance of CT and US. One reviewer (C.H.S.) extracted data from the studies, and the second reviewer (J.H.B.) double-checked the accuracy of the extracted data.

Quality Assessment

The methodologic quality of the included studies was independently assessed by 2 reviewers (C.H.S. and J.H.B.) by using tailored questionnaires and criteria provided by Quality Assessment of Diagnostic Accuracy Studies-2 (QUADAS-2).³³

Data Synthesis and Analyses

The diagnostic performances of CT and US were assessed as the main indices for this meta-analysis. First, a meta-analysis for all of the included studies was performed by using level-by-level and patient-based analyses. Second, we performed meta-analyses on the basis of the central and lateral neck levels.

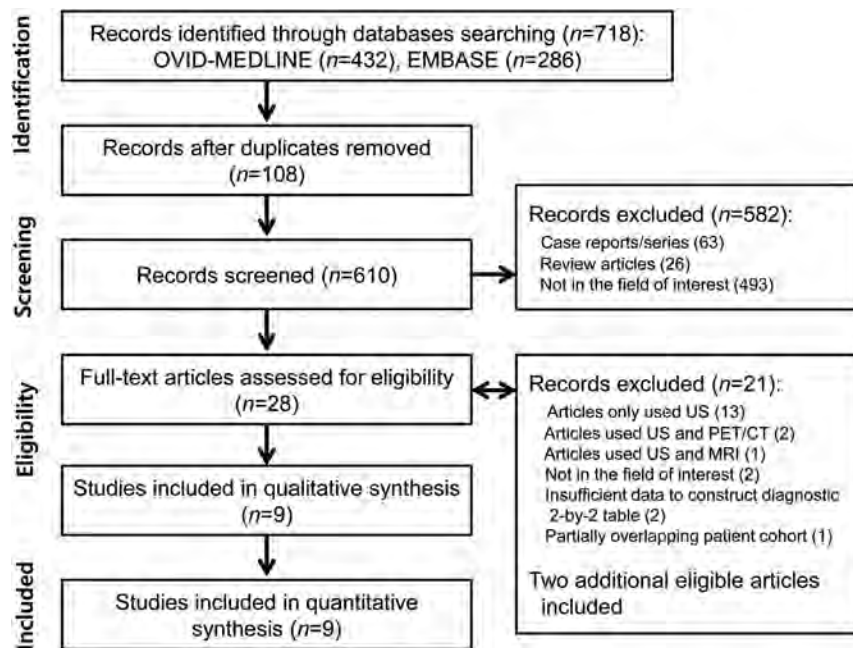


FIG 1. Flow diagram of the study selection process.

Heterogeneity among the studies was determined by using the Higgins I^2 statistics (0%–40%, might not be significant; 30%–60%, may represent moderate heterogeneity; 50%–90%, may represent substantial heterogeneity; and 75%–100%, may represent considerable heterogeneity).³⁴ When heterogeneity was noted, heterogeneity caused by a “threshold effect” was analyzed by visual assessment of the coupled forest plots of the sensitivity and the specificity. A meta-analysis of diagnostic test accuracy studies jointly analyzes a pair of outcomes (ie, sensitivity and specificity). Sensitivity and specificity are generally inversely correlated and affected by the threshold effect.^{25–27} Additionally, the Spearman correlation coefficient between the sensitivity and the false-positive rate was also obtained. A Spearman correlation coefficient of >0.6 indicates a considerable threshold effect.³⁵

The summary sensitivity and specificity values were calculated by the using hierarchic summary receiver operating characteristic (HSROC) and bivariate random-effects modeling.^{25–27} We obtained the diagnostic odds ratio, which is a single parameter of diagnostic accuracy.²⁷ The HSROC curve with a 95% confidence region and prediction region was also plotted to graphically present the results. Summarizing the results of original studies with the HSROC curve rather than by using summary points, including summary sensitivity or summary specificity, is recommended.²⁷ We obtained the area under the curve from the HSROC curve. If a test is perfectly accurate, the value of the area under the curve is 1.0 and decreases toward 0.5 as the diagnostic accuracy of the test decreases.

Publication bias was visually assessed by using the Deeks funnel plot, and the statistical significance was tested by using the Deeks asymmetry test. We used the MIDAS and METANDI modules in STATA 10.0 (StataCorp, College Station, Texas) to perform the statistical analyses.

RESULTS

Literature Search

Our study selection process is described in Fig 1. The literature search of the Ovid-MEDLINE and EMBASE data bases initially generated 718 articles, and 610 articles were screened for eligibility after removing 108 duplicates. Of the remaining articles, 582 were excluded after reviewing the titles and abstracts, including 493 articles that were not in the field of interest (ie, they did not discuss the diagnostic performance of CT for evaluating cervical lymph node metastasis in patients with papillary thyroid cancer), 63 case reports or series containing <10 relevant patients, and 26 review articles. The full texts of the remaining 28 articles were then retrieved. Searches of the bibliographies of articles identified 2 additional, eligible studies.^{14,22} Of these 30 articles, 21 were further excluded after reviewing the full text (ie, 13 studies that only used US, 2

studies that used US and PET/CT, 1 study that used US and MR imaging, 2 studies that were not in the field of interest, 2 studies that reported insufficient data to construct a diagnostic 2-by-2 table, and 1 study with a partially overlapping patient cohort). Finally, 9 eligible studies, including a total sample size of 1691 patients, were included in this meta-analysis.^{14–22}

Characteristics of the Included Studies

The detailed characteristics of the 9 included studies are summarized in the On-line Table. Three of the included studies were prospective,^{14,20,21} and the remaining 6 were retrospective.^{15–19,22} The CT criteria for cervical lymph node metastasis were similar in studies using morphologic criteria, though 4 studies added size criteria.^{14,15,20,21} The US criteria for cervical lymph node metastasis were variable. The final diagnoses of cervical lymph nodes were determined on the basis of the pathology reports of surgical specimens in all of the included studies.^{14–22} The quality of the included studies, as assessed by using QUADAS-2, was moderate overall, and all the studies satisfied ≥ 6 of the 7 items (Fig 2).³³

Diagnostic Performance of CT and US for All Cervical Lymph Nodes by Level-by-Level Analysis

Data were collected from 7 CT studies with 926 patients concerning the diagnostic performance of CT.^{14–17,19–21} The sensitivities and specificities of the individual studies were 35%–77% and 70%–96%, respectively. The Higgins I^2 statistics demonstrated a substantial heterogeneity regarding both sensitivity ($I^2 = 82.6\%$) and specificity ($I^2 = 89.7\%$). The coupled forest plots of the sensitivity and specificity revealed a threshold effect (Fig 3), and the Spearman correlation coefficient between the sensitivity and the false-positive rate was 0.807 (95% CI, 0.136–0.970), thus also indicating the presence of the threshold effect.

The pooled sensitivities and specificities of CT and US are

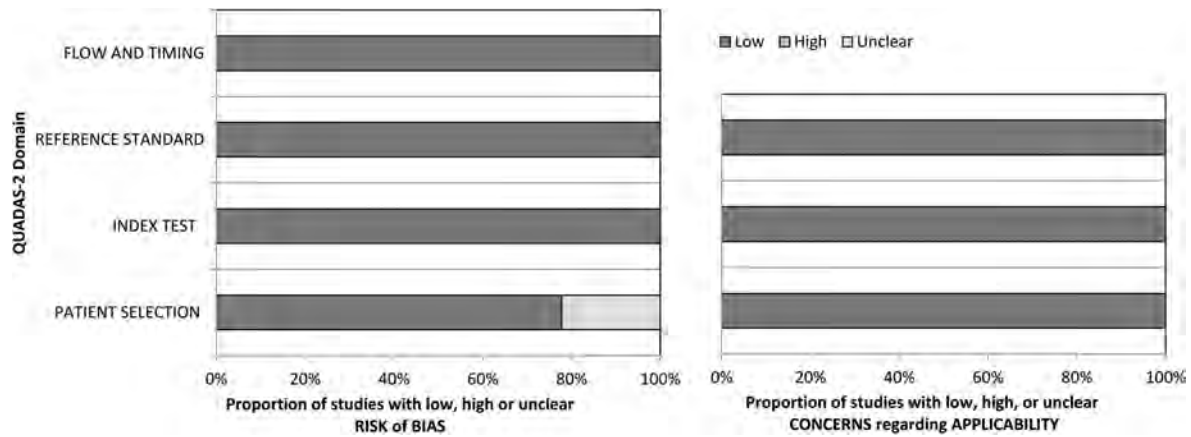


FIG 2. Quality Assessment of the Diagnostic Accuracy Studies-2 criteria for the included studies.

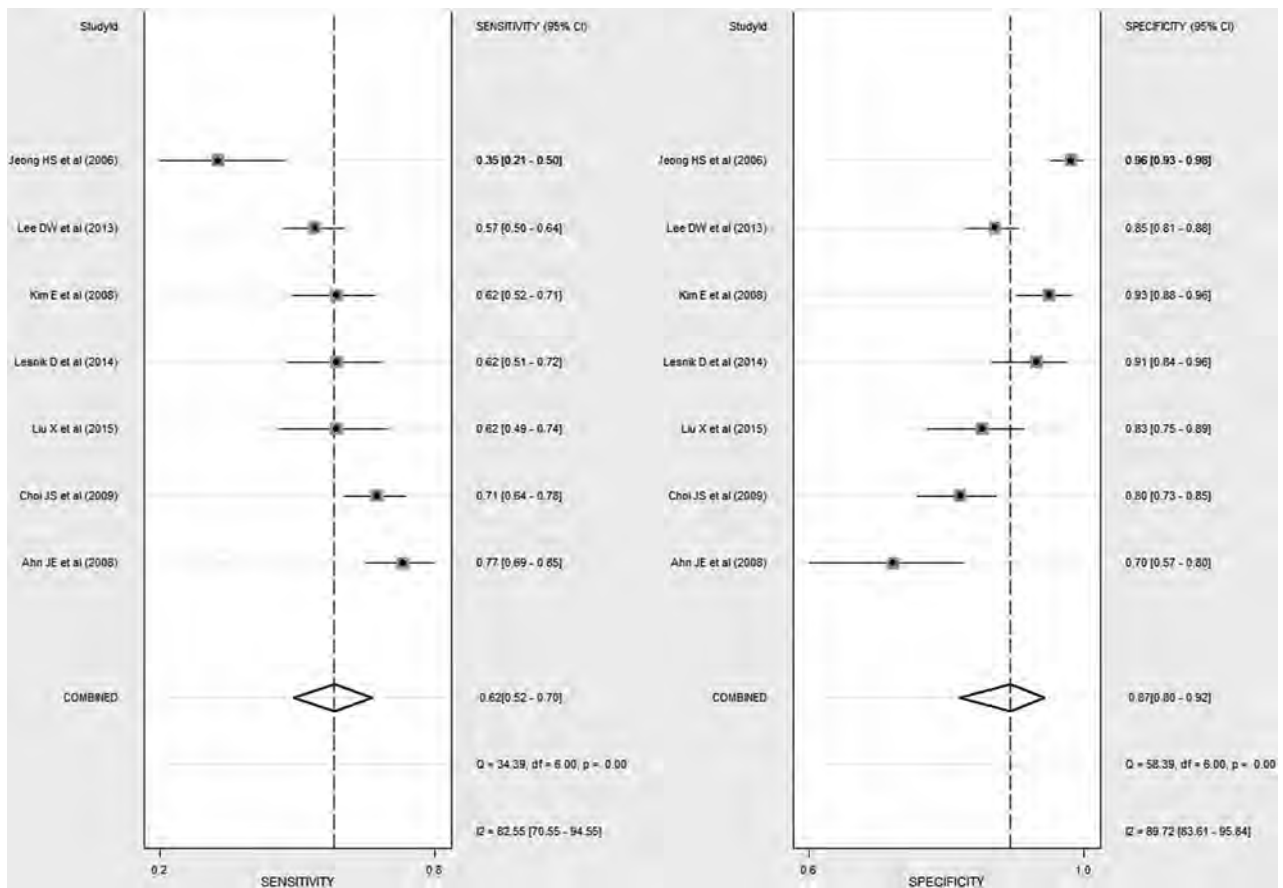


FIG 3. Coupled forest plots of the sensitivity and specificity of CT for diagnosing cervical lymph node metastasis in patients with papillary thyroid cancer. Horizontal lines indicate 95% CIs of the individual studies.

summarized in the Table. CT demonstrated a summary sensitivity of 62% (95% CI, 52%–70%) and a specificity of 87% (95% CI, 80%–92%). The diagnostic odds ratio was 11 (95% CI, 8–15). The HSROC curve was symmetric, and there was only a small difference between the 95% confidence region and the 95% prediction region, thus indicating little heterogeneity between the studies (Fig 4). The area under the HSROC curve was 0.80 (95% CI, 0.77–0.84). No significant publication bias existed among the studies ($P = .41$) (Fig 5).

Data were collected from 6 US studies with 874 patients.^{14–17,19,20}

The sensitivities and specificities of the individual studies were 40%–66% and 79%–96%, respectively. The Spearman correlation coefficient between the sensitivity and false-positive rate was 0.960 (95% CI, 0.675–0.996), thus indicating the presence of the threshold effect. US demonstrated a summary sensitivity of 51% (95% CI, 42%–60%) and a specificity of 91% (95% CI, 85%–95%). The diagnostic odds ratio was 11 (95% CI, 7–16). The area under the HSROC curve was 0.74. The summary estimates of sensitivity ($P = .127$) and specificity ($P = .351$) did not differ between CT and US.

Results of meta-analytic summary estimates of CT and US for diagnosing cervical lymph node metastasis in patients with papillary thyroid cancer by level-by-level analysis

	Meta-Analysis Summary Estimate			
	Sensitivity (95% CI)	P Value	Specificity (95% CI)	P Value
All cervical lymph nodes				
US	51% (42–60)		91% (85–95)	
CT	62% (52–70)	.127 ^a	87% (80–92)	.351 ^a
Combined CT/US	69% (61–77)	.011 ^b	81% (74–87)	.074 ^b
Lateral cervical lymph nodes				
US	71% (57–82)		85% (64–95)	
CT	70% (59–80)	.858 ^a	89% (81–94)	.792 ^a
Combined CT/US	90% (80–95)	.029 ^b	70% (43–88)	.329 ^b
Central cervical lymph nodes				
US	38% (27–52)		91% (81–96)	
CT	57% (43–69)	.088 ^a	85% (72–92)	.368 ^a
Combined CT/US	57% (45–68)	.079 ^b	83% (75–89)	.281 ^b

^a Comparison for CT vs US.

^b Comparison for combined CT/US vs US.

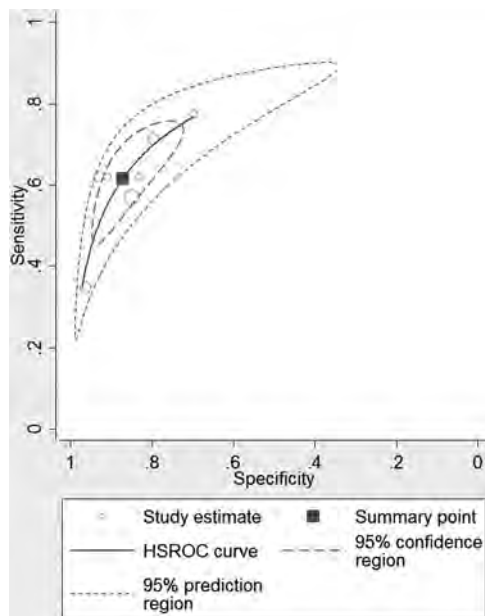


FIG 4. Hierarchic summary receiver operating characteristic curve of the performance of CT for diagnosing cervical lymph node metastasis in patients with papillary thyroid cancer.

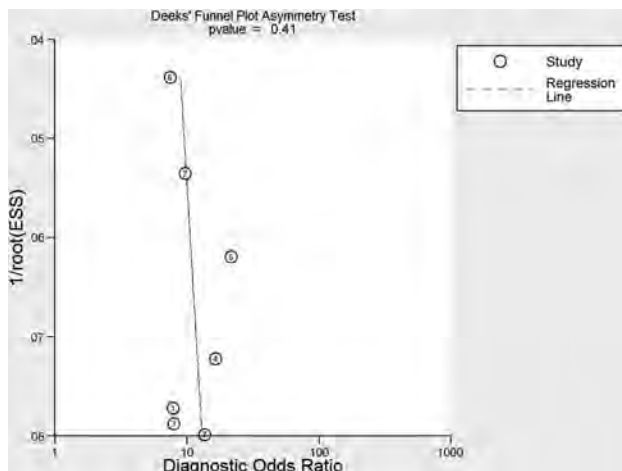


FIG 5. The Deeks funnel plot to evaluate publication bias.

Comparison of CT and US according to Lateral and Central Cervical Lymph Nodes by Level-by-Level Analysis

Concerning the lateral cervical lymph nodes, CT demonstrated a summary sensitivity of 70% (95% CI, 59%–80%) and a specificity of 87% (95% CI, 81%–94%) and US demonstrated a summary sensitivity of 71% (95% CI, 57%–82%) and a specificity of 85% (95% CI, 64%–95%) (Table). The summary estimates of sensitivity ($P = .858$) and specificity ($P = .792$) did not differ between CT and US. Regarding central cervical lymph nodes, CT demonstrated a summary sensitivity of 57% (95% CI, 43%–69%) and a specificity of 85% (95% CI, 72%–92%), and US demonstrated a summary sensitivity of 38% (95% CI, 27%–52%) and a specificity of 91% (95% CI, 81%–96%). Although the summary sensitivity of CT was higher than that of US, there was no significant difference ($P = .088$). The summary specificity ($P = .368$) did not differ between CT and US.

Added Value of Combined CT/US by Level-by-Level Analysis

Four studies reported combined CT/US for diagnosing cervical lymph node metastasis.^{16,17,19,20} The sensitivity ranged from 61% to 80%, and the lower margin of the 95% CI reached 54%. The specificity ranged from 69% to 88%, and the lower margin of the 95% CI reached 62%. Combined CT/US demonstrated a summary sensitivity of 69% (95% CI, 61%–77%) and a specificity of 81% (95% CI, 74%–87%). The summary sensitivity of combined CT/US was significantly higher than that of US ($P = .011$), though the summary specificity did not differ ($P = .074$).

Performance of CT and US for Diagnosing Cervical Lymph Node Metastasis by Patient-Based Analysis

Pooling was not performed due to the relatively small number of studies ($n = 4$) used for these analyses.^{16,18,19,22} The sensitivity of CT was variable, ranging from 31% to 59%; and the lower margin of the 95% CI reached 22%. The specificity of CT ranged from 84% to 94%, and the lower margin of the 95% CI reached 77%. The sensitivity of US was variable, ranging from 24% to 47%, and the lower margin of the 95% CI reached 17%. The specificity of US ranged from 80% to 92%, and the lower margin of the 95% CI reached 74%.

DISCUSSION

Our current systematic review with a meta-analysis demonstrated that CT showed a summary sensitivity of 62% and a specificity of 87% for diagnosing cervical lymph node metastasis in patients with papillary thyroid cancer by a level-by-level analysis. There was a positive correlation between the sensitivity and the false-positive rate (correlation coefficient of 0.807) because of the threshold effect. In terms of the comparison of CT and US, the summary estimates of the sensitivity and specificity did not differ

between CT and US for all cervical lymph nodes and lateral/central lymph nodes. However, the summary sensitivity of combined CT/US (69%) was significantly higher than that of US (51%), though the summary specificity did not differ. These results suggest that the diagnostic performances of CT and US are similar but that CT and US combined are superior to US only for the detection of cervical lymph node metastasis in patients with papillary thyroid cancer by a level-by-level analysis.

During the past decade, many studies have described the diagnostic performance of CT for cervical lymph node metastasis in patients with papillary thyroid cancer.¹⁴⁻²² CT is a standardized, objective imaging technique that is less operator-dependent compared with US. In addition, CT provides detailed axial anatomic information systematically from the base of the skull to the mediastinum, which is familiar to most thyroid surgeons. Moreover, CT can evaluate lymph nodes in the retropharyngeal, retrosternal, and mediastinal areas.²⁰ As the new American Thyroid Association guidelines suggest, CT can also be useful for evaluating the tumor extent involving the larynx, trachea, or esophagus as well as showing extranodal extension involving surrounding critical structures.⁷ Our meta-analysis revealed that the summary sensitivity of combined CT/US (69%) was significantly higher than that of US (51%) ($P = .011$). This improved sensitivity of combined CT/US allows better surgical planning and a better chance for removing all suspected cervical lymph node metastasis during surgery. Therefore, we believe that combined CT/US may have a supportive role, especially for preoperative surgical planning in patients with suspected lymph node metastasis or a high-risk of lymph node metastasis.^{16,23}

The use of iodine-based contrast materials was strongly restricted before the operation due to the concern for disturbed radioactive iodine uptake for months and the delay of radioiodine treatment.³⁶ Therefore, contrast-enhanced CT has not been recommended for the preoperative diagnosis of cervical lymph node metastasis. However, several recent studies have reported the supposition that the delay of radioiodine therapy was not necessary in patients who underwent contrast-enhanced CT because the iodine is generally cleared within 4–8 weeks in most patients, and the body iodine content is not an essential determinant of thyroid ablation.³⁷⁻⁴¹ Therefore, the benefit gained from improved anatomic imaging generally outweighs any potential risk regarding a several-week delay in radioactive iodine imaging or therapy.

In our meta-analysis, our summary estimates demonstrate consistent results despite heterogeneity. The Higgins I^2 statistic demonstrated a substantial heterogeneity in both the sensitivity ($I^2 = 82.6\%$) and specificity ($I^2 = 89.7\%$) of CT. However, there was a positive correlation between sensitivity and the false-positive rate (correlation coefficient of 0.807), which would be expected in a meta-analysis of diagnostic test accuracy studies due to the threshold effect. This correlation indicates that our heterogeneity was mainly caused by the threshold effect. CT criteria for cervical lymph node metastasis in our included studies were similar, though several studies used not only morphologic criteria but also size criteria, which may cause the threshold effect.^{26,27} Morphologic criteria include central necrosis or cystic change, strong enhancement without hilar vessel enhancement, calcification, and round shape with loss of the fatty hilum (On-line Table). The

possibility of a node with only mild enhancement would be very low for lymph node metastasis. In addition, the US criteria for cervical lymph node metastasis were also variable between studies. The US criteria included cystic change, the absence of a hilum, microcalcification, heterogeneity, and size.

We used validated systematic review methods and reported our data according to standard reporting guidelines, including the Preferred Reporting Items for Systematic Reviews and Meta-Analyses (PRISMA),⁴² the guidelines of the *Handbook for Systematic Reviews of Diagnostic Test Accuracy* by the Cochrane Collaboration,⁴³ and the guidelines of the Agency for Healthcare Research and Quality.⁴⁴ We determined the diagnostic performance of CT by using more recently developed robust methodology (ie, the HSROC model or the bivariate random-effects model).²⁵⁻²⁷ Therefore, this study, which gathered currently available evidence, was needed and will help to advance daily clinical practice.

Our study had several limitations. First, it included relatively few studies (ie, 9). In addition, the sample size of the number of included studies in the meta-analysis according to the central/lateral lymph nodes was small. Nonetheless, a small number of statistically significant differences were elucidated. Second, as addressed earlier, the CT or US criteria for cervical lymph node metastasis were similar but somewhat variable between studies because no consistent criteria have been established regarding cervical lymph node metastasis. The threshold effect is probably caused by these variable criteria. Third, 7 of 9 studies included reflect single-country data; however, these are the only available studies.^{14-19,22} Fourth, the specificity of combined CT/US is lower than that of US alone; however, it is not statistically significant.

CONCLUSIONS

The diagnostic performances of CT and US are similar, though CT and US combined are superior to US only for the detection of cervical lymph node metastasis in patients with papillary thyroid cancer by a level-by-level analysis. CT may be used as a complementary method in addition to US for diagnosing cervical lymph node metastasis in patients with papillary thyroid cancer.

REFERENCES

1. Mulla M, Schulte KM. **Central cervical lymph node metastases in papillary thyroid cancer: a systematic review of imaging-guided and prophylactic removal of the central compartment.** *Clin Endocrinol (Oxf)* 2012;76:131–36 CrossRef Medline
2. Rotstein L. **The role of lymphadenectomy in the management of papillary carcinoma of the thyroid.** *J Surg Oncol* 2009;99:186–88 CrossRef Medline
3. Sivanandan R, Soo KC. **Pattern of cervical lymph node metastases from papillary carcinoma of the thyroid.** *Br J Surg* 2001;88:1241–44 CrossRef Medline
4. Randolph GW, Duh QY, Heller KS, et al; American Thyroid Association Surgical Affairs Committee's Taskforce on Thyroid Cancer Nodal Surgery. **The prognostic significance of nodal metastases from papillary thyroid carcinoma can be stratified based on the size and number of metastatic lymph nodes, as well as the presence of extranodal extension.** *Thyroid* 2012;22:1144–52 CrossRef Medline
5. Zaydfudim V, Feurer ID, Griffin MR, et al. **The impact of lymph node involvement on survival in patients with papillary and follicular**

- thyroid carcinoma. *Surgery* 2008;144:1070–77; discussion 77–78; discussion 1077–78 CrossRef Medline
6. Mazzaferri EL, Doherty GM, Steward DL. **The pros and cons of prophylactic central compartment lymph node dissection for papillary thyroid carcinoma.** *Thyroid* 2009;19:683–89 CrossRef Medline
 7. Haugen BR, Alexander EK, Bible KC, et al. **2015 American Thyroid Association Management Guidelines for Adult Patients with Thyroid Nodules and Differentiated Thyroid Cancer: the American Thyroid Association Guidelines Task Force on Thyroid Nodules and Differentiated Thyroid Cancer.** *Thyroid* 2016;26:1–133 CrossRef Medline
 8. Wu LM, Gu HY, Qu XH, et al. **The accuracy of ultrasonography in the preoperative diagnosis of cervical lymph node metastasis in patients with papillary thyroid carcinoma: a meta-analysis.** *Eur J Radiol* 2012;81:1798–805 CrossRef Medline
 9. Ito Y, Jikuzono T, Higashiyama T, et al. **Clinical significance of lymph node metastasis of thyroid papillary carcinoma located in one lobe.** *World J Surg* 2006;30:1821–28 CrossRef Medline
 10. Sipos JA. **Advances in ultrasound for the diagnosis and management of thyroid cancer.** *Thyroid* 2009;19:1363–72 CrossRef Medline
 11. Hwang HS, Orloff LA. **Efficacy of preoperative neck ultrasound in the detection of cervical lymph node metastasis from thyroid cancer.** *Laryngoscope* 2011;121:487–91 CrossRef Medline
 12. Ha EJ, Baek JH, Lee JH. **Ultrasonography-based thyroidal and perithyroidal anatomy and its clinical significance.** *Korean J Radiol* 2015;16:749–66 CrossRef Medline
 13. Cooper DS, Doherty GM, Haugen BR, et al; American Thyroid Association (ATA) Guidelines Taskforce on Thyroid Nodules and Differentiated Thyroid Cancer. **Revised American Thyroid Association management guidelines for patients with thyroid nodules and differentiated thyroid cancer.** *Thyroid* 2009;19:1167–214 CrossRef Medline
 14. Jeong HS, Baek CH, Son YI, et al. **Integrated 18F-FDG PET/CT for the initial evaluation of cervical node level of patients with papillary thyroid carcinoma: comparison with ultrasound and contrast-enhanced CT.** *Clin Endocrinol (Oxf)* 2006;65:402–07 CrossRef Medline
 15. Ahn JE, Lee JH, Yi JS, et al. **Diagnostic accuracy of CT and ultrasonography for evaluating metastatic cervical lymph nodes in patients with thyroid cancer.** *World J Surg* 2008;32:1552–58 CrossRef Medline
 16. Kim E, Park JS, Son KR, et al. **Preoperative diagnosis of cervical metastatic lymph nodes in papillary thyroid carcinoma: comparison of ultrasound, computed tomography, and combined ultrasound with computed tomography.** *Thyroid* 2008;18:411–18 CrossRef Medline
 17. Choi JS, Kim J, Kwak JY, et al. **Preoperative staging of papillary thyroid carcinoma: comparison of ultrasound imaging and CT.** *AJR Am J Roentgenol* 2009;193:871–78 CrossRef Medline
 18. Choi YJ, Yun JS, Kook SH, et al. **Clinical and imaging assessment of cervical lymph node metastasis in papillary thyroid carcinomas.** *World J Surg* 2010;34:1494–99 CrossRef Medline
 19. Lee DW, Ji YB, Sung ES, et al. **Roles of ultrasonography and computed tomography in the surgical management of cervical lymph node metastases in papillary thyroid carcinoma.** *Eur J Surg Oncol* 2013;39:191–96 CrossRef Medline
 20. Lesnik D, Cunnane ME, Zurakowski D, et al. **Papillary thyroid carcinoma nodal surgery directed by a preoperative radiographic map utilizing CT scan and ultrasound in all primary and reoperative patients.** *Head Neck* 2014;36:191–202 CrossRef Medline
 21. Liu X, Ouyang D, Li H, et al. **Papillary thyroid cancer: dual-energy spectral CT quantitative parameters for preoperative diagnosis of metastasis to the cervical lymph nodes.** *Radiology* 2015;275:167–76 CrossRef Medline
 22. Na DK, Choi YJ, Choi SH, et al. **Evaluation of cervical lymph node metastasis in thyroid cancer patients using real-time CT-navigated ultrasonography: preliminary study.** *Ultrasonography* 2015;34:39–44 CrossRef Medline
 23. Yeh MW, Bauer AJ, Bernet VA, et al; American Thyroid Association Surgical Affairs Committee Writing Task Force. **American Thyroid Association statement on preoperative imaging for thyroid cancer surgery.** *Thyroid* 2015;25:3–14 CrossRef Medline
 24. Tunis AS, McInnes MD, Hanna R, et al. **Association of study quality with completeness of reporting: have completeness of reporting and quality of systematic reviews and meta-analyses in major radiology journals changed since publication of the PRISMA statement?** *Radiology* 2013;269:413–26 CrossRef Medline
 25. Suh CH, Park SH. **Successful publication of systematic review and meta-analysis of studies evaluating diagnostic test accuracy.** *Korean J Radiol* 2016;17:5–6 CrossRef Medline
 26. Kim KW, Lee J, Choi SH, et al. **Systematic review and meta-analysis of studies evaluating diagnostic test accuracy: a practical review for clinical researchers, part I: general guidance and tips.** *Korean J Radiol* 2015;16:1175–87 CrossRef Medline
 27. Lee J, Kim KW, Choi SH, et al. **Systematic review and meta-analysis of studies evaluating diagnostic test accuracy: a practical review for clinical researchers, part II, statistical methods of meta-analysis.** *Korean J Radiol* 2015;16:1188–96 CrossRef Medline
 28. Edge S, Byrd DR, Compton CC, et al, eds. *AJCC Cancer Staging Manual.* 7th ed. New York: Springer; 2010:87–96
 29. Som PM, Brandwein M, Lidov M, et al. **The varied presentations of papillary thyroid carcinoma cervical nodal disease: CT and MR findings.** *AJNR Am J Neuroradiol* 1994;15:1123–28 Medline
 30. Na DG, Lim HK, Byun HS, et al. **Differential diagnosis of cervical lymphadenopathy: usefulness of color Doppler sonography.** *AJR Am J Roentgenol* 1997;168:1311–16 CrossRef Medline
 31. Ying M, Ahuja A, Metreweli C. **Diagnostic accuracy of sonographic criteria for evaluation of cervical lymphadenopathy.** *J Ultrasound Med* 1998;17:437–45 Medline
 32. Rosário PW, de Faria S, Bicalho L, et al. **Ultrasonographic differentiation between metastatic and benign lymph nodes in patients with papillary thyroid carcinoma.** *J Ultrasound Med* 2005;24:1385–89 Medline
 33. Whiting P, Rutjes AW, Reitsma JB, et al. **The development of QUADAS: a tool for the quality assessment of studies of diagnostic accuracy included in systematic reviews.** *BMC Med Res Methodol* 2003;3:25 CrossRef Medline
 34. Higgins J, Green S. *Cochrane Handbook for Systematic Reviews of Interventions.* Version 5.1.0. Updated March 2011. <http://handbook.cochrane.org/>. Accessed August 15, 2015
 35. Deeks JJ, Macaskill P, Irwig L. **The performance of tests of publication bias and other sample size effects in systematic reviews of diagnostic test accuracy was assessed.** *J Clin Epidemiol* 2005;58:882–93 CrossRef Medline
 36. Spate VL, Morris JS, Nichols TA, et al. **Longitudinal study of iodine in toenails following IV administration of an iodine-containing contrast agent.** *Journal of Radioanalytical and Nuclear Chemistry* 1998;236:71–77 CrossRef
 37. Padovani RP, Kasamatsu TS, Nakabashi CC, et al. **One month is sufficient for urinary iodine to return to its baseline value after the use of water-soluble iodinated contrast agents in post-thyroidectomy patients requiring radioiodine therapy.** *Thyroid* 2012;22:926–30 CrossRef Medline
 38. Sohn SY, Choi JH, Kim NK, et al. **The impact of iodinated contrast agent administered during preoperative computed tomography scan on body iodine pool in patients with differentiated thyroid cancer preparing for radioactive iodine treatment.** *Thyroid* 2014;24:872–77 CrossRef Medline
 39. Ho JD, Tsang JF, Scoggan KA, et al. **Urinary iodine clearance following iodinated contrast administration: a comparison of euthyroid and postthyroidectomy subjects.** *J Thyroid Res* 2014;2014:580569 CrossRef Medline
 40. Mishra A, Pradhan PK, Gambhir S, et al. **Preoperative contrast-enhanced computerized tomography should not delay radioiodine ablation in differentiated thyroid carcinoma patients.** *J Surg Res* 2015;193:731–37 CrossRef Medline
 41. Tala Jury HP, Castagna MG, Fioravanti C, et al. **Lack of association**

- between urinary iodine excretion and successful thyroid ablation in thyroid cancer patients. *J Clin Endocrinol Metab* 2010;95:230–37 CrossRef Medline**
42. Liberati A, Altman DG, Tetzlaff J, et al. **The PRISMA statement for reporting systematic reviews and meta-analyses of studies that evaluate health care interventions: explanation and elaboration.** *PLoS Med* 2009;6:e1000100 CrossRef Medline
43. Deeks JJ, Bossuyt PM, Gatsonis C, eds. *Cochrane Handbook for Systematic Reviews of Diagnostic Test Accuracy*. Version 1.0.0. The Cochrane Collaboration. 2013. <http://srdta.cochrane.org/handbook-dta-reviews>. Accessed March 31, 2016
44. Trikalinos TA, Balion CM, Coleman CI, et al. **Chapter 8: meta-analysis of test performance when there is a “gold standard.”** *J Gen Intern Med* 2012;27(suppl 1):S56–66 CrossRef Medline

White Matter Injury and General Movements in High-Risk Preterm Infants

C. Peyton, E. Yang, M.E. Msall, L. Adde, R. Støen, T. Fjørtoft, A.F. Bos, C. Einspieler, Y. Zhou, M.D. Schreiber, J.D. Marks, and A. Drobyshesky



ABSTRACT

BACKGROUND AND PURPOSE: Very preterm infants (birth weight, <1500 g) are at increased risk of cognitive and motor impairment, including cerebral palsy. These adverse neurodevelopmental outcomes are associated with white matter abnormalities on MR imaging at term-equivalent age. Cerebral palsy has been predicted by analysis of spontaneous movements in the infant termed “General Movement Assessment.” The goal of this study was to determine the utility of General Movement Assessment in predicting adverse cognitive, language, and motor outcomes in very preterm infants and to identify brain imaging markers associated with both adverse outcomes and aberrant general movements.

MATERIALS AND METHODS: In this prospective study of 47 preterm infants of 24–30 weeks’ gestation, brain MR imaging was performed at term-equivalent age. Infants underwent T1- and T2-weighted imaging for volumetric analysis and DTI. General movements were assessed at 10–15 weeks’ postterm age, and neurodevelopmental outcomes were evaluated at 2 years by using the *Bayley Scales of Infant and Toddler Development III*.

RESULTS: Nine infants had aberrant general movements and were more likely to have adverse neurodevelopmental outcomes, compared with infants with normal movements. In infants with aberrant movements, Tract-Based Spatial Statistics analysis identified significantly lower fractional anisotropy in widespread white matter tracts, including the corpus callosum, inferior longitudinal and fronto-occipital fasciculi, internal capsule, and optic radiation. The subset of infants having both aberrant movements and abnormal neurodevelopmental outcomes in cognitive, language, and motor skills had significantly lower fractional anisotropy in specific brain regions.

CONCLUSIONS: Aberrant general movements at 10–15 weeks’ postterm are associated with adverse neurodevelopmental outcomes and specific white matter microstructure abnormalities for cognitive, language, and motor delays.

ABBREVIATIONS: BSID-III = *Bayley Scales of Infant and Toddler Development*, 3rd ed; FA = fractional anisotropy; FM = fidgety movements; TBSS = Tract-Based Spatial Statistics

Advances in maternal-fetal medicine and neonatology during the past 35 years have resulted in a substantial increase in survival of infants born with birth weights of <1500 g. With this increased survival, the risks for major motor, cognitive, and sen-

sory disabilities have remained high.¹ In fact, rates of cerebral palsy and visual, auditory, and intellectual disability increase with decreasing gestational age, as do rates of language, coordination, and executive function disorders.¹ Accurate diagnosis of these abnormal neurodevelopmental outcomes currently requires long-term follow-up. For example, cerebral palsy is not confi-

Received April 21, 2016; accepted after revision July 20.

From the Departments of Therapy Services (C.P.) and Pediatrics (E.Y., M.E.M., M.D.S., J.D.M.), University of Chicago, Chicago, Illinois; Department of Laboratory Medicine (L.A., T.F.), Children’s and Women’s Health, Norwegian University of Science and Technology, Trondheim, Norway; Department of Pediatrics (R.S.) and Clinics of Clinical Services (T.F.), St. Olav University Hospital, Trondheim, Norway; Division of Neonatology (A.F.B.), University of Groningen, Groningen, the Netherlands; Institute of Physiology (C.E.), Center for Physiological Medicine, Medical University of Graz, Graz, Austria; and Center for Biomedical Research Informatics (Y.Z.) and Department of Pediatrics (A.D.), NorthShore University Health System, Evanston, Illinois.

J.D. Marks and A. Drobyshesky are co-senior authors.

This study was funded in part by the Gerber Foundation (M.D.S.); American Physical Therapy Association; Section of Pediatrics research grant (C.P.); the University of Chicago–NorthShore University Health System Collaborative Research Award (A.D. and M.D.S.); the Liaison Committee among the Central Norway Regional

Health Authority and the Norwegian University of Science and Technology and the Department of Clinical Services, and Department of Pediatrics, Trondheim University Hospital, Trondheim, Norway (L.A., R.S., T.F.); and the T73 MC11047 HRSA–Department of Health and Human Services Leadership Education in Neurodevelopmental and Related Disorders Training Program (M.E.M.).

Please address correspondence to Colleen Peyton, MC1081, 5841 S Maryland Ave, Chicago, IL 60637; e-mail: colleen.peyton@uchospitals.edu

Indicates open access to non-subscribers at www.ajnr.org

Indicates article with supplemental on-line appendix and tables.

Indicates article with supplemental on-line photos.

Evidence-Based Medicine Level 2.

<http://dx.doi.org/10.3174/ajnr.A4955>

dently diagnosed until 18 months to 2 years postconceptional age. Language and cognitive delays require even more prolonged follow-up for accurate diagnosis. Accordingly, tools to predict abnormal neurodevelopmental outcomes earlier than 18 months of age would enable interventions to be targeted sooner, during times of greater brain plasticity, when a greater impact of intervention may be seen.

Abnormal neurodevelopmental outcomes have been predicted between 10 and 15 weeks' postterm age by using General Movement Assessment.² General movements are a developmentally regulated pattern of spontaneous motor activity, appearing in the embryo by 9 weeks' postconceptional age. By 50–55 weeks' postconceptional age (10–15 weeks' postterm), the predominant general movements seen are termed fidgety movements (FM), a pattern of continuous, small-amplitude movements of the neck, trunk, and limbs during wakefulness, which disappear with agitation. Most important, absence of these FM at 10–15 weeks' postterm accurately predicts the development of cerebral palsy.³ Where in the brain FM arise and how they are generated remain unclear. However, the absence of FM in infants with periventricular lesions of the corona radiata or internal capsule⁴ suggests that projections between the cortex and spinal cord may contribute to these movements. The use of General Movement Assessment to detect neurodevelopmental impairment other than cerebral palsy has been limited.

We hypothesized that the brains of very preterm (<1500 g) infants with aberrant FM differ structurally from those in infants with normal FM and that these infants are more likely to have abnormal neurodevelopmental outcomes than infants with normal movements. Accordingly, in this prospective study, we identified structural differences at term-equivalent age in the brains of infants who subsequently exhibited aberrant FM compared with those who did not. Second, we determined the extent to which aberrant FM and identified brain imaging differences were associated with abnormal neurodevelopmental outcomes in motor, cognitive, and language skills.

MATERIALS AND METHODS

Participants

Infants born at ≤31 weeks' gestational age with a birth weight of ≤1500 g who required oxygen at birth were recruited prospectively between July 2011 and March 2013 from the University of Chicago Comer Children's Hospital neonatal intensive care unit. Infants with congenital malformations, genetic syndromes, or respiratory distress severe enough that they were not expected to live (oxygenation index, ≥20) were excluded from the study. Infants who required positive pressure ventilation at term-equivalent age at the time of MR imaging were not included in the study. Informed parental consent was obtained for each infant, and ethics approval for the study was granted by the institutional review board of the University of Chicago.

General Movement Assessment

Video recordings were made by using a standardized observation system, with the infant in a state of active wakefulness at 10–15 weeks' postterm age. Raters who were General Movement Assessment-certified and blinded to the imaging and outcome data

classified the video recordings according to the Prechtl methodology.² In this study, FM were classified as normal if present (intermittent or continual) and as aberrant if abnormal (exaggerated with respect to speed and amplitude), sporadic (interspersed with long pauses), or absent.² Detailed methods are given in the Online Appendix.

MR imaging was performed at term-equivalent age. Infants were fed an hour before the scan and gently restrained, without sedation, by using a MedVac immobilization bag (CFI Medical Solutions, Fenton, Michigan).⁵ MR imaging was performed on a 3T MR imaging scanner (Achieva; Philips Healthcare, Best, the Netherlands) by using a standard head 8-channel sensitivity encoding MR imaging coil array. Acquisition schema was as follows:

3D T1-Weighted Turbo Field Echo. FOV, 192 × 144 × 124 mm; 1-mm isotropic spatial resolution; TI/TR/TE, 1100/8.0/2.9 ms; NEX, 1; turbo field echo factor, 144.

3D T2-Weighted, Turbo Spin-Echo. Same geometry and resolution as above. TR/TE, 2500/264 ms; NEX, 1; TSE factor, 100.

Single-Shot EPI Diffusion. Axial section orientation; 1.75 × 1.75 mm in-plane spatial resolution; 55 sections, 2-mm-thick; FOV, 140 × 140 mm; matrix, 80 × 80; TR/TE, 9000/47 ms; NEX, 1; sensitivity encoding, 2; 30 noncollinear diffusion directions with b-values of 0 and 750 s/mm.^{2,6}

MR Imaging Qualitative Scoring of White Matter Abnormalities

A pediatric neuroradiologist independently scored the scans and was blinded to neonatal morbidities and scores on other assessments, as previously reported.⁷ A standardized scoring system⁸ was used to grade gray and white matter pathology. The WM was scored on a scale from 1 to 3 for the following 5 areas: nature and extent of WM signal abnormality, periventricular white matter volume loss, thinning of the corpus callosum, ventricular dilation, and the presence of any cystic abnormalities. Scores of >1 on any scale were reported as abnormal. The WM pathology scores for the individual items were summed. Findings in infants with total scores of >6 were abnormal.

Measurement of Gray Matter, White Matter, and Cerebellar Volumes

Voxel-based morphometry analysis⁹ was used to investigate voxelwise regional differences in gray and white matter volume between studied cohorts of infants. Individual subject's T1- and T2-weighted images were segmented into gray matter, white matter, and CSF tissue classes by using iBEAT software (<https://www.med.unc.edu/bric/ideagroup/free-software/libra-longitudinal-infant-brain-processing-package>), designed for neonatal and infant brain segmentation.^{10,11} The automatic segmentation was followed by manual corrections and resulted gray and white matter masks that were used for voxel-based morphometry analysis, performed by using the FMRIB Software Library (FSL; www.fmrib.ox.ac.uk/fsl/). Study-specific gray and white matter templates were created. Individual subject's gray matter and white matter masks were registered to the templates. The quality of registration was confirmed by manual inspection. To avoid the effect of rapidly changing T1 and T2 contrast in neonates, we

used gray and white matter masks for analysis instead of original scans. Registered images were modulated by the Jacobian warp field, thus reflecting local expansion or shrinkage of gray or white matter volumes relative to the registration target. Cerebella were manually segmented from individual subjects' T2-weighted images, and volumes were obtained by using ITK-SNAP (www.itksnap.org).

Measurement of White Matter Microstructure

The diffusion tensor imaging data were skull-stripped, and fractional anisotropy (FA) and mean and directional diffusivity maps were calculated by using the FMRIB Diffusion Toolbox (<http://fsl.fmrib.ox.ac.uk/fsl/fslwiki/FDT>). Voxelwise statistical analysis of the DTI data was performed by using Tract-Based Spatial Statistics (TBSS; <http://fsl.fmrib.ox.ac.uk/fsl/fslwiki/TBSS>) analysis as implemented in FSL.¹² First, FA data were aligned into a common space by using nonlinear registration to the study-specific target image. The quality of registration was confirmed by manual inspection. Next, a mean FA skeleton was created, which represented the centers of all tracts common to the group. A threshold of $FA \geq 0.2$ was applied to the mean FA skeleton. Each infant's aligned FA map was then projected onto this skeleton. Individual subject's mean and directional diffusivities maps were projected to the white matter skeleton by using transformations obtained for FA maps.

The relationships among FA, General Movement Assessment (normal versus aberrant), and *Bayley Scales of Infant and Toddler Development*, 3rd ed (BSID-III)¹³ scores were assessed by using general linear model analysis, by using parameters as described above for voxel-based morphometry, and gestational age at the time of scanning was entered as a covariate.

Assessment of Neurodevelopmental Outcomes

At 18–24 months' corrected age, Cognitive, Language, and Motor outcomes were assessed with the BSID-III subscales.¹³ The assessments were performed by 2 experienced testers, unaware of the brain MR imaging findings. Because the BSID-III scores significantly underestimate cognitive and language delay by approximately 11 points,^{14–16} we designated infants with scores of ≤ 85 as having adverse neurodevelopmental outcomes.

Statistical Analysis

Continuous variables were summarized as mean (SD), and categorical variables were summarized as frequencies and percentages. Normality assumptions were assessed by using the Shapiro-Wilk test. A 2-sample *t* test or the Wilcoxon rank sum test was used to compare continuous variables, and the χ^2 test or Fisher exact test was used to compare categorical variables between normal and aberrant FM groups. A logistic regression analysis was conducted to predict adverse neurodevelopmental outcome at 2 years by using FM assessments and FA values in selected white matter tracts.

The voxelwise relationships between FM (normal-versus-aberrant) and gray and white matter volumes on voxel-based morphometry analysis and between FM and FA on TBSS analysis were assessed by using general linear regression models. Gestational age at the time of scanning was entered as a covariate. All voxelwise statistical comparisons, including TBSS and voxel-based

morphometry, were corrected for multiple comparisons by controlling the family-wise error rate, by using threshold-free cluster enhancement.¹⁷ *P* values $< .05$ were considered statistically significant.

A binary predictor was constructed from FA data in selected white matter tracts. The cutoff was determined from FA data from infants with normal neurodevelopmental outcomes, by using a threshold of 1 SD below the mean, and this cutoff was applied to FA data from all infants. ROIs ($2 \times 2 \times 2$ voxels) were selected in the splenium of the corpus callosum for Cognitive scores, in the superior longitudinal fasciculus for Language scores, and in the anterior limb of the internal capsule for Motor scores. Linear regression was performed between FA and BSID-III Cognitive scores to explore the correlation between these 2 parameters. The Pearson correlation coefficient was reported to quantify the direction and strength of the association. The sensitivity and specificity of FM and FA to predict the BSID-III were determined.

RESULTS

MR images were inspected by a board-certified pediatric neuro-radiologist for the presence of macroscopic injury and intraventricular hemorrhage (On-line Table 1). Of 60 infants enrolled, 6 were excluded due to poor image quality; additionally, 1 infant had severe posthemorrhagic ventricular dilation and was excluded due to inability to achieve satisfactory registration of brain images to the group templates. MR images of the remaining 53 infants were analyzed.

Of the 53 infants with MR imaging, 6 did not return for General Movement Assessment. Accordingly, 47 infants were analyzed (On-line Fig 1). Thirty-eight infants of these 47 (81%) had normal FM. Of the remaining 9, movements of 6 infants were classified as "sporadic"; 1, as "abnormal"; and 2, as "absent." These 9 infants were classified as having aberrant FM. These infants had significantly lower mean gestational age and mean birth weight, compared with infants having normal FM (On-line Table 1). The odds of aberrant FM classification increased by 1.96 per week for every week's decrease in gestational age (95% CI, 1.15–3.35; *P* = .014) as determined by a univariate logistic regression model.

Infants with Aberrant Fidgety Movements Do Not Differ in Gray Matter and Cerebellar Volumes

Infants with normal FM did not differ from preterm infants with aberrant FM in total brain volume (normal: 319.2 ± 10.8 mL; aberrant: 310.4 ± 17.9 mL, *P* = .683), total gray matter (normal: 166.6 ± 7.3 mL; aberrant: 166.5 ± 12.4 mL, *P* = .993), or total white matter (normal: 136.7 ± 3.0 mL; aberrant: 128.9 ± 6.4 mL, *P* = .293). No significant regional differences were found between the normal and aberrant FM groups in either cortical or subcortical gray matter volumes on voxel-based morphometry analysis. Cerebellum volumes also did not differ between the groups (16.34 ± 0.95 mL versus 15.28 ± 1.46 mL, *P* = .550). When these measurements were normalized to total brain volumes, we also found no significant differences between normal and aberrant FM groups (gray matter: normal, 0.517 ± 0.005 , versus aberrant, 0.53 ± 0.014 ; *P* = .301; white matter: normal, 0.434 ± 0.005 ,

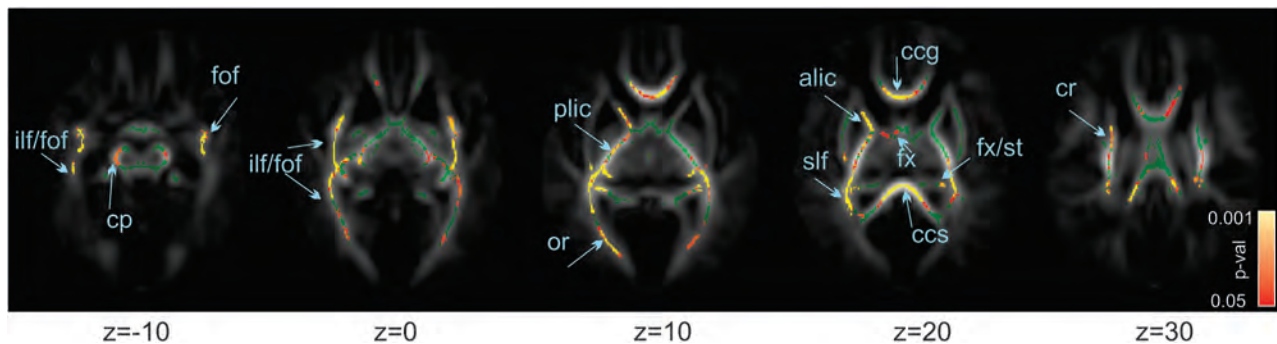


FIG 1. Differences in white matter at term-equivalent age between infants with normal and aberrant fidgety movements at 10–15 weeks. Mean FA skeleton, in green, is overlaid on the mean FA map. Superimposed are pseudocolored voxels having significantly greater anisotropy in infants with normal than in infants with aberrant fidgety movements. Color bar shows the range of *P* values represented by the pseudocolors. Significantly higher regions of FA can be observed in the splenium (ccs) and genu (ccg) of the corpus callosum, inferior (ilf) and superior longitudinal fasciculus (slf), fronto-occipital fasciculus (fof), anterior (alic) and posterior (plic) internal capsule, corona radiata (cr), cerebellar peduncles (cp), and fornix/stria terminalis (fx/st). Z represents the MR imaging axial section coordinates (zero is the center of the anterior commissure).

versus aberrant, 0.418 ± 0.013 ; $P = .295$; cerebellum: normal, 0.049 ± 0.0013 , versus aberrant, 0.0483 ± 0.034 ; $P = .89$).

While the groups did not differ in overall white matter volumes, voxel-based morphometry using the white matter mask demonstrated a significant difference between normal and aberrant FM groups: The aberrant FM group had significantly smaller volumes in the splenium of the corpus callosum and right central frontal white matter (On-line Fig 2).

Infants with Aberrant Fidgety Movements Had a Higher Burden of White Matter Abnormalities

White matter abnormalities were first assessed by using a qualitative scoring system to determine the nature of these abnormalities (see “Materials and Methods”) and their distribution between groups (On-line Table 3). Infants with aberrant FM exhibited a significantly higher incidence of white matter signal abnormalities (56%) than infants with normal FM (18%, $P = .035$). In addition, there was a significantly higher incidence of an abnormal total white matter score in the aberrant FM group (56%) than in the normal FM group (13%, $P = .014$).

Differences in white matter microstructure were next assessed. Compared with the normal FM group, the aberrant FM group had significantly lower FA values in multiple regions: the corpus callosum genu and splenium, superior and inferior longitudinal and fronto-occipital fasciculi, anterior limb of the internal capsule, corona radiata, and optic radiations (Fig 1). Most surprising, in the posterior limb of the internal capsule, infants with aberrant FM had very few voxels with significantly decreased FA. Finally, there were no FA values in the aberrant FM group greater than those in the normal FM group. The aberrant FM group demonstrated significantly higher radial diffusivity compared with the normal FM group. There was no difference in either mean diffusivity or axial diffusivity.

Aberrant Fidgety Movements at 12 Weeks Are Associated with Adverse Neurodevelopmental Outcome at 2 Years

In the time between general movement and BSID-III assessments, 3 subjects were lost to follow-up and 1 infant died. None of the infants lost to follow-up had aberrant FM. Accordingly, 43 of the initial 47 infants (91%) were available for neurodevelopmental

assessment at 2 years of age. Of the infants with normal FM, 35.1% were enrolled in early intervention programs, while 55.6% of the infants with aberrant FM were similarly enrolled. The mean age at BSID-III testing was 23.9 ± 0.6 months. Abnormal neurodevelopmental outcomes were defined by BSID-III scores being ≤ 85 for each subscale. There were 9 infants with adverse cognitive outcomes, 10 infants with adverse language outcomes, and 6 infants with adverse motor outcomes. Of infants with aberrant FM, 5 (62.5%) had adverse abnormal neurodevelopmental outcomes on at least 2 scales. In contrast, only 3 (8.8%) infants having normal FM demonstrated adverse abnormal neurodevelopmental outcomes on at least 2 scales.

Across all infants in our cohort, the mean subscale scores were the following: 99.77 ± 2.36 on the Cognitive subscale, 92.93 ± 1.51 on the Language subscale, and 98.47 ± 1.59 on the Motor subscale. Infants with normal FM scored significantly higher than infants with aberrant FM on the Cognitive subscore (101.0 ± 2.4 versus 89.4 ± 6.7 , $P = .019$) and the Motor subscore (100.8 ± 1.6 versus 83.8 ± 5.6 , $P = .019$). In addition, we observed a trend toward increased Language subscores in infants with normal FM compared with aberrant FM (93.7 ± 1.5 versus 85.9 ± 5.6 , $P = .07$).

Infant classification into normal or aberrant FM was significantly associated with normal and adverse BSID-III outcomes, respectively, on each subscale (contingency table analysis with the Fisher exact test, On-line Table 2). Furthermore, univariate binary logistic regression analysis revealed that the presence of aberrant FM significantly increased the risk of adverse neurodevelopmental outcomes in each of the Cognitive (odds ratio, 10.5; 95% CI, 2.2–50.7; $P = .003$), Language (odds ratio, 6.27; 95% CI, 1.1–20.7; $P = .04$), and Motor subscales (odds ratio, 28.5; 95% CI, 4.2–191.2; $P = .001$).

Minimal Correlation between White Matter Microstructure at Term and Neurodevelopmental Outcomes at 2 Years

No voxels demonstrated a linear relationship between FA at term and any BSID-III subscale scores on the Tract-Based Spatial Statistics analysis (On-line Fig 3). We next compared children having

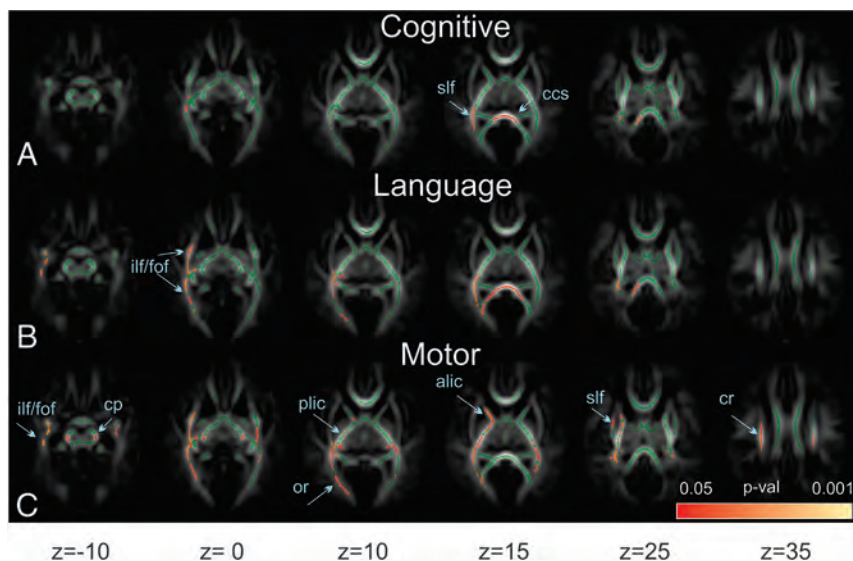


FIG 2. Differences in white matter between infants with “doubly normal” (normal fidgety movements and normal BSID-III scores) and “doubly abnormal” (aberrant fidgety movements and abnormal BSID-III scores) outcomes. The mean fractional anisotropy skeleton, in green, is overlaid on the mean fractional anisotropy map. Superimposed are pseudocolored voxels having significantly greater fractional anisotropy in “doubly normal” outcome infants than in infants with “doubly abnormal” assessments. The color bar shows the range of *P* values represented by the pseudocolors. Subscores on the BSID-III are divided into Cognitive (A), Language (B), and Motor (C) fractional anisotropy maps. Fiber tract labels are the same as in Fig 1.

normal or abnormal neurodevelopment. Infants with adverse cognitive outcomes had significantly lower FA values compared with healthy infants in the corpus callosum genu and splenium, superior and inferior longitudinal and fronto-occipital fasciculi, anterior limb of the internal capsule, and optic radiation (On-line Fig 4). There were no significant differences in FA between those who scored normally or adversely on the Language and Motor subscales of the BSID-III.

Predicting Neurodevelopmental Outcomes at 2 Years from General Movements and Neuroimaging

Because FA differences did not predict neurodevelopmental outcome, we tested whether general movements were a better predictor of neurodevelopmental outcomes. We determined the sensitivity and specificity of each FM and FA on the BSID-III subscales. A 2×2 contingency table was constructed by using normal/aberrant FM and normal/adverse neurodevelopmental outcome. To perform similar binary analyses for FA, we divided infants into low and high FA groups by using an unbiased approach as follows: We identified infants with aberrant FM and abnormal neurodevelopmental outcomes and defined them as having “doubly abnormal” outcomes. Similarly, we defined infants with normal FM and normal neurodevelopmental outcomes as having “doubly normal” outcomes. We then derived BSID-III subscale-specific Tract-Based Spatial Statistics maps by comparing the “doubly normal” and the “doubly abnormal” outcome infants (Fig 2). Using these maps, we identified the most statistically significant voxel and constructed an ROI around that voxel in a single white matter tract. The most significant voxel and associated ROI were in the splenium of the corpus callosum for Cognitive, superior longitudinal fasciculus for Language, and the posterior limb of the internal capsule for the Motor subscale. For each BSID-III sub-

scale-specific region, the mean and SD of the FA in the selected region were computed for infants with normal neurodevelopmental outcome. Infants in the entire cohort whose FA fell within 1.5 SDs of the mean had “normal FA.” The remaining infants were assigned to the “low FA” group. For the FM and FA analyses, the specificities for adverse neurodevelopmental outcome ranged between 0.83 and 0.89 (On-line Table 2). In contrast, the sensitivities of either FM or FA in predicting adverse subscale-specific neurodevelopmental outcomes were much lower, ranging between 0.36 and 0.6 (On-line Table 2).

We next tested whether combining General Movement Assessment with neuroimaging data improved prediction of neurodevelopmental outcome. A bivariate binary logistic regression model was constructed by using BSID-III scores as a response variable and FM assessment and FA values in the selected WM tracts as predictors. This analysis

failed to reveal a significant contribution of FA to the prediction of BSID-III scores in either the Cognitive, Language, or Motor subscales. These data indicate that FA does not provide data complementary to FM assessment.

Combining General Movement Assessment and Neurodevelopmental Outcomes to Identify Microstructure Differences in Specific Brain Regions

Having found that aberrant FM were associated with both abnormal microstructure and adverse neurodevelopmental outcomes, we asked whether “doubly abnormal” outcome infants had specific brain regions that differentiated them from “doubly normal” outcome infants. With respect to cognitive outcomes, “doubly abnormal” outcome infants had significantly lower FA, most strikingly in the corpus callosum and the inferior longitudinal fasciculus (Fig 2A). For language outcomes, “doubly abnormal” outcome infants exhibited significantly lower FA most strikingly in the corpus callosum, the inferior longitudinal fasciculus, and the fronto-occipital/inferior/superior longitudinal fasciculi (Fig 2B). In contrast, for motor outcomes, “doubly abnormal” outcome infants had significantly lower FA, most strikingly in the anterior and posterior limbs of internal capsule and cerebral peduncles, as well as in the optic radiation (Fig 2C) and the fronto-occipital/inferior/posterior longitudinal fasciculi. Notably, these infants did not have significant voxels in the corpus callosum (Fig 2C).

Approximately half of our infants with aberrant FM had normal neurodevelopmental outcomes. Accordingly, we sought to identify brain regions in these infants whose microstructure differentiated those with normal neurodevelopmental outcomes from those with abnormal outcomes. We compared FA in infants having aberrant FM and normal neurodevelopmental outcomes

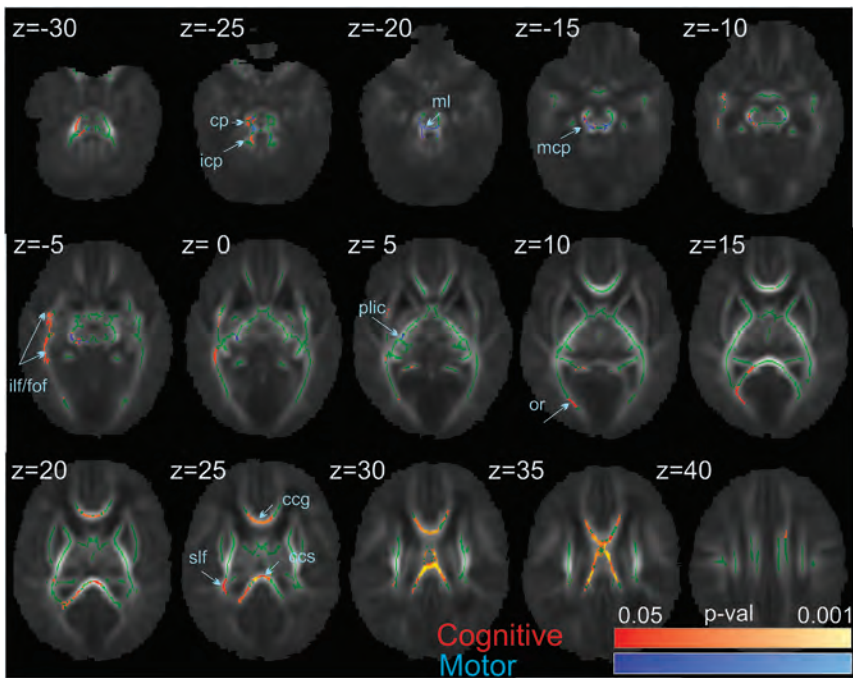


FIG 3. Differences in white matter in infants with aberrant fidgety movements between subpopulations with normal and adverse neurodevelopmental outcomes on the BSID-III. The mean fractional anisotropy skeleton, in green, is overlaid on the mean fractional anisotropy map. Superimposed are pseudocolored voxels having significantly greater fractional anisotropy in infants with normal than in those with adverse neurodevelopmental outcomes on Cognitive (in red-yellow) and Motor (in blue-light blue) BSID-III subscales. The color bar shows the range of *P* values represented by the pseudocolors. Fiber tract labels are the same as in Fig 1. Icp and mcp indicate inferior and middle cerebellar peduncles; ml, medial lemniscus.

with those with aberrant FM and adverse neurodevelopmental outcomes. In the group of infants with adverse neurodevelopmental outcomes, we, in fact, observed significantly lower FA in the Motor and Cognitive subscales. Specifically, for motor outcomes, infants had decreased FA in the motor-associated cerebellar peduncles, the medial lemniscus in the brain stem, and the posterior limb of internal capsule (Fig 3, blue). For cognitive outcomes, infants with adverse neurodevelopmental outcomes had decreased FA in corpus callosum and the associative superior and inferior longitudinal and fronto-occipital fasciculi (Fig 3, red). No differences in FA were seen on the Language subscale. These findings demonstrate that abnormal microstructure in specific brain regions identifies those infants with aberrant FM who will have abnormal neurodevelopmental outcomes.

Finally, in these children with aberrant FM, we sought to understand the impact of neurodevelopmental outcome in determining the association between FM and aberrant microstructure. Having found that in children with aberrant FM, those with adverse neurodevelopmental outcomes had significantly decreased FA compared with those with normal neurodevelopmental outcomes (Fig 2), we asked whether this latter group differed in FA from children with normal FM and normal neurodevelopmental outcomes. For cognitive outcomes, we analyzed FA in the splenium of the corpus callosum. For motor outcomes, we analyzed FA in the cerebellar peduncles. Most surprising, there was no difference in FA in either of these regions between these groups (Fig 4). The entire difference in FA, therefore, between normal

and aberrant FM is driven solely by the group having abnormal neurodevelopmental cognitive and motor outcomes.

DISCUSSION

In this prospective study, we found that preterm infants with aberrant FM at 10–15 weeks' postterm age demonstrated significantly decreased FA in multiple brain regions compared with infants with normal FM. Infants with aberrant FM were more likely to demonstrate abnormal motor, cognitive, and language outcomes at 2 years of age compared with infants with normal movement. However, among infants with aberrant FM, those with adverse neurodevelopmental outcomes could be differentiated from those with normal neurodevelopmental outcomes by differences in regional FA. In contrast to previous reports,¹⁸ we found no differences in gray matter and cerebellar volumes between groups.

Abnormal general movements have been previously associated with gross white matter abnormalities in preterm infants¹⁹ and in term infants having cerebral infarctions.²⁰ In our population, despite finding a significant proportion

of infants with aberrant FM, we observed no gross white or gray matter abnormalities, leading us to use functional and structural analyses on a voxelwise basis across the brain. Instead, we found reduced FA (due to increased radial diffusivity) in infants having aberrant FM in the corpus callosum and intrahemispheric tracts connecting the frontal, temporal, and occipital lobes. The widespread nature of this abnormality suggests that aberrant FM could arise from diffuse white matter injury. However, our infants with aberrant movements were born significantly more preterm than the rest of the cohort. While this earlier gestation raises the possibility that the presence of aberrant movement identifies less mature infants who are at increased risk for delayed white matter development, the association between aberrant movements and abnormal neurodevelopmental outcomes at 2 years of age suggests that aberrant movements even in these less mature infants confer a higher risk for abnormal outcomes.

Our dataset does not allow the identification of specific brain regions mediating FM. However, the observation that a cohort of infants totally blind from birth and without abnormalities on both brain imaging and serial neurologic examinations had delayed and exaggerated FM provides support for the role of visual pathways in the development of motor control.²¹ The widespread nature of the FA differences we observed suggests that FM may arise from connectivity among multiple brain regions, rather than a single central pattern generator, as previously hypothesized.⁴ Of note, we observed a greater burden of white matter injury in the aberrant FM group compared with the normal FM group on mul-

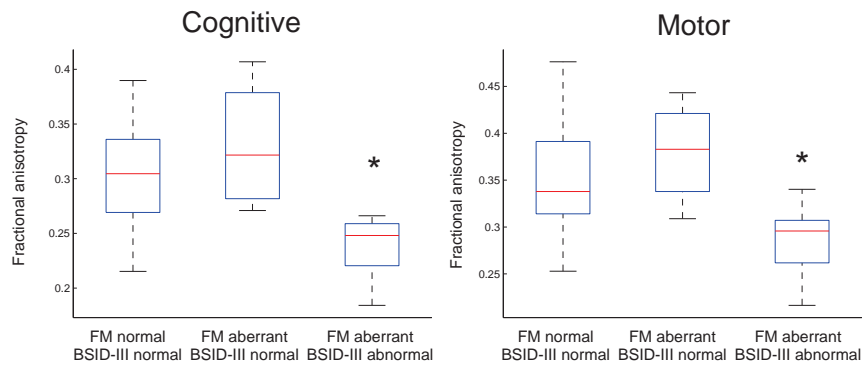


FIG 4. Mean fractional anisotropy in infants with normal and adverse neurologic outcomes. Boxplots represent the distribution of individual subject values in groups with normal fidgety movements and normal BSID-III scores, aberrant fidgety movements and normal BSID-III scores, and aberrant fidgety movements and adverse neurodevelopmental outcome as measured by BSID-III at 24 months of age. The cognitive subscale was measured in the splenium of the corpus callosum. The motor subscale was measured in the cerebellar peduncle. The asterisk indicates $P < .05$ on ANOVA, Tukey post hoc comparisons.

tiple imaging assessments: By qualitative analysis, infants with aberrant FM had an increased incidence of white matter signal abnormalities; by volumetric-based-morphometry, their corpus callosums were significantly thinner, and TBSS analysis showed a complex pattern of decreased FA. When we compared MR imaging from children with both abnormal neurodevelopmental outcomes and aberrant FM with scans from children with neither, we identified specific white matter tracts with decreased FA in subscale-specific regions: the internal capsule and corona radiata in children with poor motor performance and the corpus callosum in children with poor language or cognitive performance. This finding matches the association reported between increased mean diffusivity in the splenium of the corpus callosum with a low performance intelligence quotient in adults born preterm.²² Notably, we also observed decreased FA in the association fibers of the superior longitudinal fasciculus in children having decreased performance on any of the 3 subscales, suggesting that abnormalities in these regions presage subsequent global developmental impairment.

In this prospective study, the overall rate of cerebral palsy was low (2%) compared with the commonly reported cerebral palsy rate (3%–10%).²³ To be eligible for MR imaging at term, neonates could require only low levels of respiratory support (nasal cannula oxygen), eliminating those with more severe respiratory disease and, hence, at increased risk for abnormal neurodevelopmental outcomes. Despite the lack of major motor dysfunction, our patients still had significant differences in neurodevelopmental outcomes and brain abnormalities. Given our study design and patient population, the size of the cohort studied was not unexpectedly small. This small size may have limited the power of our statistical tests to detect significant correlations between FA and neurodevelopmental outcomes. Furthermore, although such clinical factors as birth weight, chronic lung disease, necrotizing enterocolitis, and sepsis have been noted to increase the risk of abnormal neurodevelopmental outcomes, our study size precluded using these risk factors as statistical covariates.

In our study, the total number of infants with aberrant movements composed about 20% of the cohort. Consequently, we analyzed children with absent, sporadic, and abnormal FM as a sin-

gle group and hypothesized that these infants would be at greater risk for cerebral palsy, as well as cognitive, language, and other motor disorders. Furthermore, a recent study of infants with cerebral palsy found that motor abilities did not differ between infants with sporadic or absent FM.²⁴ Studies of long-term outcomes are needed to appreciate the neurodevelopmental implications of sporadic-versus-absent FM, because their underlying mechanisms of injury may be different. Future research directions will require detailed motor assessment and correlation with long-term gross, fine, and oral motor control and language, and adaptive competencies. General Movement Assessment in preterm infants has been shown to be an

effective predictor of cerebral palsy.^{25–27} However, because only 1 infant in our cohort had cerebral palsy, we focused on determining the ability of the General Movement Assessment to predict abnormal motor performance. Notably, we found aberrant FM to be significantly and separately associated with each of the abnormal motor, language, and cognitive outcomes. Similar associations have been reported between abnormal general movements at 3 months and poor motor and cognitive outcomes at 2 years of age.^{2,28}

CONCLUSIONS

Our study emphasizes the importance of the neurobiologic substrate for aberrant FM and is an important contribution to understanding differing forms of cerebral development in early motor abilities and their developmental and adaptive correlates. Identifying specific forms of aberrant general movement with objective imaging correlates might be valuable in providing precise data on neurodevelopmental prognosis for preterm infants. The high specificity of aberrant General Movement Assessment suggests that infants at risk could be screened at 12 weeks of age. Those with aberrant FM might then benefit from MR imaging to improve prediction of adverse neurodevelopmental outcomes.

ACKNOWLEDGMENTS

We thank Randi T. Vågen and Laila Kristoffersen for their help in preparing video recordings. We also thank the infants and their families for their participation.

Disclosures: Colleen Peyton—RELATED: Grant: American Physical Therapy Section on Pediatrics.* Comments: provided salary recovery for Principal Investigator's protected research time. Christa Einspieler—UNRELATED: Employment: I am employed by the Medical University of Graz; Payment for Lectures (including service on Speakers Bureaus): General Movement Trust.* Comments: only reimbursement of travel and accommodation; Royalties: Mac Keith Press London; OTHER RELATIONSHIPS: I am a licensed tutor of the General Movement Trust, a method applied in this study. Any payment for teaching activities is received by the General Movement Trust and not by me personally. Michael D. Schreiber—RELATED: Grant: Gerber Foundation.* Ikaria*; Consulting Fee or Honorarium: Ikaria; Fees for Participation in Review Activities such as Data Monitoring Boards, Statistical Analysis, Endpoint Committees, and the Like: National Institutes of Health.* *Money paid to the institution.

REFERENCES

1. Saigal S, Doyle LW. **An overview of mortality and sequelae of preterm birth from infancy to adulthood.** *Lancet* 2008;371:261–69 CrossRef Medline
2. Einspieler C, Prechtl HF. *Prechtl's Method on the Qualitative Assessment of General Movements in Preterm, Term, and Young Infants.* London: Mac Keith Press; 2004
3. Bosanquet M, Copeland L, Ware R, et al. **A systematic review of tests to predict cerebral palsy in young children.** *Dev Med Child Neurol* 2013;55:418–26 CrossRef Medline
4. Prechtl HF. **State of the art of a new functional assessment of the young nervous system: an early predictor of cerebral palsy.** *Early Hum Dev* 1997;50:1–11 CrossRef Medline
5. Golan A, Marco R, Raz H, et al. **Imaging in the newborn: infant immobilizer obviates the need for anesthesia.** *Isr Med Assoc J* 2011; 13:663–65 Medline
6. Anjari M, Srinivasan L, Allsop JM, et al. **Diffusion tensor imaging with tract-based spatial statistics reveals local white matter abnormalities in preterm infants.** *Neuroimage* 2007;35:1021–27 CrossRef Medline
7. Woodward LJ, Anderson PJ, Austin NC, et al. **Neonatal MRI to predict neurodevelopmental outcomes in preterm infants.** *N Engl J Med* 2006;355:685–94 CrossRef Medline
8. Inder TE, Wells SJ, Mogridge NB, et al. **Defining the nature of the cerebral abnormalities in the premature infant: a qualitative magnetic resonance imaging study.** *J Pediatr* 2003;143:171–79 CrossRef Medline
9. Good CD, Johnsrude IS, Ashburner J, et al. **A voxel-based morphometric study of ageing in 465 normal adult human brains.** *Neuroimage* 2001;14:21–36 CrossRef Medline
10. Dai Y, Shi F, Wang L, et al. **iBEAT: a toolbox for infant brain magnetic resonance image processing.** *Neuroinformatics* 2013;11:211–25 CrossRef Medline
11. Wang L, Shi F, Yap PT, et al. **4D multi-modality tissue segmentation of serial infant images.** *PLoS One* 2012;7:e44596 CrossRef Medline
12. Smith SM, Jenkinson M, Johansen-Berg H, et al. **Tract-based spatial statistics: voxelwise analysis of multi-subject diffusion data.** *Neuroimage* 2006;31:1487–505 CrossRef Medline
13. Bayley N. *Bayley Scales of Infant and Toddler Development*, 3rd ed. San Antonio: Pearson Psychological Corporation; 2006
14. Anderson PJ, De Luca CR, Hutchinson E, et al; Victorian Infant Collaborative Group. **Underestimation of developmental delay by the new Bayley-III Scale.** *Arch Pediatr Adolesc Med* 2010;164:352–56 CrossRef Medline
15. Vohr BR, Stephens BE, Higgins RD, et al; Eunice Kennedy Shriver National Institute of Child Health and Human Development Neonatal Research Network. **Are outcomes of extremely preterm infants improving? Impact of Bayley assessment on outcomes.** *J Pediatr* 2012;161:222–28.e3 CrossRef Medline
16. Moore T, Johnson S, Haider S, et al. **Relationship between test scores using the second and third editions of the Bayley Scales in extremely preterm children.** *J Pediatr* 2012;160:553–58 CrossRef Medline
17. Smith SM, Nichols TE. **Threshold-free cluster enhancement: addressing problems of smoothing, threshold dependence and localisation in cluster inference.** *Neuroimage* 2009;44:83–98 CrossRef Medline
18. Spittle AJ, Doyle LW, Anderson PJ, et al. **Reduced cerebellar diameter in very preterm infants with abnormal general movements.** *Early Hum Dev* 2010;86:1–5 CrossRef Medline
19. Spittle AJ, Boyd RN, Inder TE, et al. **Predicting motor development in very preterm infants at 12 months' corrected age: the role of qualitative magnetic resonance imaging and general movements assessments.** *Pediatrics* 2009;123:512–17 CrossRef Medline
20. Guzzetta A, Mercuri E, Rapisardi G, et al. **General movements detect early signs of hemiplegia in term infants with neonatal cerebral infarction.** *Neuropediatrics* 2003;34:61–66 CrossRef Medline
21. Prechtl HF, Cioni G, Einspieler C, et al. **Role of vision on early motor development: lessons from the blind.** *Dev Med Child Neurol* 2001; 43:198–201 CrossRef Medline
22. Kontis D, Catani M, Cuddy M, et al. **Diffusion tensor MRI of the corpus callosum and cognitive function in adults born preterm.** *Neuroreport* 2009;20:424–28 CrossRef Medline
23. Winter S, Autry A, Boyle C, et al. **Trends in the prevalence of cerebral palsy in a population-based study.** *Pediatrics* 2002;110:1220–25 Medline
24. Einspieler C, Yang H, Bartl-Pokorny KD, et al. **Are sporadic fidgety movements as clinically relevant as is their absence?** *Early Hum Dev* 2015;91:247–52 CrossRef Medline
25. Adde L, Rygg M, Lossius K, et al. **General movement assessment: predicting cerebral palsy in clinical practise.** *Early Hum Dev* 2007; 83:13–18 CrossRef Medline
26. Prechtl HF, Einspieler C, Cioni G, et al. **An early marker for neurological deficits after perinatal brain lesions.** *Lancet* 1997;349: 1361–63 CrossRef Medline
27. Spittle AJ, Spencer-Smith MM, Cheong JLY, et al. **General movements in very preterm children and neurodevelopment at 2 and 4 years.** *Pediatrics* 2013;132:e452–e458 CrossRef Medline
28. Kodric J, Sustersic B, Paro-Panjan D. **Assessment of general movements and 2.5 year developmental outcomes: pilot results in a diverse preterm group.** *Eur J Paediatr Neurol* 2010;14:131–37 CrossRef Medline

Automated Processing of Dynamic Contrast-Enhanced MRI: Correlation of Advanced Pharmacokinetic Metrics with Tumor Grade in Pediatric Brain Tumors

S. Vajapeyam, C. Stamoulis, K. Ricci, M. Kieran, and T. Young Poussaint

ABSTRACT

BACKGROUND AND PURPOSE: Pharmacokinetic parameters from dynamic contrast-enhanced MR imaging have proved useful for differentiating brain tumor grades in adults. In this study, we retrospectively reviewed dynamic contrast-enhanced perfusion data from children with newly diagnosed brain tumors and analyzed the pharmacokinetic parameters correlating with tumor grade.

MATERIALS AND METHODS: Dynamic contrast-enhanced MR imaging data from 38 patients were analyzed by using commercially available software. Subjects were categorized into 2 groups based on pathologic analyses consisting of low-grade (World Health Organization I and II) and high-grade (World Health Organization III and IV) tumors. Pharmacokinetic parameters were compared between the 2 groups by using linear regression models. For parameters that were statistically distinct between the 2 groups, sensitivity and specificity were also estimated.

RESULTS: Eighteen tumors were classified as low-grade, and 20, as high-grade. Transfer constant from the blood plasma into the extracellular extravascular space (K^{trans}), rate constant from extracellular extravascular space back into blood plasma (K_{ep}), and extracellular extravascular volume fraction (V_e) were all significantly correlated with tumor grade; high-grade tumors showed higher K^{trans} , higher K_{ep} , and lower V_e . Although all 3 parameters had high specificity (range, 82%–100%), K_{ep} had the highest specificity for both grades. Optimal sensitivity was achieved for V_e , with a combined sensitivity of 76% (compared with 71% for K^{trans} and K_{ep}).

CONCLUSIONS: Pharmacokinetic parameters derived from dynamic contrast-enhanced MR imaging can effectively discriminate low- and high-grade pediatric brain tumors.

ABBREVIATIONS: IAUGC₆₀ = initial area under gadolinium curve at 60 seconds; DCE = dynamic contrast-enhanced; K_{ep} = rate constant from extracellular extravascular space back into blood plasma; K^{trans} = transfer constant from the blood plasma into the extracellular extravascular space; V_e = extracellular extravascular volume fraction; V_p = fractional blood plasma volume

Pediatric brain tumors are the most common cause of death from solid tumors, with an incidence rate of 5.57 cases per 100,000.¹ Recent advances in the molecular characterization and treatment of brain tumors² have made their proper classification by using imaging techniques critical. Conventional MR imaging is the technique of choice for preoperative diagnosis and evaluation of the child with an intracranial neoplasm because of its multipla-

nar capability and superior anatomic detail and resolution. Advanced imaging techniques such as MR perfusion are used to complement structural imaging, providing further insight into tumor physiology. In adults, dynamic contrast-enhanced (DCE) MR perfusion has been used to determine tumor grade³⁻⁵ and to distinguish pseudoprogression from tumor recurrence,⁶ thus affecting treatment.

While dynamic susceptibility contrast perfusion and DCE-MR perfusion in adult brain tumors have been extensively studied in the literature, particularly for monitoring tumor antiangiogenesis treatments,⁷⁻¹¹ DCE-MR imaging studies in pediatric brain tumors have been scarce¹²⁻¹⁸ and have not focused on tumor grading.

Multiparametric methods to characterize and monitor brain tumors have also shown great promise.^{19,20} DCE-MR imaging is particularly suited to multiparametric analyses that require image registration between modalities because it does not have geometric distortion due to susceptibility effects, unlike other advanced

Received May 11, 2016; accepted August 1.

From the Departments of Radiology (S.V., C.S., T.Y.P.) and Neurology (C.S.), Boston Children's Hospital, Boston, Massachusetts; Cancer Center (K.R.), Massachusetts General Hospital, Boston, Massachusetts; Department of Pediatric Oncology (M.K.), Dana-Farber Cancer Center, Boston, Massachusetts; and Harvard Medical School (S.V., C.S., M.K., T.Y.P.), Boston, Massachusetts.

Preliminary results previously presented at: Annual Meeting of the Radiological Society of North America, November 30 to December 5, 2014; Chicago, Illinois.

Please address correspondence to Sridhar Vajapeyam, PhD, Department of Radiology, Boston Children's Hospital, 300 Longwood Ave, Boston, MA 02115; e-mail: sridhar.vajapeyam@childrens.harvard.edu

<http://dx.doi.org/10.3174/ajnr.A4949>

MR imaging modalities such as dynamic susceptibility contrast perfusion imaging and diffusion imaging.

In this study, we retrospectively reviewed DCE perfusion data from children with newly diagnosed brain tumors during a 2-year period at our institution and analyzed the pharmacokinetic tumor permeability perfusion parameters correlating with tumor grade.

MATERIALS AND METHODS

Subjects

The study was performed with the approval of the institutional review board at the Dana Farber Cancer Institute. Children who presented with a brain mass and had undergone DCE perfusion studies were included. Of 52 patients identified with brain masses who had undergone DCE imaging, 6 patients had final diagnoses that were not brain tumors, 6 had nonenhancing tumors and therefore were not eligible for DCE-MR imaging analysis, and 2 patients were excluded due to motion. Thirty-eight patients were included in this study: 14 girls and 24 boys; age range, 0.30–18.14 years (median age, 6.01 years; mean age, 7.83 years).

MR Imaging Acquisition

All MR imaging studies were performed on a 3T scanner (Siemens, Erlangen, Germany). Standard MR imaging in all patients consisted of sagittal T1, axial T2-weighted, axial T2 FLAIR, axial diffusion-weighted, and multiplanar precontrast and postcontrast T1 images. All patients underwent a dynamic contrast-enhanced MR imaging protocol as follows:

- 1) Variable flip angle echo-spoiled gradient echo T1-mapping sequences by using flip angles of 15°, 10°, 5°, and 2°; TR = 5 seconds; TE = minimum; FOV = 240 mm; section thickness = 5 mm.

- 2) DCE-MR imaging sequence consisting of 50 phases, 7 seconds apart, with flip angle = 15°, TR = 4 seconds, TE = minimum. FOV, section thickness, and scan locations were identical to those in the T1 mapping sequences. A single bolus of gadobutrol (Gadavist, 0.1 mmol/kg body weight; Bayer Schering Pharma, Berlin, Germany) was injected 20 seconds after the start of scanning at an injection rate of 2 mL/s.

MR Imaging Postprocessing

MR images were transferred to a VersaVue workstation (iCAD, Nashua, New Hampshire) for automated processing by using OmniLook software (iCad). T1 maps were automatically calculated from the variable flip angle images²¹ to yield native T1 of the tissue. The 2-compartment Tofts model²² was used for the voxel-wise calculation of advanced pharmacokinetic parameters such as the transfer constant from the blood plasma into the extracellular extravascular space (K^{trans}), rate constant from extracellular extravascular space back into blood plasma (K_{ep}), extracellular extravascular volume fraction (V_e), fractional blood plasma volume (V_p), and initial area under gadolinium curve at 60 seconds (IAUGC₆₀). The model of Weinmann et al²³ for blood plasma concentration was used along with a relaxivity of $5.1 \text{ L} \cdot \text{mmol}^{-1} \cdot \text{s}^{-1}$ for the contrast agent.

ROIs were drawn on each section of tumor around contrast-enhancing portions of the tumor by an imaging data analyst or by a PhD scientist and verified by a Certificate of Added Qualification–certified neuroradiologist, and the mean (over voxels) and

SDs of each of the variables were recorded for statistical analysis. We included only voxels that could be fit to the model in the computation of mean and SD, excluding areas of cyst, and we took care to exclude vessels from the ROI.

Statistical Analysis

Subjects were categorized into 2 groups based on pathologic analyses consisting of low-grade (World Health Organization I and II) and high-grade (World Health Organization III and IV) tumors. All the pharmacokinetic parameters described above, along with T1 of the tissue, were compared between the 2 groups by using linear regression models with each parameter as a dependent variable (the outcome) and tumor grade as a categorical independent variable (low-grade = 0, high-grade = 1). For parameters significantly distinct between the 2 groups, sensitivity and specificity were also estimated.

Given the non-normal distribution of all parameters, summary statistics reported throughout included median and interquartile ranges. In addition, confidence intervals were estimated via bootstrapping with replacement (2000 draws).

Sensitivity and specificity were estimated as follows: First, the CIs for individual parameter medians were used for thresholding. For each parameter, there were 2 confidence intervals, 1 for the median of high-grade tumors and 1 for the median of low-grade tumors. The lower CI for intervals of statistically higher values and the upper CI for intervals of statistically lower values were used as thresholds. For example, if a parameter median was significantly higher for high-grade than low-grade tumors, then any high-grade parameter value at or above the lower CI for the group median was considered a true-positive and any value below this CI was considered a false-negative (or a false-positive for low-grade). Similarly, any low-grade parameter value at or below the upper CI for the group median was considered a true-positive, and any value above this CI was considered a false-negative (or a false-positive for high-grade).

RESULTS

Of the 38 patients who had enhancing tumors confirmed by biopsy, 18 tumors were classified as low-grade (7 pilocytic astrocytomas, 3 low-grade gliomas with piloid features, 3 low-grade gliomas, 1 low-grade ependymoma, 1 atypical meningioma World Health Organization grade II, 1 hemangioblastoma grade I, 1 ganglioglioma grade I–II, 1 low-grade histiocytic sarcoma) and 20 were classified as high-grade (11 medulloblastomas, 3 glioblastoma multiformes, 2 anaplastic ependymomas, 1 high-grade sarcoma, 1 choroid plexus carcinoma, 1 germinomatous germ cell tumor, and 1 high-grade glioma).

There was no statistically significant difference ($P = .8$) between patient age and tumor grade. For low-grade tumors, the median patient age was 5.52 years (25th to 75th quartiles = 2.62–12.97 years), and for high-grade tumors, the median patient age was 6.88 years (25th to 75th quartiles = 3.72–19.38 years).

The linear regression model results of the pharmacokinetic parameters are summarized in Table 1. The regression coefficient corresponding to tumor grade, its confidence intervals, standard error, significance (P value), and Wald statistics are included for parameters that were found to be significantly correlated with

Table 1: Summary of model permeability parameters for all imaging measures compared between high- and low-grade pediatric tumors

Parameter	Regression		Standard Error	P Value	Wald Statistic
	Coefficient	95% CI			
K^{trans}	1.54	(0.69–2.39)	0.42	<.001	13.42
K_{ep}	10.22	(6.12–14.33)	2.02	<.001	25.54
V_e	–0.11	(–0.15 to –0.06)	0.02	<.001	21.85
IAUGC ₆₀				.12	
V_p				.4	
T_{10}				.34	

Note:— T_{10} indicates T1 of tissue.

Table 2: Summary statistics, sensitivity, and specificity of permeability parameters statistically correlated with tumor grade

Parameter	Median	95% CI for		Sensitivity	Specificity
		Median	Median		
K^{trans}	L: 0.09	(0.06–0.13)		70%–72%	90%–100%
	H: 0.89	(0.57–1.85)			
K_{ep}	L: 0.66	(0.33–0.97)		70%–72%	100%
	H: 6.76	(4.99–13.95)			
V_e	L: 0.23	(0.19–0.26)		75%–78%	82%–100%
	H: 0.12	(0.11–0.15)			

Note:—L indicates low-grade; H, high-grade.

tumor grade. These included K^{trans} , K_{ep} , and V_e . Specifically, K^{trans} was statistically higher for high-grade tumors (median = 0.89, 25th to 75th quartiles = 0.46–2.67) than for low-grade tumors (median = 0.09, 25th to 75th quartiles = 0.04–0.13). K_{ep} was statistically higher for high-grade tumors (median = 6.76, 25th to 75th quartiles = 3.77–16.88) than for low-grade tumors (median = 0.66, 25th to 75th quartiles = 0.29–1.04). V_e was statistically lower for high-grade tumors (median = 0.12, 25th to 75th quartiles = 0.11–0.15) than for low-grade tumors (median = 0.23, 25th to 75th quartiles = 0.19–0.26). Information on the range, sensitivity, and specificity of these parameters is provided in Table 2.

K^{trans}

For low-grade tumors, K^{trans} was in the range of 0.02–0.52 (median = 0.09; 95% CI for the median = 0.06–0.13). For high-grade tumors, it was in the range of 0.09–6.19 (median = 0.89; 95% CI = 0.57–1.85). Based on the CI thresholds, there were 14 high-grade and 13 low-grade true-positives, resulting in a 71% (27/38) combined sensitivity of this parameter to detect high- or low-grade tumors. Individually, the sensitivity of this parameter to detect high-grade tumors was 70% (14/20), and for low-grade tumors, it was 72% (13/18). In addition, there were 2 high-grade tumors with values below the threshold for low-grade. These were considered false-positives for low-grade. There were no low-grade tumors with values above the threshold for high-grade. Consequently, the specificity of this parameter was 100% (18/18) for high-grade tumors and 90% (18/20) for low-grade tumors.

K_{ep}

For low-grade tumors, K_{ep} was in the range of 0.1–3.13 (median = 0.66; 95% CI = 0.33–0.97). For high-grade tumors, K_{ep} was in the range of 1.01–29.67 (median = 6.76; 95% CI = 4.99–13.95). Based on the CI thresholds, there were 14 high-grade and 13 low-grade true-positives, resulting in a combined sensitivity of 71% (27/

38). Individually, the sensitivity of this parameter to detect high-grade tumors was 70% (14/20) and 72% (13/18) for low-grade tumors. There were no false-positives in either group; thus, specificity was 100% (18/18) for high-grade tumors and 100% (20/20) for low-grade tumors.

V_e

For low-grade tumors, V_e was in the range of 0.11–0.48 (median = 0.23; 95% CI = 0.19–0.26). For high-grade tumors, it was in the range of 0.04–0.18 (median = 0.12; 95% CI = 0.11–0.15). Based on the CI thresholds, there were 15 high-grade and 14 low-grade true-positives, resulting in a combined sensitivity of 76% (29/38). Individually, the sensitivity of this parameter to detect high-grade tumors was 75% (15/20) and 78% (14/18) for low-grade tumors. There were 4 low-grade tumors with values below the threshold for high-grade. These were considered false-positives for high-grade. There were no false-positives for low-grade. Consequently, the specificity of this parameter for high-grade was 82% (18/22) and 100% (20/20) for low-grade.

DISCUSSION

Pediatric brain tumors encountered in a clinical setting differ significantly in tumor type from those seen in adults; therefore, predicting tumor grade by using MR imaging in a pediatric clinical setting presents a unique set of issues. While vessel permeability metrics derived from DCE-MR imaging have been associated with tumor grade in adult populations,^{24–26} such studies in pediatric brain tumors have been lacking.

Dynamic susceptibility contrast perfusion MR imaging has been studied in children by Ho et al²⁷ to associate tumor grade with maximal relative cerebral blood volume and with the post-bolus shape of the enhancement curve.²⁸ Koob et al¹⁹ used a multiparametric approach to show that the highest grading accuracy was achieved by using a combination of parameters derived from diffusion and DSC perfusion imaging. Yeom et al²⁹ used arterial spin-labeling to measure perfusion and found that maximal relative tumor blood flow of high-grade tumors was significantly higher than that of low-grade tumors.

Our results suggest that the transfer constants, both K^{trans} and K_{ep} , are significantly distinct between the low-grade and high-grade groups. Several studies have examined the role of K^{trans} and have shown K^{trans} correlates well with tumor grade, particularly in gliomas in adults.^{24–26,30–32} The role of angiogenesis in promoting leakiness of the tumor vasculature and development of new vessels is well-documented, and our findings of increased K^{trans} in higher grade tumors supports that hypothesis. K^{trans} in gliomas has also been shown to be a marker of progression^{31,33} in adults.

Our study shows that pediatric low-grade tumors in fact have a higher V_e compared with high-grade tumors, contrary to findings in adult tumors showing lower V_e in low-grade adult tumors.^{24–26} In fact, the optimal sensitivity appears to be achieved for V_e , with a combined sensitivity of 76% (compared with 71% for K^{trans} and K_{ep}) and individual sensitivities of 75% and 78%, respectively, for high- and low-grade tumors. The role of V_e , which is an indicator of extracellular extravascular space, is poorly understood in the brain tumor literature. Our findings concur with the theory that the higher cellularity in high-grade tumors would lead

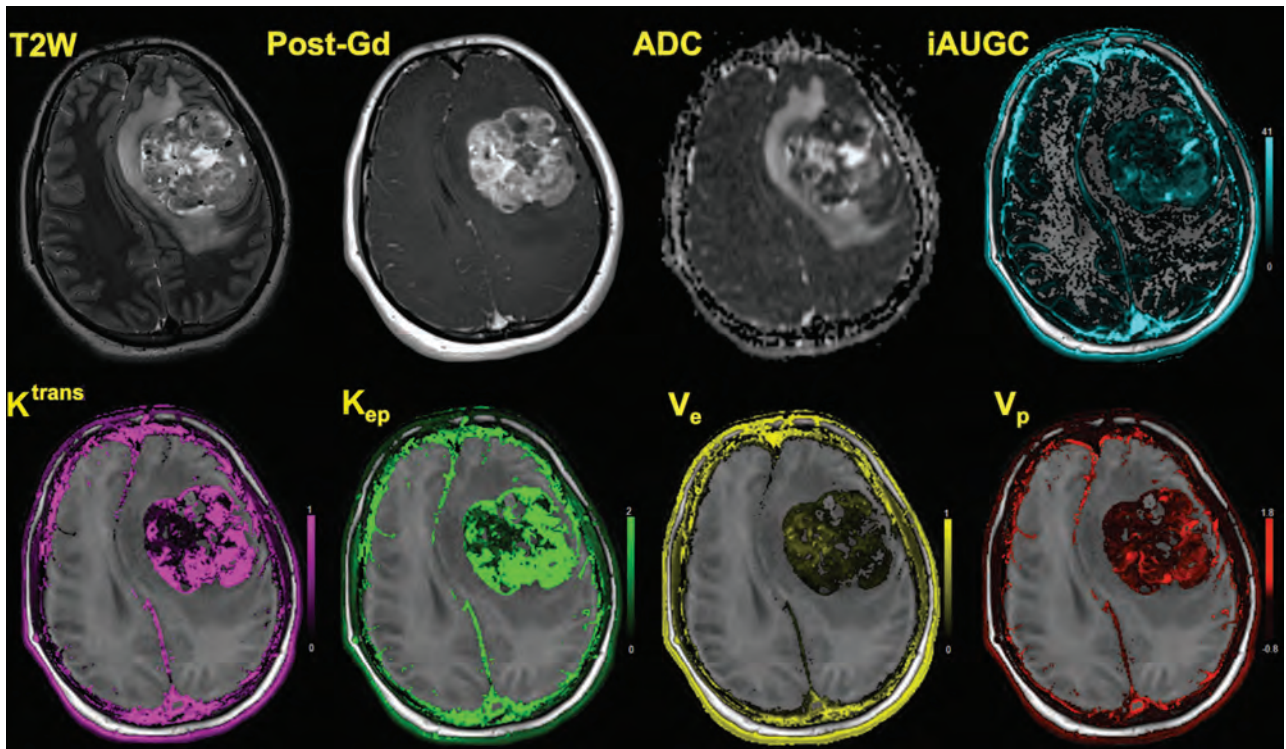


FIG 1. A 17-year-old girl with an anaplastic grade III ependymoma is shown. In addition to axial T2-weighted and axial postcontrast T1-weighted images, corresponding maps shown are ADC, $IAUGC_{60}$, K^{trans} , K_{ep} , V_e , and V_p . Axial T2 image demonstrates heterogeneous tumor in the left frontal lobe with regions of hypointensity. Axial T1 postcontrast image demonstrates heterogeneous enhancement. ADC image demonstrates regions of restricted diffusion within the tumor. High K^{trans} and K_{ep} are readily apparent in the overlaid color maps, and V_e is low.

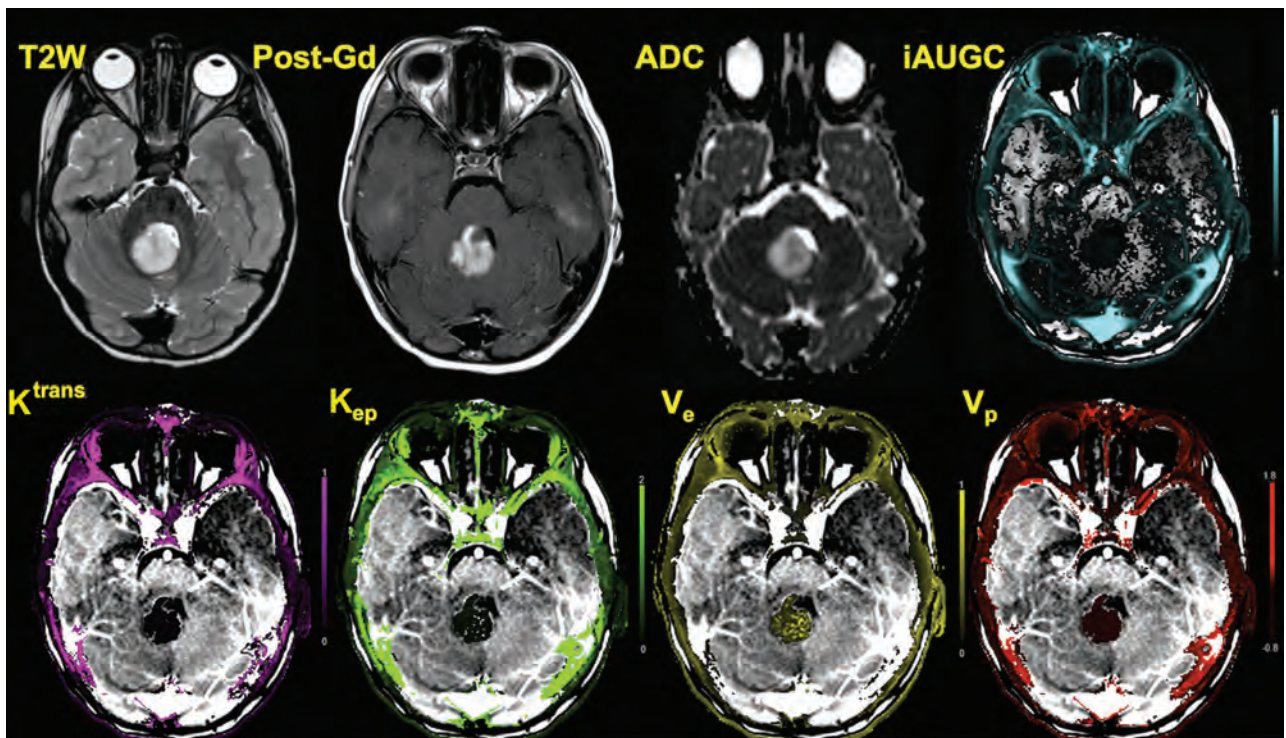


FIG 2. A 3-year-old boy with posterior fossa pilocytic astrocytoma is shown. Axial T2 image shows a T2 hyperintense mass in the vermis, which shows enhancement and increased diffusion. Permeability images show that though there is marked enhancement typical of these tumors, K^{trans} and K_{ep} are considerably lower, whereas V_e is higher throughout the tumor compared with the high-grade tumor shown in Fig 1.

to a decreased extracellular space due to the closely packed tumor cells, and hence lower V_e . As seen in Figs 1 and 2, the areas of decreased V_e also correlate with areas of decreased ADC, further confirming our hypothesis. Mills et al³⁴ however failed to find the expected correlation in a voxelwise analysis between V_e and ADC in adult glioblastoma multiformes, possibly due to the confounding effects of the heterogeneous nature of those tumors.

All 3 parameters had high specificity, in the range 82%–100%. For low-grade tumors, their specificity was 90%–100%, and for high-grade tumors, the specificity was 82%–100%. K_{ep} had the highest specificity (100%) for both grades.

One of the limitations of this study is that DCE-MR imaging-derived pharmacokinetic parameters are heavily dependent on the model and input parameters used^{12,22} and are thought to be difficult to standardize. Some of these parameters may not be as critical as previously thought. For example, Larsson et al³⁵ recently found that there was no significant difference between using T1 derived from a mapping sequence and using a fixed T1 in high-grade gliomas in adults. Because all our subjects were analyzed by using identical model parameters, this finding may not be that critical in this study. Last, the heterogeneity of tumor types and the relatively small sample in this study are also a limitation. Previous studies, however, have investigated smaller samples, so our findings are based on a comparatively larger sample. Nevertheless, this work may be validated in a larger cohort of children with pediatric brain tumors in future studies.

CONCLUSIONS

Dynamic contrast-enhanced perfusion MR imaging is useful in a clinical setting for the differential diagnosis and grading of pediatric brain tumors. Pharmacokinetic parameters such as V_e , K^{trans} , and K_{ep} can be used to differentiate low- and high-grade tumors to facilitate treatment planning and determine prognosis and have comparable specificities for tumor grade. In our study, the parameter K_{ep} had the highest specificity for both grades. Of the pharmacokinetic parameters studied, V_e offers the highest sensitivity (overall 76%) for determining tumor grade.

REFERENCES

- Ostrom QT, Gittleman H, Fulop J, et al. **CBTRUS statistical report: primary brain and central nervous system tumors diagnosed in the United States in 2008–2012.** *Neuro Oncol* 2015;17(suppl 4):iv1–iv62 CrossRef Medline
- Pollack IF. **Multidisciplinary management of childhood brain tumors: a review of outcomes, recent advances, and challenges.** *J Neurosurg Pediatr* 2011;8:135–48 CrossRef Medline
- Arevalo-Perez J, Kebede AA, Peck KK, et al. **Dynamic contrast-enhanced MRI in low-grade versus anaplastic oligodendrogliomas.** *J Neuroimaging* 2016;26:366–71 CrossRef Medline
- Zhao J, Yang ZY, Luo BN, et al. **Quantitative evaluation of diffusion and dynamic contrast-enhanced MR in tumor parenchyma and peritumoral area for distinction of brain tumors.** *PLoS One* 2015;10:e0138573 CrossRef Medline
- Zhang N, Zhang L, Qiu B, et al. **Correlation of volume transfer coefficient K^{trans} with histopathologic grades of gliomas.** *J Magn Reson Imaging* 2012;36:355–63 CrossRef Medline
- Thomas AA, Arevalo-Perez J, Kaley T, et al. **Dynamic contrast enhanced T1 MRI perfusion differentiates pseudoprogression from recurrent glioblastoma.** *J Neurooncol* 2015;125:183–90 CrossRef Medline
- Schminda KM, Prah M, Connelly J, et al. **Dynamic-susceptibility contrast agent MRI measures of relative cerebral blood volume predict response to bevacizumab in recurrent high-grade glioma.** *Neuro Oncol* 2014;16:880–88 CrossRef Medline
- Harris RJ, Cloughesy TF, Hardy AJ, et al. **MRI perfusion measurements calculated using advanced deconvolution techniques predict survival in recurrent glioblastoma treated with bevacizumab.** *J Neurooncol* 2015;122:497–505 CrossRef Medline
- Arevalo-Perez J, Thomas AA, Kaley T, et al. **T1-weighted dynamic contrast-enhanced MRI as a noninvasive biomarker of epidermal growth factor receptor VIII status.** *AJNR Am J Neuroradiol* 2015;36:2256–61 CrossRef Medline
- Jain R, Poisson LM, Gutman D, et al. **Outcome prediction in patients with glioblastoma by using imaging, clinical, and genomic biomarkers: focus on the nonenhancing component of the tumor.** *Radiology* 2014;272:484–93 CrossRef Medline
- Pope WB. **Predictive imaging marker of bevacizumab efficacy: perfusion MRI.** *Neuro Oncol* 2015;17:1046–47 CrossRef Medline
- Lam S, Lin Y, Warnke PC. **Permeability imaging in pediatric brain tumors.** *Transl Pediatr* 2014;3:218–28 CrossRef Medline
- Gururangan S, Fangusaro J, Poussaint TY, et al. **Efficacy of bevacizumab plus irinotecan in children with recurrent low-grade gliomas: a Pediatric Brain Tumor Consortium study.** *Neuro Oncol* 2014;16:310–17 CrossRef Medline
- Zukotynski KA, Fahey FH, Vajapeyam S, et al. **Exploratory evaluation of MR permeability with 18F-FDG PET mapping in pediatric brain tumors: a report from the Pediatric Brain Tumor Consortium.** *J Nucl Med* 2013;54:1237–43 CrossRef Medline
- Thompson EM, Guillaume DJ, Dosa E, et al. **Dual contrast perfusion MRI in a single imaging session for assessment of pediatric brain tumors.** *J Neurooncol* 2012;109:105–14 CrossRef Medline
- Gururangan S, Fangusaro J, Young Poussaint T, et al. **Lack of efficacy of bevacizumab + irinotecan in cases of pediatric recurrent ependymoma: a Pediatric Brain Tumor Consortium study.** *Neuro Oncol* 2012;14:1404–12 CrossRef Medline
- Gururangan S, Chi SN, Young Poussaint T, et al. **Lack of efficacy of bevacizumab plus irinotecan in children with recurrent malignant glioma and diffuse brainstem glioma: a Pediatric Brain Tumor Consortium study.** *J Clin Oncol* 2010;28:3069–75 CrossRef Medline
- Liu HL, Chang TT, Yan FX, et al. **Assessment of vessel permeability by combining dynamic contrast-enhanced and arterial spin labeling MRI.** *NMR Biomed* 2015;28:642–49 CrossRef Medline
- Koob M, Girard N, Ghattas B, et al. **The diagnostic accuracy of multiparametric MRI to determine pediatric brain tumor grades and types.** *J Neurooncol* 2016;127:345–53 CrossRef Medline
- Law M, Yang S, Wang H, et al. **Glioma grading: sensitivity, specificity, and predictive values of perfusion MR imaging and proton MR spectroscopic imaging compared with conventional MR imaging.** *AJNR Am J Neuroradiol* 2003;24:1989–98 Medline
- Fram EK, Herfkens RJ, Johnson GA, et al. **Rapid calculation of T1 using variable flip angle gradient refocused imaging.** *Magn Reson Imaging* 1987;5:201–08 CrossRef Medline
- Tofts PS. **Modeling tracer kinetics in dynamic Gd-DTPA MR imaging.** *J Magn Reson Imaging* 1997;7:91–101 CrossRef Medline
- Weinmann HJ, Laniado M, Mützel W. **Pharmacokinetics of Gd-DTPA/dimeglumine after intravenous injection into healthy volunteers.** *Physiol Chem Phys Med NMR* 1984;16:167–72 Medline
- Abe T, Mizobuchi Y, Nakajima K, et al. **Diagnosis of brain tumors using dynamic contrast-enhanced perfusion imaging with a short acquisition time.** *Springerplus* 2015;4:88 CrossRef Medline
- Li X, Zhu Y, Kang H, et al. **Glioma grading by microvascular permeability parameters derived from dynamic contrast-enhanced MRI and intratumoral susceptibility signal on susceptibility weighted imaging.** *Cancer Imaging* 2015;15:4 CrossRef Medline
- Choi HS, Kim AH, Ahn SS, et al. **Glioma grading capability: comparisons among parameters from dynamic contrast-enhanced MRI and ADC value on DWI.** *Korean J Radiol* 2013;14:487–92 CrossRef Medline
- Ho CY, Cardinal JS, Kamer AP, et al. **Relative cerebral blood volume**

- from dynamic susceptibility contrast perfusion in the grading of pediatric primary brain tumors. *Neuroradiology* 2015;57:299–306 CrossRef Medline
28. Ho CY, Cardinal JS, Kamer AP, et al. **Contrast leakage patterns from dynamic susceptibility contrast perfusion MRI in the grading of primary pediatric brain tumors.** *AJNR Am J Neuroradiol* 2016;37:544–51 CrossRef Medline
 29. Yeom KW, Mitchell LA, Lober RM, et al. **Arterial spin-labeled perfusion of pediatric brain tumors.** *AJNR Am J Neuroradiol* 2014;35:395–401 CrossRef Medline
 30. Roberts HC, Roberts TPL, Ley S, et al. **Quantitative estimation of microvascular permeability in human brain tumors: correlation of dynamic Gd-DTPA-enhanced MR imaging with histopathologic grading.** *Acad Radiol* 2002;9:S151–55 CrossRef Medline
 31. Mills SJ, Patankar TA, Haroon HA, et al. **Do cerebral blood volume and contrast transfer coefficient predict prognosis in human glioma?** *AJNR Am J Neuroradiol* 2006;27:853–58 Medline
 32. Patankar TF, Haroon HA, Mills SJ, et al. **Is volume transfer coefficient (K(trans)) related to histologic grade in human gliomas?** *AJNR Am J Neuroradiol* 2005;26:2455–65 Medline
 33. Cao Y, Nagesh V, Hamstra D, et al. **The extent and severity of vascular leakage as evidence of tumor aggressiveness in high-grade gliomas.** *Cancer Res* 2006;66:8912–17 CrossRef Medline
 34. Mills SJ, Soh C, Rose CJ, et al. **Candidate biomarkers of extravascular extracellular space: a direct comparison of apparent diffusion coefficient and dynamic contrast-enhanced MR imaging-derived measurement of the volume of the extravascular extracellular space in glioblastoma multiforme.** *AJNR Am J Neuroradiol* 2010;31:549–53 CrossRef Medline
 35. Larsson C, Kleppeto M, Grothe I, et al. **T1 in high-grade glioma and the influence of different measurement strategies on parameter estimations in DCE-MRI.** *J Magn Reson Imaging* 2015;42:97–104 CrossRef Medline

Limited Dorsal Myeloschisis and Congenital Dermal Sinus: Comparison of Clinical and MR Imaging Features

 S.M. Lee,  J.-E. Cheon,  Y.H. Choi,  I.-O. Kim,  W.S. Kim,  H.-H. Cho,  J.Y. Lee, and  K.-C. Wang



ABSTRACT

BACKGROUND AND PURPOSE: While limited dorsal myeloschisis is a distinctive form of spinal dysraphism, it may be confused with congenital dermal sinus. The aim of this study was to describe clinical and MR imaging findings of limited dorsal myeloschisis that can distinguish it from congenital dermal sinus.

MATERIALS AND METHODS: We retrospectively reviewed the clinical and MR imaging findings of 12 patients with limited dorsal myeloschisis and 10 patients with congenital dermal sinus. Skin abnormalities, neurologic deficits, and infectious complication were evaluated on the basis of clinical information. We evaluated the following MR imaging features: visibility of the tract along the intrathecal course, attachment site of the tract, level of the conus medullaris, shape of the spinal cord, and presence of intradural lesions such as dermoid/epidermoid tumors.

RESULTS: A crater covered with pale epithelium was the most common skin lesion in limited dorsal myeloschisis (10/12, 83%). Infectious complications were common in congenital dermal sinus (6/10, 60%), whereas none were found in limited dorsal myeloschisis ($P = .003$). The following MR imaging findings were significantly different between the 2 groups ($P < .05$): 1) higher visibility of the intrathecal tract in limited dorsal myeloschisis (10/12, 83%) versus in congenital dermal sinus (1/10, 10%), 2) the tract attached to the cord in limited dorsal myeloschisis (12/12, 100%) versus various tract attachments in congenital dermal sinus, 3) dorsal tenting of the cord in limited dorsal myeloschisis (10/12, 83%) versus in congenital dermal sinus (1/10, 10%), and 4) the presence of dermoid/epidermoid tumors in congenital dermal sinus (6/10, 60%) versus none in limited dorsal myeloschisis.

CONCLUSIONS: Limited dorsal myeloschisis has distinct MR imaging features: a visible intrathecal tract with dorsal tenting of the cord at the tract-cord union. Limited dorsal myeloschisis was not associated with infection and dermoid/epidermoid tumors.

ABBREVIATIONS: CDS = congenital dermal sinus; LDM = limited dorsal myeloschisis

Limited dorsal myeloschisis (LDM) is a distinct form of spinal dysraphism characterized by 2 constant features: a focal “closed” midline skin defect and a fibroneural tract connecting the skin lesion to the underlying spinal cord.^{1,2} Histologically, its tract is composed of attenuated mesenchymal (mainly fibrous) tissue and neural elements without an epithelial lining.¹⁻⁴ Because LDM has features similar to those in congenital dermal sinus

(CDS) showing a skin dimple with an associated tract extending from the skin lesion to the intraspinal space, it may be confused with CDS and has been referred to as a “dermal sinus-like stalk” or “pseudodermal sinus tract.”¹⁻⁵

Despite the resemblance between the 2 disease entities, LDM has different clinical importances compared with CDS. LDM has a closed skin defect and a solid tract without a lumen; thus, the possibility of infectious complications is extremely low.⁵ The clinical importance of LDM is related to neurologic deficits resulting from spinal cord tethering.^{1,5} By contrast, a tract of CDS with a lumen communicating with a cutaneous opening is the entry route for pathogens, consequentially leading to devastating infectious complications such as intraspinal abscess or meningitis.^{6,7} CDS requires urgent surgical removal of the tract even in asymptomatic patients to prevent potential intraspinal infection, whereas surgical intervention can be delayed in LDM to avoid complications in the neonate period.^{1,8}

Received May 9, 2016; accepted after revision August 15.

From the Departments of Radiology (S.M.L., J.-E.C., Y.H.C., I.-O.K., W.S.K., H.-H.C.), Anatomy (J.Y.L.), and Neurosurgery, Division of Pediatric Neurosurgery (J.Y.L., K.-C.W.), Seoul National University College of Medicine, Seoul, Republic of Korea; Department of Radiology (S.M.L.), Kyungpook National University Medical Center, Daegu, Korea; and Department of Radiology (H.-H.C.), Ewha Womans University Mokdong Hospital, Seoul, Republic of Korea.

Please address correspondence to Jung-Eun Cheon, MD, Department of Radiology, Seoul National University College of Medicine, 101 Daehak-ro, Jongno-gu, Seoul 110-769, Republic of Korea; e-mail: cheonje@snu.ac.kr

<http://dx.doi.org/10.3174/ajnr.A4958>

To determine the appropriate treatment strategies, one must distinguish LDM—which still is not a familiar entity—from CDS preoperatively.

Pang et al^{1,2} have reported that many cases of LDM have been misreported as CDS, despite different clinicopathologic characteristics. Furthermore, some authors have suggested that it is difficult to differentiate these 2 entities by using clinical and radiologic examinations because the entities share neuroimaging and cutaneous findings.^{3,4} To our knowledge, however, there have been no published reports regarding the comparison of the radiologic findings in LDM and CDS. The aim of this study was to describe neuroimaging findings of LDM that can distinguish it from CDS.

MATERIALS AND METHODS

Patients

The institutional review board of Seoul National University Hospital approved this study and waived the requirements for informed consent. Retrospective review of the operative record data base of all patients who underwent an operation for congenital spinal dysraphism by a pediatric neurosurgeon (K-C.W.) from January 2010 to March 2014 was performed to identify subjects. The patients with closed spinal dysraphism without a subcutaneous mass characterized by midline skin lesions and an associated tract connecting the skin lesion to the focal area of the intraspinal space were classified into LDM and CDS groups on the basis of the operative and histopathologic findings.^{1,2,4,9-11} The diagnostic criteria of LDM were as follows: 1) dural outpouching ensheathing the tract identified on tracts.

Information regarding demographic variables such as age, sex, mode of presentation, symptoms prompting neurosurgical referral, initial neurologic and physical examination findings, preoperative radiologic evaluation, urologic study, and operative findings was collected. Skin abnormalities, neurologic deficits, and infectious complications were evaluated on the basis of clinical information.

Imaging Analysis

All patients underwent preoperative lumbosacral MR imaging. MR images were acquired in both sagittal and axial planes on a 1.5T MR imaging unit. The MR image parameters were as follows: unenhanced T1-weighted (TR/TE = 500–610/10–12 ms), T2-weighted (TR/TE = 3000–3500/93–99 ms) turbo spin-echo, and postcontrast T1-weighted images (11 examinations). Other parameters included section thickness = 3 mm (sagittal), 6 mm (axial); intersection gap = 0.3 mm (sagittal), 3 mm (axial); acquisition matrix = 320 × 224–256 (sagittal), 320 × 182–205 (axial); and FOV = 18–20 × 18–20 cm (sagittal), 8–10 × 8–10 cm (axial).

The MR images, without accompanying clinical or pathologic information, were retrospectively reviewed in consensus by 2 pediatric imaging radiologists with 11 and 6 years of experience. The MR images were assessed for the following features: 1) visibility of the tract along its subcutaneous and intrathecal course, 2) attachment site of the tract, 3) the level of the conus medullaris, 4) change in the spinal cord shape, and 5) presence of an associated intradural lesion (abscess, dermoid, or epidermoid tumor or an-

other dysraphia malformation). The MR imaging findings were compared with operational and histopathologic findings. The visibility of the tract was classified into 3 types depending on the traceability of the tract on MR images based on the operative finding as the reference standard: entirely visible, round tract separate from the filum terminale or nerve roots completely traceable in its entire course; partially visible, portions of the tract detected even though the entire course was not traceable; and poorly visible, no discernable tract demonstrated along its course. The level of the conus medullaris was considered normal when it terminated at or above the L2–3 intervertebral disc level. A change in the shape of the spinal cord was assessed for dorsal tenting at the level of tract-cord union. Dorsal tenting of the spinal cord was defined as follows: The cord shape appears to be ovoid (disproportionate increase in the anteroposterior-to-transverse diameter relative to the upper and lower segments of the spinal cord) rather than round on axial images and/or to be tethered dorsally on sagittal images at the level of tract-cord union (Fig 1).

Statistical Analysis

The Fisher exact test was used to compare the male/female ratio, clinical features, and MR imaging findings between the LDM and CDS groups. The Mann-Whitney *U* test was used to compare the ages of the 2 groups. A *P* value < .05 was considered statistically significant. The data analyses were performed with the commercially available statistical software SPSS, Version 12 (IBM, Armonk, New York).

RESULTS

Clinical Findings

Twenty-two patients with surgically and histopathologically confirmed LDM (*n* = 12) and CDS (*n* = 10) were included in our study. Age at admission ranged from day of life 15 to 47 months of age (median age at presentation, 4 months; male/female ratio, 2:10) in patients with LDM. In patients with CDS, the age at admission ranged from day of life 7 to 34 months (median age at presentation, 11.5 months; male/female ratio, 6:4). There were no significant statistical differences in age at admission (*P* = .207) and in male/female ratio (*P* = .074).

In patients with LDM, the most common reason prompting a patient's referral was skin findings (11 patients, 92%). Whereas the most common reason prompting a patient's referral in patients with CDS was infection (6 patients, 60%) or skin findings (5 patients). In LDM, the most common skin lesion was a skin-covered dimple that appeared as a sunken crater covered with pearly pale epithelium (10/12, 83%) (Fig 1). The remainder showed a pinpoint pit (2/12, 17%) (Fig 2). In CDS, all patients had a pinpoint pit (10/10, 100%) (*P* < .001). The accompanying skin lesions were as follows: a crater surrounded by a capillary hemangioma (*n* = 5) and hairs emanating from the crater (*n* = 1) in LDM; and hemangioma (*n* = 4) and hypertrichosis (*n* = 1) in CDS.

The prevalence of infectious complications was higher in the CDS group than the LDM group (*P* = .003). None of the patients with LDM had infectious complications, whereas 6 of

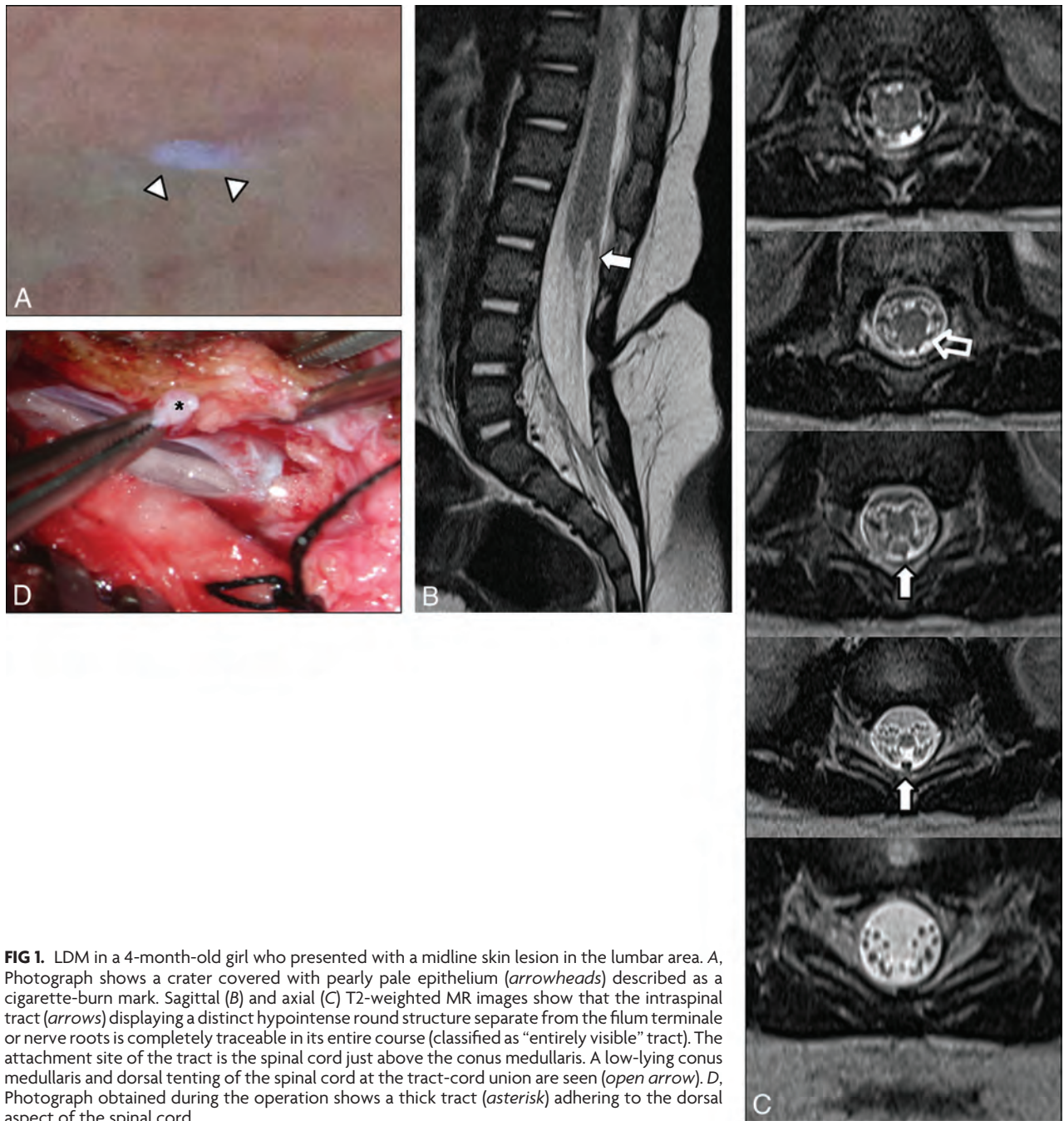


FIG 1. LDM in a 4-month-old girl who presented with a midline skin lesion in the lumbar area. *A*, Photograph shows a crater covered with pearly pale epithelium (arrowheads) described as a cigarette-burn mark. Sagittal (*B*) and axial (*C*) T2-weighted MR images show that the intraspinal tract (arrows) displaying a distinct hypointense round structure separate from the filum terminale or nerve roots is completely traceable in its entire course (classified as “entirely visible” tract). The attachment site of the tract is the spinal cord just above the conus medullaris. A low-lying conus medullaris and dorsal tenting of the spinal cord at the tract-cord union are seen (open arrow). *D*, Photograph obtained during the operation shows a thick tract (asterisk) adhering to the dorsal aspect of the spinal cord.

10 patients with CDS (60%) were admitted with infectious manifestations: fever ($n = 5$), acute meningitis ($n = 3$), recurrent meningitis ($n = 1$), skin inflammation ($n = 3$), and purulent discharge from the pit ($n = 4$). Four of 10 patients with CDS (40%) had abnormal neurologic signs and/or symptoms accompanied by an infectious complication, including 1 patient with quadriplegia and a neurogenic bladder. In patients with LDM, 2 of 12 (17%) had neurologic deficits: mild lower extremity weakness with urinary dysfunction on urodynamic studies. There was no significant difference in neurologic deficits between the 2 groups ($P = .348$).

The summary of the clinical findings in the LDM and CDS groups is presented in Table 1.

MRI Findings

Tract. The subcutaneous portions of the tracts in all cases of LDM and CDS were traceable in their entirety on MR imaging. The visibility of the tract in its intrathecal course was significantly different between the 2 groups ($P = .003$). All intrathecal tracts of LDM were either entirely visible (10/12, 83%) or partially visible (2/12, 17%) (Figs 1 and 2), whereas 5 of 10 intrathecal tracts (50%) were visible in CDS (entirely visible in 1 patient; partially visible in 4 patients). In 4 patients with CDS (40%), intrathecal tracts were poorly visible because they were indistinguishable from intradural cystic lesions and smudgy heterogeneous lesions fully filling the intrathecal space (Fig 3).

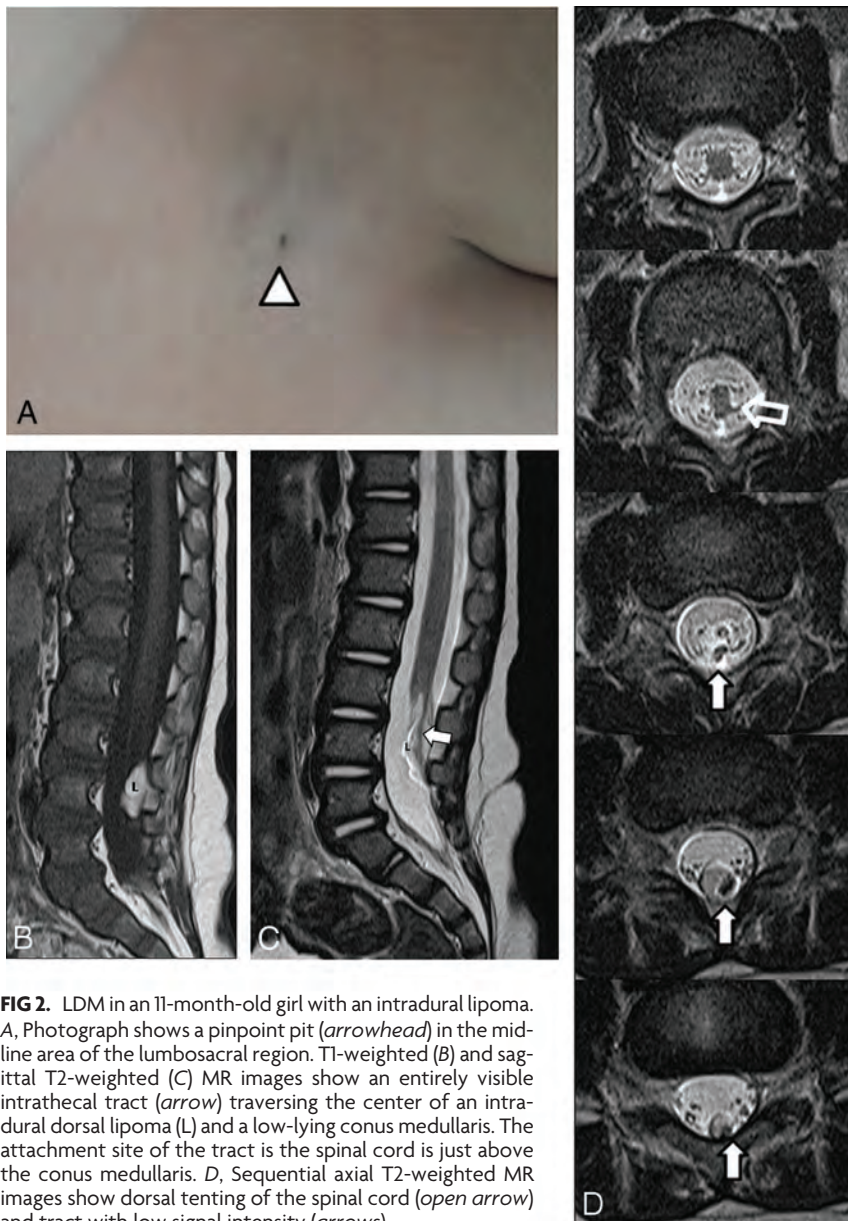


FIG 2. LDM in an 11-month-old girl with an intradural lipoma. A, Photograph shows a pinpoint pit (arrowhead) in the midline area of the lumbosacral region. T1-weighted (B) and sagittal T2-weighted (C) MR images show an entirely visible intrathecal tract (arrow) traversing the center of an intradural dorsal lipoma (L) and a low-lying conus medullaris. The attachment site of the tract is the spinal cord is just above the conus medullaris. D, Sequential axial T2-weighted MR images show dorsal tenting of the spinal cord (open arrow) and tract with low signal intensity (arrows).

Table 1: Comparison of LDM and CDS: clinical data

	LDM (n = 12)	CDS (n = 10)	P Value
Male/female	2:10	6:4	.074
Age (mo) at admission ^a	11 ± 14.2 (0.5–47)	12.9 ± 9 (0.25–34)	.207
Clinical presentation			
Skin abnormality ^b			<.0001
Skin-covered crater	10 (83%)	0	
Pit	2 (17%)	10 (100%)	
Infection ^b	0	6 (60%)	.003
Neurologic deficit ^b	2 (17%)	4 (40%)	.348

^a Data are mean value, with ranges in parentheses.

^b Data are number of patients, with percentages in parentheses.

In 1 patient with CDS, the tract was revealed to end in the dura mater at surgery and there was no tract in the intrathecal portion.

For attachment sites of the tract, a significant difference was found between the 2 groups ($P = .004$). In all 12 patients with LDM, the attachment sites of the tracts were clearly identified as a

hypointense round structure adhering to the dorsal aspect of the spinal cord above the conus medullaris on MR imaging (Figs 1 and 2). In contrast, the attachment sites of the CDS tracts were varied and were not clearly visualized on MR imaging, even in patients with visible intrathecal tracts.

Spinal Cord. While a low-lying conus medullaris, indicating a tethered cord on MR imaging, was slightly more frequent in patients with LDM (9/12, 75%) compared with those with CDS (6/10, 60%), the difference was not statistically significant ($P = .652$). Neither patients with LDM nor those with CDS had a thickened filum terminale.

For the shape of the spinal cord, a significant difference was found between LDM and CDS ($P = .001$). Ten of 12 patients with LDM (83%) had dorsal tenting of the spinal cord at the tract-cord union (Figs 1 and 2), whereas only 1 of 10 patients with CDS (10%) had that appearance. An area of CSF collection within the spinal cord, representing a syringohydromyelia, was seen in 2 of 12 patients with LDM (17%).

Intradural Lesions. For intradural lesions such as dermoid and epidermoid tumors, a significant difference was found ($P = .003$): dermoid and epidermoid tumors were present only in the CDS (6/10, 60%; 5 epidermoid tumors and 1 dermoid tumor); none of the patients with LDM had these tumors. Epidermoid tumors had variable signal intensity, most commonly isointense with CSF but sometimes having a hypointense portion on T2-weighted images. Three epidermoid tumors appeared as ring-enhancing mass lesions nearly filling the entire intrathecal space with displacement of spinal cord or nerve roots. Two of these 3 were accompanied by spinal cord edema (Fig 3). One epidermoid and 1 dermoid tumor showed smudgy heterogeneous signal intensity intermingled in the nerve roots, with diffuse enhancement in the subarachnoid space and no distinct cystic mass. These aforementioned 5 lesions were infected, with the latter 2 (1 epidermoid and 1 dermoid) found to be ruptured at the operation. The remaining extramedullary epidermoid tumor was difficult to visualize on MR imaging: It was isointense with CSF and showed the minimal deviation of nerve roots with subtle rim enhancement—and had presumably been infected.

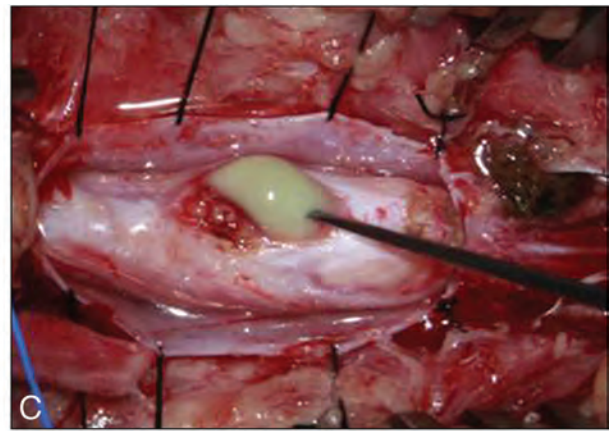


FIG 3. CDS in a 12-month-old girl who presented with fever and quadriplegia. Sagittal T2-weighted (A) and contrast-enhanced T1-weighted (B) MR images show ring-enhancing mass lesions nearly filling the entire intrathecal space (arrows), accompanied by spinal cord expansion and intramedullary thick enhancement (open arrows). There is no discernable tract in the intrathecal region on MR imaging (classified into “poorly visible”). These enhancing mass lesions (arrows) and intramedullary enhancement (open arrows) were infected epidermoid tumor and intramedullary abscess at the operation, respectively. C, Photograph obtained during the operation shows a yellowish material, representing infected epidermoid tumor.

Table 2: Visibility of tract: MRI and operative findings^a

Tract	Visibility	LDM (n = 12)	CDS (n = 10)	P Value
Subcutaneous		12 (100%)	10 (100%)	—
Intrathecal ^b	Entirely visible	10 (83%)	1 (10%)	.003
	Partially visible	2 (17%)	4 (40%)	
	Poorly visible	0 (0%)	4 (40%)	

^aData are number of patients, with percentages in parentheses.

^bBecause the tract of 1 patient with CDS was revealed to end in the dura mater at the operation and there was no tract in the intrathecal area, only 9 CDS tracts were assessed with regard to visibility and attachment site in its intrathecal portion.

In patients with LDM with a low-lying conus medullaris, 2 were found to have intradural lipomas. Of these 2 cases, 1 had a tract traversing the center of a dorsal lipoma abutting the dura mater over its whole intrathecal course (Fig 2) and 1 had a fat-lined tract not extending to the spinal cord. Intradural lipomas, running parallel to the intrathecal tract, were also identified in the 2 patients with CDS but did not extend the length of the tract.

Tables 2–5 summarize the MR imaging findings between the LDM and CDS groups compared with operative findings as a reference.

DISCUSSION

In this study, there was a significant difference in clinical and neuroimaging findings between LDM and CDS. The most common skin lesion of LDM was a crater covered with pearly pale epithelium described by previous reports as a “cigarette-burn mark.”^{1,2,12} This skin lesion was not seen in our patients with CDS. Subjects with LDM had a relatively distinct intrathecal tract that was attached to the spinal cord just above the conus medullaris and showed dorsal tenting of the cord at the tract-cord union in most cases (83%). LDM was not associated with an intradural infection or with dermoid or epidermoid tumors, unlike CDS. On

the other hand, CDS had an indistinct intrathecal tract that ended in a variable depth and rarely showed a change in shape of the spinal cord (10%). Intradural dermoid or epidermoid tumors were found in 60% of patients with CDS and were found to be infected at the operation.

These 2 entities have been described as having a different embryologic hypothesis and pathology.^{1,4,11,13} They both have been explained by abnormal neurulation during embryonic development. CDS may be the consequence of focal incomplete disjunction between the neural tube and cutaneous ectoderm, leading to a persistent epithelium-lined tract between the skin and central nervous system.^{7,11} However, some authors^{3,4} have postulated that LDM may be the result of the interposition of mesodermal cells between the neural tube and cutaneous ectoderm after separation of these 2 layers, consequently forming a solid tract composed of mesenchymal tissue with or without neural tissue.

These different embryonic errors and consequent distinctions in the histopathology may lead to differences in neuroimaging between the 2 groups. LDM has a solid tract composed of mainly attenuated fibrous tissue with variable portions of mesenchymal and neural elements—without a lumen—while CDS has a hollow tract lined by thin epithelium.^{1,3,11} Therefore, it could be postulated that visibility of the tract on MR imaging may be different between the 2 groups. In the present study, visibility of the tract was particularly different in its intrathecal portion surrounded by CSF. Most of the LDM tracts (83%) were completely visible throughout their entire course and were seen as discrete hypointense tracts in their intrathecal portion, whereas only 1 CDS tract was entirely visible among 5 tracts detectable in the intrathecal space. Even the detectable intrathecal portions of the CDS tract appeared to be subtle and relatively thin compared with LDM on

Table 3: Attachment site of tract: MRI and operative findings^a

Tract	Attachment Site	LDM (n = 12)		CDS (n = 10)		P Value
		MRI	OP	MRI	OP	
Intrathecal ^b	Conus medullaris	12 (100%)	12 (100%)	2 (20%)	3 (30%)	.004
	Filum terminale/nerve root	—	—	2 (20%)	2 (20%)	
	Dermoid/epidermoid tumor	—	—	—	4 (40%)	
	Not available ^c	—	—	5 (50%)	—	
No extension into the spinal canal	—	—	1 (10%)	1 (10%)		

Note:—Op indicates operative findings.

^a Data are number of patients, with percentages in parentheses.

^b Because the tract of 1 patient with CDS was revealed to end in the dura mater at the operation and there was no tract in the intrathecal area, only 9 CDS tracts were assessed with regard to visibility and attachment site in its intrathecal portion.

^c The attachment sites of the tracts could not be evaluated on MRI.

Table 4: Configuration of spinal cord: MRI and operative findings^a

Spinal Cord		LDM	CDS	P Value
		(n = 12)	(n = 10)	
Level of the conus medullaris	Normal	3 (25%)	4 (40%)	.652
	Low-lying	9 (75%)	6 (60%)	
Shape of the spinal cord	Dorsal tenting	10 (83%)	1 (10%)	.001

^a Data are number of patients, with percentages in parentheses.

Table 5: Intradural lesions: MRI and operative findings^a

Associated Intradural Lesions	MRI		OP		P Value
	MRI	OP	MRI	OP	
Dermoid-epidermoid	0 (0%)	0 (0%)	5 (50%)	6 (60%)	.003
Lipoma	2 (17%)	2 (17%)	2 (20%)	2 (20%)	1.000

Note:—OP indicates operative findings.

^a Data are number of patients, with percentages in parentheses.

MR imaging. The visibility of the CDS tract on MR imaging may also be influenced by the presence of a coexisting intraspinal infection as well as the innate histopathology of the tract itself. In this study, 4 CDS tracts were poorly visible due to infected intradural dermoid or epidermoid tumors fully filling the intrathecal space. These findings are consistent with some previous reports regarding the 2 groups.^{1,6,11,14}

In terms of attachment site of the tract, there was a significant difference between the 2 groups in the present study: CDS tracts ended in varying structures, including dermoid or epidermoid tumors, while all LDM tracts were attached to the spinal cord above the conus medullaris. Although some investigators have mentioned that LDM tracts can also attach to other intraspinal structures such as the arachnoid membrane, dura mater, intradural dorsal lipoma, and filum terminale,³⁻⁵ our results were consistent with the cases presented by Pang et al.¹

LDM (10/12, 83%) was significantly more likely than CDS (1/10, 10%) to be associated with a change in the shape of the spinal cord. The positive predictive value of this finding in the diagnosis of the LDM was 91% (10/11). The change in spinal cord shape, referred to as dorsal tenting of the spinal cord or a trapezoid shape of the cord-tract union by Pang et al,¹ can result from the tethering effect of the tract on the spinal cord where the tract joins it. A difference in the attachment site of the tract between the 2 groups may explain these results. However, only 1 of 3 patients with CDS with a tract attached to the spinal cord showed dorsal tenting of the spinal cord. Therefore, another factor may also influence the change in cord shape besides attachment of the tract

to the cord. As mentioned above, LDM is a solid tract composed of dense mesenchymal tissue, while CDS is a hollow tract lined with thin epithelium. The higher density of the LDM tract may lead to a more obvious tethering effect on the spinal cord where the tract joins it. Furthermore, a syringohydromyelia near the cord-tract union, which disappeared after removal of the tract, was seen in only the patients with LDM (2/12, 17%) and was presumably caused by the tethering effect of the tract.

Several studies have reported that disability is related to spinal cord tethering in many patients with LDM.^{1,3,5,15} On the other hand, CDS might rarely cause spinal cord tethering according to the report by Martinez-Lage et al,⁵ though other investigators have reported that CDS has a relatively higher rate of tethered cord, ranging from 57% to 79%.^{6,7,16} Although tethered cord syndrome is a clinical diagnosis, a tethered cord may be suggested by a low position of the conus medullaris seen on MR imaging.^{11,17-19} In the present study, the presence of a low-lying conus medullaris was not significantly different between the 2 groups, while it was slightly more frequent in patients with LDM (75%) than in those with CDS (60%). The development of cord tethering can be affected by the presence of associated lesions such as dysraphic malformations and dermoid and epidermoid tumors, as well as the tethering effect of the tract itself.²⁰ In our patients with LDM, aside from the one with intradural lipoma, the cause of the low-lying conus medullaris could not be explained in any other way besides the tethering effect of the tract itself. In contrast, dermoid or epidermoid tumors filling the entire intrathecal space seemed to tether the cord in half of our patients with CDS with a low-lying conus medullaris. Therefore, we postulate that the higher density of the tract in LDM compared with CDS may more frequently cause spinal cord tethering in the absence of an associated intradural lesion.

Dermoid tumors contain skin appendages lined with an epithelium, and epidermoid tumors consist of epidermal elements of the skin.¹¹ They commonly develop from congenital dermal-epidermal rests and could arise in the CDS as a consequence of desquamation of the tract lining, which is similar to the normal epidermis.⁶ In our study, a considerable number of patients with CDS (60%) had dermoid or epidermoid tumors in the intraspinal space. Intraspinally-extramedullary dermoid or epidermoid tumors may be difficult to visualize and could be underestimated on MR imaging.^{11,14} However, we found that 5 of the 6 patients with CDS having dermoid or epidermoid tumors at the operation had either enhancing cystic masses or smudgy enhancing lesions without a distinct mass on MR imaging. The higher sensitivity in the detection of dermoid and epidermoid tumors in our results may be from an associated intraspinal infection: The 5 aforementioned patients with CDS were admitted to the hospital with acute infectious symptoms, and all were found to have infected extramedullary dermoid or epidermoid tumors at the operation.

The craters covered with pale epithelium described as a cigarette-burn mark by previous reports were a noteworthy feature in

LDM.^{1,2,12} These served as closed skin defects, unlike the skin lesion of CDS, thus not being associated with infectious complications. We think that this skin lesion can be useful in decision-making along with the aforementioned neuroimaging findings. Two patients with LDM had a pinpoint pit, which, surprisingly, contained microscopic foci of squamous epithelium at the subcutaneous course of the tracts, but not at the intrathecal course. As in the report by Pang et al,¹ these may represent the concurrent presence of LDM and CDS sharing the same skin abnormality. We anticipate a further large study of associated dysraphic malformations of LDM.

There were several limitations in the present study. First, it was based on retrospective data collection, and patients with pathologic proof of a disease were necessarily enrolled. Second, the study population was small. Because LDM is a relatively unknown condition, it may have been misreported as another disease entity, including tethered spinal cord or CDS previously. This study can provide insight into CDS-mimicking lesions for radiologists. Further studies with a larger patient population are needed to confirm our findings.

CONCLUSIONS

LDM has a distinct intrathecal tract that attaches to the spinal cord above the conus medullaris and shows characteristic dorsal tenting of the cord at the tract-cord union. LDM is not associated with dermoid and epidermoid tumors. In patients with the aforementioned neuroimaging findings who have experienced no infectious complications since birth, the possibility of an LDM may be high. In addition, the presence of the characteristic skin lesion of LDM, referred to as the cigarette-burn mark, may be helpful in distinguishing it from CDS.

REFERENCES

1. Pang D, Zovickian J, Wong ST, et al. **Limited dorsal myeloschisis: a not-so-rare form of primary neurulation defect.** *Childs Nerv Syst* 2013;29:1459–84 CrossRef Medline
2. Pang D, Zovickian J, Oviedo A, et al. **Limited dorsal myeloschisis: a distinctive clinicopathological entity.** *Neurosurgery* 2010;67:1555–79; discussion 79–80 CrossRef Medline
3. van Aalst J, Beuls EA, Cornips EM, et al. **The spinal dermal-sinus-like stalk.** *Childs Nerv Syst* 2009;25:191–97 CrossRef Medline
4. De Vloot P, Lagae L, Sciote R, et al. **Spinal dermal sinuses and dermal sinus-like stalks analysis of 14 cases with suggestions for embryologic mechanisms resulting in dermal sinus-like stalks.** *Eur J Paediatr Neurol* 2013;17:575–84 CrossRef Medline
5. Martinez-Lage JF, Almagro MJ, Ferri-Ñíguez B, et al. **Spinal dermal sinus and pseudo-dermal sinus tracts: two different entities.** *Childs Nerv Syst* 2011;27:609–16 CrossRef Medline
6. Barkovich AJ, Edwards M, Cogen PH. **MR evaluation of spinal dermal sinus tracts in children.** *AJNR Am J Neuroradiol* 1991;12:123–29 Medline
7. Ackerman LL, Menezes AH. **Spinal congenital dermal sinuses: a 30-year experience.** *Pediatrics* 2003;112:641–47 CrossRef Medline
8. Cornips EM, Weber JW, Vles JS, et al. **Pseudo-dermal sinus tract or spinal dermal-sinus-like stalk?** *Childs Nerv Syst* 2011;27:1189–91; author reply 93 CrossRef Medline
9. Tortori-Donati P, Rossi A, Cama A. **Spinal dysraphism: a review of neuroradiological features with embryological correlations and proposal for a new classification.** *Neuroradiology* 2000;42:471–91 CrossRef Medline
10. van Aalst J, Beuls EA, Cornips EM, et al. **Anatomy and surgery of the infected dermal sinus of the lower spine.** *Childs Nerv Syst* 2006;22:1307–15 CrossRef Medline
11. Schwartz E, Barkovich J. **Congenital anomalies of the spine.** In: Barkovich J, Raybaud C, eds. *Pediatric Neuroimaging*. 5th ed. Philadelphia: Lippincott Williams & Wilkins; 2012
12. Schropp C, Sørensen N, Collmann H, et al. **Cutaneous lesions in occult spinal dysraphism: correlation with intraspinal findings.** *Childs Nerv Syst* 2006;22:125–31 CrossRef Medline
13. Rajpal S, Salamat MS, Tubbs RS, et al. **Tethering tracts in spina bifida occulta: revisiting an established nomenclature.** *J Neurosurg Spine* 2007;7:315–22 CrossRef Medline
14. Tisdall MM, Hayward RD, Thompson DN. **Congenital spinal dermal tract: how accurate is clinical and radiological evaluation?** *J Neurosurg Pediatr* 2015;15:651–56 CrossRef Medline
15. Kaffenberger DA, Heinz ER, Oakes JW, et al. **Meningocele manqué: radiologic findings with clinical correlation.** *AJNR Am J Neuroradiol* 1992;13:1083–88 Medline
16. Radmanesh F, Nejat F, El Khashab M. **Dermal sinus tract of the spine.** *Childs Nerv Syst* 2010;26:349–57 CrossRef Medline
17. Jones BV. **Tethered spinal cord.** In: Donnelly LF, ed. *Diagnostic Imaging Pediatrics*. 2nd ed. Salt Lake City, Utah: Amirsys; 2012:12
18. Bui CJ, Tubbs RS, Oakes WJ. **Tethered cord syndrome in children: a review.** *Neurosurg Focus* 2007;23:E2 Medline
19. Warder DE, Oakes WJ. **Tethered cord syndrome and the conus in a normal position.** *Neurosurgery* 1993;33:374–78 CrossRef Medline
20. Geyik M, Alptekin M, Erkuclu I, et al. **Tethered cord syndrome in children: a single-center experience with 162 patients.** *Childs Nerv Syst* 2015;31:1559–63 CrossRef Medline

Associations between Measures of Structural Morphometry and Sensorimotor Performance in Individuals with Nonspecific Low Back Pain

K. Caeyenberghs, M. Pijnenburg, N. Goossens, L. Janssens, and S. Brumagne



ABSTRACT

BACKGROUND AND PURPOSE: To date, most structural brain imaging studies in individuals with nonspecific low back pain have evaluated volumetric changes. These alterations are particularly found in sensorimotor-related areas. Although it is suggested that specific measures, such as cortical surface area and cortical thickness, reflect different underlying neural architectures, the literature regarding these different measures in individuals with nonspecific low back pain is limited. Therefore, the current study was designed to investigate the association between the performance on a sensorimotor task, more specifically the sit-to-stand-to-sit task, and cortical surface area and cortical thickness in individuals with nonspecific low back pain and healthy controls.

MATERIALS AND METHODS: Seventeen individuals with nonspecific low back pain and 17 healthy controls were instructed to perform 5 consecutive sit-to-stand-to-sit movements as fast as possible. In addition, T1-weighted anatomic scans of the brain were acquired and analyzed with FreeSurfer.

RESULTS: Compared with healthy controls, individuals with nonspecific low back pain needed significantly more time to perform 5 sit-to-stand-to-sit movements ($P < .05$). Brain morphometric analyses revealed that cortical thickness of the ventrolateral prefrontal cortical regions was increased in patients with nonspecific low back pain compared with controls. Furthermore, decreased cortical thickness of the rostral anterior cingulate cortex was associated with lower sit-to-stand-to-sit performance on an unstable support surface in individuals with nonspecific low back pain and healthy controls ($r = -0.47, P < .007$). In addition, a positive correlation was found between perceived pain intensity and cortical thickness of the superior frontal gyrus ($r = 0.70, P < .002$) and the pars opercularis of the inferior ventrolateral prefrontal cortex ($r = 0.67, P < .004$). Hence, increased cortical thickness was associated with increased levels of pain intensity in individuals with nonspecific low back pain. No associations were found between cortical surface area and the pain characteristics in this group.

CONCLUSIONS: The current study suggests that cortical thickness may contribute to different aspects of sit-to-stand-to-sit performance and perceived pain intensity in individuals with nonspecific low back pain.

ABBREVIATIONS: DASS-21 = Depression Anxiety Stress Scale; NPRS = numeric pain rating scale; NSLBP = nonspecific low back pain; ODI = Oswestry Disability Index; STSTS = sit-to-stand-to-sit

Nonspecific low back pain (NSLBP) refers to low back pain that is not attributable to a specific cause. This category of low back pain disorders includes almost all low back pain symp-

toms.¹⁻³ Despite much effort in the development of treatment strategies for this large population,⁴ the effects of current NSLBP interventions are rather small. Therefore, understanding the underlying neural basis of NSLBP is crucial.

Previous imaging studies showed structural alterations in cortical and subcortical brain regions in individuals with NSLBP. However, mixed findings were obtained. Both increases and decreases in gray matter volume in different brain

Received January 5, 2015; accepted after revision August 18, 2016.

From the School of Psychology (K.C.), Faculty of Health Sciences, Australian Catholic University, Sydney, New South Wales, Australia; Department of Rehabilitation Sciences (M.P., N.G., L.J., S.B.), Katholieke Universiteit Leuven, Leuven, Belgium; and Hasselt University (L.J.), Biomedical Research Institute, Diepenbeek, Belgium.

K. Caeyenberghs and M. Pijnenburg are co-first authors.

This work was supported by the Agency for Innovation by Science and Technology-Flanders (<http://www.iwt.be>) (PhD fellowship to Madelon Pijnenburg and PhD fellowship to Nina Goossens, grant No. 141037) and by the Research Foundation Flanders (<http://www.fwo.be>) (postdoctoral fellowship: Lotte Janssens, grant No. 12M9815N).

The funders had no role in study design; collection, analysis, and interpretation of data; in the writing of the manuscript; or in the decision to submit the manuscript for publication.

Please address correspondence to Madelon Pijnenburg, MD, Katholieke Universiteit Leuven, University of Leuven, Faculty of Kinesiology and Rehabilitation Sciences, Department of Rehabilitation Sciences, Research Group for Musculoskeletal Rehabilitation, Tervuursevest 101, Bus 1501 B-3001 Leuven; e-mail: m.pijnenburg@fontys.nl

Indicates open access to non-subscribers at www.ajnr.org

Indicates article with supplemental on-line table.

<http://dx.doi.org/10.3174/ajnr.A5020>

regions were found in individuals with NSLBP compared with healthy controls. Volumetric alterations in individuals with NSLBP were observed, for example, in the dorsolateral prefrontal cortex,⁵⁻⁷ in the somatosensory cortex,^{6,8,9} in the temporal lobes,^{6,8} and in the thalamus.⁵⁻⁷ Together, most gray matter alterations in NSLBP, either reduced or increased, are observed in areas related to sensorimotor control. These alterations in sensorimotor-related areas are indicative of impaired sensorimotor performance, as observed in individuals with NSLBP with behavioral measures.¹⁰⁻¹² For example, individuals with NSLBP need notably more time to perform 5 consecutive sit-to-stand-to-sit (STSTS) movements compared with healthy controls.¹³ This STSTS task necessitates optimal sensorimotor control, which requires an efficient processing of sensory and motor information across the brain.¹⁴ However, nearly all structural brain imaging studies in NSLBP and in sensorimotor control have evaluated volumetric changes.⁵⁻⁹ Only 1 study in patients with Parkinson disease investigated how structural morphometry was associated with motor performance, showing an association between cortical thinning of the sensory parietotemporal areas and motor deficits.¹⁵ However, in NSLBP, cortical thickness and cortical surface area have been relatively understudied, while these 2 aspects of brain structure may be crucial to functional connectivity.

Cortical thickness and cortical surface area have a distinct genetic origin,^{16,17} a contrasting phylogeny,¹⁸ and different developmental trajectories.¹⁹ In addition, it is suggested that cortical thickness and cortical surface area reflect different aspects of the underlying neural architecture.²⁰ More specifically, cortical surface area is primarily determined by the number of columns within a cortical region, whereas cortical thickness is thought to reflect the number of cells within these cortical columns.^{18,21} Therefore, evaluation of cortical surface area and cortical thickness as separate measures can provide interesting additional knowledge on the neural mechanisms of NSLBP and sensorimotor tasks. These measures of structural morphometry can be computed by a surface-based analysis method called FreeSurfer (<http://surfer.nmr.mgh.harvard.edu>).²²

With the FreeSurfer analysis suite, 2 recent studies^{23,24} have provided evidence for alterations in cortical thickness in individuals with NSLBP compared with healthy controls. Although, Kong et al,²³ found increased cortical thickness in the bilateral primary somatosensory cortex, somatotopically associated with the lower back, in individuals with NSLBP, Dolman et al,²⁴ demonstrated that the differences in cortical thickness between individuals with NSLBP and healthy controls disappeared when controlling for age. Nevertheless, little research has been done on the associations with sensorimotor control and pain by using both surface area and cortical thickness. Therefore, this study was designed to investigate the distinct relation between the STSTS performance and the cortical surface area and cortical thickness in individuals with NSLBP and healthy controls. An association between cortical thinning of sensorimotor brain areas and a longer duration to perform 5 consecutive STSTS movements was hypothesized. This correlation analysis was performed to reveal the potential different contributions of the 2 nonvolumetric parameters to sensorimotor control. In addition, considering recent

findings,^{23,24} we hypothesized subtle cortical thinning in both sensorimotor- and pain-related brain regions in individuals with NSLBP compared with healthy controls.

MATERIALS AND METHODS

Participants

Thirty-four subjects were studied, including 17 subjects with NSLBP (11 women and 6 men) and 17 age-matched (± 2 years) healthy individuals (12 women and 5 men). Data from the same cohort were previously reported.^{25,26} Subjects with NSLBP were recruited consecutively from 2012 to 2013, as they responded to flyers in various settings (ie, academic [University Hospital Leuven] or community [sport clubs]), physician referrals (speciality care), mailings, and the Internet advertisements. Subjects with NSLBP were included under the following conditions: 1) they were between 20 and 50 years of age, 2) had experienced at least 6 months of disabling NSLBP (Oswestry Disability Index, Version 2 [adapted Dutch version, ODI-2]²⁷ of $>12\%$), 3) were not taking heavy opioids or drugs, 4) did not have vestibular and/or self-reported specific balance problems that precluded participation in the study procedure, 5) had no previous history of brain injury or other neurologic disorders, 6) had no neck problems (Neck Disability Index²⁸ of $<6\%$), 7) had no previous major trauma and/or operation of the spine or lower limbs, and 8) met the standard "MR safety" bench test criteria (eg, no claustrophobia, no metal implants in body). Six left-handed participants (2 patients with NSLBP and 4 healthy controls) were included in the study; however, the removal of left-handed participants did not change the results on group differences in structural morphometry and correlation analyses. All participants gave their written informed consent before the study. The study conformed to the principles of the Declaration of Helsinki (1964) and its later amendments; was approved by the local Ethics Committee of Biomedical Sciences, University Hospital Leuven, Belgium (s53802); and was registered at www.clinicaltrials.gov with the identification number NCT01540617.

Description of Measures

Pain Characteristics. The pain characteristics are defined by the numeric pain rating scale (NPRS) of the back, scores on the ODI-2, and the number of years of NSLBP. The NPRS back pain scores (0, no pain, to 10, worst pain) during the last month (NPRS_{back} usual) and at the moment of testing (NPRS_{back} current) were reported. These scores are well-validated measures to define the intensity of NSLBP.²⁹

Sit-to-Stand-to-Sit Task. The equipment, paradigm parameters, and dependent variables of the STSTS task were identical to those in previous studies.^{13,26} The participants were instructed to sit barefoot on a stool that was placed on a 6-channel force plate (Bertec, Columbus, Ohio) with their arms relaxed alongside their bodies and their vision occluded with nontransparent goggles. The stool height was adjusted for each participant to assure an angle of 90° in both hips and knees. After 15 seconds of usual sitting (no instructions on posture were given), participants were asked to perform 5 consecutive STSTS movements with a full range of motion as fast as possible. An investigator stood near the

participant to prevent actual falls. The force plate registered anteroposterior center-of-pressure displacements. The center-of-pressure displacements were sampled at 500 Hz by using a Micro1401 data acquisition system and Spike2 software (Cambridge Electronic Design, Cambridgeshire, UK). This protocol was performed with the feet placed on both a stable (force plate itself) and an unstable support surface (50-cm length \times 41-cm width \times 6-cm thickness [Balance Pad Elite; Airex, Sins, Switzerland], on the force plate). The total duration of the 5 consecutive STSTS movements was calculated on the basis of the anteroposterior center-of-pressure displacement. The starting- and end-points of the task were defined by the mean value of the center of pressure during usual sitting before and after the task. The STSTS task has shown good test-retest reliability (intraclass correlation coefficient = 0.84–0.94).^{30,31}

Depression Anxiety Stress Scale. Finally, a short version of the Depression Anxiety Stress Scale (DASS-21) was administered.³² This is a set of 3 self-report scales designed to measure the negative emotional states of depression, anxiety, and stress. Subjects are asked to use the 4-point severity/frequency scales to rate the extent to which they have experienced each state during the past week. Scores for depression, anxiety, and stress are calculated by summing the scores for the relevant items.

MR Imaging Acquisition and Analysis

MR images were acquired with a 3T Achieva scanner (Philips Healthcare, Best, the Netherlands) equipped with a 32-channel standard head coil. High-resolution whole-brain T1-weighted anatomic scans were obtained with a 3D turbo field echo sequence (voxel size = 0.98 \times 0.98 \times 1.2 mm³, TR = 9.59 ms, TE = 4.6 ms, flip angle = 8°, 182 coronal sections, FOV = 250 \times 250 \times 218 mm³, and matrix = 256 \times 256 mm²). All T1-weighted anatomic scans were checked by a radiologist to assure that no brain lesions were present.

The structural images were analyzed with the FreeSurfer analysis suite, which is documented and freely available for download on-line. A technical description of the FreeSurfer procedures can be found in previous publications.^{33–42} The whole-brain analysis was performed with additional computing resources from the high-performance computing Tier1 cluster at the University of Ghent (<http://ugent.be/hpc/en>). The FreeSurfer analysis suite is a multistep procedure that consists of the following: 1) removal of nonbrain tissue by using a hybrid watershed/surface deformation procedure (skull stripping),⁴² 2) automated transformation to Talairach space, 3) subject-specific parcellation of the subcortical white matter and deep gray matter volumetric structures,^{36,43} and 4) calculation of cortical surface area and cortical thickness from all vertices within the 34 cortical parcellations per hemisphere.⁴⁴ Results of each subject were carefully visually inspected to ensure the accuracy of the skull stripping, segmentation, and cortical surface reconstruction. Where needed, the appropriate manual corrections were performed as explained by the FreeSurfer Tutorial (<http://surfer.nmr.mgh.harvard.edu/fswiki/FsTutorial>). In some datasets, it appeared that the skull strip left a lot of dura. However, it did not affect the surfaces following the gray and white matter borders. The averaged values across hemispheres were calculated and used in the statistical analysis to reduce the number of comparisons.

Table 1: Characteristics of the participants^a

Characteristic	NSLBP Group (n = 17)	Healthy Group (n = 17)	P Value
Age (yr)	33.3 \pm 7.9	31.8 \pm 8.2	.582
Sex (male/female)	6/11	5/12	.724
Height (cm)	173.0 \pm 6.4	169.1 \pm 6.4	.087
Weight (kg)	72.7 \pm 10.6	64.9 \pm 10.2	.036
BMI (kg/m ²)	24.2 \pm 2.8	22.6 \pm 2.7	.090
ODI-2	20.6 \pm 7.6	0	NA
Years of NSLBP	9.8 \pm 8.2	0	NA
NPRS _{back} usual	4.5 \pm 2.0	0	NA
NPRS _{back} current	2.0 \pm 2.0	0	NA

Note:—BMI indicates body mass index; NA, not applicable.

^a Data are presented as mean \pm SD. Significance level is $P < .05$.

Statistical Analysis

Unpaired *t* tests were used to calculate group differences in characteristics of the participants. To determine whether an interaction effect of the Group \times Support Surface was present in the STSTS performance, we performed a 2 \times 2 repeated-measures ANOVA with Group as the between-subject factor (NSLBP group and healthy control group) and Support Surface as the within-subject factor (stable support surface and unstable support surface). The significance level for group differences in characteristics and STSTS performance was set at $P < .05$. MANCOVA was used to contrast cortical thickness and surface area measurements from each cortical parcellation by Group while controlling for age. The Bonferroni correction was applied to correct for multiple comparisons, resulting in an adjusted *P* value of $< .001$ (.05/34) for group differences in structural morphometry.

In addition, for each cortical parcellation from the morphologic measurement differences between groups, we also conducted post hoc power analyses by using G*Power, Version 3.1.9.2 (<http://www.softpedia.com/get/Science-CAD/G-Power.shtml>; with power [1- β] set at 0.80 and $\alpha = .05$, 2-tailed), to determine whether negative findings could be attributed to a limited sample size. The Outliers Labeling Rule (with a *g*-factor of 2.2)⁴⁵ was applied to detect outliers from both the STSTS data and the structural morphometry parameters. These values were excluded pair-wise from the correlation analysis. Relationships between STSTS performance and pain scores on one hand and the characteristics of morphometry on the other hand were examined by using partial (controlling for age) Spearman correlations across the total group and within each of the groups (individuals with NSLBP and healthy controls) in regions with significant group differences only. The *P* values reported for correlations were uncorrected for multiple comparisons with a statistical threshold of $P < .01$. These analyses, while showing a consistent trend, should be considered exploratory. The statistical analysis was performed with SPSS 22 (IBM, Armonk, New York).

RESULTS

Characteristics of the Participants

In accordance with the inclusion criteria, individuals with NSLBP reported scores above zero on the parameters of NSLBP-related disability and pain intensity (ODI-2, NPRS_{back} usual and NPRS_{back} current), whereas all healthy individuals scored zero on these parameters (Table 1). No significant differences in demographic characteristics were found between the in-

dividuals with NSLBP and healthy controls ($P > .05$), except for weight (NSLBP, 72.7 ± 10.6 kg; healthy controls, 64.9 ± 10.2 kg; $P = .036$) (Table 1). According to the cutoff scores of the DASS-21, 3 individuals with NSLBP showed moderate-to-severe depression, 4 individuals with NSLBP showed moderate-to-severe anxiety, and 5 individuals with NSLBP showed moderate-to-severe stress, whereas all controls scored zero on the 3 scales of the DASS-21.

Sit-to-Stand-to-Sit Task

A significant main effect of the factors Group ($F = 11.348$, $P = .002$) and Surface ($F = 6.29$, $P = .017$) was observed in the duration of performing 5 consecutive STSTS movements. More specifically, individuals with NSLBP needed significantly more time to perform the STSTS task on stable and unstable support surfaces (stable, 18.1 ± 6.9 seconds; unstable, 16.8 ± 5.9 seconds) compared with healthy controls (stable, 12.9 ± 2.5 seconds; unstable, 11.5 ± 2.0 seconds) ($P = .002$). Moreover, a significant decrease in the duration of the STSTS task was found on unstable support surfaces compared with the stable conditions, irrespective of Group ($P = .017$). No interaction effect between the factors Group and Surface was present ($P > .05$).

Contribution of Weight

Because a significant difference in weight was found between subjects with NSLBP and healthy controls, post hoc correlation anal-

yses were performed to determine whether weight was associated with pain scores, structural morphometry measures, and STSTS performance. Our results revealed a significant positive correlation between the number of episodes of NSLBP and weight ($r = 0.357$, $P = .038$). No significant correlations between weight and the other measures of pain could be demonstrated (Table 2). Also, the weight of the participants was not significantly correlated with the total time needed to perform the STSTS task on stable and unstable support surfaces or with the structural morphometry ($P > .05$). Therefore, weight was not included in the subsequent analysis.

Structural Morphometry

MANCOVA of the cortical parcellations between subjects with NSLBP and healthy controls (On-line Tables 1 and 2 and Fig 1), including age as a covariate in the model, showed cortical thickening in the individuals with NSLBP in the pars opercularis and pars triangularis of the inferior ventrolateral prefrontal cortex ($P < .001$). These brain regions did retain significance after correcting for multiple comparisons. Using a less stringent threshold of $P < .01$ (indicated by footnote *a* in On-line Table 1), we observed a cortical thickening trend in the NSLBP group in the cuneus ($P < .003$), fusiform gyrus ($P < .004$), inferior parietal gyrus ($P < .002$), lateral orbitofrontal cortex ($P < .004$), posterior cingulate gyrus ($P < .008$), superior frontal gyrus ($P < .01$), superior temporal gyrus ($P < .006$), and transverse temporal gyrus ($P < .004$) and a cortical thinning trend in the rostral anterior cingulate gyrus ($P < .009$) and the insula ($P < .002$).

Within these regions, we checked for correlations to depression, anxiety, and stress (as measured by the DASS-21) to exclude the possibility that the significant group differences in cortical thickness may be explained by differences in emotional states. Only 1 significant positive correlation within the patient group

Table 2: Relationships between weight and measures of pain

Measure of Pain	Spearman Correlation	
	Coefficient	P Value
NPRS _{back} usual	0.314	.071
NPRS _{back} current	0.323	.630
Years of NSLBP	0.303	.082
No. of episodes of NSLBP	0.357	.038

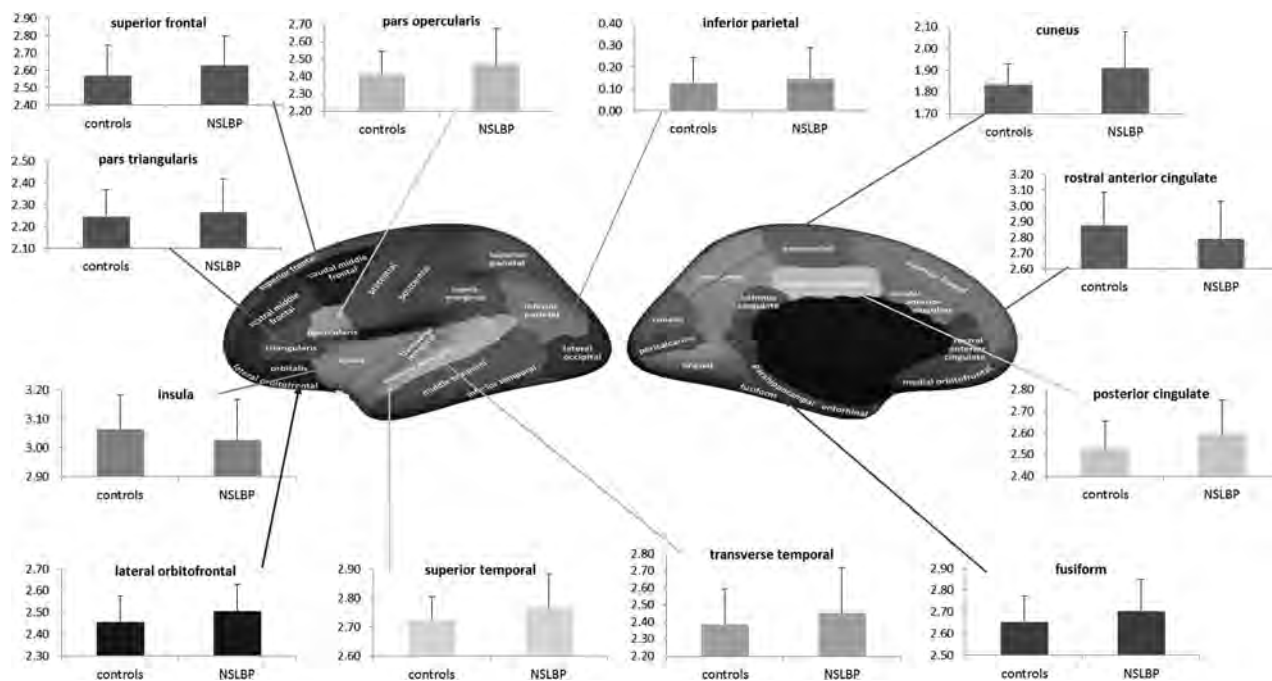


FIG 1. Significant group differences (after correcting for age) in cortical thickness.

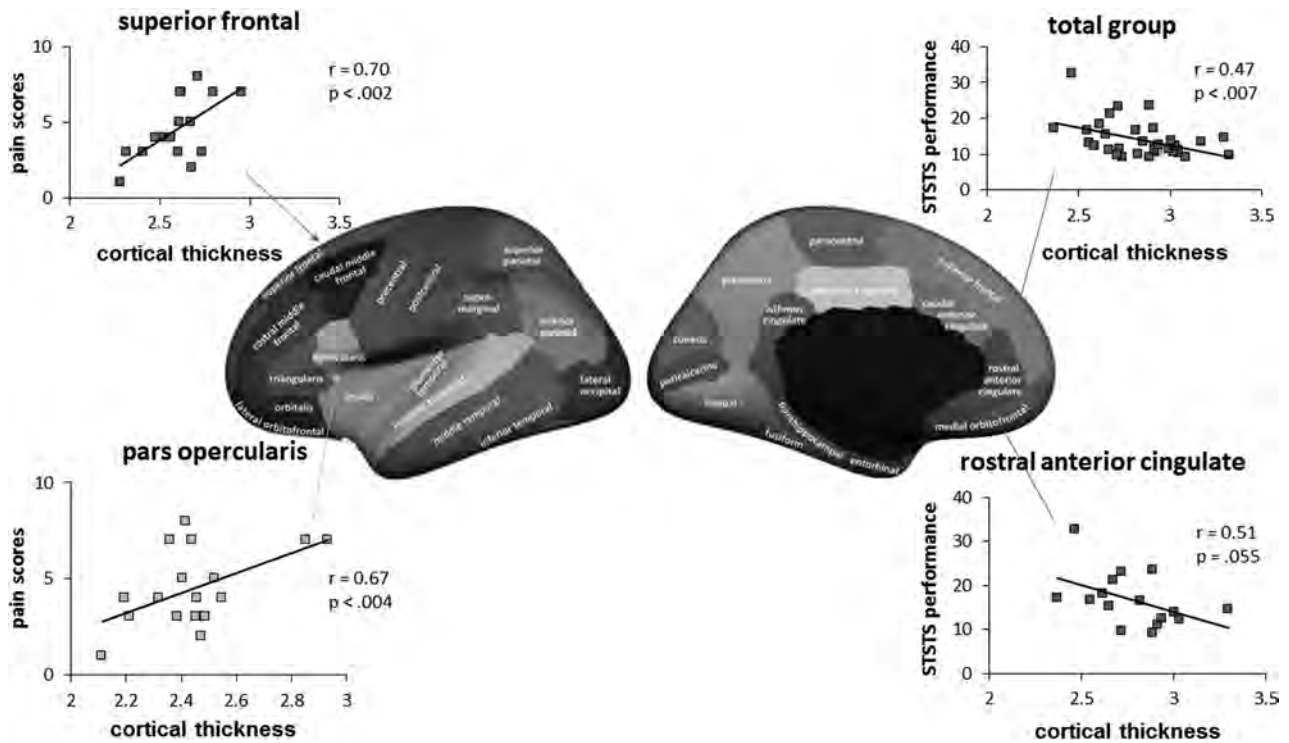


FIG 2. Scatterplots indicating the relationship between cortical thickness and STSTS performance and the pain-intensity score.

between the Depression Scale and cortical thickness was observed for the superior temporal gyrus ($r = 0.66, P < .007$).

No significant differences in cortical surface area between individuals with NSLBP and healthy controls could be demonstrated ($P > .001$, On-line Table 2). On-line Table 2 also shows the sample sizes required to find statistically significant differences in surface area between the groups for each cortical parcellation. The numbers needed per group ranged from 41 to 29,790. These results show that sample size would have to increase up to at least 41 for surface area measurements for group differences to reach statistical significance at the .05 level. Thus, it is likely that our negative findings for surface area can be attributed to a limited sample size.

Association between Cortical Thickness and the Sit-to-Stand-to-Sit Performance

Relationships (corrected for age) between STSTS performance and cortical thickness were investigated in regions with significant group effects. The duration to perform 5 consecutive STSTS movements on an unstable support surface was negatively correlated with the cortical thickness of the rostral anterior cingulate ($r = -0.47, P < .007$) within the total group (Fig 2). In other words, decreased cortical thickness of the rostral anterior cingulate cortex was associated with a longer duration of the STSTS task on an unstable support surface (lower performance). To some extent, this correlation coefficient between cortical thickness and STSTS performance was valid only for the NSLBP group ($r = -0.51, P = .055$).

Association between Structural Morphometry and Pain Characteristics

Within the group of individuals with NSLBP, significant positive correlations (as shown in Fig 2) were found between the NPRS

back pain score (indexed by the NPRS_{back} usual) and the cortical thickness of the superior frontal gyrus ($r = 0.70, P < .002$) and the pars opercularis of the inferior ventrolateral prefrontal cortex ($r = 0.67, P < .004$). In other words, increased cortical thickness of the superior frontal gyrus and pars opercularis of the inferior ventrolateral prefrontal cortex was associated with an increased level of pain intensity in the individuals with NSLBP. No significant correlations were found between cortical surface area and the pain characteristics in this group of individuals with NSLBP.

DISCUSSION

This study is the first one correlating structural morphometrics with STSTS performance in patients with chronic pain, more specifically NSLBP. Brain morphometric analyses revealed that cortical thickness of the ventrolateral prefrontal cortical regions was increased in patients with NSLBP compared with controls. This increased cortical thickness was positively correlated with increased pain scores in the NSLBP group. Our behavioral results showed that individuals with NSLBP needed significantly more time to perform 5 consecutive STSTS movements on stable and unstable support surfaces. In addition, decreased cortical thickness of the rostral anterior cingulate cortex was associated with lower STSTS performance on unstable support surfaces.

Increased Cortical Thickness in Ventrolateral Prefrontal Cortical Regions: Association with Pain Intensity

Numerous studies with voxel-based morphometry have examined alterations of gray matter densities within specific brain regions in chronic pain conditions (for meta-analyses, see Pan et al,⁴⁶ and Smallwood et al).⁴⁷ However, surface-based features, such as cortical thickness and surface area, are more direct mea-

asures of cortical morphometry than the gray matter density values used in voxel-based morphometry.^{34,48} To our knowledge, no study to date has examined these 2 measures in a group of individuals with chronic pain. So far, only 2 studies have investigated cortical thickness in individuals with NSLBP by using the FreeSurfer analysis suite. One study demonstrated an increased cortical thickness of the primary somatosensory cortex, more specifically the area somatotopically representing the lower back.²³ In another study, group comparisons revealed cortical thickening in the right rostral middle frontal gyrus and a trend toward cortical thickening in the right paracentral lobule in patients with chronic low back pain. These regions did not retain significance after correcting for age. These previous findings of cortical thickening comport with our results. Our analyses, after correcting for age, revealed cortical thickening in individuals with NSLBP in the pars opercularis and pars triangularis, which together form the mid-portion of the ventrolateral prefrontal cortex. The changes identified in the ventrolateral prefrontal cortical regions in our group of subjects with NSLBP have face validity—that is, these brain regions appear to play an important role in the cognitive regulation of pain and emotion.^{49,50} Several voxel-based morphometry studies have identified changes in the ventrolateral prefrontal cortex in patients with other chronic pain conditions, such as migraine.^{51,52} Experimental pain studies with functional imaging techniques have also demonstrated altered activation of the same brain regions.⁵³

The ventrolateral prefrontal cortex has also been reported to be involved in patients with anxiety, depressive symptoms, or stress.^{54,55} However, with the DASS-21, we checked whether the group results could be explained by depression, anxiety, or stress. We found only 1 significant positive correlation between cortical thickness of the superior temporal gyrus and the depression scale score. The present results convincingly show the important involvement of the ventrolateral prefrontal regions in pain processing. We have also found changes in cortical thickness in other structures known to be associated with pain processing and modulation, including the orbitofrontal regions, cingulate cortex, insula, and inferior parietal lobule. However, these regions did not survive Bonferroni correction.

Moreover, our results revealed that the pattern of specific alterations in brain morphology was directly related to the intensity of pain (ie, the increase in cortical thickness of the pars opercularis of the inferior frontal gyrus corresponded to greater pain). Correlation analyses revealed that increased cortical thickness was related to higher pain intensity scores in the NSLBP group. Our results are consistent with those in a previous study of Schmidt-Wilcke et al, 2006,⁶ in patients with chronic back pain in which brain regions showing an increase in gray matter density (such as the left thalamus and left putamen) coincided with increasing pain intensity.

Our findings of the relation between increased cortical thickness and increased pain scores in patients with NSLBP may reflect the consequence of a reorganization process of brain regions involved in a disproportionate number of signals of pain, emotion, and cognition. It can be suggested that this increased cortical thickness of the ventrolateral prefrontal cortex can eventually be normalized by specific and targeted training.⁵⁶ Limited evidence

available in the literature^{57,58} shows that treating chronic pain with cognitive behavioral therapy can lead to alterations in prefrontal brain regions and that the changes in these prefrontal regions correlate with clinical improvement. Whether morphologic changes can be normalized needs to be addressed in further research.

Decreased Cortical Thickness in the Rostral Anterior Cingulate Cortex: Relationship with Sensorimotor Performance

The changes in morphology correlated not only with pain scores but also with functional changes in sensorimotor control. Our behavioral results revealed that the NSLBP group required significantly more time to perform the STSTS task on both stable and unstable support surfaces compared with the healthy controls. This result is in agreement with previous studies.^{13,26} The STSTS task on an unstable support surface is ultimately challenging the sensorimotor system (including the proprioceptive system) because this condition requires additional reweighting of the proprioceptive signals due to the decreased reliability of proprioceptive signals from the ankle region.⁵⁹ Proprioception can be defined as “the unconscious perception of movement and spatial orientation arising from stimuli within the body,”⁶⁰ and the unstable support surface forces the central nervous system to down-weight the less reliable ankle muscle proprioception and consequently to up-weight the proprioceptive input from more proximal segments, to provide optimal postural control.^{59,61} Nevertheless, a faster performance on an unstable support surface compared with the stable condition was observed. Because of the nonrandomized order of these conditions, this is possibly due to a learning effect. Despite this limitation, the individuals with NSLBP needed more time to perform 5 consecutive STSTS movements compared with controls, in both conditions.

This finding fits with previous ones.¹³ The decreased performance on a sensorimotor task in individuals with NSLBP, as represented by the increased duration of the STSTS task, fits within the findings of previous studies showing impaired sensorimotor control in individuals with NSLBP.^{10,62} Indeed, the STSTS task requires optimal sensorimotor control, for example, in terms of postural control.⁶³ Recently, an association was observed between the proprioceptive reweighting capacity and microstructural integrity of the superior cerebellar peduncle in individuals with NSLBP. This finding suggests a neural basis for sensorimotor impairments.²⁵ In this current study, the association between the sensorimotor STSTS task and structural morphometry in terms of cortical surface area and cortical thickness in individuals with NSLBP and healthy controls was investigated. Evaluation of these nonvolumetric parameters as separate measures, reflecting different aspects of the underlying neural architecture, is important in investigating what drives sensorimotor tasks.

In the present study, decreased cortical thickness of the rostral anterior cingulate cortex was associated with lower STSTS performance on unstable support surfaces. This correlation was significant within the total group, and a trend within the group of the patients with NSLBP was found. The anterior cingulate cortex is considered part of the general pain matrix^{64,65} and has been im-

plicated in anticipation of pain and affective processing of pain.⁶⁶ Structural alterations in the anterior cingulate cortex have been reported in a wide range of chronic pain conditions.^{46,47} The anterior cingulate cortex is also the brain region that most consistently shows activation in response to acute pain stimuli.⁶⁶ To our knowledge, this is the first time that an association between the cortical thickness of the anterior cingulate cortex and performance on a sensorimotor task in individuals with NSLBP and healthy controls has been observed.

Of note, our statistical analyses (group comparisons and correlation analyses) revealed only significance for cortical thickness. In light of the radial unit hypothesis,^{18,67} our significant cortical thickness findings may reflect abnormalities in the number or size of the neuronal cell bodies within the cortical mini-columns of the ventrolateral prefrontal cortical regions in patients with NSLBP. In contrast, the absence of cortical surface area findings does not support individuals with NSLBP possibly having abnormal proliferation or decline in the number of cortical minicolumns. However, the power of our study was probably not enough to detect a significant group difference in surface area. While our sample size was similar to that in prior studies investigating differences in brain structure in patients with chronic pain,^{46,47} we also performed post hoc power analyses to determine whether negative findings for surface area could be attributed to the low sample size. We demonstrated that for most cortical parcellations, at least 41 subjects were required per group to observe significant differences in surface area. To precisely interpret these findings with respect to their functional significance, further research addressing the relationship between cerebral micro- and macrostructures as well as brain function is clearly necessary.

Limitations

The main shortcoming of our study was the small sample size, especially for the numerous correlations performed from the FreeSurfer output. Replication of the present morphologic findings with a larger sample is warranted. Moreover, future studies in a large number of participants should also stratify the groups by age rather than controlling for age in the statistical analyses. Another limitation of the present study pertains to the correlative nature of our study. The correlation coefficients computed between pain scores and brain morphometry provided us information about the nature of the relations between these variables but did not allow tests of strong causal inference. To achieve the latter, a longitudinal study is necessary. Finally, the inclusion of other dynamic sensorimotor tasks, such as gait, could further clarify the different aspects of sensorimotor control.

CONCLUSIONS

In the present study, patients with NSLBP showed alterations of cortical thickness in brain regions that play an important role in the cognitive regulation of pain, as well as an impaired STSTS performance compared with healthy controls. Cortical thickening was associated with increased pain intensity in the individuals with NSLBP. In addition, decreased cortical thickness of the rostral anterior cingulate cortex was correlated with lower STSTS performance on an unstable support surface. These findings

suggest that in addition to measures of volume, cortical thickness may provide a more complete understanding of the central basis of sensorimotor tasks, more specifically in the NSLBP population.

ACKNOWLEDGMENTS

The authors are grateful to the study volunteers for their participation.

Disclosures: Madelon Pijnenburg—RELATED: Grant: Agency for Innovation by Science and Technology—Flanders, Comments: PhD fellowship; Lotte Janssens—RELATED: Grant: Research Foundation Flanders, Comments: postdoctoral fellowship with grant number 12M9815N; Nina Goossens—RELATED: Grant: Agency for Innovation by Science and Technology—Flanders, Comments: PhD fellowship.

REFERENCES

1. Waddell G. 1987 Volvo award in clinical sciences: a new clinical model for the treatment of low-back pain. *Spine (Phila Pa 1976)* 1987;12:632–44 CrossRef Medline
2. Airaksinen O, Brox JI, Cedraschi C, et al. Chapter 4: European guidelines for the management of chronic nonspecific low back pain. *Eur Spine J* 2006;15(suppl 2):S192–300 CrossRef Medline
3. Hancock MJ, Maher CG, Laslett M, et al. Discussion paper: what happened to the 'bio' in the bio-psycho-social model of low back pain? *Eur Spine J* 2011;20:2105–10 CrossRef Medline
4. Balagué F, Mannion AF, Pellisé F, et al. Non-specific low back pain. *Lancet* 2012;379:482–91 CrossRef Medline
5. Apkarian AV, Sosa Y, Sonty S, et al. Chronic back pain is associated with decreased prefrontal and thalamic gray matter density. *J Neurosci* 2004;24:10410–15 CrossRef Medline
6. Schmidt-Wilcke T, Leinisch E, Gänssbauer S, et al. Affective components and intensity of pain correlate with structural differences in gray matter in chronic back pain patients. *Pain* 2006;125:89–97 CrossRef Medline
7. Ivo R, Nicklas A, Dargel J, et al. Brain structural and psychometric alterations in chronic low back pain. *Eur Spine J* 2013;22:1958–64 CrossRef Medline
8. Baliki MN, Schnitzer TJ, Bauer WR, et al. Brain morphological signatures for chronic pain. *PLoS One* 2011;6:e26010 CrossRef Medline
9. Mao C, Wei L, Zhang Q, et al. Differences in brain structure in patients with distinct sites of chronic pain: a voxel-based morphometric analysis. *Neural Regen Res* 2013;8:2981–90 CrossRef Medline
10. Brumagne S, Janssens L, Knapen S, et al. Persons with recurrent low back pain exhibit a rigid postural control strategy. *Eur Spine J* 2008;17:1177–84 CrossRef Medline
11. Laird RA, Gilbert J, Kent P, et al. Comparing lumbo-pelvic kinematics in people with and without back pain: a systematic review and meta-analysis. *BMC Musculoskelet Disord* 2014;15:229 CrossRef Medline
12. Ruhe A, Fejer R, Walker B. Center of pressure excursion as a measure of balance performance in patients with non-specific low back pain compared to healthy controls: a systematic review of the literature. *Eur Spine J* 2011;20:358–68 CrossRef Medline
13. Claeys K, Dankaerts W, Janssens L, et al. Altered preparatory pelvic control during the sit-to-stance-to-sit movement in people with non-specific low back pain. *J Electromyogr Kinesiol* 2012;22:821–28 CrossRef Medline
14. Hall LM, Brauer S, Horak F, et al. Adaptive changes in anticipatory postural adjustments with novel and familiar postural supports. *J Neurophysiol* 2010;103:968–76 CrossRef Medline
15. Lyoo CH, Ryu YH, Lee MS. Cerebral cortical areas in which thickness correlates with severity of motor deficits of Parkinson's disease. *J Neurol* 2011;258:1871–76 CrossRef Medline
16. Panizzon MS, Fennema-Notestine C, Eyer LT, et al. Distinct genetic influences on cortical surface area and cortical thickness. *Cereb Cortex* 2009;19:2728–35 CrossRef Medline

17. Winkler AM, Kochunov P, Blangero J, et al. **Cortical thickness or grey matter volume? The importance of selecting the phenotype for imaging genetics studies.** *Neuroimage* 2010;53:1135–46 CrossRef Medline
18. Rakic P. **Specification of cerebral cortical areas.** *Science* 1988;241:170–76 CrossRef Medline
19. Wierenga LM, Langen M, Oranje B, et al. **Unique developmental trajectories of cortical thickness and surface area.** *Neuroimage* 2014;87:120–26 CrossRef Medline
20. Rakic P. **Defects of neuronal migration and the pathogenesis of cortical malformations.** *Prog Brain Res* 1988;73:15–37 CrossRef Medline
21. Rakic P. **Evolution of the neocortex: a perspective from developmental biology.** *Nat Rev Neurosci* 2009;10:724–35 CrossRef Medline
22. Fischl B. **FreeSurfer.** *Neuroimage* 2012;62:774–81 CrossRef Medline
23. Kong J, Spaeth RB, Wey HY, et al. **S1 is associated with chronic low back pain: a functional and structural MRI study.** *Mol Pain* 2013;9:43 CrossRef Medline
24. Dolman AJ, Loggia ML, Edwards RR, et al. **Phenotype matters: the absence of a positive association between cortical thinning and chronic low back pain when controlling for salient clinical variables.** *Clin J Pain* 2014;30:839–45 CrossRef Medline
25. Pijnenburg M, Caeyenberghs K, Janssens L, et al. **Microstructural integrity of the superior cerebellar peduncle is associated with an impaired proprioceptive weighting capacity in individuals with non-specific low back pain.** *PLoS One* 2014;9:e100666 CrossRef Medline
26. Pijnenburg M, Brumagne S, Caeyenberghs K, et al. **Resting-state functional connectivity of the sensorimotor network in individuals with non-specific low back pain and the association with the sit-stand-to-sit task.** *Brain Connect* 2015;5:303–11 CrossRef Medline
27. Fairbank JC, Pynsent PB. **The Oswestry Disability Index.** *Spine (Phila Pa 1976)* 2000;25:2940–52; discussion 2952 CrossRef Medline
28. Vernon H, Mior S. **The Neck Disability Index: a study of reliability and validity.** *J Manipulative Physiol Ther* 1991;14:409–15 Medline
29. Jensen MP, Karoly P, Braver S. **The measurement of clinical pain intensity: a comparison of six methods.** *Pain* 1986;27:117–26 CrossRef Medline
30. Smeets RJ, Hijdra HJ, Kester AD, et al. **The usability of six physical performance tasks in a rehabilitation population with chronic low back pain.** *Clin Rehabil* 2006;20:989–97 CrossRef Medline
31. Simmonds MJ, Olson SL, Jones S, et al. **Psychometric characteristics and clinical usefulness of physical performance tests in patients with low back pain.** *Spine (Phila Pa 1976)* 1998;23:2412–21 CrossRef Medline
32. Lovibond PF, Lovibond SH. **The structure of negative emotional states: comparison of the Depression Anxiety Stress Scales (DASS) with the Beck Depression and Anxiety Inventories.** *Behav Res Ther* 1995;33:335–43 CrossRef Medline
33. Dale AM, Fischl B, Sereno MI. **Cortical surface-based analysis, I: segmentation and surface reconstruction.** *Neuroimage* 1999;9:179–94 CrossRef Medline
34. Fischl B, Dale AM. **Measuring the thickness of the human cerebral cortex from magnetic resonance images.** *Proc Natl Acad Sci U S A* 2000;97:11050–55 CrossRef Medline
35. Fischl B, Liu A, Dale AM. **Automated manifold surgery: constructing geometrically accurate and topologically correct models of the human cerebral cortex.** *IEEE Trans Med Imaging* 2001;20:70–80 CrossRef Medline
36. Fischl B, van der Kouwe A, Destrieux C, et al. **Automatically parcellating the human cerebral cortex.** *Cereb Cortex* 2004;14:11–22 CrossRef Medline
37. Fischl B, Sereno MI, Dale AM. **Cortical surface-based analysis, II: inflation, flattening, and a surface-based coordinate system.** *Neuroimage* 1999;9:195–207 CrossRef Medline
38. Fischl B, Sereno MI, Tootell RB, et al. **High-resolution intersubject averaging and a coordinate system for the cortical surface.** *Hum Brain Mapp* 1999;8:272–84 Medline
39. Fischl B, Salat DH, van der Kouwe AJ, et al. **Sequence-independent segmentation of magnetic resonance images.** *Neuroimage* 2004;23(suppl 1):S69–84 CrossRef Medline
40. Han X, Jovicich J, Salat D, et al. **Reliability of MRI-derived measurements of human cerebral cortical thickness: the effects of field strength, scanner upgrade and manufacturer.** *Neuroimage* 2006;32:180–94 CrossRef Medline
41. Jovicich J, Czanner S, Greve D, et al. **Reliability in multi-site structural MRI studies: effects of gradient non-linearity correction on phantom and human data.** *Neuroimage* 2006;30:436–43 CrossRef Medline
42. Ségonne F, Dale AM, Busa E, et al. **A hybrid approach to the skull stripping problem in MRI.** *Neuroimage* 2004;22:1060–75 CrossRef Medline
43. Fischl B, Salat DH, Busa E, et al. **Whole brain segmentation: automated labeling of neuroanatomical structures in the human brain.** *Neuron* 2002;33:341–55 CrossRef Medline
44. Desikan RS, Ségonne F, Fischl B, et al. **An automated labeling system for subdividing the human cerebral cortex on MRI scans into gyral based regions of interest.** *Neuroimage* 2006;31:968–80 CrossRef Medline
45. Hoaglin DC, Ingelwicz B. **Fine tuning some resistant rules for outlier labeling.** *J Am Statist Ass* 1987;82:1147–49 CrossRef
46. Pan PL, Zhong JG, Shang HF, et al. **Quantitative meta-analysis of grey matter anomalies in neuropathic pain.** *Eur J Pain* 2015;19:1224–31 CrossRef Medline
47. Smallwood RD, Laird AR, Ramage AE, et al. **Structural brain anomalies and chronic pain: a quantitative meta-analysis of gray matter volume.** *J Pain* 2013;14:663–75 CrossRef Medline
48. Lerch JP, Evans AC. **Cortical thickness analysis examined through power analysis and a population simulation.** *Neuroimage* 2005;24:163–73 CrossRef Medline
49. Lee MC, Tracey I. **Imaging pain: a potent means for investigating pain mechanisms in patients.** *Br J Anaesth* 2013;111:64–72 CrossRef Medline
50. Wager TD, Davidson ML, Hughes BL, et al. **Prefrontal-subcortical pathways mediating successful emotion regulation.** *Neuron* 2008;59:1037–50 CrossRef Medline
51. Rocca MA, Ceccarelli A, Falini A, et al. **Brain gray matter changes in migraine patients with T2-visible lesions: a 3-T MRI study.** *Stroke* 2006;37:1765–70 CrossRef Medline
52. Valfrè W, Rainero I, Bergui M, et al. **Voxel-based morphometry reveals gray matter abnormalities in migraine.** *Headache* 2008;48:109–17 Medline
53. Wiech K, Kalisch R, Weiskopf N, et al. **Anterolateral prefrontal cortex mediates the analgesic effect of expected and perceived control over pain.** *J Neurosci* 2006;26:11501–09 CrossRef Medline
54. Brody AL, Barsom MW, Bota RG, et al. **Prefrontal-subcortical and limbic circuit mediation of major depressive disorder.** *Semin Clin Neuropsychiatry* 2001;6:102–12 CrossRef Medline
55. Shiba Y, Santangelo AM, Roberts AC. **Beyond the medial regions of prefrontal cortex in the regulation of fear and anxiety.** *Front Syst Neurosci* 2016;10:12 CrossRef Medline
56. O’Sullivan K, Dankaerts W, O’Sullivan L, et al. **Cognitive functional therapy for disabling nonspecific chronic low back pain: multiple case-cohort study.** *Phys Ther* 2015;95:1478–88 CrossRef Medline
57. Jensen KB, Kosek E, Wicksell R, et al. **Cognitive behavioral therapy increases pain-evoked activation of the prefrontal cortex in patients with fibromyalgia.** *Pain* 2012;153:1495–503 CrossRef Medline
58. Seminowicz DA, Shpaner M, Keaser ML, et al. **Cognitive-behavioral therapy increases prefrontal cortex gray matter in patients with chronic pain.** *J Pain* 2013;14:1573–84 CrossRef Medline
59. Kiers H, Brumagne S, van Dieën J, et al. **Ankle proprioception is not targeted by exercises on an unstable surface.** *Eur J Appl Physiol* 2012;112:1577–85 CrossRef Medline
60. Stedman TL. *The American Heritage Stedman’s Medical Dictionary.* Boston: Houghton Mifflin Co; 2005

61. Isableu B, Vuillerme N. **Differential integration of kinaesthetic signals to postural control.** *Exp Brain Res* 2006;174:763–68 CrossRef Medline
62. Claeys K, Brumagne S, Dankaerts W, et al. **Decreased variability in postural control strategies in young people with non-specific low back pain is associated with altered proprioceptive reweighting.** *Eur J Appl Physiol* 2011;111:115–23 CrossRef Medline
63. Lord SR. **Aging and falls: causes and prevention.** *J Musculoskelet Neuronal Interact* 2007;7:347 Medline
64. Peyron R, Laurent B, Garcia-Larrea L. **Functional imaging of brain responses to pain: a review and meta-analysis (2000).** *Neurophysiol Clin* 2000;30:263–88 CrossRef Medline
65. May A. **Chronic pain may change the structure of the brain.** *Pain* 2008;137:7–15 CrossRef Medline
66. Schmidt-Wilcke T. **Neuroimaging of chronic pain.** *Best Pract Res Clin Rheumatol* 2015;29:29–41 CrossRef Medline
67. Rakic P. **Radial unit hypothesis of neocortical expansion.** *Novartis Found Symp* 2000;228:30–42; discussion 42–52 Medline

Dynamic Contrast-Enhanced MR Perfusion of Intradural Spinal Lesions

V. Cuvinciuc, M. Viallon, I. Barnaure, M.I. Vargas, K.-O. Lovblad, and S. Haller



ABSTRACT

SUMMARY: Fifteen patients with intradural spinal lesions were examined with an optimized dynamic contrast-enhanced MR perfusion sequence at 1.5T and 3T. SNR and mean contrast-to-noise ratio were better on 3T compared with 1.5T ($P \leq .05$). The goodness of fit of the Tofts and Tofts extended pharmacokinetic models was similar between 1.5T and 3T. Thus, dynamic contrast-enhanced MR perfusion of intradural spinal canal lesions is technically feasible at 1.5T and 3T, with better image quality at 3T.

ABBREVIATIONS: AUC = area under the curve; CNR = contrast-to-noise ratio; DCE = dynamic contrast-enhanced; k^{trans} = volume transfer constant; v_e = extravascular extracellular volume fraction; v_p = blood plasma fraction

Unlike the brain, the spinal cord is examined only by a few advanced imaging techniques; only diffusion-weighted imaging has attracted clinical interest,¹ while spectroscopy remains challenging to implement.² In humans, MR perfusion studies of spinal cord lesions are limited to very few related articles^{3,4} using DSC MR perfusion in the cervical region. However, the susceptibility artifacts and its semiquantitative nature limit this technique. Dynamic contrast-enhanced (DCE) perfusion uses a spoiled fast T1 gradient-echo sequence less sensitive to susceptibility artifacts and with higher spatial resolution. It is also a quantitative technique, not using a contralateral reference tissue.

To the best of our knowledge, our article describes, for the first time, the use of DCE MR perfusion for the evaluation of intradural spinal lesions in humans. Our purpose was to discuss the technical feasibility, pitfalls, and potential clinical advantages.

MATERIALS AND METHODS

Patients

The study was approved by the ethics committee of Geneva University Hospitals, and informed consent of patients was waived. We have included 15 patients (11 men, 4 women; mean age, 48.7 years; age range, 24–72 years) with various intradural spinal lesions (On-line Table 1). Patients with bone lesions were not included.

MR Imaging Examination

The examinations were randomly performed on 2 MR imaging machines, 1.5T Aera (Siemens, Erlangen, Germany) (7 patients) and a 3T Magnetom Trio (Siemens).

T1 mapping was based on 2 T1 acquisitions with 2° and 15° flip angles. The dynamic acquisition was performed in the sagittal plane with a T1 volumetric interpolated breath-hold examination sequence with the following parameters for the 1.5T scanner: TR, 4.55 ms; TE, 1.63 ms; number of averages, 1; FOV, 220 mm; matrix, 154 × 192; flip angle, 12°; 20 sections; thickness, 3-mm; generalized autocalibrating partially parallel acquisition accelerator factor, 2; temporal resolution, 9.5 seconds; total acquisition time, 6 minutes and 3 seconds. The parameters were slightly adapted for the 3T scanner as follows: TR, 5.03 ms; TE, 1.74 ms; number of averages, 1; FOV, 220 mm; matrix, 138 × 192; flip angle, 12°; 20 sections; thickness, 3 mm; generalized autocalibrating partially parallel acquisition accelerator factor, 2; temporal resolution, 7.8; total acquisition time, 5 minutes and 12 seconds. The contrast injection was started after 2–3 measurements; we used a power injector with a 3-mL/s gadobutrol 0.1-mmol/kg bolus (Gadovist, 1.0 mmol/mL; Bayer Schering Pharma, Berlin, Germany), followed by a 3-mL/s saline flush.

The MR imaging protocol also included standard clinical se-

Received June 8, 2016; accepted after revision August 3.

From the Departments of Neuroradiology (V.C., I.B., M.I.V., K.-O.L., S.H.) and Radiology (M.V.), Geneva University Hospitals, Geneva, Switzerland; Centre d'Imagerie Rive Droite (V.C.), Geneva, Switzerland; Université de Lyon, INSA de Lyon, Université Jean-Monnet, CHU de Saint-Etienne, CREATIS CNRS 5220, INSERM 1206, F-42055, Saint-Etienne, France (M.V.); and Affidea Centre de Diagnostique Radiologique de Carouge (S.H.), Geneva, Switzerland.

Paper previously presented at: European Congress of Neuroradiology, September 28 to October 1, 2013; Frankfurt, Germany.

Please address correspondence to Victor Cuvinciuc, MD, Centre d'Imagerie Rive Droite, Rue Chantepoulet 21, 1201 Geneva, Switzerland; e-mail: v.cuvinciuc@cirg.ch

Indicates article with supplemental on-line tables.

Indicates article with supplemental on-line photos.

<http://dx.doi.org/10.3174/ajnr.A4995>

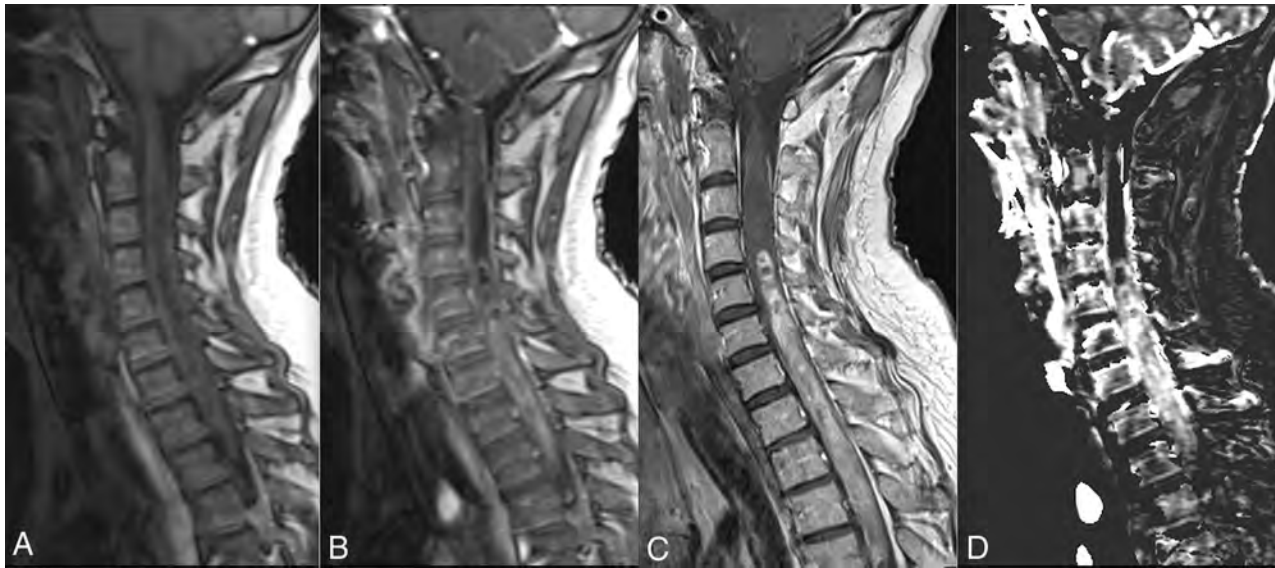


FIG 1. Spinal cord glioblastoma. Baseline (A) and timeframe after enhancement (B) of DCE perfusion show a spinal cord mass at the cervico-thoracic junction. C, Gadolinium-enhanced sagittal T1 spin-echo image shows a contrast-enhanced mass with necrotic/cystic areas. D, V_p map based on the Tofts extended pharmacokinetic modeling shows increased plasmatic volume, suggesting increased neoangiogenesis.

quences (T1, T2, and T1 after the gadolinium injection used for DCE perfusion). At the thoracic level, prevertebral saturation bands were used to compensate for the heart and large-vessel pulsations.

All images were inspected to detect relevant motion artifacts and to identify the contrast enhancement of the lesion, by V.C., a board-certified neuroradiologist with 2 years of experience in DCE MR perfusion imaging and 7 years of experience in neuroradiology.

Image Reconstruction

The data were reconstructed by using commercially available software (Olea Sphere 2.2; Olea Medical, La Ciotat, France). The analysis was performed by 1 reader (V.C.) unaware of the diagnosis at the moment of the analysis. No relevant movement artifacts were encountered; a movement-correction algorithm was applied to compensate for slight physiologic movements. The best vascular input function was selected automatically (usually in the vertebral, intercostal, or lumbar arteries or in the basivertebral veins) and checked visually. Model-independent analysis was performed, and maps of the area under the curve (AUC) of gadolinium were obtained. Pharmacokinetic modeling by using Tofts and Tofts extended models was also performed to derive maps of volume transfer constant (K^{trans}) and extravascular extracellular volume fraction (v_e); for the Tofts extended model, maps of blood plasma fraction (v_p) were also obtained. Maps of χ^2 (expressing the goodness of fit) were obtained for both models.

Image Review and Analysis

2D ROIs were drawn around the enhancing lesions on AUC maps, verified on coregistered gadolinium-enhanced T1 images, and copied on all timeframes of DCE perfusion. The SNR of DCE images was computed by dividing the mean intensity of the ROI baseline voxels by the SD of a large ROI drawn in the air. Relative signal enhancement was computed by dividing the difference between peak signal and mean baseline signal by the mean baseline

signal. The mean contrast-to-noise ratio (CNR) was computed by dividing the difference between the mean intensity of the ROI voxels after gadolinium injection and the mean baseline voxels, by the SD of a large ROI drawn in the air.

ROIs were copied on all the other maps (K^{trans} , v_e , v_p , χ^2). Only voxels with v_e or v_p values between 0 and 1 were used for analysis. Mean values, SD, and 95% confidence intervals were recorded for each of the parameters. SNR, relative signal enhancement, CNR, and χ^2 were compared by using unpaired 2-tailed *t* tests with different variances.

RESULTS

All examinations were technically correct, without significant motion artifacts and with clearly visible contrast enhancement on dynamic series.

SNR and mean CNR were better on 3T compared with 1.5T (On-line Fig 1; $P \leq .05$); relative signal enhancement was similar ($P = .4$).

The goodness of fit was similar for both pharmacokinetic models for most lesions (χ^2 between 100 and 450), except for hemangioblastomas (χ^2 between 450 and 13,000); for a patient with a hemangioblastoma (No. 11), the parametric maps based on the Tofts extended model could not be obtained at all. Goodness of fit was not significantly different between 1.5T and 3T ($P = .09$ for the Tofts model and $P = .1$ for Tofts extended model).

The values of model-free AUC and various pharmacokinetic parameters for all the patients are presented in On-line Tables 2 and 3. Some examples of pathologies are presented in Fig 1 (spinal cord glioblastoma) and in the On-line Figs 2–4 (meningioma and schwannoma, respectively; enhancement curves of representative cases of all the pathologies studied).

DISCUSSION

In this study, we report our preliminary results of DCE perfusion MR imaging for intradural spinal lesions at 1.5T and 3T. Previous

reports^{3,4} have used DSC MR perfusion only at the cervical level; its implementation at the dorsal level is difficult because of the susceptibility artifacts of the lungs and the relatively low spatial resolution compared with the size of the spinal cord. We have used DCE perfusion at any level of the spinal canal, with clearly visible contrast enhancement of the lesions and without relevant motion artifacts at both 1.5 and 3T.

The higher SNR and CNR found in our study at 3T compared with 1.5T, in the context of similar mean relative signal enhancement increase of the explored lesions at both magnetic fields, are coherent with the well-known accepted superiority of 3T already reported by previous studies.⁵ This signal increase could be used to decrease section thickness, increase in-plane resolution, or decrease acquisition time.

The AUC is a model-free parameter that describes the uptake of gadolinium in the tissue of interest, and it has been shown to depend on the blood flow, vessel permeability, and interstitial space.⁶ AUC has the advantages of not requiring a vascular input function and not depending on complex pharmacokinetic modeling.

Pharmacokinetic modeling is needed to obtain parameters better describing the microvascular environment of the lesions (ie, capillary permeability, plasma volume, extravascular extracellular space, and so forth).⁷ This modeling is challenging because it depends on good quality of the sequence (high spatial and temporal resolution), few movement artifacts, and good vascular input function. We did not encounter any relevant movement artifacts. The movement-correction algorithm of the software compensated for some slight movement; the best vascular input function was selected automatically by the software for all patients as the earliest and highest enhancement in the examined area. In our study, the goodness of fit was similar between 1.5T and 3T for both models. χ^2 was similar for most lesions (between 100 and 450), except for hemangioblastomas (between 450 and 13,000). Hemangioblastomas have an abundant expression of vascular endothelial growth factor, responsible for increased vascularization and permeability.⁸ A higher temporal resolution could be necessary to properly analyze the microcirculation of such hypervascular lesions.

The limits of our preliminary study are the following: First, the relatively low number of patients implies that any differentiation among various lesions based on DCE parameters should be con-

firmed in larger studies. Second, the differences in 3T versus 1.5T could partly be related to the heterogeneous nature of the lesions, their location, and the inherent differences of the MR imaging protocols, bores, and coils; further studies are necessary to establish whether this technical superiority of 3T compared with 1.5T results in superior clinical results. Third, the DCE protocol increases the total acquisition time of the MR imaging examination by about 8 minutes; therefore, the diagnostic utility of these new sequences should be better established. Nonetheless, we are confident that DCE perfusion could become a valuable adjunct in a spinal cord MR imaging protocol due to the paucity of advanced MR images available at this level and the potential richness of the information obtained on DCE perfusion.

CONCLUSIONS

DCE perfusion for intradural spinal canal lesions is feasible at 1.5T and 3T, with a better quality at 3T. In our opinion, DCE has the potential to become a valuable tool for the advanced imaging of the spinal cord and could be confirmed by further studies.

REFERENCES

1. Andre JB, Bammer R. **Advanced diffusion-weighted magnetic resonance imaging techniques of the human spinal cord.** *Top Magn Reson Imaging* 2010;21:367–78 CrossRef Medline
2. Hock A, Henning A, Boesiger P, et al. **(1)H-MR spectroscopy in the human spinal cord.** *AJNR Am J Neuroradiol* 2013;34:1682–89 CrossRef Medline
3. Liu X, Germin BI, Ekholm S. **A case of cervical spinal cord glioblastoma diagnosed with MR diffusion tensor and perfusion imaging.** *J Neuroimaging* 2011;21:292–96 CrossRef Medline
4. Liu X, Kolar B, Tian W, et al. **MR perfusion-weighted imaging may help in differentiating between nonenhancing gliomas and non-neoplastic lesions in the cervicomedullary junction.** *J Magn Reson Imaging* 2011;34:196–202 CrossRef Medline
5. Ethofer T, Mader I, Seeger U, et al. **Comparison of longitudinal metabolite relaxation times in different regions of the human brain at 1.5 and 3 Tesla.** *Magn Reson Med* 2003;50:1296–301 CrossRef Medline
6. Evelhoch JL. **Key factors in the acquisition of contrast kinetic data for oncology.** *J Magn Reson Imaging* 1999;10:254–59 Medline
7. Tofts PS. **Modeling tracer kinetics in dynamic Gd-DTPA MR imaging.** *J Magn Reson Imaging* 1997;7:91–101 CrossRef Medline
8. Berkman RA, Merrill MJ, Reinhold WC, et al. **Expression of the vascular permeability factor/vascular endothelial growth factor gene in central nervous system neoplasms.** *J Clin Invest* 1993;91:153–59 CrossRef Medline

First-Pass Contrast-Enhanced MRA for Pretherapeutic Diagnosis of Spinal Epidural Arteriovenous Fistulas with Intradural Venous Reflux

S. Mathur, S.P. Symons, T.J. Huynh, P. Muthusami, W. Montanera, and A. Bharatha



ABSTRACT

BACKGROUND AND PURPOSE: Spinal epidural AVFs are rare spinal vascular malformations. When there is associated intradural venous reflux, they may mimic the more common spinal dural AVFs. Correct diagnosis and localization before conventional angiography is beneficial to facilitate treatment. We hypothesize that first-pass contrast-enhanced MRA can diagnose and localize spinal epidural AVFs with intradural venous reflux and distinguish them from other spinal AVFs.

MATERIALS AND METHODS: Forty-two consecutive patients with a clinical and/or radiologic suspicion of spinal AVF underwent MR imaging, first-pass contrast-enhanced MRA, and DSA at a single institute (2000–2015). MR imaging/MRA and DSA studies were reviewed by 2 independent blinded observers. DSA was used as the reference standard.

RESULTS: On MRA, all 7 spinal epidural AVFs with intradural venous reflux were correctly diagnosed and localized with no interobserver disagreement. The key diagnostic feature was arterialized filling of an epidural venous pouch with a refluxing radicular vein arising from the arterialized epidural venous system.

CONCLUSIONS: First-pass contrast-enhanced MRA is a reliable and useful technique for the initial diagnosis and localization of spinal epidural AVFs with intradural venous reflux and can distinguish these lesions from other spinal AVFs.

ABBREVIATIONS: SDAVF = spinal dural arteriovenous fistula; SEAVF = spinal epidural arteriovenous fistula

Spinal epidural or extradural arteriovenous shunting lesions, commonly described as spinal epidural AVFs (SEAVFs), are rare and poorly understood vascular lesions of the spine. These have been described in the literature as case reports or in a few small case series. Their presentation can overlap with that of the more common spinal dural AVFs (SDAVFs) if there is associated intradural venous reflux and congestive myelopathy.^{1,2} Compared with SDAVFs, the angioarchitecture of SEAVFs with intradural reflux is usually more complex, with the radicular vein arising from the arterialized epidural venous system and with a greater likelihood of multiple arterial feed-

ers and draining veins.¹ Diagnosis on noninvasive imaging could alert the angiographer about this. In addition, because the point of reflux into the radicular vein may be at a different level than the arterialized epidural pouch, preangiographic diagnosis may guide DSA for use of appropriate fields of view and delayed runs if required. It could also forewarn the interventional radiologist and/or surgeon to potential greater difficulty in curing these lesions because, in addition to disconnection of the fistula with radicular refluxing vein, obliteration of the arterialized epidural pouch is typically required. In addition, the cross-sectional nature of MRA could depict the involved portion of the epidural venous system in a complementary fashion to DSA, with the ability to view the venous pouch in multiple planes. As such, newer treatments like percutaneous embolization of the epidural venous pouch may benefit from MRA depiction of the lesion.³ The purpose of this study was to evaluate the performance of first-pass contrast-enhanced MRA to diagnose and localize SEAVFs with intradural venous reflux and distinguish them from other spinal AVFs by using DSA as the criterion standard.

MATERIALS AND METHODS

Study Patients

Approval for this retrospective study was obtained from the local institutional research ethics board of St. Michael's Hospital. Forty-

Received June 13, 2016; accepted after revision August 16.

From the Division of Diagnostic and Interventional Neuroradiology, Department of Medical Imaging (S.M., T.J.H., P.M., W.M., A.B.), St. Michael's Hospital, University of Toronto, Toronto, Ontario, Canada; and Division of Neuroradiology, Department of Medical Imaging (S.M., S.P.S., T.J.H.) and Department of Otolaryngology–Head and Neck Surgery (S.P.S.), Sunnybrook Health Sciences Centre, University of Toronto, Toronto, Ontario, Canada.

Paper previously presented, in part, at: Annual Meeting of the American Society of Neuroradiology, May 23–26, 2016; Washington, DC.

Please address correspondence to Aditya Bharatha, MD, FRCPC, Division of Diagnostic and Interventional Neuroradiology, Department of Medical Imaging, St. Michael's Hospital, 30 Bond St, Room 3-077CC, Toronto, ON M5B 1W8, Canada; e-mail: BharathaA@smh.ca

Indicates article with supplemental on-line table.

<http://dx.doi.org/10.3174/ajnr.A5008>

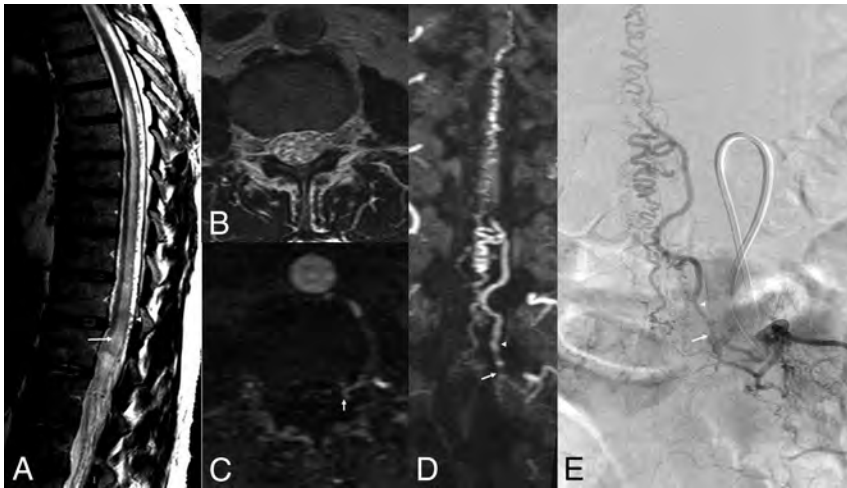


FIG 1. Imaging features of an SDAVF. Sagittal T2WI (A) shows high signal in cord (arrow) and serpiginous flow voids (arrowhead). The ventral epidural space is clear on axial T2WI (B). Axial (C) and coronal (D) reconstructions of MRA-MIP show tuft of vessels at the left L2 dural sleeve (arrow) corresponding to the site of fistula (arrow) on frontal projection on DSA (E). The radicular vein is shown by arrowhead on images D and E.

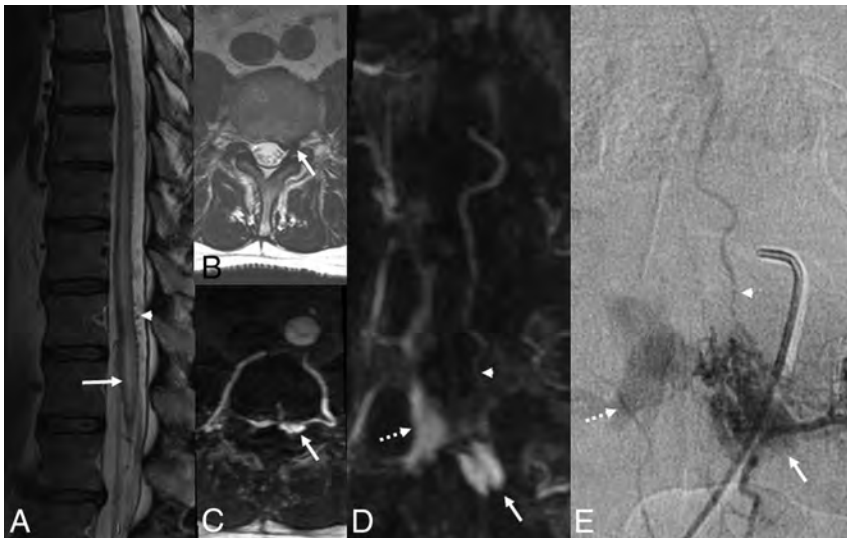


FIG 2. Patient 1. Imaging features of SEAVF with intradural venous reflux. Sagittal T2WI (A) shows high signal in cord (arrow) and serpiginous flow voids (arrowhead). Axial T2WI (B) and axial reconstruction of MRA-MIP (C) show the arterialized left anterolateral epidural venous pouch (arrow). Coronal reconstruction of MRA-MIP (D) and frontal projection on DSA (E) show arterialized contralateral epidural veins (dashed arrow) and the radicular vein (arrowhead) arising from the superior aspect of the venous pouch (arrow).

two consecutive patients referred to the St. Michael's Hospital Neurovascular Program with a clinical and/or radiologic suspicion of spinal AVF during the study period (2000–2015) underwent pretherapeutic MR imaging, MRA, and DSA at a single institution. Clinical suspicion was based on typical clinical history of progressive myelopathy and suggestive MR imaging features including nonresolving or progressive cord edema, cord enhancement, and intradural serpentine flow voids and/or enhancing vascularity. Patients with a history of treated spinal AVF were excluded. Between MR imaging, MRA, and DSA studies, patients did not receive any treatment for a spinal AVF.

Note: Some study patients from our data base have been included in another research paper testing a different research ques-

tion (“First-Pass Contrast-Enhanced MR Angiography in Evaluation of Treated Spinal Arteriovenous Fistulas: Is Catheter Angiography Necessary?” [also in this issue of *AJNR*]).

MR Imaging and MRA Technique

All patients underwent conventional whole-spine MR imaging on a 1.5T Inera Achieva (Philips, Best, the Netherlands), using a dedicated 5-channel spinal coil with the patient in the supine position, including standard sagittal T2WI, sagittal T1WI, axial T2WI, post-contrast sagittal T1WI, and axial T1WI.

First-pass or bolus-chase contrast-enhanced MRA was performed by using a timed-run technique. The sagittal plane was selected on 3 plane localizers with a field of view of 33 cm (craniocaudal), extending approximately from T3 to L4 vertebral levels. The selection of field of view was based on the clinical/radiologic suspicion of the location of the fistula. After intravenous injection of a 2-mL test bolus of contrast agent, the time taken for filling of the abdominal aorta on MR fluoroscopy was used as delay time for acquisition. Thereafter, 18 mL of contrast agent was administered intravenously at 2 mL/s injection rate by using a 2-cylinder MR compatible injector (Spectris; MedRad, Indianola, Pennsylvania) followed by a 20-mL saline bolus. Studies used gadolinium-based contrast agents, including Omniscan (gadodiamide; GE Healthcare, Piscataway, New Jersey) or, more recently, MultiHance (gadobenate dimeglumine; Bracco Diagnostics, Princeton, New Jersey). Manually triggered, single-phase, 3D acquisition was performed with 400×512 matrix and 0.82×1.08 mm in-plane resolution reconstructed to

0.64×0.64 mm with 0.9-mm section thickness. Scan parameters were: TR = 5.4 ms, TE = 1.76 ms, flip angle = 30° , NEX = 1, overcontiguous sections with scan time of 47 seconds. Automated postprocessing produced background subtracted image sets with multiplanar MIPs.

DSA Technique

Spinal DSA examinations were performed on a dedicated bipolar neuroangiographic system (Artis; Siemens, Erlangen, Germany) via a femoral approach under general or local anesthesia. Multiple selective arterial injections with iodinated contrast agent (Omnipaque 300; GE Healthcare) were performed into the arteries likely to supply the spinal AVF. Magnification, oblique, and



FIG 3. Montage of SEAVFs (patients 2–7). A, Sagittal T2 showing edematous cord with perimedullary flow voids. B, Contrast-enhanced MRA and C, DSA show arterialized epidural venous pouch (arrow), refluxing radicular vein (arrowhead), and additional arterialized epidural veins (dashed arrow). Note that the refluxing radicular vein arises from the arterialized epidural venous pouch except in patient 2, where it arises from the arterialized epidural veins superior to the level of pouch.

high-frame-rate angiography were used where appropriate. The arteries expected to be supplying an AVF based on the MRA findings were catheterized early during the procedure. After identification of the fistula, contralateral injection at the same level and bilateral injections at least 2 vertebral levels above and below the site of the fistula were performed. A complete spinal angiography was undertaken if the AVF was not identified at the anticipated level or MRA was negative for spinal AVF.

Imaging Analysis

Review of MR imaging and MRA studies was independently performed by 2 experienced neuroradiologists (S.P.S. and A.B.) with 13 and 7 years of experience, respectively, without knowledge of the DSA findings or diagnosis.

On the MRA study, the observers made a positive or negative diagnosis of SEAVF with intradural venous reflux and noted the location with regard to vertebral level and side. The presence or absence and location (vertebral level, right/left, ventral/dorsal) of arterialized epidural venous pouch and re-

flux into the radicular vein as well as presence or absence of additional arterialized epidural veins were noted. The readers had access to source images as well as multiplanar reformats on dedicated workstations.

On conventional MR imaging studies, the presence or absence of intradural serpentine flow voids, T2 hyperintensity of the spinal cord, and cord enhancement were recorded.

Upon completion of review of MR imaging and MRA studies, the observers recorded their findings on DSA studies, including presence or absence of a SEAVF with intradural venous reflux, the location, and key angioarchitectural features of the lesion. The observers again reviewed the conventional MR images to retrospectively identify the arterialized epidural venous pouch. DSA was used as the criterion standard.

RESULTS

There were 31 patients positive for spinal AVFs, of which 7 (23%) were SEAVFs with intradural (radicular/perimedullary) venous reflux. The clinical and MRA findings of these 7 patients are summarized in the On-line Table. The average age of patients was 62 years (range, 54–75 years), and all patients were male. All patients presented with progressive paraparesis. Urinary bladder dysfunction was present in 4 of 7 patients. History of trauma or neurofibromatosis was not recorded for any of the patients. The average duration of symptoms was 4.4 months (range, 0.5–12 months). The average time between MRA and DSA studies was 5 days (range, 0–19 days).

On MRA, the correct diagnosis of SEAVF with intradural venous reflux was successfully made for 7 patients. MRA accurately distinguished SEAVFs with intradural venous reflux from other spinal AVFs (20 SDAVFs, 3 perimedullary spinal AVFs, 1 AVF of filum terminale) (Fig 1) and from the 11 patients with negative DSA with 100% sensitivity, specificity, positive predictive value, and negative predictive value. Lesion localization with respect to vertebral level and location within the spinal canal (right/left, ventral/dorsal) of the epidural venous pouch and connection with the radicular vein was correct in all the cases. However, additional feeders from the contralateral side in 2 cases, with multiple levels in 1 case, that were not identified on MRA were identified on DSA. The radicular vein was correctly detected on MRA as arising from the arterialized epidural pouch (6 cases) or epidural venous system at a different level (1 case). In addition to the epidural venous pouch, vessels conforming to the shape of the epidural venous system were correctly identified to demonstrate arterialized filling

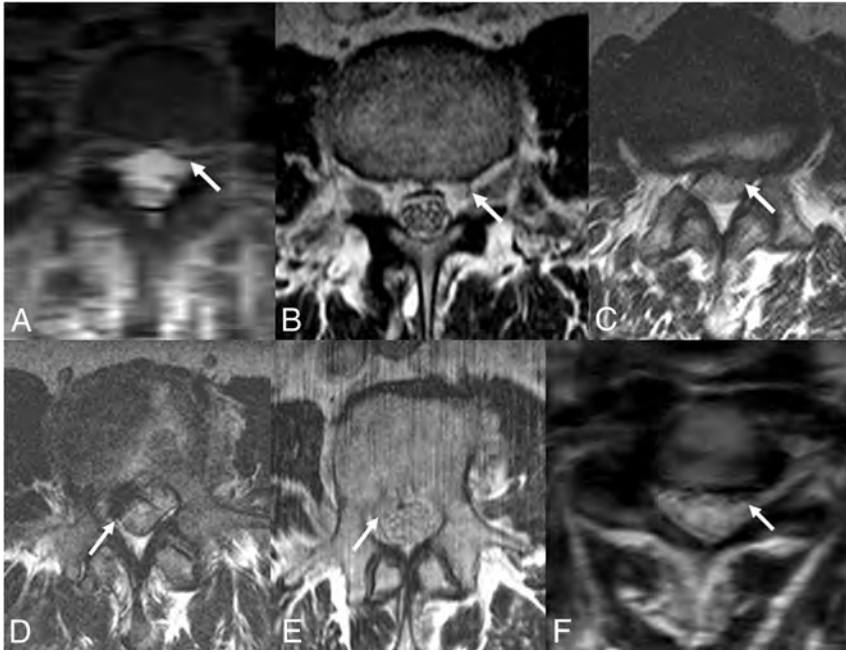


FIG 4. Epidural venous pouch on T2WI (patients 2–7). Epidural venous pouch (*arrow*) on axial T2WI. The pouch is a subtle finding with variable signal and simulates disc herniation and, therefore, is hard to identify without MRA correlation.

in 4 of 7 cases, which matched the catheter angiographic findings. There was no interobserver disagreement. The key diagnostic features of SEAVF distinguishing it from SDAVF were arterialized epidural venous pouch and a refluxing radicular vein from the arterialized epidural pouch or arterialized epidural veins (at a different level) (Figs 2 and 3).

All MRA studies in the patient population achieved arterial phase imaging except 1. In this particular case, MRA was motion-degraded with mild venous contamination, which was identified by epidural filling at all scanned levels; no spinal AVF was found on DSA.

On MR imaging, T2 hyperintensity of cord, perimedullary serpentine flow voids, and patchy mild cord enhancement were seen in all 7 (100%) patients. All (24/24, 100%) of the remaining spinal AVFs demonstrated T2 hyperintensity of cord, perimedullary serpentine flow voids, and patchy mild cord enhancement. No significant difference was found in these conventional MR imaging features of SEAVF with intradural reflux compared with other spinal AVFs ($P > .05$).

In addition, the epidural arterialized venous pouch seen on MRA studies was retrospectively identified in all cases on conventional MR images. On T2WI, compared with the signal intensity of paraspinal muscles, the pouch was hyperintense in 5 patients and hypointense in 2 patients (Figs 2 and 4). The variable signal and resemblance to disc herniation makes the pouch a subtle finding and difficult to identify without MRA correlation. The MR imaging was negative for epidural hematoma in all the cases.

DISCUSSION

SEAVFs with intradural venous reflux are distinct from the more common SDAVFs. SDAVFs are typically lesions with a single site of fistula at the dural sleeve covering the nerve root, commonly with a single radiculomeningeal artery feeder and draining intradural radicular vein refluxing into the perimedullary venous system. Perimedullary and filum terminale fistulas are variants in

which the connection is intradural between radiculopial or radiculomedullary artery and intradural vein, without proximal filling of the epidural system. In SEAVF, which is another variant, the fistula is located in the epidural space and may be associated with 1 or multiple feeding arteries and drain into the epidural venous system.¹ These can be asymptomatic because of an antireflux mechanism at the dural sleeve related to inherent narrowing and a zigzag course of the radicular vein while crossing the dura.⁴ Failure of the antireflux mechanism and/or increased venous pressures due to thrombosis of other outflow veins can result in reflux into radicular and perimedullary veins and venous congestion of the cord causing myelopathy.² Intradural reflux from the epidural venous system can occur far from the epidural fistula site, which was seen in 1 case in our study and has been described previously.⁵ Multiple feeders were seen less frequently in our study (2 of 7 cases)

compared with previous reports.^{1,6} Another way these lesions can manifest is by radiculopathy or myelopathy due to direct compression of nerve roots or cord by enlarged epidural veins;^{7,8} however, this presentation is not discussed in our paper, which focuses on patients who present with congestive myelopathy simulating SDAVF. Because of the difference in angioarchitecture of SEAVFs with intradural venous reflux compared with SDAVFs, the approach to treating these lesions can be different and may be more challenging. Both surgery and endovascular embolization have been described, and a combination of these techniques has also been used.^{1,5,6,9} Percutaneous embolization of the epidural venous pouch has also been described.³ Pretherapeutic localization and diagnosis through the use of noninvasive imaging may be helpful in expediting subsequent DSA and for planning treatment.

It is unclear if SEAVFs are congenital or acquired; however, association with previous surgery and trauma^{10,11} as well as neurofibromatosis^{12,13} has been reported. None of the patients in our study had any such clinical history. In a study by van Rooij et al,¹⁴ 6% of the spinal AVFs in the study cohort were found to be SEAVFs, compared with 23% found in our study. A literature review of 45 ventral SEAVFs performed by Kiyosue et al⁶ found that SEAVFs are more common among older males (M:F ratio, 2.4:1; average age, 63.9 years) in the lumbar spine, with progressive myelopathy being the most common symptom, which is similar to the results in our study. In their review, the average duration of symptoms was 10 months,⁶ greater than our study (4.4 months).

The clinical and conventional MR imaging findings (cord congestion, enhancement, and serpentine flow voids) in SDAVFs and SEAVFs with intradural reflux are similar^{1,2} because of the similar underlying pathomechanism of venous congestive myelopathy present in both conditions. However, our study indicates that MRA can reliably distinguish these lesions. The key diagnostic

features of SEAVFs on MRA are the presence of an arterialized epidural venous pouch and/or filling of the epidural venous system and a refluxing radicular vein. Conversely, in SDAVF, there is a tuft of vessels at the dural sleeve leading to the refluxing radicular vein without arterialized epidural pouch/veins (Fig 1). Although the arterialized epidural venous pouch in SEAVFs could be seen in retrospect on conventional MR images in our study, it was a subtle finding that would be difficult to pick up prospectively. The signal characteristics of the venous pouch on MR imaging were variable, likely because of variable or turbulent flow, adding to the difficulty in identification.

Many studies have proved the utility of MRA for evaluation of SDAVFs, which facilitates the subsequent conventional angiography.¹⁵⁻¹⁷ Rangel-Castilla et al¹⁸ found DynaCT (Siemens) useful in evaluation of SEAVFs and proposed a novel classification system for these lesions. To the best of our knowledge, our study is the first to evaluate the diagnostic performance of MRA in pretherapeutic noninvasive evaluation of SEAVF with intradural reflux. Our findings suggest high accuracy and reliability of MRA for detection and localization of these lesions and distinguishing them from SDAVFs. This may assist in treatment planning. In 2 cases, additional feeders were identified with DSA, which highlights the limitation of MRA in delineating small vessels.

Limitations of our study include its retrospective design causing selection bias and the small number of patients because of the rarity of this condition. The study was focused toward diagnosis and localization of the lesions and did not attempt to completely characterize the angioarchitecture on MRA, for which DSA remains mandatory. The MRA technique used in the study is a single-phase first-pass MRA technique rather than multiphase time-resolved MRA. This is not a major limitation because although the time-resolved techniques may provide more temporal information, they are limited by lower spatial resolution; hence, we prefer to use first-pass contrast-enhanced MRA. In addition, we have been able to obtain reasonably consistent arterial phase imaging by using this technique at our institute.

CONCLUSIONS

First-pass contrast-enhanced MRA is a reliable and useful technique for the initial diagnosis and localization of spinal epidural AVFs with intradural venous reflux and can distinguish them from spinal dural AVFs.

REFERENCES

- Silva N Jr, Januel AC, Tall P, et al. **Spinal epidural arteriovenous fistulas associated with progressive myelopathy. Report of four cases.** *J Neurosurg Spine* 2007;6:552-58 CrossRef Medline
- Krings T, Mull M, Bostroem A, et al. **Spinal epidural arteriovenous fistula with perimedullary drainage. Case report and pathomechanical considerations.** *J Neurosurg Spine* 2006;5:353-58 CrossRef Medline
- Ramanathan D, Levitt MR, Sekhar LN, et al. **Management of spinal epidural arteriovenous fistulas: interventional techniques and results.** *J Neurointerv Surg* 2014;6:144-49 CrossRef Medline
- Tadie M, Hemet J, Aaron C, et al. **Le dispositif protecteur anti-reflux des veines de la moelle.** *Neurochirurgie* 1979;25:28-30
- Pirouzmand F, Wallace MC, Willinsky R. **Spinal epidural arteriovenous fistula with intramedullary reflux. Case report.** *J Neurosurg* 1997;87:633-35 CrossRef Medline
- Kiyosue H, Tanoue S, Okahara M, et al. **Spinal ventral epidural arteriovenous fistulas of the lumbar spine: angioarchitecture and endovascular treatment.** *Neuroradiology* 2013;55:327-36 CrossRef Medline
- Willinsky R, terBrugge K, Montanera W, et al. **Spinal epidural arteriovenous fistulas: arterial and venous approaches to embolization.** *AJNR Am J Neuroradiol* 1993;14:812-17 Medline
- Asai J, Hayashi T, Fujimoto T, et al. **Exclusively epidural arteriovenous fistula in the cervical spine with spinal cord symptoms: case report.** *Neurosurgery* 2001;48:1372-75; discussion 1375-76 CrossRef Medline
- Clarke MJ, Patrick TA, White JB, et al. **Spinal extradural arteriovenous malformations with parenchymal drainage: venous drainage variability and implications in clinical manifestations.** *Neurosurg Focus* 2009;26:E5 CrossRef Medline
- Lim SM, Choi IS. **Spinal epidural arteriovenous fistula: a unique pathway into the perimedullary vein. A case report.** *Interv Neuroradiol* 2009;15:466-69 Medline
- Khalidi A, Hacein-Bey L, Origitano TC. **Spinal epidural arteriovenous fistula with late onset perimedullary venous hypertension after lumbar surgery: case report and discussion of the pathophysiology.** *Spine (Phila Pa 1976)* 2009;34:E775-79 CrossRef Medline
- Hoffman HB, Bagan M. **Cervical epidural arteriovenous malformation occurring with a spinal neurofibroma. Case report.** *J Neurosurg* 1967;26:346-51 CrossRef Medline
- Kähärä V, Lehto U, Ryymin P, et al. **Vertebral epidural arteriovenous fistula and radicular pain in neurofibromatosis type I.** *Acta Neurochir (Wien)* 2002;144:493-96 CrossRef Medline
- van Rooij WJ, Sluzewski M, Majoie CB. **Spinal dural arteriovenous fistulas with primary epidural shunting.** *Eur J Radiol Extra* 2007;62:39-41 CrossRef
- Farb RI, Kim JK, Willinsky RA, et al. **Spinal dural arteriovenous fistula localization with a technique of first-pass gadolinium-enhanced MR angiography: initial experience.** *Radiology* 2002;222:843-50 CrossRef Medline
- Lindenholz A, TerBrugge KG, van Dijk JM, et al. **The accuracy and utility of contrast-enhanced MR angiography for localization of spinal dural arteriovenous fistulas: the Toronto experience.** *Eur Radiol* 2014;24:2885-94 CrossRef Medline
- Saindane AM, Boddu SR, Tong FC, et al. **Contrast-enhanced time-resolved MRA for pre-angiographic evaluation of suspected spinal dural arterial venous fistulas.** *J Neurointerv Surg* 2015;7:135-40 CrossRef Medline
- Rangel-Castilla L, Holman PJ, Krishna C, et al. **Spinal extradural arteriovenous fistulas: a clinical and radiological description of different types and their novel treatment with Onyx.** *J Neurosurg Spine* 2011;15:541-49 CrossRef Medline

First-Pass Contrast-Enhanced MR Angiography in Evaluation of Treated Spinal Arteriovenous Fistulas: Is Catheter Angiography Necessary?

S. Mathur, S.P. Symons, T.J. Huynh, T.R. Marotta, R.I. Aviv, and A. Bharatha



ABSTRACT

BACKGROUND AND PURPOSE: Catheter angiography is typically used for follow-up of treated spinal AVFs. The purpose of this study was to determine the diagnostic performance and utility of first-pass contrast-enhanced MRA in the posttreatment evaluation of spinal AVFs compared with DSA.

MATERIALS AND METHODS: A retrospective review was performed of all patients at our tertiary referral hospital (from January 2000 to April 2015) who underwent spine MR imaging, first-pass contrast-enhanced MRA, and DSA after surgical and/or endovascular treatment of a spinal AVF. Presence of recurrent or residual fistula on MRA, including vertebral level of the recurrent/residual fistula, was evaluated by 2 experienced neuroradiologists blinded to DSA findings. Posttreatment conventional MR imaging findings were also evaluated, including presence of intramedullary T2 hyperintensity, perimedullary serpentine flow voids, and cord enhancement. The performance of MRA and MR imaging findings for diagnosis of recurrent/residual fistula was determined by using DSA as the criterion standard.

RESULTS: In total, 28 posttreatment paired MR imaging/MRA and DSA studies were evaluated in 22 patients with prior spinal AVF and 1 patient with intracranial AVF with prior cervical perimedullary venous drainage. Six image sets of 5 patients demonstrated recurrent/residual disease at DSA. MRA correctly identified all cases with recurrent/residual disease with 1 false-positive (sensitivity, 100%; specificity 95%; $P < .001$), with correct localization in all cases without interobserver disagreement. Conventional MR imaging parameters were not significantly associated with recurrent/residual spinal AVF.

CONCLUSIONS: First-pass MRA demonstrates high sensitivity and specificity for identifying recurrent/residual spinal AVFs and may potentially substitute for DSA in the posttreatment follow-up of patients with spinal AVFs.

ABBREVIATION: SAVF = spinal AVF

Spinal AVFs (SAVFs) can cause radicular/perimedullary venous reflux and present with progressive myelopathy due to cord congestion. The goal of treatment is to disconnect the refluxing vein to protect the cord from further damage. The most common vascular lesion to present in this fashion is

the spinal dural AVF. However, similar clinical and radiologic appearances can occur with intracranial dural fistulas draining into the spinal venous system, epidural fistulas with intrathecal venous reflux as well as perimedullary and filum terminale fistulas. Prevalence of recurrent or residual fistulas after treatment of SAVFs ranges from 3.4% to 27.8% and is associated with progressive myelopathy and morbidity.¹ Fistula recurrence may occur early within 1 month after treatment or present in delayed fashion years after successful treatment.¹ Conventional spine MR imaging findings of SAVF, including perimedullary flow voids, intramedullary T2 hyperintensity, and cord enhancement, are not reliable markers of residual/recurrent fistula.^{2,3} Using clinical symptoms alone to assess for residual or recurrent disease may result in delayed diagnosis and irreversible progression of symptoms.⁴ Therefore, posttherapy evaluation of patients with previously treated SAVF is commonly performed to ensure complete fistula occlusion.

Received June 14, 2016; accepted after revision August 9.

From the Division of Diagnostic and Interventional Neuroradiology, Department of Medical Imaging (S.M., T.J.H., T.R.M., A.B.), St. Michael's Hospital, University of Toronto, Toronto, Ontario, Canada; and Division of Neuroradiology, Department of Medical Imaging (S.M., T.J.H., R.I.A., S.P.S.) and Department of Otolaryngology—Head and Neck Surgery (S.P.S.), Sunnybrook Health Sciences Centre, University of Toronto, Toronto, Ontario, Canada.

Paper previously presented in part at: Annual Meeting of the American Society of Neuroradiology, April 25–30, 2015; Chicago, Illinois.

Please address correspondence to Aditya Bharatha, MD, FRCPC, Department of Medical Imaging, St. Michael's Hospital, 30 Bond St, Room 3-077CC, Toronto, ON, Canada M5B 1W8; e-mail: bharathaa@smh.ca

Indicates article with Supplemental online table.

<http://dx.doi.org/10.3174/ajnr.A4971>

DSA remains the criterion standard test; however, it is an invasive test associated with some procedural risks.⁵ Spine MRA may be a useful noninvasive tool for initial posttreatment evaluation of SAVFs and may have the potential to be a substitute for DSA for this indication.^{3,4,6} In this study, we evaluated the performance of MRA for identifying recurrent/residual SAVF posttreatment, compared with DSA and conventional MR imaging findings.

MATERIALS AND METHODS

Patients

After institutional ethics board approval, we retrospectively reviewed all consecutive patients (from January 2000 to April 2015) who underwent spine MR imaging, including MRA and DSA at our institution (St. Michael's Hospital). Patients were included in the study if they had imaging as part of follow-up of a treated SAVF (including spinal dural, epidural, perimedullary, and filum terminale AVFs) and/or for suspected residual/recurrent SAVF posttreatment. At our tertiary care referral hospital, patients routinely have DSA after SAVF treatment to confirm absence of residual fistula. MR imaging/MRA is typically performed at 1–6-month follow-up, depending on neurosurgeon and/or protocolling neuroradiologist preference, or earlier if there is clinical concern, with subsequent DSA performed as clinically indicated. There were no treatments for SAVFs between the MR imaging/MRA and DSA studies. For the purposes of this study, MR imaging/MRA studies were compared with the DSA performed closest to the date of the MR imaging/MRA study. Patient demographics and days between MR imaging/MRA, DSA, and treatments were retrieved from retrospective chart review.

Note: Some study subjects from our data base have been included in another research paper testing a different research question (“First-Pass Contrast-Enhanced MR Angiography for Pretherapeutic Diagnosis of Spinal Epidural Arteriovenous Fistulas with Intradural Venous Reflux,” also in this issue).

MR Imaging and MRA Technique

All MR imaging and MRA studies were performed on a 1.5T system (Intera Achieva; Philips Healthcare, Best, the Netherlands) by using a dedicated 5-channel spine coil in supine position. Conventional whole-spine MR imaging sequences included sagittal T2WI, sagittal T1WI, axial T2WI, and postcontrast sagittal and axial T1WI.

First-pass MRA was performed by using a manually triggered timed-delay technique. Three-plane spine localizers were obtained, and the sagittal plane was selected for imaging. The FOV was 33 cm craniocaudally, and imaged location was selected by a neuroradiologist based on the location of the treated SAVF. Studies were performed by using gadolinium-based contrast agents including Omniscan (gadodiamide; GE Healthcare, Piscataway, New Jersey) or, more recently, MultiHance (gadobenate dimeglumine; Bracco Diagnostics, Princeton, New Jersey). Acquisition delay time was determined by using a 2-mL IV contrast test bolus, and peak enhancement of the abdominal aorta was measured by using 2D MR fluoroscopy. This was followed by intravenous injection of 18 mL of contrast agent at 2 mL/s injection rate by using an MR compatible power injector (Spectris; Medrad, Indianola, Pennsylvania) followed by 20-mL saline bolus. This imaging pro-

col was used for all patients. Manually triggered, single-phase, 3D acquisition was performed with scan parameters as follows: 400 × 512 matrix, 0.82 × 1.08 mm in-plane resolution reconstructed to 0.64 × 0.64 mm with 0.9-mm section thickness, TR = 5.4 ms, TE = 1.76 ms, flip angle = 300, NEX = 1, overcontiguous sections, and scan time of 47 seconds. Background subtracted image sets with multiplanar MIP images were obtained by automated postprocessing.

DSA Technique

A dedicated biplanar neuroangiographic system (Artis; Siemens, Erlangen, Germany) was used for the spinal DSA examinations. A femoral approach was used under general or local anesthesia. Iodinated contrast agent (Omnipaque 300; GE Healthcare) was selectively injected bilaterally into segmental arteries at the level of the treated fistula and also at least 2 vertebral levels above and below the site of the fistula. Magnification, oblique and high frame rate angiography were used, as appropriate. 3D DSA was occasionally used to define the angioarchitecture. If the site of treated fistula was unclear, angiographers were encouraged to inject into the site suspected for fistula on MRA, and if unsuccessful, complete spinal angiography was performed.

Imaging Analysis

Two experienced neuroradiologists (S.P.S. and A.B.) with 13 and 7 years of experience, respectively, reviewed all posttreatment MR imaging and MRA studies. Readers were blinded to DSA findings and diagnosis, but had access to pretreatment MR imaging and MRA images while reviewing the studies. For MRA studies, the readers noted the presence or absence of an SAVF and the level and side of the fistula if present. The presence of a residual/recurrent fistula was based on the visualization of arterially enhancing prominent intradural veins on the source images of the MRA sequence. The level and side of the fistula were determined on MRA by looking for the point of fistulization (commonly seen as a small tuft of vessels in the foraminal region) and for the level at which the proximal part of the draining intradural (radicular) vein appeared. For conventional MR imaging studies, readers were asked to evaluate pre- and posttreatment MR imaging findings, including presence or absence of 1) intramedullary T2 hyperintensity, 2) perimedullary serpentine flow voids, and 3) cord enhancement. After making their observations on MR imaging and MRA studies, the readers reviewed the DSA images for presence or absence of SAVF and noted the level and side of fistula if present.

Statistical Analysis

For descriptive statistics, categorical variables are presented as percentages, and continuous variables are presented as medians with interquartile range. Diagnostic performances with 95% CI of MRA and MR imaging were calculated by using DSA as the reference standard. Fisher exact and χ^2 tests were used to identify associations for categorical data where appropriate. Statistical significance was defined as $P < .05$ for all tests. Statistical analyses were performed by using MedCalc for Windows, version 12.5 (MedCalc Software, Mariakerke, Belgium) and R, version 3.1.1 (R Foundation, <http://www.r-project.org/>).

RESULTS

In total, 23 patients (median age, 62 years; interquartile range, 54–69 years; 19 male [83%]) fulfilled the study inclusion criteria. Five patients had 2 sets of MR imaging/MRA and DSA studies, yielding a total of 28 paired posttreatment studies. The median time (interquartile range) interval between treatment and MRA, MRA and DSA, and treatment and DSA was 80 (11–277) days, 53 (2–122) days, and 3 (1–20) days, respectively. Of the 23 patients with AVF, there were 16 spinal dural AVFs, 4 spinal epidural AVFs, 1 perimedullary AVF, 1 filum terminale fistula, and 1 patient with an intracranial dural AVF, all presenting with perimedullary venous congestion and myelopathy.

All patients underwent surgical treatment of the fistula, aside from 1 patient in whom a combined endovascular and surgical procedure was performed. Previously treated AVF levels were at C4 ($n = 1$), C7 ($n = 1$), T5 ($n = 2$), T9 ($n = 4$), T12 ($n = 4$), L1 ($n = 1$), L2 ($n = 2$), L3 ($n = 3$), L4 ($n = 2$), S5 ($n = 1$), filum terminale ($n = 1$), and intracranial ($n = 1$).

Diagnosis and Localization of Residual or Recurrent SAVF on MRA

There were 6 image sets of residual/recurrent SAVF in 5 patients, which are summarized in the On-line Table. All 6 (100%) cases of residual/recurrent SAVF were correctly identified on MRA by the 2 study readers as identified by arterial phase perimedullary venous enhancement within enlarged intradural perimedullary vessels (Fig 1). Of 22 cases without residual/recurrent fistula at DSA, 21 of 22 (95%) were correctly identified on MRA to not demonstrate a residual/recurrent fistula (Fig 2). One of the 22 (5%) cases demonstrated a false-positive on MRA, as demonstrated by subtle enhancement of perimedullary veins thought to be abnormal, but no shunt was present at follow-up comprehensive DSA (Fig 3). All available pretreatment MRA identified the fistula. Pretreatment MRA for 4 patients was not available (3 positive for residual/recurrent disease and the false-positive case). The readers were still able to accurately distinguish residual/recurrent shunts from cured lesions (except for the 1 false-positive case) based on presence/absence of arterialized perimedullary veins. Overall sensitivity and specificity of MRA compared with DSA were 100% (95% CI, 42%–100%) and 95% (95% CI, 77%–100%), respectively. Localization of the recurrent/residual fistula was correct in 100% of the cases. On MRA, there was no interobserver disagreement related to the presence or localization of residual/recurrent SAVF.

Conventional MR Imaging Findings

Pretreatment MR imaging was unavailable in 3 of the patients with residual/recurrent fistulas. Four pre- and posttreatment MR imaging datasets were available for comparison for patients with recurrent/residual AVF. All cases had pretreatment perimedullary flow voids, of which 3 (75%) remained stable at posttreatment MR imaging and 1 (25%) showed decrease. Two of 4 cases demonstrated cord edema and enhancement pretreatment, of which 1 demonstrated stability posttreatment and 1 showed mild reduction.

Pre- and posttreatment MRIs were available for review for 21 cases negative for recurrent/residual AVF on DSA (at the median

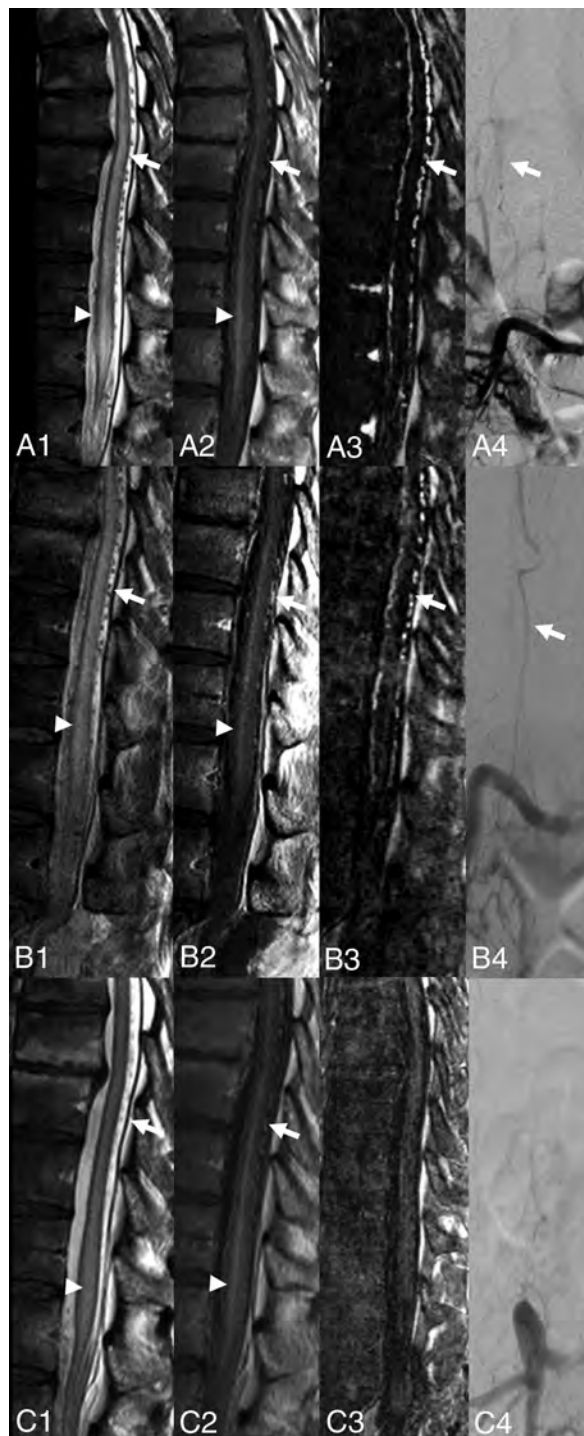


FIG 1. Spinal epidural AVF with intradural venous drainage (patient 4). Sagittal T2, postgadolinium T1, MRA MIP, and frontal DSA images pretreatment (A1–4), after first attempted surgical disconnection (B1–4), and after second surgical disconnection (C1–4), respectively. Pretreatment study shows T2 cord hyperintensity and enhancement (A1–2, arrowheads) with surrounding enhancing perimedullary flow voids (A1–2, arrows). MRA shows arterial enhancement of intradural veins (A3, arrow). DSA confirmed the AVF (A4, arrow indicates the arterIALIZED radicular vein). Postsurgical study after attempted AVF disconnection (B1–4) shows findings unchanged compared with the pretreatment study, consistent with residual AVF. Second postsurgical study shows persistent T2 cord hyperintensity and enhancement (C1–2, arrowheads) with decreased size of perimedullary veins (C1–2, arrows). MRA and DSA (C3–4) confirm absence of arterIALIZED intradural veins, consistent with a successful surgical disconnection.

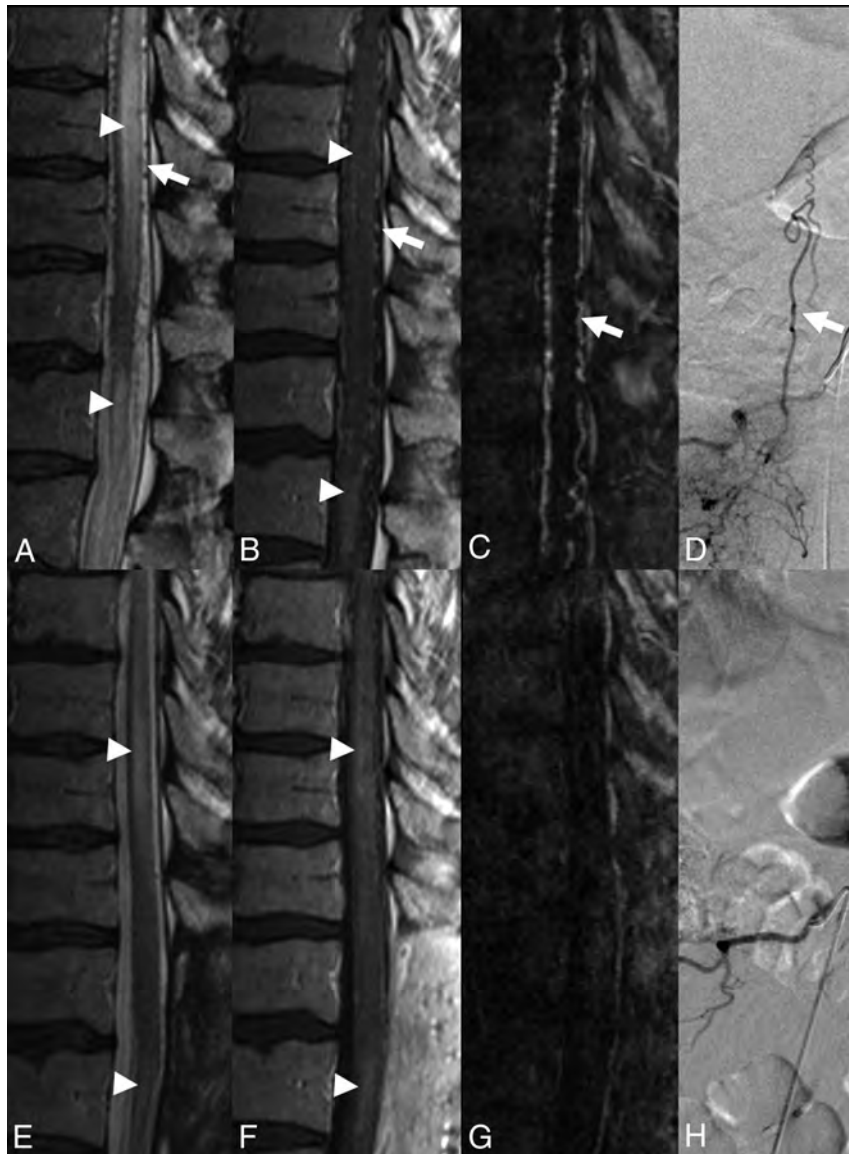


FIG 2. Spinal dural AVF in a 50-year-old man with 6 months of progressive lower extremity paraplegia. Pretreatment sagittal T2 (A) and postcontrast T1 (B) show abnormal perimedullary vessels (A, arrow), which enhance postcontrast (B, arrow), in addition to intramedullary T2 hyperintensity (A, arrowheads) with mild patchy intramedullary enhancement (B, arrowheads). Pretreatment sagittal MRA MIP (C) demonstrates arterially enhancing perimedullary veins (C, arrow). Right L1 segmental artery injection–frontal projection DSA demonstrates retrograde drainage into radicular vein (D, arrow). After surgical disconnection, there is reduction in intramedullary T2 hyperintensity (E, arrowheads) and perimedullary flow voids, with persistent cord enhancement (F, arrowheads) and lack of arterially enhancing perimedullary veins on MRA (G). Successful fistula disconnection was confirmed on repeat DSA (H).

follow-up time of 80 days). All of these had perimedullary flow voids, cord edema, and enhancement on pretreatment MR imaging. After successful treatment, 10 (47.6%) showed decrease, 1 (4.8%) showed stability, and 10 (47.6%) showed absence of perimedullary flow voids. The cord edema decreased in 17 (81%) cases, remained stable in 2 (9.5%), and completely resolved in 2 (9.5%). The cord enhancement decreased in 10 (48%) cases and remained stable in the remaining 11 (52%).

There was significant overlap in the conventional MR imaging appearances of successfully and unsuccessfully treated spinal fistulas. None of the conventional MR imaging parameters were significantly associated with recurrent/residual AVF (all $P > .05$).

DISCUSSION

Our results provide further evidence of the utility of MRA in the posttreatment evaluation of patients with SAVFs.^{2,3,7,8} All cases of recurrent/residual SAVF in our study were confirmed by DSA and demonstrated abnormal arterial enhancement of perimedullary serpentine vessels on MRA (sensitivity of 100%). Both readers correctly identified the level of the fistula, including the level of the recurrent/residual fistula, without interobserver disagreement. One false-positive study was noted on MRA (specificity of 95%), which was primarily due to poor timing of the acquisition relative to the contrast bolus, resulting in venous contamination and enhancement of normal draining perimedullary veins mimicking arterialized veins. In that particular case, further review of



FIG 3. False-positive on MRA. 78-year-old man with prior surgical disconnection of a spinal dural AVF at left T5 level presented with worsening gait spasticity confounded by history of Parkinson disease. Few dorsal perimedullary flow voids were noted on the sagittal T2 (A, arrow), which enhanced on the postcontrast T1 study (B, arrow). Mild intramedullary enhancement was also noted on the postcontrast T1 (B, arrowhead). On MRA (C), there was faint enhancement of the perimedullary veins (C, arrow), which led to the suspicion of residual/recurrent fistula. No fistula was found at subsequent DSA (not shown). The findings on MR imaging and MRA were presumed to be residual changes from prior fistula. Mild enhancement of the perimedullary veins may be a result of venous contamination of contrast bolus, as suggested by enhancement of the basivertebral veins (C, arrowhead).

the first-pass MRA source images revealed diffuse enhancement of the epidural veins at all levels, indicating that the study was timed too late, into the venous phase, likely causing the false-positive diagnosis. If this finding is observed, it should prompt consideration of a repeat study with strict attention to arterial phase timing. Apart from this single case, no other study was affected by contrast timing problems, indicating that the technique is generally robust.

The results of our study are consistent with previous MRA studies evaluating patients post-SAVF treatment.^{2,3,7} Mascalchi et al² demonstrated the ability of 2D and 3D phase-contrast MRA and 3D time-resolved MRA to correctly identify residual/recurrent fistula in 7 of 30 patients post-SAVF treatment (MRA sensitivity of 100%). In their study, however, not all patients with negative MRA were evaluated with DSA; therefore, the diagnostic performance of MRA cannot be assessed from their study. They reported 1 patient with progressive myelopathy 2 months after an initial negative MRA study, which was later proved to be a recurrent/residual fistula at DSA. This recurrence may have represented an MRA false-negative, reducing sensitivity, and the authors hypothesize that may have been the result of insufficient flow sensitivity or spatial resolution of their MRA technique.² Our technique used first-pass contrast-enhanced MRA, which has a

higher spatial resolution than current time-resolved methods. Kaufmann et al⁷ evaluated 8 of 34 patients post-SAVF treatment with manually triggered first-pass MRA. One of 8 patients showed mild increased perimedullary vascularity on MRA, but was found to be negative at DSA, consistent with a false-positive. A separate patient showed moderate increased perimedullary vascularity on MRA, which was later proved positive for recurrence at DSA. MRA was normal in the remaining 6 patients, of whom 2 were confirmed DSA negative. Ali et al³ described agreement between time-resolved MRA and DSA in their series of 3 patients post-SAVF treatment, 1 of whom had a recurrence. An advantage of our current study is that it is the largest series in which all patients with or without residual/recurrent SAVF on posttreatment MRA also had DSA as the criterion standard. All patients also had a uniform MRA protocol; specifically, a first-pass, gadolinium-enhanced, manually triggered 3D-acquisition technique.

Our findings together with the reported literature suggest high sensitivity and specificity of MRA for detection of residual/recurrent fistulas, which is likely improved with modern MRA techniques.^{9,10} High sensitivity in particular is needed, given the screening nature of the study with use of DSA to confirm the findings and evaluate the precise angioarchitecture of the residual lesion. Ensuring consistent arterial phase acquisition of first-pass MRA without venous contamination is important and remains a potential limitation of first-pass MRA that may result in decreased specificity of first-pass MRA, as demonstrated by our false-positive and possibly by the case from Kaufmann et al.⁷ Use of time-resolved MRA may help improve specificity; however, there remains a balance between the need for temporal resolution needed to identify true arterial enhancement versus the spatial resolution needed to visualize and identify the level of the fistula.³

Similar to previous studies evaluating post-SAVF treatment conventional MR imaging findings,^{2,6,7,11} we noted that none of the conventional MR imaging features demonstrated statistical significance for predicting recurrent/residual SAVF. Several studies have noted that intramedullary T2 hyperintensity usually reduces or resolves within months to years after treatment; however, it may be persistent after successful treatment.^{6,12} Similar findings may be seen with cord enhancement and perimedullary flow voids.^{2,6,7,11} Although improvement or resolution of conventional MR imaging findings may be associated with successful treatment, these findings may take time to resolve, and none are accurate enough to exclude residual/recurrent fistula.^{2,13} In contrast, our study demonstrates that MRA may more directly identify residual/recurrent disease either immediately after treatment or on follow-up. MRA may also identify enhancing perimedullary vessels not apparent on standard sagittal T2 sequences.⁷

A recent meta-analysis of 35 post-SAVF treatment studies including 1112 patients demonstrated a 96.6% and 72.2% initial fistula occlusion for patients treated with surgical and endovascular methods, respectively.¹ Recurrences may be early (ie, < 1 month) or late (up to several years). Willinsky et al⁶ hypothesized in 1995 that with advances in MRA, DSA may not be required for posttreatment follow-up of SAVFs. The high sensitivity of MRA for recurrent/residual disease in our study lends further support to this concept. Presently, MRA facilitates and does not replace DSA. Our study suggests MRA may potentially reduce the need

for DSA in follow-up of treated fistulas for most patients who do not have residual/recurrent disease. If a residual fistula is suspected on postoperative MRA, DSA will be required, but may be facilitated by allowing a more targeted study with fewer injections aimed at the predicted level of the lesion on MRA, which may occur at a different level from the original location. This approach may potentially enable reduction of DSA procedural and fluoroscopic times and volume of contrast administered and further reduces the risks associated with potentially lengthy complete spinal angiographic examinations.^{5,6,14}

This study is primarily limited by a relatively small sample size, particularly with the limited number of recurrent/residual fistula; however, this is not unexpected given the rare nature of the disease. The retrospective nature of this study may also have resulted in a selection bias. Further prospective study of MRA in posttreatment patients with SAVF would be beneficial.

CONCLUSIONS

First-pass contrast-enhanced MRA demonstrates high sensitivity and specificity for identifying recurrent/residual SAVF and may potentially substitute for DSA in the posttreatment follow-up of patients with SAVF; however, prospective confirmation in a larger study is needed.

Disclosures: Thomas Marotta—UNRELATED: Consultancy: Pipeline, Comments: proctor; Patents (planned, pending or issued): Evasc Medical Systems, Comments: eCLIPS; Stock/stock options: Evasc Medical Systems, Comments: eCLIPS.

REFERENCES

1. Bakker NA, Uyttenboogaart M, Luijckx GJ, et al. **Recurrence rates after surgical or endovascular treatment of spinal dural arteriovenous fistulas.** *Neurosurgery* 2015;77:137–44; discussion 144 CrossRef Medline
2. Mascalchi M, Ferrito G, Quilici N, et al. **Spinal vascular malformations: MR angiography after treatment.** *Radiology* 2001; 219:346–53 CrossRef Medline
3. Ali S, Cashen TA, Carroll TJ, et al. **Time-resolved spinal MR angiography: initial clinical experience in the evaluation of spinal arteriovenous shunts.** *AJNR Am J Neuroradiol* 2007;28:1806–10 CrossRef Medline
4. Brinjikji W, Nasr DM, Morris JM, et al. **Clinical outcomes of patients with delayed diagnosis of spinal dural arteriovenous fistulas.** *AJNR Am J Neuroradiol* 2016;37:380–86 CrossRef Medline
5. Forbes G, Nichols DA, Jack CR Jr, et al. **Complications of spinal cord arteriography: prospective assessment of risk for diagnostic procedures.** *Radiology* 1988;169:479–84 CrossRef Medline
6. Willinsky RA, terBrugge K, Montanera W, et al. **Posttreatment MR findings in spinal dural arteriovenous malformations.** *AJNR Am J Neuroradiol* 1995;16:2063–71 Medline
7. Kaufmann TJ, Morris JM, Saladino A, et al. **Magnetic resonance imaging findings in treated spinal dural arteriovenous fistulas: lack of correlation with clinical outcomes.** *J Neurosurg Spine* 2011;14: 548–54 CrossRef Medline
8. Condette-Auliac S, Boulin A, Roccatagliata L, et al. **MRI and MRA of spinal cord arteriovenous shunts.** *J Magn Reson Imaging* 2014;40: 1253–66 CrossRef Medline
9. Amarouche M, Hart JL, Siddiqui A, et al. **Time-resolved contrast-enhanced MR angiography of spinal vascular malformations.** *AJNR Am J Neuroradiol* 2015;36:417–22 CrossRef Medline
10. Lindenholz A, TerBrugge KG, van Dijk JM, et al. **The accuracy and utility of contrast-enhanced MR angiography for localization of spinal dural arteriovenous fistulas: the Toronto experience.** *Eur Radiol* 2014;24:2885–94 CrossRef Medline
11. Song JK, Viñuela F, Gobin YP, et al. **Surgical and endovascular treatment of spinal dural arteriovenous fistulas: long-term disability assessment and prognostic factors.** *J Neurosurg Spine* 2001;94:199–204 CrossRef
12. Horikoshi T, Hida K, Iwasaki Y, et al. **Chronological changes in MRI findings of spinal dural arteriovenous fistula.** *Surg Neurol* 2000;53: 243–49 CrossRef Medline
13. Morris JM. **Imaging of dural arteriovenous fistula.** *Radiol Clin North Am* 2012;50:823–39 CrossRef Medline
14. Luetmer PH, Lane JJ, Gilbertson JR, et al. **Preangiographic evaluation of spinal dural arteriovenous fistulas with elliptic centric contrast-enhanced MR angiography and effect on radiation dose and volume of iodinated contrast material.** *AJNR Am J Neuroradiol* 2005; 26:711–18 Medline

Comparison of Time-Resolved and First-Pass Contrast-Enhanced MR Angiography in Pretherapeutic Evaluation of Spinal Dural Arteriovenous Fistulas

S. Mathur, A. Bharatha, T.J. Huynh, R.I. Aviv, and S.P. Symons

ABSTRACT

BACKGROUND AND PURPOSE: Different MRA techniques used to evaluate spinal dural arteriovenous fistulas offer unique advantages and limitations with regards to temporal and spatial resolution. The purpose of this study was to compare the efficacy and interobserver agreement of 2 commonly used contrast-enhanced spinal MRA techniques, multiphase time-resolved MRA and single-phase first-pass MRA, in assessment of spinal dural arteriovenous fistulas.

MATERIALS AND METHODS: Retrospective review of 15 time-resolved and 31 first-pass MRA studies in patients with clinical suspicion of spinal dural arteriovenous fistula was performed by 2 independent, blinded observers. DSA was used as the reference standard to compare the diagnostic performance of the 2 techniques.

RESULTS: There were 10 cases of spinal dural arteriovenous fistula in the time-resolved MRA group and 20 in the first-pass MRA group. Time-resolved MRA detected spinal dural arteriovenous fistulas with sensitivity and specificity of 100% and 80%, respectively, with 100% correct-level localization rate. First-pass MRA detected spinal dural arteriovenous fistulas with sensitivity and specificity of 100% and 82%, respectively, with 87% correct-level localization rate. Interobserver agreement for localization was excellent for both techniques; however, it was higher for time-resolved MRA. In 5 cases, the site of fistula was not included in the FOV, but a prominent intradural radicular vein was observed at the edge of the FOV.

CONCLUSIONS: Multiphase time-resolved MRA and single-phase first-pass MRA were comparable in diagnosis and localization of spinal dural arteriovenous fistulas and demonstrated excellent interobserver agreement, though there were more instances of ambiguity in fistula localization on first-pass MRA.

ABBREVIATIONS: FP-MRA = first-pass MRA; SDAVF = spinal dural arteriovenous fistula; TR-MRA = time-resolved MRA

Spinal dural arteriovenous fistulas (SDAVFs) represent an abnormal connection between a radiculomeningeal artery and a radicular vein, typically on the dural sleeve adjacent to the nerve root. The arterialized radicular vein causes regurgitation of blood flow to the perimedullary venous plexus, resulting in increased venous pressure and congestion.¹ Although SDAVFs are a treatable cause of myelopathy,² the diagnosis remains challenging because the clinical and conventional MR imaging features are non-

specific. As a result, misdiagnosis and delay in diagnosis are common, which may result in additional disability.³

MRA is useful for confirming the diagnosis and for localizing SDAVFs to expedite DSA.^{4,5} DSA is ultimately the “criterion standard” for diagnosis of this condition, but the number of injections and the time required to perform this study can be reduced with the knowledge of the level involved, provided by MRA. The contrast-enhanced spinal MRA techniques useful for evaluation of SDAVFs are broadly of 2 types: first-pass and time-resolved. These differ with regards to temporal and spatial resolution. The purpose of this study was to compare the efficacy and interobserver agreement of multiphase time-resolved MRA (TR-MRA) and single-phase first-pass MRA (FP-MRA) in assessment of SDAVFs.

MATERIALS AND METHODS

Patient Cohort

Research ethics review board approval was obtained for this retrospective study from both the Sunnybrook Health Sciences Cen-

Received June 30, 2016; accepted after revision August 12.

From the Division of Neuroradiology, Department of Medical Imaging (S.M., T.J.H., R.I.A., S.P.S.) and Department of Otolaryngology–Head and Neck Surgery (S.P.S.), Sunnybrook Health Sciences Centre, Toronto, Ontario, Canada; and Division of Diagnostic and Interventional Neuroradiology, Department of Medical Imaging (S.M., A.B., T.J.H.), St. Michael's Hospital, Toronto, Ontario, Canada.

Paper previously presented in part at: Annual Meeting of the American Society of Neuroradiology, April 25–30, 2015; Chicago, Illinois.

Please address correspondence to Sean P. Symons, MD, 2075 Bayview Ave, AG31D, Toronto, ON, Canada M4N 3M5; e-mail: sean.symons@sunnybrook.ca

<http://dx.doi.org/10.3174/ajnr.A4962>

tre and St. Michael's Hospital. From January 2000 to April 2015, all patients who were referred to the medical imaging departments of the 2 participating sites with a clinical suspicion of SDAVF and underwent conventional spine MR imaging, contrast-enhanced TR-MRA or FP-MRA, and DSA were included in the study. Patients with a history of treated SDAVF were excluded. On retrospective review of imaging and clinical data bases, 58 patients were found to satisfy these criteria.

Patients found to have SDAVF variants on DSA including epidural AVF, perimedullary AVF, spinal cord AVM, and filum terminale AVF were excluded ($n = 12$) because they were unequally distributed in the TR-MRA and FP-MRA groups (1 and 11, respectively). This yielded a total of 15 and 31 patients in the TR-MRA and FP-MRA groups, respectively.

MR Imaging and MRA Technique

Conventional whole-spine MR imaging was performed on a 1.5T scanner (Twinspeed [GE Healthcare, Milwaukee, Wisconsin] and Intera Achieva [Philips Healthcare, Best, the Netherlands]) by using dedicated 8-channel and 5-channel spinal coils for the TR-MRA and FP-MRA groups, respectively, with the patient in the supine position. The sequences included standard sagittal and axial T2WI, sagittal T1WI, and postcontrast sagittal and axial T1WI. Routine measures to minimize degree of motion were used for MR imaging and MRA, such as patient instruction/education, stabilization in the scanner, and sedation if required.

TR-MRA was performed by using the vendor-provided time-resolved imaging of contrast kinetics, or TRICKS, sequence. Sagittal plane was selected on 3 plane localizers with FOV of 30 cm (craniocaudal) extending approximately from T4 to L4 vertebral levels. The selection of FOV was based on the clinical/radiologic suspicion of the location of fistula. After acquisition of a mask, intravenous injection of 10 mL of gadolinium-based contrast agent (gadobutrol [Gadavist; Bayer Schering Pharma, Berlin, Germany]) was performed at 1.5 mL/s injection rate by using a 2-cylinder MR compatible injector (Spectris; MedRad, Indianola, Pennsylvania) followed by 25-mL saline bolus. Manual triggering was performed with no delay. Three-dimensional acquisition was performed with 320×160 matrix and 1.4×1.2 mm in-plane resolution with 3-mm section thickness. Parameters of TR = 3.5–4 ms, TE = 1–1.5 ms, flip angle = 35° , NEX = 0.5, and no section gap were used. Twenty phases were obtained with 24 scan locations in each phase. The total scan time was 54 seconds, with temporal resolution of 2.2 seconds. Automated postprocessing produced background subtracted image sets for each of the 20 phases with multiplanar and cine MIPs.

FP-MRA was performed by using a manually triggered timed-run technique. Sagittal plane was selected on 3 plane localizers with FOV of 33 cm extending approximately from T3 to L4 vertebral levels. The selection of FOV was based on the clinical/radiologic suspicion of the location of fistula. Acquisition delay time was determined by using a 2-mL intravenous contrast test bolus and measuring peak enhancement of the abdominal aorta using MR fluoroscopy. This was followed by intravenous administration of 18 mL of contrast agent at 2 mL/s injection rate by using a 2-cylinder MR compatible injector (Spectris) followed by 20-mL saline bolus. Gadolinium-based contrast agent, including Omnis-

can (gadodiamide; GE Healthcare) or more recently MultiHance (gadobenate dimeglumine; Bracco Diagnostics, Princeton, New Jersey), was used. Single-phase 3D acquisition was performed with 400×512 matrix and 0.82×1.08 mm in-plane resolution reconstructed to 0.64×0.64 mm with 0.9-mm section thickness. Scan parameters were TR = 5.4 ms, TE = 1.76 ms, flip angle = 30° , NEX = 1, and overcontiguous sections with scan time of 47 seconds. Automated postprocessing generated background subtracted image sets and multiplanar MIPs.

DSA Technique

Spinal DSA examinations were performed on a dedicated biplanar neuroangiographic system via a femoral approach under general or local anesthesia. Multiple selective arterial injections with iodinated contrast agent (Omnipaque 300; GE Healthcare) were performed on the segmental arteries likely to supply an SDAVF. Magnification, oblique, or high frame rate angiography was used where appropriate. The angiographers first targeted the arteries expected to be supplying a fistula based on the MRA findings. Once the fistula was identified, further bilateral injections to include at least 2 vertebral levels above and below the identified fistula were performed. If the fistula was not identified at the anticipated level or MRA was negative for SDAVF, complete spinal angiography was performed.

Imaging Analysis

MR imaging and MRA images were reviewed independently by 2 experienced neuroradiologists (S.P.S. and A.B.) with 13 and 7 years of experience, respectively, who were blinded to the DSA findings.

On the MRA study, the observers made positive or negative diagnosis of SDAVF and noted the level and side of fistula if present. The observers also noted the useful signs in localization of SDAVF on MRA.

In cases where fistulas were found to be located outside the FOV, the observation of "inability to localize fistula in the MRA study" and "suspicion of fistula lower than the FOV" by the readers was considered as correct reading for the purpose of analysis. If the location of fistula was suspected at 2 levels by either of the readers, and even if 1 of the levels was correct, this ambiguity was considered an unsuccessful localization or incorrect reading. Localization within 1 vertebral level was considered as correct reading.

Information regarding the diagnosis and localization of the SDAVF was also recorded from the original clinical report of the study issued by the staff radiologist.

The readings on conventional MR images included presence or absence of intradural serpentine flow voids, T2 hyperintensity of the spinal cord, and cord enhancement.

After the readings on MR imaging and MRA studies had been completed, the observers reviewed the DSA images for presence or absence of SDAVF and noted the level and side of fistula if present. The clinical imaging reports were also retrospectively reviewed.

Statistical Analysis

The statistical measures of performance of the 2 MRA techniques and the specific signs were calculated by using DSA as the refer-

ence standard. Sensitivity and specificity of the 2 MRA techniques were compared by using test of proportions. Cohen κ coefficients were calculated to measure interobserver agreement. Values of κ of 0.21–0.4, 0.41–0.6, 0.61–0.8, and 0.81–1 were considered fair, moderate, substantial, and nearly perfect, respectively. Fisher or χ^2 test was used for categoric or dichotomous data as appropriate. Wilcoxon rank sum test was used for continuous data. Statistical significance was defined as $P < .05$. All statistical analyses were performed by using MedCalc for Windows, version 12.5 (MedCalc Software, Mariakerke, Belgium), and R, version 3.2.3 (R Foundation, <http://www.r-project.org/>).

RESULTS

Of 46 patients with suspected SDAVF (median age, 64 years; range, 40–89 years; 33 [72%] male), 15 were evaluated with TR-MRA and 31 with FP-MRA. DSA identified the presence of SDAVF in 30 of 46 (65%) patients, 10 of 15 (67%) in the TR-MRA group and 20 of 31 (64%) in the FP-MRA group. In 16 patients without evidence of SDAVF on DSA, the final diagnosis was in-

fected/inflammatory myelitis ($n = 4$), neoplasm ($n = 3$), cavernous malformation ($n = 3$), subdural hemorrhage without underlying lesion ($n = 1$), intracranial dural AVF causing myelopathy ($n = 1$), idiopathic syrinx ($n = 1$), and prominent veins/venous varix without cause identified ($n = 3$). The median time interval between MRA and DSA examinations was 5 days (interquartile range, 2–12 days). There were no significant differences between the age, sex, days between MRA and DSA, level of the fistula identified on DSA, and proportion of conventional MR imaging signs between the patients in the TR-MRA and FP-MRA groups (all $P > .05$; Table 1).

The observers recorded that the following signs on MRA were useful for localization of SDAVF: 1) smudge of enhancement in the region of nerve root dural sleeve connected to a branch of the segmental artery, 2) prominent intradural radicular vein, and 3) early draining radicular vein (only on TR-MRA) (Figs 1 and 2). In FP-MRA, the early draining vein sign is not useful for fistula localization because it is a single (arterial) phase technique with radicular and perimedullary veins enhancing simultaneously.

The diagnostic performance of TR-MRA and FP-MRA for diagnosis of SDAVF is summarized in Table 2.

In the TR-MRA group, there was 1 false-positive diagnosis (Fig 3, *Top*) and no incorrect localization of SDAVF with no interobserver disagreement. In the FP-MRA group, there were 2 false-positive diagnoses (Fig 3, *Bottom*), and in 2 cases, fistula was localized to more than 1 level. There were 2 instances of interobserver disagreements.

There were no significant differences in the sensitivity and specificity for diagnosis ($P > .05$) and accuracy of localization ($P = .50$) of SDAVF for the 2 techniques.

In 5 of 20 (25%) patients in the FP-MRA group, the site of the fistula iden-

Table 1: Patient characteristics and frequency of conventional MRI findings

Characteristic	TR-MRA ($n = 15$)	FP-MRA ($n = 31$)	P
Age (median [IQR])	57 (54–65)	66 (56–74)	.152
Male sex (no. [%])	9 (60%)	24 (77%)	.219
Days between DSA and MRA (median [IQR])	6 (4–12)	5 (1–10)	.340
DSA evidence of SDAVF	10 (67%)	20 (64%)	.886
Level of fistula identified on DSA			.515
C6–C7	1	0	
T1–T3	0	0	
T4–T6	2	4	
T7–T9	3	4	
T10–T12	3	3	
L1–L3	1	4	
L4–L5	0	1	
Sacrum/pelvis	0	4	
Conventional MR signs in DSA-positive cases			
Cord T2 hyperintensity	10/10 (100%)	20/20 (100%)	1.000
Serpentine flow voids	10/10 (100%)	20/20 (100%)	1.000
Cord enhancement	9/10 (90%)	20/20 (100%)	.333

Note:—IQR indicates interquartile range.

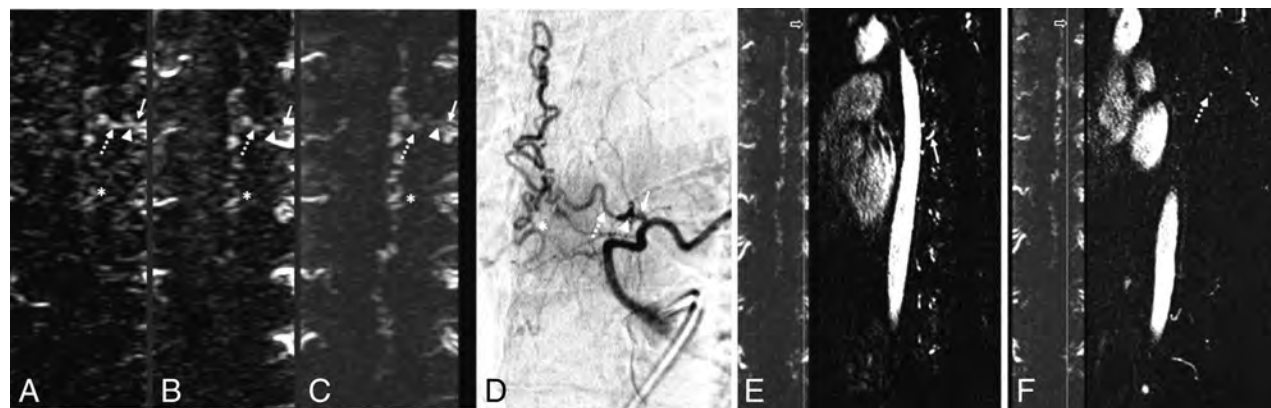


FIG 1. Imaging features of SDAVF on TR-MRA. Representative images of the coronal MIP TR-MRA images in early arterial phase (A–C) demonstrate early draining vein (*dashed arrow*) and smudge of enhancement at the dural sleeve (*arrowhead*) connected to the radiculomeningeal artery (*arrow*) with progressive enhancement of the arterIALIZED perimedullary veins (*asterisk*). Findings can be correlated on oblique frontal projection on DSA (D). E and F demonstrate correlation on source sagittal images; reference line on coronal images is marked by the *hollow arrow*. The radiculomeningeal artery at the dural sleeve (*arrow*, E) and prominent draining radicular vein (*dashed arrow*, F) are seen on sagittal images.

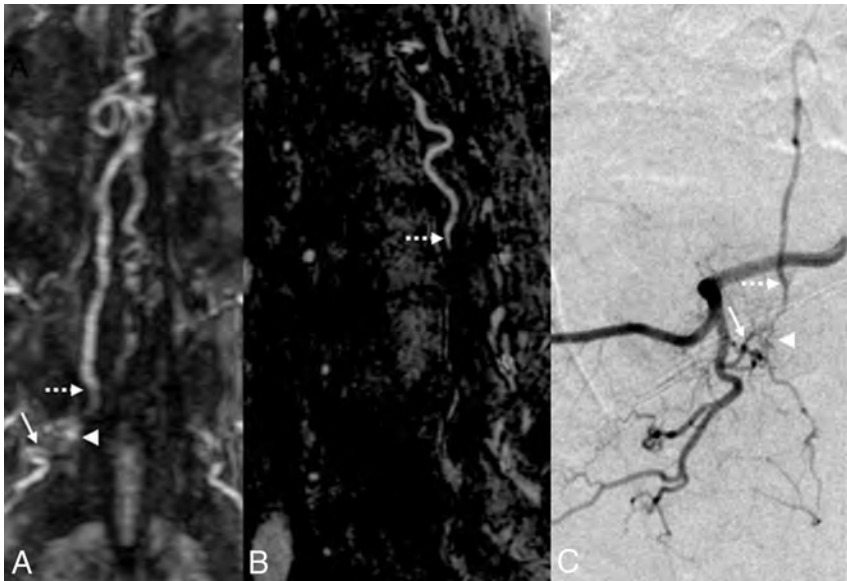


FIG 2. Imaging features of SDAVF on FP-MRA. Coronal (A) and sagittal (B) MIP FP-MRA images demonstrate a prominent arterial network along the dural sleeve (*arrowhead*) connected to the radiculomeningeal artery (*arrow*), indicating the level of the fistula. A prominent radicular draining vein (*dashed arrow*) is noted extending superiorly from the same level. Findings correlated on oblique frontal projection DSA image (C).

Table 2: Diagnostic performance of TR-MRA and FP-MRA compared with DSA, and interobserver agreement

	TR-MRA (95% CI)	FP-MRA (95% CI)
Diagnosis of SDAVF		
Sensitivity	100% (59%–100%)	100% (76%–100%)
Specificity	80% (28%–99%)	82% (48%–98%)
Positive predictive value	91% (59%–100%)	91% (71%–99%)
Negative predictive value	100% (28%–100%)	100% (55%–100%)
κ Agreement	1.0 (1.0–1.0)	1.0 (1.0–1.0)
Localization		
Reader accuracy to within 1 level of DSA ^a	100% (72%–100%)	87% (62%–96%)
κ Agreement	1.0 (1.0–1.0)	0.87 (0.70–1.00)

^a When SDAVF location within the FOV ($n = 15$); in 5 cases where the fistula was beyond the FOV, at least 1 of the observers suspected fistula outside FOV on MRA.

tified on DSA was beyond the FOV. This was suggested on MRA by incompletely imaged prominent enhancing intradural radicular vein (Fig 4). Based on this imaging feature, both readers suspected the level of the fistula was inferior to FOV in 4 of 5 patients, whereas only 1 reader suspected the fistula was beyond the FOV in 1 patient.

No fistula level was reported in the clinical report of 1 of 10 (10%) TR-MRA cases. In cases where the level of the fistula was described in the clinical report, there was perfect agreement between the reported level and the research readings. On the clinical reports in the FP-MRA group, the neuroradiologist did not specify the level of fistula in 5 cases, and in 1 case, fistula level was incorrectly identified. For cases where a fistula level was identified in the clinical report, there was near perfect agreement with the research reading ($\kappa = 0.94$).

DISCUSSION

DSA is the “criterion standard” for diagnosis and characterization of SDAVFs. However, it is an invasive technique that involves radiation and injection of iodinated contrast and is associated with a relatively high complication rate (0.3%–2.63%).⁶ Non-

selective spinal DSAs may be time-consuming and labor-intensive and may require multiple sessions to adequately localize a lesion. A major advantage of adding MRA to the imaging work-up is localization before DSA. Several studies have shown that conventional MR imaging is not helpful in fistula localization.^{7,8} MRA has proved useful to guide DSA and reduce the number of catheterized vessels, radiation, and contrast dose.^{4,5}

Contrast-enhanced MRA techniques used for evaluation of SDAVFs can be broadly classified as single-phase first-pass (or bolus-chase) technique and multiphase time-resolved technique. The selection of the technique in an institute is usually based on the preference of the neuroradiologist/neurosurgeon and feasibility. Contrast-enhanced TR-MRA uses modified k -space sampling to provide dynamic vascular imaging with a trade-off of spatial resolution.⁹ In our study, the temporal resolution of TR-MRA was 2.2 seconds with 1.4×1.2 mm in-plane resolution and 3-mm section thickness. Contrast-enhanced FP-MRA captures the arterial phase of contrast injection by manual or automated triggering at a predetermined scan delay time and provides static images with higher spatial resolution, which in our study was 0.82×1.08 mm in-plane resolution (reconstructed to 0.64×0.64 mm) with 0.9-mm section thickness.^{4,10}

Lim et al⁹ compared these techniques for evaluation of extracranial internal carotid arteries. Sandhu et al¹¹ found better identification of perforators of the leg by using bolus-chase MRA compared with TR-MRA. Oda et al¹² found that 3T dynamic contrast-enhanced MRA may be more reliable compared with CTA. To the best of our knowledge, our study is the first to compare single- and multiphase spinal MRA techniques for evaluation of SDAVFs with interobserver agreement analysis.

In our study, the sensitivity and specificity of 100% and 80% of TR-MRA for detection of SDAVFs and 100% accuracy in localization within one vertebral level is similar to previous studies. Saindane et al⁵ reported the sensitivity and specificity of 88% and 90%, respectively, for detection of SDAVF and correct localization in 6 of 7 cases. In the study by Ali et al,¹³ the spinal AVFs were correctly diagnosed and localized in all 6 patients by using TR-MRA. Amarouche et al¹⁴ found 98% sensitivity and 63% specificity for detection of spinal vascular malformations, with correct localization within 1 vertebral level in 39 of 47 SDAVFs.

The performance of FP-MRA in diagnosis of SDAVFs in our

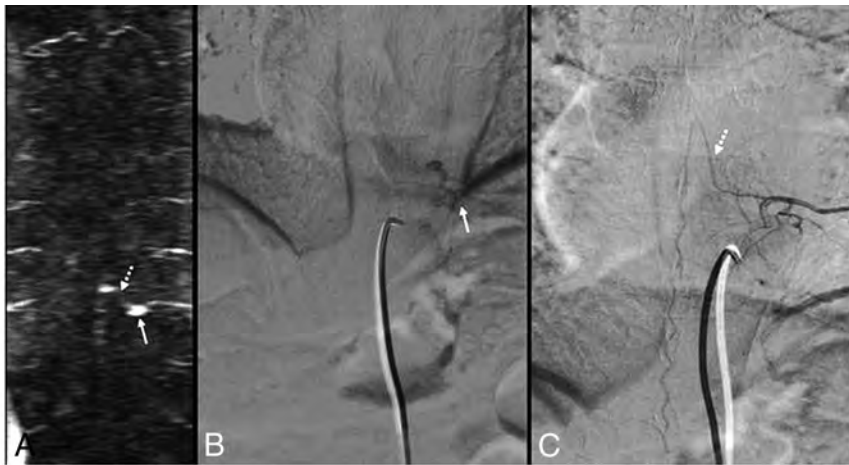


FIG 3. *Top*, Pitfalls in TR-MRA interpretation. Coronal MIP TR-MRA image (A) with enhancing structure at dural sleeve (arrow) mistaken for level of fistula and arterIALIZED intradural vessel (dashed arrow) mistaken for radicular vein. On frontal projection DSA images (B and C) these structures are found to be a venous varix and artery of Adamkiewicz, respectively. *Bottom*, Pitfalls in FP-MRA interpretation. Sagittal T2WI (A) and enhanced sagittal T1WI (B) show abnormal signal intensity (arrow, A) and mild enhancement (arrow, B) with lower thoracic cord extending to conus. There are enhancing intradural vessels in this region (dashed arrow, B). On sagittal (C and D) and axial (E) FP-MRA images, arterIALIZED structure at dural sleeve (arrow) and arterIALIZED intradural vessel (dashed arrow) are noted. This was found to be the artery of Adamkiewicz on DSA (F). The cord lesion was later diagnosed as astrocytoma on pathology.

study was comparable with prior studies. Saraf-Lavi et al⁸ found up to 100% sensitivity and 82% specificity in diagnosis. All 31 patients positive for spinal vascular lesions demonstrated enlarged perimedullary blood vessels in the study by Mull et al.¹⁵ Spinal AVF was diagnosed correctly in 20 of 22 patients in the study by Luetmer et al.⁴

The accuracy of lesion localization within 1 vertebral level with FP-MRA in our study (when lesion was within the FOV) was 87%, which is comparable with previous studies: 81% (Lindenholz et al¹⁶, $n = 53$), 73% (Saraf-Lavi et al⁸, $n = 20$), 100% (Mull et al¹⁵, $n = 19$), 93% (Luetmer et al⁴, $n = 14$), 100% (Farb et al¹⁰, $n = 9$), and 100% (Vargas et al¹⁷, $n = 4$).

The 1 false-positive TR-MRA diagnosis of SDAVF was due to

a venous varix at a neural foramen simulating smudge of enhancement and the adjacent artery of Adamkiewicz mimicking an arterIALIZED radicular vein (Fig 3, *Top*). In 1 case of false-positive diagnosis in the FP-MRA group, the artery of Adamkiewicz was misinterpreted as an arterIALIZED radicular vein (Fig 3, *Bottom*), and in the other case, prominent venous channels were mistaken for arterIALIZED intradural veins on a technically limited study. In this particular case, MRA was motion degraded with some venous contamination, which was identified by diffuse epidural venous filling. No other study suffered from this technical limitation.

Although no significant difference was found between the 2 techniques in diagnosis and localization of SDAVFs in our study, there were more occurrences of uncertainty in fistula localization

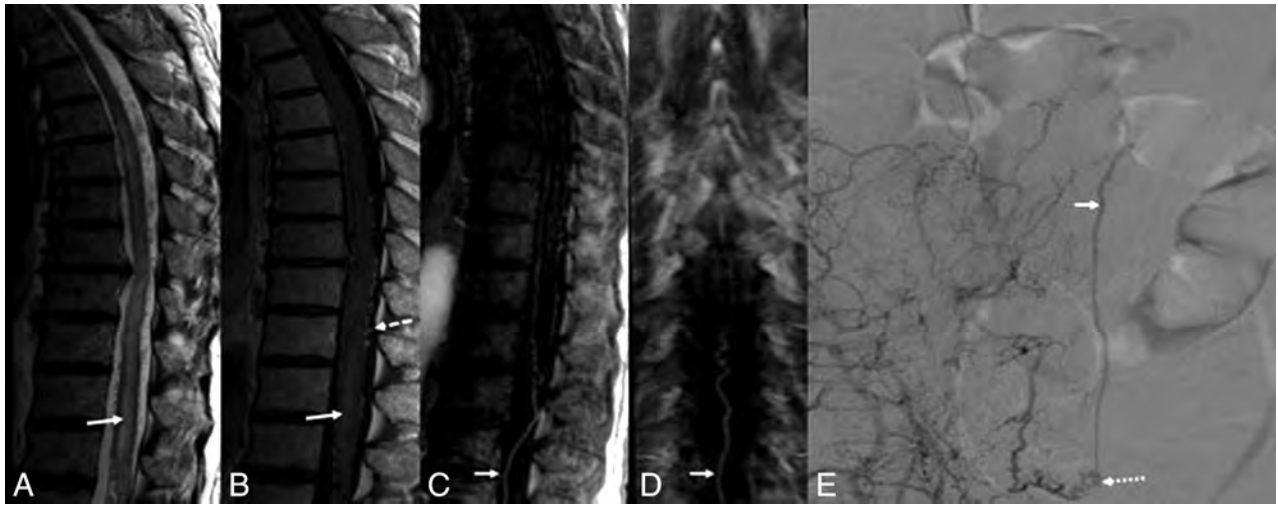


FIG 4. “Curvilinear radicular vein at the edge of the FOV”—useful sign to suspect fistula inferiorly. Sagittal T2WI (A) and enhanced sagittal T1WI (B) show abnormal signal intensity (arrow, A) and mild enhancement (arrow, B) within lower thoracic cord extending in to conus with enhancing perimedullary vessels (dashed arrow, C). On sagittal (C) and coronal (D) FP-MRA images, site of fistula inferior to FOV was suspected due to the presence of prominent arterialized vessel at the lower end of the FOV (arrow). Fistula inferior to the FOV was confirmed on DSA (dashed arrow, E) with arterIALIZED radicular vein (arrow, E).

on FP-MRA compared with TR-MRA. The ambiguity in localization in 2 cases of FP-MRA was due to a smudge of enhancement at the dural sleeve suspected by at least 1 of the observers. In the authors’ opinion, the reason for this error was poor fat suppression and lack of temporal resolution on this technique. No such ambiguity was seen with TR-MRA. TR-MRA also benefits from shorter acquisition time and no requirement for contrast bolus timing.

Amarouche et al¹⁴ suggested that it would be useful to determine interobserver agreement for MRA in spinal vascular lesions. We found nearly perfect interobserver agreement of both the techniques for diagnosis and localization of SDAVFs.

The signs on MRA useful for the localization of SDAVF correspond to the angioarchitecture of these lesions. The observers found that the prominent draining radicular vein sign was difficult to identify in the mid/upper thoracic and cervical region, which correlated to the normal anatomy of the spinal venous system. The smudge of enhancement at the dural sleeve could be subtle, but connection to a radiculomeningeal artery confirmed the presence of the fistula. Lindenholz et al¹⁶ highlighted the fact that the arterial network at the dural sleeve is difficult to identify, and this could result in a gap because the vessels are too small. Although arterIALIZED intradural veins are seen in both techniques, TR-MRA is optimal for delineation of the early draining vein due to its dynamic nature.

TR-MRA and FP-MRA are both limited by FOV, which has been reported by other investigators.^{4,5,16} In our study, in 5 cases in the FP-MRA group where the fistula was not covered by FOV, at least 1 of the observers suspected a lower level of fistula based on the presence of linear/curvilinear intradural radicular vein at the edge of FOV, and we believe that the presence of this sign in a suspected case of SDAVF should prompt further investigation at levels inferior to the FOV. The higher frequency of nonlocaliza-

tion of fistula in clinical reports in the FP-MRA group is probably due to more fistulas located outside FOV and in the upper thorax in this group.

Limitations of our study include the small number of patients with this rare condition. The small study population results in large confidence intervals. Confirmation in a large prospective study would be ideal, however, difficult given the rarity of this condition. Future studies could also compare these 2 techniques in assessment of intracranial lesions. The retrospective design of our study may result in selection bias. Comparison may also be limited because patients in the FP-MRA and TR-MRA groups were different.

CONCLUSIONS

TR-MRA and FP-MRA were comparable in diagnosis and localization of SDAVFs and demonstrate excellent interobserver agreement, though there were more instances of ambiguity in fistula localization on first-pass MRA.

REFERENCES

- Hurst RW, Kenyon LC, Lavi E, et al. Spinal dural arteriovenous fistula: the pathology of venous hypertensive myelopathy. *Neurology* 1995;45:1309–13 CrossRef Medline
- Atkinson JL, Miller GM, Krauss WE, et al. Clinical and radiographic features of dural arteriovenous fistula, a treatable cause of myelopathy. *Mayo Clin Proc* 2001;76:1120–30 CrossRef Medline
- Brinjikji W, Nasr DM, Morris JM, et al. Clinical outcomes of patients with delayed diagnosis of spinal dural arteriovenous fistulas. *AJNR Am J Neuroradiol* 2016;37:380–86 CrossRef Medline
- Luetmer PH, Lane JJ, Gilbertson JR, et al. Preangiographic evaluation of spinal dural arteriovenous fistulas with elliptic centric contrast-enhanced MR angiography and effect on radiation dose and volume of iodinated contrast material. *AJNR Am J Neuroradiol* 2005;26:711–18 Medline
- Saindane AM, Boddu SR, Tong FC, et al. Contrast-enhanced time-resolved MRA for pre-angiographic evaluation of suspected spinal

- dural arterial venous fistulas.** *J Neurointerv Surg* 2014;7:135–40 CrossRef Medline
6. Willinsky RA, Taylor SM, TerBrugge K, et al. **Neurologic complications of cerebral angiography: prospective analysis of 2,899 procedures and review of the literature.** *Radiology* 2003;227:522–28 CrossRef Medline
 7. Geibprasert S, Pongpech S, Jiarakongmun P, et al. **Cervical spine dural arteriovenous fistula presenting with congestive myelopathy of the conus.** *J Neurosurg Spine* 2009;11:427–31 CrossRef Medline
 8. Saraf-Lavi E, Bowen BC, Quencer RM, et al. **Detection of spinal dural arteriovenous fistulae with MR imaging and contrast-enhanced MR angiography: sensitivity, specificity, and prediction of vertebral level.** *AJNR Am J Neuroradiol* 2002;23:858–67 Medline
 9. Lim RP, Shapiro M, Wang EY, et al. **3D time-resolved MR angiography (MRA) of the carotid arteries with time-resolved imaging with stochastic trajectories: comparison with 3D contrast-enhanced bolus-chase MRA and 3D time-of-flight MRA.** *AJNR Am J Neuroradiol* 2008;29:1847–54 CrossRef Medline
 10. Farb RI, Kim JK, Willinsky RA, et al. **Spinal dural arteriovenous fistula localization with a technique of first-pass gadolinium-enhanced MR angiography: initial experience.** *Radiology* 2002;222:843–50 CrossRef Medline
 11. Sandhu GS, Rezaee RP, Wright K, et al. **Time-resolved and bolus-chase MR angiography of the leg: branching pattern analysis and identification of septocutaneous perforators.** *AJR Am J Roentgenol* 2010;195:858–64 CrossRef Medline
 12. Oda S, Utsunomiya D, Hirai T, et al. **Comparison of dynamic contrast-enhanced 3T MR and 64-row multidetector CT angiography for the localization of spinal dural arteriovenous fistulas.** *AJNR Am J Neuroradiol* 2014;35:407–12 CrossRef Medline
 13. Ali S, Cashen TA, Carroll TJ, et al. **Time-resolved spinal MR angiography: initial clinical experience in the evaluation of spinal arteriovenous shunts.** *AJNR Am J Neuroradiol* 2007;28:1806–10 CrossRef Medline
 14. Amarouche M, Hart JL, Siddiqui A, et al. **Time-resolved contrast-enhanced MR angiography of spinal vascular malformations.** *AJNR Am J Neuroradiol* 2015;36:417–22 CrossRef Medline
 15. Mull M, Nijenhuis RJ, Backes WH, et al. **Value and limitations of contrast-enhanced MR angiography in spinal arteriovenous malformations and dural arteriovenous fistulas.** *AJNR Am J Neuroradiol* 2007;28:1249–58 CrossRef Medline
 16. Lindenholz A, TerBrugge KG, van Dijk JMC, et al. **The accuracy and utility of contrast-enhanced MR angiography for localization of spinal dural arteriovenous fistulas: the Toronto experience.** *Eur Radiol* 2014;24:2885–94 CrossRef Medline
 17. Vargas MI, Nguyen D, Viallon M, et al. **Dynamic MR angiography (MRA) of spinal vascular diseases at 3T.** *Eur Radiol* 2010;20:2491–95 CrossRef Medline

Henry J.M. Barnett

Henry J.M. Barnett, neurologist, known as Barney, was born in Newcastle-Upon-Tyne, United Kingdom, in 1922 and died in Toronto, Canada, on October 20, 2016. He was best known for randomized stroke-prevention trials: aspirin effectiveness to prevent stroke,¹ lack of effectiveness of cerebral bypass,² and effectiveness of carotid endarterectomy.³ Part of the success of these trials came from Barney's understanding of the value of an angiographic core lab for the studies; the success of the North American Symptomatic Carotid Endarterectomy Trial (NASCET) came, in part, from the core lab's insistence on consistent, reproducible stenosis quantification.

He was honored: Companion of the Order of Canada (the closest Canadian award to a UK knighthood), Honorary Doctor of Science at Oxford University, Stroke Research Award of Sweden's Karolinska Institute, and honorary membership in foreign medical societies including the Royal Society of Medicine (United Kingdom), Russian Academy of Medical Science, Indian Academy of Neurology, Hungarian Neurosurgical Society, and more.

He completed medical school at the University of Toronto in 1944, followed by Toronto residencies in medicine and neurology and then fellowships at Oxford and Queen Square. At Queen Square, he overlapped with Charlie Drake, a neurosurgery fellow. They developed both professional and personal relationships, with their families intertwined ever since (some of his grandchildren are Drakes).

In the late 1960s, he moved from Toronto's Sunnybrook Hospital to join Drake in London, Ontario, to form an innovative combined university clinical neurosciences department. After I was recruited there in 1976, I saw a special atmosphere of combining neurology and neurosurgery into one academic department, plus neuropathology and neuroradiology. The CNS department's academics gave it a prominent place at the university table beside medicine and surgery; neurology was not considered merely to be one of many subsets of medicine or neurosurgery one of surgery.

As Editor-in-Chief of *Stroke*, Barney was careful to recuse himself from manuscripts sent from his own department. As I worked closely with Barney, I saw a master at work. He was on a first-name basis with those at the highest levels of NINDS, the Medical Research Council of Canada (now CIHR), and the Heart and Stroke Foundation of Canada (HSFC). NASCET received the largest NIH grant to date for foreign research. He was instrumental in including the word "stroke" in HSFC's name, unlike the American Heart Association. He proposed a new London Research Institute with unique governance separate from both hospital and university. His fundraising abilities were formidable. He visited the Conservative Premier of Ontario and returned with a large grant supporting the planned institute, now named for John Robarts, a former premier who experienced a series of debilitating strokes. Then, Barney visited the Liberal Prime Minister of Canada, who added another large contribution.

Every few days, without prior notice, we in neuroradiology were summoned to Barney's office to display innovative interventional materials and images of successful interventional neurora-



diology cases for yet another visiting leader of industry, wealthy potential donor, and even the American ambassador. One time, the CEO of a multinational company was flown in from Europe and diverted from New York for an urgent consultation with Barney in London after a spell in his overseas office. We fit in a same-day CT and IV DSA (it was 1982); Barney gave him a clean bill of health, and he left town with a seat on the Institute's board after pledging a six-figure donation. We can claim that our neuroradiology work enabled the founding of the Robarts Research Institute.

Barney had diverse connections. In the early 1990s, he was a stroke consultant for the famous Lubavitcher Rebbe, who had a stroke in New York. After Barney was called at Princeton, he was escorted to New York by police, who closed the Lincoln Tunnel to get him quickly to the Rebbe. That night, I received a FedEx package containing a CT with instructions to phone my interpretation to Barney. A few months later, Barney was invited to a wedding of one of the Rebbe's family members in a Manhattan square just beneath the languishing Rebbe's hospital window. Barney told me that he and Mayor Rudy Giuliani were the only ones in the crowd not wearing black coats and fedoras.

Although Barney is known for his work regarding stroke, earlier in his career, he contributed to spinal cord disease research by his discovery and report of posttraumatic syringomyelia.⁴ Even without his work on stroke, he was already a recognized syrinx expert, especially for his monograph *Syringomyelia*.⁵

He was seriously interested in birds and preserving nature. As a boy, he skipped Sunday school to frequent Toronto lagoons with his binoculars. During his career, he would tell various foreign hosts that he wished to see local birds and would often be led on a bird walk by an ornithology institute director or university biology chair. He was an advocate of the Nature Conservancy of Canada (NCC) for the Happy Valley Forest in King Township, north of Toronto, where he owned property acquired when his children were young. He passed on his passion for nature in forests, ponds,

and meadows to his children, grandchildren, and great-grandchildren. NCC published his detailed blog of flora and fauna.⁶ His successful campaign for preservation included hosting a Canadian Prime Minister in his own living room to drum up support. He was able to personally enable NCC with preservation of areas that housed threatened plant and animal species.

REFERENCES

1. Canadian Cooperative Stroke Study Group. **A randomized trial of aspirin and sulfinpyrazone in threatened stroke.** *N Engl J Med* 1978; 299:53–59 CrossRef Medline
2. EC/IC Bypass Study Group. **Failure of extracranial-intracranial arterial bypass to reduce the risk of ischemic stroke. Results of an international randomized trial.** *N Engl J Med* 1985;313:1191–200 CrossRef Medline
3. North American Symptomatic Carotid Endarterectomy Trial Collaborators. **Beneficial effect of carotid endarterectomy in symptomatic patients with high-grade carotid stenosis.** *N Engl J Med* 1991;325: 445–53 CrossRef Medline
4. Barnett HJ, Jousse AT, Morley TP, et al. **Post-traumatic syringomyelia.** *Paraplegia* 1971;9:33–37 CrossRef Medline
5. Barnett HJ, Foster JB, Hodgson P, eds. *Syringomyelia*. London: Saunders; 1973
6. Barnett HJ. Land Lines. Nature Conservancy of Canada blog. <http://www.natureconservancy.ca/en/blog/authors/dr-henry-barnett.html>. Accessed November 17, 2016

A.J. Fox

Department of Neuroradiology
Sunnybrook Health Sciences Centre
University of Toronto
Toronto, Canada

<http://dx.doi.org/10.3174/ajnr.A5046>

Celebrating 35 Years of the AJNR

January 1982 edition

Dural Arteriovenous Malformation of the Major Venous Sinuses: An Acquired Lesion

Mohammad V. Chaudhary,^{1,2}
Ved P. Sachdev,³
Soo H. Cho,⁴
Imre Wetzner, Jr.,⁵
Smiljan Puljic,⁶
Yun Peng Huang⁷

Arteriovenous malformations of the dura are thought to be congenital. However, angiographic investigations of four patients who, after a head injury, developed dural arteriovenous fistulae with features of congenital malformations suggest that these abnormal communications may also be acquired. Thrombosis or thrombophlebitis in the dural sinus or vein may be the primary event in their formation. The pathogenesis is probably "growth" of the dural arteries normally present in the walls of the sinuses during the organization of an intraluminal thrombus. This may result in a direct communication between artery and vein or sinus, establishing an abnormal shunt. Ultimate fibrosis of the sinus wall and intraluminal thrombosis may be the factors responsible for the spontaneous disappearance of such malformations.

Most dural arteriovenous malformations (AVMs) that involve the major venous sinuses present either spontaneously or as incidental findings during arteriography performed for other reasons. They occur predominantly in women over age 40 years [1]. The angiomatous network, multiple feeding arteries, numerous arteriovenous (AV) shunts, and occasional association with cerebral arteriovenous malformations [2], as well as a few cases reported in children [3], suggest that these AVMs are congenital. Thrombosis of the draining sinus or vein is thought to be responsible for the occasional spontaneous disappearance of these lesions [4, 5].

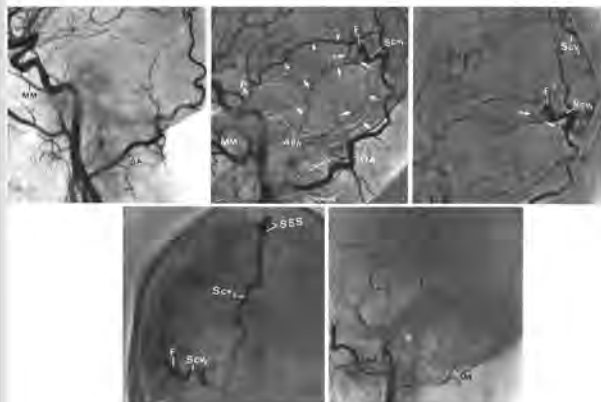
Our experience with four patients who, after a head injury, developed dural AV fistulae with features of congenital malformations prompted a review of the literature and this report. In two of our four cases, transverse and sigmoid sinus abnormalities were demonstrated angiographically before the AV fistulae developed. In case 3, angiography 2 years earlier for unrelated reasons was normal; no AV shunt was seen. Although in case 4, there was no angiographic evidence of a dural fistula before head injury, the posttraumatic onset of symptoms and the angiographic findings strongly suggested that this lesion had been acquired.

Cases 1 and 3 were studied by serial angiography with selective internal, external, and common carotid injections, while stereo angiography with selective and superselective catheterization of the sinus was performed in cases 2 and 4. The first three patients underwent periodic angiography for up to 4 years, and the AV shunts were spontaneously occluded.

Case Reports

Case 1

A 56-year-old woman was admitted for headaches and dizzy spells rapidly to rule out transient ischemic attacks with normal EEGs. She had mild diabetes, cavendish headaches, and dizzy spells to disorientation. She was brought to the emergency room after a head injury 2 months before over the right occipital/parietal area, was confused and disorient-



Received May 7, 1981; accepted after revision September 8, 1981.

Presented at the annual meeting of the American Society of Neuroradiology, Chicago, April 1981.

¹Department of Radiology, Mount Sinai Hospital, New York, NY 10029.

²Department of Radiology, New York Medical College, Westchester County Medical Center, Valhalla, NY 10595. Address reprint requests to M. V. Chaudhary (present address).

³Department of Neurosurgery, Mount Sinai Hospital, New York, NY 10029.

⁴AJNR 3:13-19, January/February 1982.

⁵1595-B105/82, 0301-0313 \$00.00.

© American Roentgen Ray Society.

Bulging Lumbar Intervertebral Disk: Myelographic Differentiation from Herniated Disk with Nerve Root Compression

Stephen A. Kieffer,¹
Richard G. Sherry,^{1,2}
David E. Weinstein,^{1,3}
Robert B. King⁴

Deformities of the lateral margins of the contrast material-filled lumbar thecal sac are common findings at myelography in patients with low back pain, but not all such deformities are due to herniated disks. Differentiation at Amipaque myelography between a diffusely bulging disk (unlikely to cause nerve root compression) and a herniated disk (which typically causes nerve root compression) is based on the curvature and extent of the extralaminar deformity of the anterolateral margin of the contrast-filled sac and on the presence of fusiform widening of the most distal part of the affected nerve root. The deformity caused by a bulging disk is rounded, usually asymmetrical (although occasionally more prominent on one side), and does not extend above or below the disk space; the nerve root is uniform in caliber and normal in size. The deformity caused by a herniated disk is angular and extends cephalad and/or caudad to the level of the disk space; the affected nerve root is usually widened in its most distal visible part. A consecutive series of 33 patients with clinically suspected lumbar disk herniation and no previous history of back surgery underwent laminectomy. Using the criteria listed above for differentiation of bulging from herniated disk on Amipaque myelography, the myelographic diagnosis was correct in all six operatively confirmed bulging disks and in 26 (96%) of 27 operatively verified disk herniations.

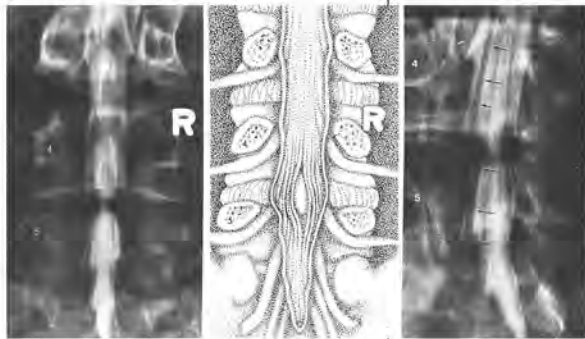
In 1934, Mixer and Barr [1] first described the clinical picture and anatomic findings of herniation of a lumbar intervertebral disk causing nerve root compression with resultant low back pain, sciatica, and weakness of the affected lower extremity. Only 2 years later, in another classical paper, Hampton and Robinson [2] described the myelographic criteria for recognizing this lesion using an oily contrast medium.

Deformities of the lateral margins of the contrast-filled lumbar thecal sac are a common finding at myelography in patients with low back pain, but not all such deformities are due to herniated disks [3-5]. Perhaps the most difficult task for the myelographer is to differentiate the extralaminar deformity produced by a bulging disk (unlikely to cause nerve root compression) from that produced by a herniated disk (which typically causes nerve root compression).

Amipaque (methylzamide, Winthrop), a nonionic water-soluble contrast medium for myelography, reliably provides delineation of the lumbar nerve roots both within the thecal sac and in the root sheaths [6, 7]. Myelography with Amipaque can directly demonstrate distal widening of a nerve root compressed by a herniated disk, thus permitting more accurate differentiation of disk herniation from disk bulging.

Materials and Methods

A consecutive series of 33 patients with clinically suspected lumbar intervertebral disk herniation and no previous history of back surgery underwent laminectomy. Amipaque lumbar myelography had been performed on all 33 shortly before laminectomy. The concentration of contrast medium introduced into the lumbar subarachnoid space varied



Comment on “Aneurysms Associated with Brain Arteriovenous Malformations”

We read with great interest the review article entitled “Aneurysms Associated with Brain Arteriovenous Malformations” by Rammos et al.¹ This article summarizes the different subtypes of intracranial aneurysms that may be associated with brain AVMs (bAVMs). We congratulate the authors for their effort to clarify the nomenclature of such aneurysms. However, we would like to raise our disagreement with the following statement: “Given that pathologic specimens of resected AVM nidi consist of a conglomerate of venous tangles and loops, implicating that venous drainage begins at the level of the nidus, intranidal aneurysms are de facto venous.” Histopathologically, the nidus has been reported to comprise both arteries and veins with disorganized walls, as well as vessels of ambiguous nature.^{2–5} Even though we agree that some intranidal aneurysms may have a venous nature and may be responsible for some bAVM bleeding events (Fig 1), in our experience, most intranidal aneurysms in bAVMs with hemorrhagic presentation are rather false aneurysms arising from the dysplastic vessels belonging to the nidus and represent the bleeding site.⁶ Indeed, as reported by numerous series,^{7,8} in patients with intracranial bAVM-related bleeding events, intranidal aneurysms are frequently observed. A higher rebleeding rate has also been reported in patients with bAVMs harboring intranidal aneurysms.⁹ Nidal aneurysms have been defined by a joint experts group as those with any portion contained in the bAVM nidus.¹⁰ As underlined by Redekop et al,⁸ these aneurysms are often seen on early phase of the DSA, before substantial venous filling, and may present a contrast media stagnation on late phase (Figs 2 and 3). Depiction of intranidal aneurysms is both difficult and subject to a high rate of interobserver disagreement. The review of Rammos et al¹ is lacking a discussion on advanced imaging tools that may help to demonstrate these aneurysms and further our understanding of their origin. Indeed, high-rate (6 frames per second or more) DSA acquisitions, 3D rotational angiography (RA), 4D-RA technology,¹¹ and ultrasensitive angiography, or even more recent algorithms used on 3D-RA such as segmentation algorithms¹² or anamorphosis algorithm,¹³ may help to depict these aneurysms more accurately. Wall enhancement of the intranidal aneurysm

on MR imaging has also been proposed as a radiologic feature that may help to confirm the bleeding site.¹⁴

Finally, we agree with Rammos et al¹ on the fact that the depiction of these intranidal aneurysms is of tremendous importance because they may prompt the interventional neuroradiologists or neurosurgeons to perform in an emergency a target treatment or whole resection of the bAVM to prevent early rebleeding.⁹

Disclosures: Frédéric Clarençon—UNRELATED: Payment for lectures including service on speakers bureaus: Medtronic. Nader Sourour—UNRELATED: Consultancy: Medtronic, Microvention; Stock/stock options: Medina/Medtronic.

REFERENCES

1. Rammos SK, Gardenghi B, Bortolotti C, et al. **Aneurysms associated with brain arteriovenous malformations.** *AJNR Am J Neuroradiol* 2016 Jun 23. [Epub ahead of print] CrossRef Medline
2. McCormick WF. **The pathology of vascular (“arteriovenous”) malformations.** *J Neurosurg* 1966;24:807–16 CrossRef Medline
3. Mandybur TI, Nazek M. **Cerebral arteriovenous malformations. A detailed morphological and immunohistochemical study using actin.** *Arch Pathol Lab Med* 1990;114:970–73 Medline
4. Jellinger K. **Vascular malformations of the central nervous system: a morphological overview.** *Neurosurg Rev* 1986;9:177–216 Medline
5. Deshpande DH, Vidyasagar C. **Histology of the persistent embryonic veins in arteriovenous malformations of brain.** *Acta Neurochir (Wien)* 1980;53:227–36 Medline
6. Mjoli N, Le Feuvre D, Taylor A. **Bleeding source identification and treatment in brain arteriovenous malformations.** *Interv Neuroradiol* 2011;17:323–30 Medline
7. Turjman F, Massoud TF, Viñuela F, et al. **Correlation of the angio-architectural features of cerebral arteriovenous malformations with clinical presentation of hemorrhage.** *Neurosurgery* 1995;37: 856–60; discussion 860–62 Medline
8. Redekop G, TerBrugge K, Montanera W, et al. **Arterial aneurysms associated with cerebral arteriovenous malformations: classification, incidence, and risk of hemorrhage.** *J Neurosurg* 1998;89: 539–46 CrossRef Medline
9. Meisel HJ, Mansmann U, Alvarez H, et al. **Cerebral arteriovenous malformations and associated aneurysms: analysis of 305 cases from a series of 662 patients.** *Neurosurgery* 2000;46:793–800; discussion 800–02 Medline
10. Atkinson RP, Awad IA, Batjer HH, et al. **Reporting terminology for brain arteriovenous malformation clinical and radiographic features for use in clinical trials.** *Stroke* 2001;32:1430–42 Medline
11. Lescher S, Gehrisch S, Klein S, et al. **Time-resolved 3D rotational angiography: display of detailed neurovascular anatomy in patients**

with intracranial vascular malformations. *J Neurointerv Surg* 2016 Aug 4. [Epub ahead of print] CrossRef Medline

12. Clarençon F, Maizeroi-Eugène F, Bresson D, et al. **Elaboration of a semi-automated algorithm for brain arteriovenous malformation segmentation: initial results.** *Eur Radiol* 2015;25:436–43 CrossRef Medline
13. Clarençon F, Maizeroi-Eugène F, Maingreaud F, et al. **Interest of convex spherical anamorphosis in better understanding of brain AVMs' angioarchitecture.** *J Neurointerv Surg* 2016;8:959–64 CrossRef Medline
14. Omodaka S, Endo H, Fujimura M, et al. **High-grade cerebral arteriovenous malformation treated with targeted embolization of a ruptured site: wall enhancement of an intranidal aneurysm as a sign of**

ruptured site. *Neurol Med Chir (Tokyo)* 2015;55:813–17 CrossRef Medline

● **F. Clarençon**

● **E. Shotar**

Department of Interventional Neuroradiology

Pitié-Salpêtrière Hospital AP-HP

Paris, France

Paris VI University (Pierre et Marie Curie University)

Paris, France

● **N.-A. Sourour**

Department of Interventional Neuroradiology

Pitié-Salpêtrière Hospital AP-HP

Paris, France

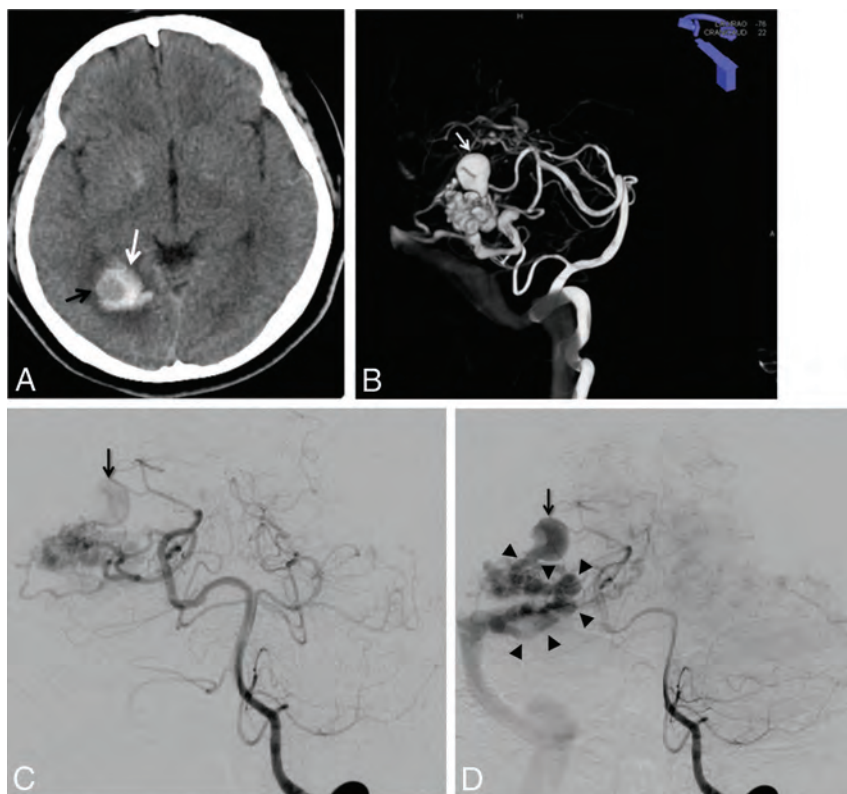


FIG 1. A, Unenhanced brain CT scan (axial section) in a 40-year-old woman with headache. Right occipital hematoma is seen (*white arrow*). Note a round hypoattenuated shape surrounded by the hematoma, corresponding to the intranidal aneurysm (*black arrow*). B, Volume rendering reconstruction from the 3D-RA acquisition through the left vertebral artery, showing a large intranidal aneurysm (*white arrow*). C and D, Left vertebral DSA in anteroposterior projection at early phase (C) and late phase (D). At early phase, an intranidal aneurysm is seen (C, *arrow*). On late phase, this nidal aneurysm appears clearly connected to the main draining vein (D, *arrowheads*), confirming the venous nature of this intranidal aneurysm.

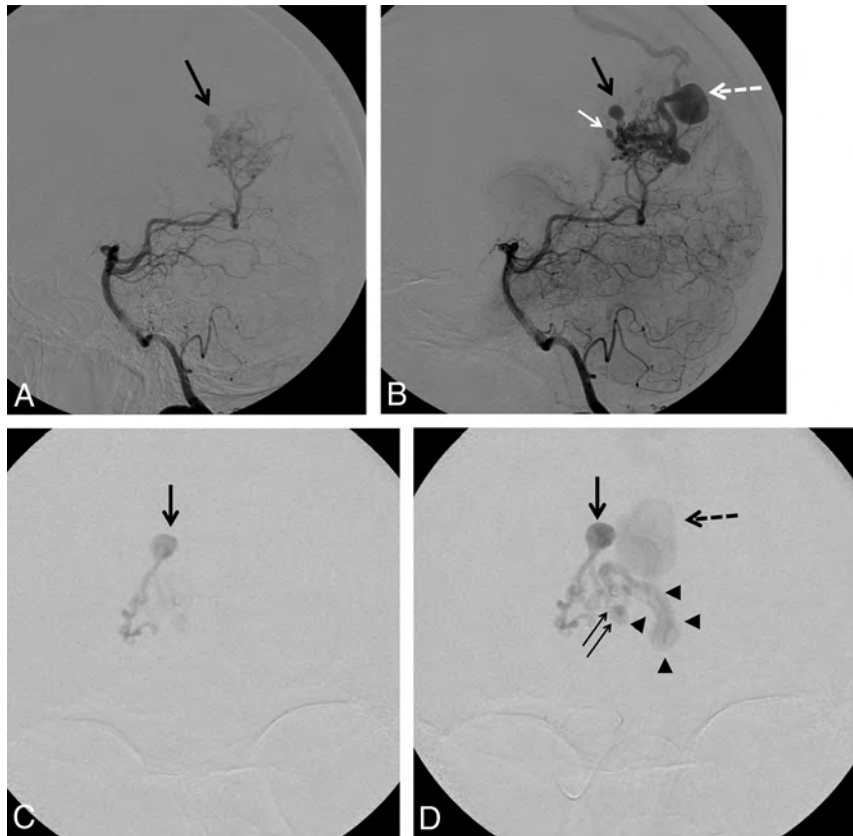


FIG 2. A and B, Left vertebral artery DSA in lateral projection in a 41-year-old woman with a ruptured right parieto-occipital bAVM. A, Early phase showing a nidus (black arrow) before filling of the draining vein. B, Intermediate phase showing a second intranidal aneurysm (white arrow) in addition to the first one (black arrow). Note a focal venous ectasia on the main draining vein (white dotted arrow). C and D, Selective DSA in anteroposterior projection from the parieto-occipital branch of the right posterior cerebral artery through a flow-dependent microcatheter. C, Early phase showing the filling of both the nidus and an intranidal aneurysm before any venous filling. D, Intermediate phase showing, in addition to the previously described intranidal aneurysm (black arrow), a second smaller nidus (double arrow) close to the origin of the main draining vein (arrowheads). Note the presence of a focal venous ectasia on the main draining vein (black dotted arrow).

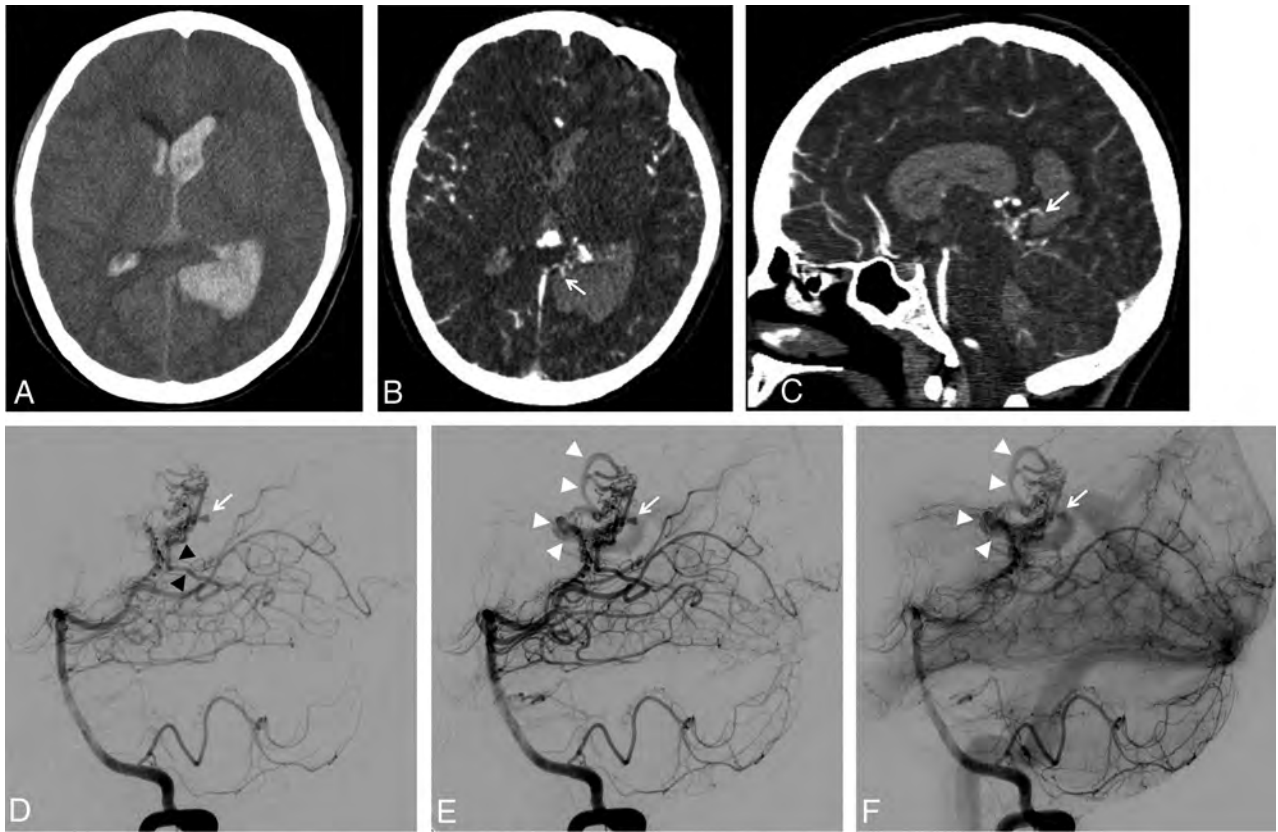


FIG 3. A, Unenhanced brain CT scan (axial section) showing a left parieto-occipital hematoma associated with intraventricular hemorrhage in a 19-year-old woman. B and C, Brain CT angiography: axial section (B) and sagittal reconstruction (C). Small false aneurysm arising from the nidus and close to the hematoma is seen on both axial and sagittal images (B and C, *white arrows*). The close relationship between the intranidal aneurysm and the hematoma suggests the aneurysm as being the cause of the bleeding. D–F, Left vertebral artery DSA in lateral projection at very early phase (D), early phase (E), and intermediate phase (F). At very early phase, opacification of the nidus is seen, supplied mainly by the left posterolateral choroidal artery (D, *black arrowheads*). Note the opacification of an intranidal aneurysm located at the posterior aspect of the nidus (D, *white arrow*) before any substantial filling of the venous drainage. At later phase, the origin of the draining vein is filling (E, *white arrowheads*) while the nidal aneurysm is still visible (E, *white arrow*). On intermediate phase, stagnation of the nidal aneurysm is seen (F, *white arrowheads*) while the venous drainage is more clearly seen (F, *white arrowheads*).

REPLY:

We greatly appreciate the thoughtful comments of the authors who raise valuable points and expand our discussion on the topic of aneurysms associated with brain AVMs (bAVMs) in their letter. We agree with the authors that in almost all ruptured bAVMs where the hemorrhage can be safely attributed to a site within the nidus (and not a prenidial aneurysm), intranidal aneurysms represent, in fact, the site of rupture of the bAVM nidus and are frequently observed as “false” aneurysms, partially filled with thrombus. We strongly believe in the use of modern angiographic techniques, particularly superselective and 3D angiography, to delineate the architecture of the nidus and, most importantly, to understand the relationship of associated aneurysms in relation to the nidus, and therefore to guide further treatment, whether endovascular or surgical. When it has been determined that the site of hemorrhage is a prenidial aneurysm (and not the nidus itself, including an intranidal aneurysm), prompt endovascular or surgical treatment should be pursued, tailored to the

angiographic features and location of the prenidial aneurysm and the clinical condition of the patient. Because the risk of early re-hemorrhage is low (in the absence of venous outflow stenosis) in bAVMs determined to have ruptured within the nidus itself (including intranidal aneurysms), the merits of expedient endovascular or surgical treatment are not clear. Equally unclear to our knowledge remains the benefit of targeted or palliative treatment (surgical or endovascular) of only part of the nidus (which may harbor intranidal aneurysms) without the complete, definitive resection of the bAVM.

S.K. Rammos

Department of Neurosurgery
Arkansas Neuroscience Institute
Little Rock, Arkansas

C. Bortolotti

Department of Neurosurgery
Istituto Di Ricovero e Cura a Carattere Scientifico
Institute of Neurological Science of Bologna
Bologna, Italy

G. Lanzino

Departments of Radiology and Neurosurgery
Mayo Clinic
Rochester, Minnesota

<http://dx.doi.org/10.3174/ajnr.A4988>

More Transparency Is Needed in the Reporting of Clinical Research Studies

We read with great interest the systematic review published very recently by Asnafi et al¹ on the efficacy and safety of the Woven EndoBridge (WEB); (Sequent Medical, Aliso Viejo, California) aneurysm embolization system for the endovascular therapy of intracranial aneurysms. Their literature search was conducted during a fairly similar period to our previously published systematic review (January 1, 2010, to October 1, 2015, versus January 1, 2010, to September 2015, respectively).² Most surprising, the authors included 15 articles while we selected only 7 articles. For 3 of these, the difference is because we selected articles with >10 patients, whereas Asnafi et al included studies with at least 5 patients. For the 5 remaining articles, we assume that we applied a more stringent study selection strategy aimed at detecting potential articles with duplicate published cases. Unlike the systematic review by Asnafi et al, we excluded the article by Papagiannaki et al,³ in which the authors stated that among their cohort of 85 patients, 22 and 24 (a total of 46 patients, 54.1%) of the patients also participated in the WEB Clinical Assessment of Intra-Saccular Aneurysm Therapy (WEBCAST) study and the French Observatory study, respectively. Our understanding is that Asnafi et al included the article by Pierot et al,⁴ which combined the 2 populations from WEBCAST and the French Observatory study and the article by Papagiannaki et al. Consequently, this meta-analysis is likely to have included the same population twice, which would make the analysis invalid. Similarly, we assume that patients from several other articles selected in the final meta-analysis, like those from Cognard et al, 2015,⁵ and Pierot et al, 2012 and 2013,^{6,7} are at great risk of having been included in other articles in the meta-analysis. On this basis, clarifications should be provided by the authors because by definition, a meta-analysis cannot include several articles with overlaps in the selected population. According to the selection criteria of our systematic review, we excluded articles potentially including the same populations.

In other systematic reviews undertaken in the field of interventional neuroradiology, we have been facing the same problem of identifying duplicate published cases because some au-

thors may publish their results in several articles. This emphasizes the need to carefully take into account several factors during the study selection process, such as the names of the authors, the location of participating centers, and the time of patient selection.

We understand that results from the same clinical research study may lead to several publications, for example, when an outcome measure is made available at different time points. However, this can be misleading within the scope of systematic reviews and the implementation of evidence synthesis methods, and may not allow a fair assessment of health technologies. This advocates for more transparency in the process of publication of clinical research studies. In practice, authors should be urged to systematically state in their article when some of their results have been partially or totally reported elsewhere.

Disclosures: Francis Turjman—UNRELATED: Consultancy: Codman, Stryker, Medtronic*; Grants/Grants Pending: Medtronic, Stryker.* *Money paid to the institution.

REFERENCES

1. Asnafi S, Rouchaud A, Pierot L, et al. **Efficacy and safety of the Woven EndoBridge (WEB) device for the treatment of intracranial aneurysms: a systematic review and meta-analysis.** *AJNR Am J Neuroradiol* 2016 Aug 11. [Epub ahead of print] Medline
2. Armoiry X, Turjman F, Hartmann DJ, et al. **Endovascular treatment of intracranial aneurysms with the WEB device: a systematic review of clinical outcomes.** *AJNR Am J Neuroradiol* 2016;37:868–72. CrossRef Medline
3. Papagiannaki C, Spelle L, Januel AC, et al. **WEB intrasaccular flow disruptor—prospective, multicenter experience in 83 patients with 85 aneurysms.** *AJNR Am J Neuroradiol* 2014;35:2106–11. CrossRef Medline
4. Pierot L, Spelle L, Molyneux A, Byrne J; WEBCAST and French Observatory Investigators. **Clinical and anatomical follow-up in patients with aneurysms treated with the WEB device: 1-year follow-up report in the cumulated population of 2 prospective, multicenter series (WEBCAST and French Observatory).** *Neurosurgery* 2016;78:133–41. CrossRef Medline
5. Cognard C, Januel AC. **Remnants and recurrences after the use of the WEB intrasaccular device in large-neck bifurcation aneurysms.** *Neurosurgery* 2015;76:522–30; discussion 530. CrossRef Medline
6. Pierot L, Liebig T, Sychra V, et al. **Intrasaccular flow-disruption treatment of intracranial aneurysms: preliminary results of a multicenter**

clinical study. *AJNR Am J Neuroradiol* 2012;33:1232–38 CrossRef Medline

7. Pierot L, Klisch J, Cognard C, et al. **Endovascular WEB flow disruption in middle cerebral artery aneurysms: preliminary feasibility, clinical, and anatomical results in a multicenter study.** *Neurosurgery* 2013;73:27–34; discussion 34–35 CrossRef Medline

 **X. Armoiry**

Hospices Civils de Lyon
Délégation à la Recherche Clinique et à l'Innovation
Cellule Innovation/UMR-CNRS 5510/MATEIS
Lyon, France

University of Warwick
Warwick Medical School, Division of Health Sciences
Coventry, England

 **F. Turjman**

 **B. Gory**

FHU IRIS, Neuroradiologie Interventionnelle
Hôpital Neurologique Pierre Wertheimer
Hospices Civils de Lyon
Lyon, France
University of Lyon 1
Lyon, France

REPLY:

We would like to thank Armoiry and colleagues for their critical analysis of our recently published systematic review. As the authors point out, there are a number of challenges to performing systematic reviews and meta-analyses of the literature in the field of interventional neuroradiology and neurosurgery.¹ This is especially true because many authors report single-center series and then a portion of those patients go on to be reported in large multi-institutional or multinational registries.

Regarding our inclusion of studies with overlapping populations, sometimes this is necessary in cases in which 1 study may focus on reporting outcomes at different time periods (ie, immediate posttreatment results versus long-term posttreatment results) or when studies focus on different outcomes (ie, morbidity and mortality versus angiographic outcomes). While patient populations may overlap, we do our best not to include overlapping results.

As stated by the authors, our systematic review and systematic reviews in the neurovascular literature in general are at risk of including overlapping patient populations. As we mentioned in our limitations section, though we were careful to exclude studies that had overlapping patient populations by examining the time periods studied and the institutions where the patients were treated, in some cases, articles were not clear as to whether patients included in their studies were included in prior publications.² In all such cases, we did attempt to contact the authors of

articles. It is important for authors of both single-center series and large multi-institutional registries to provide information regarding the potential for overlap with prior publications.

Last, we would like to congratulate Armoiry and colleagues on their systematic review of the Woven EndoBridge (WEB) aneurysm embolization system (Sequent Medical, Aliso Viejo, California).³ Their work provides an excellent and systematic overview of the current data regarding the WEB and provides important information that should be considered by all practitioners who are treating aneurysms with this device.

REFERENCES

1. Klimo P Jr, Thompson CJ, Ragel BT, et al. **Methodology and reporting of meta-analyses in the neurosurgical literature.** *J Neurosurg* 2014; 120:796–810 CrossRef Medline
2. Asnafi S, Rouchaud A, Pierot L, et al. **Efficacy and safety of the Woven EndoBridge (WEB) device for the treatment of intracranial aneurysms: a systematic review and meta-analysis.** *AJNR Am J Neuroradiol* 2016 Aug 11. [Epub ahead of print] CrossRef Medline
3. Armoiry X, Turjman F, Hartmann DJ, et al. **Endovascular treatment of intracranial aneurysms with the WEB device: a systematic review of clinical outcomes.** *AJNR Am J Neuroradiol* 2016;37:868–72 CrossRef Medline

W. Brinjikji

Department of Radiology
Mayo Clinic
Rochester, Minnesota

A. Rouchaud

Department of Interventional Neuroradiology
Hôpital Bicêtre, APHP, Paris Sud Université
Paris, France

<http://dx.doi.org/10.3174/ajnr.A4987>

Survey of Head and Neck Practice

I read with curiosity the article by Ko et al¹ regarding the survey of TNM staging by radiologists.

Two statements were made that I believe need clarification.

1) The claim is made in the “Results” that “Subspecialization in head and neck radiology was reported by 72.1% of respondents.”¹ How is this defined? Obviously, the survey results may reflect the bias of the respondents. Selecting only members of the American Society of Head and Neck Radiology is a bias. Does “subspecialization in head and neck radiology” refer to a neuro-radiology fellowship? If so, the results may be believable. Otherwise, I am skeptical that that many people are practicing head and neck radiology exclusively as a subspecialist.

2) In the “Discussion,” the authors state, “It has been reported that the short axial diameter of lymph nodes is the most accurate indicator of metastatic versus normal or reactive nodes.”¹ These data are cited from sonography² and postmortem examination³ studies, not studies of CT and MR imaging, with which most American radiologists examine head and neck cancers. In his seminal review, Peter M. Som⁴ wrote in 1987, “It should be noted that most cervical lymph nodes are ovoid or lima bean shaped, and the determination of nodal size is based on the greatest nodal diameter.” Similarly, in the largest multi-institutional study written in the radiology literature looking at head and neck lymph nodes, Curtin et al⁵ state in their methodology, “On axial images, the readers noted the largest dimension of the largest node in each zone of the neck” for their data.

It is true that there is no consensus regarding what dimension is best to assess whether a node is pathologic or not. It is also true that size criteria alone are flawed as guidelines. However, I thought that having statement number 2 above in the literature without at least some caveats would not be appropriate.

Disclosures: David Yousem—UNRELATED: Payment for Lectures (including service on Speakers Bureaus): ACR Educational Center; Royalties: Elsevier; Payment for Development of Educational Presentations: CMEInfo.com.* *Money paid to the institution.

REFERENCES

1. Ko B, Parvathaneni U, Hudgins PA, et al. **Do radiologists report the TNM staging in radiology reports for head and neck cancers? A national survey study.** *AJNR Am J Neuroradiol* 2016;37:1504–09 [CrossRef Medline](#)
2. van den Brekel MW, Castelijns JA, Snow GB. **The size of lymph nodes in the neck on sonograms as a radiologic criterion for metastasis: how reliable is it?** *AJNR Am J Neuroradiol* 1998;19:695–700 [Medline](#)
3. van den Brekel MW, Stel HV, Castelijns JA, et al. **Cervical lymph node metastasis: assessment of radiologic criteria.** *Radiology* 1990;177:379–84 [CrossRef Medline](#)
4. Som PM. **Lymph nodes of the neck.** *Radiology* 1987;165:593–600 [CrossRef Medline](#)
5. Curtin HD, Ishwaran H, Mancuso AA, et al. **Comparison of CT and MR imaging in staging of neck metastases.** *Radiology* 1998;207:123–30 [CrossRef Medline](#)

● D.M. Yousem

Division of Neuroradiology
Johns Hopkins Medical Institutions
Baltimore, Maryland

<http://dx.doi.org/10.3174/ajnr.A4985>

REPLY:

Thank you so much for your questions regarding the article related to the TNM staging by head and neck radiologists. Your first question was regarding how we determined “subspecialization in head and neck radiology.”

Subspecialization in head and neck radiology was determined based on the self-claim of the survey responders. We asked the exact question, “Are you specialized to head and neck radiology?” To this question, 72.1% of the responders answered yes. Because the survey was sent to members of the American Society of Head and Neck Radiology (ASHNR), most (if not all) of the responders were neuroradiology-fellowship trained. It is estimated that 75–80% of ASHNR members are neuroradiology-fellowship trained. Those who claimed subspecialized in head and neck radiology, however, do not necessarily practice head and neck radiology exclusively. The vast majority of them interpret general neuroradiology. The intention of the survey is to understand the current practice of neuro/head and neck radiologists regarding imaging based cancer staging, not by general radiologists.

Regarding the second question as to how we measure a cervical lymph node, I agree with Dr Yousem that the size criteria alone have limited value.¹ The reference for the statement “the shortest axial diameter of lymph nodes is the most accurate indicator of metastatic versus reactive or normal node” was supposed to be the 1990 report by van den Brekel in *Radiology*.² The article by van den Brekel² is the largest study addressing the accuracy of size criteria of 2719 lymph nodes in 71 neck dissection specimens in patients with head and neck cancer. Although the measurement was not performed on imaging, it revealed a real performance of size criteria by using the 3D measurements correlated with pathologic results in patients with head and neck cancer. They measured short axial, long axial, and longest longitudinal diameters. Based on the pathologic correlation of each lymph node, they found that a short axial diameter was the most accurate predicting presence of nodal metastasis.

Furthermore, evidence review of diagnostic accuracy of cervical lymph node metastasis by Furukawa and Anzai³ demonstrated a high sensitivity, but an extremely low specificity of 1-cm cutoff of the maximum axial diameter generally used in clinical practice.

<http://dx.doi.org/10.3174/ajnr.A5005>

On the other hand, the size cutoff when using 1-cm minimum axial diameter was associated with moderate sensitivity and specificity and overall higher accuracy compared with that of the largest axial diameter. It might be because a pathologic node is round rather than oval-shaped, as Dr. Peter Som described in 1987.⁴ Therefore, a short axial diameter reflects the presence of metastasis more accurately than a long axial diameter, as shown in a study by Steinkamp et al.⁵

However, it is customary to measure lymph nodes in a large axial diameter because that is how head and neck surgeons or oncologists palpate and document the size of nodal metastases. The goal of this survey was to access the practice variations, not to make any conclusion as to what is right or how we should measure lymph nodes. As expected, we found substantial variabilities as to how radiologists measure lymph nodes in clinical practice. The current CT allows visualization of a tumor or lymph node in any planes, as well as measurement of volume of tumor. I believe that how we measure and report tumor burden is an important question for all cancer imaging. Although we have no consensus, what is important is to understand perspectives of our colleagues of head and neck surgeons and oncology team. The authors would like to thank Dr. David Yousem for raising the interesting and important discussion.

REFERENCES

1. Don DM, Anzai Y, Lufkin RB, et al. **Evaluation of cervical lymph node metastases in squamous cell carcinoma of the head and neck.** *Laryngoscope* 1995;105:669–74 CrossRef Medline
2. van den Brekel MW, Stel HV, Castelijns JA, et al. **Cervical lymph node metastasis: assessment of radiologic criteria.** *Radiology* 1990;177:379–84 CrossRef Medline
3. Furukawa M, Anzai Y. **Diagnosis of cervical lymph node metastasis in head and neck cancer: evidence-based neuroimaging.** In Medina LS, Sanelli PC, Jarvik JG, eds. *Evidence-Based Neuroimaging Diagnosis and Treatment: Improving the Quality of Neuroimaging in Patient Care.* New York: Springer-Verlag; 2013:693–718 CrossRef
4. Som PM. **Lymph nodes of the neck.** *Radiology* 1987;165:593–600 CrossRef Medline
5. Steinkamp HJ, Hosten N, Richter C, et al. **Enlarged cervical lymph nodes at helical CT.** *Radiology* 1994;191:795–98 CrossRef Medline

Y. Anzai

Department of Radiology
University of Utah
Salt Lake City, Utah